I. SYNTHESIS AND RING-OPENING POLYMERIZATION OF CATIONIC DIVALENT METAL COMPLEXES SUPPORTED BY *NEN*-PINCER LIGANDS (E = O, S, SE)

II. SEMISYNTHESIS STRATEGIES FOR THE GENERATION OF CANNABINOIDS AND RELATED DERIVATIVES

DYLAN J. WEBB
Master of Science, Victoria University of Wellington, 2017

A thesis submitted in partial
fulfilment of the requirements for the degree of

DOCTOR OF PHILOSOPHY

in

CHEMISTRY

Department of Chemistry and Biochemistry
University of Lethbridge
LETHBRIDGE, ALBERTA, CANADA

I. SYNTHESIS AND RING OPENING POLYMERIZATION OF CATIONIC DIVALENT METAL COMPLEXES SUPPORTED BY *NEN*-PINCER LIGANDS (E = O, S, SE)

II. SEMISYNTHESIS STRATEGIES FOR THE GENERATION OF CANNABINOIDS AND RELATED DERIVATIVES

DYLAN JAMES WEBB

Date of Defence: April 5th, 2022

Dr. P. Hayes Thesis Supervisor	Professor	Ph.D
Dr. R. Boeré Thesis Examination Committee Member	Professor	Ph.D
Dr. P. Hazendonk Thesis Examination Committee Member	Associate Professor	Ph.D
Dr. R. Golsteyn Internal Examiner	Associate Professor	Ph.D
Dr. D. Morales-Morales External Examiner Universidad Nacional Autónoma de México Mexico City, Mexico	Professor	Ph.D
Dr. T. Patel Chair, Thesis Examination Committee	Associate Professor	Ph.D

Dedication

For Pam,

A constant advocate for my education

and a loving godmother

Abstract

Part I describes the synthesis of neutral bis(phosphinimine) *NEN*-pincer ligands. The ligands vary at the neutral central donor, E, the flanking aromatic group, and P-substituents. Cationic alkyl and phenoxide zinc complexes of this ligand system were synthesized to understand the steric and electronic factors that govern the complexes capacity to serve as catalysts for the ring-opening polymerization of ε-caprolactone.

Part II describes the semisynthetic strategies for the generation of the major cannabinoids (9THC and CBD), and the lower abundant cannabinoids 8THC and CBN. Lesser-known cannabinoids and related derivatives were also prepared. Their *in vitro* chemotherapeutic action to breast cancer cells is described, attempting to decipher a relationship to chemical structure. Other investigations include computational analysis and reduction of the *ortho*-quinoids. A quantitative NMR procedure was used to determine purity of cannabinoids extracted.

Compounds were characterized *via* multi-dimensional and multi-nuclear NMR spectroscopy, elemental analysis, and, where possible, single-crystal X-ray diffraction experiments.

Preface

This thesis has been written with the intention that anyone with a tertiary education in chemistry or biochemistry can understand the content. Some of the common parlance and chemical nomenclature used are not common in the English lexicon, but efforts to mitigate confusion have been implemented.

As there is an abundance of topics within this thesis, an attempt to be concise has been made; trying to highlight certain aspects in the literature, demonstrate an understanding of the current research, and explain the importance of the study from a wider point-of-view. Both Part I and Part II are structured so a larger picture is presented first, and each subsequent section narrows the scope towards the specific areas investigated for this work.

The numbering system for the compounds discussed for the introduction chapter in Part I is in Roman numerals. Any compounds synthesized in Part I have Arabic numerals. Since many of the compounds synthesized in Part II are known (*i.e.* their nomenclature has been pre-established), their commonly accepted abbreviations used in the literature, or their full chemical names, have been used. No numbering system is used for synthesized compounds in Part II, the derivatives of known compounds have abbreviations that reflect their respective derivatization. Colour has been utilized, where appropriate, to highlight the subtle changes in chemical structure.

Several aspects of this thesis were performed by collaborators, or under the supervision of other researchers. Accordingly, it is appropriate to indicate what work was not done alone. The computational analysis of 8THC (5.4.1) was conducted by Rajwinder Kur and Prof. Stacey Wetmore. The electrochemical studies and related

computational analysis (5.5.1 and 5.5.2) were conducted by Nathan Hill and Prof. René Boeré. The biological studies were conducted by Dr. DongPing Li, and the biomass of *Cannabis sativa* was provided by Prof. Igor Kovalchuk (5.8).

Some content in this thesis originated from the author's own published work, manuscripts in the process of being submitted, and manuscripts that are to be submitted, all of which has been reformatted (see sections 3.4 and 6.4 for specifics).

Acknowledgments

To my parents, Lorna and Keith: You've always encouraged me to reach my goals and aim high, you're both the reason I undertook this academic pursuit, and you are both the reason I've managed to get this far. I hope you are proud.

To Danielle: I would have never been able to work on my PhD if it were not for you. This is as much of an achievement for you as it is for me, I am sorry you have not got the recognition you deserve. I will demand to be called 'Doctor' for some time following its successful completion, for that I am not sorry.

To my Canadian friends, Ed, Daisy, Sam/Samultha/Salad-dressing/Ciggy-Sam/Dart-Cam, Jackson, Desmond, Nathan, Nolan, Eric, Felix, Ash, Francis/Franny and Brayden/Gumby: For all the necessary distractions, including Dungeons and Dragons sessions, pub drinks, rock climbing, board game and video game nights, and more pub drinks; without these I would not have survived and whether our friendship is maintained following this time in my life or not, I will always look back at it fondly.

To my lab mates both past and present, Ed, Tara, Connor, Desmond, Daisy, Sam, Jackson, Chris, and Ash: All your patience and understanding was an important factor to my success. You've all put up with me through some tough times and celebrated with me during the great times, for that I am thankful.

To the University of Lethbridge for letting me study in Canada, the University of Lethbridge Library for the resources I exploited, and to Mitacs for their funding regarding the cannabinoid work, I was able to maintain a very comfortable lifestyle thanks to them. Special mention to the Canadian Institute of Chemistry for putting on

conferences I attended and thoroughly enjoyed, those involved in organizing the Chinook Symposium, those at Rigaku who put together the remote lectures on crystallography, and Wikipedia for whom I really should donate to considering how much I used their resources.

To my supervisor, Prof. Paul Hayes: Despite trying to portray a tough exterior, you are actually a thoughtful person. Allowing and encouraging me to pursue the chemistry I enjoy saved me from burning out. I would not be the chemist I am today without a supervisor like you. Also, what happens in Colombia, stays in Colombia.

A special thanks to Prof. René Boeré, his student Nathan Hill, Prof. Stacey Wetmore, her student Rajwinder Kar, and Prof. Igor Kovalchuk and Dr. DongPing Li for being collaborators I can look up to. My knowledge of science has expanded due to your vigour and passion for your respective subjects. To Prof. René Boeré (again) and Prof. Paul Hazendonk for being fantastic committee members. To Prof. René Boeré (again!) for teaching me X-ray crystallography and helping me your spare time. I strive to be at least half as intelligent and active as you are when I'm older. To Tony Montina and Michael Opyr for doing a superb job at maintaining a state-of-art NMR facility. And finally, to Dr. Roy Golsteyn and Prof. David Morales-Morales for suffering through this thesis as my internal and external examiner, respectively.

Table of Contents

List of Tables

List of Figures

List of Schemes

List of Abbreviations

AIBN	azobisisobutyronitrile
Ar	aryl
Ar-N_3	aryl azide
b.p.	boiling point
br	broad
Bn	benzyl, or –CH_2Ph
Bu	butyl, or –C_4H_9 linear chain
C	degrees Celsius
Cat.	catalyst
COE	cyclooctene
CaH_2	calcium hydride
CBD	cannabidiol
CBD-A	cannabidiolic acid
CBE	cannabielsoin
CBG	cannabigerol
CBG-A	cannabigerolic acid
CBL	cannabicyclol
CBND	cannabinodiol
CBN	cannabinol
CBT	cannabicitran
CB_1	cannabinoid receptor 1
CB_2	cannabinoid receptor 2
$CHCl_3$	chloroform
$CDCl_3$	deuterated chloroform
CHO	cyclohexene oxide
CoA	coenzyme A
COSY	correlated spectroscopy
Cp	η^5-cyclopentadienyl ligand
CV	cyclic voltammogram
Cy	cyclohexane group, or – C_6H_{11}
CyH	cyclohexane
C_4H_4O	furan
C_4H_4S	thiophene
C_4H_4Se	selenophene
C_6H_6	benzene
C_6H_5Br	bromobenzene
C_6D_6	deuterated benzene
C_6D_5Br	deuterated bromobenzene
dbf	dibenzofuran
DCM	dichloromethane
DEPT	distortionless enhancement by polarization transfer
DFT	density functional theory
Dipp	2,6-diisopropylphenyl

Dipp-N_3	2,6-diisopropyl-1-azidophenyl
DMF	dimethylformamide
DOP	degree of polymerization
DOSY	diffusion ordered spectroscopy
DT	decatungstate
E	oxygen, sulfur, or selenium central donor
EA	elemental analysis, or combustion analysis
Et	ethyl, or $–C_2H_5$ chain
EtOAc	ethyl acetate
Et_2O	diethyl ether
equiv	equivalents
F_c	calculated structure factor
F_o	observed structure factor
FWHM	full width half maximum
G	Gibbs free energy
g	grams
GooF	goodness of fit
h	hour
HMBC	heteronuclear multiple bond coupling
HMDS	bis(trimethylsilyl)amine, or hexamethyldisilazane
HMPA	hexamethylphosphoramide
HOMO	highest occupied molecular orbital
HPLC	high pressure liquid chromatography
HSQC	heteronuclear single quantum coherence
Hz	hertz
IBX	2-iodoxybenzoic acid
^{i}Pr	isopropyl, or a $–CH(CH_3)_2$, group
J	joule
k	reaction rate constant
K	Kelvin
kcal	kilocalorie
LUMO	lowest occupied molecular orbital
MAO	methylaluminoxane
Me	methyl, or a CH_3 group
MeLi	methyl lithium
Mes	2,4,6-trimethylphenyl
Mes-N_3	2,4,6-trimethyl-1-azidophenyl
min	minutes
M_N	Number average of molecular weights
MW	molecular weight
M_W	mass average of molecular weights
m-Xy	*meta*-xylene
NacNac	1,3-diketimine ligand system
^{n}Bu	*n*-butyl
^{n}BuLi	*n*-butyllithium
NFSI	*N*-fluorobenzenesulfonimide

NMR	nuclear magnetic resonance
o	ortho
OPh	phenoxide group, or –OC6H5
ov	overlapping
o-qCBN	*ortho*-quinone-cannabinol
o-q8THC	*ortho*-quinone-Δ^8-tetrahydrocannabinol
o-q9THC	*ortho*-quinone-Δ^9-tetrahydrocannabinol
p	para
PDI	polydispersity index
PIFA	(bis(trifluoroacetoxy)iodo)benzene
Pipp	4-isopropylphenyl
Pipp-N_3	4-isopropyl-1-azidophenyl
Ph	phenyl, or a –C_6H_5, group
PLA	polylactic acid
Pm	3,5-dimethylpyrimidine
Pm-N_3	3,5-dimethyl-1-azidopyrimidine
PO	propylene oxide
ppm	parts per million
p-qCBN	*p*ara-quinone-cannabinol
p-q8THC	*para*-quinone-Δ^8-tetrahydrocannabinol
p-q9THC	*para*-quinone-Δ^9-tetrahydrocannabinol
PTFE	polytetrafluoroethylene
p-TrPh	*para*-tritylphenyl
py	pyrazole
Py	pyridine
qNMR	quantitative NMR
R	defined organic, or alkyl, group
RMO	redox molecular orbital
ROP	ring opening polymerization
ROS	reactive oxygen species
s	second or singlet (context specific)
Si-CBN	1-OSiMe3-cannabinol
Si-8THC	1-OSiMe3-Δ^8-tetrahydrocannabinol
SOMO	single occupied molecular orbital
SWV	square-wave voltammogram
t	triplet
TBDT	tetra-*n*-butylammonium decatungstate
^{t}Bu	*tert*-butyl
^{t}BuLi	*tert*-butyllithium
THC	tetrahydrocannabinol
THF	tetrahydrofuran
TLC	thin layer chromatography
TON	turnover number
Tr	trityl group –(CPh_3)

TsOH	*para*-toluenesulfonic acid
UV	ultraviolet
VT	variable temperature
$ZnEt_2$	diethyl zinc
$ZnMe_2$	dimethyl zinc
2F-CBN	2-fluoro-cannabinol
2,5-$Br_2C_4H_2S$	2,5-dibromothiophene
2,5-$Br_2C_4H_2Se$	2,5-dibromoselenophene
7THC	(−)-trans-Δ^7-tetrahydrocannabinol
8THC	(−)-trans-Δ^8-tetrahydrocannabinol
9THC	(−)-trans-Δ^9-tetrahydrocannabinol
9THC-A	(−)-trans-Δ^9-tetrahydrocannabinolic acid
10THC	(*R*,*S*)-Δ^{10}-tetrahydrocannabinol
10aTHC	*R*-Δ^{10a}-tetrahydrocannabinol
%	percent
Å	angstrom
Δ	change in or heat applied (context specific)
δ	chemical shift in ppm
°	degrees
{^{y}X}	decoupling of the y isotope of the X nuclei

Structural List of Synthesized Compounds

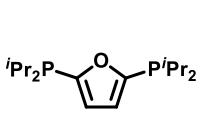

2

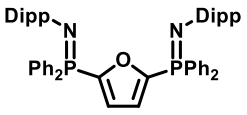

3

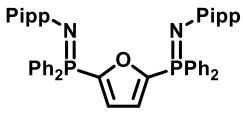

4

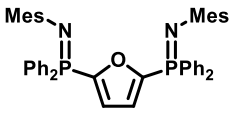

5

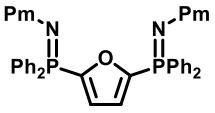

6

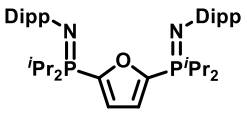

7

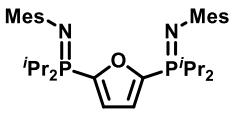

8

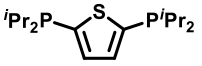

10

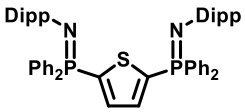

11

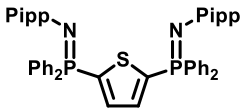

12

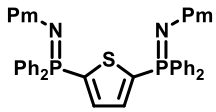

13

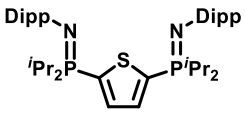

14

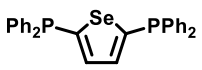

15

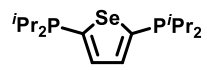

16

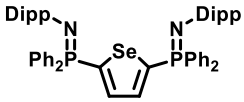

17

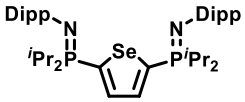

18

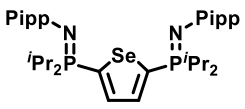

19

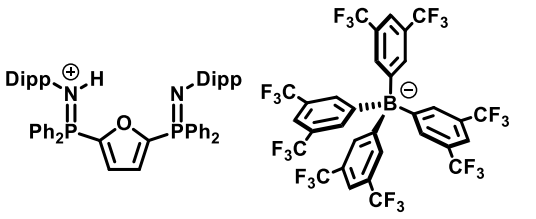

20

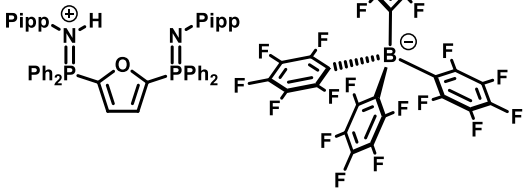

21

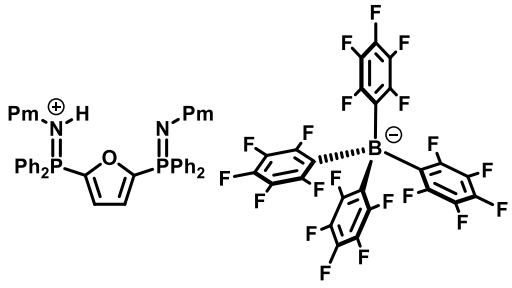

22

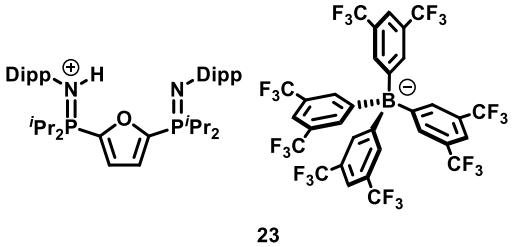

23

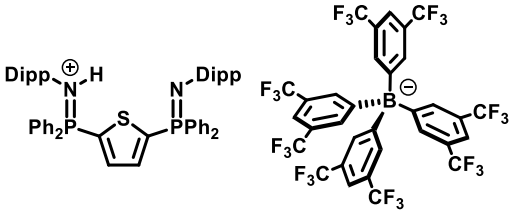

24

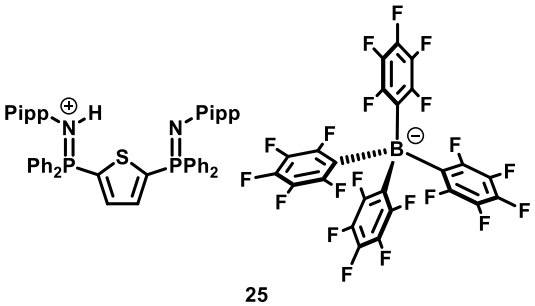

25

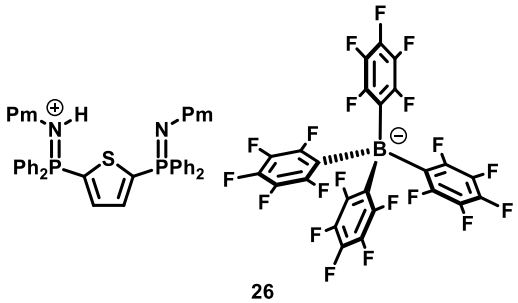

26

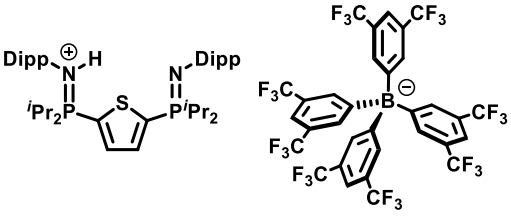

27

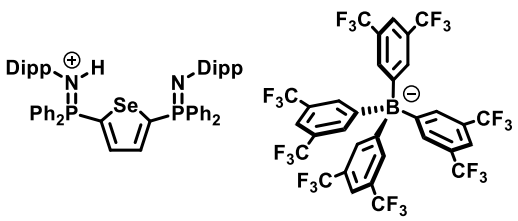

28

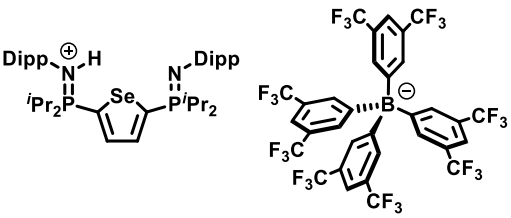

29

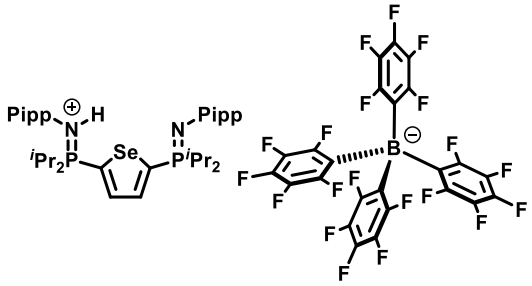

30

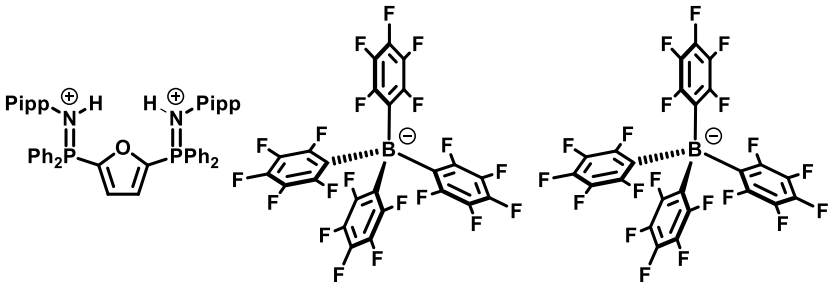

31

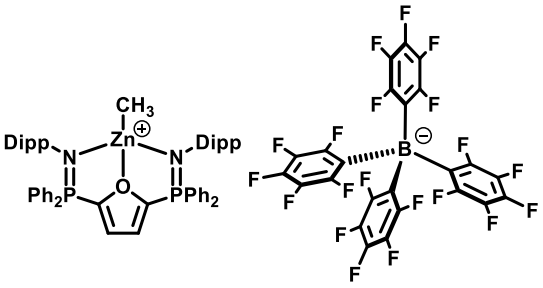

32

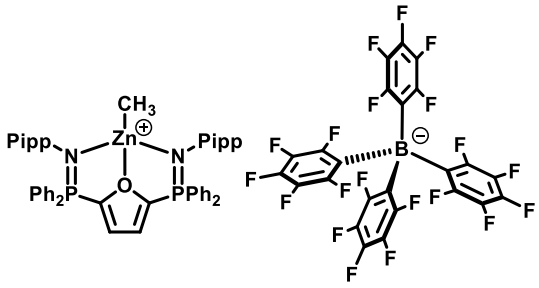

33

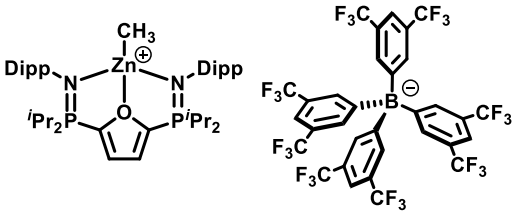

34

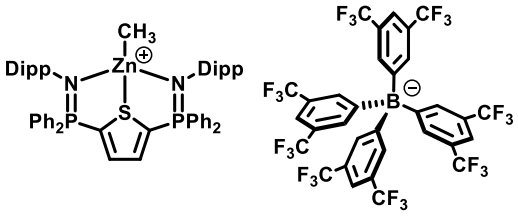

35

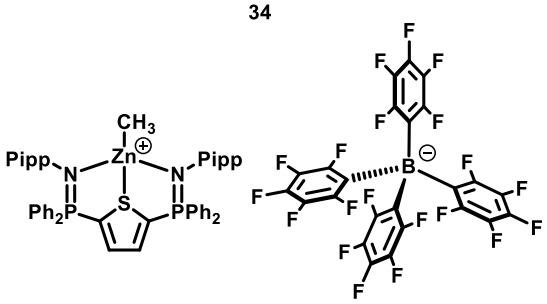

36

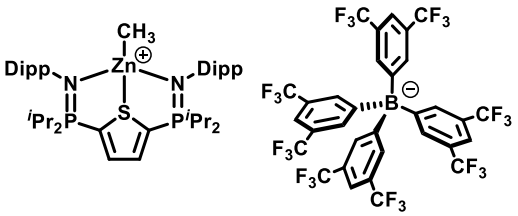

37

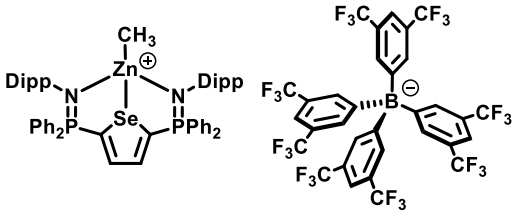

38

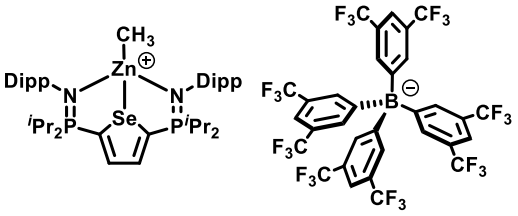

39

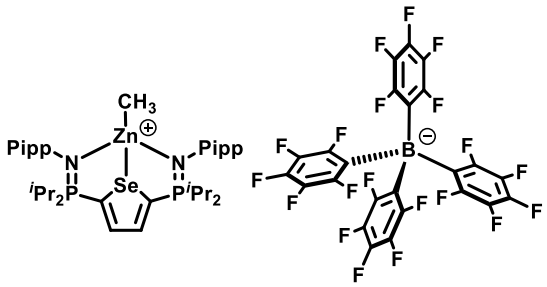

40

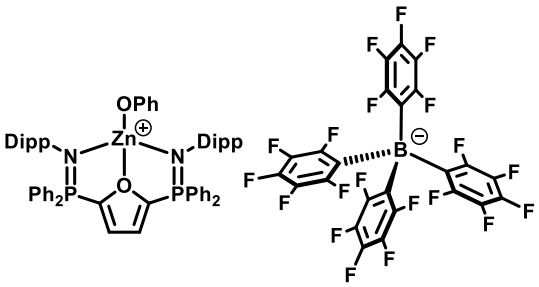

32b

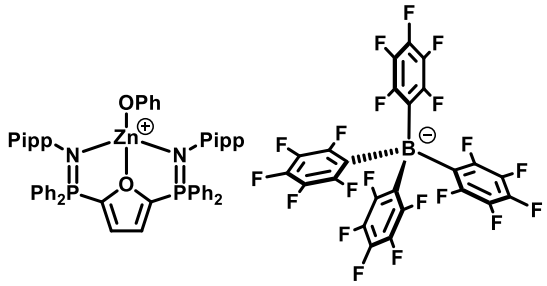

33b

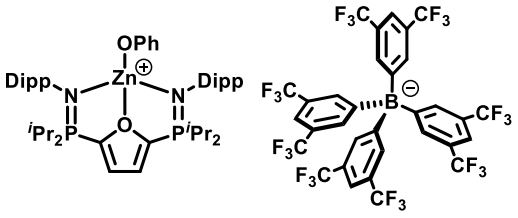

34b

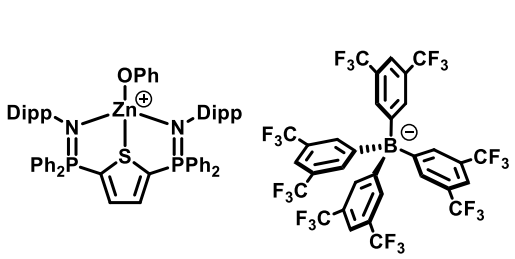

35b

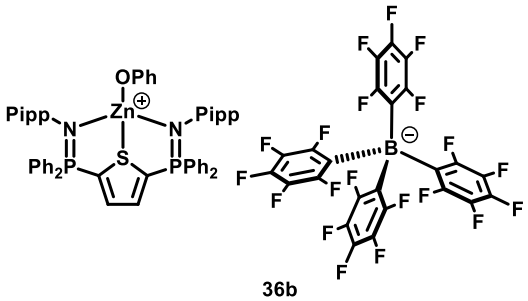

36b

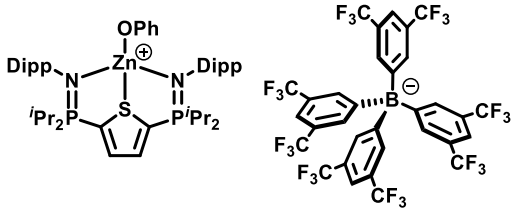

37b

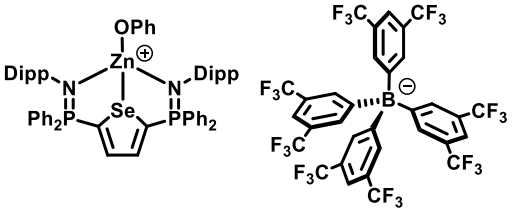

38b

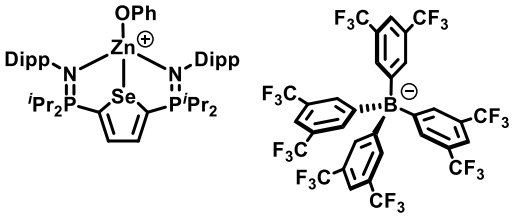

39b

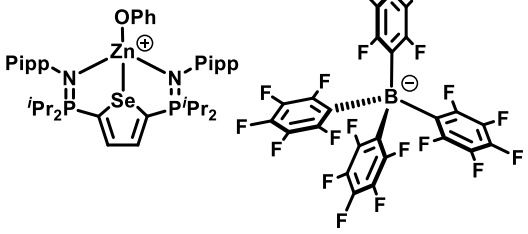

40b

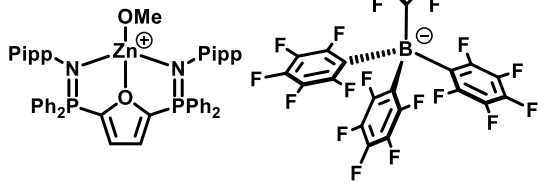

41

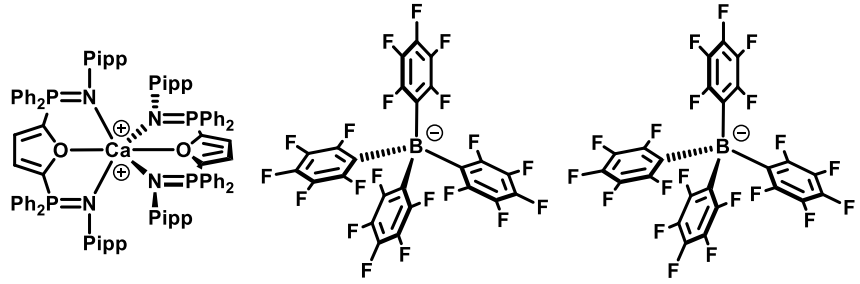

42

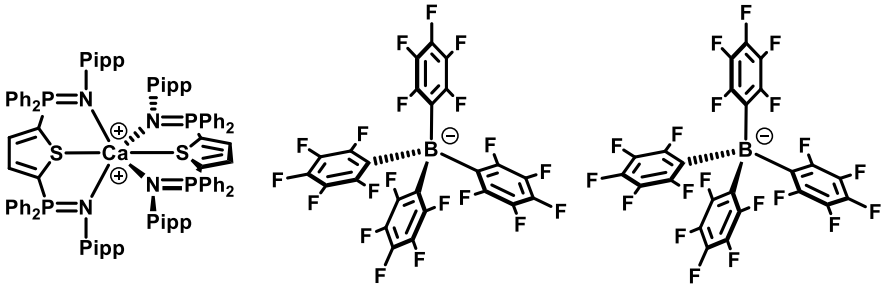

43

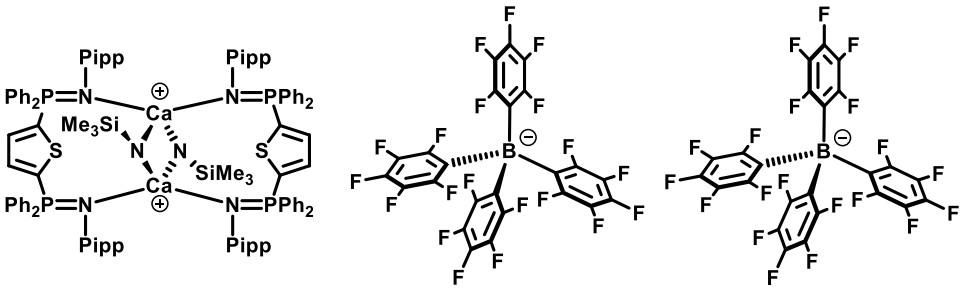

43b

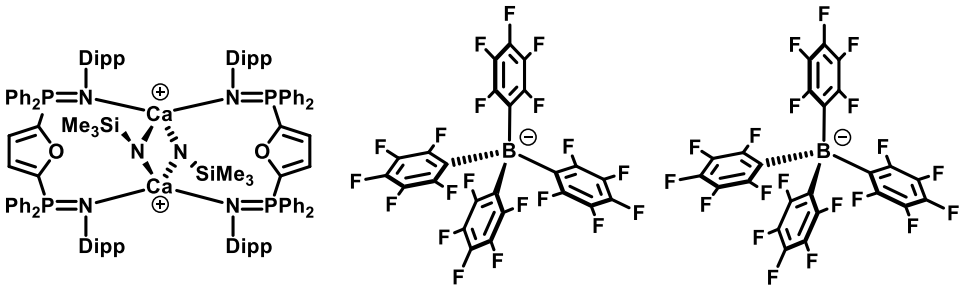

44

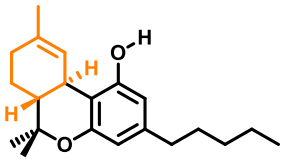

9THC

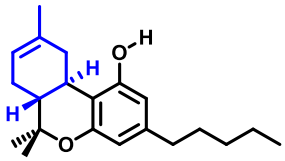

8THC

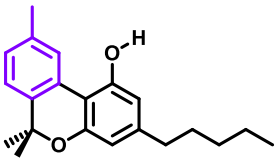

CBN

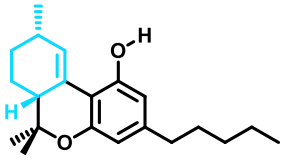

10THC

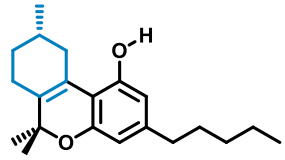

10aTHC

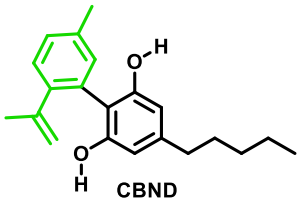

CBND

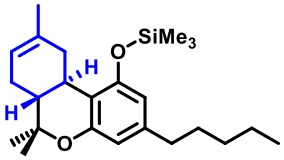

Si-8THC

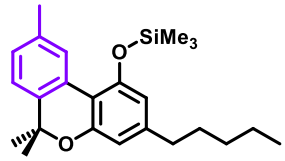

Si-CBN

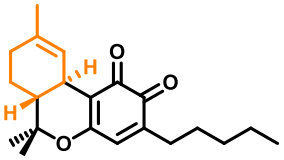

o-q9THC

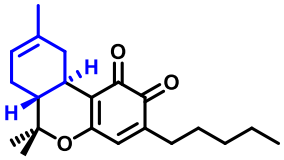

o-q8THC

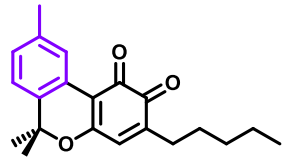

o-qCBN

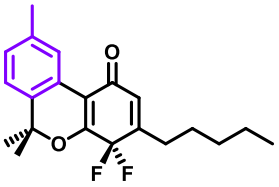

4F$_2$-CBN

I. SYNTHESIS AND RING-OPENING POLYMERIZATION OF CATIONIC DIVALENT METAL COMPLEXES SUPPORTED BY *NEN*-PINCER LIGANDS (E = O, S, SE)

Chapter 1: Introduction to Ligands and Cationic Complexes

1.1 History and Nomenclature

Chemical definitions have very specific meanings and when used incorrectly, they can lead to a great deal of confusion.[1] A few key terms will therefore be introduced now to mitigate ambiguity. *Molecule* is a general term to describe any combination of at least two atoms with a chemical bond. A *compound* is a molecule that must have at least one chemical bond between two different atoms. Therefore, all compounds are molecules, but not all molecules are compounds. A *ligand* (pronounced as either *laɪgənd* or *lɪgənd*) is a molecule that forms a bond, to a typically metallic central atom, to establish a *complex*. Complex, a term that will be used throughout Part I of this thesis, is a compound that contains a central atom surrounded by ligands. Therefore, all complexes are compounds, but not all compounds are complexes (Figure 1.1).

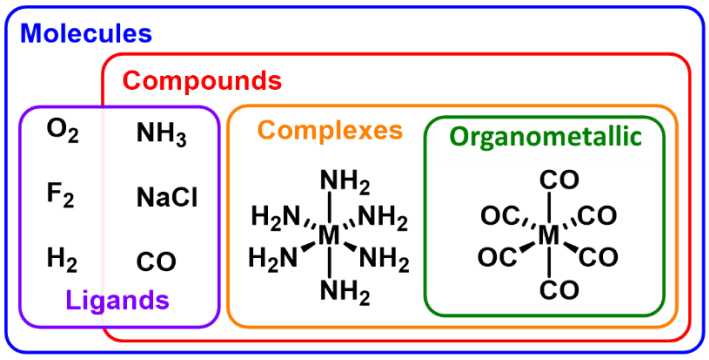

Figure 1.1: Schematic of the definitions molecule, compound, ligand, complex, and organometallic, and simple examples thereof. M = Metal.

A complex can be described based on the steric and electronic properties of the ligands themselves, as well as the electronic structure of the central atom, leading to the establishment of 'coordination' chemistry where the term *coordination complex* is often used.[2] The terms complex and coordination complex are often used interchangeably. Finally, an *organometallic complex* requires a carbon atom typically in the form of a

ligand to be bound to a metal ion. The resulting complex is referred to as an organometallic complex wherein the prefix *organo-* can be placed in front of a specific metal when that particular metal is the main subject (*e.g. organozinc* can be used for organometallic compounds where zinc is the focal and central atom).

The way a ligand generally binds to a central atom is by donating electron density to that atom. Therefore, in a coordination complex, ligands are said to be acting as Lewis bases, and the central atoms as Lewis acids.[3] They can be classified in many ways: by charge (neutral, anionic, or cationic in rare cases); by coordination number (also known as denticity, denoted with 'κ^n' where n = number of bonds formed with the central atom); or by hapticity (in which multiple atoms in a contiguous series all bind to the metal, denoted with 'η^n' where n = number of atoms in the contiguous series that are involved in binding).[4] An *ancillary* ligand, sometimes referred to as a *spectator* ligand, is a ligand that provides both a stabilizing steric and electronic environment around the central atom, but remains 'innocent' or uninvolved in a transformation the compound undergoes. Ligands which are participating in a particular chemical transformation can be called *actor* or *reactive* ligands.[5] A *substituent* is a group attached to a defined atom. This term is generally used to describe a particular feature of a ligand that can often be exchanged for other groups during their synthesis. Altering substituents is used for fine tuning steric and electronic properties of the ligand.

It is with the use of synthetic and tailor-made ancillary ligands that a metal ion can form a complex and be utilized in specified and extraordinary ways. The design of the ancillary ligand helps guide the chemical reactivity of the metal centre to yield a particular outcome. These outcomes are often only possible due to the chemical environment the ancillary ligand provides. Ligands have proved instrumental to the

solution phase reactivity of metal complexes, expanding from their early discoveries to their developments throughout the 20th and 21st centuries confirming that ligand design is a flourishing and worthwhile subject to pursue.[1, 6, 7]

The initial challenge of determining the nature of ligand coordination in aqueous solvents was overcome by Christian Wilhelm Blomstrand in 1869 with his preliminary work on water-based ammonia complexes.[8] This was further expanded upon by Alfred Werner in 1893 with the landmark discovery of hexol,[9] a coordination complex of cobalt often used to illustrate preliminary discoveries in geometry and chirality in compounds containing a metal (**I**, Figure 1.2).[10, 11]

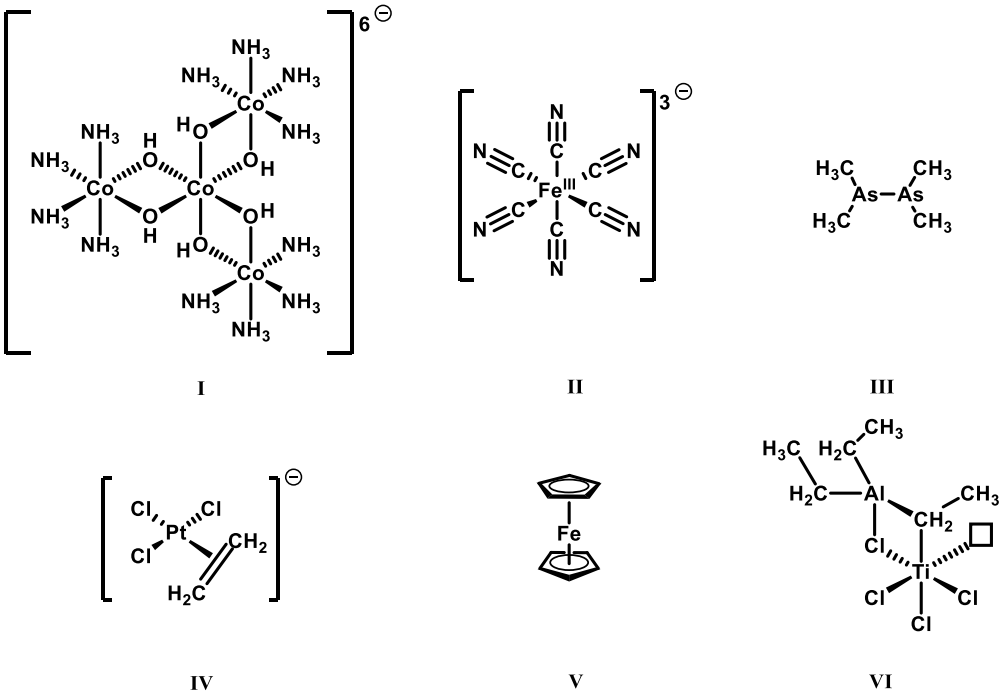

Figure 1.2: Historically significant compounds that contributed to the development of ligands and coordination chemistry.

The earliest known synthetic complex is Prussian blue,[12] or Turnbull's blue ($[Fe^{III}(CN)]^{3-}$, **II**), which is an iron ferrocyanide complex accidently made by a painter, Diesbach, in 1706 when blood tainted a dye mixing process generating a distinct blue colour instead of the intended cochineal red.[13, 14] Despite arsenic being considered a

metalloid, the arsenic containing compound, cacodyl ($(CH_3)_2AsAs(CH_3)_2$, **III**), synthesized in 1760 by Luis Claude Cadet de Gassicourt, is considered one of the earliest known organometallic compounds.[15] This discovery was followed by an organometallic complex, known as Zeise's salt ($[PtCl_3(C_2H_4)]^-$, **IV**) in 1827 named after its discoverer, William Christopher Zeise,[16] although confirmation of the exact structure and the acceptance of the η^2 bonding of the olefin ligand was not fully realized until advances in X-ray crystallography were developed in 1969.[17, 18]

Simple reactive ligands, such as C≡O by Paul Schützenberger with $Pt(CO)_2Cl_2$ in 1868[19-21] and alkyl groups, including Grignards by Auguste Victor Grignard in 1900,[22] were discovered and used to more readily generate numerous metal containing compounds. In 1951, Ferrocene ($Fe(C_5H_5)_2$, **V**) further expanded the idea of ligands involving more intricate chemical structures.[23-25] The use of ligands to alter the chemical environment of a metal centre was notably utilized in the 1963 Nobel prize in Chemistry for Karl Zieglar and Giulio Natta. Many industrial catalysts are still based upon their "Zieglar-Natta" system (an activated example, **VI**). Following Karl Zieglar and Giulio Natta's work,[26] investigations into ancillary ligands spawned the development of cyclopentadienyl ligand (Cp) systems as some of the first designed ancillary ligands which have been used to produce catalysts for the polymerization of olefins.[27-29]

The development of coordination chemistry expanded over the past 50 years, with an enormous library of unique, tailor-made, and complex ancillary ligands systems being established. Notable series of ligands, or ligand systems, designed for use as ancillary ligands include cyclopentadienyl analogues and derivatives (**VII** and **VIII**),[30,

[31] *N*-heterocyclic carbenes (**IX**),[32] and pincer ligands (**X**),[33] all of which fill various catalyst niches (Figure 1.3).

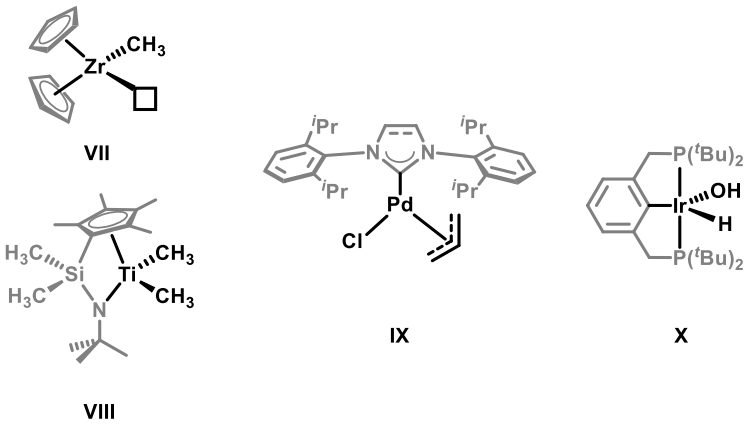

Figure 1.3: Examples of organometallic complexes that contain notable ancillary ligands systems common in homogeneous catalysis. Left to right: Cp (**VII**) and a related silyl amide containing analogue (**VIII**),[30, 31] *N*-heterocyclic carbene (**IX**),[32] and a *PCP*-pincer ligand complex (**X**).[33]

1.2 Polymerization

The process in which small molecules, monomers, bind together to form repeating units, polymers, is termed polymerization.[34-37] Two major types of polymers include homopolymers, (the polymer is made of a single monomer), and copolymers, (the polymer is made of at least two different monomers).[34-37] Natural biopolymers include deoxyribonucleic acid (DNA), silk, and rubber; a wide variety of synthetic polymers have been developed, including plastics (*e.g.* polyethylene and polypropylene) and other flexible materials (*e.g.* neoprene and nylon).

The physical properties of polymers are defined not only by the identity of the repeating monomer, but also their tacticity, which involves the relative stereochemistry of adjacent chiral centres provided by the monomer, and the polymer microstructure or physical arrangement of the monomer residues which are not always in a simple 2-dimentional chain.[38-40] Chain length, often presented as molecular weight (MW), is a microstructure feature that greatly affects the properties exhibited by the polymer.

Longer and heavier polymers generally exhibit increased melting points, impact resistance, toughness, and viscosity.[40] Due to the imperfect nature of polymerization different sized polymer chains are produced. The polydispersity index (PDI) is a value used to describe how dispersed the molecular weights of the polymers are (Figure 1.4). PDI is determined by a ratio of the mass average molecular weight (M_w) to the number average molecular weight (M_n), where a smaller and ideal PDI (closer to 1) represents a sample with more uniform chain lengths.[38-40] The degree of polymerization (DOP) is another metric used to quantify the chain length by describing how many monomer units have been incorporated into the polymer chain (Figure 1.4).[38, 39]

$$DOP = \frac{M_n}{M_0} \qquad PDI = \frac{M_w}{M_n}$$

$$M_n = \frac{\sum M_i \times n_i}{\sum n_i} \qquad M_w = \frac{\sum M_i \times w_i}{\sum w_i}$$

Figure 1.4: Equations associated with calculating DOP and PDI. M_i = mass of polymer i, n_i = number of polymer molecules, i, of a specific mass, w_i = weight fraction of polymer i, M_0 = molecular weight of the monomer.

A polymer is not always a linear chain of monomers, as there is the possibility of branching to create alternative polymer architectures. These architectures can further affect bulk physical properties like toughness and flexibility. The degree of branching can be quantified by the branching index (*g*, Figure 1.5), determined by the radius of gyration where a branched polymer has a large radius of gyration compared to an identical linear polymer. Ideally the branching index does not exceed 1 when no branching is desired. For example, low density polyethylene has more and longer branching than high density polyethylene, the long branches restrict crystallinity of the polymer, meaning low density polyethylene produces a larger radius of gyration,

compared to the tight packing observed in high density polyethylene, giving a branching index >1.[38-40]

$$s = \sqrt{\frac{\sum m_i {s_i}^2}{\sum m_i}}$$

$$g = \frac{{s_b}^2}{{s_I}^2}$$

Figure 1.5: Equations associated with calculating *g*. m_i = masses of the branching units, s_i = fixed distance from centre of mass, s_b = mean square radius of gyration of branched polymer, s_I = mean square radius of gyration of identical linear polymer.

Polymerization reactions may require a catalyst to provide better control over the initiation, propagation, and termination steps of the reaction.[34-37] Ligands on the metal centre of catalysts, along with the steric and electronic properties of ancillary ligands, greatly influence polymerization reactions. The catalyst often dictates the polymer's microstructure and tacticity, and hence, the physical properties of the polymer, by controlling how the monomers arrange themselves upon coordination and insertion.[41, 42]

1.2.1 Ring-Opening Polymerization of Lactones

A cyclic ester is called a lactone; the cyclic di-ester derived from lactic acid is named lactide (Figure 1.6).[43] Lactones are renewably sourced monomers that can be used to produce polyesters, a type of biodegradable polymer, where control over the microstructure and tacticity is accomplished with the use of a catalyst.[44] Since these monomers are cyclic compounds, the polymerization involves repeated ring-opening to generate a polymer chain, and hence, the name ring-opening polymerization (ROP). In comparison to polymers produced from olefins (Scheme 1.1), polyesters can be readily

broken down by naturally occurring processes, such as hydrolysis, cleavage of the ester groups within biological media, thermally, or with ultraviolet (UV) radiation, all of which produce smaller MW polymers or monomers that can be safely digested by microbes.[45]

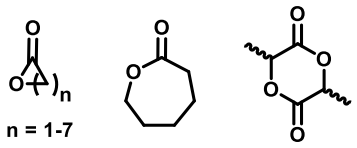

Figure 1.6: Common cyclic esters: general structure of a lactone (left), an example of a lactone, ε-caprolactone (middle), and *rac*-lactide (right).

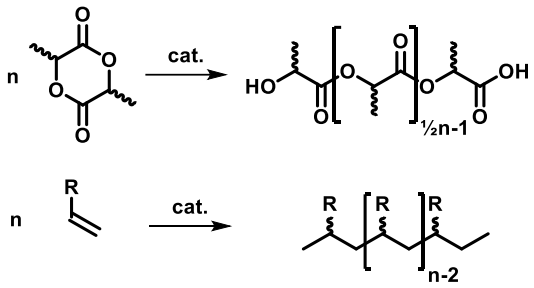

Scheme 1.1: Synthesis of PLA (top), synthesis of olefin polymer (bottom).

There are two chiral centres in lactide, giving rise to three possible stereoisomers: (*S*,*S*)-lactide (*L*-lactide), (*R*,*R*)-lactide (*D*-lactide) and (*R*,*S*)-lactide (*meso*-lactide) (Figure 1.7). A 50/50 mixture of *L*- and *D*-Lactide is known as *rac*-Lactide. Because of the variety of lactide stereoisomers, the terms to describe polymer tacticity are used, which include: isotactic (stereocentres in the same absolute configuration throughout), heterotactic (repeating pairs of stereocentres that alternate), syndiotactic (alternating stereocentres), and atactic (no pattern) (Figure 1.7). These differences in tacticity greatly influence the polymer's physical properties, such as melting point, tensile strength, viscosity, micellization, and degradation.[46-48]

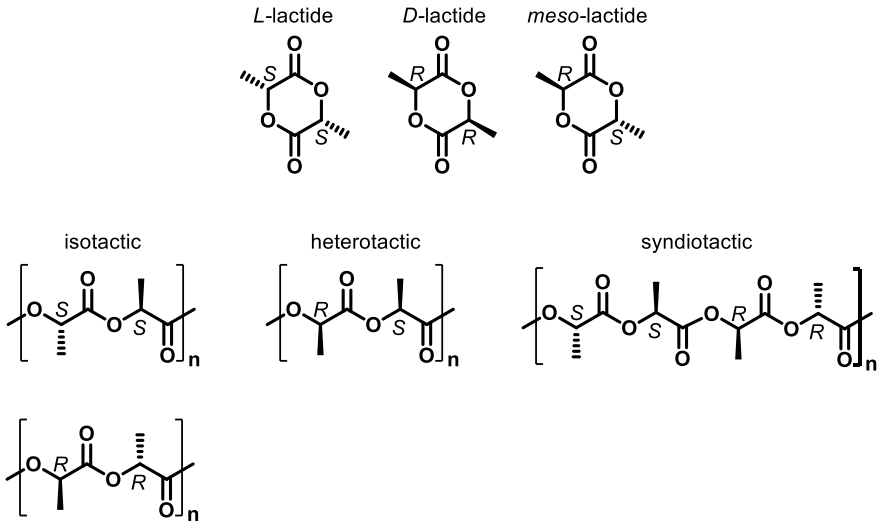

Figure 1.7: Possible isomers of lactide (top) and polylactide tacticity (bottom).

Cyclic esters undergo specific ROP mechanisms when a catalyst is used.[49] Two mechanisms for metal complex catalysed ROP are of particular interest: coordination-insertion, and chain-end activation pathways.[50] The coordination-insertion pathway involves a nucleophilic ligand provided by the catalyst to initiate ring-opening and allow propagation of the polymer (Scheme 1.2). This mechanism is highly dependent on the nature of the nucleophile and propagation occurs at the metal site. A chain-end pathway relies on the transfer of charge from the metal centre to the coordinated monomer to promote ring-opening (in the presented example the positive charge is transferred to the monomer) where propagation then occurs at the end of the chain, away from the metal site (Scheme 1.2). Both these mechanisms follow the cycle of monomer coordination, initiation (opening of the cyclic ester), propagation (the continuous activation and insertion of monomers), and termination (halting of the polymerization process). Termination often occurs due to chain-transfer reactions which transfers the growing polymer chain to available monomers, other uncoordinated polymers, solvents, or by an intentional chain-transfer agent, effectively halting polymerization.

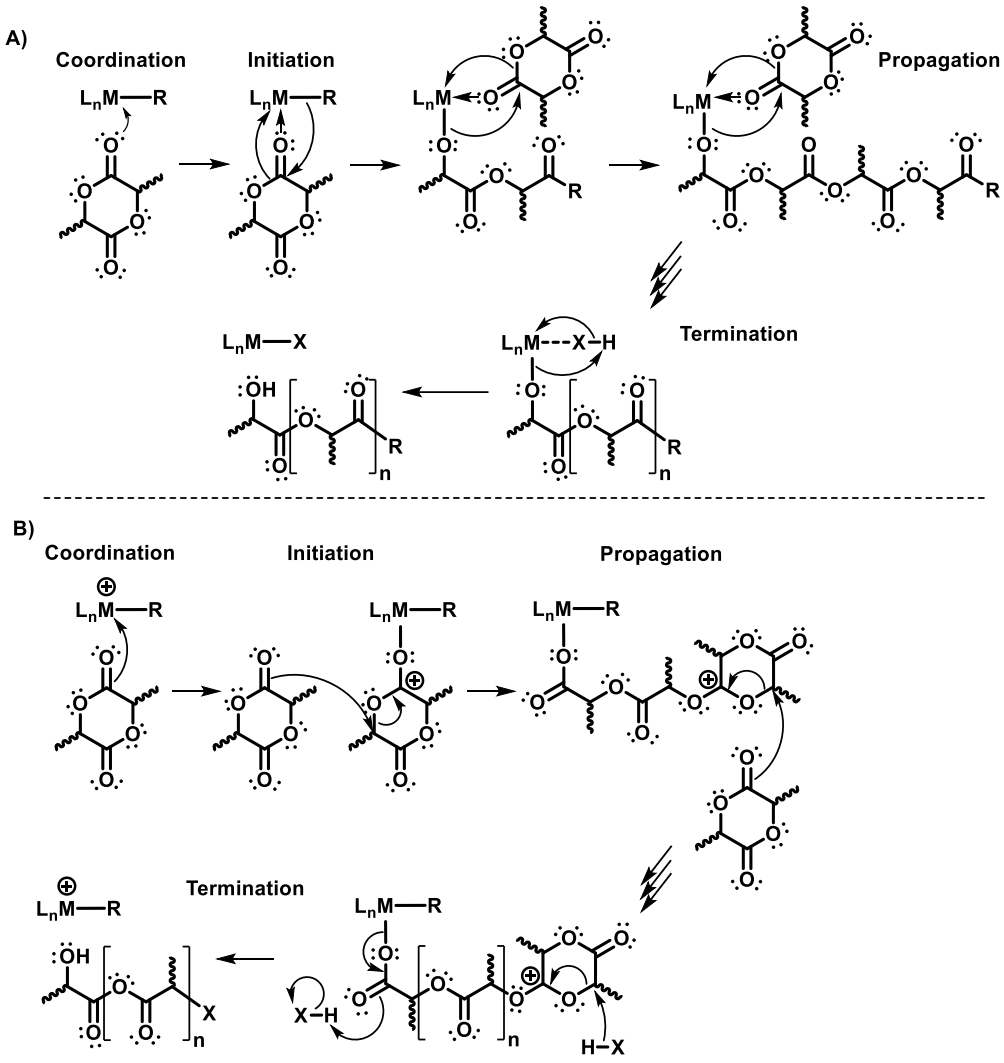

Scheme 1.2: Two common ROP mechanisms for coordination complexes with lactide. A) Coordination-insertion and B) chain-end activation mechanisms. L_n = ancillary ligand, M = metal, R = nucleophilic or non-nucleophilic ligand, X–H = quenching or chain transfer agent.

In a *living* catalyst system, termination and chain transfer reactions have been removed. The rate at which a polymer chain is initiated is much higher than the rate of propagation, resulting in more constant polymer growth. This type of catalyst requires an additive to terminate or release the polymer from the catalyst, usually quenching the catalyst. Catalysts of this type can be used to subsequently add different monomers to generate co-polymers.[51] A major problem with the mechanisms depicted in Scheme 1.2 is intra- or intermolecular transesterification where the end of the polymer *back-bites* the chain resulting in a cyclic polymer. These transesterification reactions affect the

expected PDI values by broadening the average molecule weight, the length of the polymers generated, and provide inconsistent bulk properties. An *immortal* catalysts is where termination occurs with an internal process or, if the polymer is reversibly bound to the catalyst, it can simply dissociate.[52] An immortal catalyst does not 'die' when the termination reaction occurs, and the catalyst can polymerize and continuously yield polymers if there is a sufficient monomer feedstock. They require a chain transfer agent, which is often a protic compound, so that the polymer chains can be removed from the catalyst or redistributed more evenly to give less dispersed molecular weights. For determining how efficient an immortal catalyst is, the turnover number (TON) can be used. A TON refers to the number of moles of a substrate, in this case monomer, a mole of catalyst can convert into polymer before becoming inactive due to catalyst poisoning or degradation.

Properties of the ancillary ligand, such as steric bulk, electronic environment and stereochemistry, influence the tacticity and microstructure of the polymer by altering the environment around the metal centre *via* the open coordination pocket. Solvation of the catalyst is important to allow for the homogenous reaction to occur. Issues with competitive coordination of coordinating solvents, such as tetrahydrofuran (THF), occasionally prove problematic, as they can interfere with propagation and monomer coordination. Nonpolar solvents, such as toluene, do not generally participate in competitive coordination, but solubility of the monomer and polymer can become an issue, as well as having heterogeneous mechanisms occurring.[50, 53]

1.2.2 Cationic Complexes

A cationic complex is a complex that holds an overall cationic (positive) charge; therefore, it is paired with an anion (negative), of which there are a variety.[54-56] To avoid

the anion being involved with catalysis, often a weakly coordinating anion is used. The weakly coordinating anion remains out of the coordination sphere of the metal centre due to steric bulk of the complex and/or anion and the charge is distributed over a large number of, often electronegative, atoms.[57] Introducing a cationic charge to a metal complex increases the Lewis acidity and electrophilicity of the metal centre, and as such, cationic complexes are generally quite reactive. The use of cationic complexes as single-site catalysts are heavily influenced by the ancillary ligand.[58] With respect to ROP, charge neutral metal catalysts can be hampered by limited activity.[59, 60] Cationic complexes may be more active towards ROP, especially of lactones, due to the higher electrophilicity of the metal centre which increases the affinity for the heteroatom-containing monomer.[61]

The use of cationic complexes as catalysts was first demonstrated by Zieglar-Natta type olefin polymerization catalysts. These living catalysts involve the cationic catalyst being isolated, or generated *in situ* by addition of a co-catalyst, and the nucleophilic ligand becoming incorporated into the polymer during initiation.[62-66] Cationic complexes are attractive for use in ROP catalysis as they have been shown to operate reliably, are used in industrially relevant transformations, and are continuously featured in recent literature.[61, 67-70] Included on the frontier of this work was the Hayes group who pioneered the use of cationic catalysts in the ROP of lactide, wherein great emphasis was placed upon garnering a deep understanding of the effect that various ancillary ligand architectures have on polymerization (*vide infra* 1.3.3).[61, 71, 72]

Generation of a cationic metal centre provides a vacant coordination site. They are often generated *in situ* with an activator, or co-catalyst instead of being isolated.[61] Most commonly, cationic complexes are prepared either by abstraction of a ligand using a

Lewis acid, through metathesis with an appropriate salt, or reaction with a Brønsted acid that abstracts a ligand by protonating it (Scheme 1.3).[71] The chosen approach depends on the nature of the ligand, the metal, and the ease of access to the necessary starting materials.

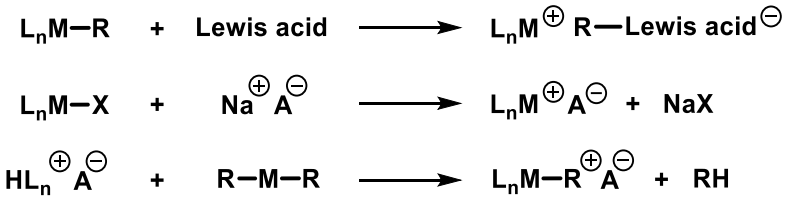

Scheme 1.3: Common routes to cationic complexes using: abstraction (top), salt metathesis (middle), and reaction with a Brønsted acid (bottom). L_n = ancillary ligand, M = metal, R = typically an organic ligand, A = anion, X = halogen.

1.3 Relevant Hayes Group Research

1.3.1 The Phosphinimine Functional Group

While phosphinimines, or iminophosphoranes, are structurally analogous to imines (R_2C=NR'; R, R' = alkyl or aryl), they are much stronger electron donors.[73] The phosphinimine moiety is capable of an ylidic resonance structure due to the presence of the phosphorous(V) atom and can therefore be drawn without a formal P=N double bond (*i.e.* R_3P^+–N^-R'; R, R' = alkyl or aryl). The phosphinimines will be portrayed akin to imines, as P–N multiple bond character has been shown to exist in the solid state (R_3P=NR'; R, R' = alkyl or aryl). Where relevant, discussion on P–N bonding is included. The substituents on phosphorous need not be the same, and they often work as linkers to other donors, thereby creating compounds that can serve as multidentate ligands. In addition, organic linkers can be incorporated into the nitrogen R' moiety, generating a multitude of possible ancillary ligand architectures. The nature of the connecting group can be distinguished by utilizing the prefixes *endo* or *exo*, which are intended to indicate if the phosphorous group is part of the linking fragment, *endo*-

phosphinimine, or acting as a terminal substituent, *exo*-phosphinimine (Figure 1.8). This distinction is made by representing *endo* as R'N=P(R)$_2$–E and *exo* as E–N=P(R)$_3$. The Hayes group has thus far used exclusively *endo*-phosphinimines.

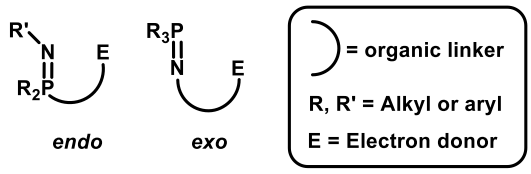

Figure 1.8: Endo and exo multidentate phosphinimines.

Unlike imines, phosphinimes do not typically participate in π-accepting interactions, and instead act as both σ and π donors through the available lone pair on nitrogen.[73] In the absence of moisture, phosphinimines tend to be more robust than their imine counterparts. This is due to, in part, the steric bulk surrounding the phosphorous(V) atom which hinders nucleophilic attack. Phosphinimines also tend to be quite stable under strongly reducing conditions.[74] Since phosphorous is an NMR active nucleus (^{31}P = 100%, I = ½), ^{31}P NMR spectroscopy has proven to be an extremely valuable tool when characterizing phosphinimine-containing ligands. This is particularly true as the ^{31}P NMR resonance in these ligands is highly sensitive to its environment, with large predictable changes observed upon coordination to a metal centre.

The Staudinger reaction, named after the German chemist Hermann Staudinger,[75] uses an organic azide to generate a phosphinimine (R_3P=NR'; R, R' = alkyl or aryl) *via* reaction with a tertiary phosphine (Scheme 1.4).[76, 77]

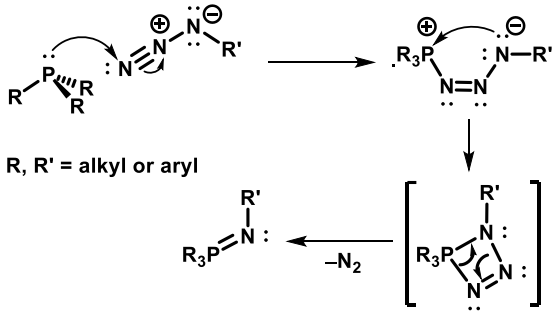

Scheme 1.4: Synthesis of a phosphinimine *via* a typical Staudinger reaction.

The first step of the Staudinger reaction is generation of a phosphazide ($R_3P–N_3–R'$; R, R' = alkyl or aryl) intermediate. Phosphazides are typically transient in nature as they are prone to extrusion of dinitrogen gas.[78] In the absence of water, no further reaction occurs. Given that the process is generally highly selective and the byproduct is a gas, often little to no purification of the phosphinimine is needed.

When an organic azide is not readily available, an alternative procedure, typically referred to as the Kirsanov reaction, can be used to prepare phosphinimines.[79] This route involves the formation of a tertiary bromophosphonium bromide ($[R_3PBr][Br]$; R = alkyl or aryl) by the addition of bromine to a phosphine. An excess of the desired alkyl or aryl amine is then added to the salt *in situ* (Scheme 1.5). The ammonium bromide side product is removed *via* standard filtration techniques. It should be noted that complex azides are continuously becoming more synthetically viable with more cost effective reagents and under increasingly safe conditions by avoiding the use of explosive and toxic organic azides.[80]

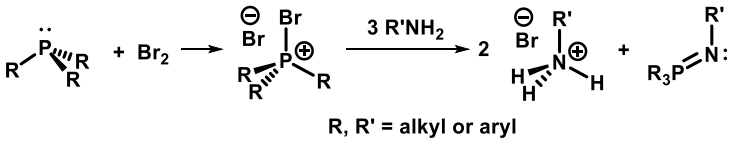

Scheme 1.5: A typical Kirsanov reaction to generate a phosphinimine.

1.3.2 Bisphosphinimine Pyrrole- and Carbazole-Based Pincer Ligands

The Hayes group has reported two families of monoanionic pincer ligands that feature two phosphinimine functionalities, denoted as bisphosphinimines. These systems incorporate carbazole (1,8-(ArN=PR_2)$_2$-3,6-dimethylcarbazole = **L_1**)[81-86] and rigid pyrrole (2,5-(4-^{i}PrC_6H_4N=PR_2)$_2$$C_4H_2$NH = **$L_2$**),[87-92] cores (Figure 1.9).

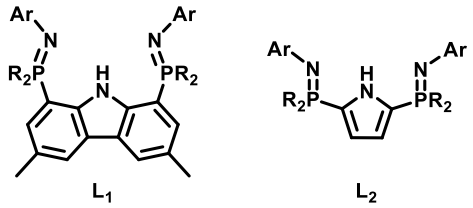

Figure 1.9: General structures of Hayes' *NNN*-pincer ligands **L_1** and **L_2**.

A notable difference between the two scaffolds is that upon coordination to a metal, **L_1** froms two 6-membered chelate rings, as opposed to two 5-membered rings when **L_2** is employed. This places the phosphorus and nitrogen substituents further from the metal centre when **L_2** is used. The consequence of increased steric crowding in **L_1** compared to **L_2** can prove beneficial, as it protects the metal centre, but can also lead to decomposition by intramolecular bond activation processes, as demonstrated in rare-earth element containing complexes.[81-86] Accordingly, **L_2** has proven to be a more ideal scaffold for stabilizing a variety of metal complexes.[87-92]

Most recently, a family of **L_2** supported rhodium complexes that engage in various reactions with small molecules have been reported. For example, reaction of **L_{2Ph}**Rh(COE), **XIa**, with H_2 gas liberates cyclooctane (COA) and affords an asymmetric dinuclear species H_2**L_{2Ph}**Rh_2, **XIb**, which contains one equivalent of H_2 as a bridging hydride (H^-) and protonated (H^+) phosphinimine (Scheme 1.6).[90] Although exposure of **XIb** to cyclooctene does not regenerate **XIa**, addition of the smaller alkene,

ethylene, affords **L$_{2Ph}$**Rh(H_2C=CH_2), **XIc**. Both complexes **XIa** and **XIc** serve as alkene and alkyne hydrogenation catalysts and **XIb** was determined to be the catalyst resting state once all of the H_2 and/or substrate has been consumed. Notably, when diphenylacetylene is hydrogenated, *trans*-stilbene is the sole alkene product. At higher temperatures, diphenylethane can be obtained.[90]

Upon replacement of the P–Ph substituents in **L$_{2Ph}$** with ^{i}Pr groups further metal ligand cooperative activation of small molecules was observed. For example, when **L$_{2iPr}$**Rh($CO)_2$, **XIIa**, is exposed to one equivalent of $B(C_6F_5)_3$, the unusual encounter complex *NN*-**L$_{2iPr}$**Rh($CO)_2B(C_6F_5)_3$, **XIIb**, wherein one CO ligand is bonded to rhodium was isolated (Scheme 1.6).[91] Although the O→B interaction is weak and can be cleaved upon addition of THF, over time in solution complete C≡O bond scission occurs, ultimately generating half an equivalent of each *NN*-**L$_{2iPr}$**Rh($CO)_2$P=O–$B(C_6F_5)_3$, **XIIc**, the monocarbonyl **L$_{2iPr}$**RhCO, **XIId**, and the borane-capped isocyanide 4-^{i}PrC_6H_4N≡C→$B(C_6F_5)_3$.[91]

When the cyclooctene complex **L$_{2iPr}$**Rh(COE), **XIIa**, was reacted with silanes, conventional Si–H oxidative addition provided the five-coordinate silyl hydride species **L$_{2iPr}$**Rh(H)SiR_3, **XIIIb**: R_3 = H_2Ph; **XIIIc**: R_3 = HPh_2; **XIIId**: R_3 = Ph_3.[92] Conversely, reaction of **L$_{2iPr}$**RhCO with $PhSiH_3$ or Ph_2SiH_2 afforded the corresponding base-stabilized silylenes **L$_{2iPr}$**Rh=Si(Ph)R(CO), **XIIIe**: R = H; **XIIIf**: R = Ph, *via* an unusual dehydrogenative process.[92]

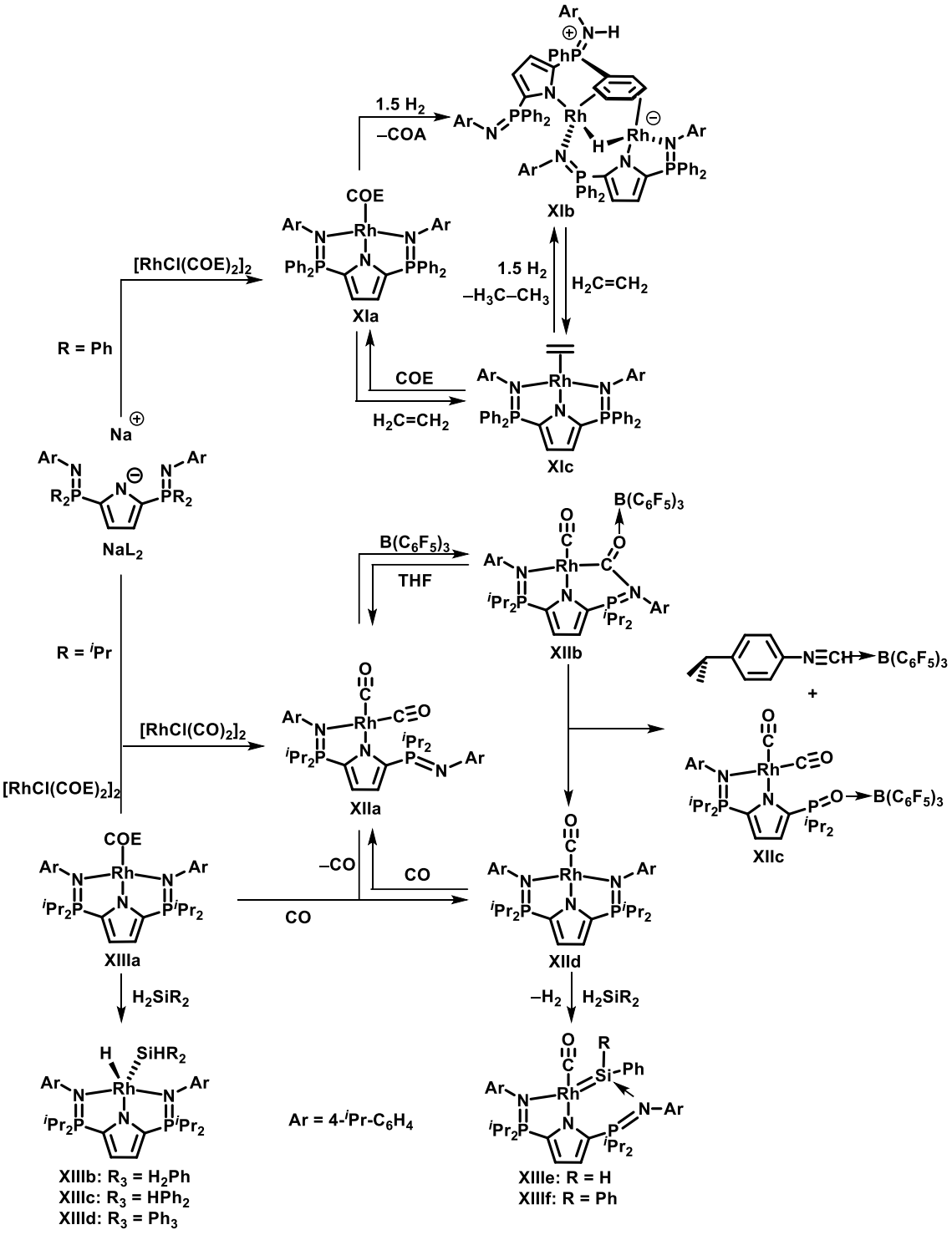

Scheme 1.6: Synthesis and reaction chemistry of rhodium complexes supported by $\mathbf{L_1}$.[90-92]

1.3.3 Mono- and Bisphosphinimine Dibenzofuran-Based Pincer Ligands

The Hayes group utilized ideas from olefin polymerization catalysts, like those derived from Ziegler-Natta catalysts, and focused on an electronically and coordinatively unsaturated metal centre to help facilitate the coordination-insertion process of ROP. To achieve this with a divalent metal, such as zinc or magnesium, a neutral ancillary ligand can be used. Accordingly, an analogous neutral ligand framework to **L$_1$**, using dibenzofuran (dbf) containing two phosphinimines at the 4 and 6 positions, 4,6-(ArN=PR$_2$)$_2$)dibenzofuran (**L$_3$**, Scheme 1.7), was developed.[96] This scaffold proved valuable for generating a large library of cationic complexes of zinc ([**L**$_3$ZnE][A], **XIVa-e**)[93-97] and magnesium ([**L**$_3$Mg^{n}Bu][A] **XV**),[98] many of which exhibited high catalytic activity for the ROP of lactones (Scheme 1.7).[93, 94] These species were prepared by treating the free neutral ligands with a Brønsted acid, affording well-behaved salts that could be isolated and stored indefinitely under an inert atmosphere. Subsequent reaction with alkylzinc or magnesium reagents cleanly afforded cationic complexes *via* an alkane elimination process.[99]

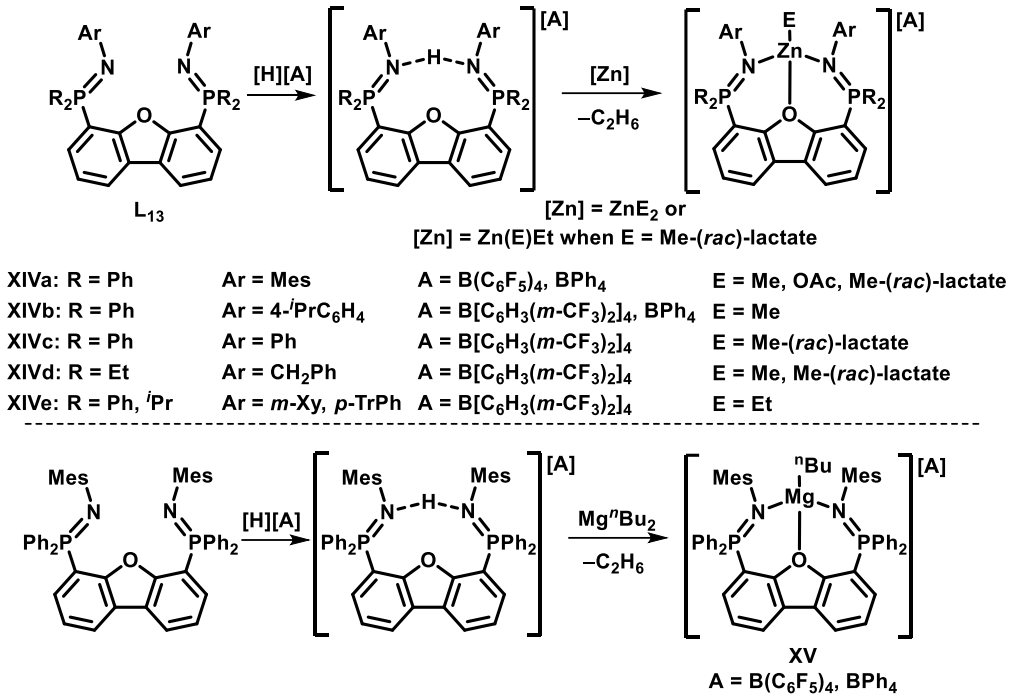

Scheme 1.7: Synthesis of cationic zinc and magnesium complexes **XIV**[93-97] and **XV**.[98] *m*-Xy = *meta*-xylene, *p*-TrPh = *para*-tritylphenyl.

Zinc complexes bearing a methyl-(*rac*)-lactate group were found to be the most active for lactide polymerization, with [$\mathbf{L_{3Bn,Et}}$Zn(lactate)][B(3,5-$(CF_3)_2C_6H_3)_4$], Bn = benzyl or –CH_2Ph, **XIVd**, capable of polymerizing 200 equivalents (90% conversion) of monomer in 20 min at 25 °C.[96] *In situ* NMR studies revealed no induction period and first-order consumption of lactide (PDI = 1.24-1.57). Polymer analysis by NMR spectroscopy, gel permeation chromatography, and MALDI-ToF mass spectrometry indicated largely atactic material with polymer chains bearing a methyl-lactate end group, suggesting a coordination-insertion mechanism. However, substantial rates of transesterification were observed, giving poorly defined microstructures. Prior to the termination reaction, additional monomer (200 equiv) was consumed giving PLA that was consistent to when 400 equiv was added in a single step displaying living catalyst characteristics. Although inert toward lactide, the magnesium complex [$\mathbf{L_{3Mes}}$Mg^{n}Bu][BPh_4], **XV**, exhibited extremely high activity with complete monomer consumption in 4 min at ambient temperature with a 0.77 mol% initiator loading for

the ROP of ε-caprolactone, producing relatively low PDI (<1.6) poly-(ε-caprolactone).[98]

Monophosphinimine dbf ligands, 4-(ArN=PR_2)dibenzofuran, **L_4**, have also been used to prepare neutral and cationic zinc complexes.[72, 100, 101] Stable neutral four-coordinate complexes **$L_{4Dipp}ZnCl_2$**, **XVIa**, **$L_{4Mes}Zn(C_6F_5)_2$**, **XVIb**, and **L_{4Dipp}**ZnEt(OTf) **XVIc**, were generated by the addition of the requisite zinc starting material to the neutral ligand (Scheme 1.8).[101] The cationic species [**L_{4Dipp}**ZnEt][A], **XVIIa**: A = $B(C_6F_5)_4$; **XVIIb**: A = SO_3CF_3, were synthesized *via* an alkane elimination process involving protonated **L_4**, akin to the zinc complexes of **L_3**.[72] Although high activity and conversion was maintained for **XVIIa-b**, the resultant PLA was atactic and suffered from bimodal and broad MW distributions.[72, 100] In an effort to impart stereochemical control during the polymerization of lactide, chirality was introduced at the phosphorous groups, giving two ligands, **$L_{4Dipp,MePh}$** and **$L_{4Mes,MePh}$**. Cationic zinc complexes [**L_4**ZnR][$B(C_6F_5)_4$], **XVIII**: R = Et; **XIX**: R = methyl-(*rac*)-lactate, were prepared from them (Scheme 1.8).[100] Although PLA was obtained under mild reaction conditions (2-4 h, 40 °C), only a slight heterotactic bias was observed.[102]

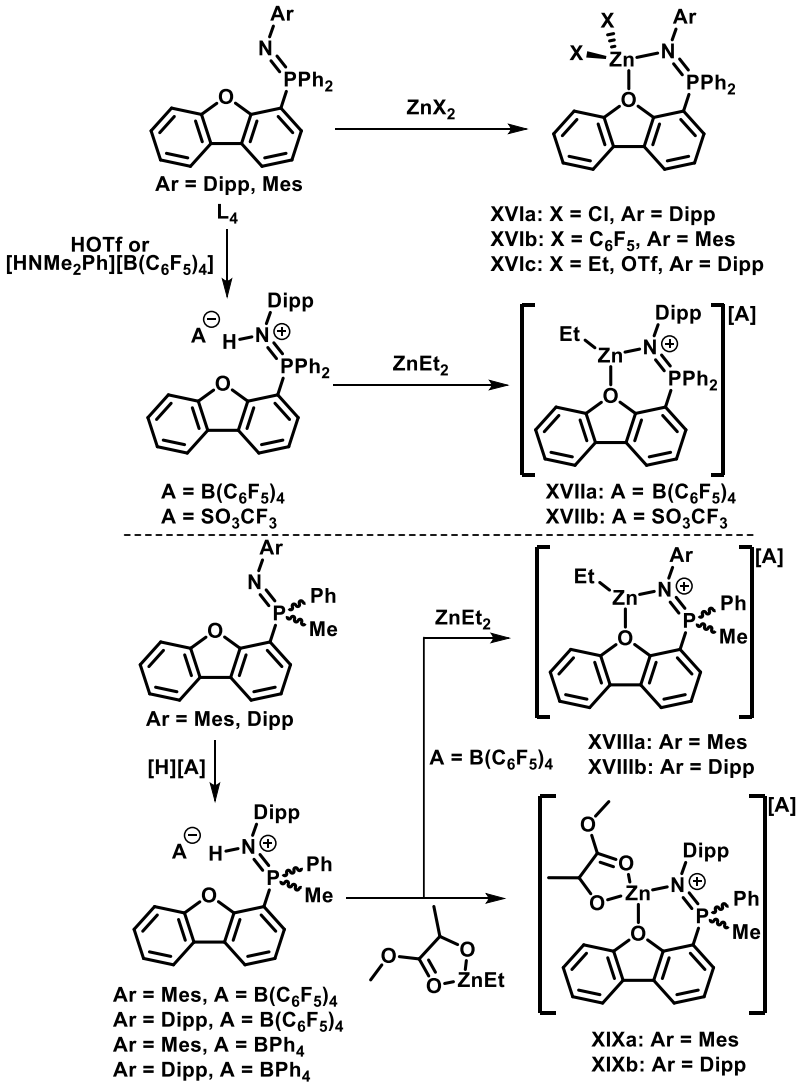

Scheme 1.8: Synthesis of neutral, cationic, and P-stereogenic zinc complexes **XVI-XIX**.[72, 100, 101]

As demonstrated by the work with **L3** and **L4**, the steric bulk provided by the Ar substituents of the phosphinimine was found to substantially influence catalytic activity. A series of experiments aimed at tuning the steric environment about the metal centre suggested that less congestion, as is the case with a benzyl group,[96] generally improved activity to an extent as complexes bearing **L3** were more active. Though the importance of the interaction between the central oxygen donor and the metal centre remains unclear. The work in Chapter 2 aimed to elucidate the relationship between this interaction and ROP activity/selectivity.

1.4 Other Notable Cationic Zinc Complexes in ROP

Apart from the contributions from the Hayes group, other ligand frameworks have been employed to stabilize cationic zinc complexes. Many of these complexes have proven effective at mediating the ROP of epoxides, lactones, and lactide. Selected complexes are highlighted below to illustrate challenges researchers have encountered and the benchmark for quality ROP in this area.

Bochmann *et al*. used their ligand system, $(MeC{=}N{-}Dipp)_2$ = **L5**, to generate several cationic zinc complexes, **L5**ZnR R = Me, Et, $N(SiMe_3)_2$ **XXa-c** (Scheme 1.9). These complexes polymerized epoxides, cyclohexene oxide (CHO) and propylene oxide (PO) at 0 °C to give polymers with high MW and PDI values (>1.8). Elevated temperatures (60 °C) were required to convert ε-caprolactone into polycaprolactone within 1 h, but with PDI values closer to 1.[103] This is an example of high reactivity that does not give rise to quality polymers as the exothermic reactions with CHO and PO produced polymers with high PDI values; the lower activity with ε-caprolactone produced far better defined polymers.

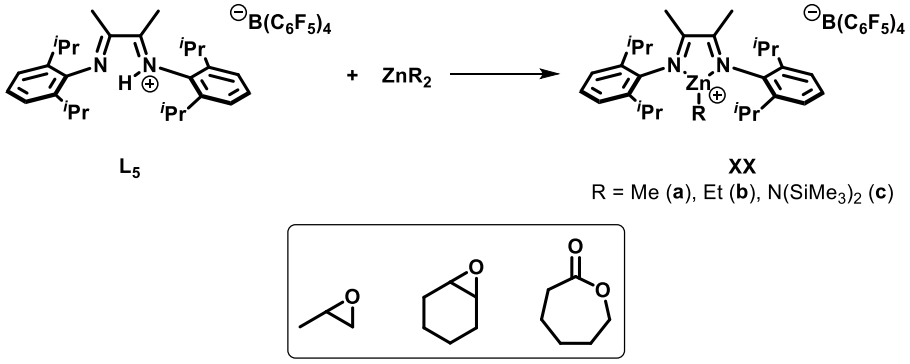

Scheme 1.9: Synthesis of complexes **XXa-c**.

Le Roux and co-workers used bis(oxazoline), **L6**, and 1,3-bis(2-pyridylmethyl)imidazolinium, **L7**, as ancillary ligands containing several variable

substituent sites. These ligands were used to give zinc alkyl complexes, $\mathbf{L_6}$ZnR R = Me, Et, (**XXIa-d**) and $\mathbf{L_7}$ZnEt(Cl) (**XXII**) (Scheme 1.10), that were treated with $B(C_6F_5)_3$ to generate zinc cations *in situ* that produced high PDI polymers (>2.1) from CHO and PO.[104] The reactions were complete within 1 min with CHO and 30 min with PO at 30 °C with yields as low as 7-25% with PO and as high as 74-100% with CHO. This is similar to Bochmann *et al.* as high PDI values were realized for a reasonably swift reaction.

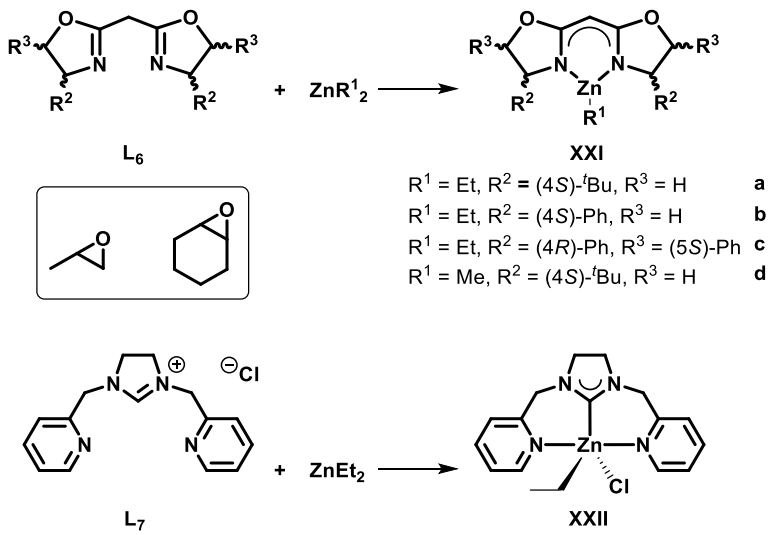

Scheme 1.10: Synthesis of complexes **XXIa-d** and **XXII**.

The 3-mesityl-1-picolylimidazolium iodide ligand, $\mathbf{L_8}$, by Tolman *et al*, was used to generate a cationic zinc complex bearing two $\mathbf{L_8}$ ligands, [($\mathbf{L_8}$)$_2$ZnI][I] (**XXIII**). Catalytic studies with **XXII** were conducted using *rac*-lactide. The ROP was performed neat (140 °C) to yield polymers with moderately broad PDI (1.78) in 5 min.[105] The metal center was still accessible to monomer despite the presence of two ligands. Since elevated temperatures are sometimes required for polymerization to transpire, a robust catalyst is often necessary, and it is possible to consider that the neutral donor portion of the ancillary ligand dissociates at these elevated temperatures.

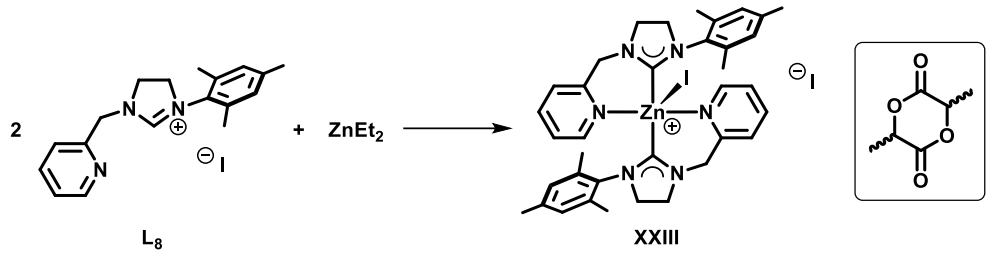

Scheme 1.11: Synthesis of complex **XXIII**.

More success was found by Aviles *et al.* when bis(Ar)acenaphthenequinonediimine, Ar = Mes, Dipp, **L9**, was used to support cationic zinc complexes [**L9**ZnMe•Et_2O][$MeB(C_6F_5)_3$], **XXIVa-b** (Scheme 1.12). This series of complexes required benzyl alcohol or (–)-menthol as a chain transfer agent. Polymerization of ε-caprolactone (2 h at 60 °C in THF) gave polymers with PDI as low as 1.07.[106] The success of this system is possibly due to the more exposed metal centre compared to others described in this section. Notably, it is not clear how much the *N*-aryl groups influenced the described activity.

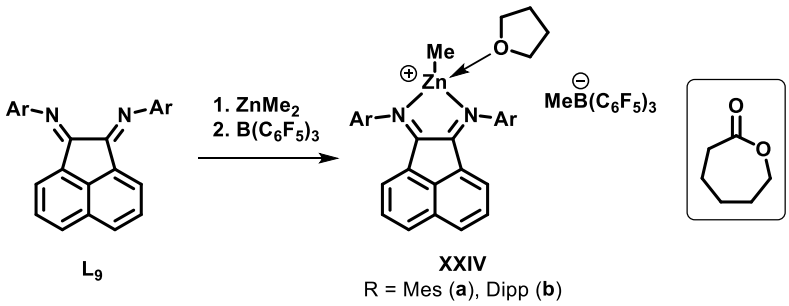

Scheme 1.12: Synthesis of complex **XXIV**.

The Schulz group used the 1,3-diketiminato (NacNac) scaffold, a well known and heavily researched ligand family, as the basis for their ligand MesN=C(Me)C(H)C(Me)=NMes, **L10**. Using **L10**, a cationic zinc complex [**L10**Zn][$Al(OC(CF_3)_3)_4$], **XXV**, which was used as a catalyst for lactide polymerization (Scheme 1.13). Elevated temperatures (160 °C) led to reaction completion in 8 min when 200 equiv of monomer was added in the absence of solvent (PDI = 1.73).[107] The

ligand, O=C(Me)C(H)C(Me)–N(H)RNMe$_2$, R = $(CH_2)_3$, $(CH_2)_2$, **L$_{11}$**, was used to synthesize zinc complexes [**L$_{11}$**Zn][Al(OC(CF$_3$)$_3$)$_4$], **XXVIa-b** (Scheme 1.13). The same reaction conditions were used for the ROP of lactide as **XXV**, after 22 min PLA with a PDI value of 1.3 was generated.[108] This is a demonstration of how ligand libraries can be refurbished for other applications and appropriate alterations can be made to select towards a particular purpose.

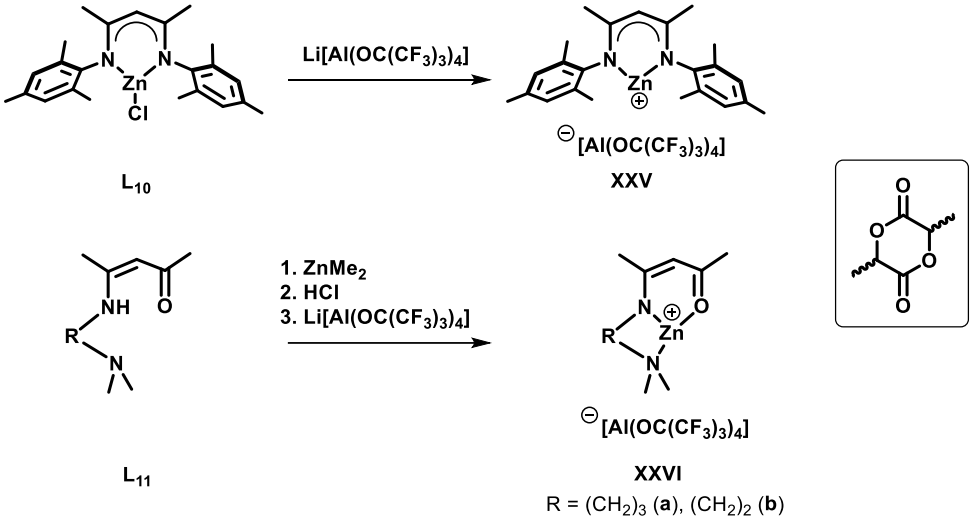

Scheme 1.13: Synthesis of complexes **XXV** and **XXVI**.

1.5 Project Aims

The Hayes group has made a pronounced effort to develop phosphinimine containing ancillary ligands (**L$_1$**-**L$_4$**). Absent from these ligands was a neutral analogue of the monoanionic pyrrole-based ligand, **L$_2$**. The smaller chelate rings formed upon coordination of **L$_2$** yielded more controlled reactivity with rhodium complexes (XI-XIII)[87-92] and more stable rare-earth species.[81-86] It is therefore reasonable to suggest that a enhanced reactivity could result with a transition from the dbf-based ligand, **L$_3$**, to a neutral pincer ligand akin to **L$_2$**.

The complexes generated using neutral ligands **L$_3$** and **L$_4$** did not provide a clear understanding of the influence that the central donor has on lactone polymerization. Solid state structures revealed substantial variation in Zn–O lengths, ranging from 3.326(1) Å in **XIVe**, 2.336(5) Å in **XIVb**, 2.60(1) Å in **XVIIb**, and 2.525(1) Å in **XIVd**. There was no discernible trend between Zn–O distance and catalyst activity and it is unclear if the solid-state structures provide meaningful information on Zn–O interactions in solution. Accordingly, it is imperative that more work be performed to elucidate whether this central donor impacts ROP catalytic performance in these systems.

A furan-based ligand structure, as opposed to the dibenzofuran-based ligands previously investigated (Figure 1.10), was targeted with the anticipation that the 5 membered chelate rings would render the metal centre more accessible, and thus, reactive. The chemical starting materials used to produce this ligand framework provides the option to easily synthesize neutral pincer ligands with different central donors (E = O, S, Se), flanking *N*-aryl groups (Ar), and substituents on the phosphorous of the phosphinimine functional groups (R, Figure 1.10). Alteration at all three sites provides an avenue for systematically optimizing the resultant cationic zinc complexes for ROP. Variation of the central chalcogen donor, E, was undertaken in an effort to learn more about the interaction between E and the metal centre. It was anticipated that by altering the central donor from oxygen to sulfur, and to selenium, a predictable trend in ROP activity would emerge. Based on hard-soft acid-base theory, oxygen is a ‘hard’ base and moving down the chalcogen group, the elements become more ‘soft’. Accordingly, one might expect stronger bonding to occur between the ‘intermediate’ zinc centre and either sulfur or selenium. If that were indeed the case, the metal centre

would be expected to be less electron deficient, and more sterically encumbered, as it would be bound more tightly by the pincer ligand.

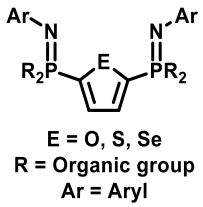

Figure 1.10: Targeted neutral bisphosphinimine *NEN*-pincer ligand system.

Zinc, compared to other metals, is plentiful, inexpensive, and better tolerated in humans compared to most other main group and transition metals. Furthermore, it has been demonstrated to be extremely promising in the research for ROP. The use of zinc will act as a direct comparison to previous work done by the Hayes group with dbf-based bisphosphinimine ligands. For this investigation, a family of neutral ligands was prepared based on work with **L3** and **L4**. From these, a wide array of cationic zinc alkyl and alkoxide complexes were synthesized by using a Brønsted acid to abstract an alkyl group off the zinc starting material and install a weakly-coordinating anion (Scheme 1.14). All complexes were characterized by multinuclear NMR spectroscopy and many by X-ray crystallography.

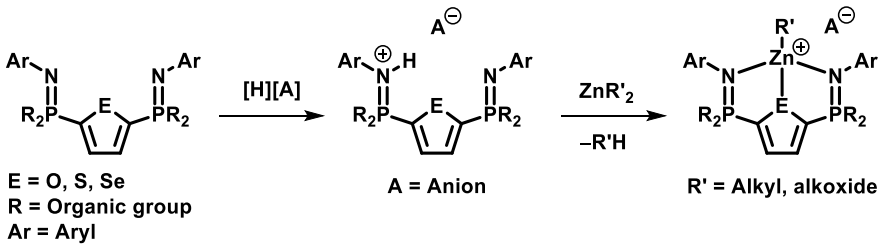

Scheme 1.14: General synthetic approach to cationic zinc complexes supported by neutral bisphosphinimine *NEN*-pincer ligands.

Chapter 2: Synthesis of Bisphosphinimine *NEN*-Pincer Ligands (E = O, S, Se) and Cationic Complexes Thereof

The synthesis of the neutral furan-, thiophene-, and selenophene-based bisphosphinimine *NEN*-pincer ligands described in this chapter, was accomplished *via* modified published routes used to access the dbf-based bisphosphinimine *NON*-pincer ligands (**L13**).[94, 96-98]

2.1 Furan-based Bisphosphinimine *NON*-Pincer Ligands

2.1.1 Furan 2,5-Bisphosphines

The furan-based (C_4H_4O) bisphosphines were made by first exposing a diethyl ether (Et_2O) solution of furan to 2 equivalents of *tert*-butyllithium (^{t}BuLi) at –78 °C. The dilithium salt of furan, $[Li]_2[C_4H_2O]$, was not isolated and was used *in situ*, as a light-yellow solution. Addition of 2 equivalents of Cl–PR_2 (R = ^{i}Pr (isopropyl, or $CH(CH_3)_2$), Ph = (phenyl, or C_6H_5)) to the cooled (–94 °C) $[Li]_2[C_4H_2O]$ solution afforded 2,5-$(PPh_2)_2C_4H_2O$ (**1**, 73.9%) and 2,5-$(P^iPr_2)_2C_4H_2O$ (**2**, 86.8%) (Scheme 2.1). $^{31}P\{^1H\}$ NMR spectroscopy was used to establish purity; compounds **1** and **2** exhibit ^{31}P NMR resonances at δ –24.71 and δ –9.91, respectively.

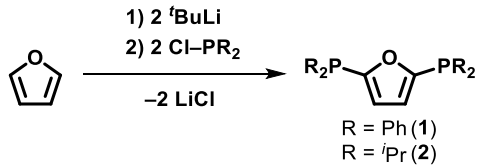

Scheme 2.1: Synthesis of furan-based bisphosphines **1** and **2**.

Compound **1** is stable under aerobic conditions; however, it is susceptible to oxidation when kept in wet solvent for a week or more. A large quantity of light-brown X-ray quality crystals of **1** was easily grown from a saturated toluene solution at

–20 °C.[109] Compound **2** was isolated as a dark-orange oil. Despite exhaustive efforts to yield compound **2** as a solid, through excessive drying and exposure to a variety of solvents, it remained an oil. The oily nature of the synthesized bisphosphines and bisphosphinimines is attributed to the isopropyl groups on phosphorous. These groups have previously proven valuable for imparting crystallinity as they increase a compound's solubility in hydrocarbon solvents.[91]

2.1.2 Furan 2,5-Bisphosphinimines

To generate a phosphinimine *via* a Staudinger reaction, an organic azide is required. Organic azides (R–N_3) are highly toxic, decompose with the violent release of nitrogen when exposed to a source of energy, and can generate explosive compounds if hydrolyzed.[110, 111] Aryl azides are partially stabilized through resonance but stability is also apparent when the carbon to nitrogen ratio is above 3. The aryl azides (Ar–N_3) used include 1-azido-2,6-diisopropylbenzene (Dipp–N_3),[112] 1-azido-4-isopropylbenzene (Pipp–N_3),[81] and 1-azido-2,4,6-trimethylbenzene (Mes–N_3),[112] all of which were generated according to reported literature procedures and isolated as red viscous liquids. In addition, 3,5-dimethyl-1-azidopyrimidine (Pm–N_3) was also used. In solution, Pm–N_3 exists in equilibrium with the tetrazole isomer, 5,7-dimethylpyrazolo-1,5a-pyrimidine *via* valence tautomerization (Scheme 2.2); it was synthesized according to reported methods.[113] The tetrazole isomer is a solid and is the predominant form in solution, so the Staudinger reaction with Pm–N_3 was monitored for at least 16 h at ambient temperature to ensure complete reaction. The Staudinger reactions that used Dipp–N_3, Pipp–N_3, or Mes–N_3 required less time to reach completion at ambient temperature.

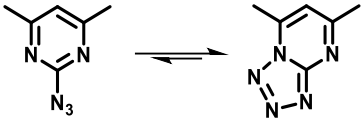

Scheme 2.2: Valence tautomerization equilibrium of Pm-N_3 and 5,7-dimethylpyrazolo-1,5a-pyrimidine.

Under an inert atmosphere of argon, 2 equivalents of Ar–N_3 were added to a toluene solution of either **1** or **2** to generate the desired neutral bisphosphinimine *NON*-pincer ligand *via* a Staudinger reaction (Scheme 1.4, 1.3.1). This procedure generated several pincer ligands, including: 2,5-(DippN=PPh_2)$_2C_4H_2O$ (**3**, 89.7%), 2,5-(PippN=PPh_2)$_2C_4H_2O$ (**4**, 92.4%), 2,5-(MesN=PPh_2)$_2C_4H_2O$ (**5**, 64.6%), 2,5-(PmN=PPh_2)$_2C_4H_2O$ (**6**, 76.4%), 2,5-(DippN=P^{i}Pr$_2$)$_2C_4H_2O$ (**7**, 79.8%), and 2,5-(MesN=P^{i}Pr$_2$)$_2C_4H_2O$ (**8**, 42.0%) (Scheme 2.3) as brown-orange solids. All compounds exhibit a single ^{31}P NMR signal: δ –22.53 (**3**), –13.42 (**4**), –25.87 (**5**), 13.30 (**6**), –3.29 (**7**), and –0.93 (**8**). The ^{31}P and ^{1}H NMR spectra were consistent with C_{2v} symmetry. All ligands would react if exposed to air or wet solvent; thus, they were stored under an inert atmosphere where they are stable indefinitely.

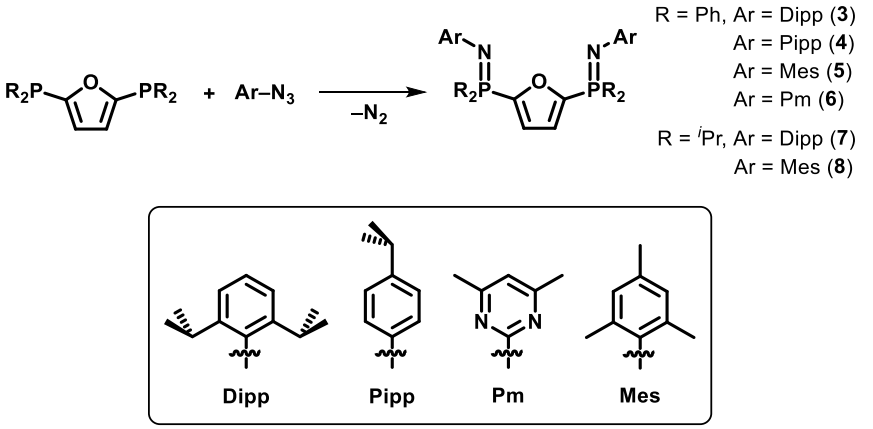

Scheme 2.3: General procedure for the synthesis of neutral furan-based bisphosphinimine ligands **3**-**8**.

A sample of bisphosphinimine **3** was dissolved in a minimum amount of toluene and kept at –30 °C wherein small X-ray quality crystals developed over a 48 h period.

Crystals of **3** grew in a monoclinic crystal system in the C2/c space group with the lattice comprising 4 molecules (Z = 4, Z' = 0.5). The compound is bisected by a 2-fold rotation axis (b-axis), and thus, the asymmetric unit is comprised of half of **3** with the rotation axis passing through O1 and the C2–C2^{i} bond (Figure 2.1).

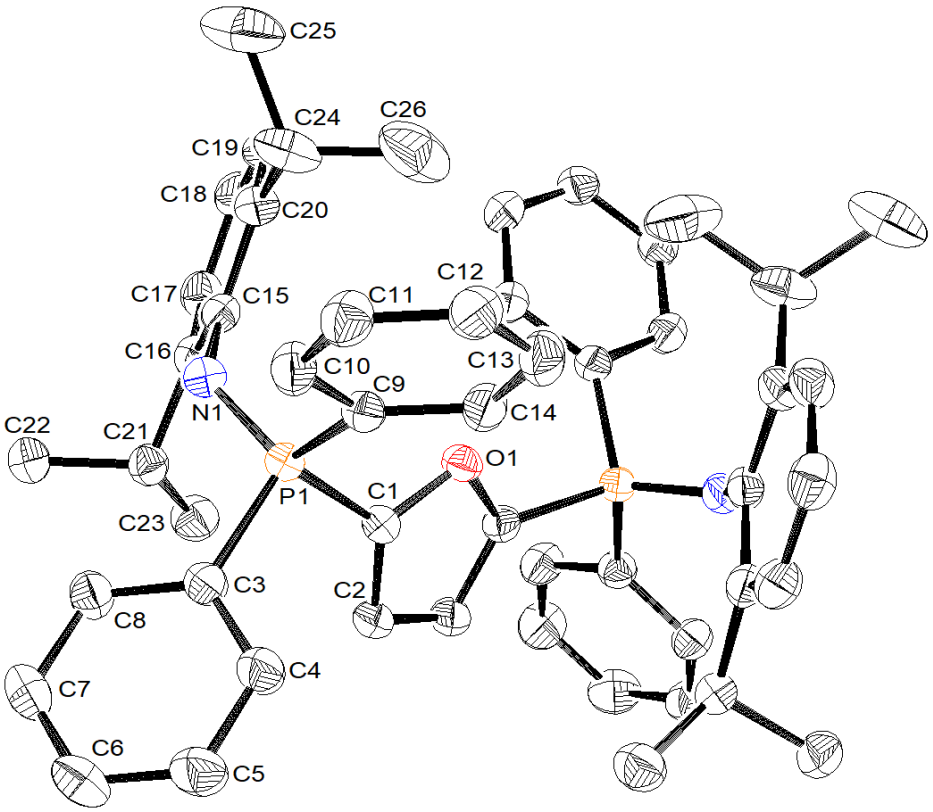

Figure 2.1: Displacement ellipsoid plot of bisphosphinimine **3**, depicted at 50% probability. The asymmetric unit (Z' = 0.5) was grown to show an entire molecule. Space group = C2/c, R_1 = 4.18%. Selected bond lengths (Å): P1–N1 = 1.549(1), N1–C15 = 1.407(2).

The $^{31}P\{^{1}H\}$ NMR spectroscopic data indicated a pronounced upfield chemical shift for compound **3** (δ –22.53) compared to **1** (δ –9.91). The X-ray structure confirmed the presence of the phosphinimine moieties which were 1.549(1) Å (P1–N1) in length. This is shorter than typical P=N bonds, which typically vary from 1.570(1) Å to 1.598(3) Å, according to solid state structures containing P=N bonds* (Figure 2.2 and Figure 2.4).

* Using ConQuest, a program used to search and retrieve information from structures submitted to the Cambridge Structural Database

Notably, those with P–N single bonds are from 1.624(2) Å to 1.694(3) Å (Figure 2.3 and Figure 2.4). The Hayes group has reported the phosphinimine bond lengths in neutral dbf-based bisphosphinimine *NON*-pincer ligands range from 1.548(1) to 1.584(1) Å;[93-97] the P=N in compound **3** lies on the shorter end of that range. The $N_{P=N}$–C_{Aryl} bonds are from 1.380(3) to 1.431(5) Å for neutral dbf-based bisphosphinimine *NON*-pincer ligands.[93-97] The $N_{P=N}$–C_{Aryl} bond distance in compound **3** is 1.407(2) Å.

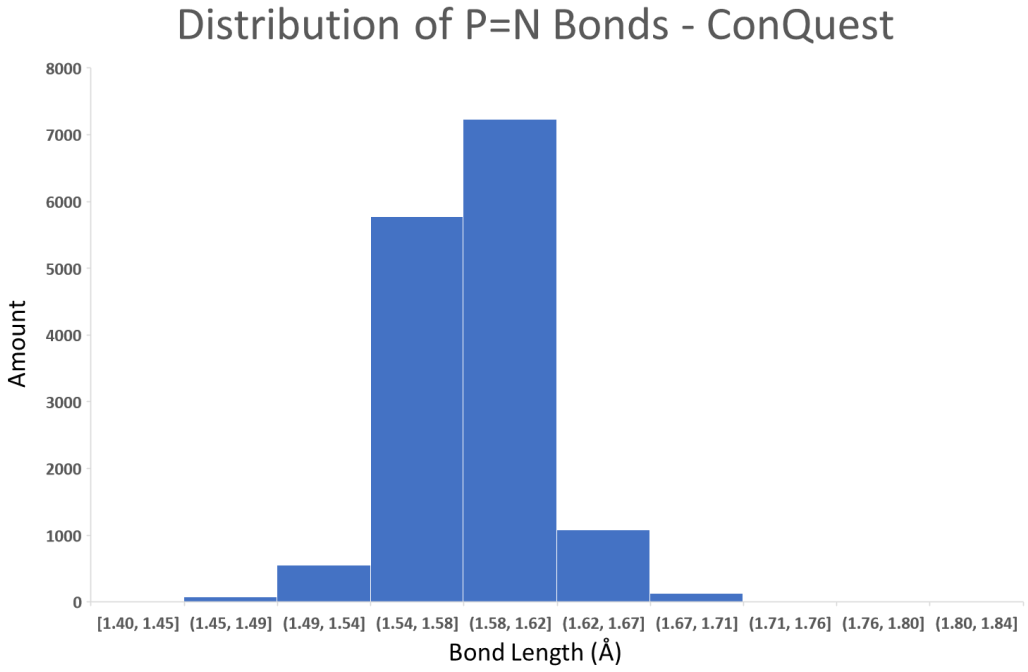

Figure 2.2: Histogram of P=N bonds reported on the Cambridge Crystallographic Data Centre (CCDC) and generated by ConQuest as of September 2021.

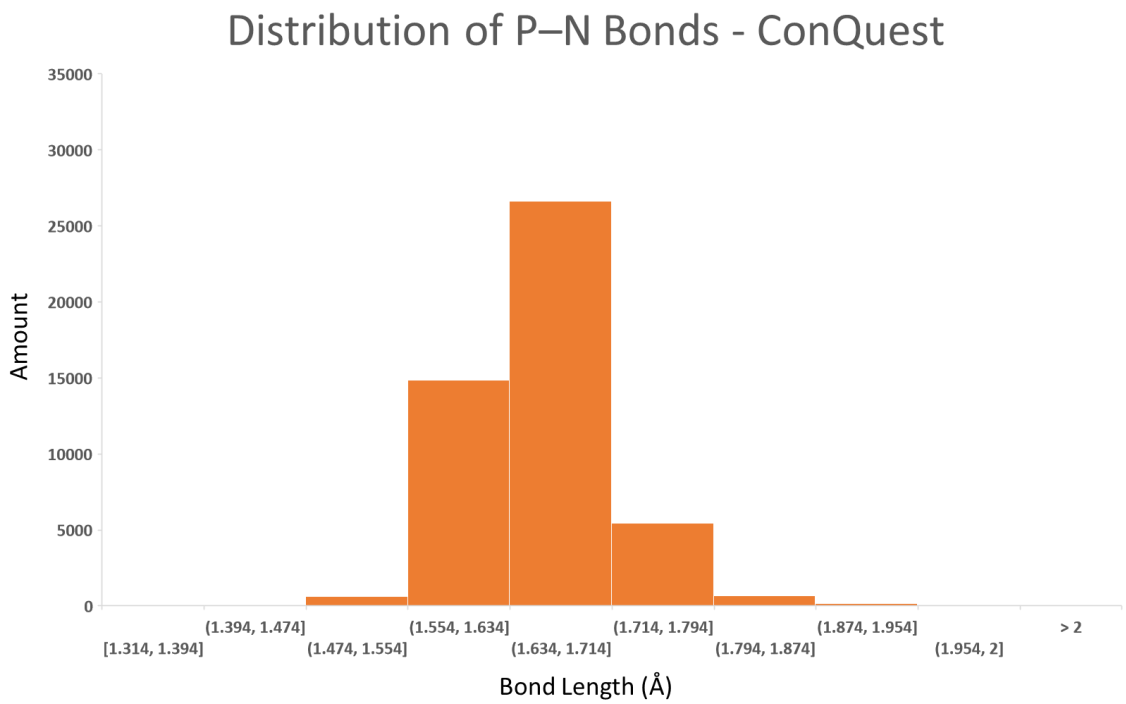

Figure 2.3: Histogram of P–N bonds reported on the Cambridge Crystallographic Data Centre (CCDC) and generated by ConQuest as of September 2021.

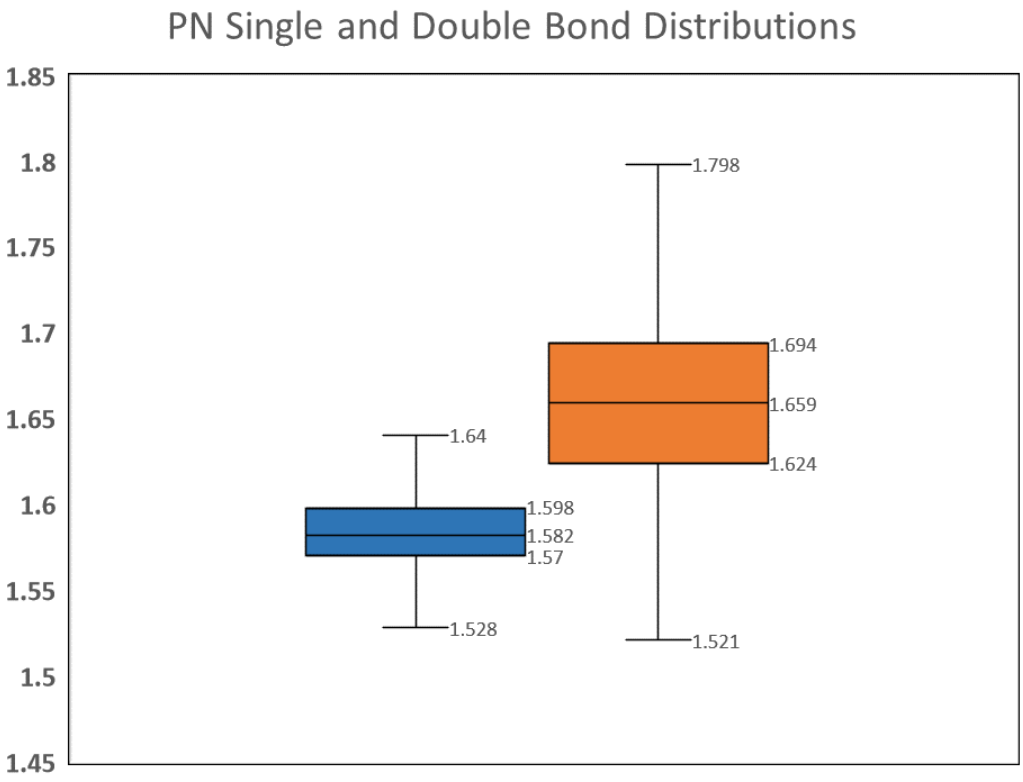

Figure 2.4: Labelled boxplot comparison of P–N bond (right, 48,586 entries) and P=N bond length (left. 14,882 entries) distributions as of September 2021.

Installing the Pm group using Pm-N_3 is relatively new to the Hayes group, and so , obtaining solid state information was sought. Bisphosphinimine **6** (2,5-(PmN=PPh_2)$_2C_4H_2O$) was soluble in many solvents where fragile crystals would grow at –30 °C. Using a minimum amount of toluene, **6** was dissolved and small X-ray quality crystals developed over a 48 h period when kept at –30 °C. Crystals of **6** grew in a monoclinic crystal system within the $P2_1/c$ space group with the lattice comprising of 8 molecules (Z = 8, Z' = 2). Two molecules comprise the asymmetric unit, of which differences in metrical parameters are not statistically significant. The P–N bond lengths range between 1.561(3) Å and 1.589(3) Å.

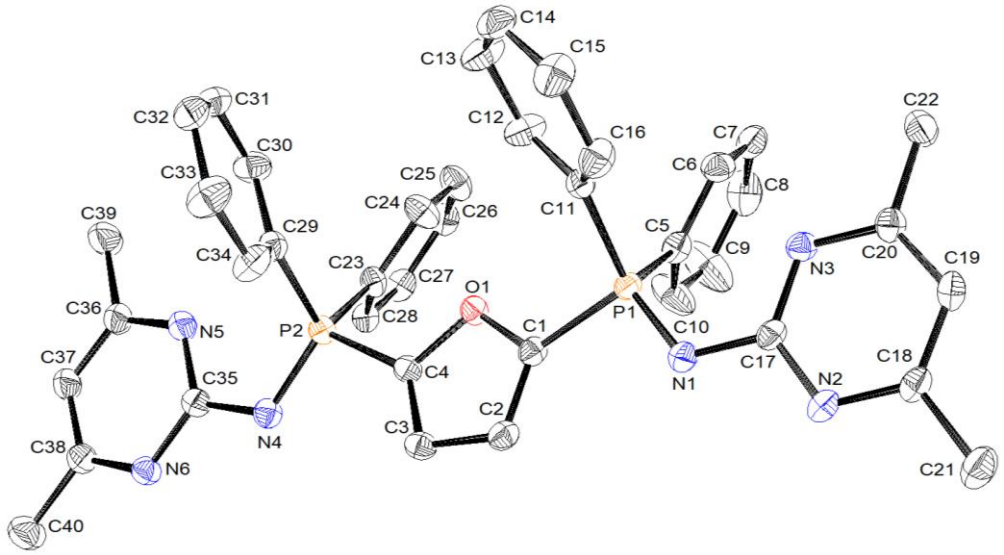

Figure 2.5: Displacement ellipsoid plot of phosphinimine **6**, depicted at 50% probability. One molecule of the asymmetric unit (Z' = 2) is shown. Space group = $P2_1/c$, R_1 = 8.34%.

Table 2.1: Selected bond lengths (Å) in compound **6**.

Atoms	Length (Å)	Atoms	Length (Å)	Atoms	Length (Å)
P1–N1	1.587(3)	**N3–C17**	1.357(6)	**N8–C57**	1.354(6)
P2–N4	1.589(4)	**N4–C35**	1.378(6)	**N9–C57**	1.340(6)
P3–N7	1.561(3)	**N5–C35**	1.357(6)	**N10–C75**	1.381(5)
P4–N10	1.589(3)	**N6–C35**	1.354(6)	**N11–C75**	1.357(5)
N1–C17	1.367(5)	**N7–C57**	1.383(6)	**N12–C75**	1.352(6)
N2–C17	1.352(5)				

Compound **8** (2,5-(MesN=P^{i}Pr$_2$)$_2$C$_4$H$_2$O) readily dissolved in pentane, and at ambient temperature, X-ray quality crystals grew within 24 h *via* the slow evaporation of solvent. Crystals of **8** grew in an orthorhombic crystal system in the $P2_12_12_1$ space group with the lattice comprising of 4 molecules (Z = 4, Z' = 1). The phosphinimine bond distances (P1–N1 1.554(2) Å, and P2–N2 1.549(2) Å) were only marginally different from each other and were similar to those in compound **3**.

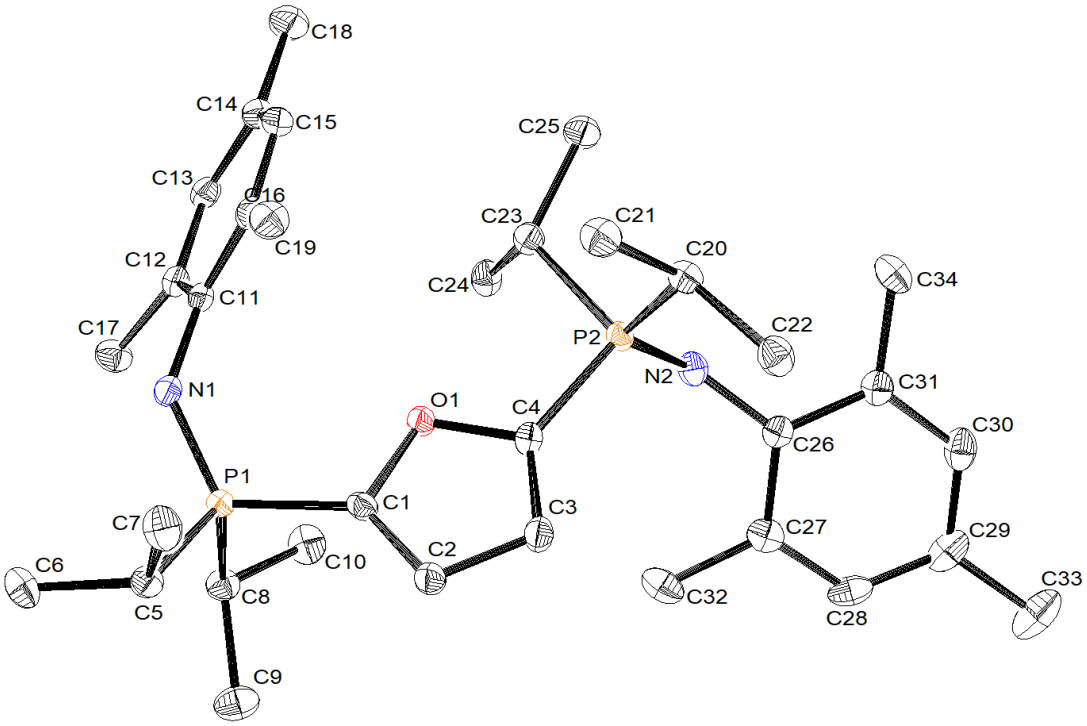

Figure 2.6: Displacement ellipsoid plot of phosphinimine **8** depicted at 50% probability. Asymmetric unit (Z' = 1) is shown. Space group = $P2_12_12_1$, R_1 = 2.86%. Selected bond distances (Å): P1–N1 = 1.554(2), P2–N2 = 1.549(2), N1–C11 = 1.400(3), N2–C26 = 1.395(3).

2.2 Thiophene-based Bisphosphinimine *NSN*-Pincer Ligands

2.2.1 Thiophene 2,5-Bisphosphines

Thiophene-based (C_4H_4S) bisphosphines were generated by introducing an Et_2O solution of either thiophene to 2 equivalents of *tert*-butyllithium (^{t}BuLi) or 2,5-dibromothiophene to 2 equivalents of ^{n}BuLi at –78 °C to generate the dilithium salt, $[Li]_2[C_4H_2S]$, in solution. Addition of 2 equivalents of Cl–PPh_2 to the cooled (–94°C)

$[Li]_2[C_4H_2S]$ solution afforded the corresponding bisphosphines, 2,5-$(PPh_2)_2C_4H_2S$ (**9**) and 2,5-$(P^iPr_2)_2C_4H_2S$ (**10**) (Scheme 2.4). $^{31}P\{^1H\}$ NMR spectroscopy showed a single resonance for both **9** and **10** at δ –16.55 and δ –0.78, respectively. Compound **9** was isolated as a beige solid, and **10** as a light-yellow liquid in appreciable yields of 94.2% and 87.1%, respectively.

When using 2,5-dibromothiophene, the lithium-halogen exchange reaction avoided competitive deprotonation of the 4 position of the thiophene ring as a mixture of 2,5-$(PR_2)_2C_4H_2S$ and 2,4-$(PR_2)_2C_4H_2S$ would often result with the rapid injection of ^{t}BuLi to thiophene. The two compounds in the mixture were corroborated by 2 inequivalent resonances in the $^{13}P\{^1H\}$ spectrum. One resonance integrated for more, at δ –0.78, and so was assigned to additions at carbons 2 and/or 5, the remaining signal at δ –2.11 was assigned to an addition at carbon 4. The evidence that 2,4-$(P^iPr_2)_2C_4H_2S$ was present in the mixture was further confirmed *via* two signals in the ^1H NMR spectrum. Two separate resonances of equal intensity attributed to the 3 and 5 positions of the thiophene ring for 2,4-$(P^iPr_2)_2C_4H_2S$ at δ 7.61 and δ 6.85, compared to δ 7.25 in 2,5-$(P^iPr_2)_2C_4H_2S$.

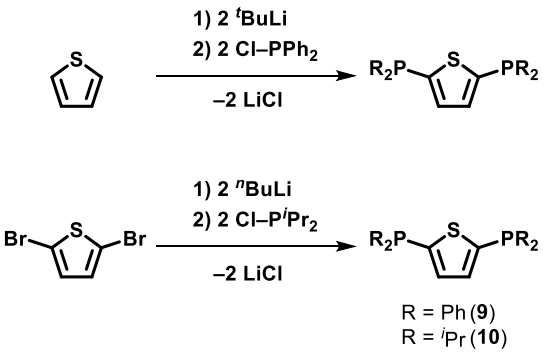

Scheme 2.4: Two routes for the synthesis of thiophene-based bisphosphines **9** and **10**.

Although compound **9** has been previously synthesized,[114] the crystal structure had not been reported. X-ray quality crystals of **9** were isolated by slowly evaporating a

concentrated solution in toluene. Crystals of **9** grew in a triclinic crystal system in the $P\bar{1}$ space group with the lattice comprising of 2 molecules (Z = 2, Z' = 1).

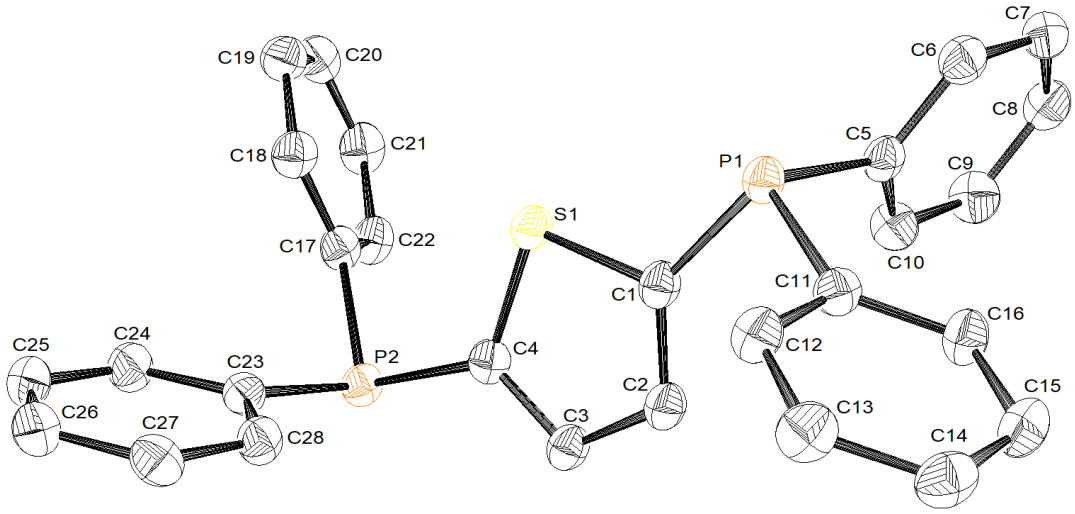

Figure 2.7: Displacement ellipsoid plot of phosphinimine **9** depicted at 50% probability. Asymmetric unit (Z' = 1) is shown. Space group = $P\bar{\mathbf{1}}$, R_1 = 5.17%.

2.2.2 Thiophene 2,5-Bisphosphinimines

To afford the desired neutral bisphosphinimine *NSN*-pincer ligands, a toluene solution of either **9** or **10** was reacted with Ar–N_3 (Ar = Dipp, Pipp, or Pm) under an inert atmosphere of argon. Several pincer ligands were generated with this method: 2,5-(DippN=PPh_2)$_2C_4H_2S$ (**11**, 82.1%), 2,5-(PippN=PPh_2)$_2C_4H_2S$ (**12**, 91.8%), 2,5-(PmN=PPh_2)$_2C_4H_2S$ (**13**, 83.8%), and 2,5-(DippN=P^{i}Pr$_2$)$_2C_4H_2S$ (**14**, 88.4%) (Scheme 2.5), all of which are yellow-orange solids. All compounds exhibit a single ^{31}P NMR signal: δ –16.39 (**11**), –7.66 (**12**), 12.69 (**13**), and 0.78 (**14**), and along with the ^{1}H NMR spectra, all ligands demonstrated C_{2v} symmetry in solution. All ligands react with water, giving the aryl amine and a phosphineoxide if exposed to air or wet solvent; thus, they were stored under an inert atmosphere where they are stable indefinitely.

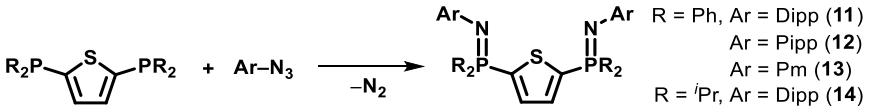

Scheme 2.5: Synthesis of thiophene-based bisphosphinimine neutral ligands **11**-**14**.

Bisphosphinimine **11** readily dissolved in toluene, and at –30 °C, X-ray quality crystals grew within 48 h. Crystals of **11** grew in a monoclinic crystal system in the C2/c space group with the lattice comprising of 4 molecules (Z = 4, Z' = 0.5). The compound is bisected by a 2-fold rotation axis (b-axis), and thus, the asymmetric unit is comprised of half of **11** with the axis passing through S1 and the bond C2–C2^{i} (Figure 2.8). Compound **11** is isostructural with **3** (2,5-(DippN=PPh$_2$)$_2$C$_4$H$_2$O), with the exception of a slightly elongated phosphinimine P–N bonds (P1–N1: 1.561(1) Å, cf. 1.549(1) Å for **3**) that still fell in the typical range for phosphinimine P=N distance.

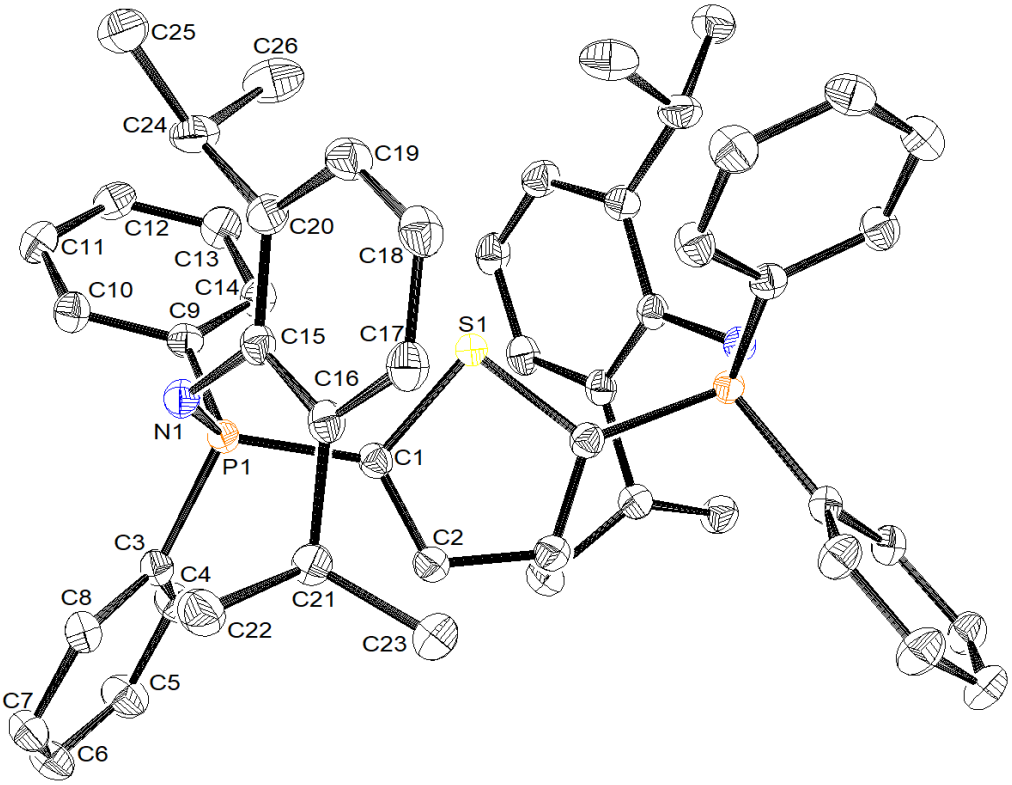

Figure 2.8: Displacement ellipsoid plot of bisphosphinimine **11** depicted at 50% probability. Asymmetric unit (Z' = 0.5) was grown to show an entire molecule. Space group = C2/c, R_1 = 3.89%. Selected bond lengths (Å): P1–N1 = 1.561(1), N1–C15 = 1.411(2).

2.3 Selenophene-based Bisphosphinimine *NSeN*-Pincer Ligands

2.3.1 Selenophene 2,5-Bisphosphines

A mixture of either 2,5-$(PR_2)_2C_4H_2Se$ and 2,4-$(PR_2)_2C_4H_2Se$ would result when exposing an Et_2O solution of selenophene (C_4H_4Se) to 2 equivalents of ^{t}BuLi followed by the addition of 2 equivalents of either Cl–PPh_2 or Cl–P^{i}Pr$_2$. To selectivity initiate at just the 2 and 5 positions of selenophene, a lithium halogen exchange reaction was exclusively used between 2,5-dibromoselenophene (2,5-$Br_2C_4H_2Se$) and ^{n}BuLi. Sequential addition of 2 equivalents of ^{n}BuLi to 2,5-$Br_2C_4H_2Se$ in Et_2O, followed by 2 equivalents of either Cl–PPh_2 or Cl–P^{i}Pr$_2$ yielded the desired bisphosphines 2,5-$(PPh_2)_2C_4H_2Se$ (**15**, 48.6%) and 2,5-$(P^iPr_2)_2C_4H_2Se$ (**16**, 83.8%) (Scheme 2.6). $^{31}P\{^1H\}$ NMR spectroscopy was used to ensure the 2,5-metalation occurred; compounds **15** and **16** exhibit ^{31}P NMR resonances at δ –13.94 and δ –7.14, respectively. $^{77}Se\{^1H\}$ NMR spectroscopy was implemented to identify the typical area the resonance of the selenophene-based ligands will occur, with δ 731.2 and δ 744.9 for **15** and **16**, respectively. Both **15** and **16** react when exposed to air or wet solvent after 48 h. Thus, they were kept under an inert atmosphere where they were stable indefinitely. Compound **15** was isolated as an oily brown liquid and dissolution of crude oily **16** in cold (0 °C) pentane provided analytically pure X-ray quality brown crystals.

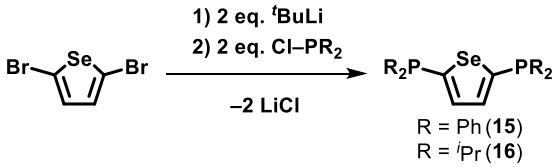

Scheme 2.6: Synthesis of selenophene-based bisphosphine.

Crystals of **16** grew in a monoclinic crystal system with the P2/c space group in the lattice comprising of 4 molecules (Z = 4, Z' = 1). There are two independent molecules

with similar metrical parameters within the unit cell. Both independent molecules are split by a 2-fold rotation axis (b-axis), and thus, the asymmetric unit is comprised of two halves of **16** with the axis passing through Se (Se1 or Se2) and the bond C2–C2^{i} or C10–C10^{i} (Figure 2.9).

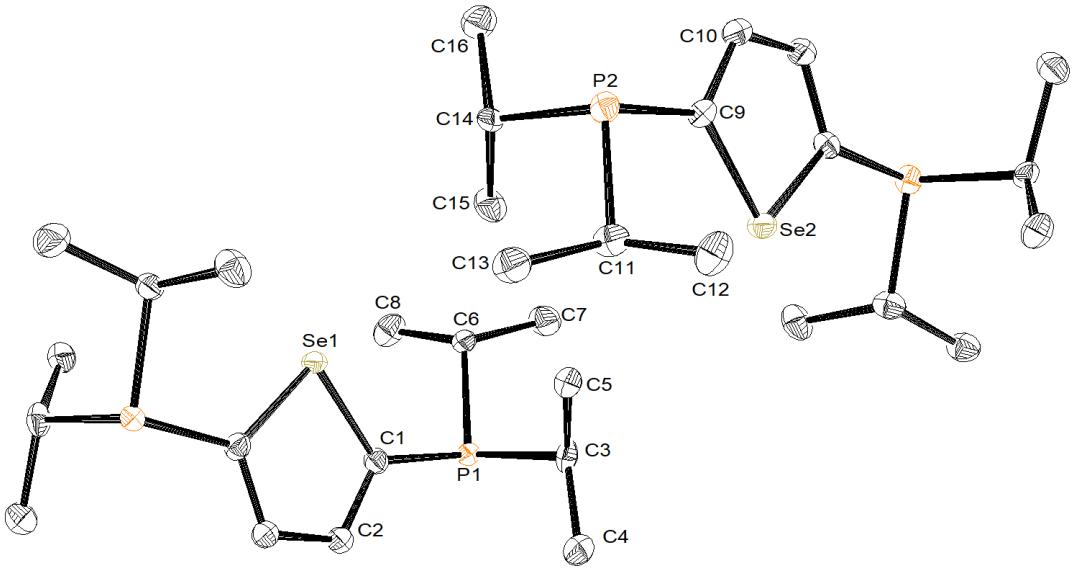

Figure 2.9: Displacement ellipsoid plot of bisphosphinimine **16** depicted at 50% probability. Asymmetric unit (Z' = 1) was grown to show molecules. Space group = P 2/c, R_1 = 4.53%.

2.3.2 Selenophene 2,5-Bisphosphinimines

A toluene solution of either **15** or **16** was reacted with Ar–N_3 (Ar = Dipp or Pipp) under an argon atmosphere. This method yielded several neutral bisphosphinimine *NSeN*-pincer ligands *via* the Staudinger reaction: (DippN=PPh_2)$_2$$C_4H_2Se$ (**17**, 70.2%), (DippN=P^{i}Pr_2)$_2$$C_4H_2Se$ (**18**, 52.2%), and (PippN=P^{i}Pr_2)$_2$$C_4H_2Se$ (**19**, 75.5%) (Scheme 2.7), all of which are yellow-brown solids. All compounds exhibit one ^{31}P NMR signal: δ –15.79 (**17**), 5.63 (**18**), and 21.04 (**19**). Much like the furan-and thiophene-based bisphosphinimines, the selenophene-based bisphosphinimines were consistent with C_{2v} symmetry in solution and would react if exposed to air or wet solvent. Of the selenophene-based ligands **17-19**, all three were crystalline and of appropriate quality to collect X-ray crystallographic data. All three bisphosphinimines,

17-19, readily dissolved in toluene, and at –30 °C, X-ray quality crystals grew within 48 h.

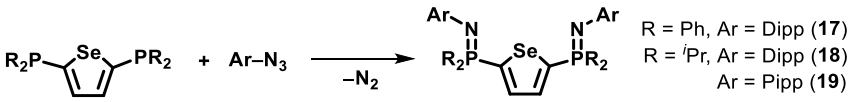

Scheme 2.7: Synthesis of selenophene-based bisphosphinimine neutral ligands.

Crystals of compound **17** grew in a triclinic crystal system in the $P\bar{1}$ space group with the lattice comprising of 2 molecules (Z = 2, Z' = 1). The phosphinimine P–N bond distances (P1–N1 1.565(2) Å, P2–N2 1.572(3) Å) are marginally different from one another and were slightly elongated compared to the analogous furan (**3**, 1.549(1) Å) and thiophene (**11**, 1.561(1) Å) analogues. There appears to be a slight elongation of the phosphinimine P–N bond distances bond with respect to the size of the central atom (*vide infra* 2.4).

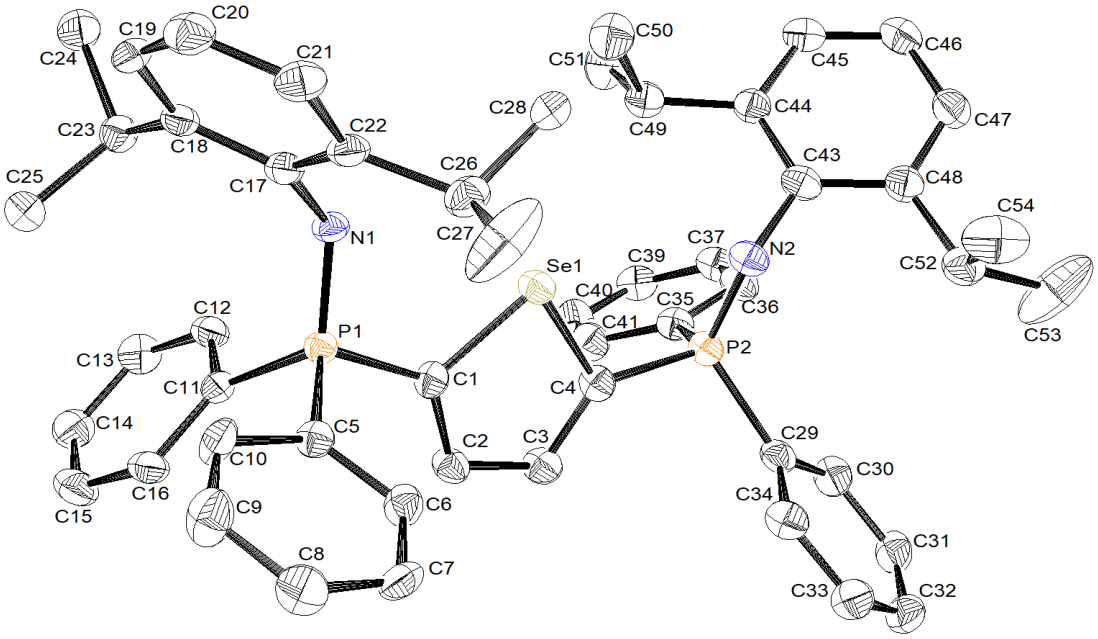

Figure 2.10: Displacement ellipsoid plot of bisphosphinimine **17** depicted at 50% probability. Asymmetric unit (Z' = 1) is shown. Space group = $P\bar{1}$, R_1 = 4.56%. Selected bond lengths (Å): P1–N1 = 1.565(2), P2–N2 = 1.572(3), N1–C17 = 1.416(3), N2–C43 = 1.411(4).

Crystals of compound **18** grew in a monoclinic crystal system in the Pn (or Pc) space group with the lattice comprising of 2 molecules (Z = 2, Z' = 1). The phosphinimine P–N bond distances (P1–N1 1.551(6) Å, and P2–N2 1.553(6) Å) are similar to compound **8** (2,5-(MesN=P^{i}Pr$_2$)$_2$C$_4$H$_2$O) which also bears isopropyl groups on phosphorous (P1–N1 1.554(2) Å, and P2–N2 1.549(2) Å).

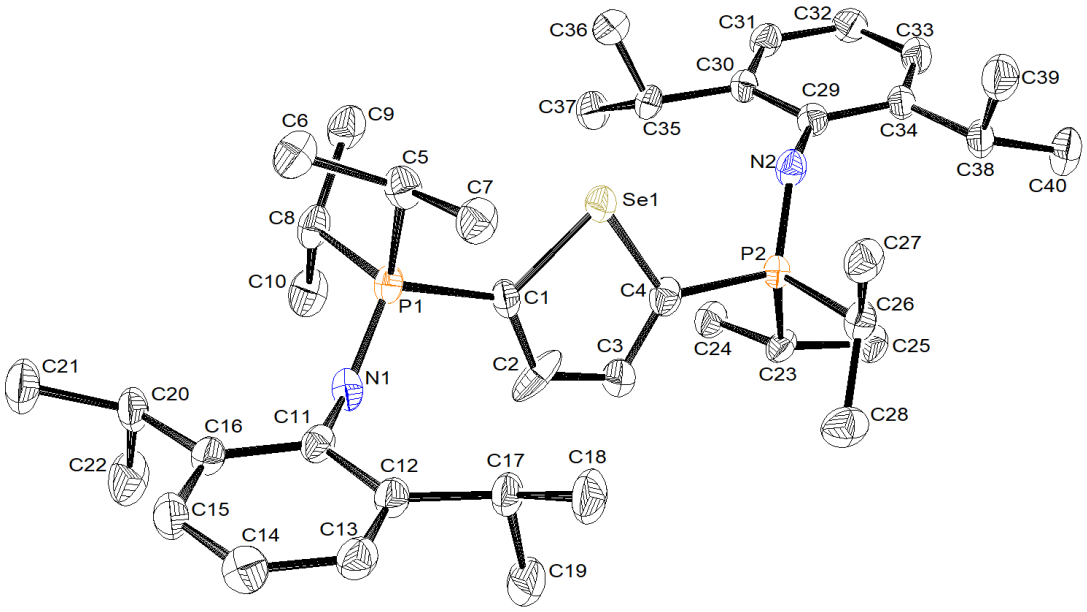

Figure 2.11: Displacement ellipsoid plot of bisphosphinimine **18** depicted at 50% probability. Asymmetric unit (Z' = 1) is shown. Space group = Pn (or Pc), R_1 = 5.58%. Selected bond lengths (Å): P1–N1 = 1.551(6), P2–N2 = 1.553(6), N1–C11 = 1.389(8), N2–C29 = 1.369(8).

Crystals of compound **19** grew in a monoclinic crystal system in the P2$_1$/c space group with the lattice comprising of 4 molecules (Z = 4, Z' =1). The phosphinimine P–N bond distances (P1–N1 1.570(3) Å, and P2–N2 1.577(3) Å) were only marginally different from one another and were slightly elongated compared to the analogous bisphosphinimine **17** (P1–N1 1.565(2) Å, and P2–N2 1.572(3) Å). Several issues arose while solving for this structure, including the N2–Pipp group which appeared over two positions. This disorder was successfully modelled using residual densities around the associated atoms. A twin was identified during refinement that pertained to 33% of the

data. It was successfully modelled which helped resolve some data and remove other space group possibilities.

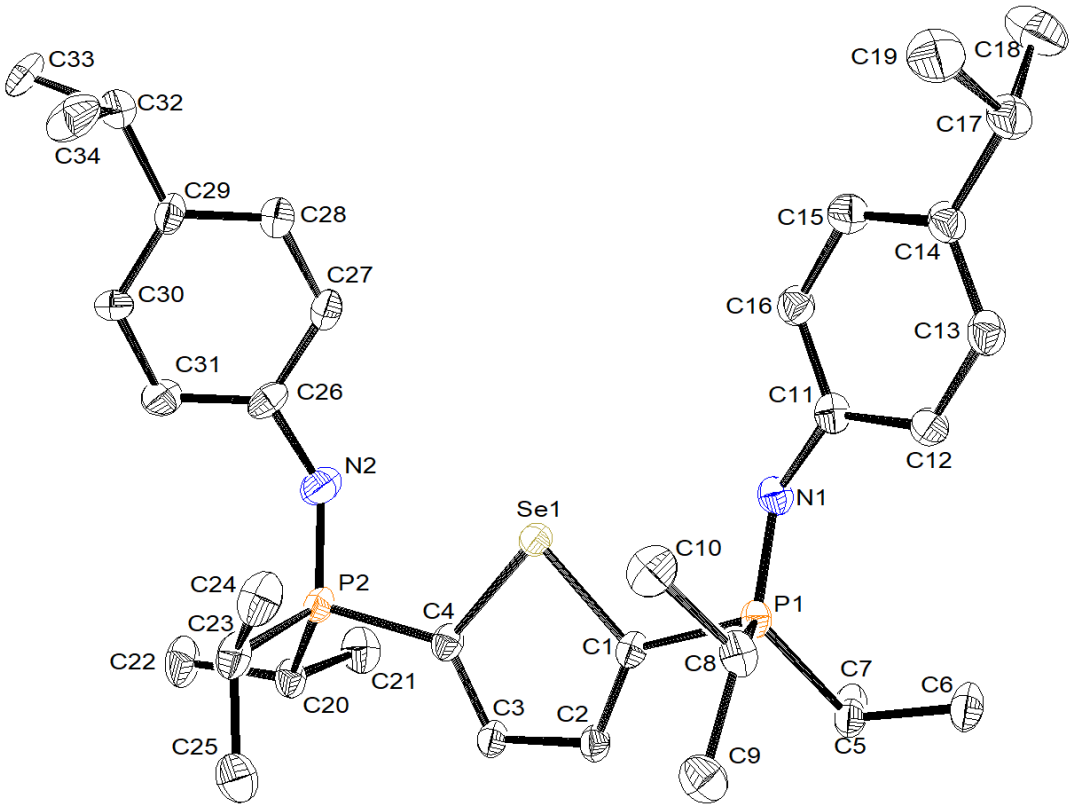

Figure 2.12: Displacement ellipsoid plot of bisphosphinimine **19** depicted at 50% probability. Asymmetric unit (Z' = 1) is shown. Space group = P $2_1/c$. R-Factor = 5.65%. Lower occupancy disordered Pipp ring not shown. Selected bond lengths (Å): P1–N1 = 1.570(3), P2–N2 = 1.577(3), N1–C11 = 1.392(5),
N2–C26 = 1.38(3), N2–C35 = 1.42(4) (from disordered model).

2.4 Other Notes on the Neutral Bisphosphinimine Ligands

The C1–E1–C4 or C1–E1–$C1^i$ (E = O, S, or Se) bond angles decreased as the size of the chalcogen increased (Table 2.2). For example, the furan-based compounds **3**, **6**, and **8**, have angles of 106.1(3)° (**3**), 105.9(3)° and 105.8(3)° (**6**), and 106.9(2)° (**8**), while the thiophene-based ligands **9** and **11**, have C1–S1–C4 angles of 92.9(1)° (**9**) and 92.8(6)° (**11**). This trend continues for the selenium-containing species **16-19**, which have C1–Se1–C4 angles of 88.8(5)° and 89.1(7)° (**16**), 86.6(1)° (**17**), 87.5(3)° (**18**), and 86.5(2)° (**19**). As the C1–E1–C4 angle contracts, the central chalcogen necessarily more

closely approaches a bound metal centre, the impact of which on lactone polymerization catalysis will be addressed in section 2.6.5. Notably the phosphinimine bond distance slightly increased with the size of the central donor when the R and Ar groups were constant (**3**, **11**, **17** where R = Ph, Ar = Dipp).

Table 2.2: Tabulated bond angles of the chalcogen ring in *NEN*-pincer neutral ligands.

Compound	Central donor (E)	C1–E1–C4, or equivalent, angle (°)	Phosphinimine P–N bond length (Å)
3	O	106.1(3)	1.549(1)
6	O	105.9(3), 105.8(3)	1.587(3), 1.589(4), 1.561(3), 1.589(3)
8	O	106.9(2)	1.554(2), 1.549(2)
9	S	92.9(1)	-
11	S	92.8(6)	1.561(1)
16	Se	88.8(5), 89.1(7)	-
17	Se	86.6(1)	1.565(2), 1.572(3)
18	Se	87.5(3)	1.551(6), 1.553(6)
19	Se	86.5(2)	1.570(3), 1.577(3)

2.5 Protonated Bisphosphinimine *NEN*-Pincer Ligands (E = O, S, Se)

The ligands **3-8**, **11-14**, and **17-18** were protonated to afford [2-(ArN(H)=PR_2)-5-(ArN=PR_2)C_4H_2E][A], according to synthetic protocols previously established in the Hayes lab.[93-98] Specifically, the requisite neutral bisphosphinimine *NEN*-pincer ligands (E = O (**3-8**), S (**11-14**), Se (**17-18**)) were combined with either *N*,*N*-dimethylanilinium tetrakis(pentalfuorophenyl)borate ([H][A] = [$HNMe_2Ph$][$B(C_6F_5)_4$]) or diethyl ether oxonium tetrakis[3,5-bis(trifluoromethyl)phenyl]borate, better known as Brookhart's acid, ([H][A] = [$(Et_2O)_2H$][$B(3,5\text{-}(CF_3)_2C_6H_3)_4$])[115] in either benzene or toluene at ambient temperature. The resultant ion pairs were generated in 2 h and proved insoluble in common aromatic solvents. Accordingly, the solvent was decanted from the oily

products, which were triturated with pentane or heptane to afford well-behaved solids of: [2-(DippN(H)=PPh_2)-5-(DippN=PPh_2)C_4H_2O][B(3,5-$(CF_3)_2C_6H_3)_4$] (**20**, 64.7%), [2-(PippN(H)=PPh_2)-5-(PippN=PPh_2)C_4H_2O][B$(C_6F_5)_4$] (**21**, 93.6%), [2-(PmN(H)=PPh_2)-5-(PmN=PPh_2)C_4H_2O][B$(C_6F_5)_4$] (**22**, 90.6%), [2-(DippN(H)=P^iPr_2)-5-(DippN=P^iPr_2)C_4H_2O][B(3,5-$(CF_3)_2C_6H_3)_4$] (**23**, 87.2%), [2-(DippN(H)=PPh_2)-5-(DippN=PPh_2)C_4H_2S][B(3,5-$(CF_3)_2C_6H_3)_4$] (**24**, 73.0%), [2-(PippN(H)=PPh_2)-5-(PippN=PPh_2)C_4H_2S][B$(C_6F_5)_4$] (**25**, 95.1%), [2-(PmN(H)=PPh_2)-5-(PmN=PPh_2)C_4H_2S][B$(C_6F_5)_4$] (**26**, 66.2%), [2-(DippN(H)=P^iPr_2)-5-(DippN=P^iPr_2)C_4H_2S][B(3,5-$(CF_3)_2C_6H_3)_4$] (**27**, 75.4%), [2-(DippN(H)=PPh_2)-5-(DippN=PPh_2)C_4H_2Se][B(3,5-$(CF_3)_2C_6H_3)_4$] (**28**, 87.6%), [2-(DippN(H)=P^iPr_2)-5-(DippN=P^iPr_2)C_4H_2Se][B(3,5-$(CF_3)_2C_6H_3)_4$] (**29**, 87.2%), and [2-(PippN(H)=P^iPr_2)-5-(PippN=P^iPr_2)C_4H_2Se][B$(C_6F_5)_4$] (**30**, 92.2%) (Scheme 2.8). All of these compounds are more intensely coloured than their neutral counterparts.

The addition of 2 equivalents of [$HNMe_2Ph$][B$(C_6F_5)_4$] to **4** (2,5-(PippN=PPh_2)$_2C_4H_2O$) in a solution of benzene at ambient temperature afforded the doubly protonated compound, [2,5-(PippN(H)=PPh_2)$_2C_4H_2O$][B$(C_6F_5)_4$]$_2$ (**31**, 77.8%) in 2 h. Compound **31** contained a single sharp signal in the $^{31}P\{^1H\}$ spectrum at δ 22.7, along with a doublet for the protonated phosphinimine N–H in the ^1H spectrum at δ 5.43 which collapsed to a singlet upon decoupling to ^{31}P.

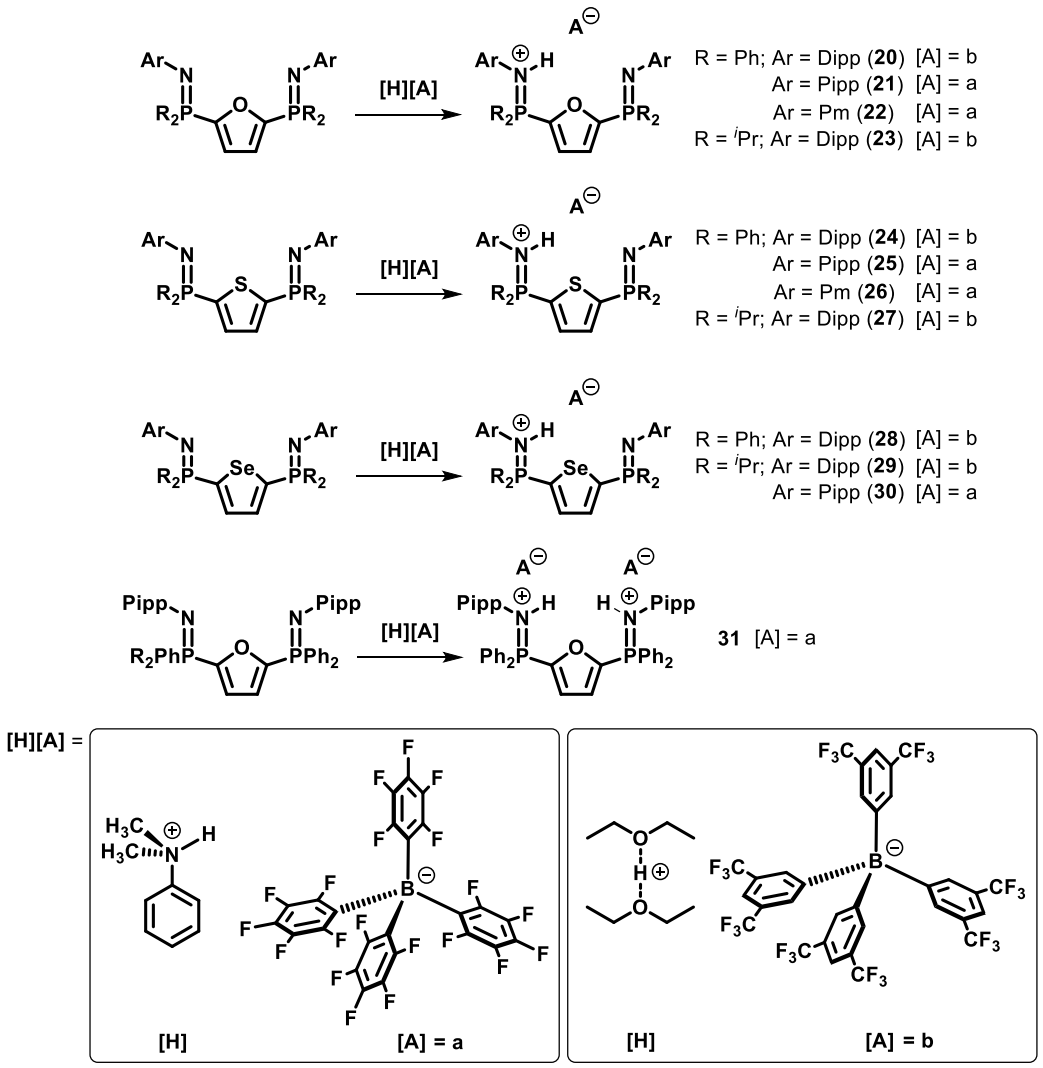

Scheme 2.8: Synthesis of protonated ligands **20**-**31**.

The addition of either Brønsted acid to a neutral bisphosphinimine protonated a single phosphinimine substituent and installed a weakly-coordinating borate anion. The large bulky fluorinated aromatic rings and lack of available orbitals on the boron centre restrict any formal bond from forming with the phosphinimine group, making the attraction electrostatic.[116] All compounds, except **24**, retained the C_{2v} symmetry in solution. Presumably the H^+ exchanges rapidly between the phosphinimine nitrogen atoms on the NMR timescale. The broad resonances observed in the ^{31}P NMR spectra, as well as broad ^{1}H signals attributed to the phosphiniminium proton are consistent with this suggestion.

The protonated Dipp (**20**, **23**, **24**, **27-29**) and Pipp (**21**, **25**, **30**) containing ligands include a broad signal in the ^{1}H NMR spectrum due to the phosphiniminium proton between δ 4.84 and δ 6.87 in $CDCl_3$ solvent. These resonances shifted further downfield in pyridine-d_5 and THF-d_8, to δ 11.82-16.36. There was no obvious correlation between phosphiniminium chemical shift and central donor, E. Compound **24** ([2-(DippN(H)=PPh_2)-5-(DippN=PPh_2)C_4H_2S][B(3,5-$(CF_3)_2C_6H_3)_4$]) is unique in that its ^{31}P{^{1}H} NMR spectrum exhibits two resonances at δ 29.47 and –15.83. Evidently the H^+ exchange between phosphinimine groups, if present, is slower than the NMR timescale. Hence, a 'free' phosphinimine and a protonated phosphiniminium can be distinguished in the ^{13}P{^{1}H} NMR spectrum. The difference of ~40-50 ppm between two phosphinimine groups of a bisphosphinimine containing complex (**L$_{2iPr}$**Rh$(CO)_2$, **XIIa** in 1.3.2) is attributed to the difference between a 'free' phosphinimine and one that is bound to a metal or H^+.[91] By comparison, compounds **22** and **26** (where Ar = Pm) exhibit relatively sharp ^{31}P{^{1}H} NMR signals at δ 10.25 (full width half maximum, FWHM, = 16.6 Hz) and δ 13.46 (FWHM = 13.9 Hz), respectively. It is postulated that the proton was exchanged between the two phosphinimines and an available nitrogen atom of the Pm group. Unfortunately, analytically pure X-ray quality material was difficult to obtain for these species.

Table 2.3: Tabulated ^{1}H and $^{31}P\{^{1}H\}$ NMR chemical shifts for the protonated phosphinimine. For reference, a sharp singlet has a FWHM of 3±1.0 Hz in ^{1}H NMR spectra and 2.44±0.61 Hz in $^{31}P\{^{1}H\}$ NMR spectra. +Compound **24** contained two peaks. *Compound **31** contained a doublet.

Compound	Solvent	^{1}H NMR shift (δ)	^{1}H shift FWHM (Hz)	$^{31}P\{^{1}H\}$ NMR shift (δ)	$^{31}P\{^{1}H\}$ shift FWHM (Hz)
20	pyridine-d_5	16.36	209	–11.64	367
21	$CDCl_3$	5.82	15.9	7.92	275
22	$CDCl_3$	-	-	10.25	16.6
23	pyridine-d_5	11.82	194	1.17	824
24	$CDCl_3$	6.87	9.30	29.47, –15.83	22.0, 36.1[+]
25	$CDCl_3$	6.40	32.4	14.8	312
26	THF-d_8	13.74	143	13.46	13.9
27	pyridine-d_5	12.54	572	7.08	719
28	pyridine-d_5	12.75	191	–8.62	1390
29	pyridine-d_5	-	-	11.07	694
30	$CDCl_3$	4.84	10.3	56.37	234
31	$CDCl_3$	5.43	3.45, 3.12[*]	22.67	2.44

Compound **25** ([2-(PippN(H)=PPh_2)-5-(PippN=PPh_2)C_4H_2S][$B(C_6F_5)_4$]) was dissolved in bromobenzene which evaporated slowly at ambient temperature to allow X-ray quality crystals of **25** to be produced. Crystals of compound **25** grew in a triclinic crystal system in the $P\overline{1}$ space group with the lattice comprising of 2 molecules (Z = 2, Z' = 1). The two phosphinimine P–N bond distances, P1–N1 = 1.621(2) Å and P2–N2 = 1.571(1) Å, differ significantly as the former is protonated, and thereby has more single bond character. Notably, H1 was successfully modelled using residual electron density (Figure 2.13). The latter phosphinimine functionality is not protonated, and as such, is similar in length to the structurally characterized neutral phosphinimines in this chapter. Typical phosphiniminium moieties have bond lengths between 1.618-1.643 Å.[72, 93-97, 100, 101] The weakly-coordinating borate anion does not interact with the protonated ligand, but hydrogen bonding was observed between N1–H1 and N2 of a neighbouring compound in the solid state.

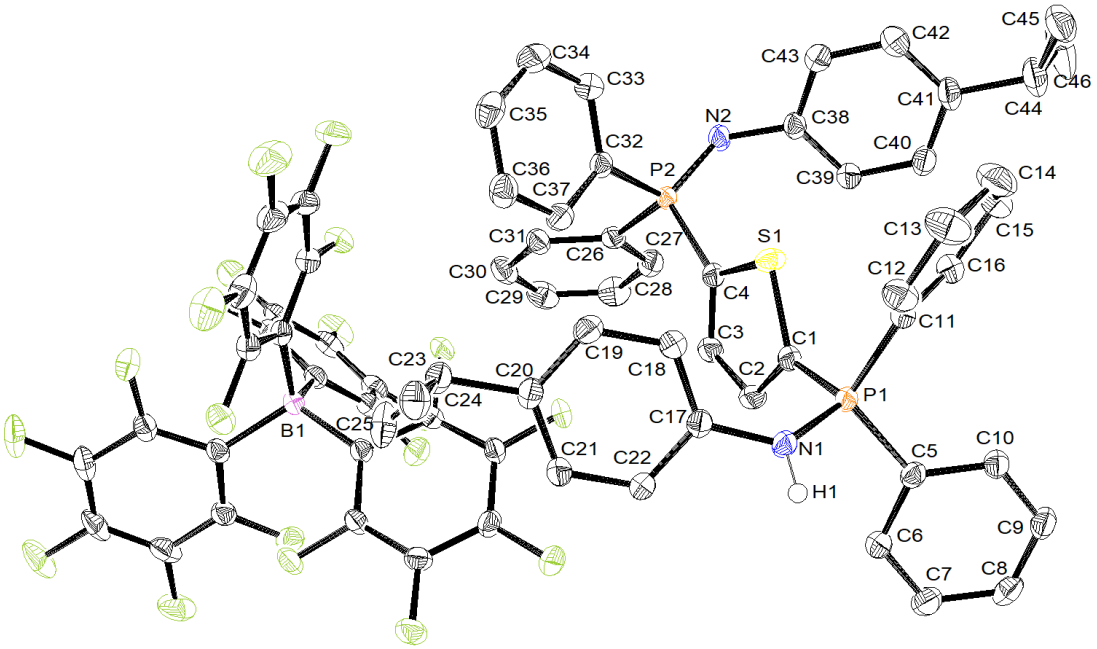

Figure 2.13: Displacement ellipsoid plot of protonated bisphosphinimine **25** depicted at 50% probability. Asymmetric unit (Z' = 1) is shown. Space group = P$\bar{1}$, R_1 = 3.96%. Selected bond lengths (Å):
P1–N1 = 1.621(2), P2–N2 = 1.571(1), N1–C17 = 1.430(2), N2–C38 = 1.413(2).
Selected bond angles (°): C1–S1–C4 = 91.93(8).

2.6 Cationic Zinc Complexes Supported by *NEN*-Pincer Ligands (E = O, S, Se)

2.6.1 Zinc Methyl Complexes

The two most available zinc alkyl compounds are dimethyl zinc ($ZnMe_2$) and diethyl zinc ($ZnEt_2$). For this project, dimethyl zinc was used as it is less expensive. In bromobenzene, a solution of 1 equivalent of $ZnMe_2$ was added to a protonated ligand [2-(ArN(H)=PR_2)-5-(ArN=PR_2)C_4H_2E][A] (**20**-**30**). No immediate change was observed and after 2 h the solvent was removed *in vacuo*. The resulting waxy solids were subjected to trituration with pentane affording pale yellow-orange powders. The protocol yielded a series of cationic zinc complexes bearing the previously described *NEN*-pincer ligands (E = O, S, Se) *via* methane elimination. The complexes synthesized include: [2,5-(DippN=PPh_2)$_2C_4H_2$OZnMe][$B(C_6F_5)_4$] (**32**, 72.9%), [2,5-(PippN=PPh_2)$_2C_4H_2$OZnMe][$B(C_6F_5)_4$] (**33**, 78.1%),

[2,5-(DippN=P^{i}Pr$_2$)$_2$C$_4$H$_2$OZnMe][B(3,5-(CF$_3$)$_2$C$_6$H$_3$)$_4$] (**34**, 87.5%) [2,5-(DippN=PPh$_2$)$_2$C$_4$H$_2$SZnMe][B(3,5-(CF$_3$)$_2$C$_6$H$_3$)$_4$] (**35**, 74.9%), [2,5-(PippN=PPh$_2$)$_2$C$_4$H$_2$SZnMe][B(C$_6$F$_5$)$_4$] (**36**, 79.9%) [2,5-(DippN=P^{i}Pr$_2$)$_2$C$_4$H$_2$SZnMe][B(3,5-(CF$_3$)$_2$C$_6$H$_3$)$_4$] (**37**, 92.7%), [2,5-(DippN=PPh$_2$)$_2$C$_4$H$_2$SeZnMe][B(3,5-(CF$_3$)$_2$C$_6$H$_3$)$_4$] (**38**, 84.4%), [2,5-(DippN=P^{i}Pr$_2$)$_2$C$_4$H$_2$SeZnMe][B(3,5-(CF$_3$)$_2$C$_6$H$_3$)$_4$] (**39**, 84.3%), and [2,5-(PippN=P^{i}Pr$_2$)$_2$C$_4$H$_2$SeZnMe][B(C$_6$F$_5$)$_4$] (**40**, 81.2%) (Scheme 2.9). A slight excess of dimethyl zinc ensured complete reaction and given the volatility of ZnMe$_2$ (b.p. = 46 °C), any residual material can be readily removed under reduced pressure. Appropriate procedures were followed when disposing of residual dimethyl zinc captured in solvent traps, such as keeping the solvent trap cold and quenching the material with isopropanol over 6 h under a blanket of argon.

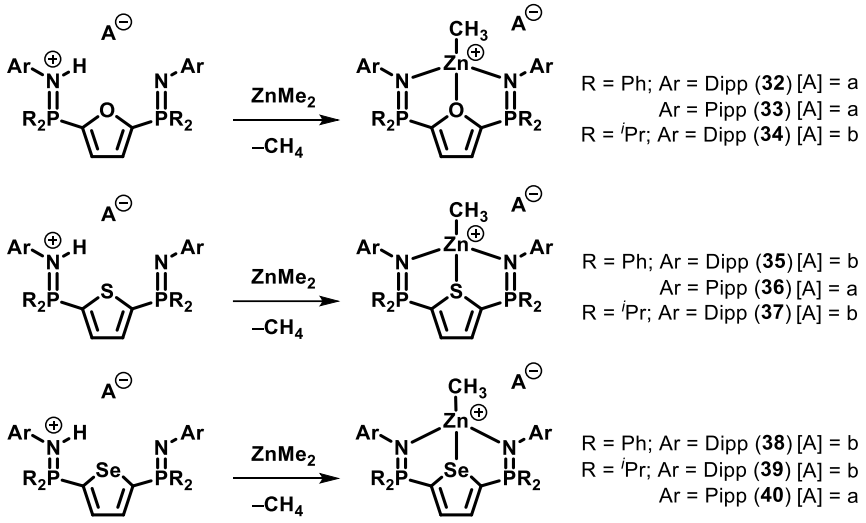

Scheme 2.9: Synthesis of cationic zinc methyl complexes **32**-**40**. a = [B(C$_6$F$_5$)$_4$], b = [B(3,5-(CF$_3$)$_2$C$_6$H$_3$)$_4$].

The products **32**-**40** were similar to the protonated ligand starting materials, in that they tenaciously retain hydrocarbon solvents which were introduced during the trituration step. The ^{11}B and ^{19}F NMR resonances for the weakly-coordinated borate

anion in all complexes remained relatively constant with respect to chemical shift, shape, and integration, within the same solvent (Table 2.4).

Table 2.4: Tabulated ^{11}B and ^{19}F NMR chemical shifts of weakly-coordinating borate anions in various deuterated solvents. a = $[B(C_6F_5)_4]$, b = $[B(3,5\text{-}(CF_3)_2C_6H_3)_4]$.

Solvent	^{11}B shift (δ) [A] = b	^{19}F shift (δ) [A] = b	^{11}B shift (δ) [A] = a	^{19}F shift (δ) [A] = a
pyridine-d_5	–4.4	–15.9	–15.9	–132.1, –162.2, –166.3
$CDCl_3$	–5.9	–16.8	–16.7	–131.6, –161.7, –165.6
THF-d_8	N/A	N/A	–18.5	–133.7, –165.9, –169.4
CD_2Cl_2	N/A	N/A	–18.5	–133.7, –166.0, –169.5

The signals in the $^{31}P\{^1H\}$ NMR spectra generally had smaller FWHM for most compounds except **33**, **36**, and **40**. All of the zinc methyl complexes **32-40** were surprisingly stable over long periods of time when kept as dried powders at ambient temperature. However, they were very sensitive to water. Degradation to various unidentified by-products was observed when these complexes were heated in solution at elevated temperatures (>100 °C) over 48 h. To decrease the broadness of the resonances, ^1H NMR spectroscopy was conducted at a range of temperatures (–80-100 °C). No temperature afforded better resolved signals for **32-39**, but for compound **40** they were considerably sharper at elevated temperatures (60 °C) attributed to an increase in the rapid exchange of the Zn–Me group between the two phosphinimines.

2.6.2 Zinc Alkoxide Complexes

The metal alkoxide complexes, EtZnOPh and MeZnOR (R = ^{i}Pr, ^{t}Bu, Ph, or Me) were synthesized by addition of 1 equivalent of the corresponding dry alcohol to 1 equivalent of dimethyl zinc or diethyl zinc diluted with toluene. Volatiles were removed *in vacuo* to give MeZnOR or EtZnOR as white powders.

Addition of MeZnOPh or EtZnOPh to a bromobenzene solution of [2-(ArN(H)=PR_2)-5-(ArN=PR_2)C_4H_2E][A] (**20**-**30**) afforded: [2,5-(DippN=PPh_2)$_2C_4H_2$OZnOPh][$B(C_6F_5)_4$] (**32b**, 72.7%), [2,5-(PippN=PPh_2)$_2C_4H_2$OZnOPh][$B(C_6F_5)_4$] (**33b**, 86.1%), [2,5-(DippN=P^{i}Pr$_2$)$_2C_4H_2$OZnOPh][$B(3,5\text{-}(CF_3)_2C_6H_3)_4$] (**34b**, 88.6%), [2,5-(DippN=PPh_2)$_2C_4H_2$SZnOPh][$B(3,5\text{-}(CF_3)_2C_6H_3)_4$] (**35b**, 90.4%), [2,5-(PippN=PPh_2)$_2C_4H_2$SZnOPh][$B(C_6F_5)_4$] (**36b**, 82.4%), [2,5-(DippN=P^{i}Pr$_2$)$_2C_4H_2$SZnOPh][$B(3,5\text{-}(CF_3)_2C_6H_3)_4$] (**37b**, 93.4%), [2,5-(DippN=PPh_2)$_2C_4H_2$SeZnOPh][$B(3,5\text{-}(CF_3)_2C_6H_3)_4$] (**38b**, 89.6%) [2,5-(DippN=P^{i}Pr$_2$)$_2C_4H_2$SeZnOPh][$B(3,5\text{-}(CF_3)_2C_6H_3)_4$] (**39b**, 71.8%) and [2,5-(PippN=P^{i}Pr$_2$)$_2C_4H_2$SeZnOPh][$B(C_6F_5)_4$] (**40b**, 90.1%) after 2 h at ambient conditions. These complexes can also be generated by addition of dried phenol to the requisite zinc alkyl complexes ([2,5-(ArN=PR_2)$_2C_4H_2$EZnMe][A]) in bromobenzene. This was a necessary route for complex **39b**, as there was considerable competition between methane and phenol elimination when MeZnOPh was employed.

The procedure to generate the cationic zinc phenoxides relied on the preferential elimination of methane to yield the desired cationic zinc alkoxide complexes. When using MeZnOR (R = ^{i}Pr or ^{t}Bu) as zinc starting materials, a mixture of products was generated. There were competing reactions with the elimination of either methane or the corresponding alcohol which could not be controlled. This was observed *via* two separate resonances in the $^{31}P\{^1H\}$ NMR spectrum, one of which was the cationic methyl complex, the other being the cationic alkoxide complex. The corresponding Zn–Me and Zn–OR (R = ^{i}Pr or ^{t}Bu) resonances were also observed in the ^{1}H NMR spectra of the reaction mixtures.

When MeZnOMe was used as the zinc starting material, the resulting reaction mixtures with the protonated ligands contained a myriad of products. When reacted with the protonated ligand **21** (**(**[2-(PippN(H)=PPh_2)-5-(PippN=PPh_2)C_4H_2O][$B(C_6F_5)_4$]) an isolatable product, [2,5-(PippN=PPh_2)$_2C_4H_2O$ZnOMe][$B(C_6F_5)_4$] (**41**) was obtained. The cationic zinc methoxide **41** degraded to various unidentified products in solution within hours and was only identified using X-ray crystallography. The cationic zinc phenoxide complexes **32b**-**40b** showed evidence of degradation after 24 h in solution and so were stored as dry solids at –30 °C. More so than the cationic zinc methyl complexes **32**-**40**, **32b**-**40b** retained solvent which may be the reason satisfactory elemental analysis (EA) values were not obtained.

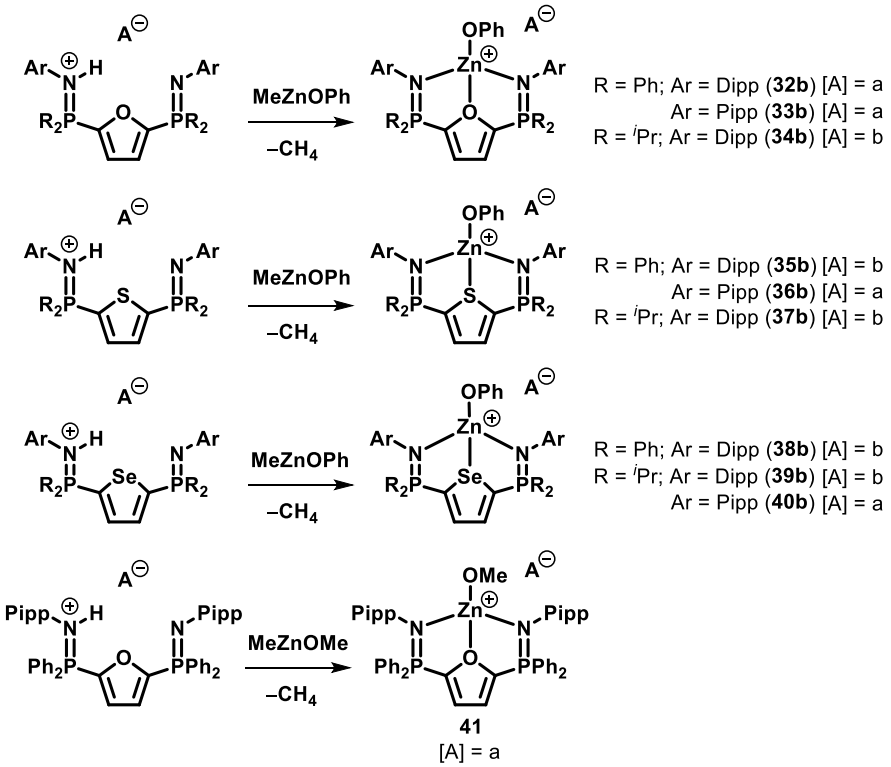

Scheme 2.10: General procedure for *in situ* generation of zinc alkoxide cationic complexes **32b**-**40b** and **41**. a = [$B(C_6F_5)_4$], b = [$B(3,5\text{-}(CF_3)_2C_6H_3)_4$].

The synthesis of lactate complexes analogous to **XIV** ([**L**$_3$ZnE][A], E = methyl-(*rac*)-lactate) was attempted, but no single product could be isolated from the reaction

mixture when MeZn(methyl-(*rac*)-lactate) was added to a bromobenzene solution of a protonated ligand (**20**-**30**).

2.6.3 Comparison of NMR Data from Cationic Zinc Complexes

The $^{31}P\{^{1}H\}$ NMR spectra of the cationic zinc methyl complexes (**32**-**40**) and cationic zinc phenoxide complexes (**32b**-**40b**), see Table 2.5, were mostly obtained in pyridine-d_5. In pyridine-d_5 singlets were observed, whereas other solvents, such as $CDCl_3$ and THF-d_8, resonances were not as well-defined. The Zinc complexes exhibited C_{2v} symmetry in solution, as indicated by the ^{1}H NMR and ^{31}P NMR spectra. However, the ^{31}P NMR spectra of **36** and **39b** contained two separate resonances and no ^{31}P signals were observed for either **33** or **40b**.

Table 2.5: Tabulated $^{31}P\{^{1}H\}$ NMR chemical shifts for the cationic zinc methyl and phenoxide complexes. For reference, a sharp singlet has a FWHM of 2.44±0.61 Hz in $^{31}P\{^{1}H\}$ NMR spectra.

Compound	Solvent	$^{31}P\{^{1}H\}$ NMR shift (δ)	$^{31}P\{^{1}H\}$ shift FWHM (δ)
32	pyridine-d_5	–23.35	2.44
33	CD_2Cl_2	NA	NA
34	pyridine-d_5	0.19	2.44
35	pyridine-d_5	–17.14	2.44
36	$CDCl_3$	26.69, –8.71	312, 299
37	pyridine-d_5	2.83	2.44
38	pyridine-d_5	–14.01	2.44
39	pyridine-d_5	7.19	336
40	$CDCl_3$	55.3	159
32b	pyridine-d_5	–23.26	447
33b	THF-d_8	18.09	2.44
34b	pyridine-d_5	–1.35	2.44
35b	pyridine-d_5	–17.05	2.44
36b	THF-d_8	–28.64	104
37b	pyridine-d_5	2.82	2.44
38b	pyridine-d_5	–14.02	2.44
39b	pyridine-d_5	5.49, 2.85	447, 447
40b	THF-d_8	NA	NA

The spin active (I = 1/2) ^{77}Se nucleus provided insight into the relationship between the central chalcogen donor and zinc. ^{77}Se{^{1}H} NMR experiments showed resonances at δ 744.93 and δ 731.17 for bisphosphines **15** and **16**. Upon oxidation of the phosphine a downfield shift in frequency of approximately 35 ppm was observed (**17**: δ 788.5, **18**: δ 764.4, and **19**: δ 812.0). Unfortunately, no ^{77}Se signals were detected for protonated ligands **28**, **29**, and **30**. Zinc complexes **39** and **39b** exhibited ^{77}Se resonances at δ 764.75 and δ 764.87, respectively. As no discernible trend was obvious upon coordination of the *NSeN*-pincer ligands to zinc it is difficult to comment upon the extent to which Se interacts with Zn in solution, or whether the presence or absence of such an interaction has a predictable impact upon metal complex reactivity.

Diffusion ordered spectroscopy experiments (DOSY) were conducted using the methyl complex **40** ([2,5-(PippN=P^{i}Pr$_2$)$_2$C$_4$H$_2$SeZnMe][B(C$_6$F$_5$)$_4$]) and the phenoxide complex **40b** ([2,5-(PippN=P^{i}Pr$_2$)$_2$C$_4$H$_2$SeZnOPh][B(C$_6$F$_5$)$_4$]). Using a DOSY, the molecular radius of a compound in solution can be calculated. Relating the results from a DOSY through the Einstein-Stokes equation gives a molecular radius of the molecule in solution (Figure 2.14).[117] This equation makes the assumption that the molecule in question is spherical. Since both **40** and **40b** are not spherical molecules, the values generated are used to determine the relative size of either molecule.

$$D = \frac{k_b T}{6\pi\mu R_0}$$

Figure 2.14: Einstein-Stokes equation. T = temperature (K), k_b = Boltzmann's constant, μ = solvent viscosity, D = diffusion constant, R_o = solute radius.

The DOSY experiment revealed self-diffusion constants of 3.648 × 10^{-9} m^{2}s^{-1} for **40** and 0.746 × 10^{-9} m^{2}s^{-1} for **40b** from the isopropyl groups at phosphorous as they gave the strongest signals. All other chemical shifts came under the same self-diffusion

constant, but their signals were diminished in comparison. Relating these values to the radius of the molecular *via* the Einstein-Stokes equation gives a radius of **40** at approximately 0.117 nm and 0.574 nm for **40b** (as a reference, 9,10-diphenylanthracene, a large flat hydrocarbon, gives a radius of 0.436 nm). This data suggests that in solution **40b** is considerably larger than **40** presumably since **40b** is dimeric in solution and **40** is monomeric.

2.6.4 Crystallographic Data from Cationic Zinc Alkoxide Complexes

Crystals of compound **41** ([2,5-(PippN=PPh_2)$_2$$C_4H_2$OZnOMe][$B(C_6F_5)_4$]) grew in a triclinic crystal system in the $P\bar{1}$ space group with the lattice comprising of 2 molecules (Z = 2, Z' = 1). This data established connectivity the Zn–OR fragment and the bisphosphinimine *NEN*-pincer ligand. In the asymmetric unit, there is one weakly-coordinating anion, as well as a disordered dichloromethane. Cavities in the centre of the a axis were responsible for the presence of another solvent of crystallization which was dealt with using the squeeze subroutine. Other sources of disorder included waving of the fluorinated rings of the borate anion.

Notable elongation of the phosphinimine P–N bonds, compared to previously discussed compounds, was observed. P1–N1, 1.600(2) Å, and P2–N2, 1.602(2) Å, were statistically indistinguishable. The $N_{P=N}$–C_{Aryl} bond lengths (N1–C38: 1.448(3) Å, and N2–C17: 1.445(3) Å) were both similar to the protonated phosphinimine $N_{P=N}$–C_{Aryl} bond length of **25** (1.430(2) Å). In the cationic zinc complexes reported by the Hayes group, the phosphinimine P–N bond lengths range between 1.586 Å and 1.611 Å, the $N_{P=N}$–C_{Aryl} between 1.437-1.473 Å, and the $N_{P=N}$–Zn from 1.972 Å to 2.367 Å (**XIVa-e** and **XVII**).[72, 93-97, 100] All of the bond lengths of **41** are within the ranges of the cationic zinc complexes reported by the Hayes group.

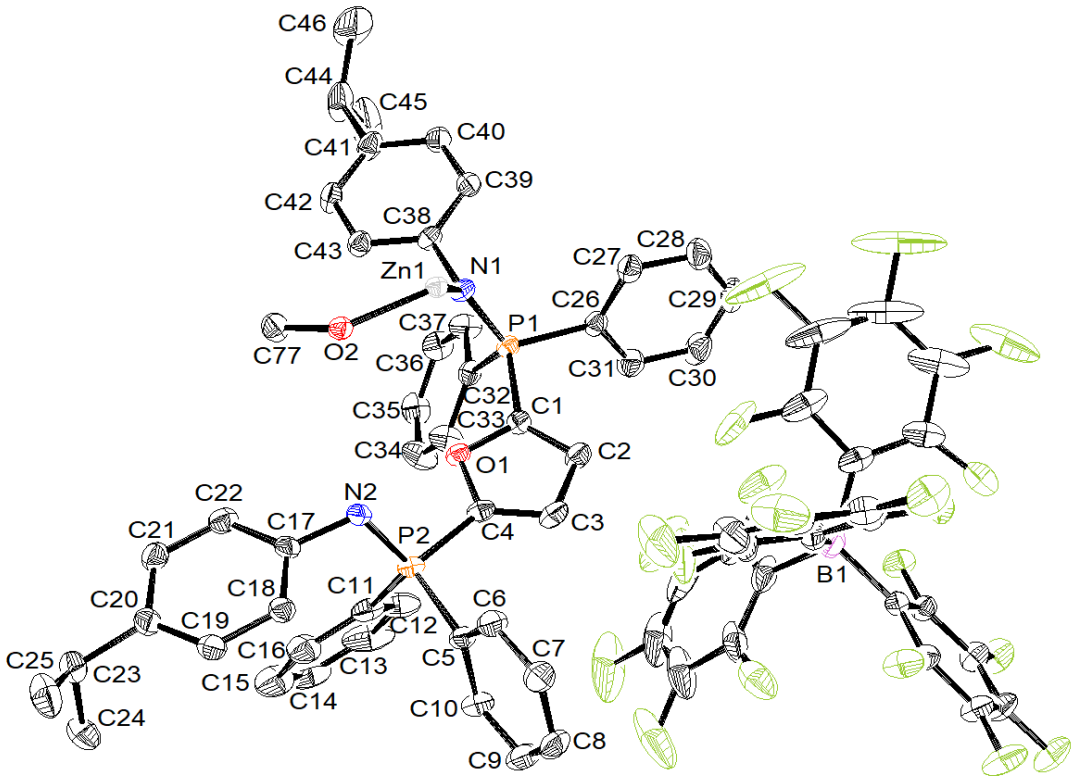

Figure 2.15: Displacement ellipsoid plot of protonated bisphosphinimine **41** depicted at 50% probability. Asymmetric unit (Z' = 1) is shown. Space group = $P\bar{1}$, R_1 = 5.12%. Solvent molecules removed for clarity.

The 'grow' function in Olex2 allowed visualization of the entire compound where two [2,5-(PippN=PPh$_2$)$_2$C$_4$H$_2$OZnOMe][B(C$_6$F$_5$)$_4$] asymmetric units interact (Figure 2.16). The zinc atom has a bond with the one of the phosphinimines (N1–Zn1: 2.025(2) Å), a bond with a phosphinimine of the nearby asymmetric unit (N2^i–Zn1: 2.029(3) Å), and the methoxide groups (O2–Zn1: 1.976(2) Å and O2^i–Zn1: 1.979(2) Å)). The bridging methoxides, visualized with two asymmetric units, give a 4-membered ring with angles O2–Zn1–O2^i = 82.78(7)° and Zn1–O2–Zn1^i = 97.22(8)°. The zinc centre retains a pseudo-tetrahedral geometry with shortened angles with the bridging methoxide groups (O2–Zn1–O2^i: 82.78(7)°) and between the two ligands (N1–Zn1–N2^i: 103.92(8)°. Whether this dimeric structure exists in solution for the methyl zinc complexes (**32**-**40**) is not fully understood; but the DOSY of **40** and **40b** suggest that the alkoxide complexes are larger than the methyl complexes in solution

and the solid-state structure of **41** provides further evidence that the alkoxide complexes are in fact dimeric.

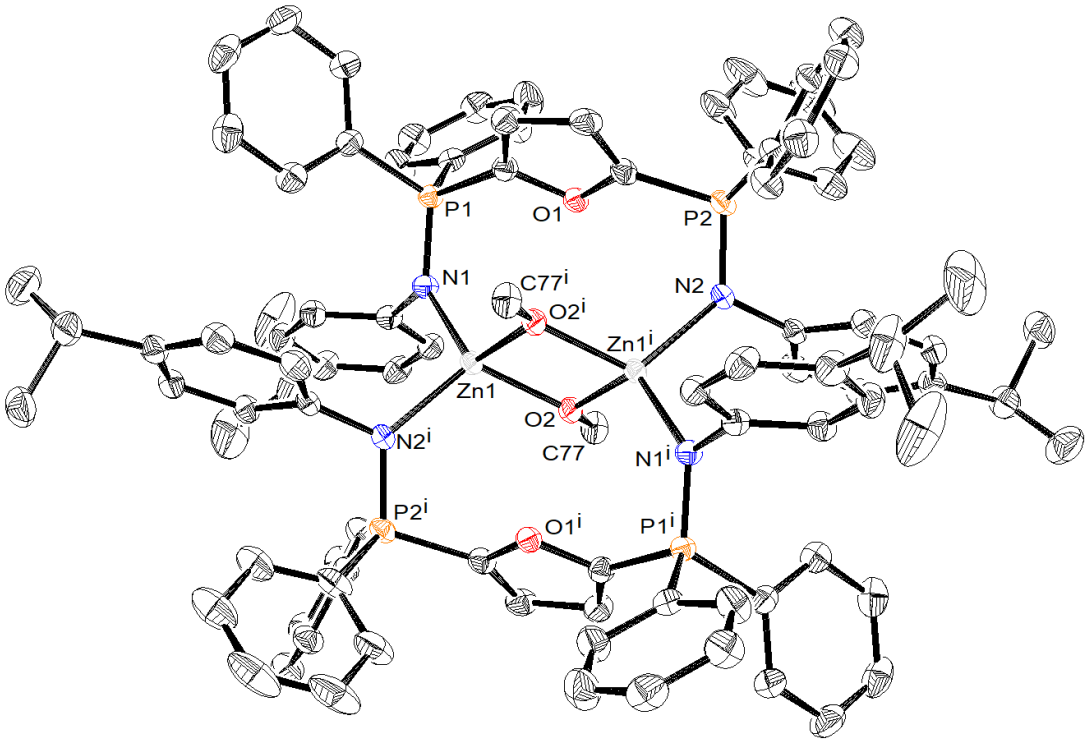

Figure 2.16: Displacement ellipsoid plot of protonated bisphosphinimine **41** depicted at 50% probability. Asymmetric unit grown to include complete molecule. Anions and solvent molecules removed for clarity.

Table 2.6: Selected bond lengths and angles in compound **41**.

Atoms	Length (Å)	Atoms	Angle (°)
P1–N1	1.600(2)	**O2–Zn1–O2^{i}**	82.78(7)
P2–N2	1.602(2)	**Zn1–O2–Zn1^{i}**	97.22(8)
N1–C38	1.448(3)	**N1–Zn1–N2^{i}**	103.92(8)
N2–C17	1.445(3)	**N1–Zn1–O2**	118.49(8)
N1–Zn1	2.025(2)	**N1–Zn1–O2^{i}**	117.73(8)
N2–Zn1^{i}	2.029(3)	**N2^{i}–Zn1–O2^{i}**	117.57(8)
O2–Zn1	1.976(2)	**N2^{i}–Zn1–O2**	116.36(8)
O2^{i}–Zn1	1.979(2)		

Fragile white crystals of complex **33b** were grown from a concentrated DCM solution stored at –30 °C for 48 h. Crystals of compound **33b** grew in a triclinic crystal system in the $P\bar{1}$ space group with the lattice comprising of 2 molecules (Z = 2, Z' = 1). The structure solution contained rotational disorder of the isopropyl groups and positional disorder of the 4-isopropylphenyl group off N1 and contained cavities that were larger than those found in **41** where several DCM molecules were removed with the squeeze subroutine. A low-quality connectivity structure was obtained (Figure 2.17 and Figure 2.18) and found to be isostructural to **41**, providing further evidence that the alkoxides are dimeric.

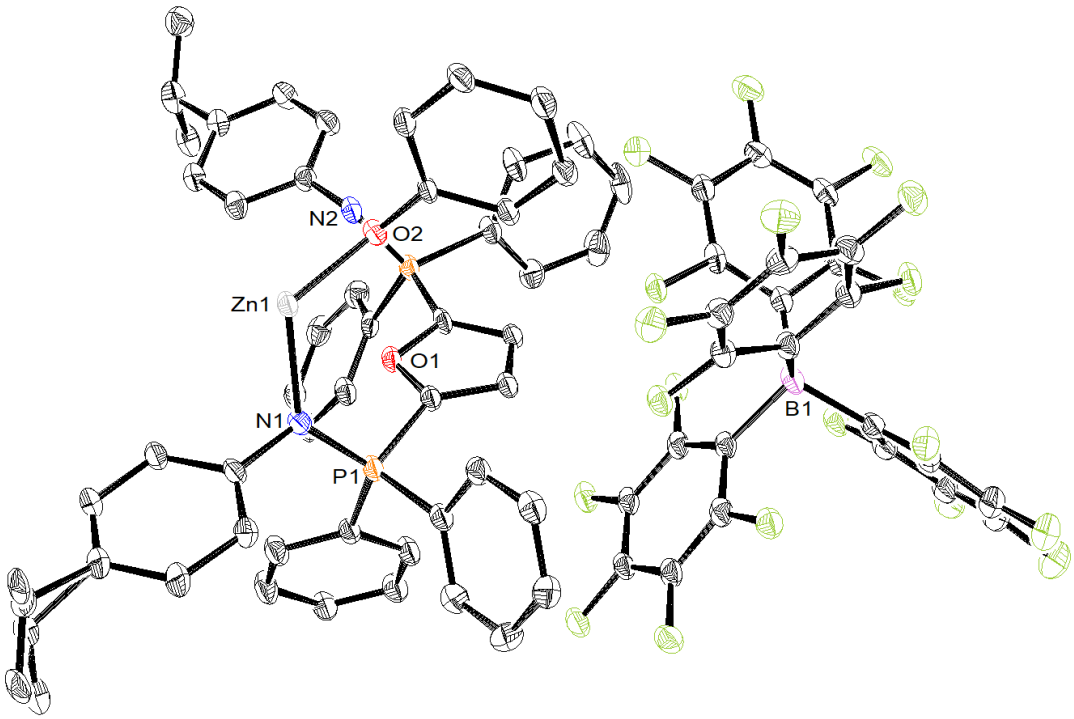

Figure 2.17: Displacement ellipsoid plot of protonated bisphosphinimine **33b** depicted at 20% probability. Asymmetric unit (Z' = 1) is shown. Space group = $P\bar{1}$.

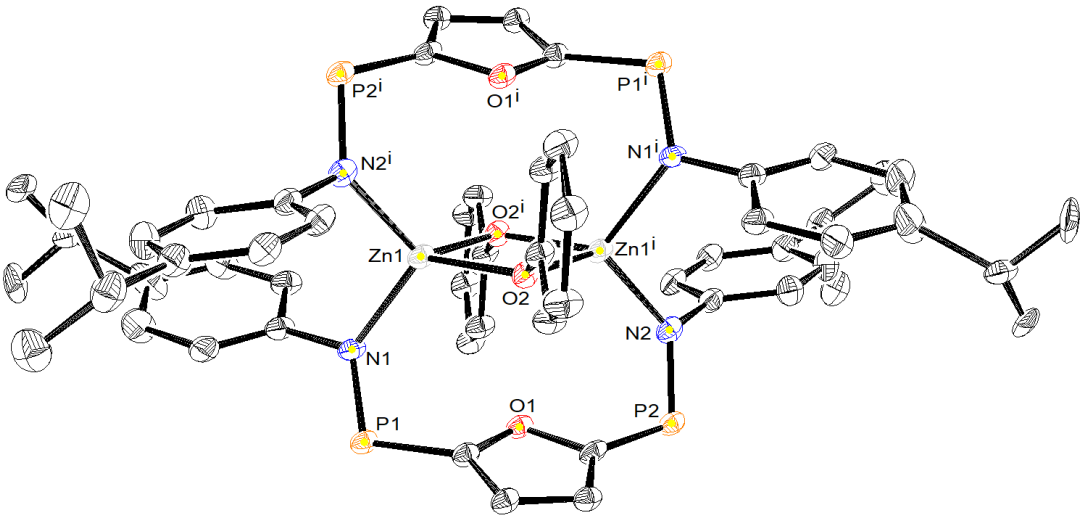

Figure 2.18: Thermal ellipsoid plot of protonated bisphosphinimine **33b** depicted at 20% probability. Asymmetric unit grown to include complete molecule. Anions and P–Ph groups removed for clarity.

2.6.5 Polymerization of ε-Caprolactone with Cationic Zinc Complexes

To ascertain the impact that the central donor (E), the aromatic group on the phosphinimine nitrogen (Ar), and the organic group on phosphorous (R) have on ROP catalysis, an ROP study was conducted. Unfortunately, when complexes **32**-**40** and **32b**-**40b** were tested as initiators for lactide polymerization at 70 °C in deuterated bromobenzene (C_6D_5Br), no reaction was observed over a 24 h period. However, activity was observed when tested with ε-caprolactone in C_6D_5Br at 70 ˚C. The activity of the catalysts was monitored over an 11 h period *via* the depletion of the monomer signal observed in the ^1H NMR spectra at δ 3.64 (ov q, $^3J_{HH}$ = 6.1 Hz, 2H, ε protons) and growth of the methylene polymer resonance (–$COOCH_2$–) at δ 3.81 (t, $^3J_{HH}$ = 6.1 Hz, 2H). These resonances are most appropriate for reaction monitoring as they are baseline resolved from all other monomer, polymer, catalyst, and residual solvent signals. To confirm that the polymerization of ε-caprolactone was catalysed by the cationic zinc complexes, control experiments with ε-caprolactone, several ligands, and protonated ligands were tested under the same conditions. These control experiments

showed no ROP of ε-caprolactone with only <5% of the monomer being consumed in all experiments.

The second-order reaction gives a rate is given by k = [catalyst][monomer]. Since the concentration of the catalyst remains relatively constant throughout the reaction and is much larger relative to the monomer, the pseudo first-order reaction rate is used, given by k' = k[catalyst]. There is an induction period occurs in the first 1.5 h reaction (or initial 10-20% of monomer consumed).

2.6.5.1 Polymerization Activity for Complexes **33**, **36**, **40**, **33b**, **36b**, and **40b** (Ar = Pipp, E = O or S, R = Ph, and E = Se, R = ^{i}Pr)

The complexes that contained the Pipp aromatic group, **33**, **36**, **40**, **33b**, **36b**, and **40b** were the first to be tested for initiating polymerization of ε-caprolactone; the results are shown in Figure 2.19. The cationic zinc methyl complexes, both **33** and **36** (Ar = Pipp, R = Ph, E = O and S, respectively), were exceptionally sluggish at k' (10^{-4}) = 0.0658 s^{-1} and 0.118 s^{-1}, but **40** (Ar = Pipp, R = ^{i}Pr, E = Se) mediated ROP at a greatly accelerated rate (k' (10^{-4}) = 1.17 s^{-1}). A similar trend was observed for the cationic zinc phenoxy complexes (**33b**, **36b**, and **40b**) wherein the rate of ROP increased as E went from O to S, and to Se (k' (10^{-4}) = 0.0118 s^{-1}, 0.137 s^{-1}, 0.469 s^{-1}) but were slower compared to their methyl counterparts. It is hypothesized that the formation of a dimeric structure in the phenoxide complexes **33b**, **36b**, and **40b**, as proposed by DOSY experiments and X-ray crystallography of **33b** and **40b**, restricted accessibility to the zinc metal centre. In comparison, the zinc methyl complexes are thought to remain as a monomer, at least in solution, and therefore contain a more accessible zinc metal centre.

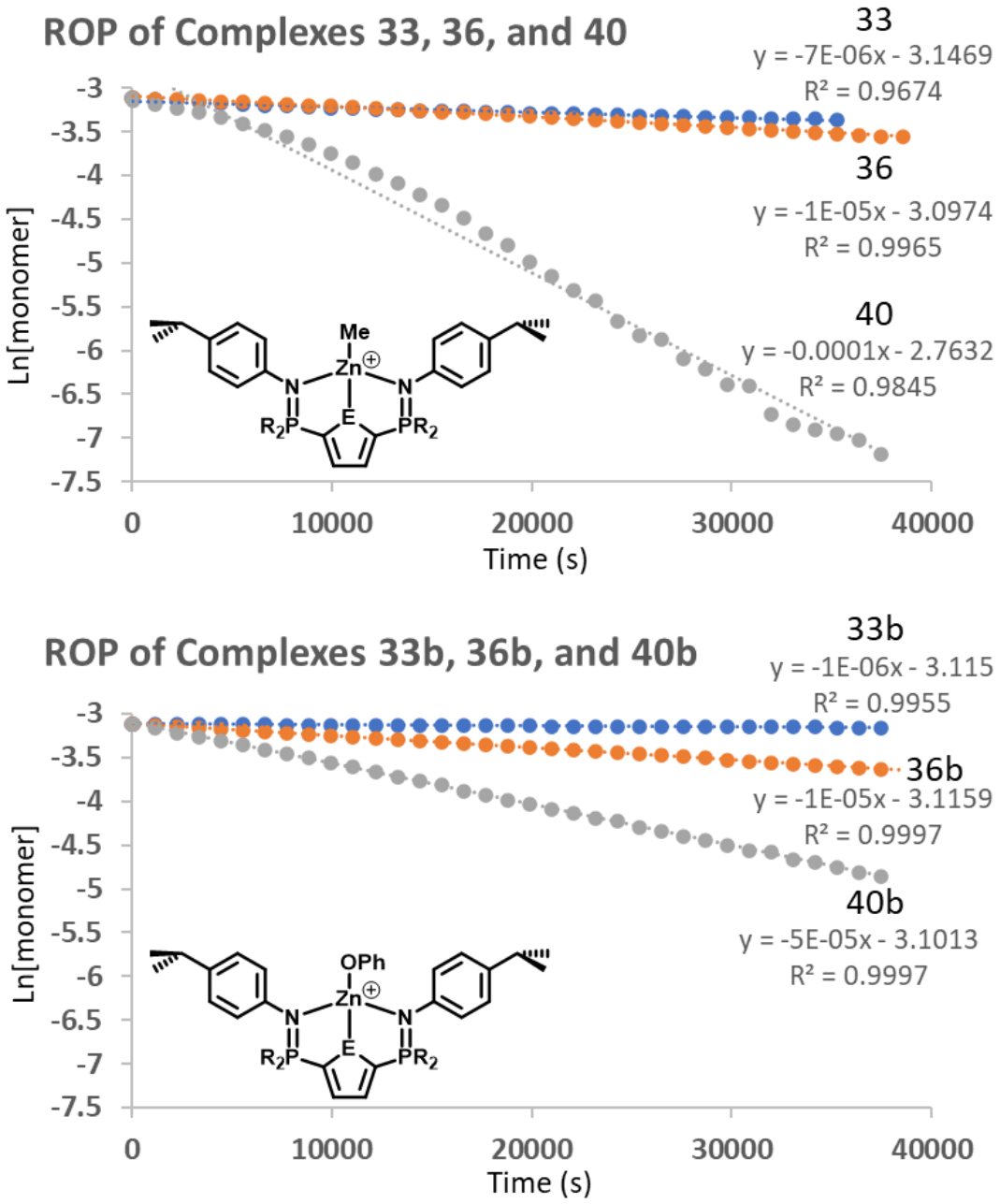

Figure 2.19: Plot of In[monomer] versus time(s) for polymerization of ε-caprolactone at 70 °C over an 11 h period. Cationic zinc methyl complexes **33**, **36**, and **40** are depicted on the top graph and cationic zinc phenoxide complexes **33b**, **36b**, and **40b** on the bottom graph. *k*' (10^{-4}) = 0.0658 s^{-1} (**33**), 0.118 s^{-1} (**36**), 1.17 s^{-1} (**40**), 0.0118 s^{-1} (**33b**), 0.137 s^{-1} (**36b**), 0.469 s^{-1} (**40b**).

2.6.5.2 Polymerization Activity for Complexes **32**, **35**, **38**, **32b**, **35b**, and **38b** (Ar = Dipp, E = O, S, or Se, R = Ph)

The complexes that contained the Dipp aromatic groups and phenyl groups on phosphorous, **32**, **35**, **38**, **32b**, **35b**, and **38b** were tested for their ability to initiate polymerization of ε-caprolactone, the results of which are shown in Figure 2.20.

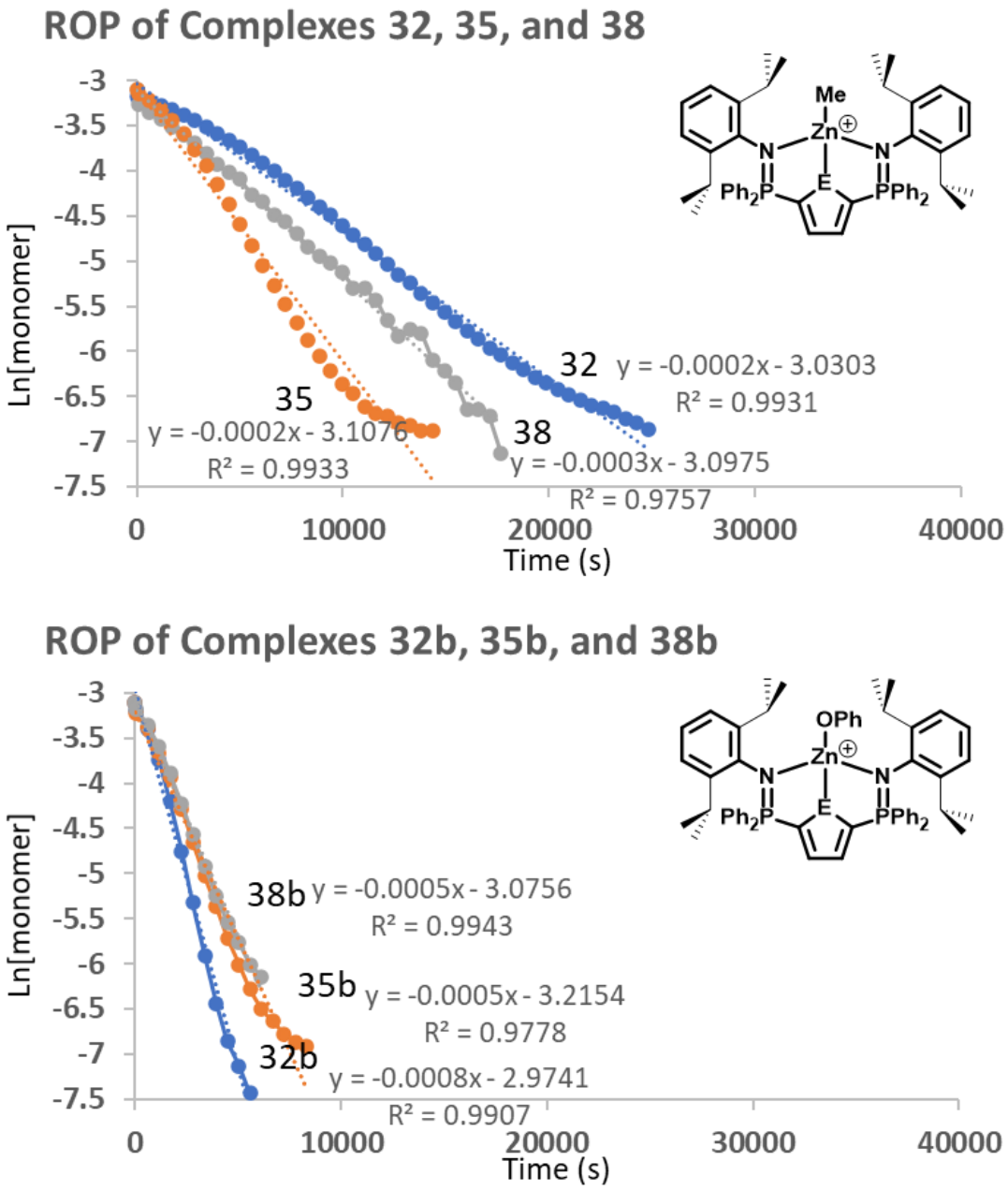

Figure 2.20: Plot of In[A] versus t for polymerization of ε-caprolactone at 70 °C over an 11 h period. Cationic zinc methyl complexes **32**, **35**, and **38** are depicted on the top graph and cationic zinc phenoxide complexes **32b**, **35b**, and **38b** on the bottom graph. *k'* (10^{-4}) = 1.63 s^{-1} (**32**), 3.00 s^{-1} (**35**), 2.10 s^{-1} (**38**), 8.33 s^{-1} (**32b**), 5.02 s^{-1} (**35b**), 5.27 s^{-1} (**38b**).

The cationic zinc methyl complexes did not display any trend in relation to the central donor, E, as the swiftest ROP occurred using **35** (*k'* (10^{-4}) = 3.00 s^{-1}) where E = S. The ROP using the cationic zinc phenoxide complexes as catalysts were notably fast in comparison, with the rate of reaction increasing from Se to S to O (*k'* (10^{-4}) = 5.27 s^{-1}, 5.02 s^{-1}, 8.33 s^{-1} (**38b**, **35b**, **32b**, respectively)).

2.6.5.3 Polymerization Activity for Complexes **34**, **37**, **39**, **34b**, **37b**, and **39b** (Ar = Dipp, E = O, S, or Se, R = ^{i}Pr)

To compare the influence of the group on phosphorous, while keeping the aryl group consistent, **34**, **37**, **39**, **34b**, **37b**, and **39b** were also tested for their ability to initiate polymerization of ε-caprolactone (Figure 2.21).

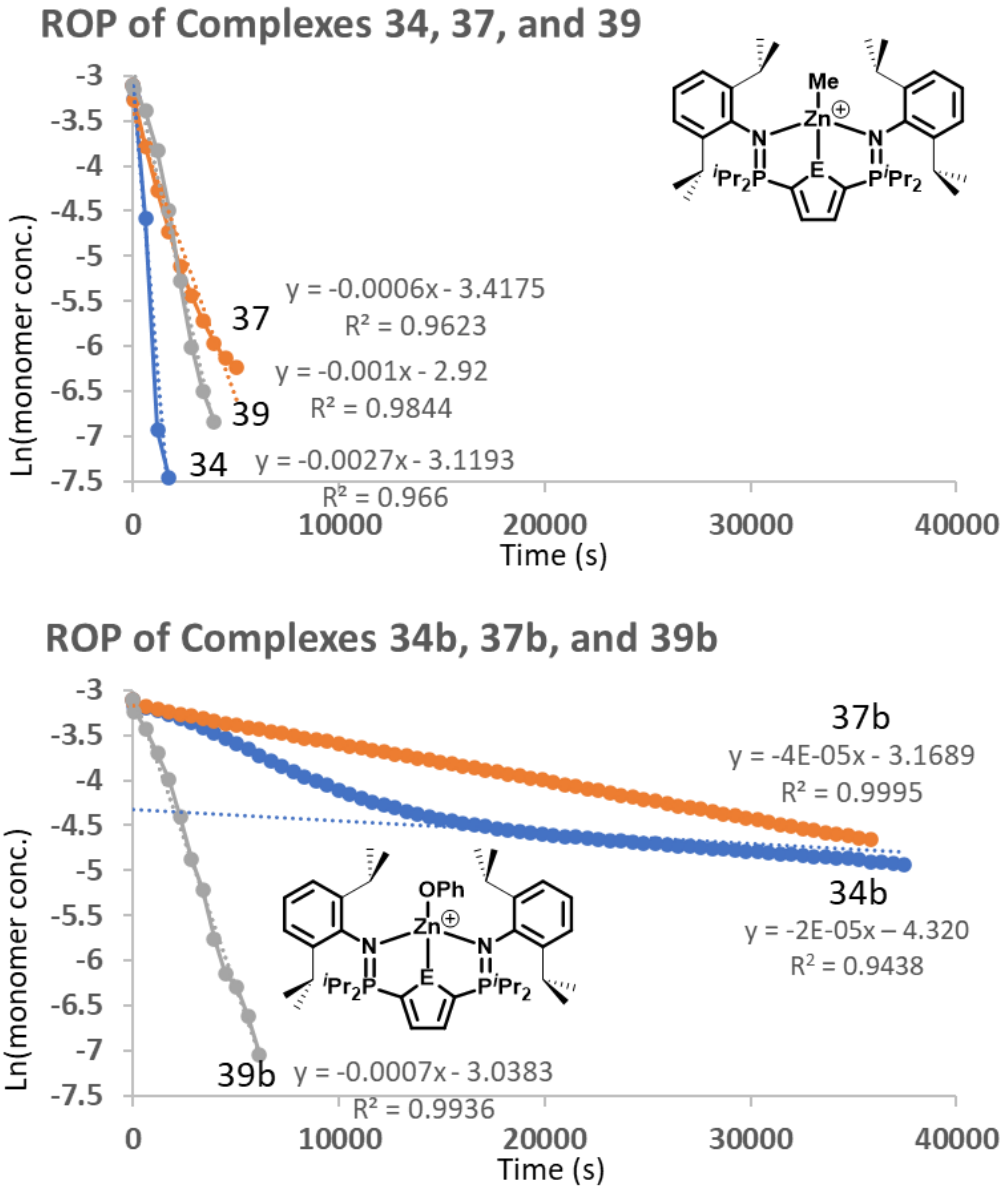

Figure 2.21: Plot of In[A] versus t for polymerization of ε-caprolactone at 70 °C over an 11 h period. Cationic zinc methyl complexes **34**, **37**, and **39** are depicted on the top graph and cationic zinc phenoxy complexes **34b**, **37b**, and **39b** on the bottom graph. k' (10^{-4}) = 27.3 s^{-1} (**34**), 6.36 s^{-1} (**37**), 10.2 s^{-1} (**39**), 0.248 s^{-1} (**34b**), 0.419 s^{-1} (**37b**), 6.56 s^{-1} (**39b**).

The cationic zinc methyl complexes catalysed ROP remarkably quickly, with the swiftest reaction rate for the investigated complexes occurring for **34** (k' (10^{-4}) = 27.3 s^{-1}, 30 min to completion) where E = O. The ROP using the cationic zinc phenoxy complexes as catalysts were mostly sluggish, except when E = Se, **39b** (k' (10^{-4}) = 6.56 s^{-1}, 1.7 h to completion).

2.6.5.4 Comparison of Polymerization Activity Data

All the rates, compound distributions, and features of the catalysts tested are displayed in Table 2.7.

Table 2.7: Tabulated results of compounds tested for ROP of ε-caprolactone at 70 °C over 11 h.

Compound	Aromatic group (Ar)	Phosphorous group (R)	Central donor (E)	Activator Ligand	Converted monomer %	1st order rate constant, *k'* (s^{-1}) (10^{-4})
33	Pipp	Ph	O	Me	23.0	0.0658
36	Pipp	Ph	S	Me	37.0	0.118
40	Pipp	iPr	Se	Me	98.3	1.17
33b	Pipp	Ph	O	OPh	5.9	0.0118
36b	Pipp	Ph	S	OPh	41.3	0.137
40b	Pipp	iPr	Se	OPh	82.7	0.469
32	Dipp	Ph	O	Me	98.1	1.63
35	Dipp	Ph	S	Me	98.0	2.10
38	Dipp	Ph	Se	Me	98.2	3.00
34	Dipp	iPr	O	Me	98.9	27.3
37	Dipp	iPr	S	Me	97.1	6.36
39	Dipp	iPr	Se	Me	98.1	10.2
32b	Dipp	Ph	O	OPh	99.0	8.33
35b	Dipp	Ph	S	OPh	98.0	5.02
38b	Dipp	Ph	Se	OPh	98.9	5.27
34b	Dipp	iPr	O	OPh	84.3	0.248
37b	Dipp	iPr	S	OPh	79.1	0.419
39b	Dipp	iPr	Se	OPh	98.1	6.56
$ZnMe_2$	-	-	-	-	33.9	0.105
MeZnOPh	-	-	-	-	98.8	28.9

As a change between chalcogen donors of a pincer ligand has not been thoroughly investigated in the literature, it was anticipated that a reliable and predictable trend would be observed between these elements. It was theorized that a better understanding of the interaction between the metal centre and the central donor M–E (E = O, S, Se) would be established by studying different chalcogen donors. Having a better understanding of the M–E interaction would help with the design of the ligand itself, as a metal centre that is bonded more tightly to the ligand is going to be better influenced by its steric bulk, providing an opportunity to develop a more refined catalytic site. A bond would also provide more electron density to the zinc centre, making it less electropositive, which would further influence its interaction with monomers. Unfortunately, X-ray quality material was not obtained, and thus, the extent of M–E interaction in the solid state was not established. In neither the ^{1}H nor $^{31}P\{^{1}H\}$ NMR spectra of the new zinc complexes, were obvious correlations between phosphorous chemical shift and interaction between the central donor, E, and zinc, observed. Unfortunately, the polymerization data did not reveal a discernible trend, despite the initial assumption that the rate of polymerization would be proportional to the size and/or electronegativity of the chalcogen donor.

All of the complexes, where Ar = Pipp, catalysed the ROP of ε-caprolactone much slower than the analogous complexes where Ar = Dipp. The consistently fast reaction rates came from the Zn–OPh complexes were R = Ph, except for **39b** (k' (10^{-4}) = 6.56 s^{-1}, R = ^{i}Pr, E = Se). The fastest Zn–OPh containing catalyst was **32b** (k' (10^{-4}) = 8.33 s^{-1}, E = O). Alkoxide ligands are known to be more effective initiating groups than alkyl ligands when this mechanism is active,[118] where aryloxides are less effective than other alkoxides.[44, 119, 120]

Generally, the zinc methyl species were more active when R = ^{i}Pr. The superior activity of catalysts with isopropyl substituents at phosphorous is likely because of greater donation to the electron deficient zinc centre compared to the more electron withdrawing phenyl groups. Generally, the zinc phenoxide species were found to be more active when R = Ph, in contrast to the zinc methyl complexes. This might be due to the dimeric structure of the Zn–OPh containing complexes being more stabilized with the more electron donating group on phosphorous, hindering access to the metal centre. While the more electron withdrawing phenyl group destabilizes the dimeric arrangement to a certain degree in solution making the zinc centre more available for catalysis. The superior activity due to the electron donation from the isopropyl groups was observed with the methyl complexes and is consistent with literature[118] as catalyst **34** was the most active (k' (10^{-4}) = 27.3 s^{-1}, E = O), proceeding to 95% completion within one hour. The most active selenophene-based containing catalysts, **39** and **39b** (k' (10^{-4}) = 10.2 s^{-1}, and 6.56 s^{-1}) where R = ^{i}Pr, were comparable.

Bochmann and co-workers generated cationic complexes with small organozinc complexes, $ZnMe_2$ and $Zn(SiMe_3)_2$, which polymerized cyclohexane oxide (CHO) within 1 h at 0 °C to yield high MW polymers, although their PDI was considerably large (>2.0).[121] To confirm that the ancillary ligand had some influence over the catalysts ability to initiate ROP, control experiments using $ZnMe_2$ and MeZnOPh were conducted (Figure 2.22). $ZnMe_2$ exhibited a similar sluggish reaction rate (k' (10^{-4}) = 0.105 s^{-1}) to several of the Pipp containing complexes tested (**33**, **36**, **33b**, and **36b**). Surprisingly, the MeZnOPh was incredibly swift, giving the fastest pseudo first-order rate constant observed (k' (10^{-4}) = 28.9 s^{-1}) with 98% consumption of monomer within 30 min. In comparison, the magnesium complex **XV** ([**L**$_3$Mg^{n}Bu][A]) which bears an ^{n}Bu ligand, was able to catalyse ROP of ε-caprolactone within 4 min and at ambient

temperature in the same catalyst loading. The presence of the ^{n}Bu group in the resulting polymer provided evidence that a coordination-insertion mechanism was operative (see A, Scheme 1.2).

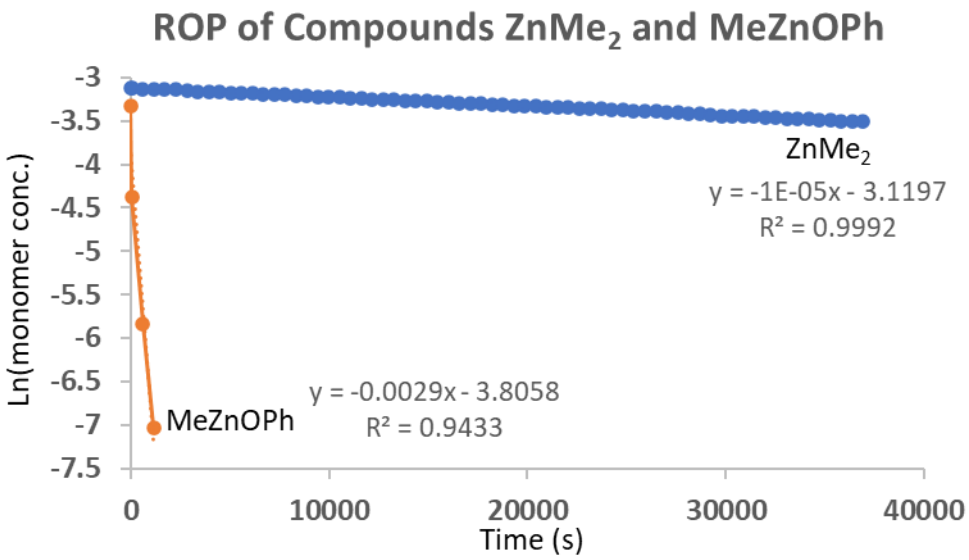

Figure 2.22: Plot of In[A] versus t for polymerization of ε-caprolactone at 70 °C over an 11 h period with $ZnMe_2$ and MeZnOPh as catalysts. k' (10^{-4}) = 0.105 s^{-1} ($ZnMe_2$), 28.9 s^{-1} (MeZnOPh).

Clearly the furan-, thiophene-, and selenophene-based bisphosphinimine *NEN*-pincer ligands greatly increased the reaction rate of ROP when using a cationic zinc methyl centre, but substantially hindered those of the cationic zinc phenoxide containing compounds, likely due to dimer formation.

The magnesium complex **XV** participates in a coordination-insertion mechanism due to the presence of the ^{n}Bu in the isolated polymer generated.[98] Since the literature suggests that alkyl groups are poor initiators,[44, 120] the Zn–OPh complexes were theorized to be more active than the Zn–Me complexes. But, with the ancillary ligand system investigated herein, the zinc methyl centre gives catalysts that are more active. Analogues complexes bearing dbf-based bisphosphinimine *NON*-pincer ligands ([**L**$_3$ZnMe][A], **XIVb**)[94] were inert to initiating ROP of lactide. The activity of complexes **32**-**40** and **32b**-**40b** could be related to the accessibility of the cationic zinc

metal centre and is independent of the substituent on zinc but mechanisms cannot be confirmed without polymer end group analysis.

2.7 Concluding Statement and Future Work with Zinc Complexes

A new neutral bisphosphinimine *NEN*-pincer ligand (2,5-(ArN=PR_2)C_4H_2E, E = O **3-8**, E = S **11-14**, and E = Se **17-18**) series has been developed. These unique ligands feature two phosphinimine functionalities which have been utilized to generate stable cationic zinc methyl and phenoxide complexes.

As the solid-state structures of the cationic zinc complexes bearing dbf-based bisphosphinimine *NON*-pincer ligands is varied, some showing bonds between Zn–O and some not, the interaction likely differs in solution and solid-state data is insufficient to ascertain the Zn–E relationship. There was no observable trend between the central ligand donors (oxygen, sulfur, selenium) and the degree if interaction with the metal centre in the complexes studied within this thesis. Therefore, no concrete statement can be made about the exact influence the central donor has on ROP. Differences were observed in the pseudo first-order rate constant in the ROP of ε-caprolactone when the central donor was changed so the Zn–E interaction is clearly important to some degree. As previously reported, a more electron donating ancillary ligand increases catalytic activity.[122-124] This is also the case with the investigated ligand system as even small change in electron donating effects, such as changing R = ^{i}Pr to R = Ph on the phosphorus atoms, caused an increase in activity for the zinc methyl complexes, and a decrease for the phenoxide complexes.

Succinct suggestions for future work include the use of cationic zinc methyl complexes bearing neutral bisphosphinimine *NEN*-pincer ligands where E = O and

R = ^{i}Pr, which produced the most active catalyst, and explore changes in the Ar substituent. Further changes of the Ar group include different steric bulk (such as Mes, Bn, or *tert*-butyl containing aryl groups). Also exploring the electron richness at the metal centre versus ROP activity by using electron withdrawing or electron donating aryl groups, with substituents such as CF_3, *tert*-butyl, or NMe_2. Work with ROP reactions with other substrates to determine which one best fits this system; cyclic ethers cyclohexene oxide (CHO) and propylene oxide (PO) are common investigative alternatives. This would be valuable because catalysts, that were shown in section 1.4, often catalysed one substrate more efficiently than others, so there could be another substrate that the system explored in Part I is more active towards.

Finally, the fact that small organozinc compounds, as simple as the zinc alkoxide starting material, MeZnOPh, was extraordinarily active at ROP is of interest, especially since it is simplistic to generate and there is a lack of literature on it and similar compounds. Generation of cationic systems of MeZnOPh and related analogues, akin to Bochmann *et al*[121] could be used to determine if a cationic zinc system lacking an ancillary ligand is more or less active and what influence that has on the polymer produced. Comparing all these results to the PDI and MW would demonstrate whether this system has any control over the physical characteristics of the polymer.

For any student reading this, if this project is adopted in the future, adhere to a single solvent system for NMR investigations, ideally pyridine-d_5, as this produced more defined resonances than other NMR solvents; and adhere to a single weakly-coordinating anion to aid with writing up and characterizations of these compounds. This ligand system is fantastic at demonstrating all the techniques required to be a

synthetic chemist and would greatly benefit any student looking at joining the Hayes group.

2.8 Cationic Calcium Complexes Supported by *NEN*-Pincer Ligands (E = O, S)

As the magnesium complex **XV** ([$\mathbf{L_3}$Mg^{n}Bu][A]) was one of the more active ROP catalysts supported by the Hayes group, analogous cationic magnesium complexes with the neutral bisphosphinimine *NEN*-pincer ligands (2,5-(ArN=PR_2)C_4H_2E, E = O, S, or Se) were sought to ascertain the differences a metal centre can have on ROP. Exploratory reactions, where Mg(^{n}Bu)$_2$ was added to a bromobenzene solution of a protonated ligand [2-(ArN(H)=PR_2)-5-(ArN=PR_2)C_4H_2E][A] (**20**-**30**), afforded a mixture of inseparable products. Calcium was then deemed a suitable replacement. Calcium is considered an alkaline earth metal, differing to the chemical similarities of zinc and magnesium.[125] The larger ionic radii of calcium atoms may also be more appropriate with the *NEN*-pincer ancillary ligand in question and mitigate the shuttling of the metal centre between phosphinimine groups which may interfere with polymerization and make the properties of the ancillary ligand more constant.

The initial challenge was to determine the appropriate calcium containing compound to be used as starting material. Ideally the starting material can undergo alkane elimination, akin to the production of **32**-**40**. Analogous alkyl calcium complexes of zinc ($CaMe_2$ or $CaEt_2$) are not readily available, nor are they well described in the literature,[126, 127] and so, alternatives were sought. The use of calcium amides was considered as amine elimination might occur upon reaction with a protonated ligand. The readily available and affordable amine bis(trimethylsilyl)amine or hexamethyldisilazane, abbreviated as HMDS–H as the amine, and HMDS as the amide, was commercially available, along with the lithium and potassium amide salt.

Addition of 2 equivalents of [K][HMDS]•THF or [K][HMDS]•Et_2O to a toluene solution of calcium diiodide afforded the calcium starting material, $Ca(HMDS)_2$•THF or $Ca(HMDS)_2$•Et_2O (yield = 69.9%), as white powders. The ^1H NMR spectra were consistent with literature and contained one equivalent of the corresponding ether from the amide salt used.[128, 129] Both calcium starting materials hydrolyse in the presence of water, and accordingly, were stored in an argon filled glove box. For added precautions, they were also kept at –30 °C.

The reaction to generate the cationic calcium complexes involved the dropwise addition of $Ca(HMDS)_2$•THF or $Ca(HMDS)_2$•Et_2O in bromobenzene to a bromobenzene solution of **21** ([2-(PippN(H)=PPh_2)-5-(PippN=PPh_2)C_4H_2O][$B(C_6F_5)_4$]) or **25** ([2-(PippN(H)=PPh_2)-5-(PippN=PPh_2)C_4H_2S][$B(C_6F_5)_4$]) at ambient temperature. No discernible change was observed. The reaction mixture was left to stir for 2 h before the volatiles were removed *in vacuo* followed by heptane triturations which gave the products of double ligand substitution, [(2,5-(PippN=PPh_2)$_2$C$_4$H$_2$O)$_2$Ca][$B(C_6F_5)_4$]$_2$ (**42**, 80.1%) and [(2,5-(PippN=PPh_2)$_2$$C_4H_2S$)$_2$Ca][$B(C_6F_5)_4$]$_2$ (**43**, 75.9%) (Scheme 2.11). Elimination of both amide ligands from the calcium starting material occurred. The excess calcium starting material was removed with triturations. Double ligand substitution was apparent in the ^1H NMR spectra of **42** and **43** which only contained resonances attributed to the ancillary ligand. Any further addition of the neutral ligand, protonated ligand, or calcium starting material or altering the stoichiometry of the reagents had no effect on the reaction outcome to complexes **42** or **43**. Much like all other cationic complexes generated in Part I of this thesis, both **42** and **43** would degrade when exposed to water or air, and so were kept under an inert atmosphere where they were stable indefinitely.

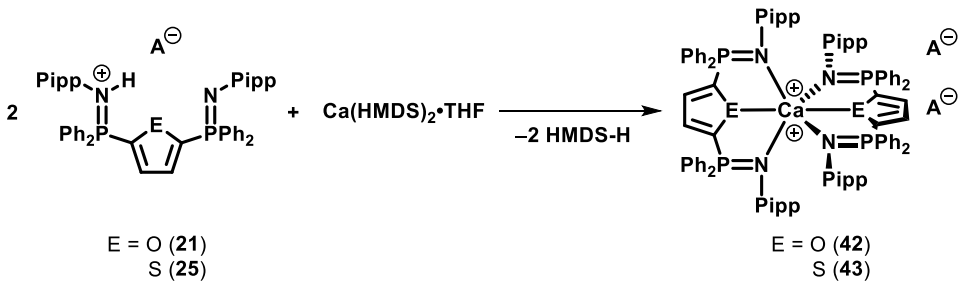

Scheme 2.11: Synthesis of dicationic calcium complexes **42** and **43**.

Crystals of compound **42** were grown from a concentrated DCM solution stored at –30 °C for 48 h. Crystals of compound **42** grew in a monoclinic crystal system in the $P2_1/n$ space group with the lattice comprising of 4 molecules (Z = 4, Z' = 1). As each molecule contained two ancillary ligands and two weakly-coordinating anions (Figure 2.23), the cell volume was notably large at 13,359.5 Å compared to the dimer **41** ([2,5-(PippN=PPh_2)$_2C_4H_2$OZnOMe][$B(C_6F_5)_4$]) (3,599.87 Å) and the phosphine **9** (2,5-(PPh_2)$_2C_4H_2$S) (1,148.66 Å).

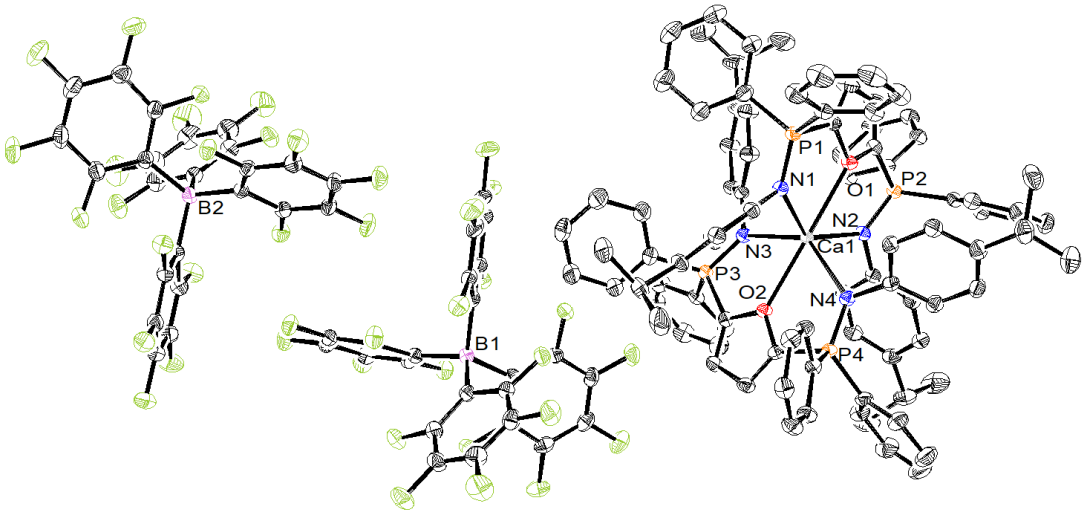

Figure 2.23: Displacement ellipsoid plot of calcium dication **42** depicted at 50% probability. Asymmetric unit (Z' = 1) is shown. Space group = $P2_1/n$, R_1 = 3.65%.

The formally dicationic calcium centre is supported by two neutral ancillary ligands. The calcium atom is 6-coordinate and has a distorted octahedral geometry as several angles are smaller than the ideal 90° in octahedral geometries (67.71-69.66°)

and some are close to, or notably larger than, 90° (92.08-97.94° and 105.09-111.93°) (Figure 2.24). All bonds with Ca1 range between 2.395(1) Å and 2.492(1) Å and all phosphinimines retain phosphinimine character with similar P–N bond lengths (1.592-1.597 Å, Table 2.8). A reported cationic calcium complex ((2-methyl-4-^{t}Bu-trispyrazolylborate)Ca(BH_4)(THF)) has Ca–N bond lengths ranging between 2.5046-2.5335 Å.[130] Complex **42** has Ca–N bond lengths more similar to a calcium complex bearing a neutral *NNN*-pincer ligand, (Ca(bis(oxazolinylphnyl)amine)($N(SiMe_3)_2$)(THF)). Where Ca–N bond lengths range from 2.3979 Å to 2.4530 Å.[131] The *NEN*-pincer ligand is more strictly acting as a pincer ligand in **42** as the ligands are in closer proximity to the calcium centre than a trispyrazolylborate ligand would be.

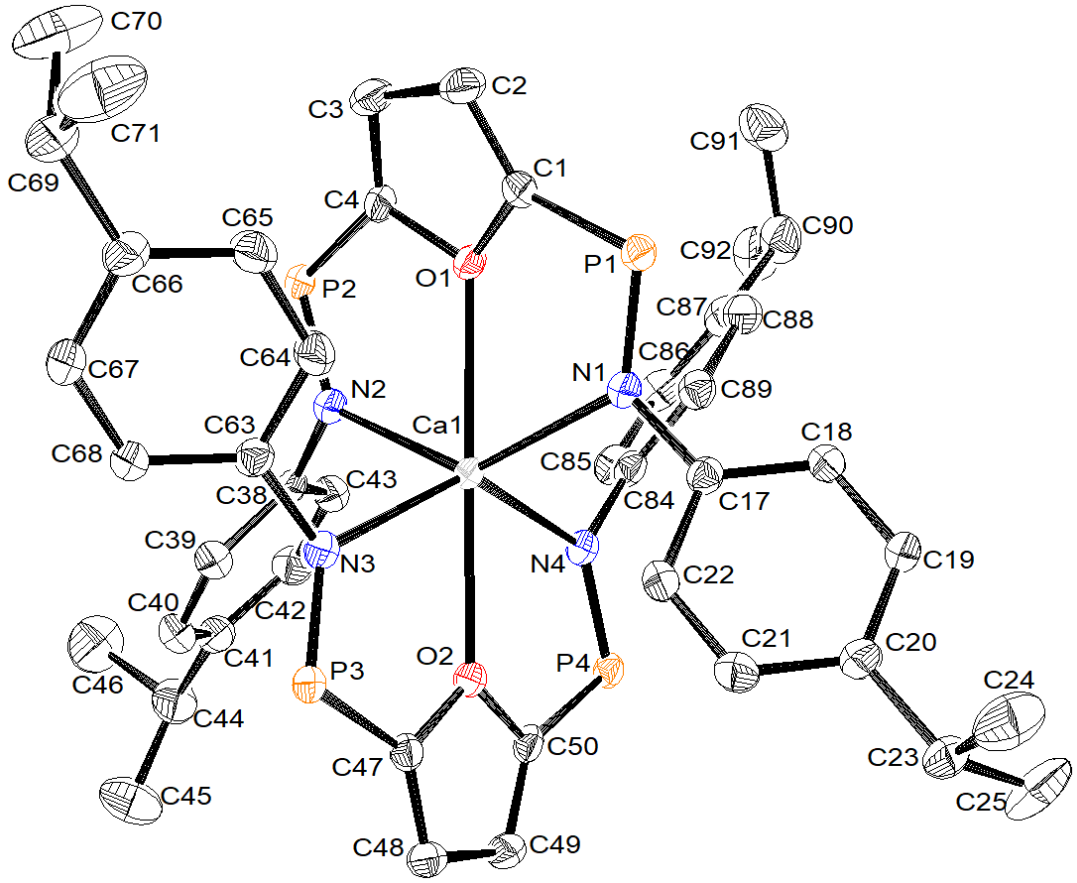

Figure 2.24: Displacement ellipsoid plot of calcium dication **42** depicted at 50% probability. Anions and phenyl groups on phosphorous removed for clarity.

Table 2.8: Selected bond lengths (Å) and angles (°) of compound **42**.

Atoms	Length (Å)	Atoms	Angle (°)	Atoms	Angle (°)
P1–N1	1.596(1)	**O1–Ca1–N1**	67.71(4)	**N2–Ca1–N3**	92.08(4)
P2–N2	1.595(1)	**O1–Ca1–N2**	69.66(4)	**N2–Ca1–N4**	95.61(4)
P3–N3	1.592(1)	**O1–Ca1–N3**	111.93(4)	**O1–Ca1–O2**	178.72(4)
P4–P4	1.597(1)	**O1–Ca1–N4**	111.22(4)	**N3–Ca1–N4**	136.15(4)
Ca1–O1	2.492(1)	**O2–Ca1–N1**	111.10(4)	**N1–Ca1–N2**	137.34(4)
Ca1–O2	2.457(1)	**O2–Ca1–N2**	111.54(4)		
Ca1–N1	2.482(1)	**O2–Ca1–N3**	67.77(4)		
Ca1–N2	2.395(1)	**O2–Ca1–N4**	69.26(4)		
Ca1–N3	2.477(1)	**N1–Ca1–N3**	105.09(4)		
Ca1–N4	2.425(1)	**N1–Ca1–N4**	97.94(4)		

When attempting to crystalize **43** by storing a concentrated solution of the complex in DCM at –30 °C for 48 h, a small number of crystals formed. The identity of the crystals was established to be $[(2,5\text{-}(PippN{=}PPh_2)_2C_4H_2S)_2CaNSiMe_3]_2[B(C_6F_5)_4]_2$ (**43b** Scheme 2.12).

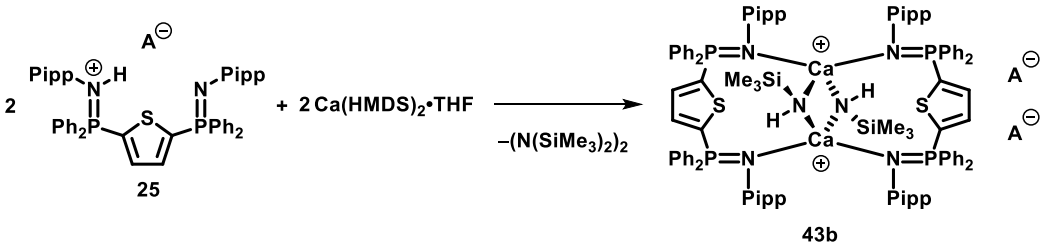

Scheme 2.12: Synthesis of dicationic calcium complex **43b** as a minor product to **43**.

Crystals of compound **43b** grew in a triclinic crystal system in the $P\bar{1}$ space group with the lattice comprising of 2 molecules (Z = 2, Z' = 1). The P–N bond lengths (1.601(2) Å and 1.598(2) Å) are slightly elongated compared to those in **42**. The calcium metal centre conforms to a pseudo-tetrahedral geometry as one angle, N3–Ca1–$N3^i$, is less than 109.5° (81.56(6)), the rest are larger than 109.5° (113.06-117.22°) (Table 2.9).

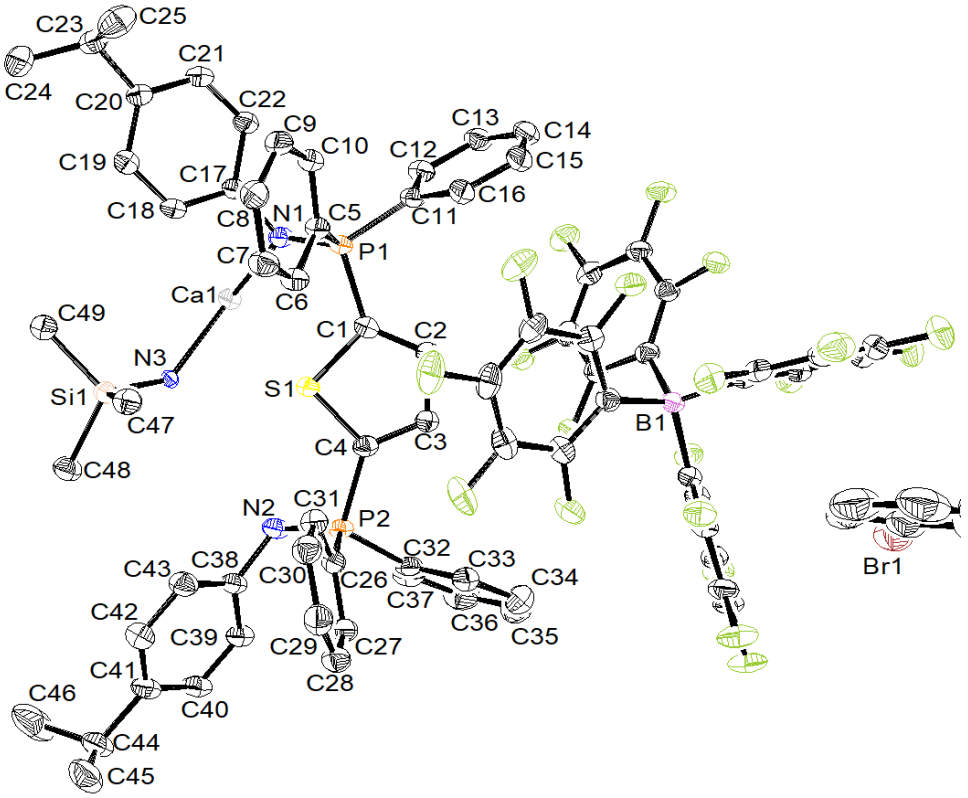

Figure 2.25: Displacement ellipsoid plot of the asymmetric unit of cationic calcium complex **43b** depicted at 50% probability. Space group = $P\bar{1}$. R_1 = 4.66%.

The 'grow' function in Olex2 allowed visualization of the entire compound (Figure 2.26). The atom N3 remains planar, with surrounding bond angles adding to 359.95° and a flat plane can be generated using Ca1, N3, Si1, $Ca1^{i}$, $N3^{i}$, and Si^{i} atoms. The crystallographic data collected for **43b** was of high quality and the depicted structure solution is of good fit, with an R_1 factor of 4.66%.

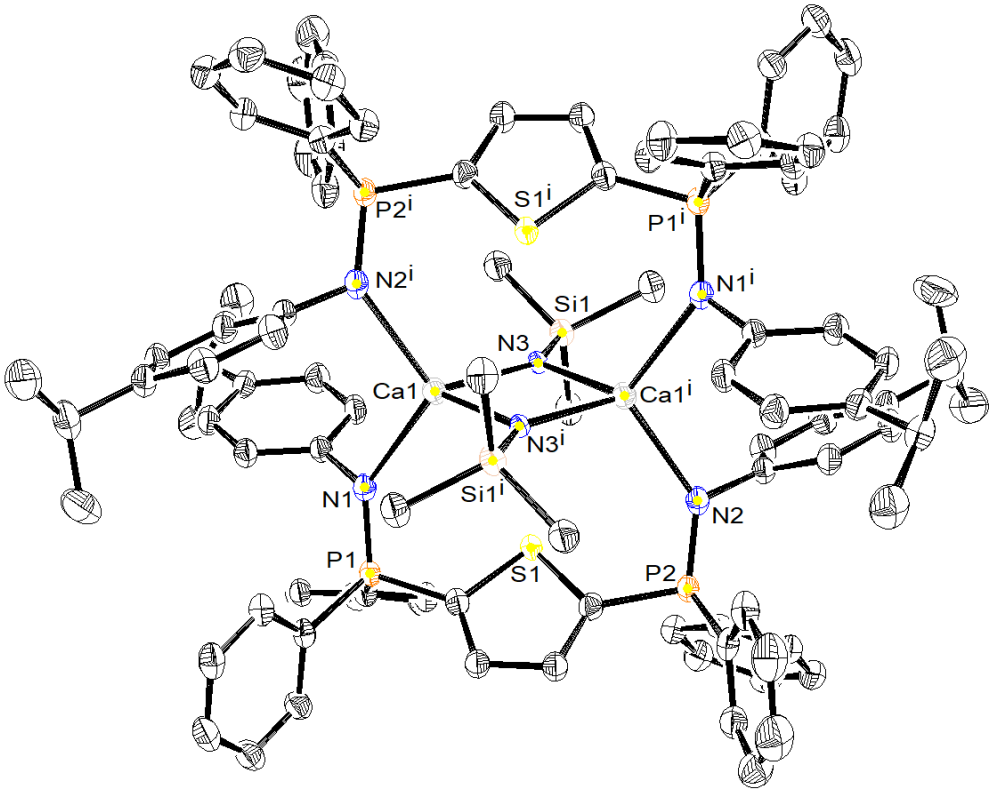

Figure 2.26: Displacement ellipsoid plot of cationic calcium complex **43b** depicted at 50% probability. Asymmetric unit grown to include complete molecule. Anions and solvent removed for clarity.

Table 2.9: Selected bond lengths (Å) and angles (°) of compound **43b**.

Atoms	Length (Å)	Atoms	Angle (°)
P1–N1	1.601(2)	**N3–Ca1–N3^{i}**	81.56(6)
P2–N2	1.598(2)	**N1–Ca1–N3**	114.29(6)
Ca1–N1	2.406(2)	**N1–Ca1–N3^{i}**	117.22(6)
Ca1–N2^{i}	2.415(2)	**N1–Ca1–N3^{i}**	117.22(6)
Ca1–N3	2.237(2)	**N2^{i}–Ca1–N3^{i}**	113.06(6)
Ca1–N3^{i}	2.264(2)	**N2^{i}–Ca1–N3**	115.22(6)
N3–Si1	1.632(2)	**Ca1–N3–Ca1^{i}**	98.35(6)
		Ca1–N3–Si1	140.04(9)
		Ca1^{i}–N3–Si1	121.56(8)

Addition of **20** to Ca(HMDS)$_2$•THF in deuterated bromobenzene at ambient temperature gave [(2,5-(DippN=PPh$_2$)$_2$C$_4$H$_2$O)$_2$CaNSiMe$_3$]$_2$[B(C$_6$F$_5$)$_4$]$_2$ (**44**) as indicated by ^{1}H, ^{13}C{^{1}H}, and ^{31}P{^{1}H} spectroscopy (Scheme 2.13). One resonance in

the $^{31}P\{^{1}H\}$ NMR spectrum was identified at δ –24.6. In the ^{1}H NMR spectrum, a single chemical environment pertaining to a $SiMe_3$ group at δ –0.01 was noted. Integrations of the resonances in the ^{1}H NMR spectrum indicated that the signal at δ –0.01 integrated for 9H. This suggested that a –$SiMe_3$ group was retained, and therefore it is postulated that **44** is isostructural to **43b**.

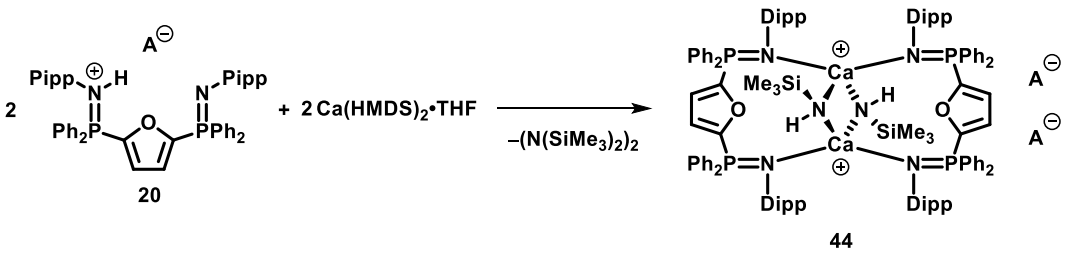

Scheme 2.13: Synthesis of dicationic calcium complex **44**.

Calcium is undoubtably cationic, but as there is only two weakly-coordinating anions, and so two anionic charges must be accounted for in the dimer. A theory is that the –$NSiMe_3$ group is in fact a –$N(H)SiMe_3$ group, although, the proton could not be found from residual densities. A possible mechanism to **44** is depicted (Scheme 2.14).

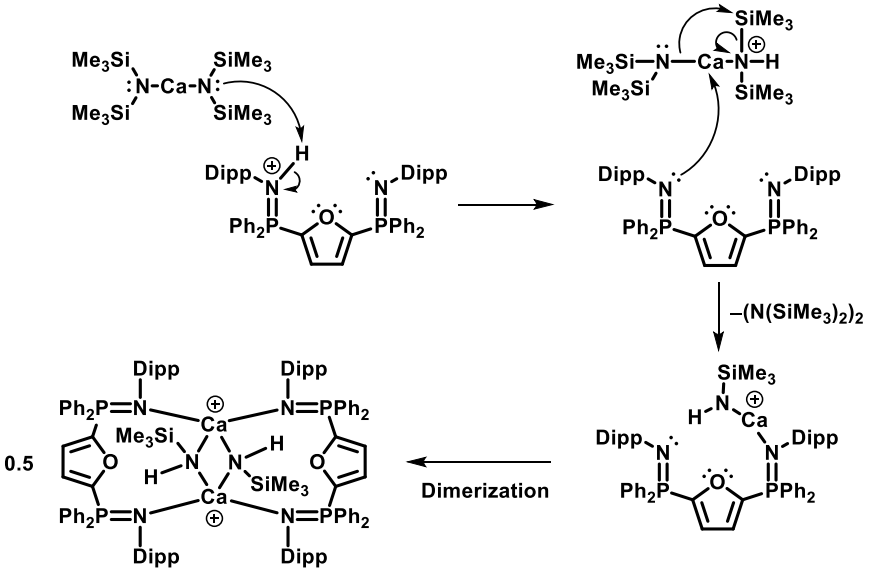

Scheme 2.14: Possible mechanism for the generation of **44** from **20**. Anions removed for clarity.

2.8.1 Concluding Statement and Future Work with Calcium Complexes

Continuing this work would involve further manipulation of the aromatic group, Ar, in attempts to reliably reproduce similar compounds to **43b** and **44**, with groups such as Mes, Bn, or *tert*-butyl containing aryl substituents which may promote or hinder formation to complexes like **42** and **43**. Also exploring the electron richness at the metal centre by using electron withdrawing or electron donating aryl groups, with substituents such as CF_3, *tert*-butyl, or NMe_2 to see if that affects the reaction outcome. Alternative amides bearing different alkyl groups may prevent dimer formation. If a monomer is generated with an accessible amide group, ROP of cyclic esters could be undertaken as amides have been reported to be good initiating groups.[103]

To avoid the congested structure in complex **42**, other group 2 elements, such as strontium and barium could be used in place of calcium as their silylamide starting materials, $Sr(N(SiMe_3)_2)_2$ and $Ba(N(SiMe_3)_2)_2$ are known.[128, 129] Both strontium and barium have larger ionic radii compared to calcium which may hinder bond formation with the phosphinimine groups of the same ligand and more reliably generate complexes akin to **43b** and **44**.

Chapter 3: Experimental and Supporting Information

3.1 Experimental Considerations

3.1.1 General Equipment

Manipulation of oxygen– and moisture–sensitive materials and reagents was carried out in the absence of air and moisture either using a double manifold vacuum line and corresponding techniques,[132] or in an MBraun Labmaster 130 glove box (argon), unless otherwise specified. All vacuum lines and glove box antechambers were evacuated using an Edwards RV12 pump. Specialty glassware designed for this work included swivel frit apparati and thick walled (5 mm) glass bombs, herein referred to as bombs, equipped with Kontes® valves. Glass utilized in experimental procedures was stored in a 115 °C oven for a minimum of 12 h or heated directly via a Bunsen burner whereupon the glass was assembled on the vacuum line or placed in the antechamber and evacuated while hot.

3.1.2 Solvents

All solvents utilized in air and moisture sensitive reactions were either obtained from an MBraun Solvent Purification System (SPS), EMD Chemicals, Inc or Millipore Sigma. Non-halogenated solvents (benzene, toluene, pentane, heptane, THF, and diethyl ether) were further degassed, dried over molecular sieves (3 Å), before being transferred to 500 mL bombs charged with Na/benzophenone for storage.[133] Halogenated solvents (chloroform, dichloromethane, and bromobenzene) were degassed before being dried and stored over CaH_2 under static vacuum in 500 mL bombs. Solvents were transferred to their receiving flask under reduced pressure and temperature (–78 °C). Solvents used in synthetic procedures that were impervious to

air and moisture were acquired from EMD Chemicals, Inc or Millipore Sigma and used without further purification. Deuterated solvents used for NMR spectroscopy were dried and stored over either Na/benzopehenone (pyridine-d_5, benzene-d_6 (C_6D_6), toluene-d_8, THF-d_8) or CaH_2 (chloroform-d_1 ($CDCl_3$), dichloromethane-d_2 (CD_2Cl_2), bromobenzene-d_5 (C_6D_5Br)). These solvents were degassed via at least three freeze-pump-thaw cycles and distilled under reduced pressure and temperature (–78 °C) into a bomb and stored under static vacuum, for the non-halogenated solvents molecular sieves (3 Å) were also added.

3.1.3 Chemical Materials

The reagents: ^{n}BuLi (1.6 M in hexanes), ^{t}BuLi (1.7 M in hexanes), MeLi (1.6 M in diethyl ether), chlorodiphenylphosphine, chlorodiisopropylphosphine, furan, thiophene, 2,5-dibromothiophene, and 2,5-dibromoselenophene, were purchased from Sigma Aldrich and $[HNMe_2Ph][B(C_6F_5)_4]$ from Alfa Aesar and used without further purification. All deuterated solvents and reagents were purchased from Cambridge Isotope Laboratories and dried *vide supra*. The following compounds were prepared according to modified literature procedures: Dipp-N_3,[112] Pipp-N_3,[81] Mes-N_3,[112] Pm-N_3,[113] 2,5–$Br_2C_4H_2Se$,[134] and $[(Et_2O)_2H][[B(C_6H_3(CF_3)_2)_4]$.[135]

3.1.4 NMR Spectroscopy

NMR spectra (^{1}H, ^{11}B{^{1}H}, ^{13}C{^{1}H}, ^{19}F{^{1}H}, ^{29}Si{^{1}H}, ^{31}P{^{1}H}, ^{77}Se{^{1}H}, ^{1}H–^{1}H COSY, ^{1}H–^{13}C HSQC, and ^{1}H–^{13}C HMBC) were acquired on a Bruker Avance II 300 MHz spectrometer (^{1}H 300.13 MHz, ^{11}B 96.251 MHz, ^{13}C 75.47 MHz, ^{19}F 282.23 MHz, ^{29}Si 59.63 MHz, ^{31}P 121.49 MHz, ^{77}Se 57.24 MHz) or a Bruker Avance III HD 700 MHz spectrometer (^{1}H 700.13 MHz, ^{13}C 176.048 MHz, ^{19}F 658.78 MHz, ^{31}P 283.42 MHz) where stated. DOSY NMR experiments were performed on a Bruker

Avance III HD 700 MHz spectrometer equipped with a gradient controller and a TXO probe with automatic tuning and a shielded z-gradient. The gradient shape was sinusoidal, and its length was 1.8 ms. The gradient strength was increased by 16 increments of 6.2% (2%–95%). The time between the midpoints of these gradients was 99.97 ms. Experiments were performed at 292 K. NMR spectroscopic data is presented in parts per million (ppm) where ^{1}H and $^{13}C\{^{1}H\}$ shifts are referenced to tetramethyl silane through internal ^{1}H and $^{13}C\{^{1}H\}$ resonance(s), respectively, of the corresponding solvent: C_6D_6 (δ 7.16 and δ 128.0), toluene-d_8 (δ 2.09, 6.98, 7.02, 7.09 and δ 20.4, 125.2, 128.0, 128.9, 137.5), $CDCl_3$ (δ 7.27 and δ 77.36), CD_2Cl_2 (δ 5.32 and δ 53.5), THF-d_8 (δ 1.73, 3.58 and δ 25.3, 67.4), pyridine-d_5 (δ 7.22, 7.58, 8.74 and δ 123.9, 135.9, 150.4), and C_6D_5Br (δ 7.28, 7.00, 6.93, and δ 122.3, 126.1, 129.3, 130.9). ^{11}B NMR spectra were referenced to an external boron trifluoride diethyl etherate sample (δ 0). ^{19}F NMR spectra were referenced to an external trifluorotoluene sample (δ –63.7). ^{29}Si NMR spectra were referenced to an external tetramethyl silane sample (δ 0). An 85% H_3PO_4 standard with an internal C_6D_6 capillary was used to reference $^{31}P\{^{1}H\}$ spectra at 0 ppm. Data for diamagnetic compounds include the following information, when appropriate, and are reported as follows: chemical shift, multiplicity (s = singlet, d = doublet, t = triplet, q = quartet, quin = quintet, sext = sextet, sp = septet, br = broad, m = multiplet, ov = overlapping, br = broad), coupling constants (Hz), integration, assignment.

3.1.5 Elemental Analysis

CHNS elemental analyses were performed on an Elementar Americas Vario MicroCube instrument. In cases when carbon percentages were low, vanadium oxide was employed as a combustion agent.

3.1.6 X-ray Crystallography

Crystals grown for X-ray diffraction analysis were coated in Paratone oil and placed on a glass slide. Close visual inspection and selection of the crystals was aided by either a standard microscope or a polarizing light microscope. The crystal chosen for diffraction analysis was placed on a MiTeGen Dual Thickness MicroMount attached to the goniometer head. The crystal was centred on a Rigaku SuperNova diffractometer equipped with a 130 Dectris Pilatus 3R 200K-A detector, Oxford CryoStream 800 cooling system,[136] and molybdenum (MOVA) radiation source (Kα = 0.71073 Å), and copper (NOVA) radiation sources (Kα = 1.5406 Å). Experiments were performed at 100 K to reduce thermal motion of the atoms. CrysAlisPro software[137] was applied to determine unit cell parameters and SHELXTL software[138, 139] using Olex2-1.3[140] and a least squares methodology for refinement with Flack[141] and Hooft[142] parameters for absolute configuration determination. Oretp3 software[143] was used for visualization of the structure solution.

3.1.7 Ring-Opening Polymerizations

All NMR-scale polymerization procedures made use of similar methods; 1.8 μmol of a given complex was weighed into an NMR tube inside an inert atmosphere glove box, and the tube was capped with a rubber NMR tube septum. Dry, distilled ε–caprolactone (20 μL, 0.18 mmol, 100 equiv) was measured under an inert atmosphere into a 20 mL scintillation vial, followed by 0.5 mL of C_6D_5Br. The 0.18 mmol L^{-1} solution was measured in a 1 mL disposable syringe and the needle inserted through the septum of the NMR tube. The NMR tube was cooled to –78 ºC, and then the solution of ε–caprolactone in C_6D_5Br was injected into the solution, freezing on the inside of the NMR tube, the cap of which was then wrapped in parafilm. Prior to this, all appropriate

instrumental parameters were set, including the high temperature of 70 ºC using a blank sample only containing the monomer solution. The tube was quickly warmed to ambient temperature immediately prior to being injected into the NMR probe. The polymerization reactions were then monitored every 10 min for 11 h maintaining a constant temperature of 70 ºC. Conversion percentages were determined by integration of the most downfield methylene resonance (–$COOCH_2$–) of the polymer (^{1}H NMR (C_6D_6): δ 3.98 (t, $^3J_{HH}$ = 6.1 Hz, 2H) relative to those of the residual monomer (^{1}H NMR (C_6D_6): δ 3.59 (t, $^3J_{HH}$ = 6.1 Hz, 2H) as these resonances were most clearly resolved from all other monomer, polymer, catalyst, and residual solvent resonances.

3.2 Synthetic Methods and Characterizations

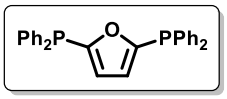

Synthesis of $(PPh_2)_2C_4H_2O$ (**1**) Diethyl ether (~40 mL) was transferred *in vacuo* to a two-necked 100 mL round-bottom flask attached to a swivel frit apparatus. Furan was injected into the flask (1.25 mL, 17.2 mmol, 0.936 g/mL), under positive argon pressure resulting in a transparent and colourless solution. The flask was cooled to –94 °C (liquid nitrogen/acetone mixture), after which ^{t}BuLi (22.2 mL, 0.0378 mol, 1.7 M) was slowly injected into the flask over the course of ~50 min. The now transparent yellow solution was then left in the cold bath to slowly warm to ambient temperature slowly followed by 3 h of constant stirring. Afterwards a pale-yellow precipitate was observed, and the flask was once again cooled to –94 °C. Cl–PPh_2 (6.48 mL, 0.0361 mol, 1.23 g/mL) was then injected into the flask over the course of 20 min. The now yellow-orange solution was then left to warm up slowly to ambient temperature while remaining in the cold bath under an argon atmosphere with constant stirring. 1 h after the injection of the phosphine, the solution turned orange-brown, and a thick precipitate formed. The reaction was left for 16 h at

ambient temperature under a flow of argon. Volatiles were removed *in vacuo* affording a brown waxy solid. Toluene (~40 mL) was then distilled into the flask, resulting in a brown opaque solution. The opaque solution was filtered through a glass frit, resulting in a transparent brown solution, and an off-white solid was collected on the frit. The solvent was removed *in vacuo*, resulting in a brown waxy solid. The product was crystallized from toluene at –30 °C as light-brown plates and the mother liquor removed by filtration to yield the desired product. Yield: 5.55 g, 73.9%. ^{1}H NMR (300 MHz, C_6D_6): δ 7.40 (m, 8H, *ortho*-Ph), 7.06-6.95 (br ov m, 12H, *meta*/*para*-Ph), 6.59 (dd, $^{3}J_{HP}$ = 4.8 Hz, $^{4}J_{HP}$ = 2.1 Hz, 2H, C_4H_2O). ^{13}C{H} NMR (75 MHz, C_6D_6): δ 158.6 (d, $^{1}J_{CP}$ = 25.6 Hz, C_2/C_5-furan), 136.8 (d, $^{2}J_{CP}$ = 6.7 Hz, *ortho*-Ph), 133.8 (d, $^{1}J_{CP}$ = 19.8 Hz, *ipso*-Ph), 128.9 (s, *para*-Ph), 128.7 (d, $^{4}J_{HP}$ = 4.6 Hz, *meta*-Ph), 123.0 (dd, $^{2}J_{CP}$ =28.1 Hz, $^{3}J_{CP}$ = 6.7 Hz, C_3/C_4-furan). ^{31}P{H} NMR (122 MHz, C_6D_6): δ –24.7 (s). Anal. Calcd for $C_{28}H_{22}OP_2$: C 77.06; H 5.08. Found: C 77.09; H 5.32.

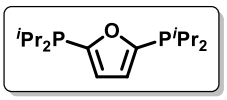

Synthesis of $(P^iPr_2)_2C_4H_2O$ (**2**) Diethyl ether (~40 mL) was transferred *in vacuo* to a two-necked 100 mL round-bottom flask attached to a swivel frit apparatus. Furan was injected into the flask (0.53 mL, 7.34 mmol, 0.936 g/mL), under positive argon pressure, resulting in a transparent and colourless solution. The flask was cooled to –94 °C (liquid nitrogen/acetone mixture), after which ^{t}BuLi (9.50 mL, 16.2 mmol, 1.7M) was slowly injected into the flask over the course of ~50 min. The still clear and colourless solution was then left in the cold bath to slowly warm to ambient temperature followed by 3 h of constant stirring. Afterwards a pale-yellow transparent solution was observed, and the flask was once again cooled to –94 °C. Cl–P^iPr_2 (2.45 mL, 15.4 mmol, 0.959 g/mL) was then injected into the flask over the course of 20 min. The solution then left to slowly warm to ambient temperature while remaining in the cold bath under an argon atmosphere with

constant stirring. Immediately after the addition the solution turned a darker shade of yellow. An hour after the injection of the phosphine, the solution was bright yellow and after 3 h eventually turned to a bright orange/red colour. After 16 h, a deep red opaque solution with orange precipitate was observed. The ether was removed under vacuum, resulting in a deep red-purple liquid, along with bright red solid stuck to the sides of the flask. Toluene was transferred to the flask under reduced pressure, resulting in a deep red/purple opaque solution. The solution was then filtered through a glass frit, resulting in a transparent deep red-purple solution. An orange solid was collected on the frit. The solvent was removed under vacuum, resulting in a red-purple liquid. The apparatus was transferred to a glove box and the liquid was washed with heptane (4 × 2 mL). The remaining heptane was removed under vacuum. This yielded an opaque red-purple liquid confirmed to be the desired product. Yield: 1.91 g, 86.8%. ^{1}H NMR (300 MHz, C_6D_6): δ 6.64 (t, 2H, $^{3}J_{HP}$ = 4.3 Hz, C_4H_2O), 2.13 (sp, 4H, $^{3}J_{HH}$ = 7.0 Hz, $CH(CH_3)_2$), 1.05 (ov dd, 24H, $^{3}J_{HP}$ = 15.9, $^{3}J_{HH}$ = 7.0 Hz, $CH(CH_3)_2$). $^{13}C\{^{1}H\}$ NMR (75 MHz, C_6D_6): δ 158.1 (dd, $^{3}J_{CP}$ = 90.2 Hz, $^{4}J_{CP}$ = 3.3 Hz, C_2/C_5-furan), 123.6 (dd, $^{2}J_{CP}$ = 64.8 Hz, $^{3}J_{CP}$ = 16.8 Hz, C_3/C_4-furan), 23.8 (d, $^{3}J_{CP}$ = 21.4 Hz, $CH(CH_3)_2$), 20.4 (dd, $^{3}J_{CP}$ = 44.8 Hz, $CH(CH_3)_2$). $^{31}P\{^{1}H\}$ NMR (122 MHz, C_6D_6): δ –9.9 (s). Anal. Calcd for $C_{16}H_{24}OP_2$: C 63.98; H 10.07. Found: C 63.41; H 9.79.

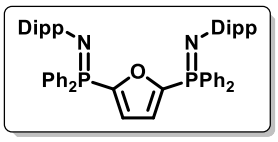

Synthesis of $(DippN{=}PPh_2)_2C_4H_2O$ (**3**) Under argon **1** (520 mg, 1.19 mmol) was added to a two-necked 50 mL round-bottom flask. Toluene (~20 mL) was distilled into the flask under *in vacuo* and the flask was then placed under an argon atmosphere. Dipp-N_3 (484 mg, 2.38 mmol) was injected into the flask under positive argon pressure, resulting in a dark-brown solution. The solution was left for 16 h at ambient temperature under constant stirring, after which no further change was observed. The solvent was removed under vacuum, yielding a dark-

brown oil, after which the oil was brought into a glove box and triturated with heptane (4 × 10 mL). The remaining heptane was removed under vacuum. This yielded a light-brown solid. Yield: 841 mg, 89.7%. ^{1}H NMR (300 MHz, C_6D_6) δ 7.62 (dd, $^{3}J_{HP}$ = 12.3 Hz, $^{3}J_{HH}$ = 7.0 Hz, 8H, *ortho*-Ph), 7.28 (m, 4H, *meta*-Dipp), 7.15–6.93 (ov m, 14H, *meta*/*para*-Ph and *para*-Dipp), 6.62 (s, 2H, $(Ph_2P{=}NDipp)_2$–C_4H_2O), 3.55 (sp, $^{3}J_{HH}$ = 6.8 Hz, 4H, Dipp-C*H*$(CH_3)_2$), 1.10 (d, $^{3}J_{HH}$ = 6.8 Hz, 24H, Dipp-CH(C*H*$_3)_2$). ^{13}C{^{1}H} NMR (75 MHz, C_6D_6) δ 155.8 (d, $^{1}J_{CP}$ = 92.1 Hz, C_2/C_5-furan), 143.5 (d, $^{2}J_{CP}$ = 17.5 Hz, *ipso*-Dipp), 143.1 (s, *ortho*-Dipp), 133.8 (d, $^{1}J_{CP}$ = 104.2 Hz, *ipso*-Ph), 132.3 (d, $^{2}J_{CP}$ = 9.8 Hz, *ortho*-Ph), 132.5 (s, *para*-Ph), 129.0 (d, $^{4}J_{CP}$ = 2.3 Hz, *meta*-Ph), 123.7 (s, *meta*-Dipp), 123.6 (m, C_3/C_4-furan), 121.0 (s, *para*-Dipp), 29.5 (s, Dipp-CH(*C*H$_3)_2$), 24.3 (s, Dipp-*C*H$(CH_3)_2$). ^{31}P{^{1}H} NMR (122 MHz, C_6D_6) δ –22.5 (s). Anal. Calcd. for $C_{52}H_{56}N_2OP_2$: C 79.36; H 7.17; N 3.56; found: C 79.31; H 7.14; N 3.49.

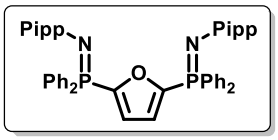

Synthesis of $(PippN{=}PPh_2)_2C_4H_2O$ (**4**) In a glove box, **1** (612 mg, 1.40 mmol) was added to a two-necked 50 mL round-bottom flask containing toluene (~20 mL). Pipp-N_3 (452 mg, 2.81 mmol) was injected into the flask under positive argon pressure, resulting in a dark-brown solution. The solution was left for 16 h at ambient temperature with constant stirring, after which no further change was observed. The solvent was removed under vacuum, yielding a dark-brown oil, after which the oil was brought into a glove box and triturated with heptane (4 × 10 mL). The remaining heptane was removed under vacuum. This yielded a light-brown solid. Yield: 911 mg, 92.4%. ^{1}H NMR (300 MHz, C_6D_6): δ 7.80 (dd, 8H, $^{3}J_{HP}$ = 12.7 Hz, $^{3}J_{HH}$ = 7.7 Hz, *ortho*-Ph), 7.24 (d, 4H, $^{3}J_{HH}$ = 7.7 Hz, *meta*-Pipp), 7.07-6.89 (ov m, 16H, *meta*/*para*-Ph, *ortho*-Pipp), 6.66 (s, 2H, C_4H_2O), 2.78 (sp, 2H, $^{3}J_{HH}$ = 6.8 Hz, Pipp-C*H*$(CH_3)_2$), 1.22 (d, 12H, $^{3}J_{HH}$ = 6.8 Hz, Pipp-CH(C*H*$_3)_2$).

$^{13}C\{^{1}H\}$ NMR (75 MHz, C_6D_6): δ 155.0 (d, J_{CP} = 42.6 Hz, C_2/C_5-furan), 149.0 (s, *ipso*-Pipp), 138.7 (s, *para*-Pipp), 132.9 (d, $^{2}J_{CP}$ = 3.9 Hz, *ortho*-Ph), 132.2 (s, *meta*-Ph), 131.1 (d, $^{1}J_{CP}$ = 49.9 Hz, *ipso*-Ph), 129.2 (s, *ortho*-Pipp), 127.6 (s, *para*-Ph), 124.3 (s, *meta*-Pipp), 123.4 (d, $^{2}J_{CP}$ = 9.7 Hz, C_3/C_4-furan), 34.2 (s, Pipp-*C*H(CH_3)$_2$), 25.0 (s, Pipp-CH(*C*H_3)$_2$). $^{31}P\{^{1}H\}$ NMR (122 MHz, C_6D_6): δ –13.4 (s). Anal. Calcd. for $C_{48}H_{44}N_2OP_2$: C 78.61; H 6.31; N 3.99; found: C 78.59; H 6.36; N 3.92.

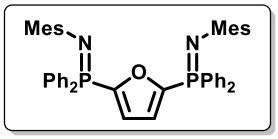

Synthesis of (MesN=PPh_2)$_2C_4H_2O$ (**5**) In a glove box, **1** (129 mg, 0.146 mmol) was added to a two-necked 50 mL round-bottom flask containing toluene (~20 mL). Mes-N_3 (102 mg, 0.292 mmol) was added to the stirring mixture, yielding a brown solution. Under constant stirring, the solution was allowed to react for 18 h at 50 ºC producing a reddish-brown solution. The solvent was removed under vacuum, producing a reddish-brown oil. The oil was left to stir in pentane overnight leaving a brown powder. The pentane was decanted and all remaining volatiles were removed *in vacuo* to yield a light-brown solid. Yield: 71.9 mg, 64.6%. ^{1}H NMR (300 MHz, C_6D_6): δ 7.68 (dd, 8H, $^{3}J_{HH}$ = 7.6 Hz, $^{3}J_{HP}$ = 12.9 Hz, *ortho*-Ph), 7.03 (t, 4H, $^{3}J_{HH}$ = 7.6 Hz, *para*-Ph), 6.96 (dd, 8H, $^{3}J_{HH}$ = 7.6 Hz, $^{3}J_{HH}$ = 2.9 Hz, *meta*-Ph), 6.54 (s, 2H, C_4H_2O), 6.94 (s, 4H, *meta*-Mes), 2.29 (d, 6H, $^{4}J_{HH}$ = 1.8 Hz, *para*-Mes-CH_3), 2.21 (s, 12H, *ortho*-Mes-CH_3). $^{13}C\{^{1}H\}$ NMR (75 MHz, C_6D_6): δ 155.1 (d, $^{1}J_{CP}$ = 45.7 Hz, C_2/C_5-furan), 143.7 (s, *ipso*-Mes), 133.0 (d, $^{1}J_{C\text{-}P}$ = 48.5 Hz, *ipso*-Ph), 131.8 (d, $^{3}J_{CP}$ = 3.3 Hz, *ortho*-Mes), 131.8 (d, $^{2}J_{CP}$ = 4.3 Hz, *ortho*-Ph), 131.1 (d, $^{4}J_{CP}$ = 1.1 Hz, *para*-Ph), 128.2 (d, $^{4}J_{CP}$ = 5.7 Hz, *meta*-Mes), 128.0 (s, *para*-Mes), 128.0 (s, *meta*-Ph), 122.2 (d, $^{2}J_{CP}$ = 10.2 Hz, C_3/C_4-furan), 21.00 (s, *ortho*-Mes), 20.6 (s, *para*-Mes). $^{31}P\{^{1}H\}$ NMR (75 MHz, C_6D_6): δ –25.9 (s). Anal. Calcd. for $C_{46}H_{44}N_2OP_2$; C 78.61; H 6.33; N 3.99; found: C 78.54; H 6.28; N 3.94.

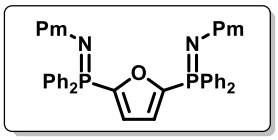

Synthesis of (PmN=PPh$_2$)$_2$C$_4$H$_2$O (**6**) In a glove box, **1** (400.0 mg, 0.917 mmol) and 3,5-dimethyl-1-tetrazolopyrimidine (273 mg, 1.83 mmol) were added to a 100 mL round-bottom flask. Toluene (~40 mL) was transferred in *vacuo* to the round-bottom flask generating a yellow suspension. The mixture was stirred at ambient temperature for 16 h under an argon atmosphere. This yielded a clear tan solution with no solid remaining. Afterwards, the toluene was removed under vacuum, resulting in a bright yellow-orange solid. Yield: 476 mg, 76.4%. ^{1}H NMR (300 MHz, C_6D_6): δ 7.85 (dd, 8H, $^3J_{HP}$ = 12.9 Hz, $^3J_{HH}$ = 7.3 Hz, *ortho*-Ph), 7.16 (m, 2H, C$_4$*H*$_2$O), 7.07-6.87 (ov m, 12H, *meta*/*para*-Ph), 5.97 (s, 2H, *para*-Pm), 2.05 (s, 12H, *meta*-Pm-C*H*$_3$). ^{13}C{^{1}H} NMR (75 MHz, C_6D_6): δ 168.2 (s, *ipso*-Pm), 167.1 (s, *meta*-Pm), 152.0 (d, $^1J_{CP}$ = 51.0 Hz, *ipso*-Ph), 133.7 (d, $^2J_{CP}$ = 7.2 Hz, *ortho*-Ph), 132.0 (d, $^3J_{CP}$ = 2.1 Hz, *meta*-Ph), 130.1 (d, $^1J_{CP}$ = 42.9 Hz), 129.0 (s, *para*-Ph), 124.7 (d, $^2J_{CP}$ = 9.9 Hz, C$_3$/C$_4$-furan), 110.0 (s, *para*-Pm), 24.0 (s, *meta*-Pm-CH$_3$). ^{31}P{^{1}H} NMR (122 MHz, C_6D_6): δ 13.3 (s). Anal. Calcd. for $C_{40}H_{36}N_6OP_2$; C 70.79; H 5.35; N 12.38; found: C 70.66; H 5.32; N 12.47.

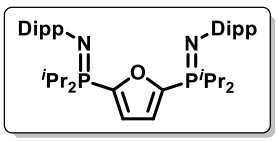

Synthesis of (DippN=P^{i}Pr$_2$)$_2$C$_4$H$_2$O (**7**) In a glove box **2** (540 mg, 1.80 mmol) was added to a two-necked 50 mL round-bottom flask containing toluene (~20 mL). Dipp-N$_3$ (731 mg, 3.60 mmol) was injected into the flask under positive argon pressure, causing the deep red solution to turn an opaque brown. Vigorous bubbling was observed. The solution was left for 16 h at ambient temperature under constant stirring, after which no change was observed. The solvent was removed under vacuum, yielding a brown waxy solid, after which the material was brought into a glove box and triturated with pentane (3 × 6 mL). The remaining pentane was removed under vacuum. This yielded a brown solid. Yield: 934 mg, 79.8%. ^{1}H NMR (300 MHz, C_6D_6) δ 7.23 (br dd, $^3J_{HH}$ = 7.2 Hz, $^5J_{HP}$ = 0.9 Hz,

4H, *meta*-Dipp), 7.09 (br dt, $^{3}J_{HH}$ = 7.2 Hz, $^{6}J_{HP}$ = 1.4 Hz, 2H, *para*-Dipp), 6.85 (br s, 2H, C_4H_2O), 3.51 (sp, $^{3}J_{HH}$ = 6.8 Hz, 4H, Dipp-C*H*$(CH_3)_2$), 2.25 (ov sp, $^{3}J_{HH}$ = 7.1 Hz, 4H, P–C*H*$(CH_3)_2$), 1.31 (d, $^{3}J_{HH}$ = 6.8 Hz, 24H, Dipp-CH(C*H*$_3)_2$), 1.11 (dd, $^{3}J_{HP}$ = 15.9 Hz, $^{3}J_{HH}$ = 7.1 Hz, 12H, P–CH(C*H*$_3)_2$), 0.91 (dd, $^{3}J_{HP}$ = 17.2 Hz, $^{3}J_{HH}$ = 7.1 Hz, 12H, P–CH(C*H*$_3)_2$). $^{13}C\{^{1}H\}$ NMR (75 MHz, C_6D_6) δ 153.4 (dd, $^{1}J_{CP}$ = 92.7, $^{4}J_{CP}$ = 2.1 Hz, C_2/C_5-furan), 145.0 (s, *ortho*-Dipp), 142.1 (d, $^{2}J_{CP}$ = 6.1 Hz, *ipso*-Dipp), 123.4 (d, $^{5}J_{CP}$ = 1.1 Hz, *para*-Dipp), 121.7 (dd, $^{2}J_{CP}$ = 12.1 Hz, $^{3}J_{CP}$ = 7.0 Hz, C_3/C_4-furan), 120.3 (d, $^{4}J_{CP}$ = 2.4 Hz, *meta*-Dipp), 29.5 (s, Dipp-*C*H$(CH_3)_2$), 28.6 (d, $^{1}J_{CP}$ = 73.4 Hz, P–*C*H$(CH_3)_2$), 24.2 (s, Dipp-CH(*C*H$_3)_2$), 16.9 (d, $^{2}J_{CP}$ = 2.1 Hz, P–CH(*C*H$_3)_2$), 15.9 (d, $^{2}J_{CP}$ = 3.6 Hz, P–CH(*C*H$_3)_2$). $^{31}P\{^{1}H\}$ NMR (122 MHz, C_6D_6) δ –3.3 (s). Anal. Calcd. for $C_{40}H_{64}N_2OP_2$: C 73.31; H 9.91; N 4.30; found: C 73.96; H 9.89; N 4.23.

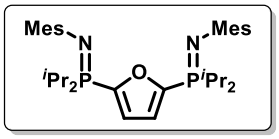

Synthesis of (MesN=P^{i}Pr$_2$)$_2$C$_4$H$_2$O (**8**) In a glove box **2** (120 mg, 0.287 mmol) was added to a two-necked 50 mL round-bottom flask containing toluene (~20 mL). Mes-N_3 (130 mg, 0.574 mmol) was added to the stirring mixture, yielding an orange-brown solution. The solution was stirred for 48 h at 70 ºC producing a red-brown solution. The solvent was removed under vacuum, affording a brown oil. The oil was dissolved in minimal pentane and left at ambient temperature where crystals grew within 24 h. The remaining pentane was decanted and the brown crystals were dried *in vacuo*. Yield: 68.4 mg, 42.0% ^{1}H NMR (700 MHz, C_6D_6): δ 7.00 (s, 4H, *meta*-Mes), 6.73 (s, 2H, C_4H_2O), 2.32 (s, 18H, *ortho*/*para*-Mes-C*H*$_3$), 2.12 (sp, 4H, $^{3}J_{HH}$ = 8.8 Hz, P–C*H*$(CH_3)_2$), 1.08 (dd, 12H, $^{3}J_{HP}$ = 23.0 Hz, $^{3}J_{HH}$ = 8.8 Hz, P–CH(C*H*$_3)_2$), 0.94 (dd, 12H, $^{3}J_{HP}$ = 24.1 Hz, $^{3}J_{HH}$ = 8.8 Hz, P–CH(C*H*$_3)_2$). $^{13}C\{^{1}H\}$ NMR (176 MHz, C_6D_6): δ 154.0 (dd, $^{4}J_{CP}$ = 2.5 Hz, J_{CP} = 2.4 Hz, C_2/C_5-furan), 145.6 (s, *para*-Mes), 131.5 (d, $^{3}J_{CP}$ = 6.6 Hz,

ortho-Mes), 129.5 (d, $^{4}J_{CP}$ = 1.5 Hz, *meta*-Mes), 127.4 (d, $^{2}J_{CP}$ = 2.8 Hz, *ipso*-Mes), 121.5 (dd, $^{2}J_{CP}$ = 18.7 Hz, $^{3}J_{CP}$ = 5.4 Hz, C_3/C_4-furan), 28.3 (d, $^{2}J_{CP}$ = 73.2 Hz, P–CH(*C*H_3)$_2$), 21.6 (s, *ortho*-Mes-CH_3), 21.3 (s, *para*-Mes-CH_3), 16.9 (d, $^{2}J_{CP}$ = 2.3 Hz, P–*C*H(CH_3)$_2$)). $^{31}P\{^{1}H\}$ NMR (283 MHz, C_6D_6): δ –0.9 (s). Anal. Calcd. for $C_{34}H_{52}N_2OP_2$: C 72.06; H 9.25; N 4.94; found: C 72.66; H 9.84; N 4.37.

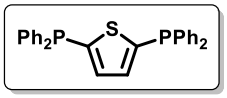

Synthesis of $(PPh_2)_2C_4H_2S$ (**9**) Diethyl ether (~40 mL) was transferred *in vacuo* to a two-necked 100 mL round-bottom flask attached to a swivel frit apparatus. Thiophene was injected into the flask (1.47 mL, 17.5 mmol, 1.05 g/mL), under positive argon pressure resulting in a transparent and colourless solution. The flask was cooled to –94 °C (liquid nitrogen/acetone mixture), after which ^{t}BuLi (22.7 mL, 0.0385 mmol, 1.7 M) was slowly injected into the flask over the course of ~50 min. The yellow slurry was then left in the cold bath to warm to ambient temperature slowly over 3 h under constant stirring. The flask was once again cooled to –94 °C. Cl–PPh_2 (6.59 mL, 36.7 mmol, 1.23 g/mL) was then injected into the flask over the course of 20 min. The dark-yellow solution was then left to warm up slowly to ambient temperature while remaining in the cold bath under an argon atmosphere with constant stirring. The reaction mixture was left for 16 h at ambient temperature under argon. Volatiles were removed *in vacuo* affording an orange waxy solid. Toluene (~40 mL) was then transferred into the flask under reduced pressure, resulting in an orange opaque solution. The solution was filtered through a glass frit, resulting in a transparent orange solution, and an off-white solid. The solvent was removed *in vacuo*, resulting in a pale-yellow oily solid. The apparatus was transferred into a glove box, where the solid was washed with heptane (4 × 10 mL), affording a pale-yellow solid. The remaining heptane was removed under vacuum. This yielded a light-yellow solid. **9** was crystallized from toluene at ambient temperature over one

week, during which the toluene evaporated, to yield X-ray quality crystals. Yield: 7.46 g, 94.2%. ^{1}H NMR (300 MHz, C_6D_6): δ 7.41 (ov m, 8H, *ortho*-Ph), 7.16 (dd, 2H, C_4H_2S, $^{3}J_{HP}$ = 4.1 Hz, $^{4}J_{HP}$ = 2.3 Hz), 6.99 (ov m, 12H, *meta*/*para*-Ph). ^{13}C {H} NMR (72 MHz, C_6D_6): δ 146.3 (d, $^{1}J_{CP}$ = 31.3 Hz, C_2/C_5-thiophene), 138.5 (d, $^{2}J_{CP}$ = 10.1 Hz, *ortho*-Ph), 137.6 (dd, $^{2}J_{CP}$ = 23.10 Hz, $^{3}J_{CP}$ = 6.6 Hz, C_3/C_4-thiophene), 133.9 (d, $^{1}J_{CP}$ = 20.0 Hz, *ipso*-Ph), 129.4 (s, *para*-Ph), 129.1 (d, $^{4}J_{HP}$ = 4.2 Hz, *meta*-Ph). ^{31}P {H} NMR (122 MHz, C_6D_6): –16.6 (s). Anal. Calcd for $C_{28}H_{22}P_2S$: C 74.32; H 4.90; S 7.09. Found: C 74.35; H 5.07; S 6.84.

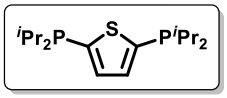

Synthesis of $(P^{i}Pr_2)_2C_4H_2S$ (**10**) Diethyl ether (~40 mL) was transferred *in vacuo* to a two-necked 100 mL round-bottom flask attached to a swivel frit apparatus. 2,5-dibromothiophene was injected into the flask (0.280 mL, 2.22 mmol, 2.14 g/mL) under positive argon pressure resulting in a transparent yellow solution. The round-bottom flask was cooled to –94 °C (liquid nitrogen/acetone mixture), after which ^{n}BuLi (1.95 mL, 4.88 mmol, 2.5M) was slowly injected over the course of 20 min. The faint yellow solution was then left in the cold bath to slowly warm to ambient temperature followed by 3 h of constant stirring. Afterwards a thick white slurry was observed, and the flask was once again cooled to –94 °C. Cl–$P^{i}Pr_2$ (0.74 mL, 4.66 mmol, 0.956 g/mL) was then injected into the flask over the course of 20 min. The solution was then left to warm to ambient temperature, after which it was stirred for 16 h under an argon atmosphere. The diethyl ether was removed under vacuum to afford an opaque yellow oil. Toluene (15 mL) was then transferred into the flask, yielding a cloudy yellow mixture. The mixture was then filtered through a glass frit, resulting in a transparent faint yellow solution. The solvent was removed *in vacuo*, giving a yellow transparent liquid. The apparatus was transferred into a glove box and the liquid was washed with heptane (4 × 2 mL). The

remaining heptane was removed under vacuum, affording the product as a transparent light-yellow liquid. Yield: 611 mg, 87.1%. ^{1}H NMR (300 MHz, C_6D_6): δ 7.25 (dd, $^{3}J_{HP}$ = 4.8, $^{4}J_{HP}$ = 2.3 Hz, 2H, C_4H_2S), 1.96 (sp, $^{3}J_{HH}$ = 6.9 Hz, 4H, $CH(CH_3)_2$), 1.02 (ov dd, $^{3}J_{HP}$ = 15.2 Hz, $^{3}J_{HH}$ = 6.9 Hz, 24H, $CH(CH_3)_2$). ^{13}C{^{1}H} NMR (75 MHz, C_6D_6) δ 143.0 (d, $^{1}J_{CP}$ = 42.0 Hz, C_2/C_5-thiophene), 137.7 (dd, $^{2}J_{CP}$ = 26.6 Hz, $^{3}J_{CP}$ = 7.6 Hz, C_3/C_4-thiophene), 25.3 (d, $^{1}J_{CP}$ = 11.2 Hz, $CH(CH_3)_2$), 20.5 (d, $^{2}J_{CP}$ = 18.8 Hz, $CH(CH_3)_2$), 19.5 (d, $^{2}J_{CP}$ = 8.3 Hz, $CH(CH_3)_2$). ^{31}P{^{1}H} NMR (122 MHz, C_6D_6) δ –0.8 (s). Anal. Calcd. for $C_{16}H_{30}P_2S$: C 60.73; H 9.56; S 10.13; found: C 61.12; H 9.53; S 10.21.

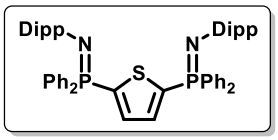

Synthesis of $(DippN{=}PPh_2)_2C_4H_2S$ (**11**) Under argon **9** (453 mg, 1.45 mmol) was added to a two-necked 50 mL round-bottom flask. Toluene (~20 mL) was distilled into the flask under vacuum. The flask was then placed under an argon atmosphere. Dipp-N_3 (591 mg, 2.91 mmol) was injected into the flask under positive argon pressure, resulting in a dark-yellow solution. The solution was stirred for 16 h at ambient temperature, after which no further change was observed. The solvent was removed under vacuum, yielding an orange oil. The oil was brought into a glove box and triturated with heptane (4 × 10 mL). The remaining heptane was removed under vacuum to yield a light-yellow solid. Yield: 945 mg, 82.1%. ^{1}H NMR (300 MHz, C_6D_6) δ 7.66 (dd, $^{3}J_{HP}$ = 12.1, $^{3}J_{HH}$ = 6.1 Hz, 8H, *ortho*-Ph), 7.23 (m, 4H, *meta*-Dipp), 7.15–6.93 (ov m, 16H, C_4H_2S and *meta*/*para*-Ph and *para*-Dipp), 3.56 (sp, $^{3}J_{HH}$ = 6.8 Hz, 4H, Dipp-$CH(CH_3)_2$), 1.08 (d, $^{3}J_{HH}$ = 6.8 Hz, 24H, Dipp-$CH(CH_3)_2$). ^{13}C{^{1}H} NMR (75 MHz, C_6D_6) δ, 143.9 (d, $^{2}J_{CP}$ = 16.2 Hz, *ipso*-Dipp), 143.0 (d, $^{3}J_{HP}$ = 7.1 Hz, *ortho*-Dipp), 142.7 (m, C_2/C_5-thiophene), 136.5 (dd, $^{2}J_{CP}$ = 10.9 Hz, $^{3}J_{CP}$ = 7.9 Hz, C_3/C_4-thiophene), 133.7 (d, $^{1}J_{CP}$ = 105.0 Hz, *ipso*-Ph), 132.2 (d, $^{2}J_{CP}$ = 9.9 Hz, *ortho*-Ph), 131.9 (s, *para*-Ph), 128.5 (d, $^{4}J_{CP}$ = 2.6 Hz,

meta-Ph), 123.7 (s, *meta*-Dipp), 120.6 (s, *para*-Dipp), 29.2 (s, Dipp-CH(CH$_3$)$_2$), 24.0 (s, Dipp-CH(CH$_3$)$_2$). ^{31}P{^{1}H} NMR (122 MHz, C_6D_6) δ –16.4 (s). Anal. Calcd. for $C_{52}H_{56}N_2P_2S$ C 77.78; H 7.03; N 3.49; S: 3.99; found: C 77.49; H 7.51; N 3.28; S 3.79.

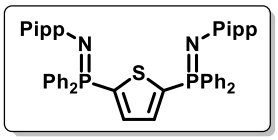

Synthesis of (PippN=PPh$_2$)$_2$C$_4$H$_2$S (**12**) In a glove box, **9** (699 mg, 1.55 mmol) was added to a two-necked 50 mL round-bottom flask containing toluene (~20 mL). Pipp-N$_3$ (498 mg, 3.09 mmol) was injected into the flask under positive argon pressure, resulting in a dark-yellow solution. The solution was stirred for 16 h at ambient temperature, after which no further change was observed. The solvent was removed under vacuum, yielding a dark-yellow oil that was brought into a glove box and triturated with heptane (4 × 10 mL). The remaining heptane was removed under vacuum to give a light-yellow solid. Yield: 1.02 g, 91.8%. ^{1}H NMR (300 MHz, C_6D_6): δ 7.79 (dd, 8H, $^3J_{HH}$ = 7.8 Hz, $^3J_{HP}$ = 12.6 Hz, *ortho*-Ph), 7.26-7.16 (ov m, 6H, C$_4$$H$$_2$S and *meta*-Pipp), 7.09-6.87 (ov m, 16H, *meta*/*para*-Ph and *ortho*-Pipp), 2.77 (sp, 2H, $^3J_{HH}$ = 6.8 Hz, Pipp-CH(CH$_3$)$_2$), 1.21 (d, 12H, $^3J_{HH}$ = 6.8 Hz, Pipp-CH(C$H$$_3$)$_2$). ^{13}C{^{1}H} NMR (75 MHz, C_6D_6): δ 149.1 (s, *ipso*-Pipp), 142.1 (d, $^1J_{CP}$ = 43.5 Hz, C$_2$/C$_5$-thiophene), 138.6 (s, *para*-Pipp), 135.8 (d, $^2J_{CP}$ = 9.5 Hz, C$_3$/C$_4$-thiophene), 131.1 (d, $^1J_{CP}$ = 49.9 Hz, *ipso*-Ph), 132.9 (d, $^2J_{CP}$ = 7.0 Hz, *ortho*-Ph), 132.6 (d, $^1J_{CP}$ = 47.7 Hz, *ipso*-Ph), 132.2 (s, *ortho*-Pipp), 129.2 (d, $^4J_{CP}$ = 5.8 Hz, *para*-Pipp), 127.5 (s, *meta*-Ph), 124.3 (d, $^3J_{CP}$ = 6.7 Hz, *meta*-Pipp), 34.2 (s, Pipp-CH(CH$_3$)$_2$), 25.0 (s, Pipp-CH(CH$_3$)$_2$). ^{31}P{^{1}H} NMR (122 MHz, C_6D_6): δ –7.7 (s). Anal. Calcd. for $C_{46}H_{44}N_2P_2S$: C 76.86; H 6.17; N 3.90; S 4.46; found: C 76.68; H 6.32; N 3.93; S 4.16.

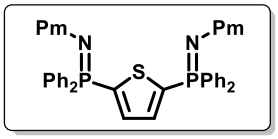

Synthesis of (PmN=PPh$_2$)$_2$C$_4$H$_2$S (**13**) In a glove box **9** (198 mg, 0.434 mmol) and 3,5-dimethyl-1-tetrazolopyrimidine

(130 mg, 0.868 mmol) were added to a 100 mL round-bottom flask. Toluene (~40 mL) was then transferred in *vacuo* to the round bottom flask. The reaction was stirred at ambient temperature for 16 h under an argon atmosphere yielding a clear mustard yellow solution along with a darker yellow-orange solid. Toluene was removed under vacuum, resulting in a bright yellow-orange solid. Yield: 249 mg, 83.8%. ^{1}H NMR (300 MHz, $CDCl_3$): δ 7.80 (dd, 8H, $^{3}J_{HH}$ = 7.2, $^{3}J_{HP}$ = 12.6 Hz, *ortho*-Ph), 7.50 (dd, 4H, $^{3}J_{HH}$ = 7.2, $^{4}J_{HH}$ = 6.3 Hz, *para*-Ph), 7.42 (td, 8H, $^{2}J_{HH}$ = 6.4 Hz, $^{4}J_{HP}$ = 2.7 Hz, *meta*-Ph), 7.25 (dd, 2H, $^{4}J_{HH}$ = 6.0 Hz, $^{6}J_{HP}$ = 3.3 Hz, *para*-Pm), 6.21 (s, 2H, C_4H_2S), 2.03 (s, 12H, *meta*-Pm-CH_3). $^{13}C\{^{1}H\}$ NMR (75 MHz, $CDCl_3$): δ 167.0 (d, $^{2}J_{CP}$ = 3.9 Hz, *ipso*-Pm), 166.6 (s, *meta*-Pm), 138.5 (dd, $^{1}J_{CP}$ = 90.7 Hz, $^{4}J_{CP}$ = 2.1 Hz, C_2/C_5-thiophene), 137.4 (dd, $^{2}J_{CP}$ = 13.1 Hz, $^{3}J_{CP}$ = 10.3 Hz, C_3/C_4-thiophene), 132.8 (d, $^{2}J_{CP}$ = 10.1 Hz, *ortho*-Ph), 132.1 (s, *para*-Ph), 129.9 (d, $^{1}J_{CP}$ = 13.0 Hz, *ipso*-Ph), 128.4 (d, $^{3}J_{CP}$ = 51 Hz, *meta*-Ph), 109.6 (s, *para*-Pm), 23.5 (s, *meta*-Pm-CH_3). $^{31}P\{^{1}H\}$ NMR (122 MHz, $CDCl_3$): δ 12.7 (s). Anal. Calcd. for $C_{40}H_{36}N_2P_2S$: C 68.94; H 5.19; N 12.19; S 4.02; found: C 69.15; H 5.22; N 12.10; S 4.61.

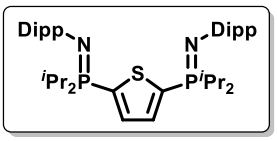

Synthesis of (DippN=P^{i}Pr$_2$)$_2$C$_4$H$_2$S (**14**) In a glove box **10** (228 mg, 0.722 mmol) was added to a two-necked 50 mL round-bottom flask containing toluene (~20 mL). Dipp-N_3 (293 mg, 1.44 mmol) was injected into the flask under positive argon pressure, resulting in a transparent bright yellow solution. Vigorous bubbling was observed. The solution was stirred for 16 h at ambient temperature, after which no change was observed. The solvent was removed under vacuum, yielding a pale-yellow fluffy power, after which the powder was brought into a glove box and washed with pentane (4 × 3 mL). The remaining pentane was removed under vacuum to afford a pale-yellow powder. Yield: 426 mg, 88.4%. ^{1}H NMR (300 MHz, C_6D_6) δ 7.13 (br d, $^{3}J_{HP}$ = 0.9 Hz, 2H, C_4H_2S), 7.06 (br m,

$^{3}J_{HH}$ = 7.0 Hz, 4H, *meta*-Dipp), 7.00 (t, $^{3}J_{HH}$ = 7.0 Hz, 2H, *para*-Dipp), 3.45 (sp, $^{3}J_{HH}$ = 6.8 Hz, 4H, Dipp-C*H*$(CH_3)_2$), 2.06 (ov sp, $^{3}J_{HH}$ = 7.0 Hz, 4H, P–C*H*$(CH_3)_2$), 1.22 (d, $^{3}J_{HH}$ = 6.8 Hz, 24H, Dipp-CH(C*H*$_3)_2$), 1.01 (dd, $^{3}J_{HP}$ = 15.7 Hz, $^{3}J_{HH}$ = 7.0 Hz, 12H, P–CH(C*H*$_3)_2$), 0.78 (dd, $^{3}J_{HP}$ = 17.2 Hz, $^{3}J_{HH}$ = 7.0 Hz, 12H, P–CH(C*H*$_3)_2$). ^{13}C NMR (75 MHz, C_6D_6): δ 145.4 (s, *ortho*-Dipp), 142.2 (d, $^{2}J_{CP}$ = 6.0 Hz, *ipso*-Dipp), 138.6 (d, $^{1}J_{CP}$ = 75.1 Hz, C_2/C_5-thiophene), 135.3 (dd, $^{2}J_{CP}$ = 11.6 Hz, $^{3}J_{CP}$ = 7.1 Hz, C_3/C_4-thiophene), 123.4 (d, $^{5}J_{CP}$ = 1.2 Hz), 120.2 (d, $^{6}J_{CP}$ = 2.4 Hz, *para*-Dipp), 29.6 (s, P–*C*H$(CH_3)_2$), 29.4 (d, $^{1}J_{CP}$ = 71.4 Hz, P–*C*H$(CH_3)_2$), 24.3 (s, Dipp-*C*H$(CH_3)_2$), 17.3 (d, $^{2}J_{CP}$ = 1.8 Hz, P–CH(*C*H$_3)_2$), 16.0 (d, $^{2}J_{CP}$ = 3.6 Hz, P–CH(*C*H$_3)_2$). ^{31}P NMR (122 MHz, C_6D_6): δ 0.8 (s). Anal. Calcd. for $C_{40}H_{64}N_2P_2S$: C 72.03; H 9.67; N 4.20; S 4.81; found: C 72.68; H 9.71; N 4.16; S 4.62.

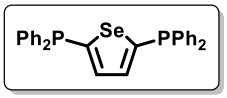

Synthesis of $(PPh_2)_2C_4H_2Se$ (**15**) Diethyl ether (~40 mL) was transferred *in vacuo* into a two-necked 100 mL round-bottom flask attached to a swivel frit apparatus. 2,5-dibromoselenophene was injected into the flask (1.42 g, 4.91 mmol) under positive argon pressure resulting in a light-yellow solution. The round-bottom flask was cooled to –78 °C, after which ^{n}BuLi (4.32 mL, 10.8 mmol, 2.5 M) was slowly injected into the flask over the course of 10 min. The faint yellow solution was then left in the cold bath to warm to ambient temperature slowly over 3 h under constant stirring. Afterwards, a thick brown slurry was observed. The flask was once again cooled to –78 °C. Cl–PPh_2 (1.87 mL, 10.30 mmol, 0.956 g/mL) was then injected into the flask over the course of 5 min. The solution was allowed to warm to ambient temperature and react for 16 h with constant stirring and under an argon atmosphere. This yielded a light brown-orange cloudy suspension. The solution was filtered through a glass frit, resulting in a transparent brown solution. The solvent was removed under vacuum, giving a brown oil. The apparatus was transferred into a glove

box and the liquid washed with heptane (4 × 3 mL). The oil was then dissolved in pentane and the resultant solution filtered through Celite to give a brown transparent solution. The remaining pentane was removed under vacuum affording a brown sticky solid. Yield: 1.19 g, 48.6%. ^{1}H NMR (300 MHz, C_6D_6) δ 7.58 (ov dd, $^{3}J_{HP}$ = 6.1 Hz, $^{4}J_{HP}$ = 2.6 Hz, 2H, C_4H_2Se), 7.53 (ov ddd, $^{3}J_{HP}$ = 7.8 Hz, $^{3}J_{HH}$ = 3.6 Hz, $^{4}J_{HH}$ = 2.2 Hz, 8H, *ortho*-Ph), 7.22-7.12 (m, 4H, *para*-Ph), 7.12-6.98 (m, 8H, *meta*-Ph). ^{13}C{^{1}H} NMR (75 MHz, C_6D_6) δ 152.9 (d, $^{1}J_{CP}$ = 37.4 Hz, C_2/C_5-selenophene), 139.5 (dd, $^{2}J_{CP}$ = 27.0 Hz, $^{3}J_{CP}$ = 8.6 Hz, C_3/C_4-selenophene), 138.6 (d, $^{1}J_{CP}$ = 10.1 Hz, *ipso*-Ph), 133.1 (d, $^{2}J_{CP}$ = 20.1 Hz, *ortho*-Ph), 128.8 (s, *para*-Ph), 128.5 (d, $^{3}J_{CP}$ = 7.1 Hz, *meta*-Ph). ^{31}P{^{1}H} NMR (122 MHz, C_6D_6) δ –13.9 (s). ^{77}Se NMR (134 MHz, C_6D_6) δ 731.1 (t, $^{2}J_{SeP}$ = 8.6 Hz). Anal. Calcd. for $C_{28}H_{22}NP_2Se$: C 67.34; H 4.44; found: C 67.10; H 4.71.

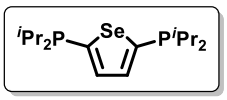

Synthesis of $(P^{i}Pr_2)_2C_4H_2Se$ (**16**) Diethyl ether (~40 mL) was transferred *in vacuo* to a two-necked 100 mL round-bottom flask attached to a swivel frit apparatus. 2,5-dibromoselenophene was injected into the flask (1.42 g, 4.91 mmol) under positive argon pressure resulting in a light-yellow solution. The round-bottom flask was cooled to –78 °C (dry ice/acetone mixture), after which ^{n}BuLi (4.32 mL, 10.8 mmol, 2.5 M) was slowly injected over the course of 10 min. The faint yellow solution was allowed to warm to ambient temperature over 3 h under constant stirring. Afterwards, a thick green-brown slurry was observed, and the flask was once again cooled to –78 °C. Cl–$P^{i}Pr_2$ (0.49 mL, 3.01 mmol, 0.956 g/mL) was then injected into the flask over the course of 5 min. The solution was allowed to warm to ambient temperature, after which the mixture was stirred for 16 h under an argon atmosphere. This yielded a brown cloudy solution. The solution was filtered through a frit, giving a transparent brown solution. The solvent was removed under vacuum,

giving in a thick brown oil. The apparatus was transferred into a glove box, and the liquid was washed with pentane (4 × 3 mL). The resulting oil was dissolved in pentane and kept at –30 °C, which yielded light-brown crystals. Yield: 249 mg, 83.8%. ^{1}H NMR (300 MHz, C_6D_6): δ 7.55 (dd, 2H, $^{3}J_{HP}$ = 6.9 Hz, $^{4}J_{HP}$ = 2.4 Hz, C_4H_2Se), 1.89 (sp, 4H, $^{3}J_{HH}$ = 6.9 Hz, C*H*$(CH_3)_2$), 1.00-1.08 (ov m, 24H, CH(C*H*$_3)_2$). ^{13}C{^{1}H} NMR (75 MHz, C_6D_6): δ 150.3 (dd, $^{1}J_{CP}$ = 47.5 Hz, $^{4}J_{CP}$ = 1.5 Hz, C_2/C_5-selenophene), 140.7 (dd, $^{2}J_{CP}$ = 29.4 Hz, $^{3}J_{CP}$ = 9.1 Hz, C_3/C_4-selenophene), 26.2-26.3 (d, $^{1}J_{CP}$ = 11.3 Hz, *C*H$(CH_3)_2$), 19.6 (d, $^{2}J_{CP}$ = 4.6 Hz, CH(*C*H$_3)_2$). ^{31}P{^{1}H} NMR (122 MHz, C_6D_6): δ 7.1 (s). ^{77}Se{^{1}H} NMR (57 MHz, C_6D_6): δ 744.9 (s). Anal. Calcd. for $C_{16}H_{30}P_2Se$: C 52.89; H 8.37; found: C 52.74; H 8.33.

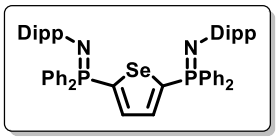

Synthesis of (DippN=PPh$_2$)$_2$C$_4$H$_2$Se (**17**) In a glove box **15** (108 mg, 0.217 mmol) was added to a two-necked 50 mL round-bottom flask with toluene (~20 mL). Dipp-N_3 (88.3 mg, 0.433 mmol) was injected into the flask under positive argon pressure, resulting in an opaque golden-brown solution. Vigorous bubbling was observed. The solution was stirred for 16 h at ambient temperature, after which an orange-brown solution was observed. The solvent was removed under vacuum yielding a dark orange-brown oil, which was washed with pentane (4 × 3 mL). The oil was dissolved in pentane and filtered through Celite, resulting in an orange-brown transparent solution. The remaining pentane was removed under vacuum yielding an orange-brown sticky solid. Yield: 259 mg, 70.2%. ^{1}H NMR (300 MHz, C_6D_6): δ 7.69 (dd, $^{3}J_{HP}$ = 12.4 Hz, $^{3}J_{HH}$ = 6.7 Hz, 8H, *ortho*-Ph), 7.20 (br ov t, 6H, *meta*-Dipp and C_4H_2Se), 7.10 (d, $^{3}J_{HH}$ = 8.4 Hz, 2H, *para*-Dipp), 7.07-6.87 (m, 12H, *para*/*meta*-Ph), 3.58 (sp, $^{3}J_{HH}$ = 6.8 Hz, 4H, Dipp-C*H*$(CH_3)_2$), 1.08 (d, $^{3}J_{HH}$ = 6.8 Hz, 24H, Dipp-CH(C*H*$_3)_2$). ^{13}C{^{1}H} NMR (75 MHz, C_6D_6): δ 150.4 (d, $^{1}J_{CP}$ = 95.8 Hz, C_2/C_5-selenophene), 144.2 (s, *ortho*-Dipp), 143.4 (d, $^{2}J_{CP}$ = 7.5 Hz,

ipso-Dipp), 138.9 (dd, $^{2}J_{CP}$ = 15.5, $^{3}J_{CP}$ = 8.9 Hz, C_3/C_4-selenophene), 134.6 (d, $^{1}J_{CP}$ = 105.5 Hz, *ipso*-Ph), 132.5 (d, $^{2}J_{CP}$ = 10.0 Hz, *ortho*-Ph), 132.0 (d, $^{4}J_{CP}$ = 2.6 Hz, *meta*-Ph), 128.9 (d, $^{3}J_{CP}$ = 12.4 Hz, *para*-Ph), 123.7 (d, $^{4}J_{CP}$ = 2.1 Hz, *meta*-Dipp), 121.0 (d, $^{5}J_{CP}$ = 3.4 Hz, *para*-Dipp), 29.52 (s, Dipp-*C*H(CH_3)$_2$), 24.35 (s, Dipp-CH(*C*H_3)$_2$). $^{31}P\{^{1}H\}$ NMR (122 MHz, C_6D_6): δ –15.8 (s). ^{31}P NMR (283 MHz, C_6D_6) δ –15.8 (s, ^{77}Se satellites: $^{2}J_{SeP}$ = 102.2 Hz). ^{77}Se NMR (134 MHz, C_6D_6): δ 764.4 (t, $^{2}J_{SeP}$ = 26.2 Hz). Anal. Calcd. for $C_{52}H_{56}N_2P_2Se$: C 73.48; H 6.64; N 3.30; found: C 74.09; H 6.60; N 3.21.

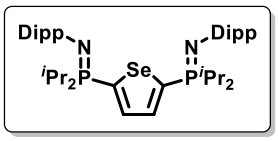

Synthesis of (DippN=P^{i}Pr$_2$)$_2$C$_4$H$_2$Se (**18**) In a glove box **16** (80.0 mg, 0.220 mmol) was added to a two-necked 50 mL round-bottom flask with toluene (~20 mL). Dipp-N_3 (118 mg, 0.578 mmol) was injected into the flask under positive argon pressure, resulting in a golden-yellow solution. Vigorous bubbling was observed. The solution was stirred for 16 h at ambient temperature. Volatiles were removed *in vacuo*. The resulting brown waxy solid was dissolved in pentane (~5 mL) and cooled to –35 °C for 48 h. Brown-yellow crystals were isolated and washed with 4 portions of cold toluene (3 mL). The product was brown-yellow rectangular block crystals. Yield: 82.1 mg, 52.2%. ^{1}H NMR (300 MHz, C_6D_6): δ 7.36 (dd, 2H, $^{3}J_{HP}$ = 5.4 Hz, $^{4}J_{HP}$ = 3.3, C_4H_2Se), 7.24 (d, $^{3}J_{HH}$ = 7.2 Hz 2H, *meta*-Dipp), 7.11 (m, 4H, *para*-Dipp), 3.57 (sp, 4H, $^{3}J_{HH}$ = 6.6 Hz, Dipp-C*H*(CH_3)$_2$), 2.12-2.13 (ov sp, 4H, P–C*H*(CH_3)$_2$), 1.31 (d, 12H, $^{3}J_{HH}$ = 6.6 Hz, Dipp-CH(C*H*$_3$)$_2$), 1.11 (dd, 12H, $^{3}J_{HP}$ = 15.6 Hz, $^{3}J_{HH}$ = 6.9 Hz, P–CH(C*H*$_3$)$_2$), 0.91 (dd, 24H, $^{3}J_{HH}$ = 6.9, $^{3}J_{HP}$ = 17.1 Hz, P–CH(C*H*$_3$)$_2$). ^{13}C NMR (75 MHz, C_6D_6): δ 145.0 (d, *ortho*/*ipso*-Dipp), 144.9 (s, *ipso*-Dipp), 141.7 (d, $^{1}J_{CP}$ = 24.0 Hz, C_2/C_5-selenophene), 136.6 (dd, $^{3}J_{CP}$ = 27.0, $^{2}J_{CP}$ = 54.0 Hz, C_3/C_4-selenophene), 122.9 (s, *meta*-Dipp), 119.7 (d, $^{5}J_{CP}$ = 3.0 Hz, *para*-Dipp), 29.0 (s, P–*C*H(CH_3)$_2$), 28.9 (d, $^{5}J_{CP}$ = 6.9 Hz,

Dipp-CH(CH_3)$_2$), 23.8 (s, P–CH(CH_3)$_2$), 16.2 (d, $^2J_{CP}$ = 9.0 Hz, P–CH(CH_3)$_2$). $^{31}P\{^1H\}$ NMR (122 MHz, C_6D_6): δ 5.6 (s).$^{77}Se\{^1H\}$ NMR (57 MHz, C_6D_6): δ 788.3 (s). Anal. Calcd. for $C_{40}H_{64}N_2P_2Se$: C 67.30; H 9.04; N 3.92; found: C 67.09; H 8.94; N 3.92.

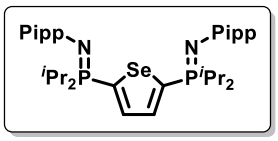

Synthesis of (PippN=P^{i}Pr$_2$)$_2$C$_4$H$_2$Se (**19**) In a glove box, **16** (117 mg, 0.322 mmol) was added to a two-necked round-bottom flask containing toluene (~20 mL). Pipp-N_3 (136 mg, 0.845 mmol) was injected into the flask under positive argon pressure, resulting in a dark-yellow solution. The solution was stirred for 16 h at ambient temperature, after which no further change was observed. The solvent was removed under vacuum, yielding a dark-yellow oil. The oil was brought into a glove box and triturated with heptane (4 × 10 mL). The remaining heptane was removed under vacuum to give a light-yellow solid. Yield: 153 mg, 75.5%. ^1H NMR (300 MHz, C_6D_6): δ 7.48 (dd, 2H, $^4J_{HP}$ = 3.4 Hz, $^3J_{HP}$ = 5.2 Hz, C_4H_2Se), 7.14 (ov m, 4H, *ortho*/*meta*-Pipp), 2.83 (sp, 2H, $^3J_{HH}$ = 6.9 Hz, Pipp-C*H*(CH_3)$_2$), 2.05 (ov sp, 4H, P–C*H*(CH_3)$_2$), 1.27 (s, 12H, Pipp-CH(C*H*$_3$)$_2$), 1.06 (dd, 12H, $^3J_{HH}$ = 6.9, $^3J_{HP}$ = 15.7 Hz, P–CH(C*H*$_3$)$_2$), 0.94 (dd, 12H, $^3J_{HP}$ = 16.1 Hz, $^3J_{HH}$ = 6.9 Hz, P–CH(C*H*$_3$)$_2$). $^{13}C\{^1H\}$ NMR (75 MHz, C_6D_6): δ 150.3 (s, *ipso*-Pipp), 147.0 (d, $^1J_{CP}$ = 45.9 Hz, C_2/C_5-selenophene), 138.2 (dd, $^2J_{CP}$ = 15.0 Hz, $^3J_{CP}$ = 8.5 Hz, C_3/C_4-selenophene), 137.9 (s, *para*-Pipp), 127.4 (s, *meta*-Pipp), 124.4 (d, $^3J_{CP}$ = 3.3 Hz, *ortho*-Pipp), 34.2 (s, Pipp-*C*H(CH_3)$_2$), 27.8 (d, $^1J_{CP}$ = 40.0 Hz, P–*C*H(CH_3)$_2$), 25.1 (s, Pipp-CH(*C*H$_3$)$_2$) 17.3 (d, $^2J_{CP}$ = 5.1 Hz, P–CH(*C*H$_3$)$_2$), 16.5 (d, $^2J_{CP}$ = 5.1 Hz, P–CH(*C*H$_3$)$_2$). $^{31}P\{^1H\}$ NMR (122 MHz, C_6D_6): δ 21.0 (s). $^{77}Se\{^1H\}$ NMR (57 MHz, C_6D_6): δ 812.0 (s). Anal. Calcd. for $C_{34}H_{52}N_2P_2Se$: C 64.85; H 8.32; N 4.45; found: C 64.65; H 8.38; N 4.38.

Synthesis of [(DippN(H)=PPh_2)(DippN=PPh_2)C_4H_2O][B(3,5-$(CF_3)_2C_6H_3)_4$] (**20**) In a

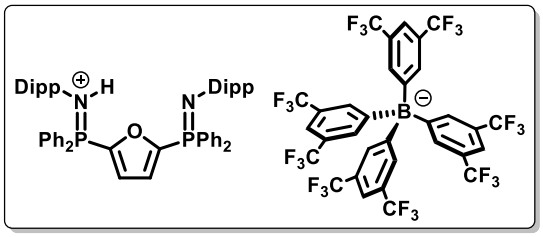

glove box, **3** (40.0 mg, 0.0508 mmol) and Brookhart's acid (51.4 mg, 0.0508 mmol), were added to a 20 mL scintillation vial, followed by ~5 mL of toluene or benzene. The reaction was left at ambient temperature for 2 h under an argon atmosphere with constant stirring. This yielded a clear solution with an orange oil. The solvent was decanted, and the oil washed with four ~1 mL portions of pentane or heptane. Excess solvent was removed under vacuum, resulting a dark-orange sticky solid. Yield: 55.3 mg, 64.7%. ^{1}H NMR (pyridine-d_5, 300 MHz): δ 16.36 (br s, 1H, *H*–N=P), 8.44 (br s, 8H, *ortho*-[B($C_6H_3(CF_3)_2)_4$]), 7.83 (br s, 4H, *para*-[B($C_6H_3(CF_3)_2)_4$]), 7.78 (dd, 8H, $^{3}J_{HP}$ = 12.3, $^{3}J_{HH}$ = 7.0 Hz, *ortho*-Ph), 7.73 (m, 4H, *para*-Ph), 7.67 (br ov m, 2H, C_4H_2O), 7.49 (td, 8H, $^{3}J_{HH}$ = 7.0 Hz, $^{3}J_{HH}$ = 2.9 Hz, *meta*-Ph), 7.31 (m, 4H, *meta*-Dipp), 7.20 (m, 2H, *para*-Dipp), (4H, $^{3}J_{HH}$ = 6.8 Hz, Dipp-*C*H($CH_3)_2$), 0.98 (d, 24H, $^{3}J_{HH}$ = 7.0 Hz, Dipp-CH(C*H*$_3)_2$). ^{11}B{^{1}H} NMR (96 MHz, pyridine-d_5): δ –5.91 (s). ^{13}C{^{1}H} NMR (176 MHz, pyridine-d_5): δ 162.5 (1:1:1:1 q, $^{1}J_{CB}$ = 49.4 Hz, *ipso*-[B(*C*$_6$H$_3$(CF$_3$)$_2$)$_4$]), 144.1 (d, $^{2}J_{CP}$ = 13.3 Hz, *ipso*-Dipp), 139.2 (br m, C_3/C_4-furan), 134.8 (s, *ortho*-[B(*C*$_6$H$_3$(CF$_3$)$_2$)$_4$]), 133.3 (s, *para*-Ph), 132.3 (d, $^{2}J_{CP}$ = 31.8 Hz, *ortho*-Ph), 130.3 (s, *para*-Dipp), 129.8 (q, $^{1}J_{CF}$ = 115.5 Hz, *C*F$_3$-[B(C$_6$H$_3$(*C*F$_3$)$_2$)$_4$]), 129.4 (s, *meta*-Dipp), 129.2 (s, *meta*-Ph), 128.5 (s, *meta*-[B(*C*$_6$H$_3$(CF$_3$)$_2$)$_4$]), 126.1 (d, $^{1}J_{CP}$ = 102.7 Hz, *ipso*-Ph), 119.4 (s, *ortho*-Dipp), 118.1 (m, *para*-[B(C$_6$H$_3$(*C*F$_3$)$_2$)$_4$]), 28.9 (s, Dipp-*C*H(CH$_3$)$_2$), 23.5 (s, Dipp-CH(*C*H$_3$)$_2$). Note: C_2/C_5-thiophene were not observed. ^{19}F{^{1}H} NMR (282 MHz, pyridine–d_5): δ –62.07 (s). ^{31}P{^{1}H} NMR (282.42 MHz, pyridine–d_5): δ –11.6 (br). Anal. Calcd. for $C_{84}H_{57}BF_{24}N_2OP_2$: C 61.55; H 3.50; N 1.71; found: C 62.05; H 3.95; N 2.00.

Synthesis of [(PippN(H)=PPh_2)(PippN=PPh_2)C_4H_2O][$B(C_6F_5)_4$] (**21**) In a glove box, **4**

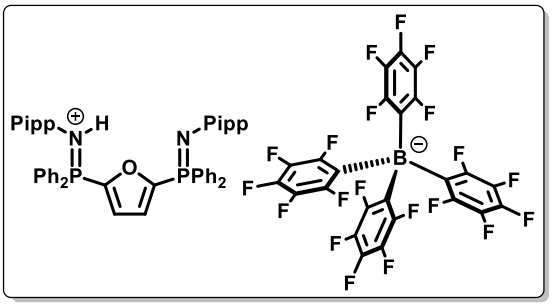

(193 mg, 0.275 mmol) and [$HNMe_2Ph$][$B(C_6F_5)_4$] (220 mg, 0.275 mmol) were added to a 20 mL scintillation vial followed by ~5 mL of benzene. The reaction was stirred at ambient temperature for 2 h under an argon atmosphere. This yielded a dark-orange oil. The solvent was decanted, and the oil washed with four ~1 mL portions of pentane. Excess solvent was removed under vacuum, resulting in an orange sticky solid. Yield: 356 mg, 93.6%. ^{1}H NMR (300 MHz, $CDCl_3$): δ 7.75 (t, 4H, $^{3}J_{HH}$ = 7.8 Hz, *para*-Ph), 7.62 (dd, 8H, $^{3}J_{HH}$ = 7.3 Hz, $^{3}J_{HP}$ = 11.8 Hz, *ortho*-Ph), 7.51 (m, 8H, *meta*-Ph), 7.11 (s, 2H, C_4H_2O), 6.92 (d, 4H, $^{3}J_{HH}$ = 8.1 Hz, *ortho*-Pipp), 6.65 (d, 4H, $^{3}J_{HH}$ = 8.1 Hz, *meta*-Pipp), 5.82 (br s, 1H, *H*–N=P), 2.78 (sp, 2H, $^{3}J_{HH}$ = 6.7 Hz, Pipp-C*H*$(CH_3)_2$), 1.15 (d, $^{3}J_{HH}$ = 6.7 Hz, 12H, Pipp-CH(C*H*$_3)_2$). ^{11}B{^{1}H} NMR (96 MHz, $CDCl_3$): δ –16.72 (s). ^{13}C{^{1}H} NMR (75 MHz, $CDCl_3$): δ 148.5 (br d, J_{CP} = 53.6 Hz, C_2/C_5-furan), 144.2 (s, *ipso*-Ph), 143.8 (s, *para*-Pipp), 139.9 (d, $^{2}J_{CP}$ = 37.6 Hz, *ipso*-Pipp), 135.4 (s, *para*-Ph), 132.7 (d, $^{2}J_{CP}$ = 5.9 Hz, *ortho*-Ph), 130.4 (d, $^{3}J_{CP}$ = 3.0 Hz, *meta*-Ph), 127.8 (s, *ortho*-Pipp), 126.9 (dd, $^{2}J_{CP}$ = 9.1 Hz, $^{3}J_{CP}$ = 7.9 Hz, C_3/C_4-furan), 122.2 (s, Pipp *meta*), 33.5 (s, Pipp-*C*H$(CH_3)_2$), 24.09 (s, Pipp-CH(*C*H$_3)_2$). ^{19}F{^{1}H} NMR (282 MHz, $CDCl_3$): δ –131.56 (d, 8F, *ortho*-C_6F_5), –161.72 (t, 4F, *para*-C_6F_5), –165.61 (t, 8F, *meta*-C_6F_5). ^{31}P{^{1}H} NMR (122 MHz, $CDCl_3$): δ 7.9 (br s). Anal. Calcd. for $C_{70}H_{45}BF_{20}N_2OP_2$: C 60.80; H 3.28; N 2.03; found: C 60.46; H 3.27; N 2.03.

Synthesis of [(PmN(H)=PPh_2)(PmN=PPh_2)C_4H_2O][$B(C_6F_5)_4$] (**22**) In a glove box, **6**

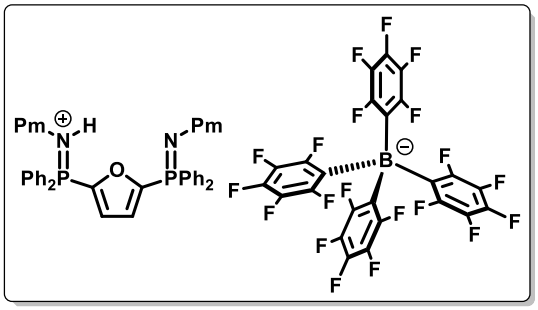

(157 mg, 0.231 mmol) and [$HNMe_2Ph$][$B(C_6F_5)_4$] (185 mg, 0.231 mmol) were added to a 20 mL scintillation vial followed by ~3 mL of toluene. A faint yellow solution was visible immediately after the addition of the solvent. The reaction was stirred at ambient temperature for 2 h under an argon atmosphere. This yielded a dark-yellow oil. A clear toluene layer was seen on top with a small dark-yellow oil layer underneath. The solvent was decanted, and the oil washed with four 3 mL portions of toluene followed by two 3 mL portions of heptane. The remaining heptane was removed under vacuum to give a golden yellow solid. Yield: 272.8 mg, 90.6%. ^{1}H NMR (300 MHz, $CDCl_3$): δ 7.55-7.12 (br ov m, 20H, *ortho*/*meta*/*para*-Ph), 6.82 (s, 2H, C_4H_2O), 6.41 (s, 2H, *para*-Pm), 2.20 (s, 12H, *meta*–CH_3-Pm). Note: *H*–N=P was not observed. ^{11}B{^{1}H} NMR (96 MHz, $CDCl_{38}$): δ –16.69 (s). ^{13}C{^{1}H} NMR (176 MHz, $CDCl_3$): δ 168.1 (s, *meta*-Pm), 152.5 (d, $^{1}J_{CP}$ = 63.2, C_2/C_5-furan), 133.6 (s, *para*-Ph), 132.8 (d, $^{3}J_{CP}$ = 2.3 Hz, *meta*-Ph), 128.9 (d, $^{2}J_{CP}$ = 8.0 Hz, *ortho*-Ph), 128.7 (d, $^{1}J_{CP}$ = 52.7 Hz *ipso*-Ph), 128.0 (m, C_3/C_4-furan), 111.2 (s, *para*-Pm), 22.3 (s, *meta*-CH_3-Pm). Note: *ipso*-Pm was not observed. ^{19}F{^{1}H} NMR (282 MHz, $CDCl_3$): δ –131.63 (d, 8F, *ortho*-C_6F_5), –162.10 (t, 4F, *para*-C_6F_5), –165.84 (t, 8F, *meta*-C_6F_5). ^{31}P{^{1}H} NMR (122 MHz, $CDCl_3$): δ 10.3 (s). Anal. Calcd. for $C_{64}H_{37}BF_{20}N_6OP_2$: C 56.57; H 2.74; N 6.19; found: C 56.42; H 2.70; N 6.15.

Synthesis of [(DippN(H)=P^{i}Pr$_2$)(DippN=P^{i}Pr$_2$)C$_4$H$_2$O][B(3,5-(CF$_3$)$_2$C$_6$H$_3$)$_4$] (**23**) In a

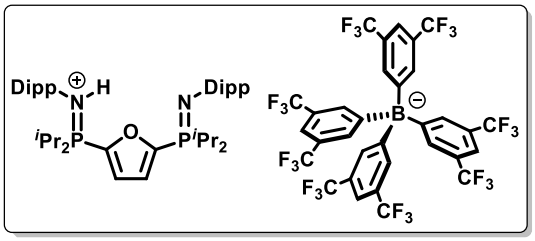

glove box, **7** (113 mg, 0.173 mmol) and Brookhart's acid (176 mg, 0.173 mmol) were added to a 20 mL scintillation vial, followed by ~5 mL of toluene. The reaction was stirred at ambient temperature for 2 h under an argon atmosphere. This yielded a clear solution with a bright-orange oil. The solvent was decanted, and the oil washed with four ~1 mL portions of pentane. Excess solvent was removed under vacuum, resulting in an orange sticky solid. Yield: 228.6 mg, 87.2%. ^{1}H NMR (300 MHz, pyridine-d_5) δ 11.82 (br s, 1H, *H*–N=P), 8.44 (br s, 8H, *ortho*-[B(C$_6$*H*$_3$(CF$_3$)$_2$)$_4$]), 7.83 (br s, 4H, *meta*-[B(C$_6$*H*$_3$(CF$_3$)$_2$)$_4$]), 7.62 (br s, 2H, C$_4$*H*$_2$O), 7.27 (ov m, 4H, *meta*-Dipp), 7.17 (ov s, 2H, *para*-Dipp), 3.51 (sp, $^3J_{HH}$ = 6.7 Hz, 4H, Dipp-C*H*(CH$_3$)$_2$), 2.79 (br sp, 4H, P–C*H*(CH$_3$)$_2$), 1.35 (ov dd, $^3J_{HP}$ = 16.7 Hz, $^3J_{HH}$ = 7.1 Hz, 12H, P–CH(C*H*$_3$)$_2$), 1.25 (ov d, $^3J_{HH}$ = 6.8 Hz, 6H, P–CH(C*H*$_3$)$_2$), 1.19 (ov d, $^3J_{HH}$ = 7.0 Hz, 30H, Dipp- and P–CH(C*H*$_3$)$_2$). ^{11}B{^{1}H} NMR (96 MHz, pyridine-d_5): δ –5.91 (s). ^{13}C{^{1}H} NMR (75 MHz, pyridine-d_5) δ 163.1 (1:1:1:1 q, $^1J_{CB}$ = 49.8 Hz, *ipso*-[B(*C*$_6$H$_3$(CF$_3$)$_2$)$_4$]), 144.0 (br s, *ipso*-Dipp), 135.8 (s, *ortho*-[B(*C*$_6$H$_3$(CF$_3$)$_2$)$_4$]), 130.5 (q, $^1J_{CF}$ = 2.8 Hz, *C*F$_3$-[B(C$_6$H$_3$(*C*F$_3$)$_2$)$_4$]), 130.1 (q, $^1J_{CF}$ = 2.9 Hz, *C*F$_3$-[B(C$_6$H$_3$(*C*F$_3$)$_2$)$_4$]), 129.5 (d, $^2J_{CP}$ = 56.0 Hz, C$_3$/C$_4$-furan), 127.3 (s, *meta*-[B(C$_6$H$_3$(*C*F$_3$)$_2$)$_4$]), 126.2 (s, *para*-Dipp), 124.2 (s, *meta*-Dipp), 120.1 (s, *ortho*-Dipp), δ 118.8 (t, $^3J_{CF}$ = 4.1 Hz, *para*-[B(*C*$_6$H$_3$(CF$_3$)$_2$)$_4$]), 29.5 (s, P–*C*H(CH$_3$)$_2$), 28.8 (s, Dipp-CH(*C*H$_3$)$_2$), 27.8 (s, Dipp-CH(*C*H$_3$)$_2$), 24.3 (s, Dipp-*C*H(CH$_3$)$_2$), 17.0 (d, $^2J_{CP}$ = 2.1 Hz, P–CH(*C*H$_3$)$_2$), 16.2 (d, $^2J_{CP}$ = 3.3 Hz, P–CH(*C*H$_3$)$_2$). Note: C$_2$/C$_5$-furan was not observed. ^{19}F{^{1}H} NMR (282 MHz, pyridine-d_5): δ –62.06 (s). ^{31}P{^{1}H} NMR (122 MHz, pyridine-d_5): δ 1.17 (br s). Anal. Calcd. for C$_{72}$H$_{77}$BF$_{24}$N$_2$OP$_2$: C 57.08; H 5.12; N 1.85; found: C 57.19; H 5.31; N 1.84.

Synthesis of [(DippN(H)=PPh_2)(DippN=PPh_2)C_4H_2S][B(3,5-$(CF_3)_2C_6H_3)_4$] (**24**) In a

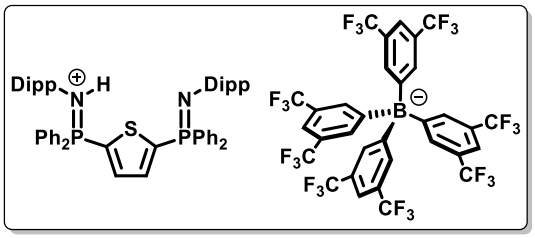

glove box, **11** (103 mg, 0.128 mmol) and Brookhart's acid (130 mg, 0.128 mmol) were added to a 20 mL scintillation vial, followed by ~5 mL of toluene. The reaction was stirred at ambient temperature for 2 h under an argon atmosphere. This yielded a bright-orange solution. The solvent was removed under vacuum, resulting in a bright yellow powder. Yield: 156.0 mg, 73.0%. ^{1}H NMR (300 MHz, $CDCl_3$): δ 7.79 (br, 2H, *para*-Dipp), 7.72 (br s, 8H, *ortho*-[B($C_6H_3(CF_3)_2)_4$]), 7.58 (br ov m, 2H, C_4H_2S), 7.56 (br ov m, 8H, *meta*-Ph), 7.51 (br s, 4H, *para*-[B($C_6H_3(CF_3)_2)_4$]), 7.48 (br, 4H, *para*-Ph), 7.35 (br d, 8H, $^3J_{HP}$ = 4.2 Hz, *ortho*-Ph), 7.08 (br d, 2H, $^3J_{HH}$ = 7.0 Hz, *meta*-Dipp), 6.98 (br d, 2H, $^3J_{HH}$ = 7.0 Hz, *para*-Dipp), 6.87 (br, 1H, *H*–N=P), 3.16 (br sp, 2H, Dipp-*C*H($CH_3)_2$), 2.84 (br sp, 2H, Dipp-*C*H($CH_3)_2$), 0.84 (ov d, 12H, $^3J_{HH}$ = 7.0 Hz, Dipp-CH(C*H*$_3)_2$), 0.80 (ov d, 12H, $^3J_{HH}$ = 7.0 Hz, Dipp CH(C*H*$_3)_2$). ^{11}B{^{1}H} NMR (96 MHz, pyridine-d_5): δ –5.91 (s). ^{13}C{^{1}H} NMR (176.05 MHz, $CDCl_3$): δ 161.7 (1:1:1:1 q, $^1J_{CB}$ = 49.4 Hz, *ipso*-[B(*C*$_6$H$_3$($CF_3)_2)_4$]), 134.8 (s, *ortho*-[B(*C*$_6$H$_3$($CF_3)_2)_4$]), 132.3 (br m, C_3/C_4-thiophene), 129.3 (ov m, *meta*-Dipp), 129.3 (ov d, $^2J_{CP}$ = 22.9 Hz, *ortho*-Dipp), 128.8 (s, *para*-Dipp), 125.2 (q, $^1J_{CF}$ = 115.5 Hz, *C*F_3-[B(C_6H_3(*C*$F_3)_2)_4$]), 124.2 (d, $^1J_{CP}$ = 116.3 Hz, *ipso*-Ph) 122.2 (s, *meta*-[B(*C*$_6$H$_3$($CF_3)_2)_4$]), 117.5 (s, *para*-[B(C_6H_3(*C*$F_3)_2)_4$]), 29.4 (s, $^2J_{CP}$ = 120.0 Hz, Dipp-*C*H($CH_3)_2$), 22.71 (m, Dipp-CH(*C*H$_3)_2$). Note: *ipso* Dipp, and C_2/C_5-thiophene were not observed. ^{19}F{^{1}H} NMR (282 MHz, pyridine-d_5) δ –62.06 (s). ^{31}P{^{1}H} NMR (282.42 MHz, $CDCl_3$): δ 29.5 (s, Dipp–NH=P+), –15.83 (s, Dipp–N=P). Anal. Calcd. for $C_{84}H_{69}BF_{24}N_2P_2S$: C 60.51; H 4.17; N 1.68; S 1.92; found: C 60.55; H 4.01; N 1.53; S 1.49.

Synthesis of [(PippN(H)=PPh_2)(PippN=PPh_2)C_4H_2S][$B(C_6F_5)_4$] **(25)** In a glove box, **12**

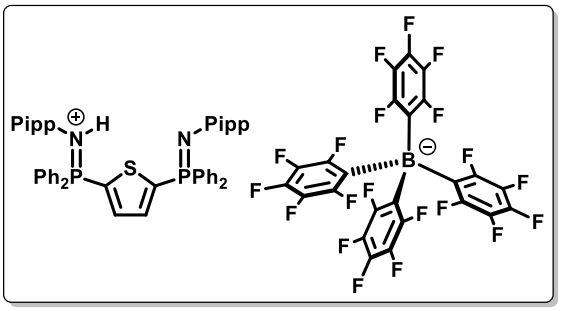

(249 mg, 0.346 mmol) and [$HNMe_2Ph$][$B(C_6F_5)_4$] (278 mg, 0.346 mmol) were added to a 20 mL scintillation vial followed by ~5 mL of benzene. The reaction was stirred at ambient temperature for 2 h under an argon atmosphere. This yielded a dark-red oil. The solvent was decanted, and the oil washed with four ~1 mL portions of pentane. Excess solvent was removed under vacuum, resulting a bright yellow solid. Yield: 460.0 mg, 95.1%. ^{1}H NMR (300 MHz, $CDCl_3$): δ 7.72 (t, 4H, $^3J_{HH}$ = 7.7 Hz, *para*-Ph), 7.62 (dd, 8H, $^3J_{HH}$ = 7.1 Hz, $^3J_{HP}$ = 11.1 Hz, *ortho*-Ph), 7.54 (m, 8H, *meta*-Ph), 7.44 (m, 2H, C_4H_2S), 6.96 (d, 4H, $^3J_{HH}$ = 8.2 Hz, *ortho*-Pipp), 6.62 (d, 4H, $^3J_{HH}$ = 8.2 Hz, *meta*-Pipp), 6.40 (br s, 1H, *H*–N=P), 2.80 (sp, 2H, $^3J_{HH}$ = 6.6 Hz, Pipp-C*H*$(CH_3)_2$), 1.16 (d, $^3J_{HH}$ = 6.6 Hz, 12H, Pipp-CH(C*H*$_3)_2$). ^{11}B{^{1}H} NMR (96 MHz, $CDCl_3$): δ –16.73 (s). ^{13}C{^{1}H} NMR (75 MHz, $CDCl_3$): δ 149.0 (br, C_2/C_5-furan), 143.1 (s, *para*-Pipp), 137.9 (s, *ipso*-Pipp), 135.2 (s, *para*-Ph), 132.8 (d, $^2J_{CP}$ = 5.1 Hz, *ortho*-Ph), 130.4 (d, $^3J_{CP}$ = 3.1 Hz, *meta*-Ph), 127.7 (s, *meta*-Pipp), 123.0 (s, *ortho*-Pipp), 121.2 (s, *ipso*-Ph), 33.5 (s, Pipp-*C*H$(CH_3)_2$), 24.1 (s, Pipp-CH(*C*$H_3)_2$). Note: C_3/C_4-furan was not observed. ^{19}F{^{1}H} NMR (282 MHz, $CDCl_3$): δ –131.63 (d, 8F, *ortho*-C_6F_5), –161.73 (t, 4F, *para*-C_6F_5), –165.59 (t, 8F, *meta*-C_6F_5). ^{31}P{^{1}H} NMR (122 MHz, $CDCl_3$): δ 14.8 (br s). Anal. Calcd. for $C_{70}H_{45}BF_{20}N_2P_2S$: C 60.10; H 3.24; N 2.00; S 2.29; found: C 59.87; H 3.24; N 1.93; S 2.38.

Synthesis of [(PmN(H)=PPh_2)(PmN=PPh_2)C_4H_2S][$B(C_6F_5)_4$] (**26**) In a glove box, **13**

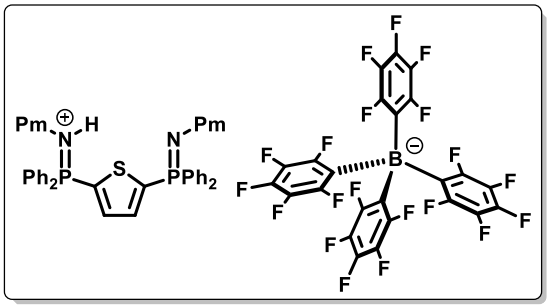

(30.0 mg, 0.0432 mmol) and [$HNMe_2Ph$][$B(C_6F_5)_4$] (35.0 mg, 0.0432 mmol) were toluene added to a 20 mL scintillation vial followed by ~3 mL of toluene creating a light-yellow solution. The reaction was stirred at ambient temperature for 2 h under an argon atmosphere. This yielded a dark-yellow oil. The mixture was left to settle for 16 h. The solvent was decanted, and the oil washed with toluene (4 × 3 mL) followed heptane (2 × 3 mL). The remaining heptane was removed under vacuum to afford a golden yellow coloured solid. Yield: 0.0402 mg, 66.2%. ^{1}H NMR (300 MHz, THF-d_8): δ 13.74 (br s, 1H, *H*–N=P), 7.75 (dd, 8H, $^3J_{HH}$ = 7.2 Hz, $^3J_{HP}$ = 6.0 Hz, *ortho*-Ph), 7.61 (t, 4H, $^3J_{HH}$ = 7.2 Hz, *para*-Ph), 7.53 (d, 2H, $^4J_{HH}$ = 6.0 Hz, *para*-Pm), 7.48 (td, 8H, $^3J_{HH}$ = 3.3, $^3J_{HH}$ = 7.8 Hz, *meta*-Ph), 6.51 (s, 2H, C_4H_2S), 2.19 (s, 12H, *meta*-CH_3-Pm). ^{11}B{^{1}H} NMR (96 MHz, THF-d_8): δ –18.45 (s). ^{13}C{^{1}H} NMR (176 MHz, THF-d_8): δ 168.4 (s, *meta*-Pm), 163.0 (br, *ipso*-Pm), 140.0 (m, C_3/C_4-thiophene), 136.8 (br, C_2/C_5-thiophene), 134.1 (s, *para*-Ph), 133.6 (d, $^3J_{CP}$ = 42 Hz, *ortho*-Ph), 129.8 (d, $^3J_{CP}$ = 51 Hz, *meta*-Ph), 110.5 (s, *para*-Pm), δ 128.5 (d, *ipso*-Ph), 22.4 (s, *meta*-CH_3 Pm). ^{19}F{^{1}H} NMR (282 MHz, THF-d_8): δ –133.70 (d, 8F, *ortho*-C_6F_5), –165.92 (t, 4F, *para*-C_6F_5), –169.42 (t, 8F, *meta*-C_6F_5). ^{31}P{^{1}H} NMR (122 MHz, THF-d_8): δ 13.5 (s).

Synthesis of [(DippN(H)=P^iPr_2)(DippN=P^iPr_2)C_4H_2S][$B(3,5\text{-}(CF_3)_2C_6H_3)_4$] (**27**) In a

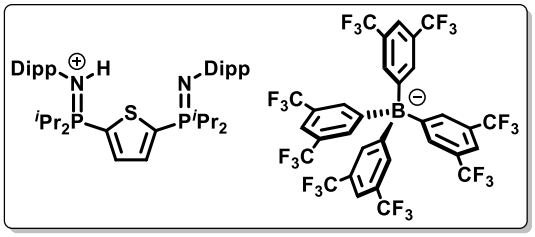

glove box, **14** (142 mg, 0.212 mmol) and Brookhart's acid (215 mg, 0.212 mmol) were added to a 20 mL scintillation vial, followed by ~5 mL of toluene. The reaction was stirred at ambient temperature for 2 h

under an argon atmosphere giving a clear solution and a bright yellow-orange oil. The solvent was decanted, and the oil washed with pentane (4 × 1 mL). Excess solvent was removed under vacuum, resulting in a bright yellow powder. Yield: 244.8 mg, 75.4%. ^{1}H NMR (300 MHz, pyridine-d_5) δ 12.54 (br s, 1H, *H*–N=P), 8.44 (br s, 8H, *ortho*-[B(C$_6$*H*$_3$(CF$_3$)$_2$)$_4$]), 7.91 (br s, 2H, C$_4$*H*$_2$S), 7.83 (s, 4H, *meta*-[B(C$_6$*H*$_3$(CF$_3$)$_2$)$_4$]), 7.26 (ov t, $^{3}J_{HH}$ = 6.6 Hz, 4H, *meta*-Dipp), 7.17 (br ov, 2H, *para*-Dipp), 3.51 (sp, $^{3}J_{HH}$ = 6.7 Hz, 4H, Dipp-C*H*(CH$_3$)$_2$), 2.86 (br s, 4H, P–C*H*(CH$_3$)$_2$), 1.36 (ov dd, $^{3}J_{HP}$ = 16.6, $^{3}J_{HH}$ = 7.0 Hz, 12H, P–CH(C*H*$_3$)$_2$), 1.23 (ov d, $^{3}J_{HH}$ = 6.8 Hz, 36H, Dipp and P–CH(C*H*$_3$)$_2$). ^{11}B{^{1}H} NMR (96 MHz, pyridine-d_5): δ –5.91 (s). ^{13}C{^{1}H} NMR (75 MHz, pyridine-d_5): δ 163.1 ((1:1:1:1 q, $^{1}J_{CB}$ = 50.0 Hz, *ipso*-[B(*C*$_6$H$_3$(CF$_3$)$_2$)$_4$]), 144.2 (br s, *ipso*-Dipp), 135.7 (ov s, *ortho*-[B(*C*$_6$H$_3$(CF$_3$)$_2$)$_4$]), 130.9 (br s, *para*-Dipp), 130.4 (q, $^{1}J_{CF}$ = 2.8 Hz, *C*F$_3$-[B(C$_6$H$_3$(*C*F$_3$)$_2$)$_4$]), 130.0 (q, $^{1}J_{CF}$ = 2.9 Hz, *C*F$_3$-[B(C$_6$H$_3$(*C*F$_3$)$_2$)$_4$]), 129.8-129.3 (br m C$_3$/C$_4$-thiophene), 127.3 (s, *meta*-[B(*C*$_6$H$_3$(CF$_3$)$_2$)$_4$]), 124.3 (s, *para*-[B(*C*$_6$H$_3$(CF$_3$)$_2$)$_4$]), 120.0 (s, *ortho*-Dipp), 118.6 (t, $^{3}J_{CF}$ = 4.0 Hz, *meta*-Dipp), 29.6 (s, P-*C*H(CH$_3$)$_2$), 28.7 (s, Dipp-CH(*C*H$_3$)$_2$), 24.3 (s, Dipp-*C*H(CH$_3$)$_2$), 17.1 (d, $^{2}J_{CP}$ = 1.7 Hz, P–CH(*C*H$_3$)$_2$), 16.31 (d, $^{2}J_{CP}$ = 3.0 Hz, P–CH(*C*H$_3$)$_2$). Note: C$_2$/C$_5$-selenophene was not observed. ^{19}F{^{1}H} NMR (282 MHz, pyridine-d_5): δ –62.06 (s). ^{31}P{^{1}H} NMR (122 MHz, pyridine-d_5): δ 7.1 (s). Anal. Calcd. for C$_{72}$H$_{77}$BF$_{24}$N$_2$P$_2$S: C 56.48; H 5.07; N 1.83; S 2.09; found: 56.28; H 5.04; N 1.81; S 2.24.

Synthesis of [(DippN(H)=PPh$_2$)(DippN=PPh$_2$)C$_4$H$_2$Se][B(3,5-(CF$_3$)$_2$C$_6$H$_3$)$_4$] (**28**) In a

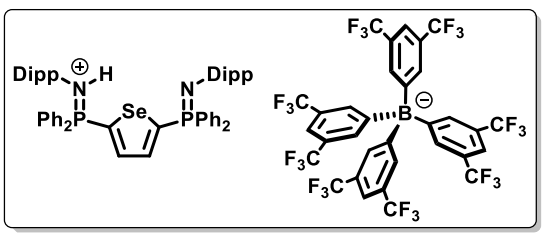

glove box, **17** (44.4 mg, 0.0522 mmol) and Brookhart's acid (52.9 mg, 0.0522 mmol) were added to a 20 mL scintillation vial, followed by ~5 mL of toluene. The reaction was stirred at ambient temperature for

2 h under an argon atmosphere. This yielded a clear solution with a brown oil. The solvent was decanted, and the oil washed with pentane (4 × 1 mL). Excess solvent was removed under vacuum, resulting in a brown chucky solid. Yield: 78.4 mg, 87.6%. ^{1}H NMR (300 MHz, pyridine-d_5): δ 12.75 (br s, 1H, *H*–N=P), 8.44 (br s, 8H, *ortho*-[B(C$_6$*H*$_3$(CF$_3$)$_2$)$_4$]), 7.84 (br t, $^{3}J_{HP}$ = 9.9 Hz, 12H, *meta*-[B(C$_6$*H*$_3$(CF$_3$)$_2$)$_4$] and *ortho*-Ph), 7.76 (dd, $^{3}J_{HP}$ = 7.1, $^{4}J_{HP}$ = 3.5 Hz, 2H, C$_4$*H*$_2$Se), 7.64 (ov m, 4H, *para*-Ph), 7.51 (br td, $^{3}J_{HH}$ = 7.4 Hz, $^{4}J_{HP}$ = 3.0 Hz, 8H, *meta*-Ph), 7.28 (ov m, $^{3}J_{HH}$ = 7.4 Hz, 2H, *para*-Dipp), 7.18 (ov t, $^{3}J_{HH}$ = 7.4 Hz, 4H, *meta*-Dipp), 3.51 (sp, $^{3}J_{HH}$ = 6.8 Hz, 4H, Dipp-C*H*(CH$_3$)$_2$), 0.99 (ov d, $^{3}J_{HH}$ = 6.8 Hz, 24H, Dipp-CH(*CH*$_3$)$_2$)). ^{11}B{^{1}H} NMR (96 MHz, pyridine-d_5): δ –5.91 (s). ^{13}C{^{1}H} NMR (75 MHz, pyridine-d_5): δ 163.1 (1:1:1:1 q, $^{1}J_{CB}$ = 49.7 Hz, *ipso*-[B(*C*$_6$H$_3$(CF$_3$)$_2$)$_4$]), 144.8 (d, $^{2}J_{CP}$ = 6.2 Hz, *ipso*-Dipp), 141.1 (br s, C$_3$/C$_4$-selenophene), 135.8 (ov s, *ortho*-[B(*C*$_6$H$_3$(CF$_3$)$_2$)$_4$]), 133.6 (d, $^{4}J_{CP}$ = 2.1 Hz, *para*-Dipp), 133.1 (d, $^{3}J_{CP}$ = 10.2 Hz, *meta*-Dipp), 131.7 (d, $^{1}J_{CP}$ = 87.8 Hz, *ipso*-Ph), 130.5 (q, $^{1}J_{CF}$ = 2.7 Hz, *C*F$_3$-[B(C$_6$H$_3$(*C*F$_3$)$_2$)$_4$]), 130.1 (q, $^{1}J_{CF}$ = 2.9 Hz, *C*F$_3$-[B(C$_6$H$_3$(*C*F$_3$)$_2$)$_4$]), 129.7 (d, $^{2}J_{CP}$ = 22.9, *ortho*-Dipp), 127.3 (s, *meta*-[B(*C*$_6$H$_3$(CF$_3$)$_2$)$_4$]), 126.2 (s, *meta*-Dipp), 123.7 (ov s, *para*-[B(C$_6$H$_3$(*C*F$_3$)$_2$)$_4$]), 118.77 (m, $^{3}J_{CF}$ = 3.7 Hz, *para*-[B(C$_6$H$_3$(*C*F$_3$)$_2$)$_4$]), 30.48 (s, Dipp-*C*H(CH$_3$)$_2$), 24.29 (s, Dipp-CH(*C*H$_3$)$_2$). Note: C$_2$/C$_5$-selenophene was not observed. ^{19}F{^{1}H} NMR (282 MHz, pyridine-d_5): δ –62.06 (s). ^{31}P{^{1}H} NMR (122 MHz, pyridine-d_5): δ –8.6 (br s). Anal. Calcd. for C$_{84}$H$_{69}$BF$_{24}$N$_2$P$_2$Se: C 58.86; H 4.06; N 1.63; found: C 58.79; H 4.14; N 1.73.

Synthesis of [(DippN(H)=P^{i}Pr$_2$)(DippN=P^{i}Pr$_2$)C$_4$H$_2$Se][B(3,5-(CF$_3$)$_2$C$_6$H$_3$)$_4$] (**29**) In a

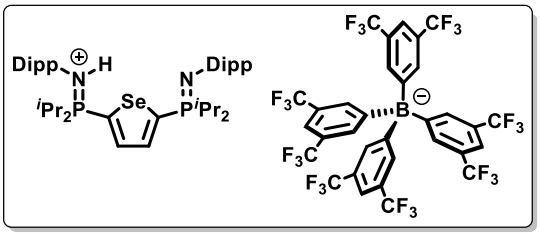

glove box, **18** (106 mg, 0.148 mmol) and Brookhart's acid (150 mg, 0.148 mmol) were added to a 20 mL scintillation vial, followed by ~5 mL of toluene. The reaction was stirred at ambient temperature for 2 h under an argon atmosphere. This yielded a clear solution with a brown-beige oil. The solvent was decanted, and the oil washed with pentane (4 × 1 mL). Excess solvent was removed under vacuum, resulting in a beige-peachy solid. Yield: 206.3 mg, 87.2%. ^{1}H NMR (300 MHz, pyridine-d_5): δ 8.44 (br s, 8H, *ortho*-[B(C$_6$*H*$_3$(CF$_3$)$_2$)$_4$]), 8.19 (br s, 2H, C$_4$*H*$_2$Se), 7.83 (s, 4H, *meta*-[B(C$_6$*H*$_3$(CF$_3$)$_2$)$_4$]), 7.26 (ov m, 6H, *meta*/*para*-Dipp), 3.51 (sp, $^3J_{HH}$ = 6.8 Hz, 4H, Dipp-C*H*(CH$_3$)$_2$), 2.90 (br s, 4H, P–C*H*(CH$_3$)$_2$), 1.53-1.25 (m, 24H, P–CH(C*H*$_3$)$_2$), 1.21 (d, $^2J_{HH}$ = 6.8 Hz, 24H, Dipp-CH(C*H*$_3$)$_2$). Note: *H*–N=P signal was not observed. ^{11}B NMR (96 MHz, pyridine-d_5): δ –4.76 (s). ^{13}C NMR (75 MHz, pyridine-d_5): δ 163.1 (1:1:1:1 q, $^1J_{CB}$ = 49.8 Hz, *ipso*-[B(*C*$_6$H$_3$(CF$_3$)$_2$)$_4$]), 135.8 (s, *ortho*-[B(*C*$_6$H$_3$(CF$_3$)$_2$)$_4$]), 131.1-129.4 (m, *C*F$_3$-[B(C$_6$H$_3$(*C*F$_3$)$_2$)$_4$]), 130.0-127.3 (br, m C$_3$/C$_4$-selenophene), 129.6 (s, *meta*-Dipp), 129.1 (s, *para*-Dipp), 127.3 (s, *meta*-[B(*C*$_6$H$_3$(CF$_3$)$_2$)$_4$]), 120.1 (s, *ortho*-Dipp), 118.8 (t, $^3J_{CF}$ = 4.1 Hz, *para*-[B(*C*$_6$H$_3$(CF$_3$)$_2$)$_4$]), 29.7 (s, Dipp-*C*H(CH$_3$)$_2$), 28.9 (s, P–*C*H(CH$_3$)$_2$), 24.4 (s, Dipp-CH(*C*H$_3$)$_2$), 16.9 (d, $^1J_{CP}$ = 49.2 Hz, P–CH(*C*H$_3$)$_2$), Note: Dipp *ipso*, and C$_2$/C$_5$-selenophene signals were not observed. ^{19}F NMR (282 MHz, pyridine-d_5): δ –60.92 (s). ^{31}P NMR (122 MHz, pyridine-d_5): δ 11.07 (br s). Anal. Calcd. for C$_{72}$H$_{77}$BF$_{24}$N$_2$P$_2$Se: C 54.80; H 4.92; N 1.78; found: C 54.76; H 4.96; N 1.76.

Synthesis of [(PippN(H)=P^{i}Pr$_2$)(PippN=P^{i}Pr$_2$)C$_4$H$_2$Se][B(C$_6$F$_5$)$_4$] (**30**) In a glove box,

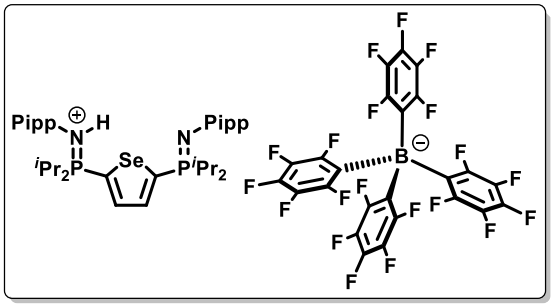

19 (50.6 mg, 0.0800 mmol) and [HNMe$_2$Ph][B(C$_6$F$_5$)$_4$] (99.8 mg, 0.120 mmol) were added to a 20 mL scintillation vial followed by ~5 mL of toluene. The reaction was stirred at ambient temperature for 2 h under an argon atmosphere. This yielded a dark-yellow oil. The solvent was decanted, and the oil was with 4 portions of pentane (~1 mL). Excess solvent was removed under vacuum, resulting in a yellow solid. Yield: 106.6 mg, 92.2%. ^{1}H NMR (300 MHz, CDCl$_3$): δ 8.10 (dd, 2H, $^{3}J_{HP}$ = 3.9 Hz, $^{4}J_{HP}$ = 5.0 Hz, C$_4$*H*$_2$Se), 7.19 (d, 4H, $^{3}J_{HH}$ = 7.9 Hz, *ortho*-Pipp), 6.90 (d, 4H, $^{3}J_{HH}$ = 7.9 Hz, *meta*-Pipp), 4.84 (br s, 1H, *H*–N=P), 2.89 (ov sp, 6H, Pipp-C*H*(CH$_3$)$_2$ and P–C*H*(CH$_3$)$_2$), 1.30 (ov m, 36H, Pipp-CH(C*H*$_3$)$_2$ and P–CH(C*H*$_3$)$_2$). ^{11}B{^{1}H} NMR (96 MHz, CDCl$_3$): δ –16.68 (s). ^{13}C{^{1}H} NMR (75 MHz, CDCl$_3$): δ 148.2 (br m, C$_3$/C$_4$-selenophene), 142.6 (br m, C$_2$/C$_5$-selenophene), 128.9 (d, $^{2}J_{CP}$ = 27.7 Hz, *ipso*-Pipp), 128.8 (s, *meta*-Pipp), 124.2 (s, *ortho*-Pipp), 33.3 (s, Pipp-*C*H(CH$_3$)$_2$), 25.6 (d, $^{1}J_{CP}$ = 41.1 Hz, P–*C*H(CH$_3$)$_2$), 23.9 (s, Pipp-CH(*C*H$_3$)$_2$) 15.6 (m, P–CH(*C*H$_3$)$_2$). ^{19}F{^{1}H} NMR (282 MHz, CDCl$_3$): δ –131.58 (d, 8F, *ortho*-C$_6$*F*$_5$), –161.15 (t, 4F, *para*-C$_6$*F*$_5$), –165.30 (t, 8F, *meta*-C$_6$*F*$_5$). ^{31}P{^{1}H} NMR (122 MHz, CDCl$_3$): δ 56.4 (s). Anal. Calcd. for C$_{58}$H$_{53}$BF$_{20}$N$_2$P$_2$Se: C 53.19; H 4.08; N 2.14; found: C 53.12; H 4.13; N 2.06.

Synthesis of [(PippN(H)=PPh$_2$)$_2$C$_4$H$_2$O][B(C$_6$F$_5$)$_4$]$_2$ (**31**) In a glove box, **4** (54.0 mg, 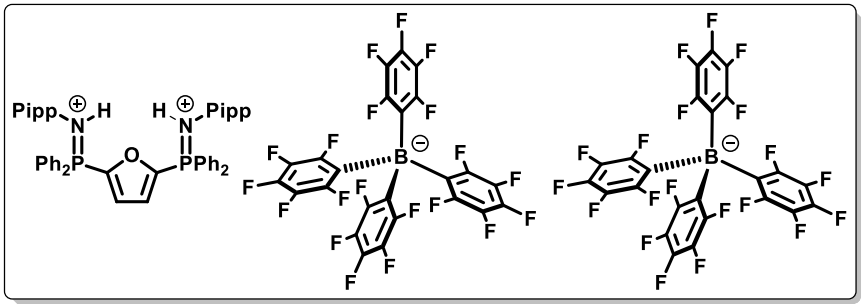

0.0768 mmol) and [HNMe$_2$Ph][B(C$_6$F$_5$)$_4$] (123 mg, 0.154 mmol) were added to a 20 mL scintillation vial followed by ~5 mL of benzene. The reaction was stirred at ambient temperature for 2 h under an argon atmosphere. This yielded a dark-brown oil. The solvent was decanted, and the oil washed with 4 portions of pentane (~1 mL). Excess solvent was removed under vacuum affording a light-brown solid. Yield: 127.0 mg, 79.8%. ^{1}H NMR (300 MHz, CDCl$_3$): δ 7.92 (m, 4H, *para*-Ph), 7.72-7.51 (ov m, 16H, *ortho*/*meta*-Ph), 7.35 (s, 2H, C$_4$*H*$_2$O), 7.02 (d, 4H, $^3J_{HH}$ = 8.2 Hz, *ortho*-Pipp), 6.59 (d, 4H, $^3J_{HH}$ = 8.2 Hz, *meta*-Pipp), 5.43 (d, 2H, $^2J_{HP}$ = 11.0 Hz, *H*–N=P), 2.81 (sp, 2H, $^3J_{HH}$ = 6.6 Hz, Pipp-C*H*(CH$_3$)$_2$), 1.14 (d, $^3J_{HH}$ = 6.6 Hz, 12H, Pipp-CH(C*H*$_3$)$_2$). ^{11}B{^{1}H} NMR (96 MHz, CDCl$_3$): δ –16.73 (s). ^{13}C{^{1}H} NMR (75 MHz, CDCl$_3$): δ 148.1 (s, *para*-Pipp), 143.2 (br d, $^1J_{CP}$ = 52.0 Hz, C$_2$/C$_5$-furan), 137.9 (s, Ph-*para*), 133.1 (d, $^3J_{CP}$ = 2.9 Hz, *meta*-Ph), 131.2 (d, $^2J_{CP}$ = 4.7 Hz, *ortho*-Ph), 131.0 (br, *ipso*-Pipp), 129.0 (br, C$_3$/C$_4$-furan), 128.6 (s, *ortho*-Pipp), 120.9 (s, *meta*-Pipp), 33.6 (s, Pipp-*C*H(CH$_3$)$_2$), 23.8 (s, Pipp-CH(*C*H$_3$)$_2$). Note: *ipso*-Ph was not observed. ^{19}F{^{1}H} NMR (282 MHz, CDCl$_3$): δ –131.55 (d, 8F, *ortho*-C$_6$*F*$_5$), –161.21 (t, 4F, *para*-C$_6$*F*$_5$), –165.31 (t, 8F, *meta*-C$_6$*F*$_5$). ^{31}P{^{1}H} NMR (122 MHz, CDCl$_3$): δ 22.7 (s). Anal. Calcd. for C$_{94}$H$_{46}$B$_2$F$_{40}$N$_2$OP$_2$: C 54.73; H 2.25; N 1.36; found: C 54.87; H 2.36; N 1.38.

Synthesis of [(DippN=PPh$_2$)$_2$C$_4$H$_2$OZnMe][B(C$_6$F$_5$)$_4$] (**32**) In a glove box, **20** (35.9 mg,

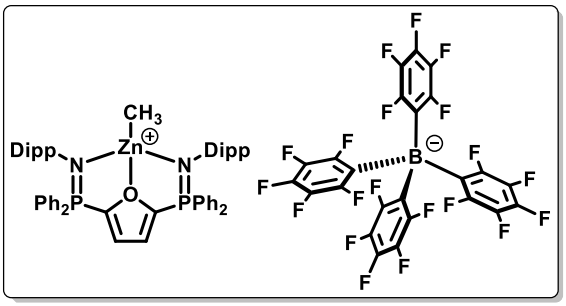

0.0245 mmol) was added to a 20 mL scintillation vial, followed by 5 mL of bromobenzene, resulting in a yellow solution. Dimethyl zinc (29.4 μL, 0.0245 mmol, 1.2 M) was slowly injected into the stirring solution over a period of 5 min. Immediately afterwards a bright orange-red solution was observed, along with a small amount of bubbling. The solution was stirred for 2 h under an argon atmosphere. An orange solution resulted, to which pentane (~2 mL) was added. The mixture was allowed to stir for 30 min. The solvent was then removed under vacuum, resulting in a thick dark-orange oil. The oil was washed with three portions of pentane (3 mL), and the remaining pentane was removed under vacuum, giving a peach-orange solid. Yield: 27.9 mg, 72.9%. ^{1}H NMR (300 MHz, pyridine-d_5): δ 7.78 (dd, $^3J_{HH}$ = 13.6 Hz, $^3J_{HH}$ = 7.0 Hz, 8H, *meta*-Ph), 7.54 (dt, $^3J_{HH}$ = 13.6 Hz, $^4J_{HH}$ = 3.2, 4H, *para*-Ph), 7.42 (td, $^3J_{HP}$ = 7.0 Hz, $^3J_{HH}$ = 3.2 Hz, 8H, *ortho*-Ph), 7.21-7.13 (ov m, 4H, *meta*-Dipp), 7.10 (dd, $^2J_{HP}$ = 9.6 Hz, $^3J_{HP}$ = 2.9 Hz, 2H, C$_4$*H*$_2$O), 7.06 (s, 2H, *para*-Dipp), 3.59 (sp, $^3J_{HH}$ = 6.7 Hz, 4H, Dipp-C*H*(CH$_3$)$_2$), 1.05 (d, $^3J_{HH}$ = 6.9 Hz, 24H, Dipp-CH(C*H*$_3$)$_2$), –0.16 (s, 3H, Zn–C*H*$_3$). ^{11}B{^{1}H} NMR (96 MHz, pyridine-d_5): δ –15.94 (s). ^{13}C{^{1}H} NMR (75 MHz, pyridine-d_5): δ 144.2 (s, *ortho*-Dipp), 143.3 (d, $^2J_{CP}$ = 7.4 Hz, *ipso*-Dipp), 133.0 (d, $^1J_{CP}$ = 107.3 Hz, *ipso*-Ph), 132.5 (d, $^2J_{CP}$ = 10.3 Hz, *meta*-Ph), 131.1 (s, *para*-Ph), 129.4 (d, $^3J_{CP}$ = 12.8 Hz, *ortho*-Ph), 127.9 (s, *para*-Dipp), 123.5 (s, *meta*-Dipp), 29.5 (s, Dipp-*C*H(CH$_3$)$_2$), 24.3 (s, Dipp-CH(*C*H$_3$)$_2$), –17.1 (s, Zn–C*H*$_3$). Note: C$_{2\text{-}5}$-furan were not observed. ^{19}F{^{1}H} NMR (282 MHz, pyridine-d_5): δ –132.13 (s, 8F, *ortho*-F), –162.18 (t, 4F, $^3J_{FF}$ = 20.9 Hz, *para*-F), –166.29 (t, 8F, $^3J_{FF}$ = 18.2 Hz,

meta-F). $^{31}P\{^{1}H\}$ NMR (122 MHz, pyridine-d_5): δ –23.4 (s). Anal. Calcd. for $C_{77}H_{54}BF_{24}N_2P_2OZn$: C 59.81; H 3.85; N 1.81; found: C 59.79; H 3.84; N 1.80.

Synthesis of $[(PippN{=}PPh_2)_2C_4H_2OZnMe][B(C_6F_5)_4]$ (**33**) In a glove box, **21** (50.0 mg, 0.0362 mmol) was added to a 20 mL scintillation vial followed by 5 mL of bromobenzene, resulting in a yellow solution. Dimethyl zinc (30.0 μL, 0.0398 mmol, 1.2 M) was slowly injected into the stirring solution over a period of 5 min. Immediately afterwards, the solution became less yellow in which an oil formed over 10 min. The solution was stirred for 2 h under an argon atmosphere. Pentane (~2 mL) was added to the vial and the mixture stirred for 30 min, after which the solvent was decanted, and the resulting oil further washed with three portions of pentane (3 mL). The remaining volatiles were removed *in vacuo* to afford a pale-yellow solid. Yield: 60.5 mg, 78.1%. ^{1}H NMR (300 MHz, CD_2Cl_2): δ 7.81-7.61 (ov m, 12H, *para*/*ortho*-Ph), 7.54 (m, 8H, *meta*-Ph), 7.13 (s, 2H, C_4H_2O), 6.89 (d, 4H, $^{3}J_{HH}$ = 8.0 Hz, *ortho*-Pipp), 6.76 (d, 4H, $^{3}J_{HH}$ = 8.0 Hz, *meta*-Pipp), 2.76 (sp, 2H, $^{3}J_{HH}$ = 6.8 Hz, Pipp-C*H*$(CH_3)_2$), 1.15 (d, $^{3}J_{HH}$ = 6.8 Hz, 12H, Pipp-CH(C*H*$_3)_2$), –1.11 (s, 3H, Zn–C*H*$_3$). $^{11}B\{^{1}H\}$ NMR (96 MHz, CD_2Cl_2): δ –18.46 (s). $^{13}C\{^{1}H\}$ NMR (75 MHz, CD_2Cl_2): δ 147.2 (s, *ipso*-Pipp), 134.5 (s, *para*-Ph), 133.7 (d, $^{2}J_{CP}$ = 9.8 Hz, *ortho*-Ph), 132.5 (s, *para*-Pipp), 130.2 (d, $^{1}J_{CP}$ = 130.2 Hz, *ipso*-Ph), 130.2 (d, $^{3}J_{CP}$ = 12.8 Hz, *meta*-Ph), 129.5 (m, C_2/C_5-furan), 127.8 (s, *meta*-Pipp), 127.8 (s, *ortho*-Pipp), 126.9-126.1 (br ov m, C_3/C_4-furan and *ortho*-Pipp), 34.5 (s, *C*H$(CH_3)_2$), 24.7 (s, CH(*C*H$_3)_2$), –15.1 (s, ZnC*H*$_3$). $^{19}F\{^{1}H\}$ NMR (282 MHz, CD_2Cl_2): δ –133.71 (d, 8F, *ortho*-C_6F_5), –165.98 (t, 4F, *para*-C_6F_5), –169.45 (t, 8F, *meta*-C_6F_5). $^{31}P\{^{1}H\}$

NMR (122 MHz, CD_2Cl_2): δ was not observed. Anal. Calcd. for $C_{71}H_{47}BF_{20}N_2OP_2Zn$: C 58.32; H 3.24; N 1.92; found: C 58.19; H 3.35; N 2.24.

Synthesis of [(DippN=P^{i}Pr$_2$)$_2$C$_4$H$_2$OZnMe][B(3,5-(CF$_3$)$_2$C$_6$H$_3$)$_4$] (**34**) In a glove box, 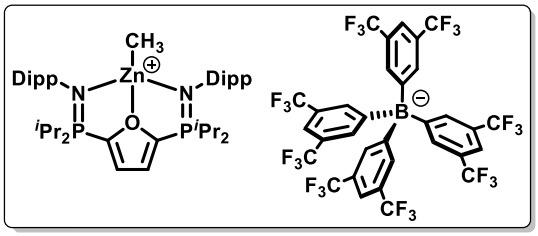

23 (43.4 mg, 0.0286 mmol) was added to a 20 mL scintillation vial followed by 5 mL of bromobenzene, resulting in a yellow-peach solution. Dimethyl zinc (24.0 μL, 0.0286 mmol, 1.2 M) was slowly injected into the stirring solution over a period of 5 min. A small amount of bubbling was observed. The solution was stirred for 2 h under an argon atmosphere. Pentane (~2 mL) was added to the now pink solution and the mixture was stirred for 30 min. The solvent was removed under vacuum resulting in a red oil. The oil was washed with three portions of pentane (3 mL), and the remaining pentane removed under vacuum to give a pink-peach coloured powder. Yield: 39.9 mg, 87.5%. ^{1}H NMR (300 MHz, pyridine-d_5): δ 8.43 (s, 8H, *ortho*-[B(C$_6$*H*$_3$(CF$_3$)$_2$)$_4$]), 7.83 (s, 4H, *meta*-[B(C$_6$*H*$_3$(CF$_3$)$_2$)$_4$]), 7.60 (s, 2H, C$_4$*H*$_2$O), 7.33 (s, 2H, *meta*-Dipp), 7.24 (s, 2H, *meta*-Dipp), 7.06 (t, $^3J_{HH}$ = 7.4 Hz, 2H, *para*-Dipp), 3.61 (sp, $^3J_{HH}$ = 6.7 Hz, 4H, Dipp-*C*H(CH$_3$)$_2$), 2.63 (d sp, $^1J_{HP}$ = 14.1 Hz, $^3J_{HH}$ = 7.0 Hz, 4H, P–C*H*(CH$_3$)$_2$), 1.36 (d, $^3J_{HH}$ = 7.0 Hz, 6H, P–CH(C*H*$_3$)$_2$), 1.30 (ov d, $^3J_{HH}$ = 5.3 Hz, 30H, Dipp and P–CH(C*H*$_3$)$_2$), 1.15 (dd, $^3J_{HP}$ = 17.3 Hz, $^3J_{HH}$ = 7.0 Hz, 12H, P–CH(C*H*$_3$)$_2$), –0.14 (s, 3H, Zn–C*H*$_3$). ^{11}B{^{1}H} NMR (96 MHz, pyridine-d_5): δ –4.41 (s). ^{13}C{^{1}H} NMR (75 MHz, pyridine-d_5) δ 163.2 (1:1:1:1 q, $^1J_{CB}$ = 49.8 Hz, *ipso*-[B(*C*$_6$H$_3$(CF$_3$)$_2$)$_4$]), 153.7 (dd, $^1J_{CP}$ = 93.8 Hz, $^4J_{CP}$ = 2.2 Hz, C$_2$/C$_5$-furan), 145.7 (s, *ortho*-Dipp), 142.4 (d, $^2J_{CP}$ = 6.0 Hz, *ipso*-Dipp), 135.8 (s, *ortho*-[B(*C*$_6$H$_3$(CF$_3$)$_2$)$_4$]), 130.6 (m, *C*F$_3$-[B(*C*$_6$H$_3$(CF$_3$)$_2$)$_4$]), 130.5 (q, $^1J_{CF}$ = 2.8 Hz, *C*F$_3$-[B(C$_6$H$_3$(*C*F$_3$)$_2$)$_4$]), 130.1 (q, $^1J_{CF}$ = 2.8 Hz, *C*F$_3$-[B(C$_6$H$_3$(*C*F$_3$)$_2$)$_4$]), 129.7 (m, *C*F$_3$-[B(C$_6$H$_3$(*C*F$_3$)$_2$)$_4$]), 129.5 (d,

$^{1}J_{CP}$ = 56.1 Hz, P–*C*H(CH$_3$)$_2$), 127.9 (s, *para*-Dipp), 127.4 (s, *meta*-[B(C$_6$H$_3$(*C*F$_3$)$_2$)$_4$]), 123.5 (s, *meta*-Dipp), 122.0 (dd, $^{2}J_{CP}$ = 12.2 Hz, $^{3}J_{CP}$ = 7.0 Hz, C$_3$/C$_4$-furan), 119.9 (d, $^{5}J_{CP}$ = 2.2 Hz, *para*-Dipp), 118.8 (d, $^{3}J_{CF}$ = 3.8 Hz, *para*-[B(*C*$_6$H$_3$(CF$_3$)$_2$)$_4$]), 29.4 (s, P–*C*H(CH$_3$)$_2$), 29.2 (s, Dipp-CH(*C*H$_3$)$_2$), 28.3 (s, Dipp-CH(*C*H$_3$)$_2$), 24.3 (s, Dipp-*C*H(CH$_3$)$_2$), 17.1 (d, $^{2}J_{CP}$ = 2.1 Hz, P–CH(*C*H$_3$)$_2$), 16.1 (d, $^{2}J_{CP}$ = 3.6 Hz, P–CH(*C*H$_3$)$_2$), –16.7 (s, Zn–*C*H$_3$). ^{19}F{^{1}H} NMR (282 MHz, pyridine- d_5): δ –62.07 (s). ^{31}P{^{1}H} NMR (122 MHz, pyridine-d_5): δ 0.2 (s). Anal. Calcd. for C$_{73}$H$_{79}$BF$_{24}$N$_2$OP$_2$Zn: C 54.99; H 4.99; N 1.76; found: C 54.41; H 4.62; N 1.39.

Synthesis of [(DippN=PPh$_2$)$_2$C$_4$H$_2$SZnMe][B(3,5-(CF$_3$)$_2$C$_6$H$_3$)$_4$] (**35**) In a glove box, **24**

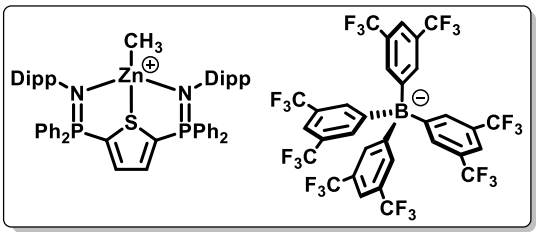

(60.1 mg, 0.0360 mmol) was added to a 20 mL scintillation vial, followed by 5 mL of bromobenzene, resulting in a yellow solution. Dimethyl zinc (30.05 μL, 0.0360 mmol, 1.2 M) was slowly injected into the stirring solution over a period of 5 min. A gradual colour change to pale yellow-green, along with effervescence, was observed over the next 30 min. The solution was stirred for 2 h under an argon atmosphere. Pentane (~2 mL) was added to the dark-green solution after which the mixture was stirred for 30 min. The solvent was removed under vacuum resulting in a thick dark green-brown oil. The oil was washed with three portions of pentane (3 mL), and the remaining pentane was removed under vacuum, yielding a brown solid. Yield: 47.0 mg, 74.9%. ^{1}H NMR (300 MHz, pyridine-d_5): δ 8.44 (s, 8H, *ortho*-[B(C$_6$*H*$_3$(CF$_3$)$_2$)$_4$]), 7.84 (ov m, 12H, *meta*-Ph and *meta*-[B(C$_6$*H*$_3$(CF$_3$)$_2$)$_4$]), 7.52 (ov d, $^{3}J_{HH}$ = 7.4 Hz, 4H, *para*-Ph), 7.49-7.38 (m, 8H, *ortho*-Ph), 7.35 (dd, $^{3}J_{HP}$ = 5.3, $^{4}J_{HP}$ = 3.3 Hz, 2H, C$_4$*H*$_2$S), 7.18 (ov s, 4H, *meta*-Dipp), 7.07 (t, $^{3}J_{HH}$ = 8.5 Hz, 2H, *para*-Dipp), 3.59 (sp, $^{3}J_{HH}$ = 6.9 Hz, 4H, Dipp-C*H*(CH$_3$)$_2$), 1.02 (d, $^{3}J_{HH}$ = 6.9 Hz, 24H, Dipp-CH(C*H*$_3$)$_2$), –0.09 (s, 3H, Zn–C*H*$_3$). ^{11}B{^{1}H} NMR

(96 MHz, pyridine-d_5): δ –5.91 (s). $^{13}C\{^1H\}$ NMR (75 MHz, pyridine-d_5): δ 143.5 (d, $^2J_{CP}$ = 7.4 Hz, *ipso*-Dipp), 135.0 (br s, *ortho*-Dipp), 134.6 (s, *meta*-[B($C_6H_3(CF_3)_2)_4$]), 133.9 (d, $^1J_{CP}$ = 106.5 Hz, *ipso*-Ph), 132.8 (s, *para*-Dipp), 132.7 (s, *meta*-Ph), 132.3 (s, *meta*-Dipp), 132.3-131.1 (br m, C_2/C_5-furan), 132.0-130.5 (m, CF_3-[B($C_6H_3(CF_3)_2)_4$]), 129.4 (d, $^1J_{CP}$ = 12.6 Hz, *ortho*-Ph), 127.33 (s, *ipso*-[B($C_6H_3(CF_3)_2)_4$]), 120.8 (s, *meta*-Dipp), 118.8 (s, *para*-[B($C_6H_3(CF_3)_2)_4$]), 29.5 (s, Dipp-$CH(CH_3)_2$), 24.4 (s, Dipp-$CH(CH_3)_2$), –13.0 (s, Zn–CH_3). Note: *ipso*-[B($C_6H_3(CF_3)_2)_4$] and $C_{2/5}$-thiophene resonances were not observed. $^{19}F\{^1H\}$ NMR (282 MHz, pyridine-d_5): δ –62.07 (s). $^{31}P\{^1H\}$ NMR (122 MHz, pyridine-d_5): δ –17.1 (s). Anal. Calcd. for $C_{85}H_{71}BF_{24}N_2P_2SZn$: C 58.45; H 4.10; N 1.60; S 1.84; found: C 58.89; H 4.18; N 1.63; S 1.44.

Synthesis of [(PippN=$PPh_2)_2C_4H_2S$ZnMe][B($C_6F_5)_4$] (**36**) In a glove box, **25** (50.0 mg, 0.0357 mmol) was added to a 20 mL scintillation vial, followed by 5 mL of bromobenzene, resulting in a yellow solution. Dimethyl zinc (33.0 μL, 0.0393 mmol, 1.2 M) was slowly injected into the stirring solution over a period of 5 min. Immediately after, the solution became less yellow, and an oil formed over 10 min. The reaction was stirred for 2 h with no significant change observed. Pentane (~2 mL) was added to the vial and the mixture stirred for 30 min after which the solvent was decanted, and the resulting oil washed with three portions of pentane (3 mL). The remaining volatiles were removed *in vacuo* to give a pale-yellow solid. Yield: 61.5 mg, 79.9%. ^1H NMR (300 MHz, d_8-THF): δ 7.9-7.4 (br ov m, 20H, *ortho*/*meta*/*para*-Ph), 7.3 (m, 2H, C_4H_2S), 7.0-6.7 (br ov m, 8H, Pipp *ortho*/*meta*), 2.8 (sp, $^3J_{HH}$ = 6.9 Hz, 2H, Pipp-$CH(CH_3)_2$), 1.14 (d, $^3J_{HH}$ = 6.9 Hz, 12H, Pipp-$CH(CH_3)_2$), –1.18 (s, 3H, Zn–CH_3).

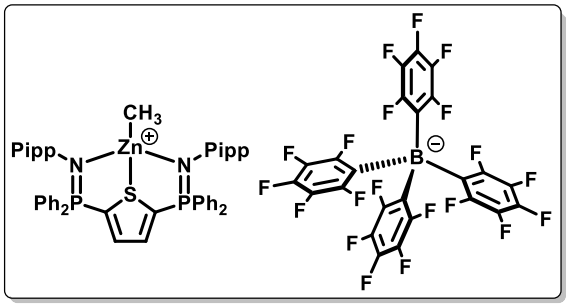

^{11}B NMR (96 MHz, d_8-THF): δ –18.45 (s). ^{13}C{H} NMR (75 MHz, d_8-THF): δ 135.5-133.1 (br ov m, *ortho*/*para*-Ph), 131.9 (d, $^3J_{HP}$ = 95.8, *ipso*-Ph), 130.2 (d, $^3J_{CP}$ = 12.1 Hz, *meta*-Ph), 128.6 (*para*-Pipp), 128.0 (s, *meta*-Pipp), 127.7 (m, *ortho*-Pipp), 34.5 (s, Pipp-*C*H(CH$_3$)$_2$), 24.7 (s, Pipp-CH(*C*H$_3$)$_2$), –14.60 (s, Zn–C*H*$_3$). Note: *ipso*-Pipp and C$_{2\text{-}5}$-thiophene carbons were not observed. ^{19}F NMR (282 MHz, d_8-THF): δ –133.70 (s, 8F, *ortho*-C$_6$F$_5$), –165.98 (br, 4F, *para*-C$_6$F$_5$), –169.45 (br, 8F, *meta*-C$_6$F$_5$). ^{31}P{H} NMR (CDCl$_3$): δ 26.7 (br s), –8.71 (br s). Anal. Calcd. for C$_{70}$H$_{45}$BF$_{20}$N$_2$P$_2$SZn: C 57.68; H 3.20; N 1.89; S 2.17; found: C 57.10; H 3.62; N 1.81; S 2.29.

Synthesis of [(DippN=P^{i}Pr$_2$)$_2$C$_4$H$_2$SZnMe][B(3,5-(CF$_3$)$_2$C$_6$H$_3$)$_4$] (**37**) In a glove box,

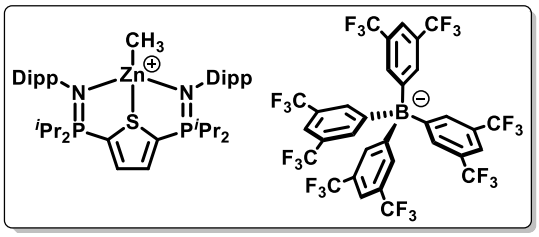

27 (71.8 mg, 0.0510 mmol) was added to a 20 mL scintillation vial, followed by 5 mL of bromobenzene, resulting in a yellow solution. Dimethyl zinc (43.0 μL, 0.0510 mmol, 1.2 M) was slowly injected into the stirring solution over a period of 5 min. A small amount of bubbling was observed. The solution was stirred for 2 h under an argon atmosphere. Pentane (~2 mL) was added, and the mixture stirred for 30 min. The solvent was removed under vacuum resulting in an orange-yellow oil. The oil was washed with three portions of pentane (3 mL), and the remaining pentane was removed under vacuum. This gave a yellow-peach powder. Yield: 76.1 mg, 92.7%. ^{1}H NMR (300 MHz, pyridine-d_5): δ 8.43 (s, 8H, *ortho*-[B(C$_6$*H*$_3$(CF$_3$)$_2$)$_4$]), 7.83 (s, 4H, *para*-[B(C$_6$*H*$_3$(CF$_3$)$_2$)$_4$]), 7.74–7.63 (m, 2H, C$_4$*H*$_2$S), 7.33-7.24 (m, 4H, *meta*-Dipp), 7.06 (t, $^3J_{HH}$ = 7.6 Hz, 2H, *para*-Dipp), 3.62 (br d, $^3J_{HH}$ = 6.9 Hz, 4H, Dipp-C*H*(CH$_3$)$_2$), 2.61 (d sp, $^3J_{HP}$ = 14.0 Hz, $^3J_{HH}$ = 6.9 Hz, 4H, P–C*H*(CH$_3$)$_2$), 1.35 (d, $^3J_{HH}$ = 7.0 Hz, 6H, P–CH(C*H*$_3$)$_2$), 1.28 (d, $^3J_{HH}$ = 6.9 Hz, 30H, Dipp and P–CH(C*H*$_3$)$_2$), 1.12 (dd, $^3J_{HP}$ = 17.3 Hz, $^3J_{HH}$ = 6.9 Hz, 12H, P–CH(C*H*$_3$)$_2$),

–0.15 (s, 3H, Zn–CH_3). $^{11}B\{^1H\}$ NMR (96 MHz, pyridine-d_5): δ –4.39 (s). $^{13}C\{^1H\}$ NMR (75 MHz, pyridine-d_5): δ 163.1 (1:1:1:1 q, $^1J_{CB}$ = 49.7 Hz, *ipso*-[B($C_6H_3(CF_3)_2)_4$]), 146.1 (d, $^2J_{CP}$ = 8.1 Hz, *ortho*-Dipp), 142.6 (t, $^3J_{CP}$ = 5.4 Hz, *ipso*-Dipp), 139.0 (d, $^1J_{CP}$ = 77.6 Hz, C_2/C_5-thiophene), 135.8 (s, *ortho*-[B($C_6H_3(CF_3)_2)_4$]), 131.7 (d, $^2J_{CP}$ = 88.2 Hz, C_3/C_4-thiophene), 130.5 (q, $^1J_{CF}$ = 2.8 Hz, CF_3-[B($C_6H_3(CF_3)_2)_4$]), 130.1 (q, $^1J_{CF}$ = 2.8 Hz, CF_3-[B($C_6H_3(CF_3)_2)_4$]), 127.3 (s, *meta*-[B($C_6H_3(CF_3)_2)_4$]), 123.5 (s, *meta*-Dipp), 119.9 (br d, $^5J_{CP}$ = 1.9 Hz, *para*-Dipp), 118.8 (br t, $^3J_{CF}$ = 3.8 Hz, *para*-[B($C_6H_3(CF_3)_2)_4$]), 30.1 (s, Dipp-CH($CH_3)_2$), 29.6 (s, Dipp-CH$(CH_3)_2$), 29.2 (s, Dipp-CH($CH_3)_2$), 29.0 (s, Dipp-CH($CH_3)_2$), 24.5 (s, P–CH$(CH_3)_2$), 24.4 (s, P–CH$(CH_3)_2$), 17.6 (d, $^2J_{CP}$ = 1.7 Hz, P–CH($CH_3)_2$), 17.4 (d, $^2J_{CP}$ = 1.6 Hz, P–CH($CH_3)_2$), 16.4 (d, $^2J_{CP}$ = 3.5 Hz, P–CH($CH_3)_2$), 16.3 (d, $^2J_{CP}$ = 3.6 Hz, P–CH($CH_3)_2$), –16.9 (s, Zn–CH_3). $^{19}F\{^1H\}$ NMR (282 MHz, pyridine-d_5): δ –60.55 (s). $^{31}P\{^1H\}$ NMR (122 MHz, pyridine-d_5): δ 2.8 (s). Anal. Calcd. for $C_{73}H_{79}BF_{24}N_2P_2SZn$: C 54.44; H 4.94; N 1.74; S 1.99; found: C 53.89; H 4.41; N 1.37; S 1.49.

Synthesis of [(DippN=P$Ph_2)_2C_4H_2$SeZnMe][B(3,5-$(CF_3)_2C_6H_3)_4$] (**38**) In a glove box,

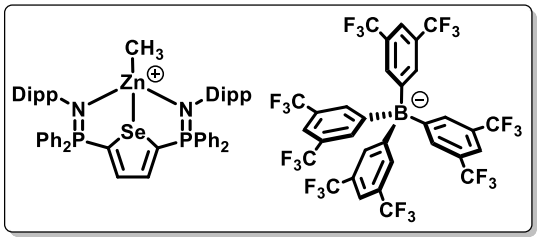

28 (30.9 mg, 0.0180 mmol) was added to a 20 mL scintillation vial, followed by 5 mL of bromobenzene, resulting in a golden-brown solution. Dimethyl zinc (15.0 μL, 0.0180 mmol, 1.2 M) was slowly injected into the stirring solution over a period of 5 min, after which a small amount of bubbling was observed. The solution was stirred for 2 h under an argon atmosphere. Pentane (~2 mL) was added to the brown solution and the mixture was allowed to stir for 30 min. The solvent was then removed under vacuum resulting in a thick dark-brown oil. The oil was washed with pentane (3 × 3 mL), and the remaining solvent

removed under vacuum to afford a brown solid. Yield: 28.4 mg, 84.4%. ^{1}H NMR (300 MHz, pyridine-d_5) δ 8.44 (s, 8H, *ortho*-[B(C$_6$*H*$_3$(CF$_3$)$_2$)$_4$]), 7.87 (dd, $^{3}J_{HH}$ = 7.2 Hz, $^{3}J_{HP}$ = 5.7 Hz, 8H, *ortho*-Ph), 7.83 (s, 4H, *meta*-[B(C$_6$*H*$_3$(CF$_3$)$_2$)$_4$]), 7.67-7.61 (m, 2H, C$_4$*H*$_2$Se), 7.54 (br td, $^{3}J_{HH}$ = 7.2 Hz, $^{5}J_{HP}$ = 1.1 Hz, 4H, *para*-Ph), 7.45 (br td, $^{3}J_{HH}$ = 7.2, $^{4}J_{HP}$ = 2.9 Hz, 8H, *meta*-Ph), 7.20 (ov d, $^{3}J_{HH}$ = 7.0 Hz, 4H, *meta*-Dipp), 7.06 (br td, $^{3}J_{HH}$ = 7.0 Hz, $^{5}J_{HP}$ = 1.9 Hz, 2H, *para*-Dipp), 3.61 (sp, $^{3}J_{HH}$ = 6.7 Hz, 4H, Dipp-C*H*(CH$_3$)$_2$), 1.03 (d, $^{3}J_{HH}$ = 6.7 Hz, 24H, Dipp-CH(C*H*$_3$)$_2$), –0.14 (s, 3H, Zn–C*H*$_3$). ^{1}H{^{31}P} NMR (300 MHz, pyridine-d_5): δ 8.43 (br s, 8H, *ortho*-[B(C$_6$*H*$_3$(CF$_3$)$_2$)$_4$]), 7.86 (ov d, $^{3}J_{HH}$ = 8.1 Hz, 8H, *ortho*-Ph), 7.83 (ov s, 4H, *meta*-[B(C$_6$*H*$_3$(CF$_3$)$_2$)$_4$]), 7.62 (s, 2H, C$_4$*H*$_2$Se), 7.54 (t, $^{3}J_{HH}$ = 7.5 Hz, 4H, *para*-Ph), 7.45 (br t, *J* = 7.2 Hz, 8H, *meta*-Ph), 7.20 (ov d, $^{3}J_{HH}$ = 7.5 Hz, 4H, *meta*-Dipp), 7.07 (t, $^{3}J_{HH}$ = 7.5 Hz, 2H, *para*-Dipp), 3.61 (sp, $^{3}J_{HH}$ = 6.7 Hz, 4H, Dipp-C*H*(CH$_3$)$_2$), 1.04 (d, $^{3}J_{HH}$ = 6.8 Hz, 24H, Dipp-CH(C*H*$_3$)$_2$), –0.14 (s, 3H, Zn–C*H*$_3$). ^{11}B{^{1}H} NMR (96 MHz, pyridine-d_5): δ –5.91 (s). ^{13}C{^{1}H} NMR (75 MHz, pyridine-d_5): δ 163.1 (1:1:1:1 q, $^{1}J_{CB}$ = 49.8 Hz, *ipso*-[B(*C*$_6$H$_3$(CF$_3$)$_2$)$_4$]), 143.6 (d, $^{2}J_{CP}$ = 7.5 Hz, *ipso*-Dipp), 139.8-138.9 (m, C$_3$/C$_4$-selenophene), 135.8 (s, *ortho*-[B(*C*$_6$H$_3$(CF$_3$)$_2$)$_4$]), 134.7 (d, $^{1}J_{CP}$ = 134.7 Hz, *ipso*-Ph), 132.7 (s, *meta*-Dipp), 132.6 (s, *para*-Dipp), 131.0 (s, *ortho*-Ph), 130.5 (q, $^{1}J_{CF}$ = 2.7 Hz, *C*F$_3$-[B(C$_6$H$_3$(*C*F$_3$)$_2$)$_4$]), 130.1 (q, $^{1}J_{CF}$ = 2.9 Hz, *C*F$_3$-[B(C$_6$H$_3$(*C*F$_3$)$_2$)$_4$]), 129.4 (d, $^{2}J_{CP}$ = 12.8 Hz, *ortho*-Dipp), 127.3 (s, *meta*-[B(*C*$_6$H$_3$(CF$_3$)$_2$)$_4$]), 126.2 (s, *meta*-Ph), 123.8 (s, *para*-[B(C$_6$H$_3$(*C*F$_3$)$_2$)$_4$]), 120.84 (s, *para*-Ph), 118.8 (t, $^{3}J_{CF}$ = 4.2 Hz, *para*-[B(C$_6$H$_3$(*C*F$_3$)$_2$)$_4$]), 29.5 (s, Dipp-*C*H(CH$_3$)$_2$), 24.4 (s, Dipp-CH(*C*H$_3$)$_2$), –16.7 (s, Zn–*C*H$_3$). Note: C$_2$/C$_5$-selenophene were not observed. ^{19}F{^{1}H} NMR (282 MHz, pyridine-d_5): δ –62.07 (s). ^{31}P{^{1}H} NMR (122 MHz, pyridine-d_5): δ –14.0 (s). Anal. Calcd. for C$_{85}$H$_{71}$BF$_{24}$N$_2$P$_2$SeZn: C 56.92; H 3.99; N 1.56; found: C 56.62; H 3.64; N 1.79.

Synthesis of [(DippN=P^{i}Pr$_2$)$_2$C$_4$H$_2$SeZnMe][B(3,5-(CF$_3$)$_2$C$_6$H$_3$)$_4$] (**39**) In a glove box,

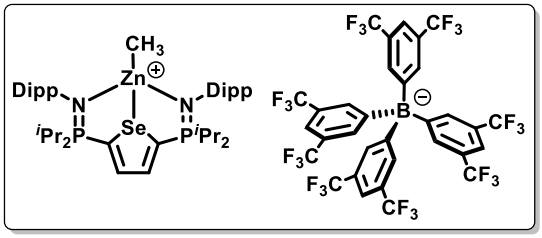

29 (51.8 mg, 0.0328 mmol) was added to a 20 mL scintillation vial, followed by 5 mL of bromobenzene, resulting in a brown solution. Dimethyl zinc (27.4 μL, 0.0328 mmol, 1.2 M) was slowly injected into the stirring solution over a period of 5 min. A small amount of bubbling was observed. The solution was stirred for 2 h under an argon atmosphere. Pentane (~2 mL) was added to the brown-orange solution and the mixture was allowed to stir for 30 min. The solvent was removed under vacuum resulting in a thick dark orange-brown oil. The oil was washed with three portions of pentane (3 mL), and the remaining pentane removed under vacuum to afford a caramel coloured solid. Yield: 45.8 mg, 84.3%. ^{1}H NMR (300 MHz, pyridine-d_5): δ 8.43 (br s, 8H, *ortho*-[B(C$_6$*H*$_3$(CF$_3$)$_2$)$_4$]), 7.93 (br s, 2H, C$_4$*H*$_2$Se), 7.83 (s, 4H, *meta*-[B(C$_6$*H*$_3$(CF$_3$)$_2$)$_4$]), 7.25 (br d, 4H, *meta*-Dipp), 7.08 (t, $^3J_{HH}$ = 7.2 Hz, 2H, *para*-Dipp), 3.63 (sp, $^3J_{HH}$ = 6.7 Hz, 4H, P–C*H*(CH$_3$)$_2$), 2.64 (br sp, $^3J_{HH}$ = 6.1 Hz, 4H, Dipp-C*H*(CH$_3$)$_2$), 1.35 (ov d, $^3J_{HH}$ = 6.7 Hz, 12H, P–CH(C*H*$_3$)$_2$), 1.27 (ov d, $^3J_{HH}$ = 6.1 Hz, 24H, Dipp-CH(C*H*$_3$)$_2$), 1.17 (dd, $^3J_{HP}$ = 17.1 Hz, $^3J_{HH}$ = 6.7 Hz, 12H, P–CH(C*H*$_3$)$_2$), –0.15 (s, 3H, Zn–C*H*$_3$). ^{11}B{^{1}H} NMR (96 MHz, pyridine-d_5): δ –4.41 (s). ^{13}C{^{1}H} NMR (75 MHz, pyridine-d_5): δ 163.1 (1:1:1:1 q, $^1J_{CB}$ = 49.9 Hz, *ipso*-[B(*C*$_6$H$_3$(CF$_3$)$_2$)$_4$]), 142.8 (br s, *ipso*-Dipp), 132.3 (s, *ortho*-[B(*C*$_6$H$_3$(CF$_3$)$_2$)$_4$]), 131.7 (d, $^2J_{CP}$ = 88.5 Hz, C$_3$/C$_4$-selenophene), 131.0-129.5 (m, *C*F$_3$-[B(C$_6$H$_3$(*C*F$_3$)$_2$)$_4$]), 129.1 (s, *para*-Dipp), 127.9 (s, *meta*-Dipp), 127.3 (s, *meta*-[B(*C*$_6$H$_3$(CF$_3$)$_2$)$_4$]), 120.1 (s, *ortho*-Dipp), 118.7 (t, $^3J_{CF}$ = 3.9 Hz, *para*-[B(*C*$_6$H$_3$(CF$_3$)$_2$)$_4$]), 29.6 (d, $^1J_{CP}$ = 68.8 Hz, P–CH(*C*H$_3$)$_2$), 24.5 (s, Dipp-*C*H(CH$_3$)$_2$), 17.0 (d, $^2J_{CP}$ = 83.9 Hz, P–CH(*C*H$_3$)$_2$). –18.01 (s, Zn–*C*H$_3$). Note: C$_2$/C$_5$-selenophene were not observed. ^{19}F{^{1}H} NMR (282 MHz, pyridine-d_5): δ –60.56 (s). ^{31}P{^{1}H} NMR (122 MHz, pyridine-d_5): δ 7.2 (s). ^{77}Se{^{1}H}

NMR (134 MHz, pyridine-d_5) δ 764.8 (br m). Anal. Calcd. for $C_{73}H_{61}BF_{24}N_2P_2SeZn$: C 52.90; H 4.80; N 1.69; found: C 53.37; H 4.77; N 1.70.

Synthesis of $[(PippN{=}P^iPr_2)_2C_4H_2SeZnMe][B(C_6F_5)_4]$ (**40**) In a glove box, **30** (100.0

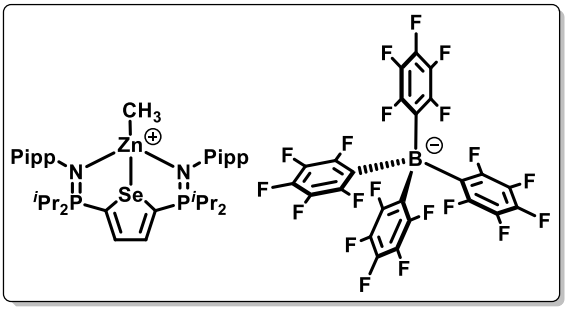

mg, 0.0764 mmol) was added to a 20 mL scintillation vial, followed by 5 mL of bromobenzene, resulting in a brown solution. Dimethyl zinc (63.4 μL, 0.0764 mmol, 1.2 M) was slowly injected into the stirring solution over a period of 5 min. A small amount of bubbling was observed. The solution was stirred for 2 h under an argon atmosphere. Pentane (~2 mL) was added to the brown-orange solution and mixture was allowed to stir for 30 min. The solvent was removed under vacuum resulting in a thick dark orange-brown oil. The oil was washed with three portions of pentane (3 mL), and the remaining solvent removed under vacuum to give caramel coloured solid. Yield: 94.6 mg, 81.2%. Resonances were better resolved at 60 °C for ^{1}H and ^{13}C{^{1}H} experiments, all others were run at ambient temperature. ^{1}H NMR (300 MHz, d_8-THF): δ 8.12 (br, 2H, C_4H_2Se), 6.98 (br, 4H, *ortho*-Pipp), 6.83 (br, 4H, *meta*-Pipp), 2.88 (br ov, 4H, P–C*H*$(CH_3)_2$), 2.73 (br ov, 2H, Pipp-C*H*$(CH_3)_2$), 1.32 (ov m, 24H, P–CH(C*H*$_3)_2$), 1.10 (d, 12H, $^3J_{HH}$ = 6.6 Hz, Pipp-CH(C*H*$_3)_2$), –0.15 (s, 1-2H, Zn–C*H*$_3$). ^{11}B{^{1}H} NMR (96 MHz, d_8-THF): δ –18.32 (s). ^{13}C{^{1}H} NMR (75 MHz, $CDCl_3$): δ 149.6 (br d, *ipso*-Pipp), 137.7 (br m, C_3/C_4-selenophene), 137.4 (br d, C_2/C_5-selenophene), 128.7 (s, *para*-Pipp), 128.3 (s, *meta*-Pipp), 124.7 (s, *ortho*-Pipp), 33.5 (s, Pipp-*C*H$(CH_3)_2$), 27.4 (m, P–*C*H$(CH_3)_2$), 24.5 (s, Pipp-CH(*C*H$_3)_2$) 16.42 (m, P–CH(*C*H$_3)_2$), –14.99 (s, Zn–*C*H$_3$). ^{19}F{^{1}H} NMR (282 MHz, d_8-THF): δ –133.54 (s, 8F, *ortho*-C_6F_5), –166.27 (t, 4F, $^3J_{FF}$ = 20.1 Hz, *para*-C_6F_5), –169.73 (t, 8F,

$^{3}J_{FF}$ = 18.9 Hz, *meta*-C_6F_5). $^{31}P\{^{1}H\}$ NMR (122 MHz, $CDCl_3$): 55.3 (br s). Anal. Calcd. for $C_{59}H_{55}BF_{20}N_2P_2SeZn$: C 51.01; H 3.99; N 2.02; found: C 50.93; H 3.65; N 1.97.

Synthesis of $[(DippN{=}PPh_2)_2C_4H_2OZnOPh][B(C_6F_5)_4]$ (**32b**) In a glove box,

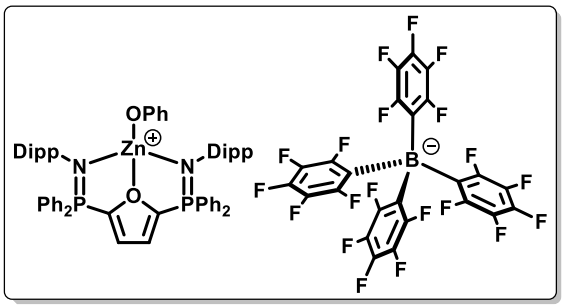

bromobenzene (~3 mL) was added to a 20 mL scintillation vial containing **20** (42.2 mg, 0.0288 mmol) and MeZnOPh (5.00 mg, 0.0288 mmol). A yellow solution was visible immediately after the addition of the solvent. The solution was stirred for 2 h under an argon atmosphere, after which a transparent orange-yellow solution was observed. The solvent was then removed under vacuum resulting in a thick red-orange oil. The oil was washed with pentane (3 × 3 mL), and the remaining pentane was removed *in vacuo* to afford an orange-red solid. Yield: 34.0 mg, 72.7%. ^{1}H NMR (300 MHz, pyridine-d_5): δ 7.78 (dd, $^{3}J_{HP}$ = 12.9 Hz, $^{3}J_{HH}$ = 7.2 Hz, 8H, *ortho*-Ph), 7.53 (dt, $^{3}J_{HH}$ = 7.6 Hz, $^{5}J_{HP}$ = 6.3 Hz, 4H, *para*-Ph), 7.41 (td, $^{3}J_{HH}$ = 7.4 Hz, $^{4}J_{HP}$ = 3.1 Hz, 8H, *meta*-*P*h), 7.31 (t, $^{3}J_{HH}$ = 7.8 Hz, 2H, *meta*-OC_6H_5), 7.23 (ov m, C_4H_2O), 7.20 (ov s, 2H, *para*-Dipp), 7.12 (ov t, $^{3}J_{HH}$ = 8.7 Hz, 4H, *meta*-Dipp), 7.05 (ov s, 2H, *ortho*-OC_6H_5), 6.85 (t, $^{3}J_{HH}$ = 7.1 Hz, 1H, *para*-OC_6H_5), 3.59 (sp, $^{3}J_{HH}$ = 6.8 Hz, 4H, Dipp-C*H*$(CH_3)_2$), 1.04 (d, $^{3}J_{HH}$ = 6.8 Hz, 24H, Dipp-CH(C*H*$_3)_2$). $^{11}B\{^{1}H\}$ NMR (96 MHz, pyridine-d_5): δ –14.45 (s). $^{13}C\{^{1}H\}$ NMR (75 MHz, pyridine-d_5): δ 156.6 (dd, $^{1}J_{CP}$ = 116.1 Hz, $^{4}J_{CP}$ = 4.3 Hz, C_2/C_5-furan), 145.0 (s, *ortho*-Dipp), 144.1 (d, $^{2}J_{CP}$ = 7.3 Hz, *ipso*-Dipp), 133.8 (d, $^{1}J_{CP}$ = 111.7 Hz, *ipso*-Ph), 133.5 (ov d, $^{2}J_{CP}$ = 2.8 Hz, C_3/C_4-furan), 133.3 (d, $^{2}J_{CP}$ = 10.3 Hz, *meta*-Ph), 133.1 (s, *meta*-OC_6H_5),), 132.0 (s, *ortho*-OC_6H_5),), 131.4 (s, *para*-Dipp), 130.3 (d, $^{2}J_{CP}$ = 12.7 Hz, *ortho*-Ph), 128.73 (s, *para*-OC_6H_5), 124.6 (s, *meta*-Dipp), 121.6 (d, $^{5}J_{CP}$ = 2.9 Hz, *para*-Dipp), 30.3 (s, Dipp-*C*H$(CH_3)_2$), 25.2 (s, Dipp-CH(*C*H$_3)_2$). Note:

ipso-OC_6H_5 was not observed. $^{19}F\{^1H\}$ NMR (282 MHz, pyridine-d_5): δ –130.61 (d, $^3J_{FF}$ = 9.1 Hz, 8F, *ortho*-C_6F_5), –160.63 (t, $^3J_{FF}$ = 20.9 Hz, 4F, *para*-C_6F_5), –164.74 (t, $^3J_{FF}$ = 18.2 Hz, 8F, *meta*-C_6F_5). $^{31}P\{^1H\}$ NMR (122 MHz, pyridine-d_5): δ –23.26 (s).

Synthesis of [(PippN=PPh_2)$_2C_4H_2$OZnOPh][$B(C_6F_5)_4$] (**33b**) In a glove box,

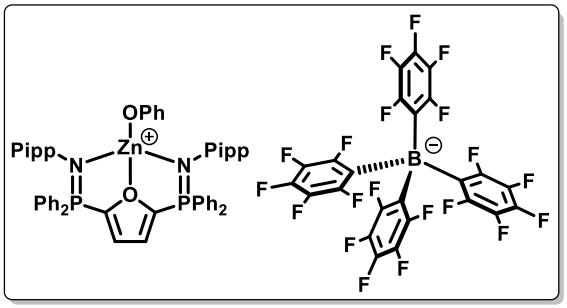

bromobenzene (~3 mL) was added to a 20 mL scintillation vial containing **21** (78.0 mg, 0.0560 mmol) and EtZnOPh (11.0 mg, 0.0560 mmol). The solution turned from yellow to transparent over a 1 h period. The solution was stirred for 2 h under an argon atmosphere, during which a light-yellow oil formed. The excess solvent was decanted, and the remaining volatiles were removed *in vacuo* giving an off-white solid which was washed with pentane (3 × 3 mL). The residual pentane was removed *in vacuo* to afford an off-white solid. Yield: 74.3 mg, 86.1%. Crystals were grown from a saturated solution in DCM at –30 °C. ^1H NMR (300 MHz, THF-d_8): δ 7.73 (t, $^3J_{HH}$ = 7.6, 4H, *para*-Ph), 7.42 (td, $^3J_{HH}$ = 7.6, $^4J_{HP}$ = 3.1 Hz, 8H, *meta*-*P*h), 7.20 (dd, $^3J_{HP}$ = 12.1, $^3J_{HH}$ = 7.6 Hz, 8H, *ortho*-Ph), 7.01 (s, 2H, C_4H_2O), 6.94 (s, 5H, Zn–OC_6H_5), 6.63 (d, 4H, $^3J_{HH}$ = 7.7 Hz, *ortho*-Pipp), 5.96 (d, 4H, $^3J_{HH}$ = 7.7 Hz, *meta*-Pipp), 2.74 (sp, $^3J_{HH}$ = 6.8 Hz, 4H, Pipp-C*H*$(CH_3)_2$), 1.08 (d, $^3J_{HH}$ = 6.8 Hz, 24H, Pipp-CH(C*H*$_3)_2$). $^{11}B\{^1H\}$ NMR (96 MHz, THF-d_8): δ –18.45 (s). $^{13}C\{^1H\}$ NMR (75 MHz, THF-d_8): δ 162.2 (s, *ipso*-OC_6H_5), 149.1 (br d, $^1J_{CP}$ = 111.1, C_2/C_5-furan), 146.7 (s, *para*-Pipp), 141.0 (d, $^2J_{CP}$ = 93.7 Hz, *ipso*-Pipp), 135.5 (s, *para*-Ph), 134.5 (d, $^2J_{CP}$ = 3.1 Hz, *ortho*-Ph), 131.1 (s, *ortho*-OC_6H_5), 130.5 (d, $^3J_{CP}$ = 2.9 Hz, *meta*-Ph), 130.4 (br m, C_3/C_4-furan), 129.0 (s, *meta*-Pipp), 128.1 (s, *ortho*-Pipp), 125.6 (d, $^1J_{CP}$ = 72.7 Hz, *ipso*-Ph), 123.3 (s, *meta*-OC_6H_5), 121.9 (s, *para*-OC_6H_5), 34.4 (s, Pipp *C*H$(CH_3)_2$), 24.4 (s, Dipp CH(*C*H$_3)_2$). $^{19}F\{^1H\}$ NMR (282 MHz, THF-d_8): δ –133.69 (t, $^3J_{FF}$ = 9.1 Hz,

8F, *ortho*-C_6F_5), –165.90 (t, $^3J_{FF}$ = 20.9 Hz, 4F, *para*-C_6F_5), –169.38 (t, $^3J_{FF}$ = 18.2 Hz, 8F, *meta*-C_6F_5). $^{31}P\{^1H\}$ NMR (122 MHz, THF-d_8): δ –18.1 (s). Anal. Calcd. for $C_{84}H_{61}BF_{24}N_2O_2P_2Zn$: C 58.50; H 3.57; N 1.62; found: C 58.90; H 3.21; N 1.67.

Synthesis of [(DippN=P^{i}Pr$_2$)$_2$C$_4$H$_2$OZnOPh][B(3,5-(CF$_3$)$_2$C$_6$H$_3$)$_4$] (**34b**) In a glove box,

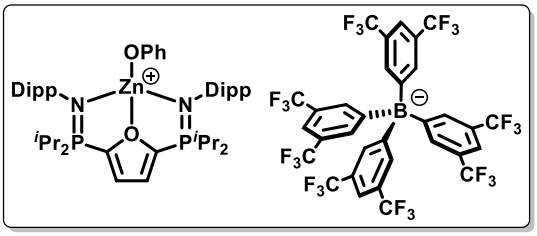

bromobenzene (~3 mL) was added to a 20 mL scintillation vial containing **23** (33.2 mg, 0.0219 mmol) and MeZnOPh (3.80 mg, 0.0219 mmol). An orange-brown solution was visible immediately after the addition of the solvent. The solution was stirred for 2 h under an argon atmosphere, after which a transparent orange solution was observed. The solvent was then removed under vacuum resulting in a thick brown-orange oil. The oil was washed with pentane (3 × 3 mL), and the remaining solvent removed under vacuum to give an orange-brown solid. Yield: 32.5 mg, 88.6%. ^1H NMR (300 MHz pyridine-d_5): δ 8.42 (s, 8H, *ortho*-[B(C$_6H_3$(CF$_3$)$_2$)$_4$]),, 7.83 (s, 4H, *para*-[B(C$_6H_3$(CF$_3$)$_2$)$_4$]), 7.39-7.28 (m, 6H, *meta/para*-Dipp), 7.24 (ov m, 2H, C$_4H_2$O), 7.16 (ov m, 2H, *ortho*-OC$_6H_5$), 7.07 (br t, $^3J_{HH}$ = 7.2 Hz, 2H, *meta*-OC$_6H_5$), 6.87 (br s, 1H, *para*-OC$_6H_5$), 3.64 (br sp, $^3J_{HH}$ = 6.5 Hz, 4H, P–*C*H(CH$_3$)$_2$), 2.75-2.50 (ov m, 4H, Dipp-C*H*(CH$_3$)$_2$), 1.29 (ov d, $^3J_{HH}$ = 6.3 Hz, 24H, Dipp-CH(C*H*$_3$)$_2$), 0.86 (br d, $^3J_{HH}$ = 6.6 Hz, 24H, P–CH(C*H*$_3$)$_2$). $^{11}B\{^1H\}$ NMR (96 MHz, pyridine-d_5): δ –5.92 (s). $^{13}C\{^1H\}$ NMR (75 MHz, pyridine-d_5): δ 163.1 (1:1:1:1 q, $^1J_{CB}$ = 51.6 Hz, *ipso*-[B(*C*$_6$H$_3$(CF$_3$)$_2$)$_4$), 153.7 (d, $^1J_{CP}$ = 93.7 Hz, C$_2$/C$_5$-furan), 145.7 (s, *ortho*-Dipp), 142.4 (d, $^2J_{CP}$ = 5.8 Hz, *ipso*-Dipp), 135.8 (s, *ortho*-[B(C$_6$H$_3$(*C*F$_3$)$_2$)$_4$]), 130.9 (br m, $^1J_{CF}$ = 3.6 Hz, *C*F$_3$-[B(C$_6$H$_3$(*C*F$_3$)$_2$)$_4$]), 130.6 (s, *meta*-Dipp), 130.6-130.3 (m, *C*F$_3$-[B(C$_6$H$_3$(*C*F$_3$)$_2$)$_4$]), 130.1 (br m, $^1J_{CF}$ = 3.7 Hz, *C*F$_3$-[B(C$_6$H$_3$(*C*F$_3$)$_2$)$_4$]), 129.9-129.3 (m, *C*F$_3$-[B(C$_6$H$_3$(*C*F$_3$)$_2$)$_4$]), 127.3 (s, *meta*-[B(*C*$_6$H$_3$(CF$_3$)$_2$)$_4$]), 124.0 (ov s, *para*-O*C*$_6$H$_5$), 123.5 (s, *meta*-Dipp), 119.9 (ov

s, *para*-Dipp), 119.9 (ov s *ortho*/*meta*-OC_6H_5), 118.7 (s, *para*-[B(C_6H_3(CF_3)$_2$)$_4$]), 29.4 (s, Dipp-CH(CH_3)$_2$), 29.2 (s, P–CH(CH_3)$_2$), 28.3 (s, P–CH(CH_3)$_2$), 24.3 (s, Dipp-CH(CH_3)$_2$), 17.11 (s, P–CH(CH_3)$_2$), 16.12 (s, P–CH(CH_3)$_2$). Note: *ipso*-OC_6H_5 was not observed. $^{19}F\{^1H\}$ NMR (282 MHz, pyridine-d_5): δ –62.10 (s). $^{31}P\{^1H\}$ NMR (122 MHz, pyridine-d_5) δ –1.4 (s).

Synthesis of [(DippN=PPh_2)$_2$$C_4H_2$SZnOPh][B(3,5-($CF_3$)$_2$$C_6H_3$)$_4$] (**35b**) In a glove box,

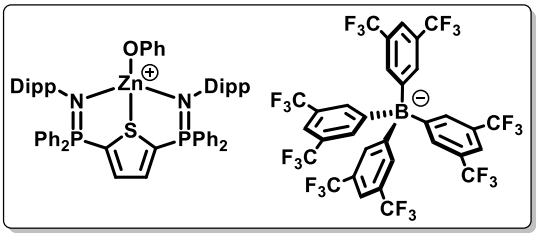

bromobenzene (~3 mL) was added to a 20 mL scintillation vial containing **25** (31.2 mg, 0.0193 mmol) and MeZnOPh (3.30 mg, 0.0193 mmol). A yellow solution was visible immediately after the addition of the solvent. A gradual colour change was observed over the next 30 min as the yellow solution turned bright-orange in colour and a small amount of bubbling was observed. The solution was stirred for 2 h under an argon atmosphere, during which no change was observed. The solvent was then removed under vacuum resulting in a thick orange-brown oil. The oil was washed with pentane (3 × 3 mL), and the remaining pentane was removed under vacuum to yield a brown-orange solid. Yield: 31.8 mg, 90.4%. ^1H NMR (300 MHz, pyridine-d_5): δ 8.44 (br s, 8H, *ortho*-[B(C_6H_3(CF_3)$_2$)$_4$]), 7.87 (ov d, $^3J_{HH}$ = 7.1 Hz, 4H, *meta*-[B(C_6H_3(CF_3)$_2$)$_4$]), 7.83 (ov s, 8H, *ortho*-Ph), 7.52 (t, $^3J_{HH}$ = 7.2 Hz, 4H, *para*-Ph), 7.46 (td, $^3J_{HH}$ = 9.4 Hz, $^4J_{HP}$ = 4.7 Hz, 8H, *meta*-Ph), 7.36 (ov dd, $^3J_{HP}$ = 5.2 Hz, $^4J_{HP}$ = 3.3 Hz, 2H, C_4H_2S), 7.29 (ov t, $^3J_{HH}$ = 7.4 Hz, 2H, *meta*-OC_6H_5), 7.22 (ov s, 1H, *ortho*-OC_6H_5), 7.18 (ov t, $^3J_{HH}$ = 6.8 Hz, 4H, *meta*-Dipp), 7.07 (td, $^3J_{HH}$ = 6.8, $^5J_{HP}$ = 4.1 Hz, 2H, *para*-Dipp), 6.81 (t, $^3J_{HH}$ = 6.7 Hz, 1H, *para*-OC_6H_5), 3.60 (t, $^3J_{HH}$ = 6.8 Hz, 4H, Dipp-CH(CH_3)$_2$), 1.03 (d, $^3J_{HH}$ = 6.8 Hz, 24H, Dipp-CH(CH_3)$_2$). $^{11}B\{^1H\}$ NMR (96 MHz, pyridine-d_5): δ –4.40 (s). $^{13}C\{^1H\}$ NMR (75 MHz, pyridine-d_5): δ 163.2 (1:1:1:1 q, $^1J_{CB}$ = 49.8 Hz, *ipso*-[B(C_6H_3(CF_3)$_2$)$_4$), 144.6

(dd, $^{1}J_{CP}$ = 19.5, $^{4}J_{CP}$ = 1.6 Hz, C_2/C_5-thiophene), 143.5 (d, $^{2}J_{CP}$ = 7.5 Hz, *ipso*-Dipp), 139.5 (br s, *ortho*-Dipp), 137.8-137.0 (m, C_3/C_4-thiophene), 135.8 (s, *ortho*-[B(C_6H_3(*C*F_3)$_2$)$_4$]), 133.9 (d, $^{1}J_{CP}$ = 106.8 Hz, *ipso*-Ph), 132.8 (d, $^{3}J_{CP}$ = 10.2 Hz, *meta*-Ph), 132.7 (m, *ortho*/*meta*-O*C*$_6H_5$), 130.6 (s, *para*-Ph), 130.6 (q, $^{1}J_{CF}$ = 2.7 Hz, *C*F_3-[B(C_6H_3(*C*F_3)$_2$)$_4$]), 130.1 (q, $^{1}J_{CF}$ = 5.3 Hz, *C*F_3-[B(C_6H_3(*C*F_3)$_2$)$_4$]), 129.4 (d, $^{2}J_{CP}$ = 12.6 Hz, *ortho*-Ph), 127.3 (s, *meta*-[B(*C*$_6H_3$(CF_3)$_2$)$_4$]), 123.8 (s, *para*-Dipp), 123.6 (s, *para*-O*C*$_6H_5$), 120.8 (d, $^{5}J_{CP}$ = 3.0 Hz, *meta*-Dipp), 118.7 (d, $^{3}J_{CF}$ = 4.0 Hz, *para*-[B(C_6H_3(*C*F_3)$_2$)$_4$]), 29.5 (s, Dipp-*C*H(CH_3)$_2$), 24.4 (s, Dipp-CH(*C*H_3)$_2$). Note: *ipso*-OC_6*H*$_5$ was not observed. ^{19}F{^{1}H} NMR (282 MHz, pyridine-d_5): δ –60.55 (s). ^{31}P{^{1}H} NMR (122 MHz, pyridine-d_5): δ –17.1 (s).

Synthesis of [(PippN=PPh_2)$_2$$C_4H_2$SZnOPh][B($C_6F_5$)$_4$] (**36b**) In a glove box,

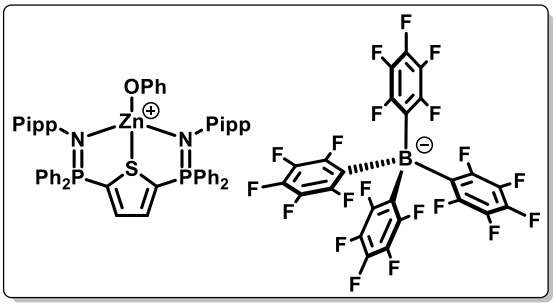

bromobenzene (~3 mL) was added to a 20 mL scintillation vial containing **25** (56.0 mg, 0.0400 mmol) and EtZnOPh (7.50 mg, 0.0400 mmol). The solution turned from yellow to colourless over a 1 h period. The solution was stirred for 2 h under an argon atmosphere. Heptane (5 mL) was added which caused an off-white solid to precipitate. The excess solvent was decanted, and the remaining volatiles were removed *in vacuo* giving an off-white solid which was washed with pentane (3 × 3 mL). The remaining pentane was removed *in vacuo* which afforded an off-white solid. Yield: 51.3 mg, 82.4%. ^{1}H NMR (300 MHz, THF-d_8): δ 7.89 (br ov m, 8H, *ortho*-Ph) 7.77 (br ov m, 4H, *para*-Ph), 7.61 (br ov m, 8H, *meta*-Ph), 7.45 (br ov m, 2H, *ortho*-OC_6*H*$_5$), 7.26 (br ov m, 2H, *meta*-OC_6*H*$_5$), 7.25 (br ov m, 2H, C_4*H*$_2$S), 6.91 (br ov m, 4H, *ortho*-Pipp), 6.82 (br ov m, 1H, *para*-OC_6*H*$_5$), 6.68 (br ov m, 4H, *meta*-Pipp), 2.75 (sp, $^{3}J_{HH}$ = 6.9 Hz, 4H, Dipp C*H*(CH_3)$_2$), 1.12 (d, $^{3}J_{HH}$ = 6.9 Hz, 24H, Dipp CH(C*H*$_3$)$_2$).

$^{11}B\{^{1}H\}$ NMR (96 MHz, THF-d_8): δ –18.45 (s). $^{13}C\{^{1}H\}$ NMR (75 MHz, THF-d_8) δ 134.7 (s, *ortho*-OC_6H_5), 131.7 (s, *meta*-OC_6H_5), 130.4 (s, *meta*-Ph), 130.2 (s, *para*-Ph), 128.0 (s, *para*-OC_6H_5), 127.7 (s, *meta*-Pipp), 123.65 (s, *ortho*-Pipp), 120.1 (s, *para*-OC_6H_5). Note $C_{2\text{-}5}$-thiophene, *ipso*-Ph, *ipso*-OC_6H_5, *ipso*-Pipp, and *para*-Pipp were not observed. $^{19}F\{^{1}H\}$ NMR (282 MHz, THF-d_8): δ –133.69 (t, $^{3}J_{FF}$ = 9.1 Hz, 8F, *ortho*-C_6F_5), –165.97 (t, $^{3}J_{FF}$ = 20.9 Hz, 4F, *para*-C_6F_5), –169.45 (t, $^{3}J_{FF}$ = 18.2 Hz, 8F, *meta*-C_6F_5). $^{31}P\{^{1}H\}$ NMR (122 MHz, THF-d_8): δ –28.6 (br s). Anal. Calcd. for $C_{76}H_{49}BF_{20}N_2OP_2SZn$: C 58.65; H 3.17; N 1.80; S 2.06; found: C 58.31; H 3.22; N 2.06; S 2.54.

Synthesis of [(DippN=P^{i}Pr$_2$)$_2$C$_4$H$_2$SZnOPh][B(3,5-(CF$_3$)$_2$C$_6$H$_3$)$_4$] (**37b**) In a glove box,

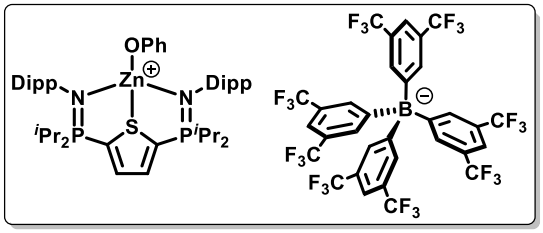

bromobenzene (~3 mL) was added to a 20 mL scintillation vial containing **27** (22.1 mg, 0.0137 mmol) and MeZnOPh (2.40 mg, 0.0137 mmol). An orange solution was visible immediately after the addition of the solvent. The solution was stirred for 2 h under an argon atmosphere, after which a transparent orange solution was observed. The solvent was then removed under vacuum resulting in a thick brown-yellow oil. The oil was washed with pentane (3 × 3 mL), and the remaining pentane was removed under vacuum giving a brown-yellow solid. Yield: 22.6 mg, 93.4%. ^{1}H NMR (300 MHz, pyridine-d_5) δ 8.44 (br s, 8H, *ortho*-[B(C_6H_3(CF$_3$)$_2$)$_4$]), 7.83 (s, 4H, *meta*-[B(C_6H_3(CF$_3$)$_2$)$_4$]), 7.68 (br s, 2H, C_4H_2S), 7.31 (ov t, $^{3}J_{HH}$ = 8.0 Hz, 2H, *para*-Dipp), 7.14 (ov d, $^{3}J_{HH}$ = 7.5 Hz, 4H, *meta*-Dipp), 7.06 (t, $^{3}J_{HH}$ = 7.3 Hz, 2H, *meta*-OC_6H_5), 6.94 (s, 1H, *para*-OC_6H_5), 6.87 (br t, $^{3}J_{HH}$ = 6.6 Hz, 2H, *ortho*-OC_6H_5), 3.62 (sp, $^{3}J_{HH}$ = 6.8 Hz, 4H, Dipp-C*H*(CH$_3$)$_2$), 2.61 (d sp, $^{3}J_{HP}$ = 14.6, $^{3}J_{HH}$ = 7.1 Hz, 4H P–C*H*(CH$_3$)$_2$), 1.34 (ov d, $^{3}J_{HH}$ = 6.6 Hz, 12H, P–CH(C*H*$_3$)$_2$), 1.28 (ov d, $^{3}J_{HH}$ = 6.6 Hz, 24H, Dipp-CH(C*H*$_3$)$_2$), 1.12 (dd, $^{3}J_{HP}$ = 17.2,

$^{3}J_{HH}$ = 6.6 Hz, 12H, P–CH(CH_3)$_2$). ^{11}B{^{1}H} NMR (96 MHz, pyridine-d_5): δ –4.41 (s). ^{13}C{^{1}H} NMR (75 MHz, pyridine-d_5): δ 163.1 (1:1:1:1 q, $^{1}J_{CB}$ = 49.8 Hz, *ipso*-[B(C_6H_3(CF$_3$)$_2$)$_4$), 146.1 (s, *ortho*-Dipp), 142.6 (d, $^{2}J_{CP}$ = 5.9 Hz, *ipso*-Dipp), 139.0 (d, $^{1}J_{CP}$ = 77.4 Hz, C_2/C_5-thiophene), 135.8 (s, *ortho*-[B(C_6H_3(*C*F$_3$)$_2$)$_4$]), 131.7 (d, $^{2}J_{CP}$ = 88.4 Hz, C_3/C_4-thiophene), 130.6 (m, *C*F$_3$-[B(C_6H_3(*C*F$_3$)$_2$)$_4$]), 130.5 (s, *meta*-Dipp), 130.5 (q, $^{1}J_{CF}$ = 2.8 Hz, *C*F$_3$-[B(C_6H_3(*C*F$_3$)$_2$)$_4$]), 130.1 (q, $^{1}J_{CF}$ = 2.9 Hz, *C*F$_3$-[B(C_6H_3(*C*F$_3$)$_2$)$_4$]), 129.9 (s, *meta*-O*C*$_6$H$_5$), 129.4 (m, *C*F$_3$-[B(C_6H_3(*C*F$_3$)$_2$)$_4$]), 129.4 (s, *para*-O*C*$_6$H$_5$), 129.1 (s, *ortho*-O*C*$_6$H$_5$), 127.3 (s, *meta*-[B(*C*$_6$H$_3$(CF$_3$)$_2$)$_4$]), 123.5 (s, *meta*-Dipp), 119.9 (d, $^{5}J_{CP}$ = 2.1 Hz, *para*-Dipp), 119.1-118.2 (m, *para*-[B(C_6H_3(*C*F$_3$)$_2$)$_4$]), 30.0 (s, P–*C*H(CH$_3$)$_2$), 29.6 (s, Dipp-*C*H(CH$_3$)$_2$), 29.0 (s, P–*C*H(CH$_3$)$_2$), 24.4 (s, Dipp-CH(*C*H$_3$)$_2$), 17.4 (d, $^{2}J_{CP}$ = 1.5 Hz, P–CH(*C*H$_3$)$_2$), 16.3 (d, $^{2}J_{CP}$ = 3.5 Hz, P–CH(*C*H$_3$)$_2$). Note: *ipso*-O*C*$_6$H$_5$ was not observed. ^{19}F{^{1}H} NMR (282 MHz, pyridine-d_5): δ –60.56 (s). ^{31}P{^{1}H} NMR (122 MHz, pyridine-d_5): δ 2.8 (s).

Alternate synthesis: In a glove box, bromobenzene (~3 mL) was added to a 20 mL scintillation vial containing **37** (24.9 mg, 0.0155 mmol), and phenol (1.5 mg, 0.0155 mmol). Immediately after the addition of the solvent, a bright yellow solution was observed along with slight bubbling. The solution was stirred for 2 h under an argon atmosphere, after which a transparent orange solution was observed. The solvent was then removed under vacuum resulting in a thick brown-yellow oil. The oil was washed with pentane (3 × 3 mL), and the remaining pentane was removed under vacuum to afford a brown-yellow solid. Yield: 23.8 mg, 87.3%.

Synthesis of [(DippN=PPh$_2$)$_2$C$_4$H$_2$SeZnOPh][B(3,5-(CF$_3$)$_2$C$_6$H$_3$)$_4$] (**38b**) In a glove box, bromobenzene (~3 mL) was added to a 20 mL scintillation vial containing **28** (23.4 mg, 0.0137 mmol) and MeZnOPh (2.40 mg, 0.0137 mmol). A golden-brown solution was visible immediately after the addition of the solvent. The solution was stirred for 2 h under an argon atmosphere, after which a transparent orange solution was observed. The solvent was then removed under vacuum resulting in a thick brown-orange oil. The oil was washed with pentane (3 × 3 mL), and the remaining pentane was removed under vacuum to give an orange-brown solid. Yield: 22.9 mg, 89.6%. ^{1}H NMR (300 MHz, pyridine-d_5): δ 8.44 (s, *ortho*-[B(C$_6$*H*$_3$(CF$_3$)$_2$)$_4$]), 7.88 (ov d, $^4J_{HH}$ = 7.5 Hz, 4H, *meta*-[B(C$_6$*H*$_3$(CF$_3$)$_2$)$_4$]), 7.83 (s, 8H, *ortho*-Ph), 7.68-7.61 (m, 2H, C$_4$*H*$_2$Se), 7.57-7.49 (m, 4H, *para*-Ph), 7.46 (ov m, 8H, *meta*-Ph), 7.29 (t, $^3J_{HH}$ = 7.6 Hz, 4H, *meta*-Dipp), 7.17 (ov m, 6H, *para*-Dipp and *ortho*-OC$_6$*H*$_5$), 7.06 (t, $^3J_{HH}$ = 7.6 Hz, 2H, *meta*-OC$_6$*H*$_5$), 6.80 (t, $^3J_{HH}$ = 6.8 Hz, 1H, *para*-OC$_6$*H*$_5$), 3.61 (t, $^3J_{HH}$ = 6.8 Hz, 4H, Dipp-C*H*(CH$_3$)$_2$), 1.03 (d, $^3J_{HH}$ = 6.8 Hz, 24H, Dipp-CH(C*H*$_3$)$_2$). ^{11}B{^{1}H} NMR (96 MHz, pyridine-d_5): δ –5.91 (s). ^{13}C{^{1}H} NMR (75 MHz, pyridine-d_5): δ 163.1 (1:1:1:1 q, $^1J_{CB}$ = 48.9 Hz, *ipso*-[B(*C*$_6$H$_3$(CF$_3$)$_2$)$_4$), 144.6 (s, *ortho*-Dipp), 143.6 (d, $^2J_{CP}$ = 6.4 Hz, *ipso*-Dipp), 139.4 (dd, $^2J_{CP}$ = 14.4, $^3J_{CP}$ = 10.4 Hz, C$_3$/C$_4$-selenophene), 135.8 (s, *ortho*-[B(C$_6$H$_3$(*C*F$_3$)$_2$)$_4$]), 134.4 (d, $^1J_{CP}$ = 106.0 Hz, *ipso*-Ph), 132.7 (d, $^3J_{CP}$ = 10.6 Hz, *meta*-Ph), 131.2-130.9 (m, $^1J_{CF}$ = 5.1 Hz, *C*F$_3$-[B(C$_6$H$_3$(*C*F$_3$)$_2$)$_4$]), 130.6 (s, *para*-Ph), 130.5-130.3 (m, $^1J_{CF}$ = 2.4 Hz, *C*F$_3$-[B(C$_6$H$_3$(*C*F$_3$)$_2$)$_4$]), 130.0 (m, $^1J_{CF}$ = 3.7 Hz, *C*F$_3$-[B(C$_6$H$_3$(*C*F$_3$)$_2$)$_4$]), 129.5 (s, *ortho*-OC$_6$*H*$_5$), 129.3 (d, $^2J_{CP}$ = 12.3 Hz, *ortho*-Ph), 129.1 (s, *meta*-OC$_6$*H*$_5$), 127.3 (s, *meta*-[B(*C*$_6$H$_3$(CF$_3$)$_2$)$_4$]), 126.2 (s, *para*-OC$_6$*H*$_5$), 123.7 (s, *para*-Dipp), 120.8 (s, *meta*-Dipp), 118.7 (s, *para*-[B(C$_6$H$_3$(*C*F$_3$)$_2$)$_4$]), 29.5 (s, Dipp-*C*H(CH$_3$)$_2$), 24.4 (s,

Dipp-CH(CH$_3$)$_2$). Note: C$_2$/C$_5$-selenophene and *ipso*-OC$_6$$H_5$ was not observed. ^{19}F{^{1}H} NMR (282 MHz, pyridine-d_5): δ –62.07 (s). ^{31}P{^{1}H} NMR (122 MHz, pyridine-d_5): δ –14.0 (s).

Synthesis of [(DippN=P^{i}Pr$_2$)$_2$C$_4$H$_2$SeZnOPh][B(3,5-(CF$_3$)$_2$C$_6$H$_3$)$_4$] (**39b**) In a glove box, bromobenzene (~3 mL) was added to a 20 mL scintillation vial containing **29** (31.9 mg, 0.0202 mmol) and MeZnOPh (3.5 mg, 0.0202 mmol). An orange-brown solution was visible immediately after the addition of the solvent, along with slight bubbling. The solution was stirred for 2 h under an argon atmosphere with constant stirring, after which a transparent brown solution was observed. The solvent was then removed under vacuum resulting in a thick brown oil. The oil was washed with pentane (3 × 3 mL), and the remaining pentane was removed under vacuum yielding a brown solid. This material contained a mix of **39** and the desired compound **39b**, as indicated by the peak observed at δ –0.15 (s, 2H, Zn–CH_3) in the ^{1}H NMR spectrum. Thus, phenol (0.500 mg, 0.00510 mmol), was added the vial containing the brown solid, to which bromobenzene (~3 mL) was also added, yielding a transparent brown solution. The solution was stirred for an additional 16 h under an argon atmosphere, during which no change was observed. The solvent was then removed under vacuum resulting in a thick brown oil. The oil was washed with pentane (3 × 3 mL), and the remaining pentane was removed under vacuum affording a brown solid. Yield: 25.1 mg, 71.8%. ^{1}H NMR (300 MHz, pyridine-d_5): δ 8.44 (br s, 8H, *ortho*-[B(C$_6$$H_3$(CF$_3$)$_2$)$_4$]), 7.89 (dd, $^3J_{HP}$ = 5.2, $^4J_{HP}$ = 3.4 Hz, 2H, C$_4$$H_2$Se), 7.83 (br s, 4H, *para*-[B(C$_6$$H_3$(CF$_3$)$_2$)$_4$]), 7.68 (m, 2H, *ortho*-OC$_6$$H_5$), 7.58-7.52 (m, 2H, *meta*-OC$_6$$H_5$), 7.30 (ov m, 4H, *meta*-Dipp), 7.06 (br t, $^3J_{HH}$ = 7.5, 2H, *para*-Dipp), 6.79 (br t, J = 6.5 Hz, 1H, *para*-OC$_6$$H_5$), 3.66 (ov sp, $^3J_{HH}$ = 6.8 Hz, 4H, Dipp-CH(CH$_3$)$_2$),

2.60 (ov sp, $^{3}J_{HH}$ = 7.0 Hz, 4H, P–C*H*(CH_3)$_2$), 1.32 (ov m, 36H, Dipp and P–CH(C*H*$_3$)$_2$), 1.15 (ov dd, $^{3}J_{HP}$ = 17.2 Hz, $^{3}J_{HH}$ = 7.1 Hz, 12H, P–CH(C*H*$_3$)$_2$). ^{11}B{^{1}H} NMR (96 MHz, pyridine-d_5): δ –5.92 (s). ^{13}C{^{1}H} NMR (75 MHz, pyridine-d_5): δ 163.1 (1:1:1:1 q, $^{1}J_{CB}$ = 49.9 Hz, *ipso*-[B(*C*$_6$H$_3$(CF_3)$_2$)$_4$), 146.2 (s, *ipso*-O*C*$_6$H$_5$), 145.5 (s, *ortho*-Dipp), 142.6 (m, *ipso*-Dipp), 139.0 (d, $^{1}J_{CP}$ = 77.3Hz, C_2/C_5-selenophene), 137.4 (dd, $^{2}J_{CP}$ = 13.2 Hz, $^{3}J_{CP}$ = 6.6 Hz, C_3/C_4-selenophene), 135.8 (s, *ortho*-[B(C_6H_3(*C*F_3)$_2$)$_4$]), 132.3 (s, *meta*-O*C*$_6$H$_5$), 131.1 (s, *para*-O*C*$_6$H$_5$), 131.0 (m, *C*F_3-[B(C_6H_3(*C*F_3)$_2$)$_4$]), 130.1 (q, $^{1}J_{CF}$ = 2.8 Hz, *C*F_3-[B(C_6H_3(*C*F_3)$_2$)$_4$]), 129.9 (s, *ortho*-O*C*$_6$H$_5$), 129.1 (s, *ortho*-O*C*$_6$H$_5$), 127.9 (s, *para*O*C*$_6$H$_5$), 127.3 (s, *meta*-[B(*C*$_6$H$_3$(CF_3)$_2$)$_4$]), 123.6 (s, *meta*-Dipp), 119.9 (br s, *para*-Dipp), 118.8 (br m, *para*-[B(C_6H_3(*C*F_3)$_2$)$_4$]),), 30.1 (s, P–*C*H(CH_3)$_2$), 30.0 (s, P–*C*H(CH_3)$_2$), 29.5 (s, Dipp-*C*H(CH_3)$_2$), 29.2 (s, P–*C*H(CH_3)$_2$), 29.0 (s, P–*C*H(CH_3)$_2$), 24.5 (s, Dipp-CH(*C*H$_3$)$_2$), 24.4 (s, Dipp-CH(*C*H$_3$)$_2$), 17.6 (d, $^{2}J_{CP}$ = 1.5 Hz, P–CH(*C*H$_3$)$_2$), 17.4 (d, $^{2}J_{CP}$ = 1.6 Hz, P–CH(*C*H$_3$)$_2$), 16.4 (d, $^{2}J_{CP}$ = 3.5 Hz, P–CH(*C*H$_3$)$_2$), 16.3 (d, $^{2}J_{CP}$ = 3.6 Hz, P–CH(*C*H$_3$)$_2$). ^{19}F NMR (282 MHz, pyridine-d_5) δ –62.06 (s). ^{31}P{^{1}H} NMR (122 MHz, pyridine-d_5): δ 5.5 (s, 71.4%), 2.85 (s, 28.6%). ^{77}Se{^{1}H} NMR (134 MHz, pyridine-d_5) δ 764.9 (t, $^{2}J_{SeP}$ = 12.8 Hz).

Synthesis of [(PippN=P^{i}Pr$_2$)$_2$C$_4$H$_2$SeZnOPh][B(C$_6$F$_5$)$_4$] (**40b**) In a glove box,

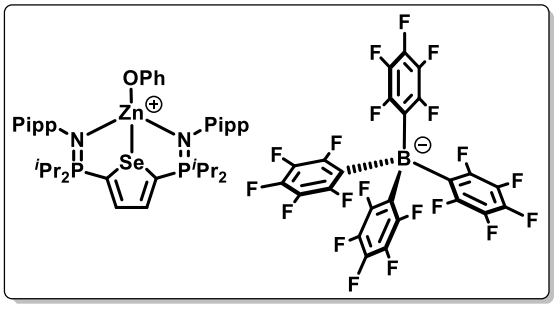

bromobenzene (~3 mL) was added to a 20 mL scintillation vial containing **30** (70.6 mg, 0.054 mmol) and MeZnOPh (10.1 mg, 0.054 mmol). The solution was stirred for 48 h under an argon atmosphere, during which a light-yellow oil formed. The excess solvent was decanted, and the remaining volatiles were removed *in vacuo* giving a yellow solid which was washed with pentane (3 × 3 mL). The remaining solvent was removed *in vacuo* to afford a yellow solid. Yield: 78.0 mg, 90.1%. ^{1}H NMR (300 MHz,

THF-d_8): δ 8.20 (br, 2H, C_4H_2Se), 7.69 (br ov m, 1H, *para*-OC_6H_5), 7.50 (br ov m, 2H, *meta*-OC_6H_5), 7.28 (br ov m, 2H, *ortho*-OC_6H_5), 7.05 (br ov m, 4H, *ortho*-Pipp), 6.89 (br ov m, 4H, *meta*-Pipp), 3.00 (br ov, 4H, P–C*H*$(CH_3)_2$), 2.80 (br ov, 2H, Pipp-C*H*$(CH_3)_2$), 1.29 (br ov, 24H, P–CH(C*H*$_3)_2$, 1.19 (br ov, 12H, Pipp-CH(C*H*$_3)_2$). $^{11}B\{^1H\}$ NMR (96 MHz, THF-d_8): δ –18.45 (s). $^{13}C\{^1H\}$ NMR (75 MHz, THF-d_8): δ 149.4 (br d, $^1J_{CP}$ = 102.0, C_2/C_5-selenophene), 139.4 (br d, $^2J_{CP}$ = 102.8 Hz, *ipso*-Pipp), 138.1 (br s, *para*-OC_6H_5), 136.7 (br s, *para*-Pipp), 132.6 (br s, *para*-OC_6H_5), (br s, *ortho*-OC_6H_5), 129.2 (br s, *meta*-Pipp), 129.0 (br s, *ortho*-Pipp), 124.3 (s, *meta*-OC_6H_5), 124.3 (br s), 34.5 (m, P–*C*H$(CH_3)_2$), 27.1 (m, Dipp-*C*H$(CH_3)_2$), 24.7 (s, Dipp-CH(*C*H$_3)_2$), 16.41 (m, P–*C*H$(CH_3)_2$). Note: C_3/C_4-selenophene was not observed. $^{19}F\{^1H\}$ NMR (282 MHz, THF-d_8) δ –133.69 (d, $^3J_{FF}$ = 9.1 Hz, 8F, *ortho*-C_6F_5), –165.90 (t, $^3J_{FF}$ = 20.9 Hz, 4F, *para*-C_6F_5), –169.38 (t, $^3J_{FF}$ = 18.2 Hz, 8F, *meta*-C_6F_5). $^{31}P\{^1H\}$ NMR (122 MHz, THF-d_8): δ 55.4 (br), 24.0 (br).

Synthesis of $Ca(HMDS)_2$•THF In a glove box, calcium diiodide (0.818 g, 0.00278 mol) and 2 equiv of THF solvated potassium hexamethyldisilazane, [K][HMDS]•THF (1.512 g, 0.00557 mol), were added to a swivel frit apparatus equipped with 100 mL round-bottom flasks. Toluene (~50 mL) was transferred *in vacuo* to the mixture. The reaction was stirred for 48 h under argon during which a light-yellow slurry formed. The mixture was filtered using and the volatiles removed *in vacuo* to yield a thick yellow oil. In a glove box, hexanes were added to the oil. Vigorous stirring afforded an off-white powder. The powder was triturated with hexanes (3 × 10 mL) and the volatiles removed *in vacuo* to give $Ca(HMDS)_2$•THF. Spectra were consistent with literature.[128, 129] Yield: 0.84 g, 69.9%. ^1H NMR (300 MHz, C_6D_6) δ 3.56 (m, 4H, C_2/C_5-THF), 1.23 (m, C_3/C_4-THF), 0.38 (s, 18H, HMDS), 0.26 (s, 18H, HMDS).

Important notes: [K][HMDS]•THF was a solid obtained from a 1.0 M solution of [K][HMDS] in THF. This reaction is extremely sensitive to the halide salt and the solvent used due to the insolubility of the group 2 salts. For exact reproduction of this reaction do not substitute the halide salt or the solvent. The same procedure can be undertaken using a Et_2O solvated [K][HMDS] salt.

Synthesis of [((PippN=PPh$_2$)$_2$C$_4$H$_2$O)$_2$Ca][B(C$_6$F$_5$)$_4$]$_2$ (**42**) In a glove box, **21** (85.0 mg, 0.0615 mmol) was added to a 20 mL scintillation vial, followed by Ca(HMDS)$_2$•Et$_2$O (53.0 mg, 0.123 mmol) and ~5 mL of toluene. The light-yellow mixture was stirred for 2 h with no significant change. Volatiles were removed *in vacuo* and the resulting oil was washed with three portions of pentane (3 mL). The remaining volatiles were removed *in vacuo* to give a pale-yellow solid. Crystals were grown from a saturated DCM solution stored at –30 °C Yield: 138.1 mg, 80.1%. ^{1}H NMR (300 MHz, CD_2Cl_2): δ 7.70 (t, 8H, $^{3}J_{HH}$ = 6.7 Hz, *para*-Ph), 7.44 (m, 16H, *meta*-Ph), 7.26 (dd, 16H, $^{3}J_{HH}$ = 7.4 Hz, $^{3}J_{HP}$ = 12.3 Hz, *ortho*-Ph), 7.01 (s, 4H, C$_4$*H*$_2$O), 6.72 (d, 8H, $^{3}J_{HH}$ = 7.8 Hz, *ortho*-Pipp), 6.40 (d, 8H, $^{3}J_{HH}$ = 7.8 Hz, *meta*-Pipp), 2.63 (sp, 4H, $^{3}J_{HH}$ = 6.6 Hz, Pipp-C*H*(CH$_3$)$_2$), 0.99 (d, 24H, $^{3}J_{HH}$ = 6.6 Hz, Pipp-CH(C*H*$_3$)$_2$). ^{11}B{^{1}H} NMR (96 MHz, CD_2Cl_2) δ –16.67 (s). ^{13}C{^{1}H} NMR (75 MHz, CD_2Cl_2): δ 149.5 (br m, C$_2$/C$_5$-furan), 144.4 (s, *ipso*-Pipp), 135.0 (s, *para*-Ph), 133.30 (d, $^{2}J_{CP}$ = 3.7 Hz, *ortho*-Ph), 130.3 (d, $^{4}J_{CP}$ = 2.9 Hz, *meta*-Ph), 128.5 (s, *meta*-Pipp), 126.5 (d, $^{1}J_{CP}$ = 35.4 Hz, *ipso*-Ph), 124.9 (m, C$_3$/C$_4$-furan), 123.2 (s, *ortho*-Pipp), 33.3 (s, Pipp-*C*H(CH$_3$)$_2$), 24.0 (s, Pipp-CH(*C*H$_3$)$_2$). Note: *ipso*-Pipp resonance was not observed. ^{19}F{^{1}H} NMR (282 MHz, CD_2Cl_2): δ –132.24 (s, 8F,

ortho-C_6F_5), –162.63 (t, 4F, $^3J_{FF}$ = 20.1 Hz, *para*-C_6F_5), –166.34 (t, 8F, $^3J_{FF}$ = 18.9 Hz, *meta*-C_6F_5). $^{31}P\{^1H\}$ NMR (122 MHz, CD_2Cl_2): δ 14.2 (s). Anal. Calcd. for $C_{140}H_{88}B_2CaF_{40}N_4O_2P_4$: C 59.97; H 3.16; N 2.00; found: C 59.55; H 3.35; N 1.97.

Synthesis of $[((PippN{=}PPh_2)_2C_4H_2S)_2Ca][B(C_6F_5)_4]_2$ **(43)** In a glove box, **25** (100.0 mg,

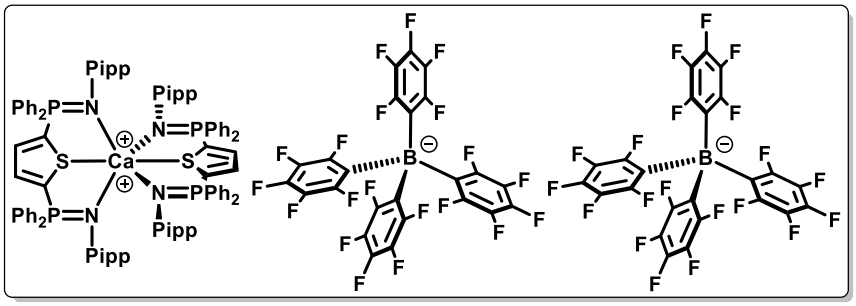

0.0710 mmol) was added to a 20 mL scintillation vial, followed by $Ca(HMDS)_2$•THF (15.0 mg, 0.036 mmol) and ~5 mL of toluene. The orange solution was stirred for 2 h with no significant change. Volatiles were removed *in vacuo* and the resulting oil was further washed with three portions of pentane (3 mL). The remaining volatiles were removed *in vacuo* to yield a yellow-orange solid. Yield: 77.5 mg, 75.9%. ^1H NMR (300 MHz, d_8-THF): δ 7.83 (dd, 16H, $^3J_{HH}$ = 7.6 Hz, $^3J_{HP}$ = 12.5 Hz, *ortho*-Ph), 7.61-7.41 (ov m, 28H, *para*/*meta*-Ph and C_4H_2S), 6.79 (d, 8H, $^3J_{HH}$ = 7.8 Hz, *ortho*-Pipp), 6.62 (d, 8H, $^3J_{HH}$ = 7.8 Hz, *meta*-Pipp), 2.70 (sp, 4H, $^3J_{HH}$ = 6.7 Hz, Pipp-C*H*$(CH_3)_2$), 1.14 (d, 24H, $^3J_{HH}$ = 6.7 Hz, Pipp-CH(C*H*$_3)_2$). $^{11}B\{^1H\}$ NMR (96 MHz, d_8-THF): δ –18.48 (s). $^{13}C\{^1H\}$ NMR (75 MHz, d_8-THF): δ 147.7 (br m, *ipso*-Pipp), 142.5 (br m, C_2/C_5-thiophene), 138.5 (s, *para*-Pipp), 137.9 (br m, C_3/C_4-thiophene), 133.4 (d, $^2J_{CP}$ = 3.9 Hz, *ortho*-Ph), 132.5 (s, *para*-Ph), 132.1 (d, $^1J_{CP}$ = 37.7 Hz, *ipso*-Ph), 128.6 (d, $^4J_{CP}$ = 2.9 Hz, *meta*-Ph), 127.1 (s, *meta*-Pipp), 123.2 (d, $^3J_{CP}$ = 11.0 Hz, *ortho*-Pipp), 34.42 (s, Pipp-*C*H$(CH_3)_2$), 24.6 (s, Pipp-CH(*C*H$_3)_2$). $^{19}F\{^1H\}$ NMR (282 MHz, d_8-THF): δ –133.71 (s, 8F, *ortho*-C_6F_5), –165.91 (t, 4F, $^3J_{FF}$ = 20.1 Hz, *para*-C_6F_5), –169.44 (t, 8F, $^3J_{FF}$ = 18.9 Hz, *meta*-C_6F_5). $^{31}P\{^1H\}$ NMR (122 MHz, d_8-THF): δ –9.4 (s). Anal. Calcd. for $C_{140}H_{88}B_2CaF_{40}N_4P_4S_2$: C 59.29; H 3.13; N 1.98; S 2.26 found: C 58.80; H 3.69; N 2.57; S 2.49.

Synthesis of [((DippN=PPh$_2$)$_2$C$_4$H$_2$O)$_2$CaNSiMe$_3$]$_2$[B(C$_6$F$_5$)$_4$]$_2$ (**44**) In a glove box, **20**

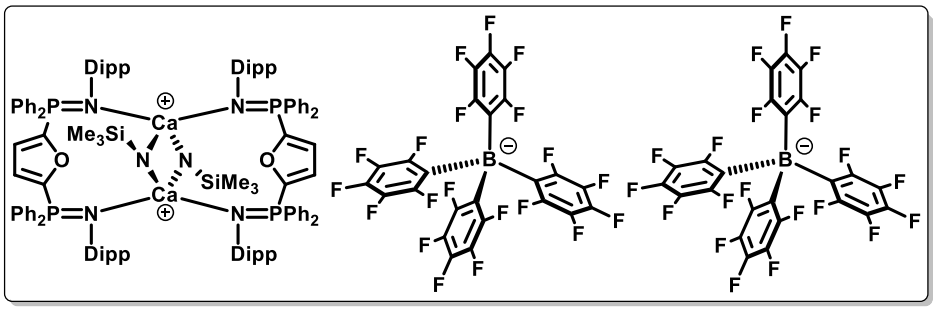

(40.0 mg, 0.0273 mmol) was added to an NMR tube followed by Ca(HMDS)$_2$•THF (12.0 mg, 0.0273 mmol) and ~0.5 mL of THF-d_8. The orange solution became crimson within 10 min and was monitored over 2 h *via* ^{31}P{^{1}H} NMR spectroscopy at which starting material resonances had vanished. Volatiles were removed *in vacuo* and the resulting red oil was washed with three portions of pentane (3 mL). The remaining volatiles were removed *in vacuo* to provide a red solid. Yield: 70.2 mg, 79.9%. ^{1}H NMR (300 MHz, THF-d_8): δ 7.53 (ov m, 24H, *ortho*/*para*-Ph), 7.38 (td, 16H, $^3J_{HH}$ = 7.7 Hz, $^3J_{HP}$ = 4.5 Hz, *meta*-Ph), 6.86 (m, 12H, *meta*/*para*-Dipp), 6.68 (m, 4H, C$_4$*H*$_2$O), 3.25 (sp, 8H, $^3J_{HH}$ = 6.4 Hz, Dipp-C*H*(CH$_3$)$_2$), 0.83 (d, 48H, $^3J_{HH}$ = 6.4 Hz, Dipp-CH(C*H*$_3$)$_2$), –0.01 (s, 18H, N–Si(C*H*$_3$)$_3$). ^{11}B{^{1}H} NMR (96 MHz, THF-d_8) δ –18.46 (s). ^{13}C{^{1}H} NMR (75 MHz, THF-d_8): δ 155.8 (d, $^2J_{CP}$ = 47.7 Hz, *ipso*-Dipp), 144.1 (s, *ortho*-Dipp), 143.0 (d, $^1J_{CP}$ = 18.8 Hz, C$_2$/C$_5$-furan), 133.7 (d, $^1J_{CP}$ = 49.2 Hz, *ipso*-Ph), 132.8 (d, $^2J_{CP}$ = 10.2 Hz, *ortho*-Ph), 132.6 (d, $^4J_{CP}$ = 2.9 Hz, *para*-Ph), 129.5 (d, $^3J_{CP}$ = 11.1 Hz, *meta*-Ph), 123.23 (m, *meta*/*para*-Dipp), 120.3 (m, C$_3$/C$_4$-thiophene), 29.5 (s, Dipp-*C*H(CH$_3$)$_2$), 24.06 (s, Dipp-CH(*C*H$_3$)$_2$), 5.45 (s, N–Si(*C*H$_3$)$_3$). ^{19}F{^{1}H} NMR (282 MHz, THF-d_8): δ –133.71 (s, 8F, *ortho*-C$_6$F$_5$), –165.98 (t, 4F, $^3J_{FF}$ = 20.1 Hz, *para*-C$_6$F$_5$), –169.48 (t, 8F, $^3J_{FF}$ = 18.9 Hz, *meta*-C$_6$F$_5$). ^{29}Si{^{1}H} NMR (59 MHz, d_8-THF) δ –16.85. ^{31}P{^{1}H} NMR (122 MHz, THF-d_8): δ –24.6 (s). Anal. Calcd. for C$_{158}$H$_{130}$B$_2$Ca$_2$F$_{20}$N$_4$O$_2$P$_4$Si$_2$: C 60.08; H 4.15; N 1.77; found: C 59.49; H 3.67; N 2.14.

3.3 X-ray Crystal Data Tables

Table 3.1: X-ray crystallography data of $(DippN{=}PPh_2)_2C_4H_2O$ (**3**) and $(PmN{=}PPh_2)_2C_4H_2O$ (**6**).

Identification code	PH18049	ph18082
Empirical formula	$C_{52}H_{56}N_2OP_2$	$C_{40}H_{36}N_6OP_2$
Formula weight	786.92	678.69
Temperature/K	108.4(2)	293(2)
Crystal system	monoclinic	monoclinic
Space group	C2/c	$P2_1/c$
a/Å	23.3449(3)	15.4768(3)
b/Å	9.77621(10)	15.6589(3)
c/Å	19.7871(2)	29.2604(5)
α/°	90	90
β/°	101.9326(11)	93.845(2)
γ/°	90	90
Volume/$Å^3$	4418.34(9)	7075.3(2)
Z	4	8
$\rho_{calc}g/cm^3$	1.183	1.274
μ/mm^{-1}	1.188	1.438
F(000)	1680.0	2848.0
Crystal size/mm^3	0.3 × 0.2 × 0.1	0.2 × 0.1 × 0.05
Radiation	Cu Kα (λ = 1.54184)	CuKα (λ = 1.54184)
2Θ range for data collection/°	7.742 to 160.632	8.042 to 162.24
Index ranges	$-29 \le h \le 29$, $-12 \le k \le 11$, $-24 \le l \le 25$	$-19 \le h \le 19$, $-13 \le k \le 19$, $-36 \le l \le 36$
Reflections collected	35733	30331
Independent reflections	4812 [R_{int} = 0.0296, R_{sigma} = 0.0136]	14551 [R_{int} = 0.0392, R_{sigma} = 0.0511]
Data/restraints/parameters	4812/0/262	14551/0/891
Goodness-of-fit on F^2	1.085	1.088
Final R indexes [I>=2σ (I)]	R_1 = 0.0418, wR_2 = 0.1097	R_1 = 0.0834, wR_2 = 0.2338
Final R indexes [all data]	R_1 = 0.0428, wR_2 = 0.1103	R_1 = 0.0955, wR_2 = 0.2401
Largest diff. peak/hole / e $Å^{-3}$	0.49/-0.41	0.91/-0.49

Table 3.2: X-ray crystallography data of $(MesN=P^{i}Pr_2)_2C_4H_2O$ (**8**) and $(PPh_2)_2C_4H_2S$ (**9**).

Identification code	PH20003	PH18063
Empirical formula	$C_{34}H_{52}N_2OP_2$	$C_{28}H_{22}P_2S$
Formula weight	566.71	452.45
Temperature/K	100.00(10)	110.6(8)
Crystal system	orthorhombic	triclinic
Space group	$P2_12_12_1$	P-1
a/Å	8.09960(10)	9.1754(2)
b/Å	15.7433(3)	10.9959(3)
c/Å	25.5186(5)	13.0490(3)
α/°	90	111.585(2)
β/°	90	92.306(2)
γ/°	90	107.736(2)
Volume/$Å^3$	3253.99(10)	1148.65(5)
Z	4	2
$\rho_{calc}g/cm^3$	1.157	1.308
μ/mm^{-1}	1.414	2.657
F(000)	1232.0	472.0
Crystal size/mm^3	0.6 × 0.5 × 0.3	0.25 × 0.2 × 0.1
Radiation	Cu Kα (λ = 1.54184)	Cu Kα (λ = 1.54184)
2Θ range for data collection/°	6.596 to 149.854	7.396 to 160.668
Index ranges	$-10 \le h \le 10$, $-18 \le k \le 19$, $-24 \le l \le 31$	$-11 \le h \le 11$, $-12 \le k \le 14$, $-16 \le l \le 16$
Reflections collected	17820	25817
Independent reflections	6164 [R_{int} = 0.0239, R_{sigma} = 0.0222]	4995 [R_{int} = 0.0493, R_{sigma} = 0.0355]
Data/restraints/parameters	6164/0/366	4995/0/280
Goodness-of-fit on F^2	1.130	1.065
Final R indexes [I>=2σ (I)]	R_1 = 0.0286, wR_2 = 0.0844	R_1 = 0.0517, wR_2 = 0.1502
Final R indexes [all data]	R_1 = 0.0290, wR_2 = 0.0846	R_1 = 0.0572, wR_2 = 0.1541
Largest diff. peak/hole / e $Å^{-3}$	0.26/-0.27	0.79/-0.53

Table 3.3: X-ray crystallography data of (DippN=PPh_2)$_2C_4H_2S$ (**11**) and (P^iPr_2)$_2C_4H_2Se$ (**16**).

Identification code	PH19012	PH19005
Empirical formula	$C_{104}H_{112}N_4P_4S_2$	$C_{16}H_{30}P_2Se$
Formula weight	1605.97	363.30
Temperature/K	99.98(10)	100.0(2)
Crystal system	monoclinic	monoclinic
Space group	C2/c	P2/c
a/Å	23.9121(3)	13.7471(4)
b/Å	9.75930(10)	6.4235(2)
c/Å	19.2860(2)	20.5973(6)
α/°	90	90
β/°	100.1990(10)	93.932(2)
γ/°	90	90
Volume/Å^3	4429.57(9)	1814.55(9)
Z	2	4
ρ_{calc}g/cm^3	1.204	1.330
μ/mm^{-1}	1.606	4.347
F(000)	1712.0	760.0
Crystal size/mm^3	0.4 × 0.3 × 0.15	0.5 × 0.1 × 0.1
Radiation	Cu Kα (λ = 1.54184)	Cu Kα (λ = 1.54184)
2Θ range for data collection/°	7.512 to 160.69	6.444 to 161.23
Index ranges	-30 ≤ h ≤ 30, -12 ≤ k ≤ 12, -18 ≤ l ≤ 24	-17 ≤ h ≤ 17, -8 ≤ k ≤ 7, -26 ≤ l ≤ 25
Reflections collected	25270	20877
Independent reflections	4831 [R_{int} = 0.0298, R_{sigma} = 0.0201]	3942 [R_{int} = 0.0304, R_{sigma} = 0.0205]
Data/restraints/parameters	4831/0/262	3942/0/181
Goodness-of-fit on F^2	1.102	1.156
Final R indexes [I>=2σ (I)]	R_1 = 0.0389, wR_2 = 0.1032	R_1 = 0.0453, wR_2 = 0.1217
Final R indexes [all data]	R_1 = 0.0409, wR_2 = 0.1046	R_1 = 0.0582, wR_2 = 0.1273
Largest diff. peak/hole / e Å^{-3}	0.46/-0.55	0.51/-0.61

Table 3.4: X-ray crystallography data of (DippN=PPh_2)$_2C_4H_2Se$ (**17**) and (DippN=P^{i}Pr$_2$)$_2C_4H_2Se$ (**18**).

Identification code	PH20010	PH19011
Empirical formula	$C_{52}H_{56}N_2P_2Se$	$C_{40}H_{64}N_2P_2Se$
Formula weight	849.88	713.83
Temperature/K	99.99(10)	100.01(10)
Crystal system	triclinic	monoclinic
Space group	P-1	Pn
a/Å	8.9063(3)	8.2082(2)
b/Å	15.1038(6)	27.5965(4)
c/Å	17.4097(4)	9.5740(2)
α/°	108.416(3)	90
β/°	97.799(2)	113.004(2)
γ/°	92.183(3)	90
Volume/Å^3	2193.27(13)	1996.22(8)
Z	2	2
ρ_{calc}g/cm^3	1.287	1.188
μ/mm^{-1}	2.126	2.229
F(000)	892.0	764.0
Crystal size/mm^3	0.1 × 0.05 × 0.03	1 × 0.05 × 0.03
Radiation	Cu Kα (λ = 1.54184)	Cu Kα (λ = 1.54184)
2Θ range for data collection/°	6.19 to 148.456	9.614 to 161.694
Index ranges	-8 ≤ h ≤ 11, -16 ≤ k ≤ 11, -19 ≤ l ≤ 21	-8 ≤ h ≤ 10, -35 ≤ k ≤ 34, -11 ≤ l ≤ 12
Reflections collected	8700	21986
Independent reflections	5667 [R_{int} = 0.0220, R_{sigma} = 0.0272]	7348 [R_{int} = 0.0537, R_{sigma} = 0.0531]
Data/restraints/parameters	5667/0/522	7348/26/422
Goodness-of-fit on F^2	1.049	1.065
Final R indexes [I>=2σ (I)]	R_1 = 0.0456, wR_2 = 0.1304	R_1 = 0.0558, wR_2 = 0.1516
Final R indexes [all data]	R_1 = 0.0483, wR_2 = 0.1328	R_1 = 0.0586, wR_2 = 0.1548
Largest diff. peak/hole / e Å^{-3}	0.81/-0.50	1.16/-0.83

Table 3.5: X-ray crystallography data of (PippN=P^{i}Pr$_2$)$_2$C$_4$H$_2$Se (**19**) and [(PippN(H)=PPh$_2$)(PippN=PPh$_2$)C$_4$H$_2$S][A] (**25**).

Identification code	TWIN_twin1_hklf4	PH18084
Empirical formula	$C_{34}H_{52}N_2P_2Se$	$C_{70}H_{45}BF_{20}N_2P_2S$
Formula weight	629.67	1398.89
Temperature/K	100.0(2)	112.4(4)
Crystal system	monoclinic	triclinic
Space group	$P2_1/c$	P-1
a/Å	12.0624(3)	10.26140(10)
b/Å	23.8990(6)	16.07790(10)
c/Å	11.9583(4)	19.2278(2)
α/°	90	102.8480(10)
β/°	100.958(3)	94.8320(10)
γ/°	90	94.6160(10)
Volume/Å^3	3384.47(17)	3065.71(5)
Z	4	2
ρ_{calc}g/cm^3	1.236	1.515
μ/mm^{-1}	2.564	1.918
F(000)	1336.0	1420.0
Crystal size/mm^3	0.3 × 0.1 × 0.05	0.15 × 0.1 × 0.1
Radiation	Cu Kα (λ = 1.54184)	Cu Kα (λ = 1.54184)
2Θ range for data collection/°	10.24 to 161.52	6.496 to 160.554
Index ranges	-15 ≤ h ≤ 14, -30 ≤ k ≤ 29, -14 ≤ l ≤ 12	-11 ≤ h ≤ 13, -20 ≤ k ≤ 20, -22 ≤ l ≤ 24
Reflections collected	18411	43024
Independent reflections	6080 [R_{int} = 0.0733, R_{sigma} = 0.0397]	13237 [R_{int} = 0.0396, R_{sigma} = 0.0406]
Data/restraints/parameters	6080/197/448	13237/0/873
Goodness-of-fit on F^2	1.099	1.065
Final R indexes [I>=2σ (I)]	R_1 = 0.0565, wR_2 = 0.1971	R_1 = 0.0396, wR_2 = 0.0989
Final R indexes [all data]	R_1 = 0.0623, wR_2 = 0.2125	R_1 = 0.0463, wR_2 = 0.1023
Largest diff. peak/hole / e Å^{-3}	1.31/-1.01	0.45/-0.40

Table 3.6: X-ray crystallography data of [(PippN=PPh_2)$_2C_4H_2OZnOMe$][A] (**41**) and [((PippN=PPh_2)$_2C_4H_2O$)$_2$Ca][A]$_2$ (**42**).

Identification code	PH19013	PH18092
Empirical formula	$C_{77}H_{52}BBrF_{20}N_2O_2P_2Zn$	$C_{140}H_{88}B_2CaF_{40}N_4O_2P_4$
Formula weight	1635.23	2803.72
Temperature/K	100.01(10)	114(1)
Crystal system	triclinic	monoclinic
Space group	P-1	$P2_1/n$
a/Å	15.4748(2)	25.82769(11)
b/Å	15.9484(2)	18.32973(7)
c/Å	16.3909(2)	28.38988(13)
α/°	68.5570(10)	90
β/°	84.3240(10)	96.2821(4)
γ/°	72.9640(10)	90
Volume/Å^3	3599.87(8)	13359.48(10)
Z	2	4
ρ_{calc}g/cm^3	1.509	1.394
μ/mm^{-1}	2.431	1.819
F(000)	1648.0	5688.0
Crystal size/mm^3	0.05 × 0.05 × 0.05	0.2 × 0.2 × 0.1
Radiation	Cu Kα (λ = 1.54184)	Cu Kα (λ = 1.54184)
2Θ range for data collection/°	6.824 to 160.792	6.876 to 160.662
Index ranges	-19 ≤ h ≤ 11, -20 ≤ k ≤ 17, -20 ≤ l ≤ 20	-32 ≤ h ≤ 32, -23 ≤ k ≤ 23, -35 ≤ l ≤ 36
Reflections collected	50607	127435
Independent reflections	15527 [R_{int} = 0.0377, R_{sigma} = 0.0383]	28983 [R_{int} = 0.0363, R_{sigma} = 0.0311]
Data/restraints/parameters	15527/0/970	28983/0/1746
Goodness-of-fit on F^2	1.047	1.055
Final R indexes [I>=2σ (I)]	R_1 = 0.0512, wR_2 = 0.1308	R_1 = 0.0365, wR_2 = 0.0926
Final R indexes [all data]	R_1 = 0.0560, wR_2 = 0.1345	R_1 = 0.0416, wR_2 = 0.0952
Largest diff. peak/hole / e Å^{-3}	1.23/-0.88	0.70/-0.44

Table 3.7: X-ray crystallography data of $[((PippN{=}PPh_2)_2C_4H_2S)_2CaNSiMe_3]_2[A]_2$ (**43b**).

Identification code	PH19002
Empirical formula	$C_{158}H_{116}B_2Br_2Ca_2F_{40}N_6P_4S_2Si_2$
Formula weight	3364.34
Temperature/K	100.00(16)
Crystal system	triclinic
Space group	P-1
a/Å	12.8644(3)
b/Å	16.9624(4)
c/Å	17.4238(2)
α/°	81.7654(16)
β/°	85.8432(17)
γ/°	83.917(2)
Volume/Å^3	3735.34(14)
Z	1
ρ_{calc}g/cm^3	1.496
μ/mm^{-1}	3.023
F(000)	1706.0
Crystal size/mm^3	0.1 × 0.1 × 0.05
Radiation	Cu Kα (λ = 1.54184)
2Θ range for data collection/°	6.85 to 161.506
Index ranges	$-12 \le h \le 16$, $-21 \le k \le 21$, $-22 \le l \le 22$
Reflections collected	49107
Independent reflections	15839 [R_{int} = 0.0395, R_{sigma} = 0.0354]
Data/restraints/parameters	15839/0/989
Goodness-of-fit on F^2	1.063
Final R indexes [I>=2σ (I)]	R_1 = 0.0466, wR_2 = 0.1295
Final R indexes [all data]	R_1 = 0.0527, wR_2 = 0.1370
Largest diff. peak/hole / e Å^{-3}	1.50/-1.57

3.4 Publications and Presentations Arising from Part I

Webb, D. J; Wheaton, C. A; Hayes, P. G. Cationic Zinc Complexes of Phosphinimine-Containing *NON*-Pincer Ligands. Invited submission to Inorganic syntheses

- Consists of most work in 2.1 through 2.2

Webb, D. J; Hayes, P. G. On the Coordination Chemistry of Bis- and Trisphosphinimine Containing Ligands. *Comprehensive Coordination Chemistry III*. **2021**, 1, Pg 131-157.

- Content has been reformatted for 1.3

Webb, D. J; Cruz-Milette, D. E; Hayes, P. G. The Synthesis of Phosphinimine Containing *NEN*-Pincer Ligands (E = O, S, Se) and their Corresponding Cationic Zinc Complexes. To be submitted to European Journal of Inorganic Chemistry.

- Consists of most work with zinc depicted in Chapter 2.

II. SEMISYNTHESIS STRATEGIES FOR THE GENERATION OF CANNABINOIDS AND RELATED DERIVATIVES

Chapter 4: Introduction to Cannabinoid Semisynthesis

4.1 Natural Products

For commercial purposes, a natural product contains ingredients that are sourced from nature. In the context of chemistry, a natural product is a compound produced by an organism,[144, 145] and refers to purified organic compounds that were isolated from the organism that produced the compounds *via* primary or secondary metabolism.[146, 147] An organism will utilize primary metabolites for intrinsic functions (growth, development, reproduction), while secondary metabolites serve extrinsic functions and affect other organisms.[148] Secondary metabolites may not be wholly necessary for the organism's survival, but are utilized due to their notable influence on their ecological environment, whether it be cytotoxic to competing organisms, as pheromones, or as nutrient transport. Often, the exact function of secondary metabolites is not explicitly known, and they may have numerous purposes.[149-151]

Natural selection led to the development of complex biological machinery to synthesize extremely unique chemicals.[152, 153] This results in natural products having chemical manifolds which often contain several chiral centres and functional groups that are exceedingly difficult to create by artificial methods. As the diverse structures of natural products typically have unique influences on biological systems,[154] drug discovery has been possible with the identification and testing of various natural products. One such example is paclitaxel, or Taxol®, which is a natural product extracted from the Pacific yew tree, *Taxus brevifolia* (Figure 4.1).[155] Taxol is used by the organism to repel pests, but it was also revealed to be effective as an anti-cancer medication, and is now prominently used in chemotherapy.[156, 157]

Figure 4.1: Image of the Pacific yew[158] with the chemical structure of paclitaxel.

4.1.1 Isolation Methods

An organism does not generally require secondary metabolites in high concentrations for the desired advantageous effects to be realized. Therefore, a primary issue with natural products is their lack of availability. An organism, such as the Pacific yew tree, produces as little as 0.001-0.01% of Taxol® per dry bark weight (about 0.66 g per tree).[159] Other notable organisms include marine sponges, who produce a diverse array of chemicals in low quantities.[160] In fact, 0.91 kg of *Hyrtios erectus* yields only 41.1 mg of bioactive compounds (>0.0001%).[161] For effective research and commercial use of natural products, a larger, and more viable source is required. Accordingly, several methods have been developed to obtain natural products, all of which come with benefits and downfalls.

4.1.1.1 Direct Extraction

Typically, the initial discovery and complete characterization of a natural product requires isolation of the novel compound *via* straightforward and direct extraction methods. An extraction requires collection of the organism's biomass, or portions of the organism, and using various solvent systems and chromatography methods to

isolate the natural products within (Figure 4.2). A mixture of natural products can then be further separated by chromatography, or sometimes, with crystallization. The ease of isolation and purification depends highly on the natural product's structure, stability, and quantity within the organism. If the organism is a plant, the extraction can be conducted on biomass that has been removed from the organism (such as the leaves); otherwise, the process destroys the organism, as is the case for marine sponges.

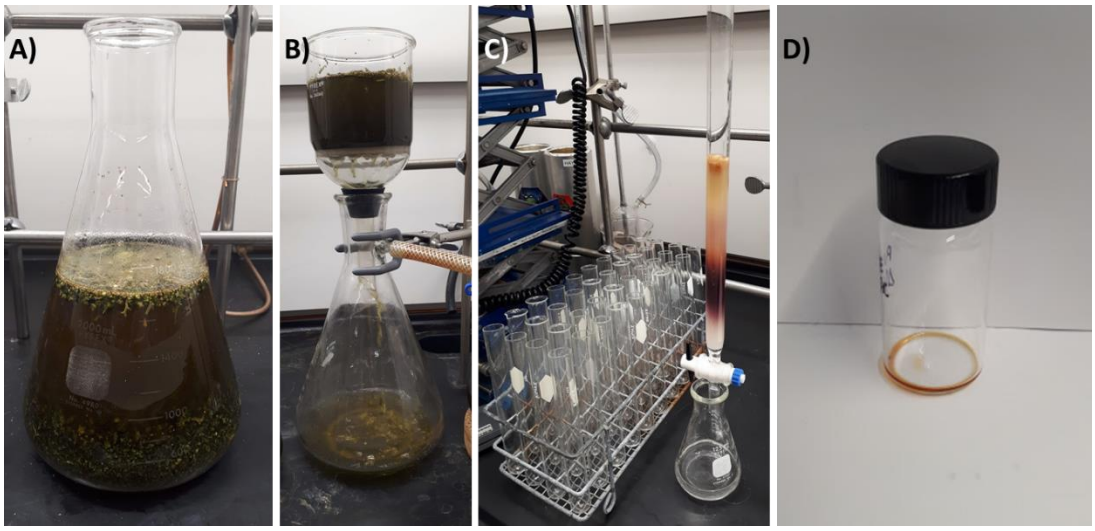

Figure 4.2: Example of a typical and simplified extraction process. A) Biomass submerged in a solvent. B) The mixture is filtered. C) Compounds separated *via* chromatography. D) A purified natural product.

Extraction uses common laboratory materials, such as commercially available solvents and drying agents, along with simplistic or chiral chromatography systems. Extraction methodologies have been crucial to the development of this field, without them natural products would not have been so readily discovered. A glaring issue is that the yield of harvested compound is completely dictated by the organism's output. Unless proper growth conditions can be ensured to promote optimal production, the yield will always be limited by the organism's natural production of the metabolite. It would not be viable, nor ethical, to destroy a large portion of marine sponges to harvest their natural products on a commercial scale; historical extraction of Taxol®

from the bark of the Pacific yew tree was a destructive process. Commercial viability of Taxol® was only achieved when alternative cultivation and extraction methods were developed.[162] Therefore, in modern times, relying solely on direct extraction is inefficient and generally reserved for initial isolation, detection, and characterization of natural products.

4.1.1.2 Total Synthesis

A natural product, if found to be medicinally relevant, often becomes an important target for total synthesis. Total synthesis involves the preparation of a compound from simple, commercially available compounds. Generally, inexpensive starting materials and procedures that involve the least number of steps, are time efficient, and incorporate strategies promoting high atom economy, are considered vital for commercial use.[163, 164] One of the earliest total synthesis challenges was reported for quinine, an anti-malaria natural product, from the cinchona tree of Peru.[165] The total synthesis of quinine was developed over a 150 year period and was a pivotal milestone in organic chemistry by stimulating discourse that furthered its development (Scheme 4.1).[166, 167]

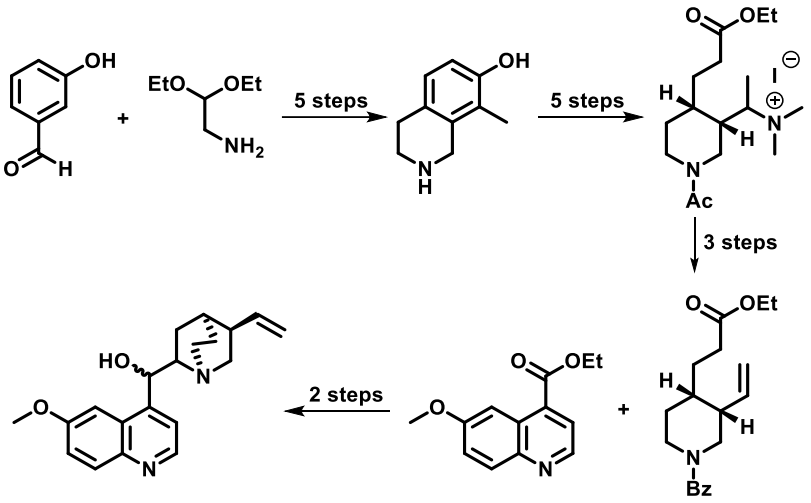

Scheme 4.1: Simplified version of the Woodward-Doering quinine total synthesis reported in 1944.[161] The desired enantiomer was isolated by chiral resolution.

When the structure of Taxol was first established following extractions from the Pacific yew in 1971,[168, 169] there was not considerable interest in its total synthesis. However, in the early 1990's its pharmaceutical importance became apparent. Many research teams worked to achieve the total synthesis of Taxol®. The 'winner' was the result of a photo finish between the Holton (first accepted article)[170, 171] and Nicolaou groups (first article to appear in print, within a week of the R. Holton group)[172] who worked independently of one another. The practices used to achieve a target natural product, such as Taxol®, have resulted in revolutionary synthetic techniques that have benefited many aspects of organic chemistry, making large scale synthesis of complex structures possible.[173, 174] Without total synthesis, the methods used in modern chemistry would be less sophisticated, and synthetic organic chemistry may have been stunted for some time. On a laboratory scale (<50 g), total synthesis can be economical, but the cost of raw materials required, and purification practices necessary to produce large amounts (>50 g) of a target natural molecule, are not usually practical. Crippling issues, such as increased exposure to toxic materials, larger quantities of dangerous chemicals, as well as high temperatures, high pressures, and expensive infrastructure, complicate the transition to large scale synthesis.

4.1.1.3 Semisynthesis

With structural knowledge of a target natural product, and an understanding of the biosynthetic pathway (the synthesis of the natural product in the organism), a strategy applying extraction and synthetic methods in tandem can be used to obtain high quantities of a natural product.[175] The biosynthesis of a natural product is usually part of a larger pathway that produces many metabolites. The other compounds on this pathway can often be isolated and extracted, from which the desired natural product

can be prepared. This approach can be extremely valuable if such precursors are more abundant than the target molecule, or cultivation of them is easier. In some cases, the precursors can be more abundant in various parts of the organism, thereby allowing high yielding extraction. In other scenarios, pathways to precursors may be mimicked *in vitro*. With Taxol®, the needles of the European yew, *Taxus baccata*, produce large quantities of the key Taxol® precursor, 10-deacetylbaccatin, which can be more easily isolated without killing the plant (Scheme 4.2).[162, 176, 177] This semisynthetic strategy for the generation of Taxol® is one of the commonly used processes.

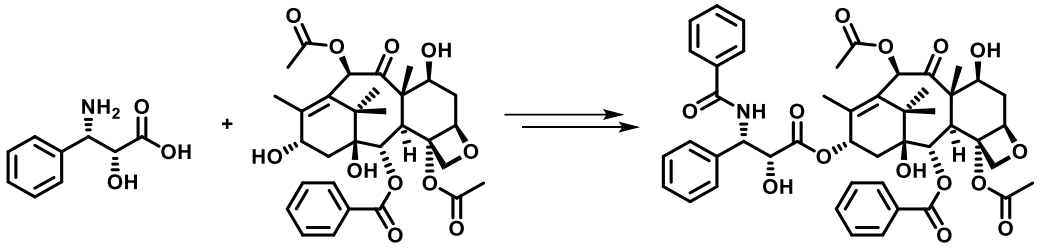

Scheme 4.2: Reaction of phenylisoserine with 10-deacetylbaccatin, which can be isolated from the European yew, to afford Taxol®.[177]

To produce practical semisynthetic strategies, a good understanding of the biosynthetic pathway, refined extraction techniques, and straightforward synthetic routes to the desired natural product are essential. This approach has led to the production of diverse families of natural products, including analogues and isomers not produced biologically, at a scale (>50 g) appropriate for commercial applications.

4.2 Cannabinoids

A cannabinoid is any chemical compound that effects the cannabinoid receptors, but the term cannabinoid is often used to describe the natural products found in common cannabis, such as *Cannabis sativa* and related strains (Figure 4.3). The largest amounts of cannabinoids are produced by the cannabis plant's flowers during maturation.

The flower bud can be clipped and dried prior to recreational use, or the cannabinoids contained within can be extracted. The term endocannabinoid is generally used for cannabinoids that are produced within the human body. Exocannabinoid, or phytocannabinoid, is the term used for cannabinoids that are not native to human biology.

Figure 4.3: Clockwise from top left: industrial hemp; cultivated *Cannabis sativa* strain; mature *Cannabis sativa*; several high CBD strains of young *Cannabis sativa*.

Cannabinoids predominantly effect two receptors, cannabinoid receptor types 1 and 2 (CB_1 and CB_2, respectively) that are present in most higher forms of life.[178] In humans both receptors exist primarily along the peripheral and central nervous systems,[179-181] but more densely in the brain and spine (Figure 4.4 and Figure 4.5).[182, 183] Both receptors are activated by endocannabinoids, including anandamide for CB_1[178] and 2-arachidonoylglycerol for CB_2[184, 185] (Figure 4.6). Other than the nervous systems,

individual distribution shows CB_2 being abundant within the immune system and related tissues[179] and CB_1 being heavily involved in metabolism[186] and the retina.[187]

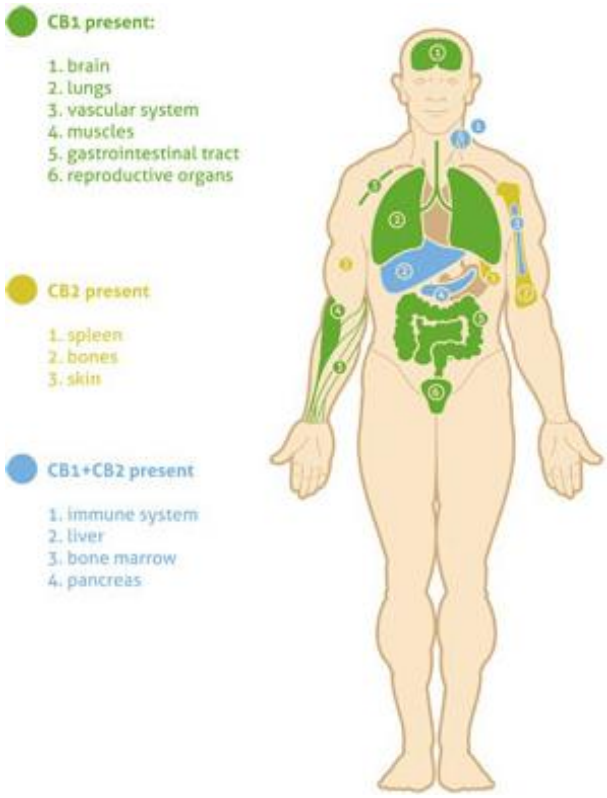

Figure 4.4: The Endocannabinoid System. CB1 and CB2 receptors in the human body. Image used with permission, no alterations made: https://www.fundacion-canna.es/en/endocannabinoid-system, Fundación CANNADistribution.

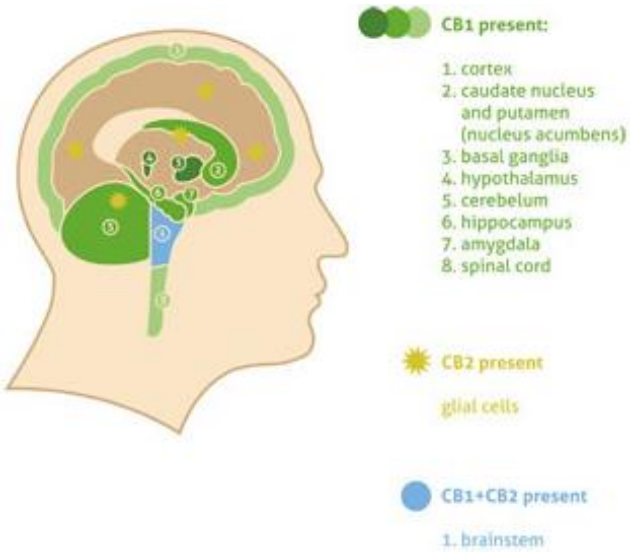

Figure 4.5: The Endocannabinoid System. CB1 and CB2 receptors in the human brain. Image used with permission, no alterations made: https://www.fundacion-canna.es/en/endocannabinoid-system, Fundación CANNADistribution

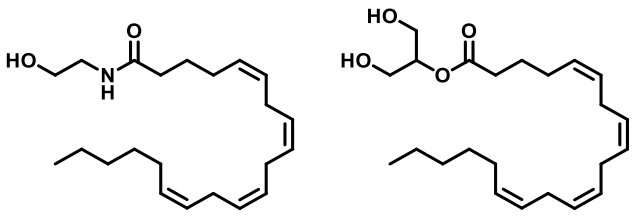

Figure 4.6: Left, anandamide; Right, 2-arachidonoylglycerol.

Cannabinoid receptor type 1 is culpable for psychoactive properties *via* presynaptic-inhibition[182, 183] and was found to be responsible for the pharmacological properties of (−)-trans-Δ^9-tetrahydrocannabinol (9THC), a potent phytocannabinoid in cannabis. The mechanism and role of cannabinoids within cells and biological systems is understandably complex, with phytocannabinoids capable of acting as agonists and antagonists, details of which are beyond the scope of this thesis. Sources covering these topics are readily available.[188-194]

Cannabis owes its medicinal and psychoactive effects to the phytocannabinoids produced by the organism, with medical uses including the treatment of nausea during chemotherapy, spasticity, and neuropathic pain.[178, 195-201] Research into the more potent properties exhibited by individual cannabinoids and their analogues is the subject of ongoing research.[202] Although at least sixty-five different phytocannabinoids have been identified, the two most notable and abundant are cannabidiol (CBD) and 9THC.[203] Other cannabinoids lack substantial research, which is a prominent subject of this thesis.

Two different numbering systems have been implemented for the naming of the dibenzopyran-based cannabinoids (the major cannabinoids). Herein, the dibenzopyran numbering system will be used if ambiguity exists. It is important to note that historically the monoterpenoid numbering system was used. Thus, both systems are presented here for completion and comparison (Figure 4.7). For example, 9THC is

called so because the alkene begins at carbon 9 (the assignment of 9 is predetermined from the dibenzopyran numbering system), hence, (−)-trans-Δ^9-tetrahydrocannabinol. Since chiral carbons exist within 9THC, the name also describes the optical activity, with a symbol denoting the counterclockwise (−) or clockwise (+) rotation of plane-polarized light. Earlier accounts have reported 9THC described as 1THC due to the monoterpenoid numbering system.[204] More recently, the simplified abbreviation of tetrahydrocannabinol, THC, is frequently used, but is too vague for this thesis.

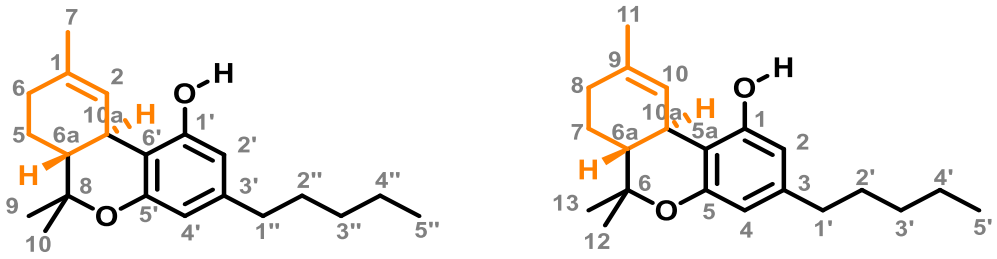

Figure 4.7: Numbering systems for 9THC. Left, previously used monoterpenoid numbering. Right, modern dibenzopyran numbering.

4.2.1 Major Cannabinoids

Herein, the phytocannabinoids will be referred to as cannabinoids. The biosynthetic pathway to the major cannabinoids (CBD and 9THC) produced by cannabis, integrates key steps in the production of isoprenoid, or terpenoid (natural products derived from five carbon isoprene molecules). Through biological machinery and selected enzymes, the major cannabinoids are generated (Scheme 4.3).[205, 206] These processes do not take place in a single portion of the cell, but instead, are spread throughout the cytosol (liquid portion within a cell), plastid (an organelle within plant and algae cells), and the apoplast (the space, including the cell wall, outside of the cell membrane). Hexanoic acid, which is likely generated from various fatty acids, is converted to a thioester (Hexanoyl-CoA, CoA = Coenzyme A), and elongated and cyclized to olivetolic acid. Through further enzymatic process, the major cannabinoids are produced, notably the

carboxylic acid analogues of 9THC and CBD (9THC-A and CBD-A, respectively). The biosynthetic pathway ends at this point; more active derivatives are generated through a decarboxylation process which is caused by heat, radiation, or long term storage.[207, 208] Alternative alkyl side chains can be introduced by the same enzymes *via* different fatty acyl-CoAs giving rise to many possible cannabinoid variations. Over time, or with intense heat and/or exposure to ultraviolet light, the major cannabinoids aromatize to afford cannabinol (CBN), which is still somewhat effective at activating the cannabinoid receptors and is often used to quantify older cannabis samples.[209, 210]

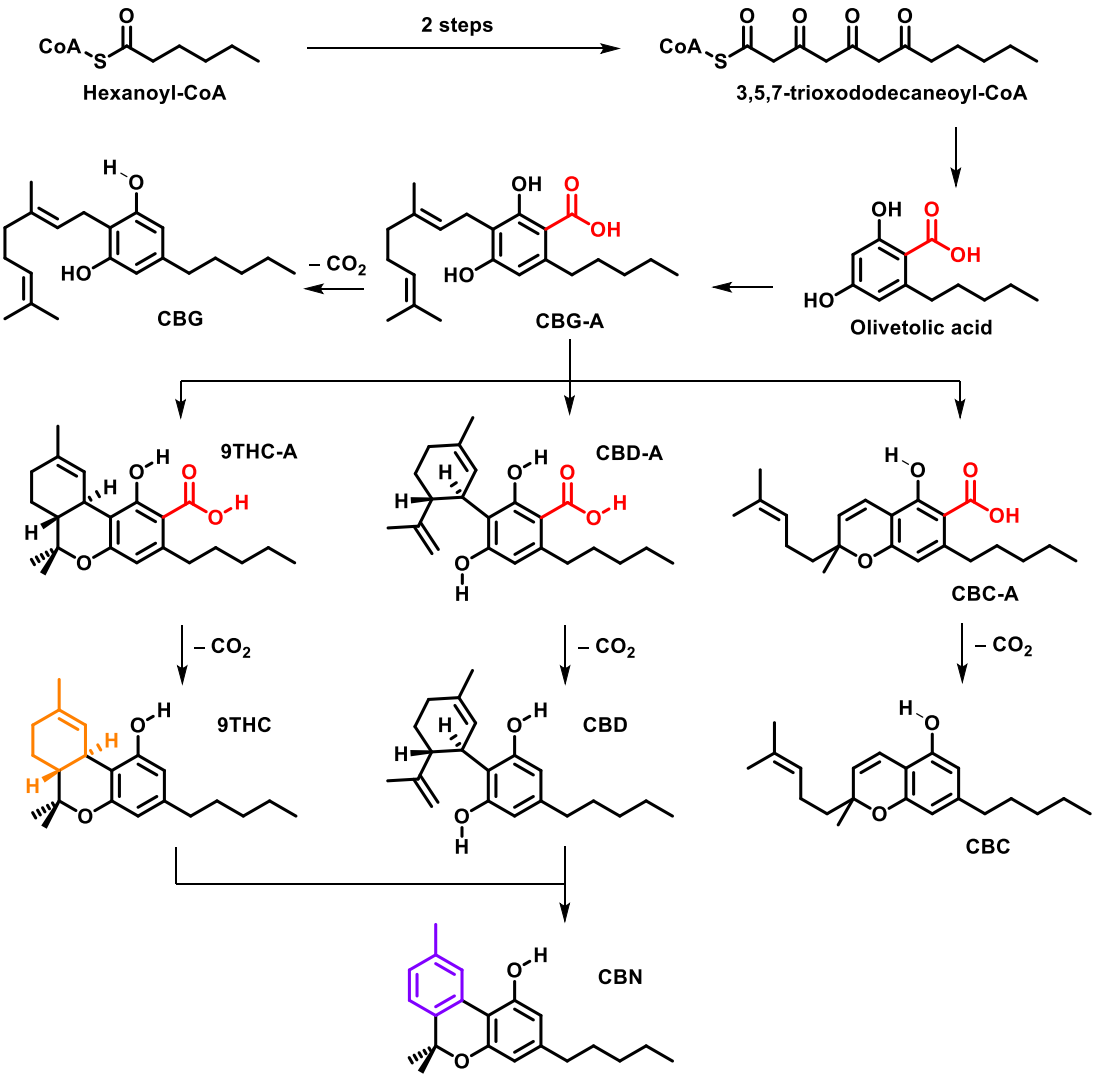

Scheme 4.3: Simplified biosynthetic pathway to the major phytocannabinoids. All processes, except decarboxylation steps, are enzyme mediated. CBG = cannabigerol, CBC = cannabichromene.

Considered a major cannabinoid, 9THC is highly sought as the primary psychoactive component of cannabis.[211] Currently, the pharmaceutical uses for 9THC include antiemetic medication (reducing nausea and vomiting),[212] and the treatment of multiple sclerosis[213] and various neurodegenerative disorders.[214] Often 9THC is used in conjunction with CBD; research into their tandem effectiveness is ongoing.[215] It has been postulated that the cannabis plant uses 9THC and 9THC-A as self-defence against insect predation and environmental stress through absorption of UV-B radiation.[216-218]

Another of the major cannabinoids, CBD, is also heavily investigated. Particular interest in CBD focuses upon clinical research, particularly for the treatment of mental disorders (such as anxiety and cognition), movement disorders, and pain. The treatment of epilepsy has proven highly effective.[219-222] Thorough conclusive results for the efficacy on other conditions are yet to be fully determined.[223] In cannabis, there is no enzyme committed to converting CBD to 9THC, but CBD does cyclize to 9THC in a Lewis acidic environment (Figure 4.8).[224-227]

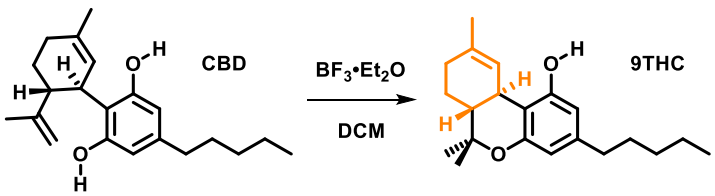

Figure 4.8: Synthetic conversion of CBD to 9THC.

4.2.2 Low Abundant Cannabinoids

The medicinal efficacy of major cannabinoids largely depends on intake, as 9THC and CBD often produce different effects when paired together and/or in varying quantities.[215] Other cannabinoids produced by cannabis also contribute to the observed medicinal effects of impure cannabis, but their specific impact on biological systems

remains largely unexplored (Figure 4.9).[205, 228] There is also a lack of research on the impact individual terpenoids found in cannabis have on biological systems.

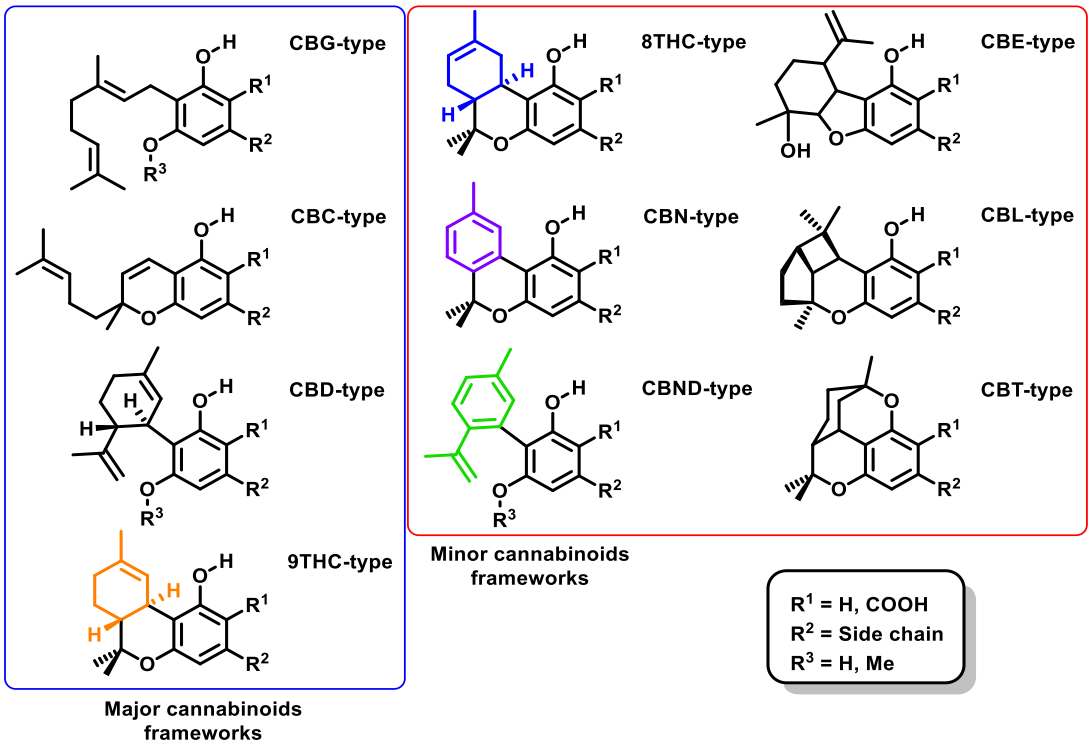

Figure 4.9: Several types of cannabinoids generated from olivetolic acid. CBE = cannabielsoin, CBL = cannabicyclol, and CBT = cannabicitran types are generated through alternative cyclizations. (−)-trans-Δ^8-tetrahydrocannabinol = 8THC, a minor side-product to 9THC. CBND = cannabinodiol, is generated similarly to CBN. Side chains vary, typically R^1 = H or COOH, R^2 = H, Me (denoted with a 'C_1' suffix), C_3H_7 (denoted with a 'V' suffix, for 'variant'), C_4H_9 (denoted with a 'C_4' suffix) or C_5H_{11} (the most common side chain), R^3 = H or Me.

Many of the less abundant compounds found in cannabis have received little attention compared to CBD and 9THC.[229-232] Because of their lower bioavailability, such cannabinoids are rarely the focus of biological studies. In order to access reasonable quantities of these compounds, selective synthesis from abundant cannabinoids, followed by careful isolation, is required. Improved methodologies for isolation of cannabinoids can often be developed from these investigations.

There is no known biosynthetic pathway that converts CBD into 9THC; the generation of these compounds occurs *via* conversion of cannabigerolic acid (CBG)

into CBD-A and 9THC-A by separately *in vivo* enzyme-catalyzed processes, and subsequent decarboxylation.[233, 234] However, a Lewis acid catalyzed method, which can be conducted at low temperatures (ideally under an inert atmosphere with dry solvents)[224-226] promotes ring closure of CBD. When heated, or in the presence of acid, the thermodynamic isomer, 8THC, is preferentially formed *via* isomerization of the double bond at position 9 to 8 (Figure 4.7).[226, 235, 236] There is no evidence to suggest that this conversion readily occurs within biological media, whether in cannabis as a biosynthetic pathway, or following human consumption of CBD or 9THC-containing products.[237] Therefore, 8THC is likely generated as a product of degradation of 9THC and CBD prior to CBN generation, or by an enzyme misusing an isoprenoid, as the alkene is established at position 9 early in the biosynthesis of tetrahydrocannabinol-based cannabinoids.[228]

8THC, much like all low abundant cannabinoids, typically exists in very low abundance (<1%). It is therefore not surprising that research on 8THC is lacking compared to 9THC, despite 8THC showing similar, or only slightly lower, biological activity.[238-241] The degradation product of 9THC, CBN, has also garnered interest from the scientific community because it exhibits different effects on cannabinoid receptors. The degradation product of CBD, CBND, has similarly received very little attention. Furthermore, neither CBN nor CBND are psychoactive, which is oft undesired for medical applications.[209, 242, 243] The other low abundant cannabinoids, CBE, CBL, and CBT, form from cyclizations of CBD, and CBE during metabolism or natural irradiation, are sparsely reported beyond detection procedures.[244, 245]

4.2.3 Synthetic Cannabinoids

Cannabinoid receptors can also be affected by synthetic cannabinoids. These synthetic compounds either mimic existing cannabinoids, whether they are exogenous or endogenous in origin, or simply act as agonists to the same receptors. These analogues can shed light on the link between chemical structure and biological activity when focused on a particular activation site.[246, 247] This structure-activity relationship is particularly important considering that chiral centres are present in most cannabinoids and there is a strong relationship between the spatial orientations of chiral centres and biological systems such as enzyme active sites.[248] Synthetic cannabinoids can be used as agonists, often with increased potency compared to natural products; as antagonists, to inhibit certain receptor outputs, which is of interest for appetite decreasing medications, or other effects not typically targeted by natural cannabinoids, including anticarcinogenic or antitumor growth.[249-251] Subtle changes to the chemical structure of cannabinoids can have an impact on efficacy and medicinal properties. In particular, the location of the double bond (typically starting at carbon 9) and the substituent at carbon 11, increase binding affinity to cannabinoid receptors. The length and makeup of the side chain at carbon 3 (see R^2 in Figure 4.9) affects potency either by restricting metabolism or changing the time bound to the cannabinoid receptors. Alterations to the phenol group at carbon 1 increase receptor selectivity.[252-254] Other additions or changes can also cause unforeseen effects.[247, 248, 255]

Derivatives such as HU-210 (Figure 4.10), which is 100 to 800 times more potent than 9THC,[256-258] and nabilone, which has been used as an antiemetic and analgesic for neuropathic pain,[259, 260] demonstrate how dramatically small changes to the typical cannabinoid structure can impact activity. A chemotherapeutic drug, HU-331, a

para-quinone derivative of cannabidiol, has demonstrated highly specific inhibition of topoisomerase II, halting DNA access and inducing antineoplastic activity (stopping abnormal growth) in cancer cells.[261, 262] To investigate such effects, it is imperative to expand the library of accessible cannabinoids.

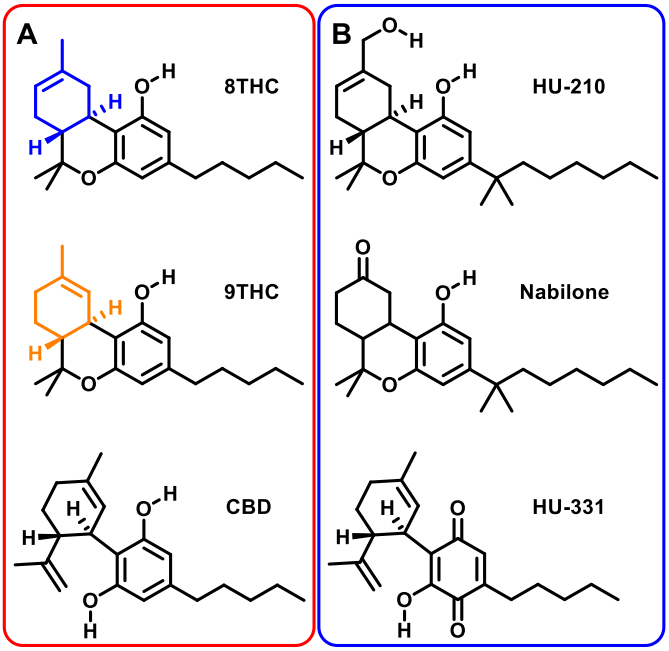

Figure 4.10: A) Prominent naturally occurring cannabinoids. B) Pharmaceutically relevant synthetic cannabinoids.

Other prominent synthetic compounds that effect the cannabinoid receptors, but do not contain the typical phytocannabinoid architecture, include aminoalkylindoles[249-251] (Figure 4.11) and eicosanoids[263] (signalling molecules, or mimics of endocannabinoids anandamide and 2-arachidonoylglycerol, Figure 4.6), the former of which is far more common.

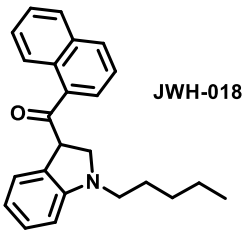

Figure 4.11: Example of an aminoalkylindoles-based synthetic cannabinoid.[264] These compounds are typically comprised of two bicyclic 'cores' with a linker between them. Variants expand on this general structure.[249-251]

4.2.3.1 Quinones

As previously mentioned, derivatization of natural products, including cannabinoids, have shown to have profound medicinal impact. One such derivatization, to include a quinone, can be considered. A quinone is generated from an aromatic group upon replacement of an even number (n) of C–H bonds by n/2 C=O functionalities. Most commonly, two carbonyl groups are formed, giving rise to 1,2- or 1,4-diones (described as *ortho*- or *para*-, respectively). These fully conjugated cyclic diones are well-known oxidizing agents as they often have facile two-step electron accepting redox processes[265, 266] which makes them effective electron transport systems in all respiring organisms.[267] Electrochemically active organic molecules have garnered attention due to their redox catalysis potential and their ability to act as co-enzymes in electron transport chains in biological systems.[268, 269] In particular, quinones have been shown to be cytotoxic towards cancer cells. [269, 270] The broad utility of quinone-containing molecules renders them attractive for use in biochemistry, encouraging exploration into their unique medicinal properties.

Para-quinone cannabinoids are more synthetically accessible than their *ortho* counterparts and are reported to be far more stable.[271] For example, Taglialatela-Scafati and co-workers showed that HU-331 can be readily prepared. They postulated a mechanism to *para*-quinones that involves a sigmatropic rearrangement of an iodine–

oxygen bond in an iodane ester which preferentially forms the *para*-quinone species (Scheme 4.4).[272] Efforts to prepare *para*-quinone analogues of cannabinoids 9THC, 8THC, and CBN, remained stunted until recently when Caprioglio and co-workers were able to isolate *para*-quinones more succinctly by using a stabilized hypervalent iodine compound, *ortho*-iodoxybenzoic acid (SIBX). All of the *para*-quinone cannabinoid analogues reduced tumour growth in mice.[273] Notably though, research by Pettus and co-workers indicates that a similar hypervalent iodine compound, *ortho*-iodoxybenzoic acid (IBX), can be used to generate *ortho*-quinones from substituted phenols when *N*,*N*-dimethylformamide (DMF) is employed as the solvent.[274] It is postulated that IBX, or some intermediate during the transformation, is stabilized in DMF, which allowed for the formation of the *ortho*-quinone (Scheme 4.4). When oxidation of the iodane ester complex can occur, as stated by Taglialatela-Scafati, the *para*-quinone forms.[272]

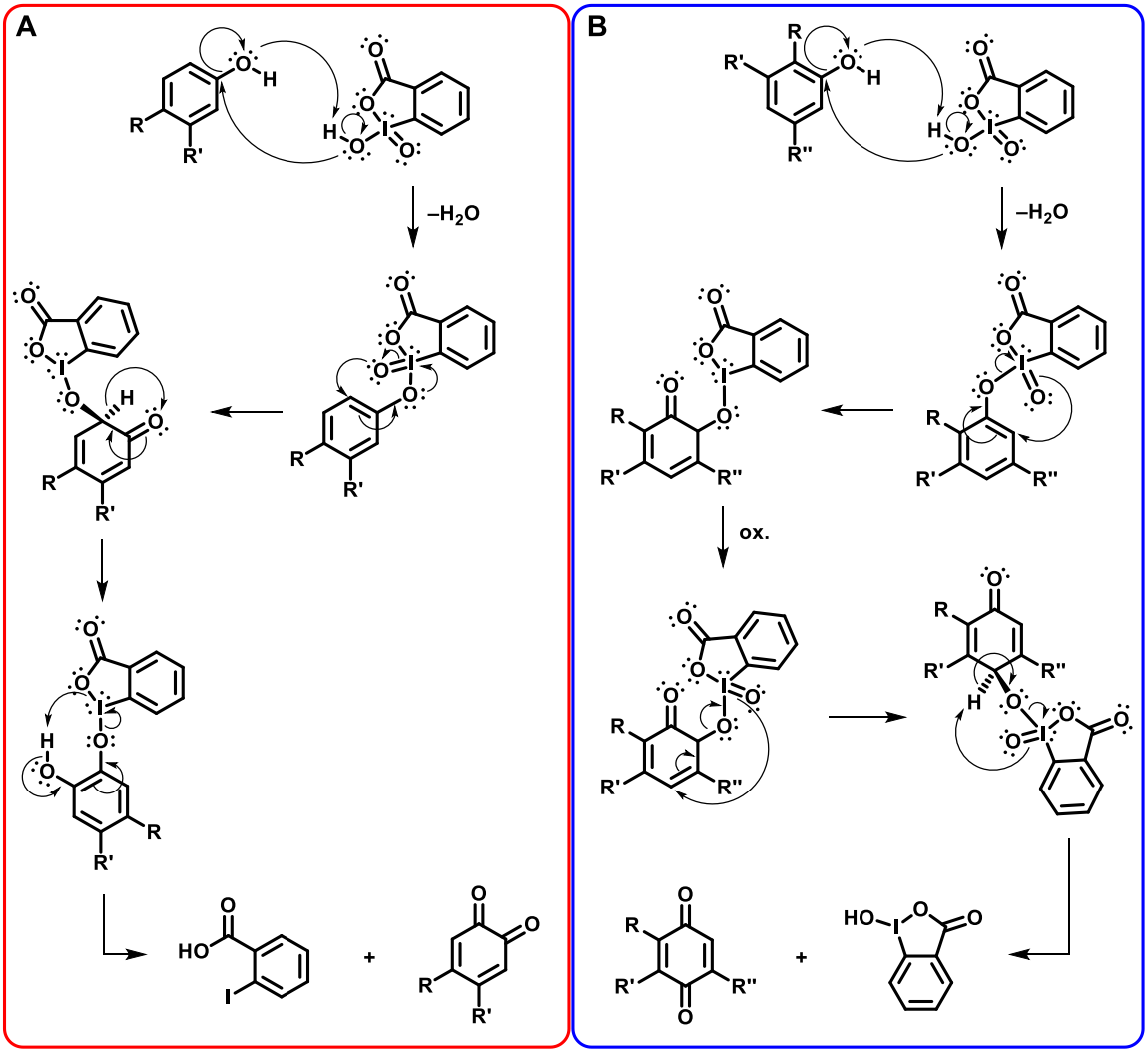

Scheme 4.4: A) Proposed mechanism by Pettus and co-workers for *ortho*-quinone generation with disubstituted phenols in DMF.[274] B) Proposed mechanism of *para*-quinone generation by Taglialatela-Scafati and co-workers in EtOAc.[272]

4.2.3.2 Fluorinated Cannabinoids

Fluorine, in the form of organofluorine, is present in an ever increasing proportion of approved drugs.[275] The incorporation of one or more fluorine atoms into natural products has garnered interest as such modifications generally improve metabolic stability, cell permeability, and/or target interactions.[276] There are two core strategies for introducing fluorine atoms into a natural product: 1) total synthesis starting from materials that contain fluorine, or that can be readily transformed into fluorine during the total synthesis; and 2) 'late-stage' fluorination where the fluorine atom is introduced

into the already synthesized or isolated molecule.[277-279] Late-stage fluorination generally involves the combination of a carbon centred nucleophile with an electrophilic fluorine source, a process often referred to as electrophilic fluorination. Although both approaches have their advantages and disadvantages, re-designing a total synthesis strategy is an extensive task. Thus, the more attractive tactic for this thesis and especially for large scale and industrial uses, is utilizing labile C–H bonds or reactive functional groups to introduce the fluorine atom at a later stage.

Fluorinated cannabinoids are relatively scarce and underdeveloped. Accordingly, there is a deficiency of thorough studies, and many reported compounds lack complete characterization. In addition, biological investigations on such species are rare, despite cannabinoids having relatively simple functional groups and structures (Figure 4.12).

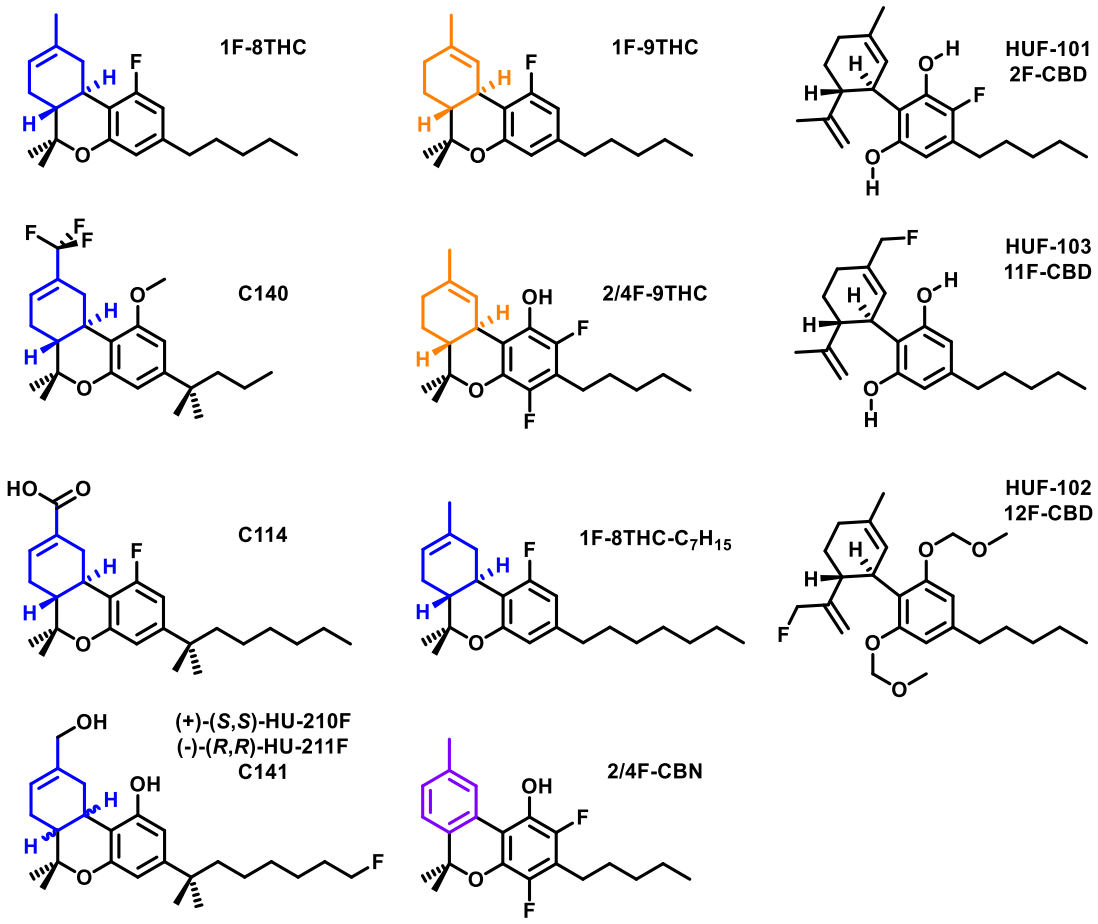

Figure 4.12: Reported fluorinated cannabinoids.

Several examples of fluorinated cannabinoids were generated using late-stage fluorination; both 1F-8THC and 1F-9THC were prepared from their parent cannabinoids using SelectFluor™.[280] The fluorinated CBD analogues (HUF-101, 102, and 103) were synthesized using 1-fluoropyridium triflate as the fluorine source.[281] 2/4F-9THC and 2/4F-CBN were synthesized from CBD and CBN, respectively using *N*-fluoro-3,5-dichloropyridium triflate as the fluorination source. In that case, however, an intractable mixture of compounds that contained F in the 2 and 4 positions of the cannabinoid were reported.[282, 283] The remaining known fluorinated cannabinoids were generated using a total synthesis approach, beginning with fluorine-containing materials. Further work beyond their synthesis is deficient.

Both 1F-8THC and 1F-9THC, which have had the hydroxyl groups replaced with fluorine, are desirable products for determining the influence of the hydroxyl group on potency and receptor selectivity. However, the reported synthesis requires multiple steps from expensive materials, and hence, little bioactivity work has been conducted.[280] It has been shown that replacement of the hydroxyl group in similar analogues decreases the selectivity to cannabinoid receptors (1F-8THC-C_7H_{15}).[284] Other evidence indicates that replacement of the aromatic ring hydrogens (2/4F-9THC and 2/4F-CBN) leads to minor receptor affinity changes.[282, 283] The features of the group at position 3 (C141) has also seen to effect receptor affinity.[285] Fluorinated CBD analogues (HUF-101, -102, and -103, Figure 4.12) have been reported to have increased potency compared to CBD in neurological based targets associated with anxiety and depression, and have neural protective properties.[281, 286] Many cannabinoid derivatives and analogues, fluorinated ones included, are frequently buried in patents and lower impact publications.[287]

The two 'hot-spots' where fluorine atoms may be introduced in late-stage fluorination are the hydroxyl group and the benzyl C–H bonds, both of which are considered targets for metabolism. As such, alteration of these sites could lengthen the compound's efficacy by restricting swift metabolic breakdown. With cannabinoids, this would involve carbon 1 (as an aryl fluoride) when switching the hydroxyl, and carbons 11 and 1' (as benzyl fluorides) when substituting the benzyl hydrogens. Replacement of the aryl protons, at carbons 2 and 4, is also attractive given the activity exhibited by the CBD analogue HUF-101.

Two recent and well described strategies for electrophilic fluorination are: 1) the use of PhenoFluor™, a commercially available, albeit expensive, series of fluorinating

compounds that have seen many uses in the literature;[288, 289] and 2) a more recent procedure that uses radical initiators to promote removal of a tertiary or benzyl C–H bonds leading to replacement of a hydrogen atom by fluorine.[290-293] The radical initiator used dictates which C–H bond is activated.[294]

4.3 Chemotherapeutic Activity

Any compound that can directly or indirectly inhibit the uncontrolled growth and proliferation of cancer cells can be considered to have a chemotherapeutic effect. Cannabinoids interact with CB_1 and CB_2, as mentioned *vide supra*, and the modes of action they take is complex.[193] Nonetheless, their lipophilic nature makes them perfect candidates for drugs, including as chemotherapeutic agents. The balanced expression of both cannabinoid receptors, as well as other associated receptors, is vital for the cell, and therefore the organism's, wellbeing. By exploiting the expression of CB_1 and CB_2, cannabinoids have been utilized for specific cell outcomes, such as the death of cancerous cells,[295] *via* proliferation and apoptosis.[296] Results differ between types of cancer,[297, 298] and so, each cancerous disease needs to be treated as an individual illness, rather than one of the same.

There are several approaches to developing a chemotherapeutic drug, but ideally potential candidates will be lipophilic, interact with receptors within cells, exhibit preferential selectivity for cancer cells, and halt the growth of cancer cells (also known as an antiproliferation effect). To design a compound that possess these qualities is understandably difficult as the inner workings of a cell are extraordinarily complex and predications on how a compound may interact with the plethora of biological machinery is exceptionally challenging. Instead, we can probe the efficacy of a library of compounds that contain certain structural motifs to ascertain what alterations to the

chemical structure exhibits the most promising antiproliferative effects. One can also exploit the chemistry within cancer cells, as they have a different internal environment than healthy cells. Differences are typically observed in pH levels,[299] redox potential from oxidative stress,[300] hypoxia,[301] membrane permeability,[302] and in the up or down regulation of specific receptors.[303-308] These qualities of cancerous cells can be used to aid in a compound's selectivity and poisonous efficacy towards them. For example, a redox active compound could be a more effective poison to a cancer cell than a healthy cell, permeability changes might allow for the drug to pass into the cell more swiftly, or the presence (or absence) of receptors may promote other cellular mechanisms to become more dominant.

4.4 Project Aims

With the increasing demand for cannabinoids from cost effective and swift methodologies, inventive setups are required.[227] Cannabinoids, notably the most pharmacologically active ones, CBD and 9THC,[309-311] are important to the medicinal industry,[195-199] and with legalization and decriminalization, the growing recreational economy.[312-316] These compounds can be used directly from plant material, or extraction techniques can be used to obtain oils that retain many of the desired cannabinoids.[317-319]

With recent changes in the legalization of recreational cannabis use in Canada, research into cannabinoids has become more viable and economic interests more apparent. Specific incubation and growth conditions are required for cannabis plants to produce large quantities of specific cannabinoids. Industrial cannabis varieties, where 9THC is less than 0.3% (i.e. hemp), have no regulations on the amount of CBD or CBD-A produced. Sourcing specific pure cannabinoids, however, can be challenging because

of cultivation restrictions and legal regulations can limit the amount that can be produced.[320] Moreover, large quantities of 9THC are not readily available, even for research, as it can only be purchased as an HPLC standard (typically 1 mL at a concentration of 1 mg/mL).[321] Therefore, *in vivo* experiments become cost prohibitive. Since hemp biomass has the potential of serving as a large source of CBD-A and CBD, a semisynthetic procedure that converts all available cannabinoids, particularly CBD-A and 9THC-A, into a single cannabinoid, is extremely attractive.

Although synthetic pathways to many cannabinoids are known, be it from total synthesis[322, 323] or through transformation from other isolated cannabinoids,[224-226] these methods usually require an extensive series of chemical reactions and/or rigorous, energy-intensive isolation procedures.[317-319] The approach of a synthetic chemist will be used for the semisynthesis and purification of known cannabinoids, as well as to enhance access to a library of synthetic cannabinoids.

Current methods for the production of 8THC include total syntheses,[324-328] as well as semisynthesis from isolated CBD.[226, 329] While both approaches serves as sources of 8THC, there is substantial room for improvement, especially with respect to an increase in generality whereby a single procedure could be applied to a wide array of cannabis extracts, regardless of overall cannabinoid content. The current work aimed to provide a straightforward semisynthetic method for the generation of 8THC from cannabis extract by using the related cannabinoids CBD-A, CBD, 9THC-A, and 9THC as precursors. If 8THC can be readily prepared from *Cannabis sativa* extracts, it will become possible to conduct more in depth research and expand our cannabinoid knowledge base.

By altering a semisynthetic procedure that targets 9THC, the degradation product CBN may also be obtained. Many other cannabinoids have also been reported, including 9THC isomers, (*R*,*S*)-Δ^{10}-tetrahydrocannabinol (10THC), *R*-Δ^{10a}-tetrahydrocannabinol (10aTHC),[204] and the degradation product of CBD, cannabinodiol (CBND).[330] None of these compounds have yet to gain substantial attention, beyond their initial discovery and identification. This is likely due to challenges associated with previously reported syntheses, as well as limited availability of characterization data, an unfortunate, but common trend in some organic chemistry circles.

Whether or not Taglialatela-Scafati and colleagues were correct with their NMR assignments of the quinones of cannabinoids made it unclear on the exact nature of the compounds synthesized. This has driven us to target the *ortho*-quinones of the cannabinoids as they may possess different cytotoxicity to the reported *para*-quinones. Accordingly, the *ortho*-quinone analogues of 9THC, the more thermodynamically stable isomer, 8THC, and the degradation product, CBN, were chosen as likely candidates to exhibit chemotherapeutic activity.

Although there are many different cell types that could be tested with the synthesized compounds, our collaborator, Prof. Igor Kovalchuk and his team, primarily focused on the antiproliferative influence of the isolated cannabinoids on breast cancer. Many of the synthesized cannabinoids throughout this project were screened for their antiproliferative efficacy, the results of which will be discussed in detail in Chapter 5.

Chapter 5: Semisynthesis of Cannabinoids and Relevant Derivatives and their Chemotherapeutic Activity

5.1 Extraction

A reported method for extracting cannabinoids involves submerging *Cannabis sativa* biomass in acetone, followed by filtration and removal of solvent to afford a crude extract or 'gum' (a term used to describe impure extract that is a dark waxy oil).[227] Silica gel chromatography, using methanol as the mobile phase, can be used to remove unwanted materials. Then, the extract is subjected to excessive heat to induce decarboxylation of the carboxylic acid derivatives of any cannabinoids in the extract. Finally, another chromatography step is employed to isolate a pure cannabinoid. This intensive procedure relies wholly on the plant to produce the particular cannabinoid of interest, requiring several purification steps and many solvents. Initially, collaborator Prof. Igor Kovalchuk, supplied an extract prepared in a similar manner,[227] but having to rely heavily on external researchers for material became troublesome. To mitigate the dependence on the Kovalchuk group to supply extract samples, an alternative extraction approach was developed so that only biomass was required for this project.

Biomass of *Cannabis sativa* contains a plethora of material. We desire the extraction solvent to contain all the cannabinoids while the unwanted material remains insoluble. Despite containing a hydroxyl group, cannabinoids are exclusively hydrophobic, and thus, water is unsuitable. Most plant material is polar, while cannabinoids are highly soluble in nonpolar solvents. Accordingly, a nonpolar solvent is most appropriate. Highly polar solvents, such as methanol and acetone, have been used in previous work[227, 331] but they tend to also extract polar contaminants. Butane

has also been used, as it is easily collected and reused, but it requires low temperatures or high pressures as it is a gas at ambient conditions.[332] Thus, toluene was chosen as a suitable extraction solvent because it is only weakly polar, recollection *via* rotary evaporation is possible, and its high boiling point (110.6 °C) means less safety issues to consider with scale up. Furthermore, toluene is a good choice for subsequent cannabinoid conversions (*vide infra*).

To scale up a procedure for industrial use, one must consider several factors. These include, but are not limited to, cost of materials and equipment, safe materials and procedures used, turnaround time, and method reliability. The idea is that the methodology is kept simple so when scaling up, complications are mitigated.

Dried cuttings of *Cannabis sativa* were crushed and submerged in 30-50 mL of toluene per gram of biomass (see 6.1.5 for details). The mixture was stirred vigorously for 30 minutes and then filtered. The solid biomass was re-extracted at least three times, after which the dark-yellow toluene fractions were combined. Although minimal colour remains in the fourth extraction, no additional cannabinoids are present. The weight of the extract obtained increases with subsequent extractions, but the quantity of cannabinoids in the extract remains unchanged after the third extraction. The volatile components were then removed *in vacuo* with a rotary evaporator to yield crude extract; the toluene was collected and reused in consecutive extractions. The ease of toluene recollection allowed for the same 4 L of toluene to be recycled throughout the entirety of this project. Ultimately, the efficiency of toluene rendered it possible to isolate crude extract the same day biomass was supplied.

The extract, a thick yellow oil, was determined to be 13-15 w/w% of the biomass (*i.e.* if 1 g of biomass is used, 130-150 mg of extract can be obtained) irrespective of the *Cannabis sativa* strain. While high CBD and CBD-A containing samples were initially used in this project, low cannabinoid containing hemp varieties also proved viable. Given that such material is not controlled by government regulations, and often disposed of, the ability to use it as a cannabinoid source is beneficial from economic and logistic perspectives, making the process much more viable on an industrial scale. During subsequent steps a small amount of toluene was always retained to facilitate transfer of solutions and minimize mechanical loss. With further drying, *via* exposure to high vacuum, a solvent-free crude extract can be obtained. The desired cannabinoids within the extract can be purified by a single silica chromatography process. Throughout this work such purification was not necessary for subsequent reactions or conversion of cannabinoids.

5.2 Decarboxylation

A decarboxylation reaction is a chemical process wherein a carbonyl group is replaced by a hydrogen and CO_2 gas is released (Scheme 5.1).

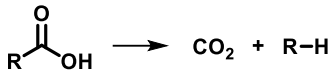

Scheme 5.1: Simplified decarboxylation reaction where R = alkyl or aryl group.

Chemically induced decarboxylations include many named reaction, all of which are radical processes,[333-335] while biochemical routes rely on enzyme catalysis.[336] Both 9THC-A and CBD-A are present in varying amounts in *Cannabis sativa*, where they slowly degrade to 9THC and CBD, respectively. This decarboxylation can be accelerated by exposure to high temperatures. While 9THC and CBD are far more

biologically active than their carboxylic acid analogues, both 9THC-A and CBD-A are solids, isolable as crystals, more abundant, and easily converted to 9THC and CBD *via* burning (hence, smoking and vaping of marijuana and related products). Since burning biomass is undesirable due to the formation of degradation by-products, controlled heating is generally used for research purposes (Scheme 5.2).

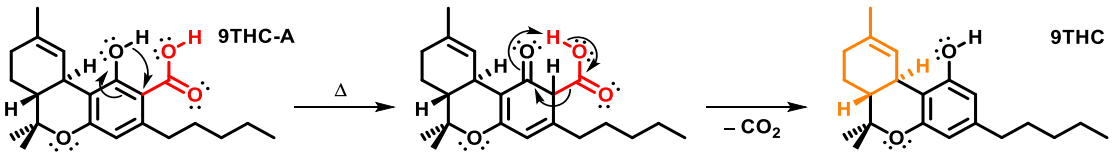

Scheme 5.2: Plausible mechanism of the decarboxylation of 9THC-A, producing 9THC.[208]

Rather than directly exposing the biomass to heat, it is preferential to conduct the decarboxylation in solution, as this allows for the extract to be directly used in other chemical transformations. The decarboxylation of 9THC-A and CBD-A occurs above 110 °C, which is beyond the boiling point of most common solvents, especially ones that can be easily removed *in vacuo*. Heating a toluene solution of extract to reflux for 3 h was not sufficient to cause complete decarboxylation; using boiling xylenes only led to 20% decarboxylation in 3 h. A thick-walled (5 mm) glass vessel designed to handle high pressures and sealed with Kontes® valves was thus used for this process. Specifically, this vessel was charged with a concentrated toluene extract solution, sealed, and heated to 130 °C with constant stirring. The sealed system maintained toluene as a liquid, allowing solution phase decarboxylation. The vessel also had substantial headspace to allow safe liberation of gaseous CO_2. Complete decarboxylation of 9THC-A and CBD-A was achieved in 3 h affording a toluene solution of 9THC and CBD (Figure 5.2 and Figure 5.1). At this point either 9THC or CBD can be isolated *via* silica column chromatography.

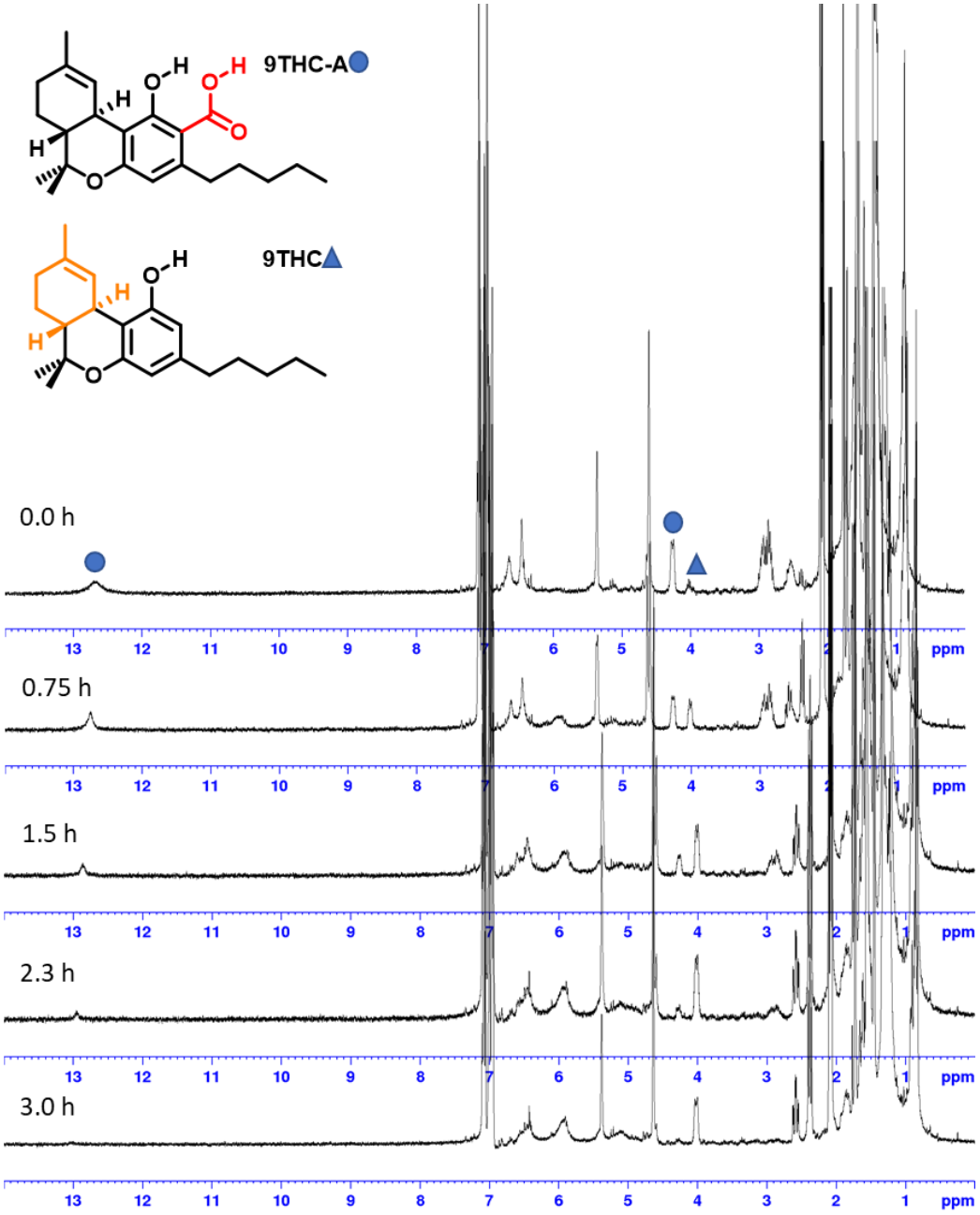

Figure 5.1: *In situ* monitoring of decarboxylation of 9THC-A in extract *via* ^{1}H NMR spectroscopy in toluene-d_8. From top to bottom: 0.0 h, 0.75 h, 1.5 h, 2.3 h, 3.0 h. Note the loss of characteristic 9THC-A signals (δ 12.96 and 4.29) and gain of 9THC signal (δ 4.02).

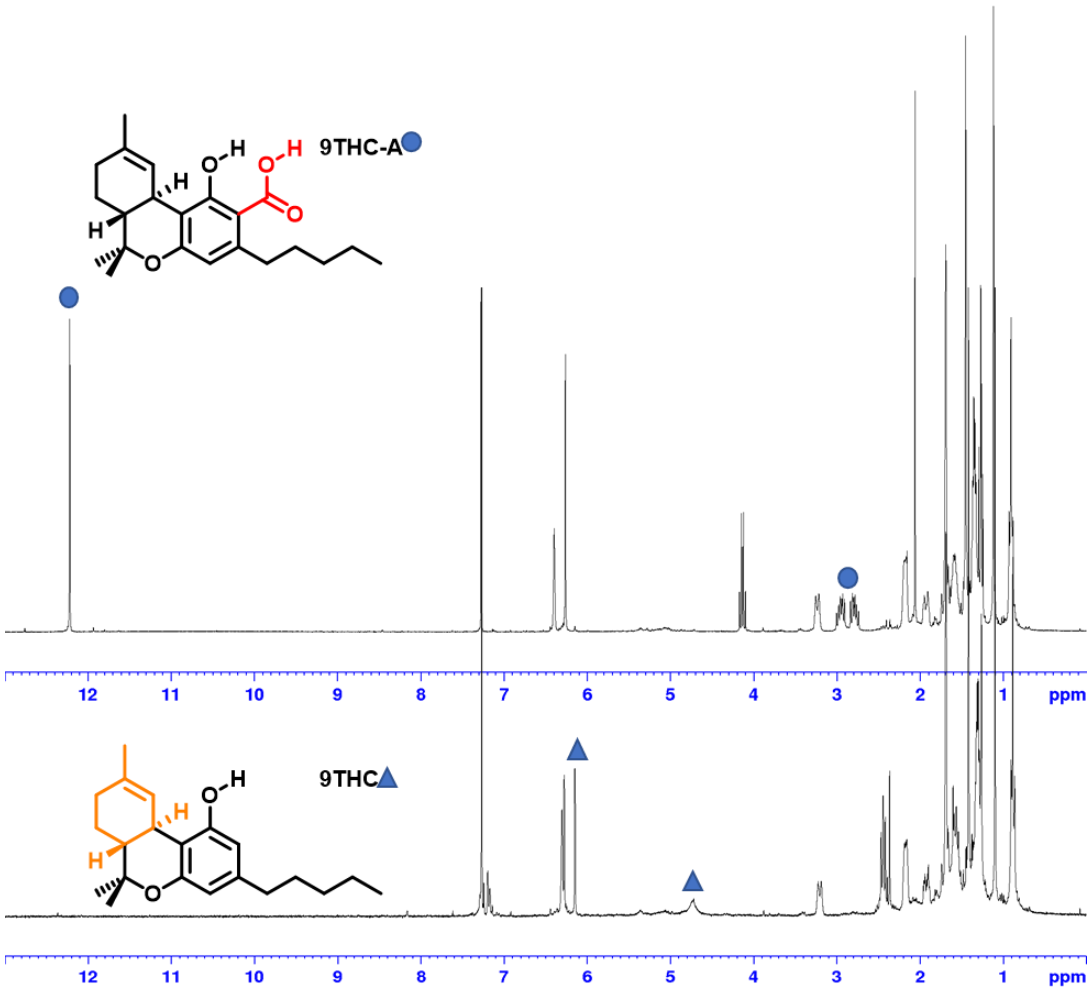

Figure 5.2: Solution phase decarboxylation of 9THC-A in extract *via* ^{1}H NMR spectroscopy in $CDCl_3$. Top: 9THC-A rich extract prior to decarboxylation. Bottom: the same extract following the solution phase decarboxylation step. No 9THC-A present due to loss of characteristic signals at δ 12.19, 2.94, and 2,78, and growth of 9THC signals notably at δ 6.14 and 4.87.

Although using high temperatures and pressures are less than ideal, the custom-designed 2 L vessel can tolerate far harsher conditions than that used for this work. The vessel size enabled biomass samples up to 100 g to be processed at a time. Steel reactors are more than capable of safely enduring such reaction conditions on an industrial scale.

5.3 Synthesis of 9THC

Even with the recent legalization of recreational cannabis in Canada, regulatory restrictions on growing *Cannabis sativa* with high quantities of 9THC for commercial cultivation and sale are still costly. As a result, strains of cannabis that possess low

9THC and high CBD concentrations are more commonly grown for such purposes. There is motivation to source pure 9THC and other cannabinoids without breaching current regulations, potentially through conversion of unregulated cannabinoids, such as CBD, into 9THC. The partnership between Prof. Igor Kovalchuk and Prof. Paul Hayes was fuelled by a desire to develop a straightforward and cheap route to 9THC from CBD. Initial efforts focused upon generating 9THC from pure CBD. Subsequent investigations aimed to obtain 9THC from CBD rich extracts.

5.3.1 Synthesis of 9THC From CBD

This work is a substantially modified version of a procedure reported by Webster *et al.*[226] That contribution showed that an acidic environment promotes ring closure of CBD to give the kinetic product, 9THC, which isomerizes over time to the thermodynamic product, 8THC. The isomerization was accelerated in the presence of water from the atmosphere or in solvent, or when the acidic environment was more concentrated. To ensure the kinetic product was isolated, and to restrict the presence of protons, which provide an avenue for isomerization, a lower temperature (–10 °C) and thoroughly dried solvent were used. In addition, the reaction was conducted under an argon atmosphere (Figure 5.3). This approach was successful, producing only a minimal quantity of 8THC (5-10%) after 2.5 h. Pure 9THC was isolated *via* silica column chromatography.

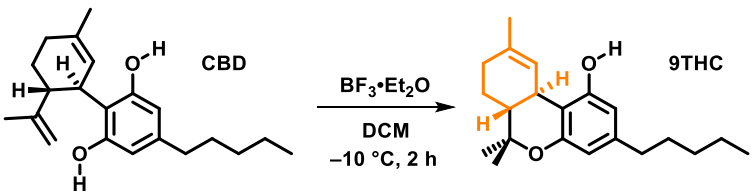

Figure 5.3: Revised method for the synthesis of 9THC from CBD.

This procedure proved to be relatively simple and other researchers have employed similar approaches.[224-226] This represents the initial work which provided inspiration for the cannabinoid research associated with this thesis.

5.3.2 Synthesis of 9THC from Extract

Rather than needing to isolate CBD prior to synthesis of 9THC, crude extract was used as the source of CBD; 9THC was isolated from the mixture following the reaction. Two different extract samples were used for this investigation: 1) high quantity CBD extract supplied by Prof. Igor Kovalchuk (from specially cultivated *Cannabis sativa*); and 2) hemp extracts that had undergone extraction and decarboxylation *vide supra*. Unless quantitative NMR (qNMR) was used to determine the exact quantity of CBD or CBD-A within a given sample (see 6.1.7), an estimate of how much BF_3•Et_2O to use had to made. The optimized procedure is described in section 6.2. In all other aspects, this method followed the same procedure as that used with pure CBD. Workup involved washing the organic phase with a saturated $NaHCO_3$ solution to neutralize the acidic solution. During liquid-liquid separation, better separation was achieved when the same saturated $NaHCO_3$ solution was employed as the aqueous phase. Otherwise, the separation of aqueous and organic fractions proved challenging and clear distinction between the aqueous and organic layers was not observed.

5.4 Synthesis of Low Abundant Cannabinoids

Low abundant cannabinoids are often overlooked and difficult to isolate due to their lack of production in cannabis. Therefore, methods for generating them from available cannabinoids were sought.

5.4.1 Synthesis of 8THC

As stated previously stated, 8THC is an isomer of 9THC that forms in very low amounts within *Cannabis sativa*. 8THC forms as a result of alternative isoprene units being introduced in the biosynthetic pathway of 9THC-A, or as part of the degradation routes of 9THC-A and 9THC. With a substantially modified version of a procedure reported by Webster *et al*,[226] a path to 8THC was explored, one that could be conducted using either pure CBD, or more ideally, from an extract containing both CBD-A and CBD.

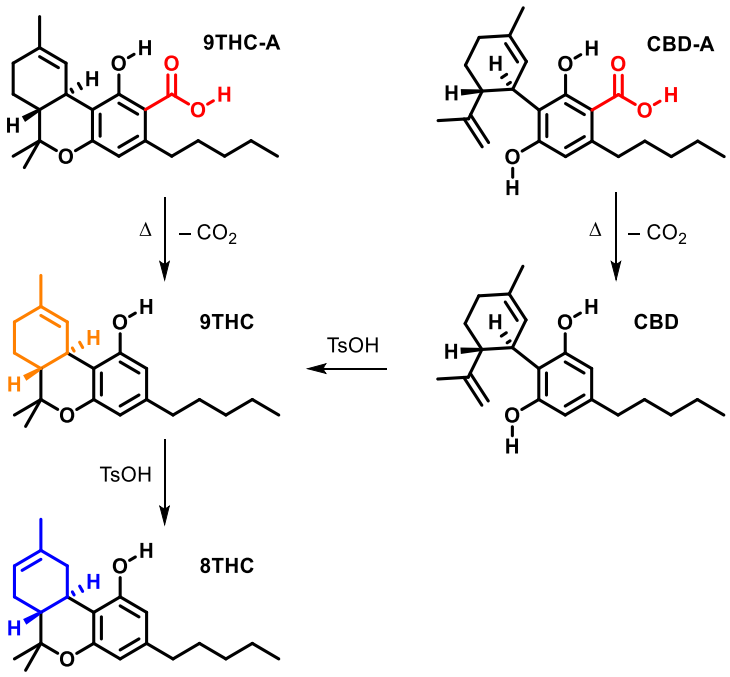

Scheme 5.3: One-pot semisynthesis of 8THC.

With pure CBD, the synthesis of 8THC was a relatively straightforward reaction. A toluene solution of CBD was added to one equivalent of the organic acid *para*-toluene sulfonic acid or tosylic acid (TsOH), after which the mixture was heated to reflux, yielding 8THC. The same reaction can be conducted using samples of extract as a source of CBD and 9THC. Since the reaction was conducted at 110 °C, a one pot process including decarboxylation was attempted. TsOH was added to the toluene

solution of crude extract containing CBD-A and 9THC-A after which decarboxylation occurred in the solution phase. Accordingly, CBD-A and 9THC-A were transformed into CBD and 9THC, respectively. All the CBD was then converted into 9THC under the acidic conditions supplied by TsOH, which in turn promoted isomerization of 9THC into the thermodynamic product 8THC (Scheme 5.3). The entire procedure can be completed in two days (day 1 = extraction, day 2 = 8THC synthesis followed by column chromatography) yielding analytically pure 8THC from *Cannabis sativa* biomass. The exact yield depended on the *Cannabis sativa* sample used and the relative concentration of CBD-A and 9THC-A (80-90%).

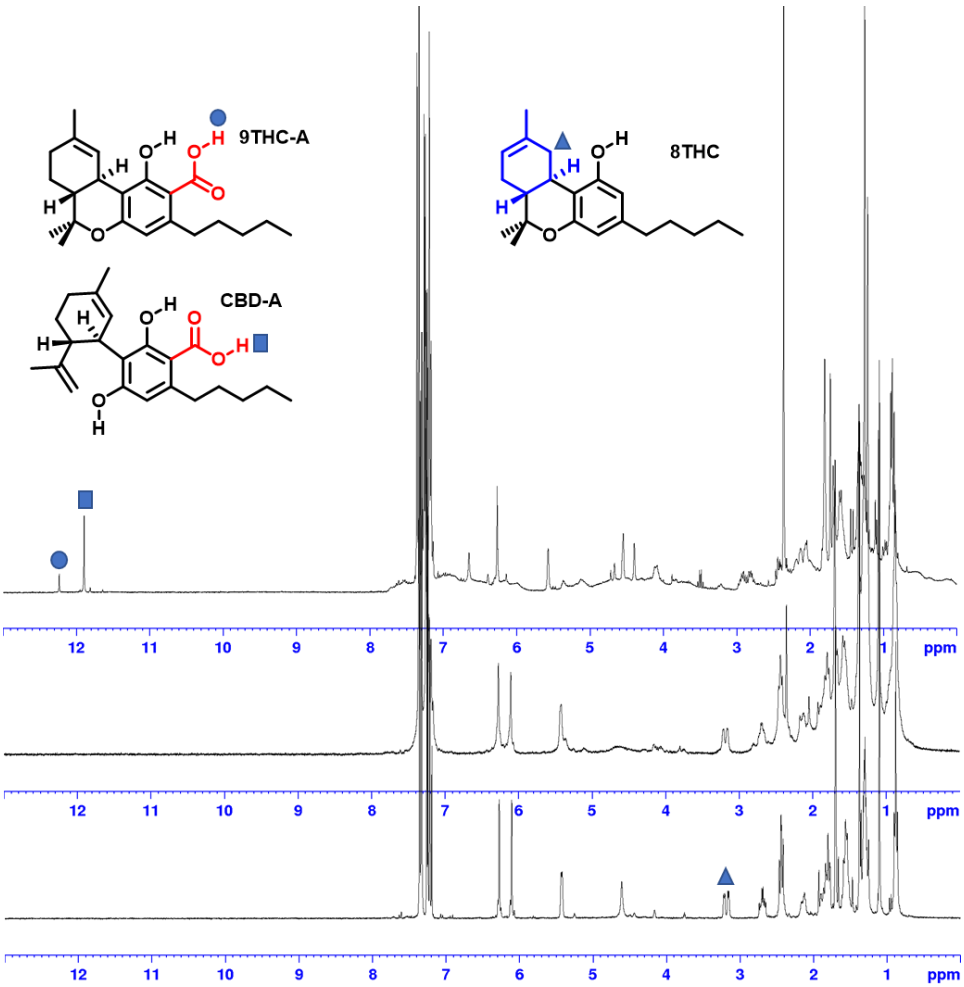

Figure 5.4: Monitoring of 8THC generation *via* ^{1}H NMR spectroscopy in $CDCl_3$. Top: 9THC-A and CBD-A rich extract prior to decarboxylation with notable signals at δ 12.19 and 11.93, respectively. Middle: the same extract after the reaction to give 8THC. Bottom: sample of 8THC following silica chromatography.

5.4.1.1 Computational Investigations

Researchers are comfortable stating 8THC is the thermodynamically favoured THC isomer as it is an experimentally verified fact. However, there is a lack of investigations into why this is the case. To ascertain the reason 8THC is thermodynamically favoured over 9THC, a computational study was conducted at the B3LYP-D3(BJ) level of theory using the 6-31+G(d,p) basis set. Models of both 9THC and 8THC, along with Δ^7-tetrahydrocannabinol (7THC), wherein the alkene is located at carbon position 7 (see Figure 4.7 for cannabinoid numbering), were built to evaluate the impact of the double bond position on the stability of the THC scaffold. To reduce the computational cost and complexity associated with the numerous degrees of freedom, the carbon chain (C1' to C5') was replaced with a methyl group in all models (Figure 5.5; see experimental section for details). Since the solvent (such as DCM, which is typically used for non-enzymatic 9THC synthesis, or toluene, which is used in this study for 8THC synthesis) did not change the predicted stability of 8THC compared to 9THC, calculations were performed in the gas-phase. It was found that 8THC is substantially more stable than both 7THC (by 19.8 kJ mol^{-1}) and 9THC (11.5 kJ mol^{-1}). 7THC was expected to have a higher ground state energy as it contains a secondary alkene, whereas both 8THC and 9THC contain more stable tertiary alkenes.

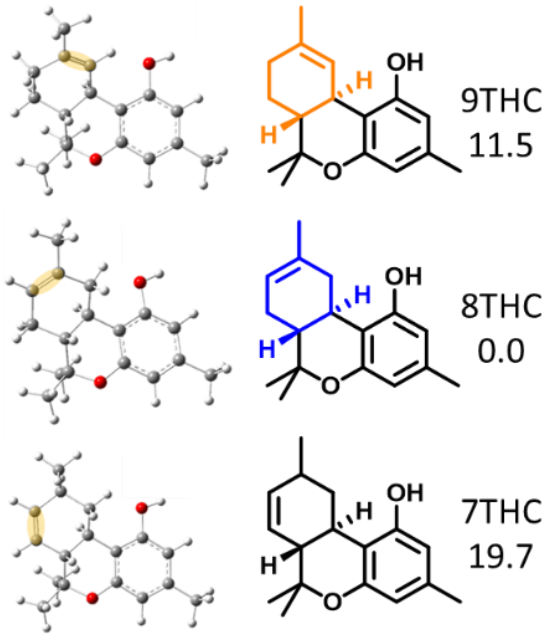

Figure 5.5: DFT optimized structures and relative energies (kJ mol^{-1}) of THC isomers considered in the present work: 8THC (top), 9THC (middle) and 7THC (bottom).

To identify the substituents or structural motifs of these cannabinoids that contribute to the observed energy difference between 8THC and 9THC, several additional models that differed by the presence of various chemical structures were utilized.

In order to determine if the energy difference between 8THC and 9THC is only observed for the naturally occurring *RR* (carbons 6a and 10a) isomers, models for all stereoisomers (*RR*, *SS*, *RS* and *SR*) of 8THC and 9THC were examined (Figure 5.6). As expected, the *SS* isomer had the same calculated ground state energy as its *RR* enantiomer. Meanwhile, the *RS* and *SR* diastereomers of 8THC and 9THC were found to be higher in energy relative to the most stable model, *RR*-8THC by between 6.0 and 29.9 kJ mol^{-1}. Notably, *SR*-9THC proved to be the lowest energy stereoisomer of 9THC. Most importantly, alkene placement at position 8 is preferred in all 4 pairs of stereoisomers (by 1.6 kJ mol^{-1} for SR and 23.9 kJ mol^{-1} for *RS*). In fact, the highest energy 8THC isomers (*SR*-8THC and *RS*-8THC) are 1.6 kJ mol^{-1} lower in energy than

the most stable 9THC isomer (*SR*-9THC). Thus, the greater stability of 8THC is not dependent upon the absolute configuration at either C6a or C10a.

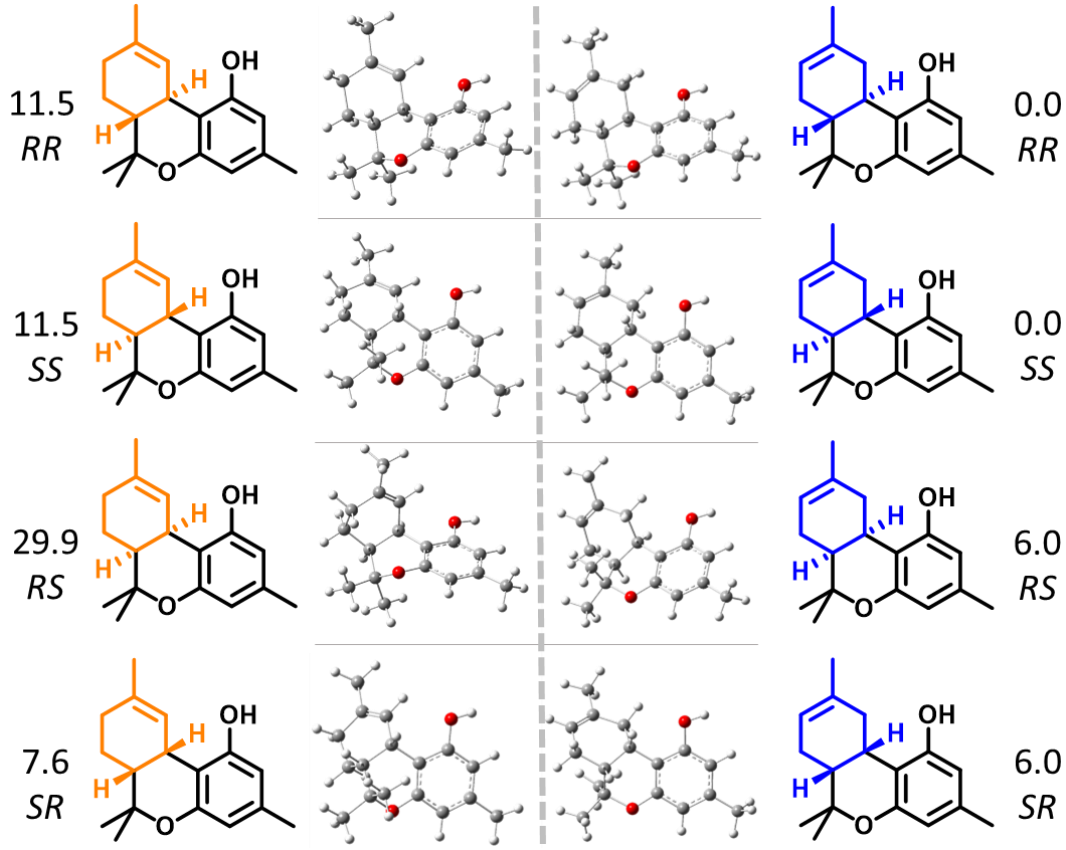

Figure 5.6: DFT structures and relative energies (kJ mol^{-1}) of THC stereoisomers of 9THC (left) and 8THC (right). From top to bottom: *RR*, *SS*, *RS*, and *SR*.

In order to ascertain if certain functional groups or structural motifs within 8THC and 9THC impact stability, or whether the same phenomenon can be observed in simple organic molecules, the relative energies of select parent octahydronaphthalene analogues were evaluated (Figure 5.7). Amongst the simplest related structures (Figure 5.7a), the most stable molecule (by 3.0 kJ mol^{-1}) positions the alkene parallel to the two fused rings (at position 8, akin to 8THC), which provides evidence that there is inherent stability with the alkene in that position. However, this also suggests that other factors and structural motifs contribute to the observed thermodynamic stability of 8THC over 9THC. To further probe the impact of additional functionalities, different

sites on the parent octahydronaphthalene were systematically altered to include features of 8THC and 9THC, including a methyl group at C9 (Figure 5.7b), the ether oxygen between carbons 5 and 6 (Figure 5.7c), the two methyl groups at position 6 (Figure 5.7d), an alkene at the 5 position (Figure 5.7e), and a fused aromatic ring (Figure 5.7f). For models that contained chiral centres, the *RR* isomer, or the stereochemistry that generated the same hydrogen orientations at 6a and 10a to that of 8THC and 9THC, was employed.

In all cases, location of the C=C functionality at C8 led to lower energy structures (by 1.2–11.5 kJ mol^{-1}). While addition of a methyl group at C9 (Figure 5.7b) did not affect the relative ground state energies, inclusion of the ether group (Figure 5.7c) decreased the stability of the structure containing the alkene at C9 by 4.7 kJ mol^{-1}. Placement of two methyl groups at C6 (Figure 5.7d) afforded nearly degenerate isomers (ΔH = 1.2 kJ mol^{-1}). Addition of a second alkene (at C5; Figure 5.7e) resulted in the largest destabilization of the 9THC model, which is 9.8 kJ mol^{-1} higher in energy than its 8THC counterpart. These energies are relatively unperturbed when the full aromatic ring (Figure 5.7f) is included (ΔH = 8.8 kJ mol^{-1}), though addition of OH at C1 and a methyl substituent at C3 (Figure 5.7g) further increases the difference in ground state energies (to 11.5 kJ mol^{-1}) in favour of 8THC. Ultimately, the enhanced unsaturation, and hence, rigidity of the central ring, appears to be the dominant contributing factor responsible for the thermodynamic preference of 8THC over 9THC (Figure 5.7e-g).

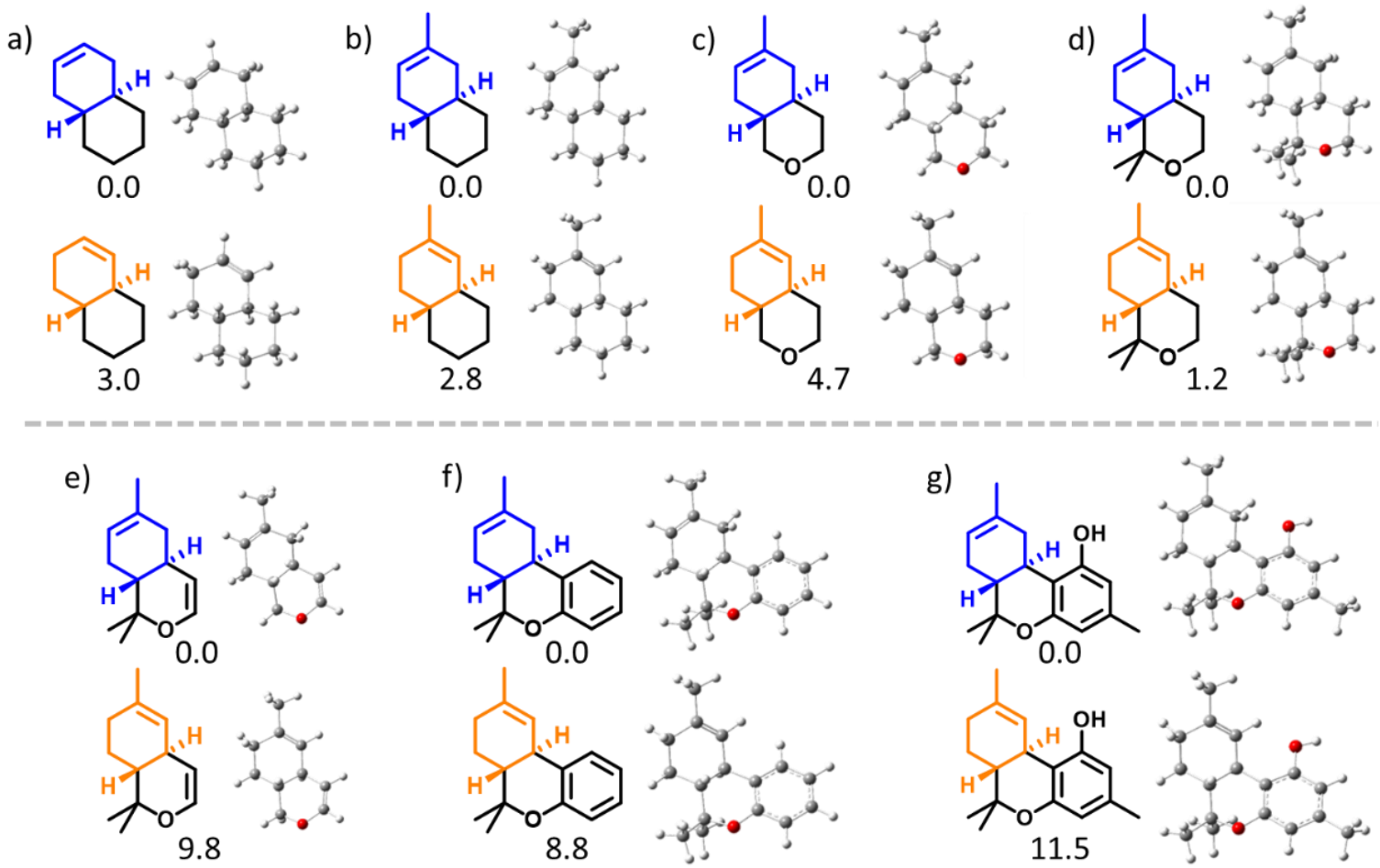

Figure 5.7: DFT structures and relative energies (kJ mol^{-1}) following addition of structural motifs to octahydronaphthalene. Top: alkene placement at position 8. Bottom: alkene placement at position 9 (a) parent octahydronaphthalene, b) methyl at 9 position, c) cyclic ether, d) methyl substituents at 6 position, e) additional alkene at 5 position, f) fused aromatic ring, alcohol at 1 position and methyl at 3 position, g) models used for 8THC and 9THC).

The impact of different substituents at position 9 was considered by replacing the methyl group (Figure 5.8a) with a hydrogen atom (8THC-H, 9THC-H; Figure 5.8b), the electron donating NMe_2, (8THC-NMe_2, 9THC-NMe_2, Figure 5.8c) and the electron withdrawing CF_3 (8THC-CF_3, 9THC-CF_3, Figure 5.8d). Switching to hydrogen did not substantially change the relative stability of 8THC vs. 9THC (<0.5 kJ mol^{-1} difference). However, substitution of methyl by NMe_2 led to a dramatic energy difference that rendered 9THC-NMe_2 28.7 kJ mol^{-1} more destabilized than 8THC-NMe_2. By contrast, CF_3 provided slight stabilization to 9THC, decreasing the relative energy difference by 1.5 kJ mol^{-1} .

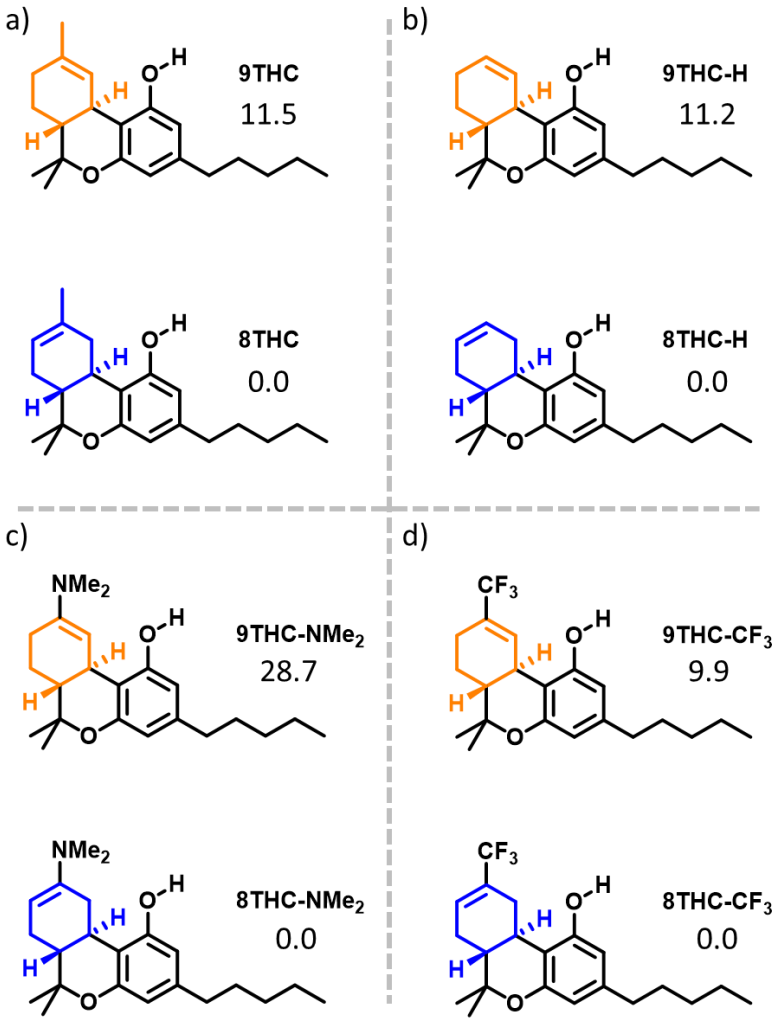

Figure 5.8: Relative energies (kJ mol^{-1}) of substitutions at carbon 9: a) methyl (8THC, 9THC); b) hydrogen (8THC-H, 9THC-H); c) dimethyl amine (8THC-NMe_2, 9THC-NMe_2); and d) trifluoromethyl (8THC-CF_3, 9THC-CF_3).

The straightforward tautomerization of 9THC was expected to proceed *via* initial protonation of C10 to create a transient tertiary carbocation (C9), followed by deprotonation of C8, re-establishing the double bond at the thermodynamically favoured site, and affording 8THC. To confirm this hypothesis, the reaction pathway was modelled using a discrete molecule of TsOH that serves as an H^+ shuttle. The calculations revealed a concerted pathway wherein TsOH simultaneously delivers a proton to C10 and abstracts H^+ from C8 (Figure 5.9). A negative reaction energy barrier of $\Delta_r G$ = –368.4 kJ mol^{-1} was predicted, indicating a thermodynamically accessible forward reaction pathway. This indicates that 9THC can favourably isomerize to 8THC in the presence of TsOH, providing a protic environment at high temperatures, which is consistent with the observed conversion in the extract reaction.

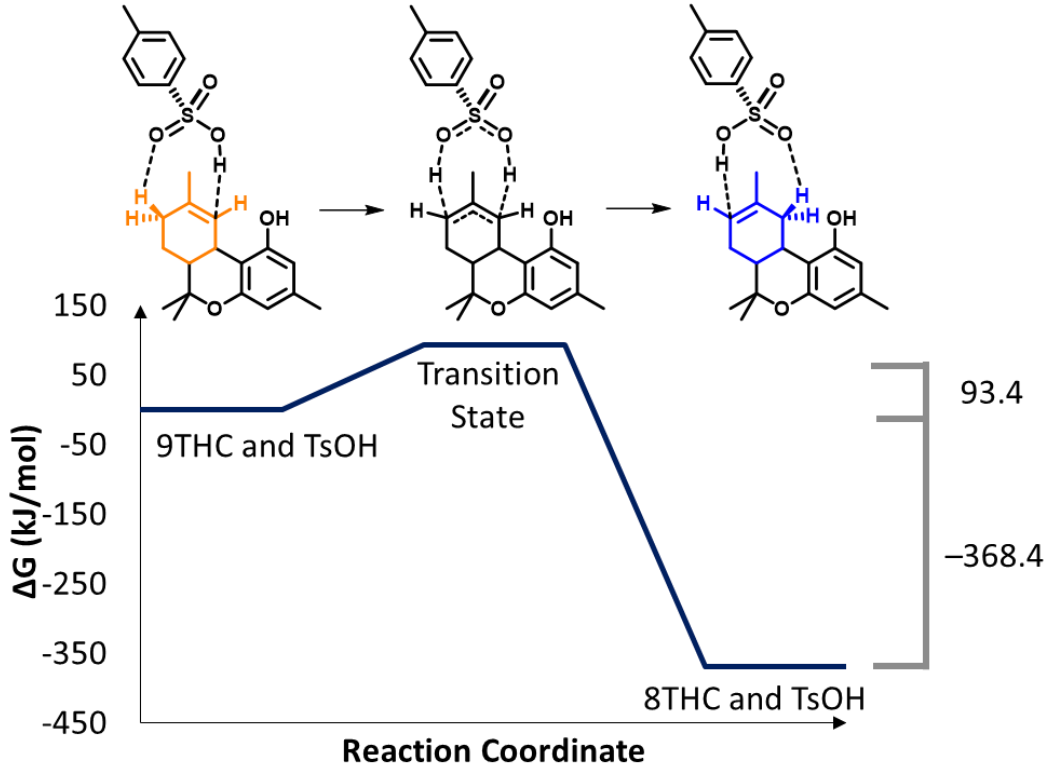

Figure 5.9: Proposed reaction pathway for the isomerization of 9THC to 8THC, in the presence of *p*-TsOH. Selected bonds (Å): a) C8–H 1.099, O···H 2.824, O–H 0.987, H···C10 2.264 b) C8···H 1.125, O···H 2.024, O···H 1.769, H···C10 1.161; c) C8···H 2.181, O–H 0.991, O···H 2.889, C10–H 1.099.

It has been demonstrated that 8THC can be quickly synthesized and isolated from cannabis extract, irrespective of CBD-A and/or 9THC-A content. The flexibility of its semisynthesis will hopefully encourage further biological testing, research, and industrial scale production from any CBD-A or 9THC-A containing crop. Although it was previously known that 8THC is thermodynamically favoured over 9THC, density functional theory (DFT) calculations provided insight into the structural motifs that contribute to its greater stability.

5.4.2 Synthesis of CBN

Applying the same approach as the one-pot synthesis used to access 8THC, a route to CBN, similar to the procedure described by Appendino *et al.*,[331] was developed. Generation of CBN, a product of 9THC degradation, occurs over time. This decomposition can be sped up with heat or UV exposure, but this is often unreliable and time consuming. Elemental iodine can promote aromatization, turning 9THC into CBN, giving iodic acid (IH) as a by-product, which in turn affords an acidic environment that promotes ring closure of CBD, generating 9THC. This feedback loop allows all available cannabinoids to eventually be converted into CBN. With the addition of elemental iodine to the decarboxylation protocol, CBN can be readily generated from a toluene solution of extract (Scheme 5.4).[227] Analytically pure samples of CBN were isolated from the extract with a single chromatography step.

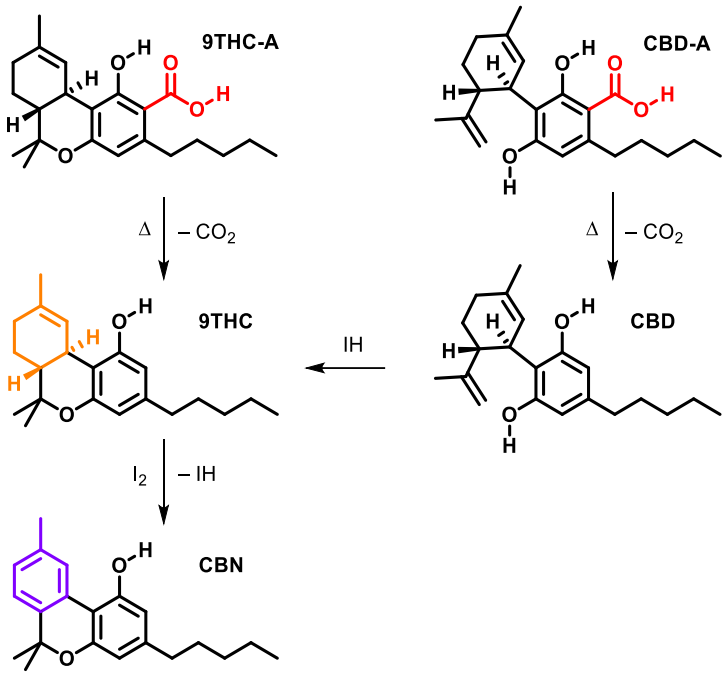

Scheme 5.4: One-pot semisynthesis of CBN.

5.4.3 Synthesis of 10THC and 10aTHC

The little-known isomer of 9THC, 10THC, first reported by Mechoulam *et al.*,[204] was generated by addition of *n*-butyl lithium (^{n}BuLi) to a solution of isolated 9THC in hexamethylphosphoramide (HMPA). The solvent, HMPA, was required to promote the separation of ^{n}BuLi oligomers in solution which increases its selectivity. Other solvents were found to be inadequate for this transformation. Deprotonation at the ring fusion, carbon 10a, followed by alkene isomerization during workup, afforded crude 10THC, from which analytically pure product can be isolated after either column chromatography or by recrystallization from hexane (at temperatures below 0 °C) to yield X-ray quality crystals (Figure 5.10). To exclusively generate 10THC, the source of 9THC had to be pure, and thus it was not feasible to conduct this procedure using an extract sample. As a consequence, and unlike that demonstrated for 8THC and CBN, this procedure cannot be considered a semisynthesis.

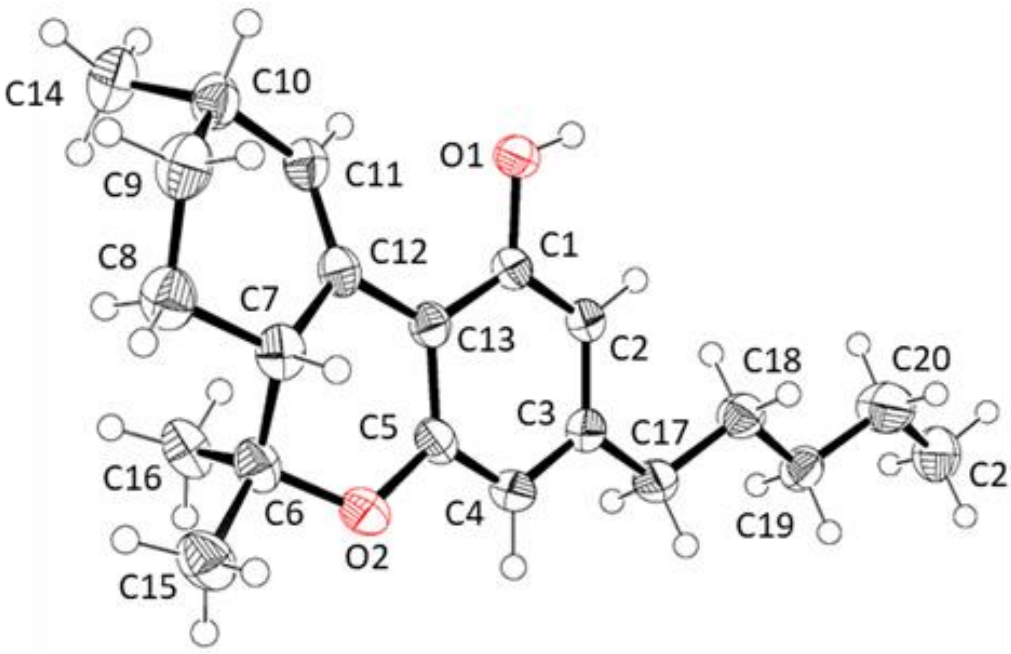

Figure 5.10: X-ray crystal structure of 10THC. Displacement ellipsoids are drawn at 50% probability. Hydrogen atoms are shown at calculated positions. Selected bond distances (Å) and angles (°): C7–C12 1.513(2), C7–C8 1.536(3), C11–C12 1.342(3), C7–C12–C11 122.17(16), C12–C11–C10 124.77(17), C11–C10–C9 110.46(17), C10–C9–C8 111.50(17), C9–C8–C7 111.73(17), C8–C7–C12 112.36(15).

In the first report of 10THC, it was proposed that its kinetic isomer contains *R* configuration at carbon 6a and *S* at carbon 9 due to the pseudo-axial geometry of the ring. Despite exhaustive efforts, all attempts to isolate the thermodynamic isomer, (*R*,*R*)-Δ^{10}-tetrahydrocannabinol, by the procedure outlined by Mechoulam *et al*. were unsuccessful. In order to confirm the stereochemistry, X-ray quality white needles of 10THC were grown from a concentrated hexanes solution stored at –20 °C. The diffraction data produced a Flack parameter of –0.06(5). This value indicated that there were only reflections associated with one enantiomer of 10THC (the other would give a value of 1), thereby verifying the absolute configuration, and confirming the synthesized 10THC sample contained the chiral centres, *S*C6a and *R*C10a (C7 and C10, respectively in Figure 5.10).

The NMR spectra acquired from samples of 10THC in $CDCl_3$, despite being sourced from crystalline material, did not indicate analytically purity. Upon further

investigation, it became apparent that over time a separate compound prevailed. The NMR spectra obtained were not consistent with 10THC; for example, no ^{1}H resonances could be attributed to the alkene proton H10. Furthermore, APT and DEPT experiments revealed two less CH resonances than expected, one more CH_2, and one more quaternary carbon than anticipated in the ^{13}C NMR spectra. Conversely, when crystals of 10THC were analysed in benzene-d_6, the data were consistent with pure 10THC. Evidently, an acid catalysed tautomerization occurs, even in chloroform, converting 10THC into 10aTHC (Scheme 5.5). Both 10THC and 10aTHC cannabinoids were comprehensively characterized in solution *via* multinuclear NMR spectroscopy.

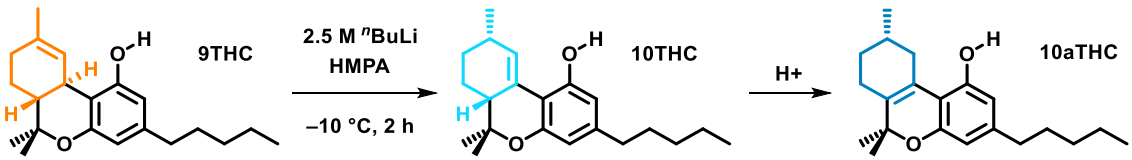

Scheme 5.5: Synthesis of 10THC and 10aTHC from 9THC.

5.4.4 Synthesis of CBND

The cannabinoid CBND was prepared by a modified literature procedure from CBN.[330] Although there are reports of CBND being synthesized,[337] they employed a total synthesis approach, rather than the desired semisynthesis route from readily available CBN. A solution of CBN in ethanol, as outlined in the initial publication describing CBND,[330] was subjected to UV irradiation, and reaction progress was followed by monitoring diagnostic CBN and CBND ^{1}H NMR resonances at δ 8.55 and 6.54 ppm, respectively, in benzene-d_6. Notably, this reaction must be conducted in a quartz reaction vessel, as the wavelength of light required to promote ring-opening is likely to be absorbed by standard borosilicate glass. A variety of optimization experiments indicated that yield and purity are greatly improved when cyclohexane

(CyH) is used as a solvent (Figure 5.11). In addition, quiescent solutions require dramatically longer reaction times (96 h, compared to 12 h) to proceed to completion.

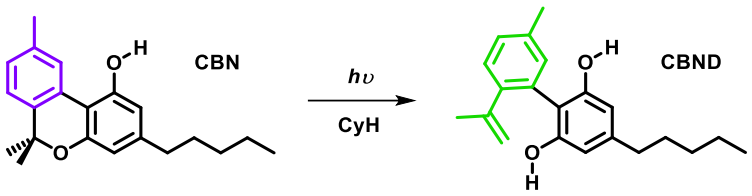

Figure 5.11: Synthesis of CBND from CBN.

Although the initial report on CBND did not include NMR characterization, a more recent article which detailed a total synthesis of CBND, provided complete, but unassigned, ^{1}H and ^{13}C NMR data.[337] Multinuclear 1D and 2D experiments afforded high quality NMR data that was readily ascribed to the relevant atoms; the resonances closely matched the unassigned signals in the literature. Surprisingly, CBND was found to be robust at elevated temperatures (70 °C) in C_6D_6, with only minor quantities of CBN and side-products observed.

5.4.5 Synthesis of Silylated Cannabinoids

To derivatize the hydroxyl group of the cannabinoid structure, addition of a silyl ether was considered as it would eliminate hydrogen bonding and permit assessment of such interactions on chemotherapeutic activity. Silyl ethers of cannabinoids, which do not occur naturally, are known,[338, 339] but much like the low abundant cannabinoids, have not been extensively studied. The most obvious route to a silyl ether from a hydroxy group is to generate an alkali metal salt of the hydroxyl group, followed by addition of a silyl chloride electrophile. Initially potassium hydride was used, but that required the reaction to be conducted in THF, resulting in a solvated salt. The potassium salt [K][HMDS] proved to be a more ideal reagent, as the salt was soluble in hydrocarbon solvents and the amine by-product was easily and safely removed *in vacuo*

to yield the potassium salts of CBN and 8THC as off-white solids. Presence of a protic environment, *e.g.* water, resulted in regeneration of the cannabinoid and a white solid, assumed to be potassium hydroxide. Therefore, these reactions were conducted under an inert atmosphere. The simple compound trimethylsilyl chloride (Cl–$SiMe_3$) was used as the silyl source for these reactions, affording the desired silyl ethers, 1-$OSiMe_3$-cannabinol (Si-CBN) and 1-$OSiMe_3$-Δ^8-tetrahydrocannabinol (Si-8THC), instantaneously, along with concomitant production of a white solid, presumed to be potassium chloride. After work-up, the silylated cannabinoids were isolated as analytically pure oils with diagnostic methyl signals in their respective ^{1}H NMR spectra at δ 0.20 and 0.24, both integrating as 9H.

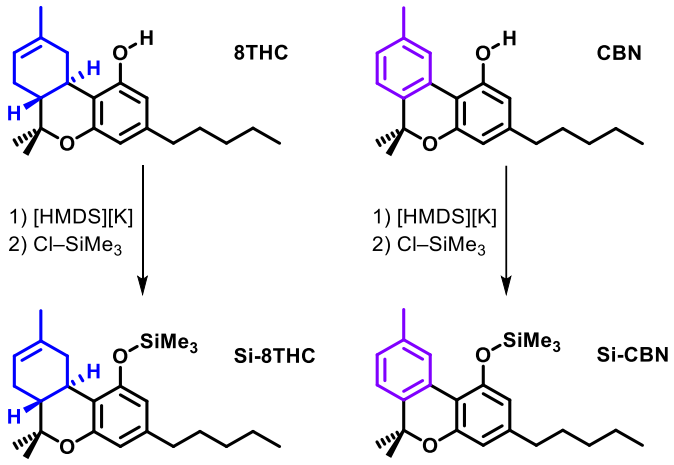

Scheme 5.6: Synthesis of silylated cannabinoids Si-8THC and Si-CBN.

5.5 *ortho*-Quinone Derivatives of Cannabinoids

The synthesis of *ortho*-quinone substituted cannabinoids from phenols, as described by Pettus and co-workers,[274] and explored recently by Kaur and Ariafard,[340] was undertaken by adding IBX in small portions over a period of 10 minutes to a solution of the relevant cannabinoid in DMF. The pale-yellow solutions slowly became dark-red over the course of 30 minutes. The resultant oils were subsequently purified by flash column chromatography to afford analytically pure samples of *ortho*-quinones:

*o*q-9THC, *o*-q8THC, and *o*-qCBN (Scheme 5.7). It was postulated that IBX, or some intermediate during the transformation, is stabilized in DMF. If the mechanism proposed by Taglialatela-Scafati and co-workers was correct, oxidation of the iodane species, which is responsible for formation of the *para*-quinone, is inhibited when DMF is employed.[272] In this work, the presence of 2-iodobenzoic acid in unpurified mixtures suggested that the mechanism proposed by Pettus and co-workers is likely operative.

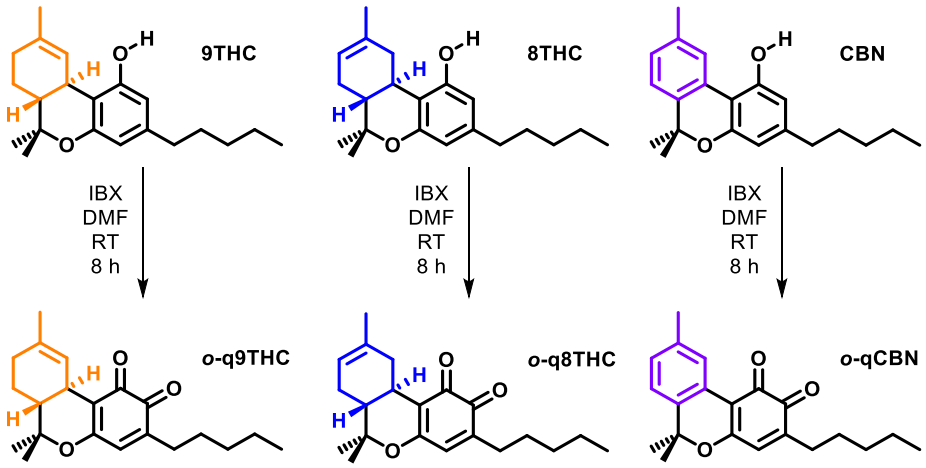

Scheme 5.7: Synthesis of *ortho*-quinone derivatives of 9THC, 8THC, and CBN.

To confirm exclusive formation of the desired *ortho* isomers, the ^{1}H and ^{13}C{^{1}H} NMR spectra of *o*-q8THC were carefully compared to the known *para* derivative (*p*-q8THC).[341] The ^{13}C{H} spectra proved to be the most useful for distinguishing between the two compounds (Figure 5.12). Specifically, carbons 1 through 4 provide diagnostic resonances with the quinone carbons in the *para* isomer shifted substantially downfield compared to *o*-q8THC (*p*-q8THC: δ 187.63 and 182.62; *o*-q8THC: 181.12 and 177.57). Previous publications on *p*-q9THC do not include ^{13}C NMR data, but do report ^{1}H spectra,[273] which notably, differ from that obtained for our synthesized *o*-q9THC. Hence, it is reasonable to assume that the described route with IBX provided exclusively *o*-q8THC and *o*-q9THC. Notably, little ambiguity exists for the ^{1}H NMR data of *p*-qCBN reported by Mechoulam as their assignment was supported by an

X-ray crystal structure.[341] As such, their ^{13}C spectra were reliable comparisons to confirm our *o*-qCBN assignments as they differed in the same ways that *o*-q8THC differed from *p*-q8THC.

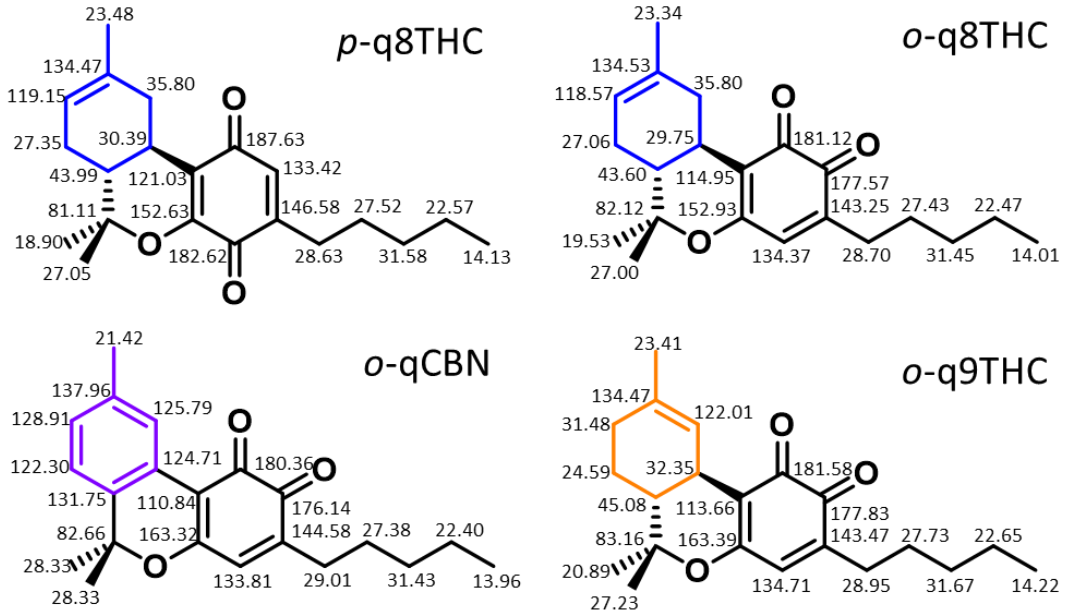

Figure 5.12: Assignment of ^{13}C NMR spectra for of *para*-quinone q8THC analogue,[341] *o*-q8THC, *o*-q9THC, and *o*-qCBN.

Taglialatela-Scafati, along with Appendino, have recently amended their previous work on *para*-quinones.[342] Specifically, they confirmed that the *ortho*-quinones were exclusively generated from the use of hypervalent iodine compounds, such as IBX. Their rationale was that the short lived λ^5-iodane intermediate restricts rearrangement so that only an *ortho*-quinone is generated. When using a hypervalent iodine that produces a sterically crowded λ^3-iodane intermediate, such as when using (bis(trifluoroacetoxy)iodo)benzene (PIFA), the *para*-quinone is generated. This supported the mechanism by Pettus and co-workers[274] as we had originally postulated. It is unfortunate that their work comes during this investigation, and it ultimately negates some of the synthesis described herein, despite our more rigorous characterizations of the *ortho*-quinones. It is important to properly characterize new

compounds to eliminate any ambiguity of assignments for future researchers. Until now the quinones of cannabinoids have been documented to an unsatisfactory level and misassignments were common.

While *o*-qCBN and *o*-q8THC are stable at elevated temperatures, and upon limited exposure to UV light, enabling storage for months without significant degradation, *o*-q9THC decomposes into a green intractable mixture within 24 h at ambient conditions. Hence, for further testing, only the former two cannabinoids were considered.

5.5.1 Voltammetry Experiments

A correlation has been found between redox potentials and cytotoxicity in quinone chemotherapeutic candidates,[343, 344] as they are known to be oxidizers, usually in two sequential one-electron steps. It was therefore of interest to explore the possibility that the reduction potentials of *o*-q8THC and *o*-qCBN could be related to their cancer cell growth inhibition efficacy (*vide infra* 5.8.4*)*. The solution electrochemistry of the two stable quinones has been investigated in preliminary fashion using the organic aprotic medium DMF at macrodisc working electrodes in order to determine the ease of electrochemical reduction independent of the strong pH dependence and coupled chemical reactions that induce a single two-electron redox process in water.[345] Cyclic voltammograms for *o*-q8THC at two scan rates are presented in Figure 5.13, and for *o*-qCBN in Figure 5.14; (for other examples of cyclic (CV) and square-wave voltammograms (SWV) see 6.1.9). The CVs show a strong dependence on reversal potentials and a weaker dependence on the scan rates (50–5000 mV/s). In addition to the expected first and second quinone reductions (labelled I and II), additional off-set anodic peaks corresponding to the observed induced process III are noted. Similar

complexity has been previously observed for 3,5-di-tertbutyl-1,2-benzoquinone and 3,6-di-tert-butyl-1,2-benzoquinone.[346-348] Process III is attributed to the irreversible oxidation of the hydroquinone anion QH^- produced by reaction of Q^{2-} with traces of water in the nominally dry solvent.

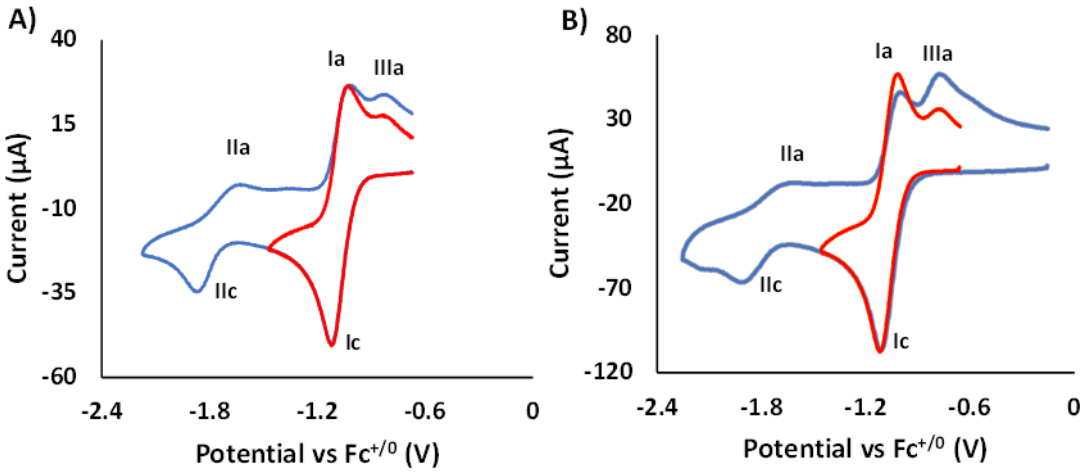

Figure 5.13: Overlays of CVs of *o*q-8THC, 5.48 mM analyte in DMF/0.4 M $[Bu_4N][PF_6]$ at a Pt macrodisc WE. Scan rates: A) 200 mV/s; B) 1000 mV/s, with differing switching potentials.

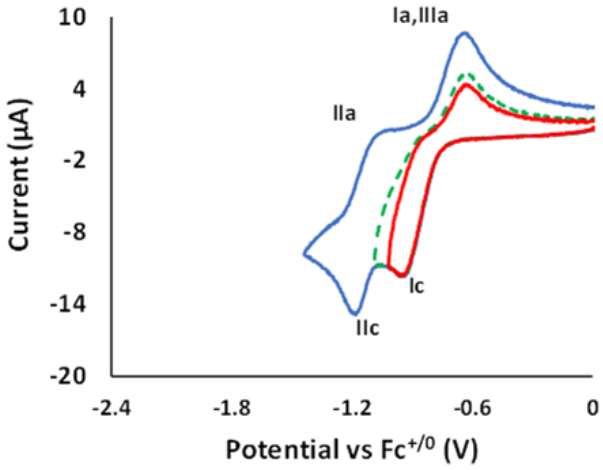

Figure 5.14: Overlay of cyclic voltammograms of *o*q-CBN, 5.53 mM analyte in DMF/0.4 M $[Bu_4N][PF_6]$ at a Pt macrodisc WE. Various switching potentials: scan rate of 50 mM/s.

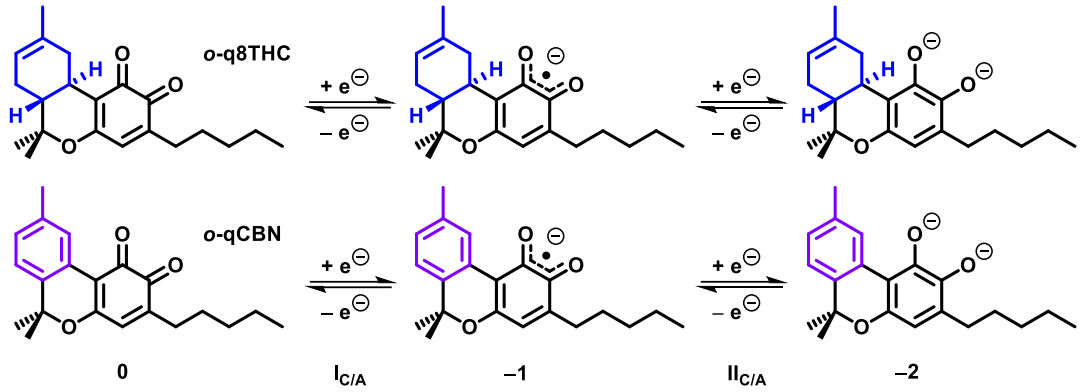

Scheme 5.8: The two-step reduction of *o*-q8THC and *o*-qCBN with labels related the description of their charge in the text and the numbered cathodic or anodic process depicted on the cyclic voltammograms.

Table 5.1: Voltammetric data for o-q8THC and o-qCBN (potentials w.r.t. to Fc+/0 at 0.0V). From CV experiments in DMF/0.4M [nBu4N][PF6], taken on a 3 mm Pt macrodisc electrode. ‡Approximate value. § E_p^{aI} and E_p^{aIII} merged into one broad peak in CV, but distinguishable in SWV.

Compound	Scan rate ($V \cdot s^{-1}$)	E_p^{cI} (V)	E_p^{aI} (V)	$\sim E_m^{I}$ (V)	E_p^{cII} (V)	E_p^{aII} (V)	$\sim E_m^{II}$, (V)	E_p^{aIII} (V)
***o*-q8THC**	0.050	−1.117	−1.023	−1.07	−1.799	−1.603	−1.76	−0.850
	0.500	−1.130	−1.024	−1.08	−1.872	−1.675 ‡	−1.82	−0.814
***o*-qCBN**	0.050	−0.943	−0.624 §	−0.90	−1.179	−1.022 ‡	−1.14	−0.624 §
	0.500	−0.966	−0.587 §	−0.91	−1.218	−1.043 ‡	−1.17	−0.587 §

The 0/−1 redox couple of *o*-q8THC (E_p^{cI} = −1.117 V) was found to be formally electrochemically irreversible, but otherwise well-defined with an I_c/I_a ratio of 0.85 (Scheme 5.8, Table 5.1). The −1/−2 redox couple (E_p^{cII} = −1.799 V) displays a greatly reduced peak potential and is chemically irreversible. For *o*-qCBN, the 0/−1 redox couple (E_p^{cI} = −0.943 V) is irreversible, as is the −1/−2 redox couple (E_p^{cII} = −1.179 V). Potentials listed are for 50 mV/s scan rates and are on the $Fc^{+/0}$ scale (Table 5.1). The reductions of *o*-qCBN are much more closely spaced than *o*-q8THC, with a peak-to-peak difference of 220 mV in *o*-qCBN versus a more typical value for quinones of 740 mV in *o*-q8THC.

The CVs recorded for *o*-q8THC were strongly reminiscent of those reported for 3,5-di-tertbutyl-1,2-benzoquinone and 3,6-di-tert-butyl-1,2-benzoquinone as reported recently by René and Evans.[348] Particularly noteworthy is the anomalously low peak current for the second reduction step compared to the expectation of 'classical' CVs of quinones. This anomalously low current for IIc was confirmed in the square wave voltammogram (SWV) (Figure 5.15). Furthermore, under the measurement conditions scanning from positive to negative, does not involve the potential for process III. This confirms the relationship of III to II, whereas if III were associated with I, it would be intercepted by this large amplitude differential technique.

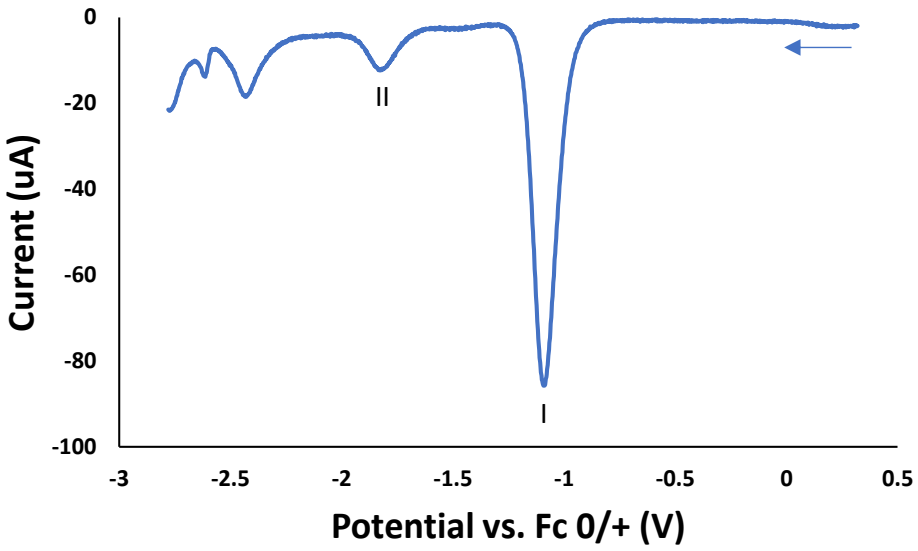

Figure 5.15: Square wave voltammogram (SWV) of *o*-q8THC in DMF containing $[Bu_4N][PF_6]$ at a Pt macrodisc electrode, scanned from the positive limit to the negative.

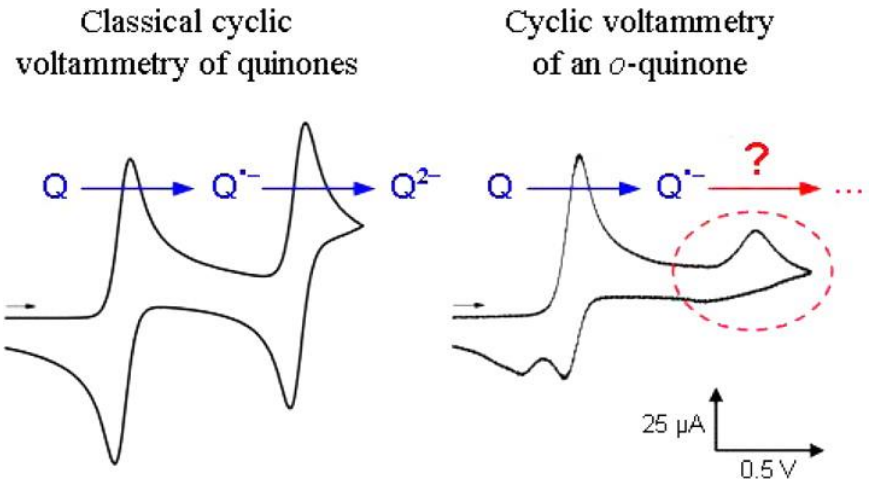

Figure 5.16: Schematic CVs representative of classical quinones and *ortho*-quinones with bulky substituents. (drawn in the American convention. Reprinted with permission from *J. Phys. Chem. C*. 2012, *116*, 14454–14460.[348] Copyright 2021 American chemical Society).

The quinone, 3,5-di-tertbutyl-1,2-benzoquinone, has been the subject of numerous investigations and reports, in part due to the importance of the precursor 3,5-ditertbutylphenol as an antioxidant, but mostly because of the surprisingly unusual appearance of its CVs, especially those undertaken in nominally dry, aprotic organic solvents.[346, 347] There is an extreme similarity to the CV trace shown of the *ortho*-quinone in Figure 5.16 (when rotated by 180°) with those for *o*-q8THC shown at various scan rates. Several possible mechanisms have been considered and debated for the unexpected behaviour in CV of such *ortho*-quinones, and it seems reasonable that such mechanisms are likely also to be operative for *o*-q8THC and *o*-qCBN. The expected classical voltammetry for two, reversible, electrochemical steps is below.

$$\text{E(I):} \qquad Q + e^- \rightleftharpoons Q^{\bullet -}$$

$$\text{E(II):} \qquad Q^{\bullet -} + e^- \rightleftharpoons Q^{2-}$$

However, in nominally dry aprotic solvents, which almost always contain some residual water, the mechanism can be modified to incorporate two chemical steps.

E(I): $Q + e^- \rightleftharpoons Q^{\bullet -}$

C(1): $Q^{\bullet -} + H_2O \rightleftharpoons Q^{\bullet -} \bullet H_2O$

E(II'): $Q^{\bullet -} \bullet H_2O + e^- \rightleftharpoons Q^{2-} \bullet H_2O$

C(2): $Q^{2-} \bullet H_2O + e^- \rightleftharpoons QH^- + OH^-$

In step C(1), the quinone radical anion complexes to water, and this has the significant thermodynamic consequence that the now-modified second reduction tends towards significantly less negative potentials. At the same time, the presence of small amounts of water in the voltammetric medium result in a distinct increase in current for the now modified second reduction. Thus, as René and Evans concluded, water is the origin of redox process III (oxidation of QH^-). In view of the extreme similarity of the CVs reported in aprotic solvents[346, 347] and the structural similarity of the *ortho*-quinones and similar redox potentials in DMF and CH_3CN, it seems reasonable to postulate that very similar mechanisms operate for the two compounds.

The SWV for *o*-qCBN (Figure 5.17) clearly shows three processes. Noteworthy in this is the clear identification of redox process II with a large intensity, comparable to that of I, and quite unlike what is observed in the SWV of *o*-q8THC. This mechanism would merge smoothly with the classical voltammetry of quinones in buffered aqueous solutions.[349-351] It is clear that some form of follow-up chemical reactions operate after E(I) in *o*-qCBN, and that these prevent the Michael-type addition reactions that lower the peak current for E(II), resulting in the two reductions to occur with a small voltage difference. Whereas the III process for *o*-q8THC is a consequence of reactivity

following E(II), and hence the voltage difference to be much higher between the two standard reductions.

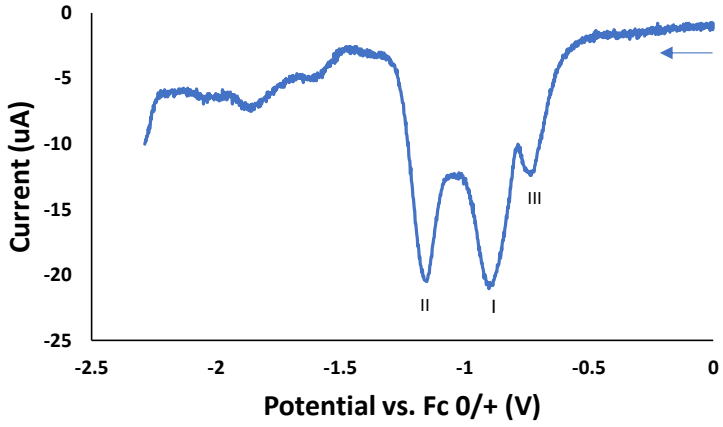

Figure 5.17: Square wave voltammogram of *o*-qCBN in DMF containing $[Bu_4N][PF_6]$ at a Pt macrodisc electrode, scanned from the positive limit to the negative.

5.5.2 Computational Analysis

A computational study of *o*-qCBN and *o*-q8THC was undertaken with full geometry optimization at the B3LYP-D3BJ/6-311+G(d,p) level of theory without solvation for the series of charge states 0, –1, and –2, but in these models the *n*-pentyl chains were truncated to methyl groups to avoid convergence issues in the doublet and triplet states. DFT calculations were conducted on models that had geometry optimization in a PCM solvent model for *N*,*N*-dimethylformamide (ε = 37.219). For the neutral species, full optimization with a PCM solvent model for *N*,*N*-dimethylformamide (ε = 37.219) was employed to ensure accuracy in the calculation of the LUMO energies. The geometries optimized with zero imaginary frequencies, indicating these are at least local minima on the potential energy surfaces. Topologically, the respective lowest unoccupied molecular orbitals of the two molecules are almost indistinguishable (Figure 5.18).

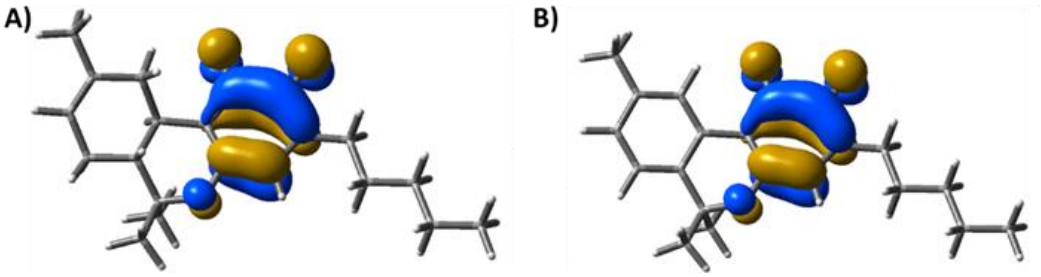

Figure 5.18: Kohn-Shahm orbital surface plots for the LUMOs of A) *o*q-8THC and B) *o*q-8CBN from DFT calculations at the B3LYP-D3BJ/6311+G(d,p) level of theory using a PCM model for DMF.

The computed orbital energies indicate that the *o*-q8THC LUMO lies 0.126 eV higher than that of *o*-qCBN, in excellent agreement with the experimental difference in the $E_p^{c\mathrm{I}}$ potentials whereby *o*-q8THC is ~0.17 V more difficult to reduce than *o*-qCBN. Further calculations indicate that there should be no intrinsic difference in the electronic structures of the 0, –1, or –2 charge states of these two quinones, so that the highly divergent voltammograms are likely to be caused by different follow-up chemical reactions. All calculations were undertaken with the program Gaussian W16 on a 12-core/16 GB personal computer and visualized using GaussView 6.0.16.

DFT calculations are only slightly affected by solvation for the neutral models of *o*-qCBN and *o*-q8THC, and hence, solvation was ignored for a follow up study of the series of ions 0, –1, or –2 charge states. The theoretical redox behavior of the two compounds was further investigated on a series of models in which the *n*-pentyl chains were truncated to methyl groups attached to the quinone rings and without a solvent model, in order to save on computational time associated with slow convergence of the pentyl chains. The redox molecular orbitals (RMO) of the *o*-q8THC and *o*-qCBN molecules are virtually indistinguishable at this level of theory. The only difference of note is that the dianion of *o*-qCBN is more stable as a triplet whereas *o*-q8THC is more stable in a singlet electronic configuration. Moreover, there is no effect of truncating the long alkyl chain to a methyl group as these RMOs do not have any coefficients

including these chains. The RMOs are highly concentrated on the *ortho*-quinone ring and extend significantly only out to the O atoms of the fused oxanes (Figure 5.19).

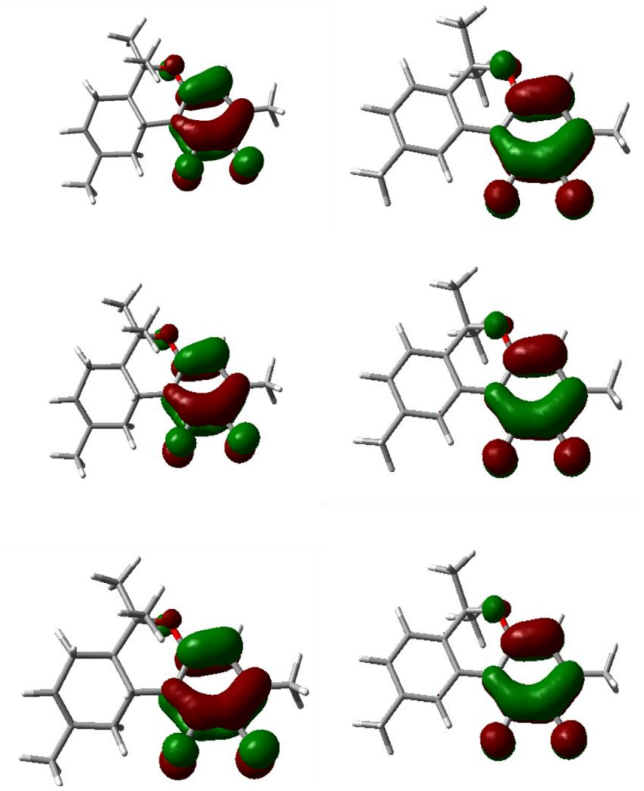

Figure 5.19: Redox molecular orbitals of *o*-q8THC (left) and *o*-qCBN (right). Top) neutral truncated LUMO; middle) anion truncated SOMO; bottom) dianion truncated HOMO.

Thus, the DFT calculations are fully consistent with the expectation that such *ortho*-quinones undergo two separate and reversible one-electron reductions, *i.e.* 'classical' quinone voltammetry in aprotic organic solvents. From an examination of RMO energies, it is noteworthy that the difference in energy between the RMOs increased from neutral to anionic to dianionic, and that in each case *o*-q8THC is computed to be the more difficult to reduce. In this regard, the more facile second experimental reduction of *o*-qCBN vs. *o*-q8THC is consistent with the calculated trends. However, the observed experimental values are probably too different to be directly explained by these theoretical considerations. Almost certainly, the large

difference in ease of the second reduction seen experimentally must be sought in mechanistic considerations and a large relative difference in reaction kinetics.

Comparison of CVs of *o*-qCBN with those of *o*-q8THC showed a dramatic difference when all experimental variables were kept constant. The peak potentials for the first reduction process $E_p^{c\mathrm{I}}$ of −0.943 V for *o*-qCBN versus −1.117 V for *o*-q8THC (50 mV/s scan rate) are readily interpretable by the slight difference in electronic structures computed by DFT methods. The former is thus about 0.17 V easier to reduce, reflecting the change from an alkyl substituent at carbon 10b in *o*-q8THC to the biphenyl architecture in *o*-qCBN. However, as the full report of the DFT study on quinone, radical anion, and dianion demonstrates, there is nothing in the electronic structure of these two quinones that explains the significant difference in the CVs beyond the first reduction.

5.6 Fluorination of CBN and 8THC

Several reactions were attempted for introducing a fluorine into the cannabinoid framework. Initially, replacement of the hydroxyl group at carbon 1 was undertaken with PhenoFluor™, a compound developed by renowned organofluorine chemist, Dr. Tobias Ritter.[352-354] The reagent was chosen to maximize step economy, as the fluorinated compound would be generated from the parent cannabinoid in a single step. PhenoFluor™ was synthesized by reported literature methods and added to either CBN or 8THC.[355] Despite exhaustive efforts and systematic fine-tuning of solvent, temperature, and time, no reaction occurred. Interestingly, related fluorinated versions of 9THC and 8THC were reported by Tobias Ritter in a patent.[280] In those examples, however, a more labile hydroxyl group had to be created, a process that greatly diminishes their practical value.

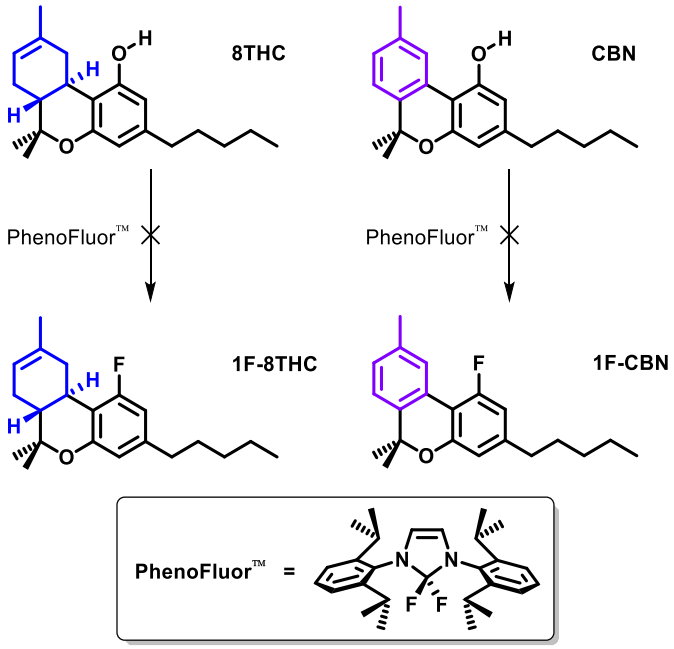

Scheme 5.9: Attempted synthesis of fluorinated 8THC and CBN using PhenoFluor™.

The second venture to fluorinate cannabinoids employed the tungsten catalyst, tetra-*n*-butylammonium decatungstate (TBDT) described by Dr. Robert Britton as capable of replacing labile benzylic C–H bonds with C–F.[290] Following literature reports, TBDT was synthesized.[356] The introduction of fluorine occurs by a radical process. The fluorine atom is provided by *N*-fluorobenzenesulfonimide (NFSI), the reaction is conducted in acetonitrile and proceeds in the presence of UV light ($\lambda = 365$ nm) which is essential for activating the catalyst. The catalyst abstracts a labile hydrogen *via* heterolytic bond cleavage, generating the necessary carbon based radical, which in turn abstracts a fluorine atom. For this reaction, NFSI possesses a labile N–F bond. The reaction was monitored by ^{19}F NMR spectroscopy. Promising results were only observed when CBN was tested. When 8THC was used a myriad of products formed. A TLC analysis concluded that separation of the closely related species would be nigh impossible. When using CBN, predominantly two products formed, but despite exhaustive efforts, they could not be separated. The two major ^{19}F NMR signals are attributed to the two possible products resulting from activation of the benzyl C–H

bonds at carbons 1’ and 11 but the exact identity of the compounds could not be confirmed (Figure 5.20).

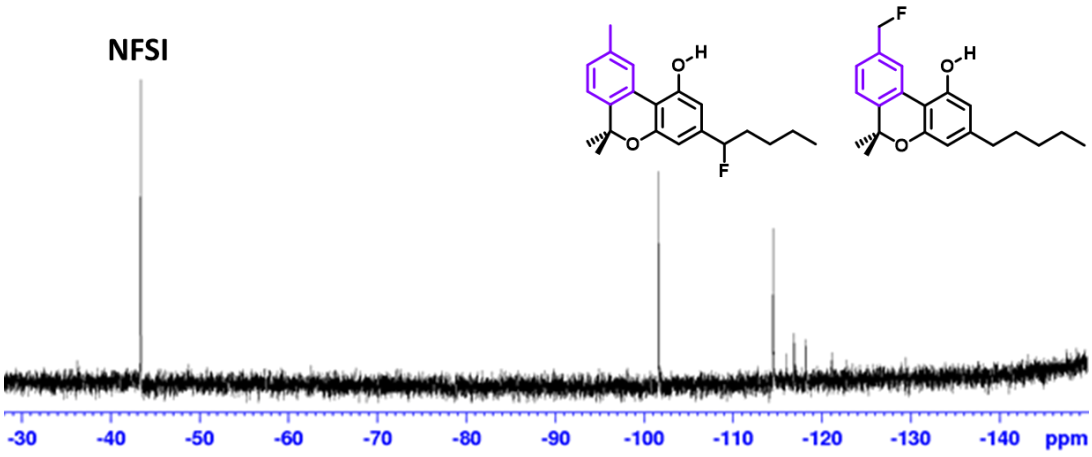

Figure 5.20: $^{19}F\{^{1}H\}$ NMR spectrum in MeCN of reaction between CBN, NFSI, and TBDT after 40 h.

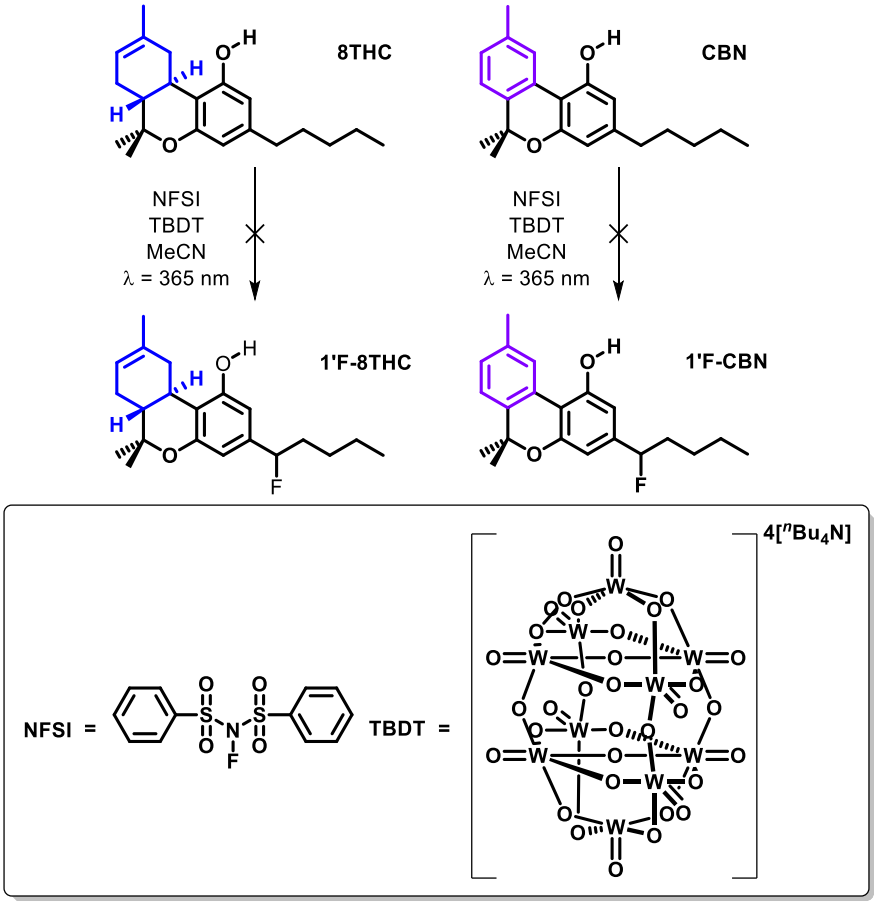

Scheme 5.10: Attempted synthesis of fluorinated 8THC and CBN using TBDT as a catalyst.

A final attempt at fluorinating cannabinoids was made using the radical initiator azobisisobutyronitrile (AIBN), also described by Britton and researchers for its utility in mediating benzyl C–H/C–F exchange, albeit less selectivly.[290] Following the reported procedure, AIBN, along with 1 equivalent of NFSI, and 3 equivalents of lithium carbonate (used to restrict formation of acetamides and protio NFSI) were combined in acetonitrile and heated to promote generation of the AIBN radical. The reaction was monitored using ^{19}F NMR spectroscopy. Unfortunately, no promising results were observed for 8THC or CBN as many inseparable products were generated. While monitoring these reactions, it was noted that all of the NFSI was consumed, and several intermediates would form and disappear over a 24 h period before NFSI was completely consumed. It was proposed that additional NFSI may promote further production of a partially generated product. Accordingly, the reaction was attempted with an excess of NFSI; fine tuning revealed three equivalents was adequate, leading to the formation of predominantly a single fluorine-containing product (Figure 5.21). This was only achieved when using CBN. A physically tall column (~0.75 m) was required for purification *via* chromatography, as several impurities with similar R_f values had to be removed from the crude product.

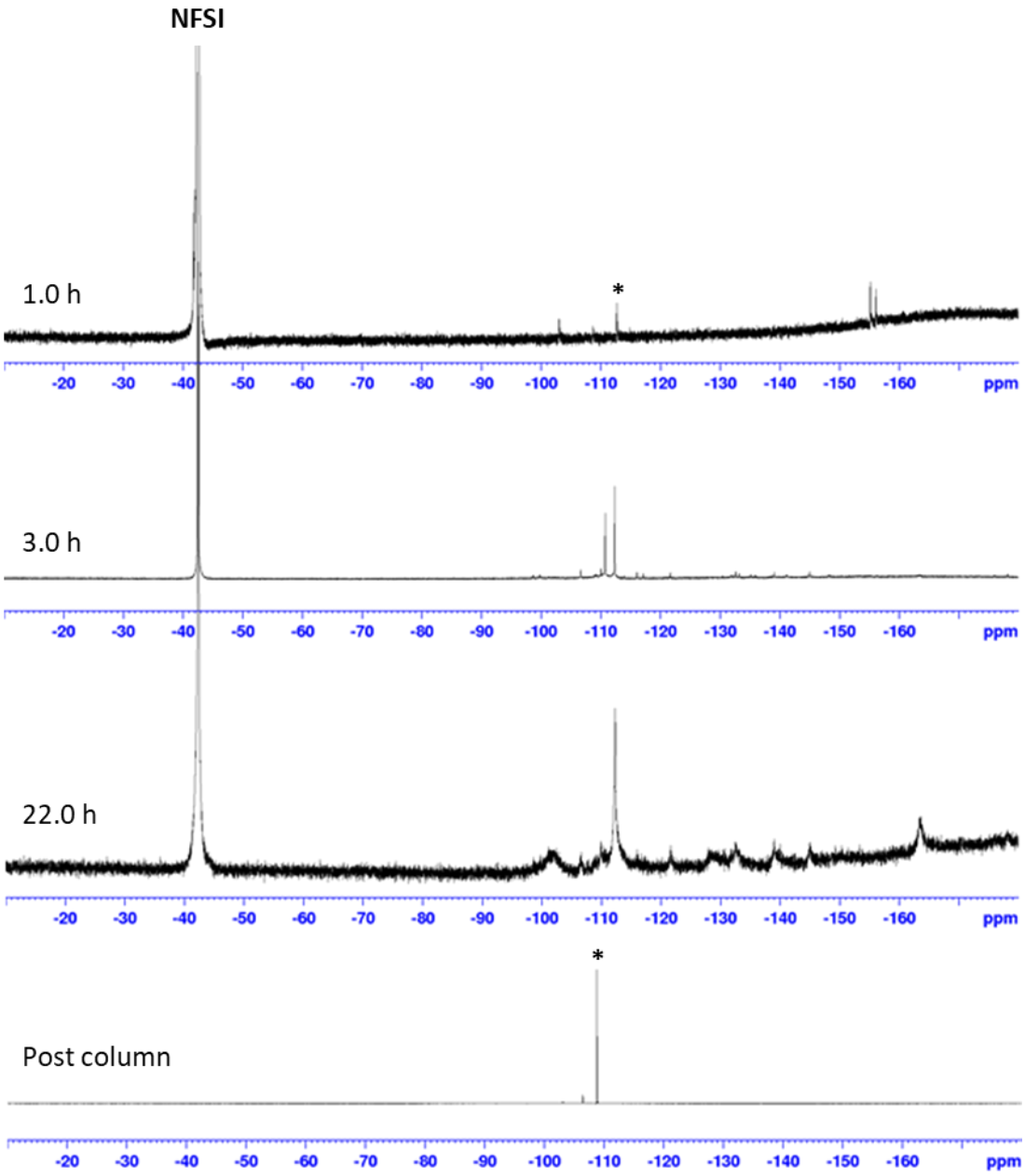

Figure 5.21: $^{19}F\{^{1}H\}$ NMR spectrum of *in situ* monitoring of reaction with CBN, NFSI, and AIBN (top to bottom) at 1 h in MeCN, 3 h in MeCN, 22 h in MeCN, and purified product post column in benzene-d_6.

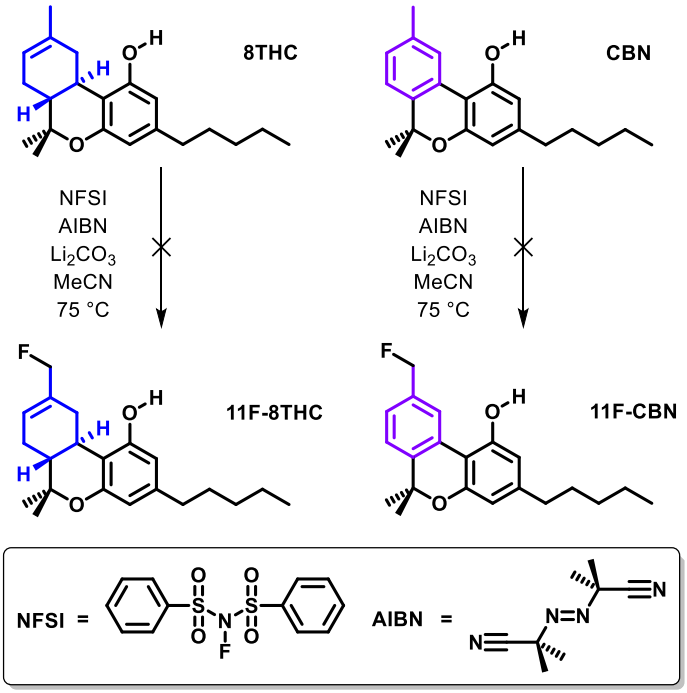

Scheme 5.11: Attempted synthesis of fluorinated 8THC and CBN using AIBN as a catalyst.

The ^{19}F NMR spectrum contained a lone singlet at δ –108.8. A proton decouple experiment, ^{19}F{^{1}H}, did not alter this resonance. ^{1}H and ^{1}H{^{19}F} NMR experiments failed to identify protons coupled to fluorine. Notably though, there were two less proton environments compared to CBN, one of which was an aromatic resonance and the other, a hydroxyl group. A ^{1}H–^{1}H COSY experiment indicated two of the four aromatic resonances, δ 6.88 and 6.66, protons at carbons 8 and 7, respectively, coupled to one other. The downfield shifted singlet at δ 8.79 was attributed to the proton at carbon 10, which is typically observed for other CBN-based compounds. The remaining signal at δ 6.01 could be attributed to a proton at either carbon 2 or 4 as this is typical for other CBN-based compounds. Using information from ^{13}C–^{19}F HSQC and ^{13}C{^{19}F} experiments (Figure 5.23), it was determined that the carbon giving rise to a ^{13}C signal at δ 110.2 had fluorine directly bound to it ($^{1}J_{CF}$ = 235.0 Hz). No other carbon atoms had a fluorine atom directly bound. The remaining ^{13}C signals that coupled to fluorine, δ 157.0, 147.4, 129.5, and 112.4, were triplets. The resonances at δ 157.0 and

147.4 exhibited $^{2}J_{CF}$ = 23.5 Hz and 24.5 Hz, respectively. The resonances at δ 129.5 and 112.4 exhibited $^{3}J_{CF}$ = 6.3 Hz and 4.2 Hz, respectively. The multiplicity of the resonance suggests that there are two chemically equivalent fluorines (Figure 5.22). The loss of an aromatic hydrogen, compared to CBN, confirms that either carbons 2 or 4 have two fluorine atoms bound to them.

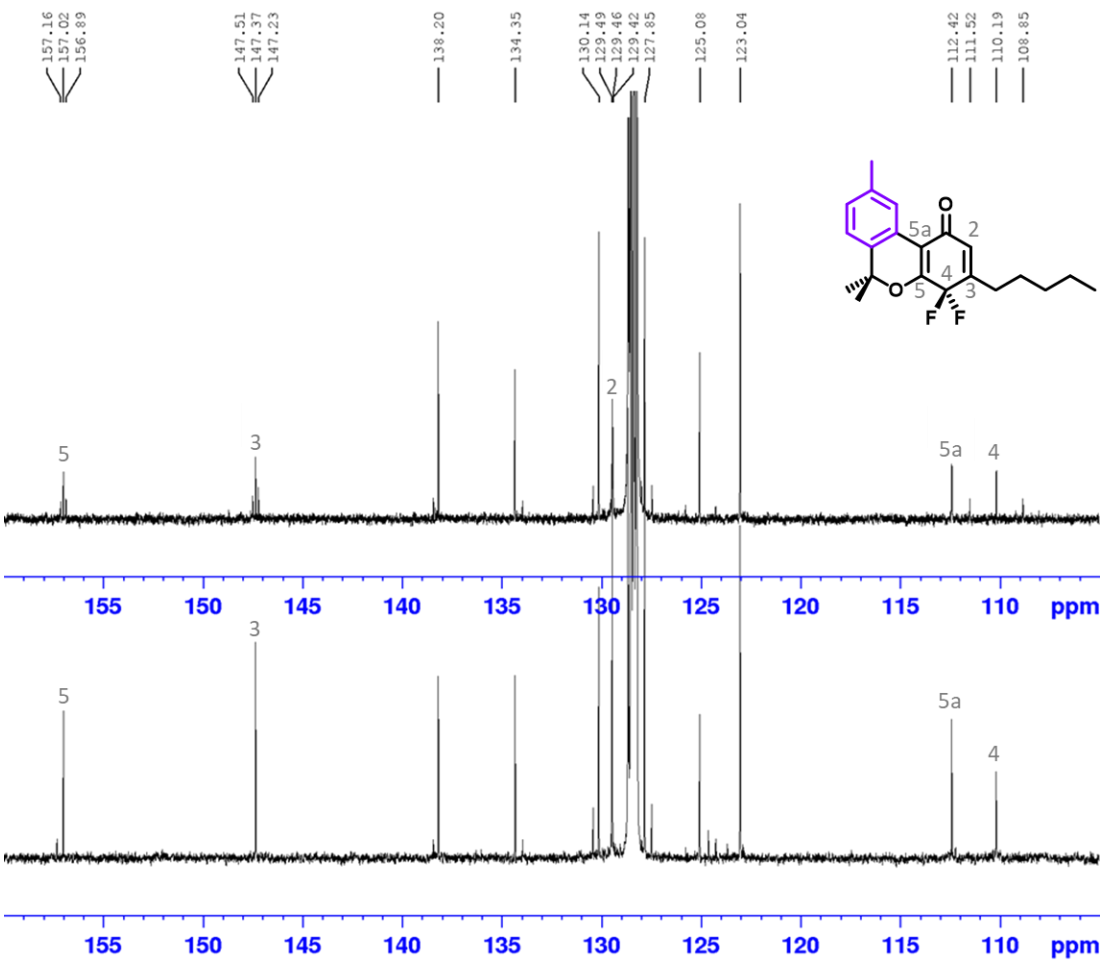

Figure 5.22: ^{13}C NMR spectra from isolated fluorinated CBN compound between 160 and 105 ppm. Top, $^{13}C\{^{1}H\}$ spectrum. Bottom, $^{13}C\{^{1}H,^{19}F\}$ spectrum.

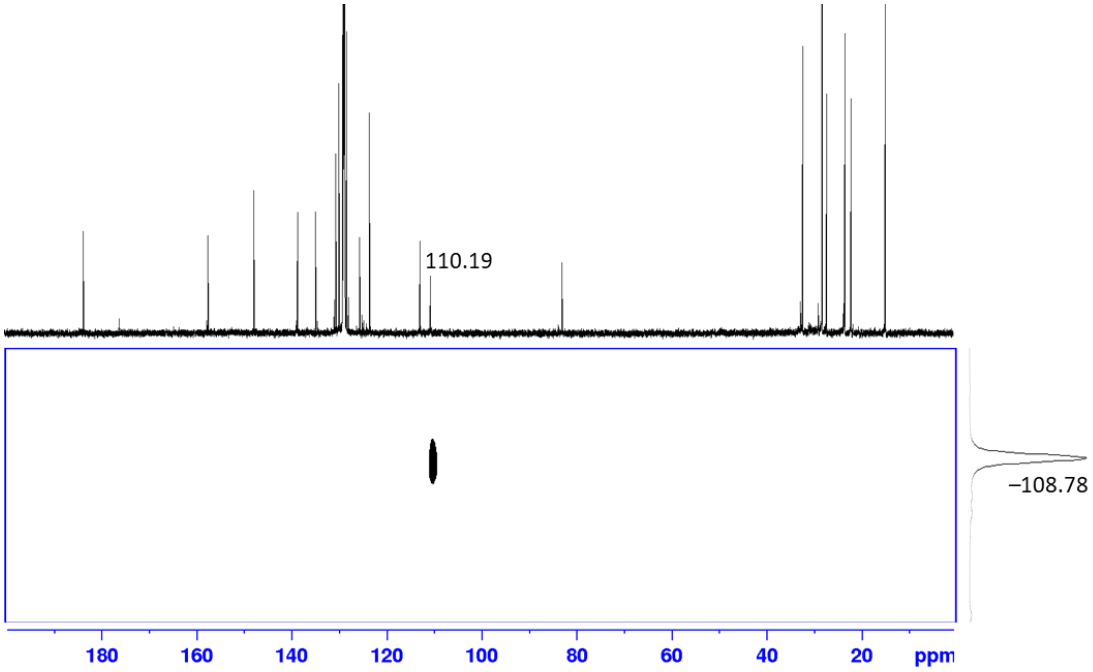

Figure 5.23: ^{13}C–^{19}F HSQC spectrum from isolated fluorinated CBN compound showing coupling between ^{19}F resonance at δ –108.8 and ^{13}C resonance at δ 110.2.

There two most downfield ^{13}C NMR resonances in THC and CBN-based cannabinoids. These are usually observed at δ ~150 and are due to carbon 1 (bound to the hydroxyl group) and carbon 5. In the $^{13}C\{^{1}H\}$ NMR spectrum collected for the fluorinated CBN product, there are two downfield ^{13}C resonances at δ 183.3 and δ 157.0. The more downfield signal is in a similar range to carbonyl carbons (C=O) of *ortho*-quinones and did not exhibit coupling to fluorine, whereas the other resonance has two bond coupling to fluorine.

It is proposed that the hydroxyl group was activated by the catalyst, extracting the hydrogen atom and generating an oxygen-based radical. Resonance of the radical through the aromatic system yields a carbon based radical on carbon 4 and a carbonyl group on carbon 1. The carbon-based radical abstracts a fluorine from NFSI to produce a fluorine on carbon 4. The remaining hydrogen on carbon 4 is cleaved and replaced with a fluorine with the second equivalent of NFSI to give the compound $4F_2$-cannabinone ($4F_2$-CBN, Figure 5.24). Therefore, δ 157.02 is carbon 5, because of the

observed $^{2}J_{CF}$. Using CBN and Si-CBN (as references) and 2-dimentional NMR spectroscopy (^{1}H–^{13}C HSQC, and ^{1}H–^{13}C HMBC), the remaining ^{13}C resonances were assigned accordingly. Notably, 4F$_2$-CBN is not the only compound that forms during this reaction (yield = 13.4%). Hence, other products of the radical reaction likely form alongside 4F$_2$-CBN.

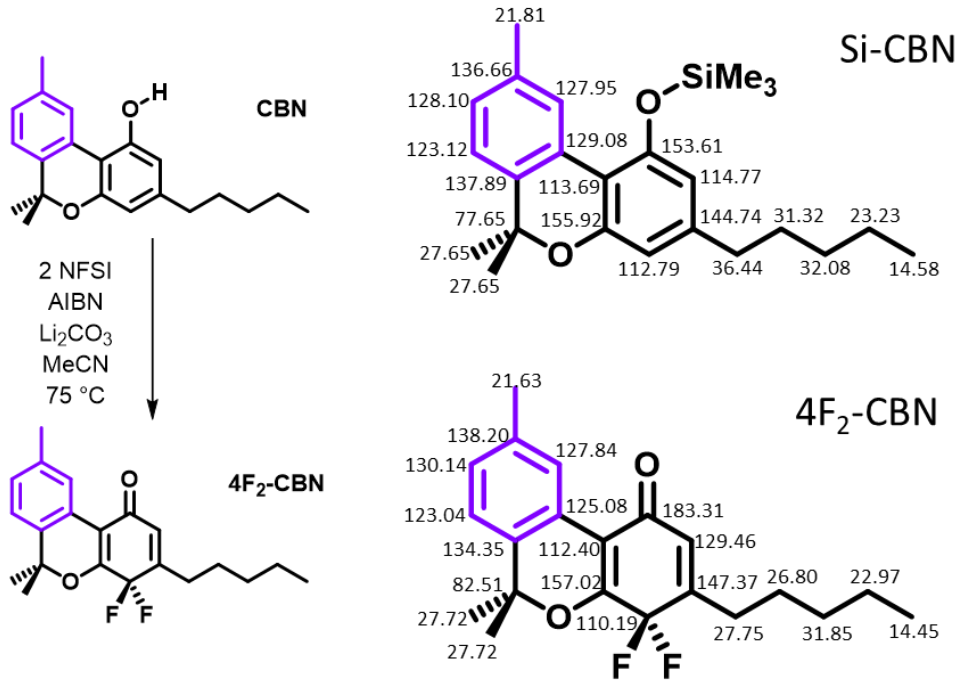

Figure 5.24: Left, synthesis of 4F$_2$-CBN. Right, ^{13}C NMR assignments of Si-CBN and 4F$_2$-CBN in benzene-d_6.

5.7 Summary of Cannabinoids Synthesized

A summary of the compounds synthesized, and the generalized routes to each, is depicted in Scheme 5.12.

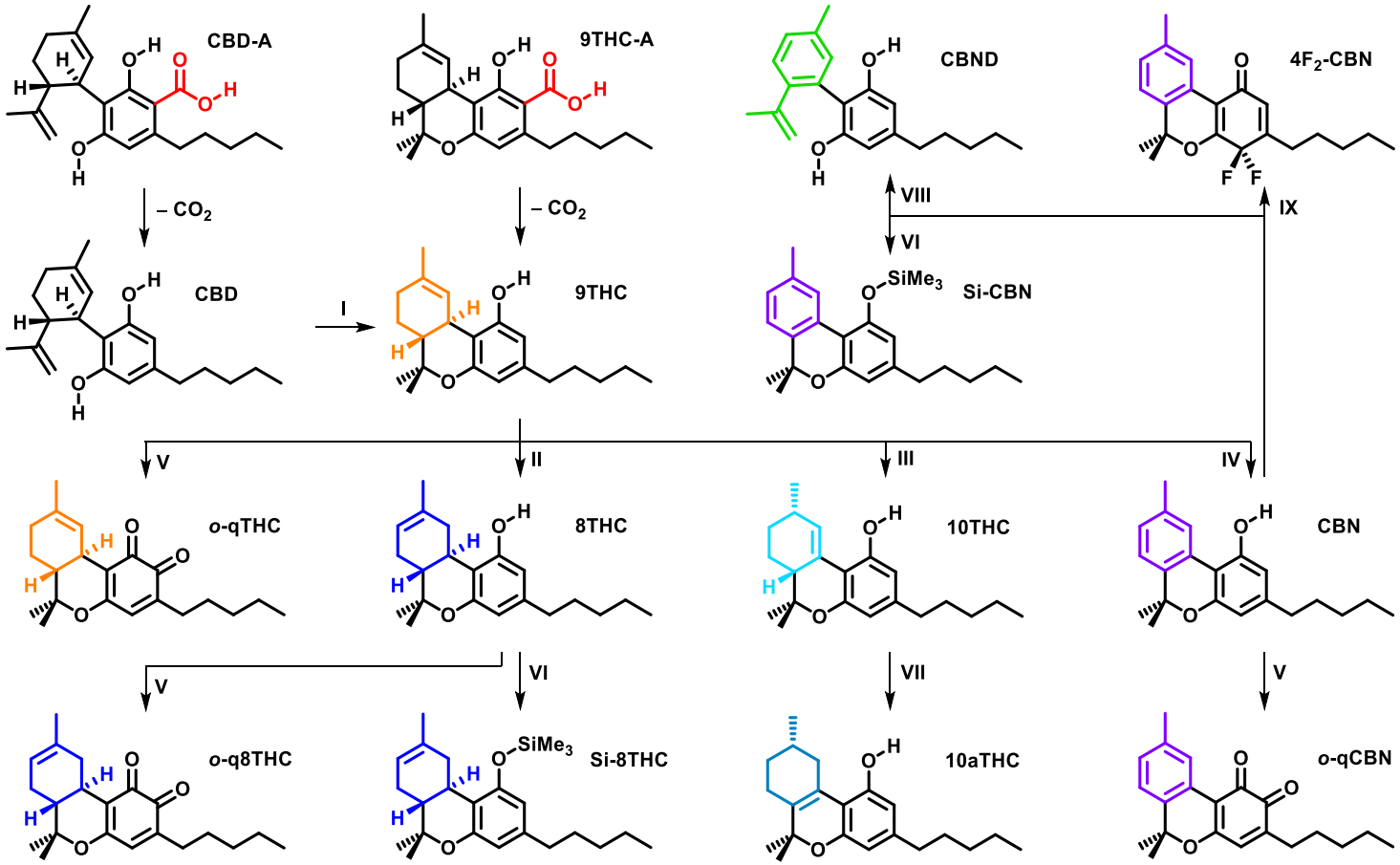

Scheme 5.12: Cannabinoid transformations discussed in this body of work. I) BF_3•Et_2O, DCM, 1.5 h, –10 °C. II) TsOH, Tol., 3 h, 135 °C. III) 2.5 M ^{n}BuLi, HMPA (hexamethylphosphoramide), 2 h, 0 °C. IV) I_2, Tol., 3 h, 135 °C V) IBX, DMF, RT, 8 h. VI) 1. [K][HMDS], Tol., 1 h, RT 2. Cl–$SiMe_3$, Tol., 1 h, RT VII) $CHCl_3$, 24 h, RT. VIII) UV radiation, CyH. IX) AIBN, 3 equiv NFSI, Li_2CO_3, CH_3CN, 16 h, 70 °C.

5.8 Chemotherapeutic Action of Isolated Cannabinoids

The chemotherapeutic action was tested against cancer cells and compared to normal cells (refer to the rest of this section and the experimental, 6.1.6, for further details). The cellular growth used to describe the chemotherapeutic effect was quantified using arbitrary units for cellular growth which were based on the absorbance measured. Not all experiments were conducted at the same time and so their units on the y-axis differ, but they all represent cellular growth. The trials with the same values and scale on the y-axis were conducted and processed in the same experiment.

5.8.1 THC-based Cannabinoids

The THC-based cannabinoids, 8THC, 9THC, 10THC, 10aTHC, and Si-8THC, were compared to one another to ascertain the influence the location of the alkene, the sp^3-hybridized carbon 9, and the hydrogen bonding have on the antiproliferative activity. The isolated compounds were tested with HCC1806 breast cancer cells, using foreskin BJ-5ta cells as the normal control (Figure 5.25).

Normal cellular growth was unperturbed for all measured compound concentrations except for 8THC at 20 μM (Figure 5.25a). With cancer cells, growth was consistent for 8THC and 9THC (Figure 5.25f and h), this would suggest their influence as antiproliferative agents are non-selective and the 8 or 9 position of the alkene does not influence their efficacy. An apparent dose-dependent relationship was observed for Si-8THC, dropping to <40% of cancer cell growth at 20 μM (Figure 5.25i). Removal of the hydroxyl group increased the antiproliferative efficacy in cancer cells compared to normal cells. The hydroxyl group likely alters the binding affinity to the cannabinoid receptors, causing one receptor to be bound preferentially.[252-254] This imbalance of receptor expression is somewhat thwarted in normal cells but is clearly less manageable

in cancer cells. By enhancing the receptor preference, antiproliferative affects are more prevalent in cancer cells.

A more pronounced dose-dependent relationship was apparent with 10THC, dropping to <33% of cellular growth at 20 μM. The most effective in this group was 10aTHC, also showing a dose-dependent relationship, dropping to <22% of cellular growth at 20 μM. (Figure 5.25j). Both the location of the alkene and sp^3-hybridized carbon 9 in 10THC and 10aTHC clearly have an impact on selectivity for cancer cell antiproliferation over normal cells. The few biological studies published on similar cannabinoids discovered that *S* configuration at carbon 9 results in higher binding affinity to CB_1 and less binding affinity to CB_2, compared to 9THC.[357, 358] Since carbon 9 in 10THC and 10aTHC is of *S* configuration, it is postulated that the different CB_1 and CB_2 binding affinities causes cancer proliferation to decrease. Isomerization to 10aTHC in biological media is likely to occur given the protic environment cancer cells generate. Thus, the activity of 10THC is likely a combination of both 10THC and any 10aTHC generated over time.

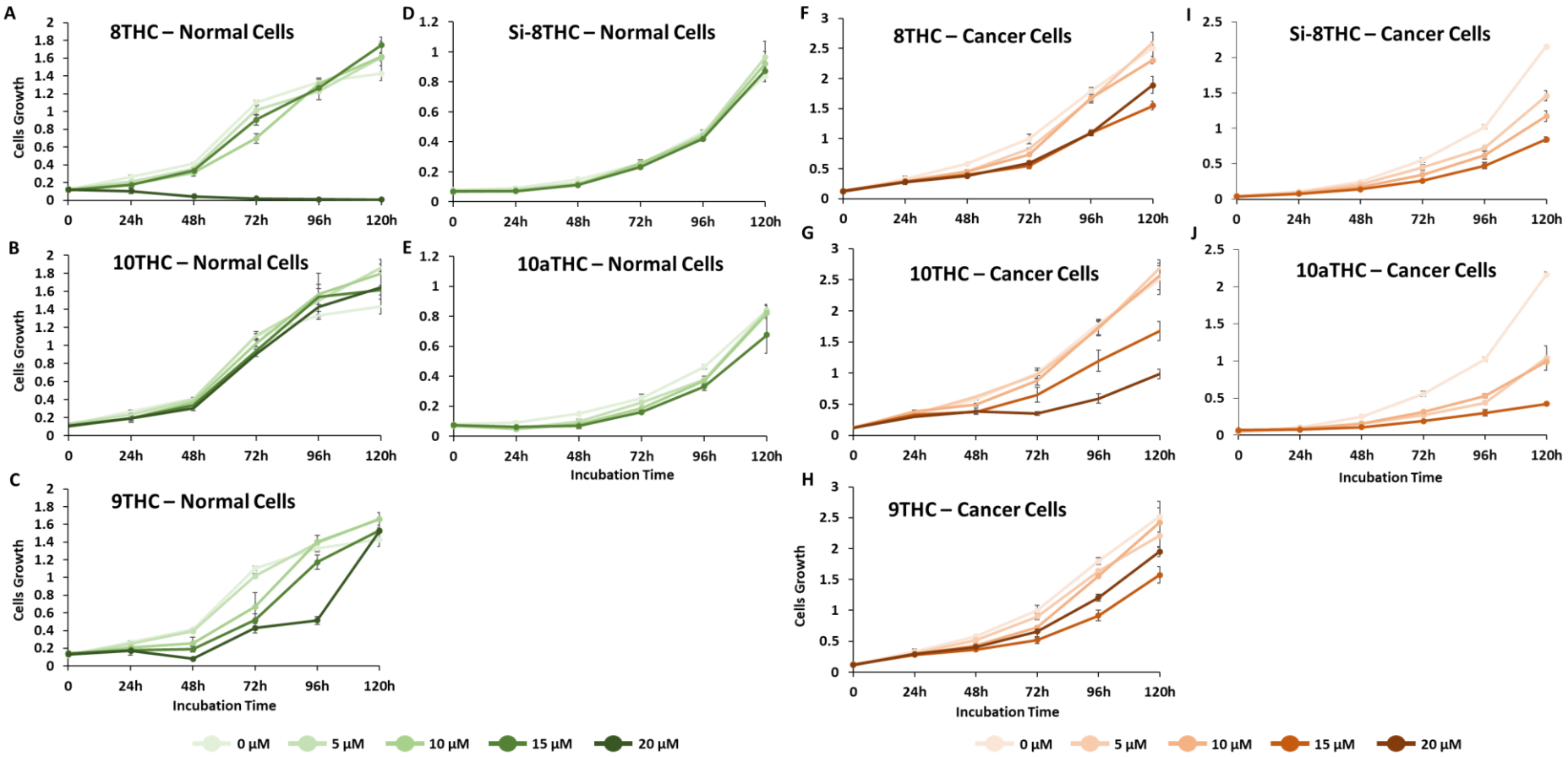

Figure 5.25: Antiproliferative effect of 8THC, Si-8THC, 10THC, 10aTHC, and 9THC on normal (A-E = BJ-5ta foreskin cells) and cancer cells (F-J = HCC1806 breast cancer cells). Data are shown as average arbitrary units of cell growth (with SD) calculated from three independent measurements tested at 24-120 h after plating. Note that Si-8THC and 10aTHC experiments were conducted separately and so their X-axes differ. Orange colours indicate cancer cells; green colours indicate normal cells.

5.8.2 CBN with Various Cancer Lines

Since CBN is known to have an antiproliferative effect,[193, 359] it was tested on IMR5 and SH-SY5Y neuroblastoma cells, A172 and M059K glioblastoma, HCC1806 breast cancer, and HB8065 liver cancer cells with foreskin BJ-5ta cells as a normal control (Figure 5.26f). Significant inhibition ($p<0.05$) of tested cells, both cancer and normal, was observed, with the exception of line M059K, which was not sensitive to the tested CBN doses. Notably, synthesized CBN required slightly higher concentration than purchased CBN to inhibit the growth of cancer cells to the same degree. This disparity is almost certainly due to the fact that synthesized CBN was slightly less pure than the purchased standard and is a testament to the importance of purity with regards to the efficacy of biological activity.

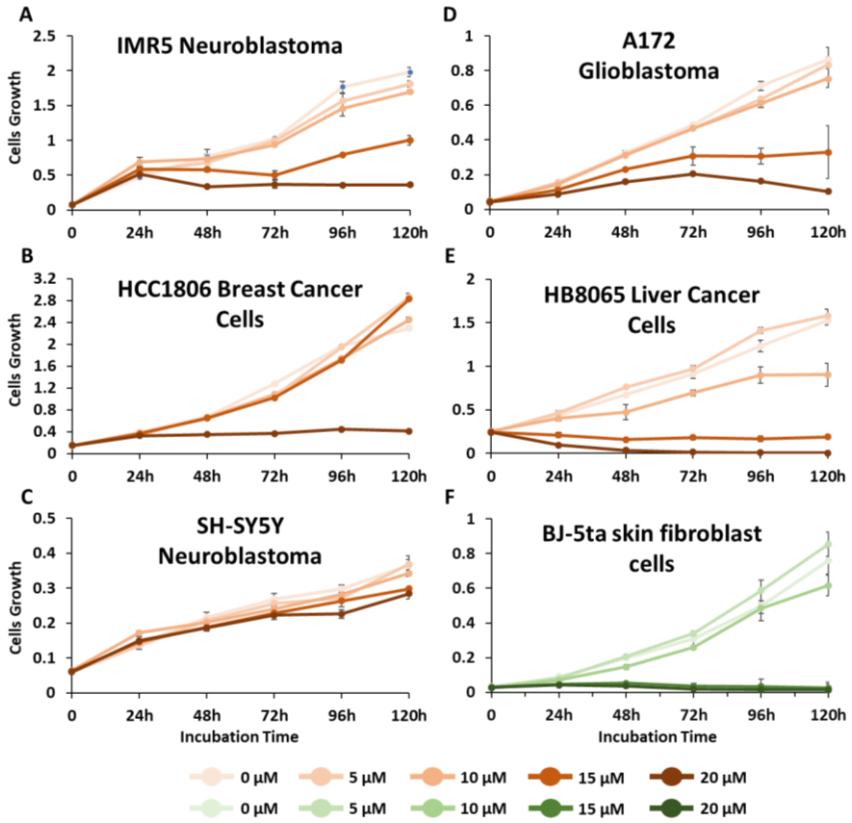

Figure 5.26: Antiproliferative effect of CBN on various cancer (IMR5, HCC1806, SH-SY5Y, A172, HB8065) and BJ-5ta normal cells. Data is shown as average arbitrary units of cell growth (with standard deviation (SD)) tested at 24-120 h after plating. Orange colours used for cancer cells; green colours used for normal cells.

5.8.3 CBD and CBN-based Cannabinoids

To assess if the loss of the cyclic ether in CBND produced a similar antiproliferative response as CBD, it was tested, and the data compared with that obtained from CBD and CBN. It was found that CBND exhibited a dose-dependent effect on proliferation of both normal and cancer cells, with cancer cells being more dramatically affected; for example, 10 μM CBND inhibited the growth of cancer cells, but spared normal cells. In comparison to CBD, CBND had a diminished effect on cell growth, a fact that was particularly prominent for normal cells, whereas CBD exhibited a more pronounced dose-dependent relationship. Among the three compounds, CBN reduced cell growth the most, and notably, exhibited a binary dose dependence wherein concentrations of 5-10 μM had little to no effect, while concentrations above 10 μM drastically inhibited cell growth, especially that of normal cells. This would indicate that the presence of two hydroxyl groups in CBD and CBND incurs a dose-dependent response to antiproliferation with no preference for normal or cancer cells

With Si-CBN, a slight dose-dependent response to cancer cells, similar to Si-8THC, was observed, dropping to <40% of cancer cell growth at 20 μM (Figure 5.27i) with no effect on normal cells. Both Si-CBN and Si-8THC possess a lagging effect where the growth of either cell line does not grow significantly until more time elapses (>72 h). Finally, the fluorinated CBN, $4F_2$-CBN, showed little response towards antiproliferation of breast cancer cells, with only minor growth inhibition above 5 μM in cancer cells (Figure 5.27j). It can be concluded that the 4 position of CBN is not imperative for receptor selectivity and the slight inhibition is likely a consequence of an absence of the hydroxyl group at carbon 1.

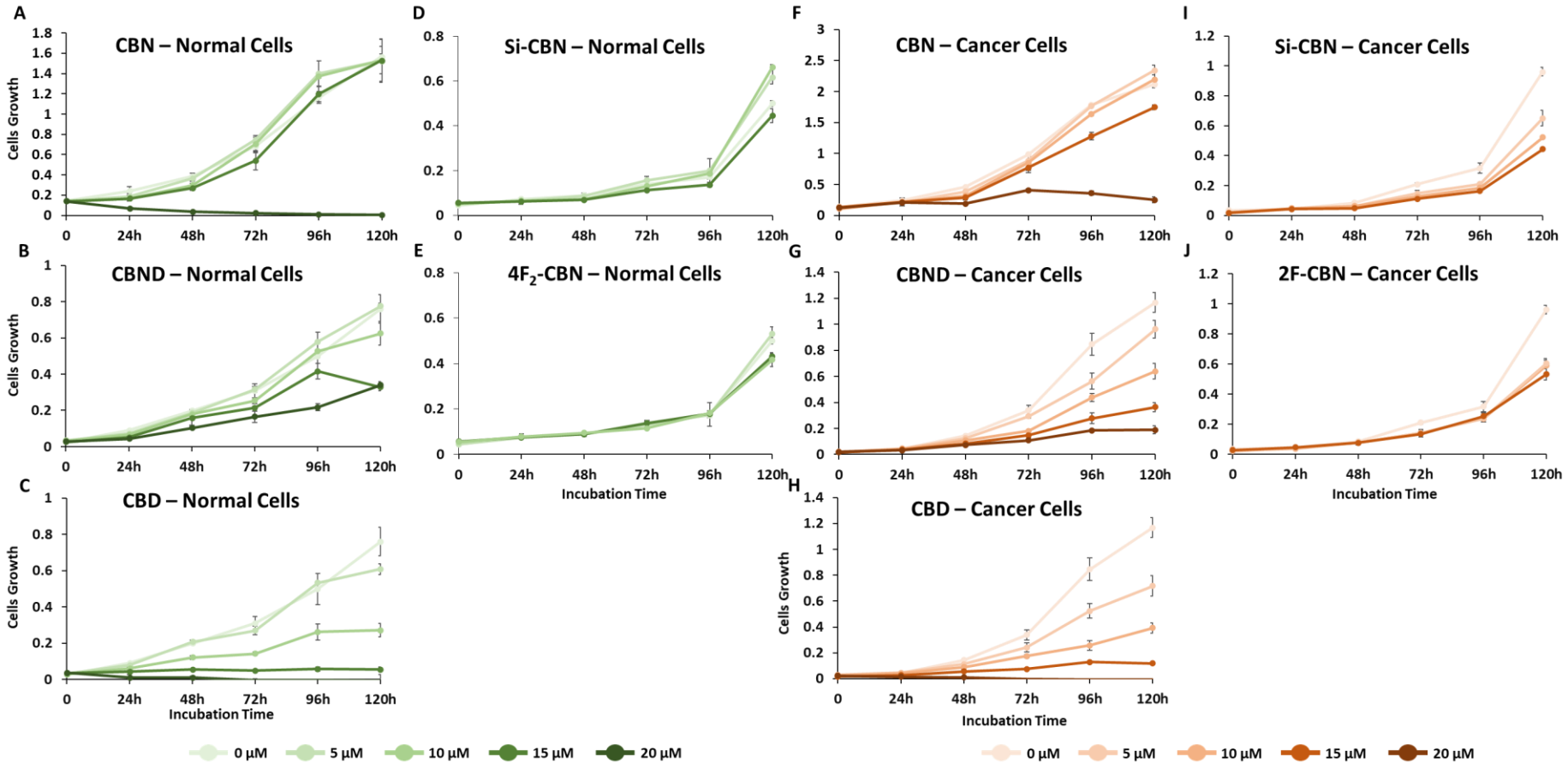

Figure 5.27: Antiproliferative effect of CBN, Si-CBN, CBND, $4F_2$-CBN, and CBD on normal (A-E = BJ-5ta foreskin cells) and cancer cells (F-J = HCC1806 breast cancer cells). Data are shown as average arbitrary units of cell growth (with SD) calculated from three independent measurements tested at 24-120 h after plating. Orange colours indicate cancer cells; green colours indicate normal cells.

5.8.4 *ortho*-Quinone Derivatives of Cannabinoids

To test whether the synthesized cannabinoid derivatives *o*-qCBN and *o*-q8THC also possess anti-cancer properties, they were exposed to HCC1806 breast cancer cells at various concentrations, alongside their respective parent compounds (CBN, 8THC, and 9THC). BJ-5ta foreskin cells (normal cells), were used as a control (Figure 5.28a-f).

Both cancer and normal cells were extremely sensitive to a 20 µM solution of CBN and *o*-qCBN (Figure 5.28a, b, g, and i). The quinone *o*-qCBN began strongly inhibiting normal cell growth above 15 µM, whereas CBN did not substantially affect normal cell growth until concentrations reached 20 µM. Intriguingly, in cancer cells, *o*-qCBN effectively inhibited cell growth at 10 µM, while CBN exhibited little effect below 20 µM. Thus, a 'sweet spot' exists at a concentration of 10 µM wherein *o*-qCBN does not affect normal cell growth to a great degree but devastates cancer cells.

Compared to either 8THC and 9THC, which were largely unproductive antiproliferative agents, the quinone *o*-q8THC annihilated growth of both normal and cancer cells from 10 µM. A low dose was used to show that at a concentration of 3 µM, cancer cell inhibition was observed while normal cells continued to flourish (Figure 5.28f and l). Despite only minor changes in their structures, both *o*-qCBN and *o*-q8THC influence cell growth differently.

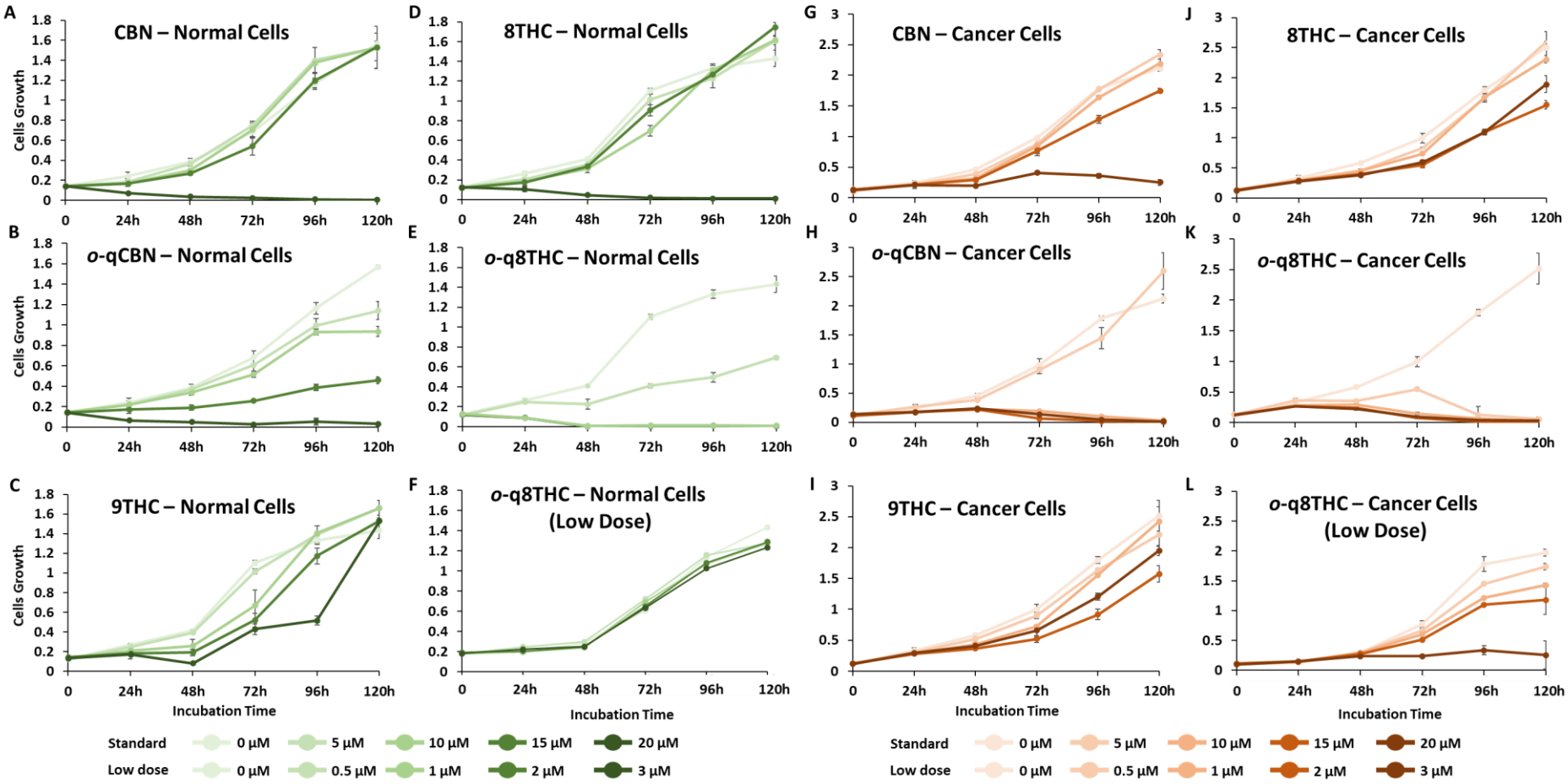

Figure 5.28: Antiproliferative effect of CBN, 8THC, 9THC, *o*-qCBN, and *o*-q8THC on normal (A-F = BJ-5ta foreskin cells) and cancer cells (G-L = HCC1806 breast cancer cells). Data are shown as average arbitrary units of cell growth (with SD) calculated from three independent measurements tested at 24-120 h after plating. Orange colours indicate cancer cells; green colours indicate normal cells. Note that data for 8THC, 9THC, and CBN are also presented in Figure 5.27.

A correlation has been found between redox potentials and cytotoxicity in quinone chemotherapeutic candidates,[343, 344] as they are known to be oxidizers, usually in two sequential one-electron steps. It was therefore of interest to explore the possibility that the reduction potentials of *o*-q8THC and *o*-qCBN could be related to their cancer cell growth inhibition efficacy. The most reactive form of a quinone in the biological cell is formed after the first reduction, the semiquinone, as the second reduction often reacts with available proton sources to generate the more benign catechol analogue.

The facile $E_p^{c\mathrm{I}}$ values of both *o*-qCBN and *o*-q8THC are consistent with their powerful cytotoxic responses to breast cancer cells at extremely low concentrations where the effect on normal cell growth is minimal. If this activity is due to *in situ* reduction to the radical anion, the slightly higher activity of the latter. Despite a more negative reduction potential, the efficacy of *o*-q8THC may be related to the different voltammetric responses observed in DMF and that follow-up reactions that deactivate the semiquinone radicals are more facile with *o*-qCBN. This results in *o*-q8THC being far more destructive; the semiquinone is more present and longer living compared to *o*-qCBN which undergoes the second reduction and deactivation *via* secondary processes more readily. Further investigation of voltammetry under biomedical conditions (aqueous buffer, with and without added O_2) are required to fully confirm this hypothesis.

The efficacy of the quinone as a chemotherapeutic drug may depend on the hypoxic nature of cancer cells.[301, 360] As a cell becomes cancerous, the cellular machinery alters, favouring certain processes and overusing others to proliferate at considerable rates. This results in a dramatic loss of available oxygen in the cell, causing hypoxia. Redox active compounds, including radicals, can be tolerated somewhat in normal cells due to

the presence of oxidizing species, such as oxygen. The lack of oxygen in cancer cells, however, results in reductive processes occurring more readily as the effective reduction potential has become more negative compared to normal cells.[361] It is this net reducing environment that is exploited in hypoxia-activated prodrugs, such as evofosfamide,[362] which is converted to a radical anion in the reducing environment of the cell, but instead of being reversibly oxidized, which happens in normal cells, the hypoxia aids in the longer life of the radical anion, therefore releasing its destructive nature.[363]

Apart from hypoxia, the chemotherapeutic activity of both *o*-qCBN and *o*-q8THC can be linked to oxidative stress. Oxidative stress is prevalent in cancer cells and is attributed to the generation of reactive oxygen species (ROS) that are destructive to biological machinery. ROS can be tolerated to certain levels; however, the first reduction, to the radical semiquinone, may perpetuate the generation of ROS beyond tolerable levels in normal and/or cancer cells, especially if radicals are already present at high concentrations, as is the case in certain cancers undergoing prevalent oxidative stress. Since the first reduction of *o*-q8THC affords a radical semiquinone that is longer lived compared to the semiquinone of *o*-qCBN, it is more capable of perpetuating ROS, leading to apoptosis.

5.8.5 Other Cell Lines

Two normal cell lines, WI-38 human lung fibroblasts and HSIEC human intestinal cells were used to test this series of cannabinoids against other biological environments where use as inflammatory agents may become important (Figure 5.29). Cell growth was completely diminished at 15 μM, somewhat diminished at 10 μM, and unhindered at 5 μM with CBN, 8THC and 9THC (Figure 5.29a, c, d, f, h, and i). For *o*-q8THC and

o-qCBN growth was completely diminished at 10 μM and 15 μM, showing that their destructive nature is generally unspecific (Figure 5.29b, e, g, and j). The WI-38 and HSIEC cells were on average more resilient to *o*-q8THC than BJ-5ta (Figure 5.29e and j) making the effective cancer death concentration of 3 μM for *o*-q8THC still impactful. Unfortunately, both WI-38 and HSIEC are less resilient than BJ-5ta with *o*-qCBN (Figure 5.29b and g) as the effective cancer death concentration of 10 μM causes death with these cell lines. As a comparison, several other cannabinoids were tested with WI-38 and HSIEC, including 10aTHC, Si-8THC, $4F_2$-CBN, and Si-CBN. Practically, all of these cannabinoids had no detrimental effect on cell growth, except for Si-CBN which inhibited growth of HSIEC at 15 μM (Figure 5.30h), and 10aTHC which had a slight dose-dependent relationship on diminishing cellular growth of HSIEC (Figure 5.30e). Investigations into the use of these and other cannabinoids isolated during this work as chemotherapeutic drugs for *in vivo* studies and other cancer lines, as well as anti-inflammatories is ongoing.

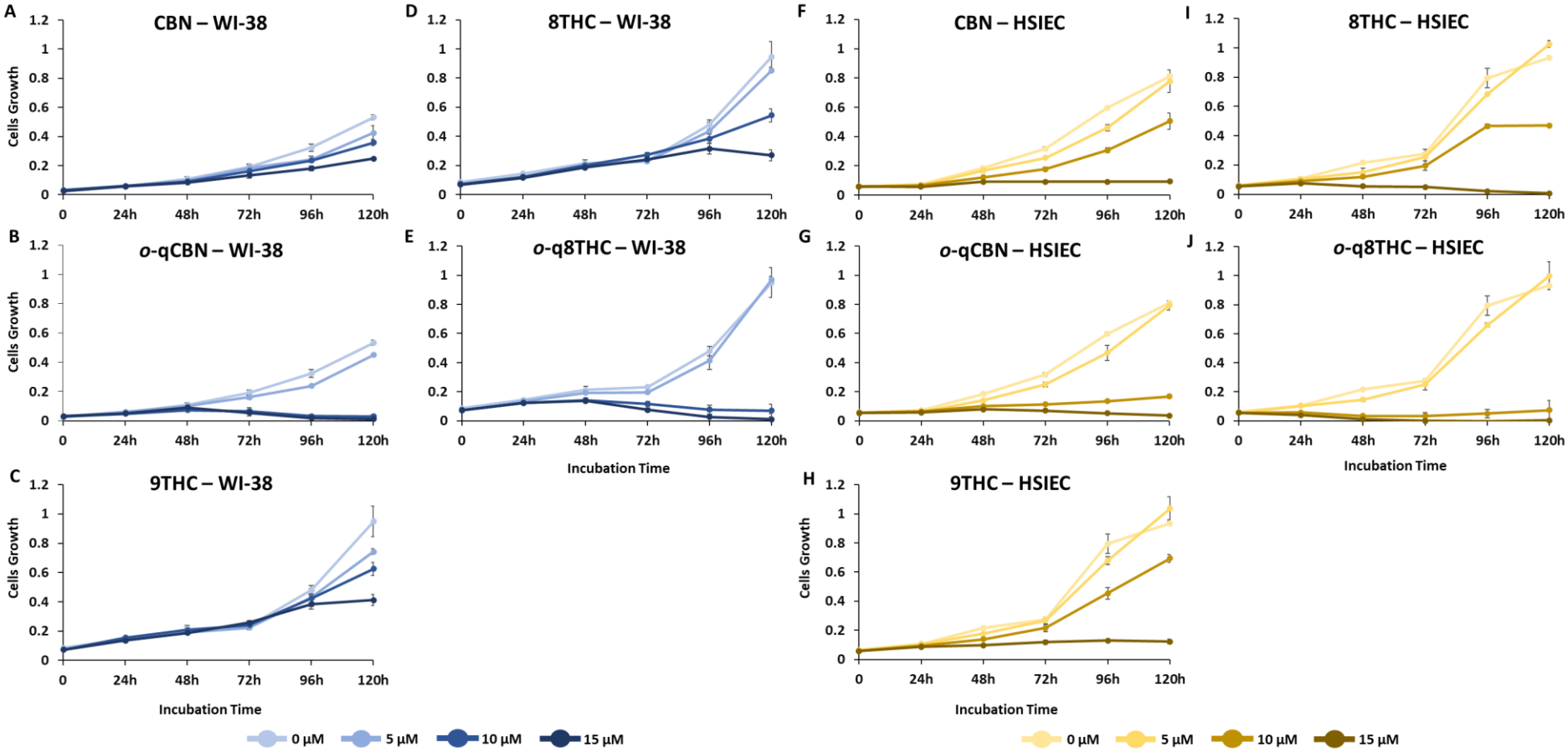

Figure 5.29: Antiproliferative effect of CBN, 8THC, 9THC, *o*-qCBN, and *o*-q8THC on human lung fibroblasts (A-E = WI-38) and human intestinal cells (F-J = HSIEC). Data are shown as average arbitrary units of cell growth (with SD) calculated from three independent measurements tested at 24-120 h after plating.

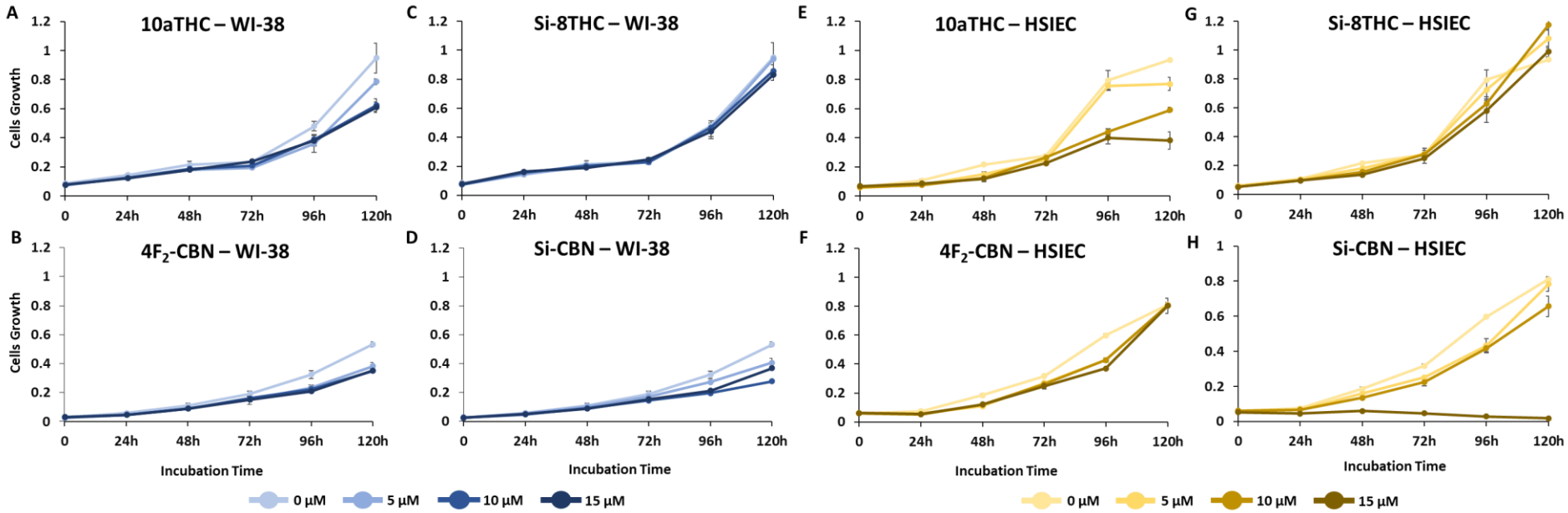

Figure 5.30: Antiproliferative effect of 10aTHC, Si-8THC, 4F_2-CBN, and Si-CBN on human lung fibroblasts (A-D = WI-38) and human intestinal cells (E-H = HSIEC). Data are shown as average arbitrary units of cell growth (with SD) calculated from three independent measurements tested at 24-120 h after plating.

5.9 Concluding Statement and Future Work with Cannabinoids

The body of work discussed in Part II of this thesis represents preliminary studies. This thesis emphasizes avenues to generate biologically relevant cannabinoids and highlights their potential as anticarcinogenic drugs. Now that semisynthetic and characterization methods have been established, a continuation of bioactivity experiments should be conducted. Breast cancer lines were targeted for this project, but many other cancers need the same attention. Particular attention should be given to 8THC and CBN for their ease of synthesis and stability, *o*-q8THC and *o*-qCBN as they were the most active towards the antiproliferation of cancer cells, and 10THC and 10aTHC for they were the most active of the THC-based compounds tested. Expanding from *in vito* studies to *in vivo* studies should be considered to investigate the efficacy of these compounds in living organisms.

The silylated cannabinoids, Si-8THC and Si-CBN although not chemically taxing to generate, could serve as opportunities to better label cannabinoids with other functionalities or attach cannabinoids to surfaces of macromolecules for timed drug delivery.

Other low abundant cannabinoids may be excellent targets for semisynthesis. The alternative cyclizations, CBT, CBL, and CBE, could be targeted and made in higher abundance so further research can be conducted (Figure 5.31). For instance, CBG gives CBL when exposed to high temperatures or acidic conditions. In the same way 8THC and CBN were targeted in this work, *Cannabis sativa* samples with CBG could be used to afford extracts with a high amount of CBL given the right conditions, such as the excessive heat provided during the decarboxylation step. In fact, it was theorized that one of the earlier fractions ($R_f \approx 0.91$) from the synthesis of CBN was CBL, but this

was not pursued to great lengths and could easily be an introduction for a student to continue this work.

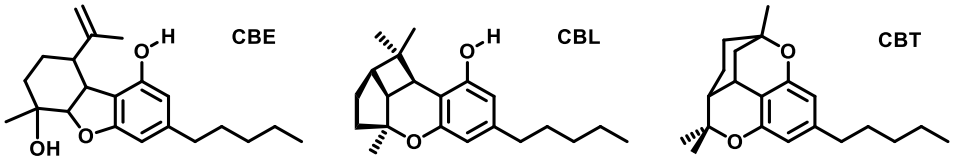

Figure 5.31: Alternative cyclized low abundant cannabinoids. CBE = cannabielsoin, CBL = cannabicyclol, and CBT = cannabicitran

Finally, further modification of cannabinoids with late-stage fluorination should be pursued as fluorine is prominent in medicinally relevant compounds. Substantial work went into attempting to control the fluorination with cannabinoids with radical initiators and other cannabinoids may be more susceptible to this modification approach, but it is likely best to protect the hydroxyl group to allow for the modification to proceed unperturbed. A plethora of protecting groups are available for hydroxyl groups.[364] Targeting carbon 1' (of the pentyl chain off carbon 3) should be a priority as literature suggests this area is vital for manipulation of the cannabinoid receptor selectivity and efficacy. As carbon 1' contains benzylic C–H bonds, a catalyst that preferentially targets this moiety should be prioritized, see Huang *et al.* for a recent review on group 10 catalyst examples investigated for this type of activation.[365]

Chapter 6: Experimental and Supporting Information

6.1 Experimental Considerations

6.1.1 General

Conditions specific to Part II are stated here. All other procedures were performed as described in Chapter 3 (*i.e.* NMR spectroscopy and X-ray crystallography).

6.1.2 Solvents

Diethyl ether was obtained from an MBraun Solvent Purification System (SPS) while petroleum ether (30-60 ˚C fraction), hexanes, *N*,*N*-dimethylformamide, and toluene were acquired from EMD Chemicals, Inc or Millipore Sigma. and used as received. Dichloromethane (DCM) was purchased from EMD Chemicals, dried over CaH_2, degassed via three freeze–pump–thaw cycles, distilled under vacuum and stored in a polytetrafluoroethylene (PTFE)-sealed glass vessel. Deuterated chloroform ($CDCl_3$) and benzene (C_6D_6) were purchased from Cambridge Isotope Laboratories, Inc. and used without further purification.

6.1.3 Chemical Materials

Cannabidiol (CBD) was purchased from CBD Okanagan (BC, Canada). Hexamethylphosphoramide, 2.5 M solution of ^{n}BuLi in hexanes, boron trifluoride etherate, *para*-toluene sulfonic acid (TsOH), and elemental iodine were purchased from Sigma-Aldrich and used without further purification. The hypervalent iodine compound, 2-iodobenzoic acid (IBX) was synthesized *via* a reported procedure and used without further purification.[366] *Cannabis sativa* was grown at a licensed research facility at the University of Lethbridge (Lethbridge, Alberta, Canada).

6.1.4 Instruments

Infrared spectra were recorded on a Bruker Tensor 37 FT Infrared spectrometer. Melting points were determined using an Electrothermal MEL-TEMP® 3.0. A Rayonet RPR-100 Photochemical Reactor was used as a UV (253 nm) source at 0.00128 W m^{-2}.

6.1.5 *Cannabis Sativa* Preparation

6.1.5.1 General Procedure for Generation of Extract

Cuttings of *cannabis sativa* (2.3 g) were crushed using a motor and pestle to generate a fine green powder. Toluene (100 mL) was added to the cuttings and the mixture was stirred for 20 min. The mixture was filtered to give a golden solution. This step was repeated twice more, thereafter the golden colour diminished greatly. The toluene washings were combined, and volatiles removed *in vacuo* to yield a thick brown oil (0.67 g, generally 13-18% of the biomass used). qNMR experiments indicated the extract was 26.0% CBD-A and 8.3% 9THC-A for this particular sample, which was grown to contain this particular ratio and percentage of major cannabinoids. The same procedure has been conducted using hemp. Wherein the extract percentage is generally similar with all extracts from *Cannabis sativa*, but the amount of cannabinoids is substantially lower in hemp. Specific examples provided in 6.2.

6.1.6 Cell Cultures and Growth Inhibition

6.1.6.1 Procedure for Cell Cultures used for Growth Inhibition

Normal human foreskin fibroblasts (BJ-5ta), purchased from American Type Culture Collection (ATCC, Manassas, USA), were cultured in Dulbecco's Modified Eagle's Medium (DMEM) supplemented with 10% fetal bovine serum (FBS) and 1%

penicillin/streptomycin (P/S). Human glioblastoma cell lines M059K, A172 and neuroblastoma cell lines SH-SY5Y, the breast cancer cell line HCC1806 and the liver cancer HB8065 cell line were purchased from American Type Culture Collection (Manassas, VA, USA). Another neuroblastoma cell line, IMR-5 was kindly provided by Dr. Aru Narendran (Arnie Charbonneau Cancer Institute, University of Calgary). M059K cells were grown in a 1:1 mixture of Dulbecco's Modified Eagle's Medium (DMEM) and Ham's F12 medium with 2.5 mM L-glutamine adjusted to contain 15 mM HEPES, 0.5 mM sodium pyruvate and 1.2 g/L sodium bicarbonate supplemented with 1% non-essential amino acids (NEAA), 10% fetal bovine serum (FBS) and 1% penicillin/streptomycin (P/S). A172 was grown in ATCC-formulated DMEM supplemented with 10% FBS and 1% P/S. HB8065 cells were grown in ATCC-formulated Eagle's Minimum Essential Medium (EMEM) supplemented with 10% FBS and 1% P/S. SH-SY5Y cells were grown in a 1:1 mixture of ATCC-formulated EMEM and F12 Medium supplemented with 10% FBS and 1% P/S. IMR-5 cells were grown in RPMI1640 medium supplemented with 2 mM L-glutamine, 1% NEAA, 10% FBS and 1% P/S. Human breast cancer cell line HCC1806 (ATCC, Manassas, USA) was grown in ATCC-formulated RPMI-1640 Medium (ATCC) containing 10% FBS. All cell lines were incubated at 37 °C in a humidified atmosphere of 5% CO_2.

6.1.6.2 Procedure for Dimethylthiazol-2-yl-2,5-diphenyltetrazolium Bromide Assay

Cells were grown to 90% confluence, 3.0×10^3 cells per well were plated in 96-well plates. After 24 hours different doses of active ingredients, including CBN (Millipore Sigma, USA), 9THC ((Millipore Sigma, USA), and synthesized CBN, 8THC, 9THC, CBND, 10THC, 10aTHC, *o*-qCBN, *o*-q8THC, Si-CBN, Si-8THC, and $4F_2$-CBN were added into the plates. The plates were incubated for 120 h, taking

samples for analysis every 24 h. The 3-(4,5-dimethylthiazol-2-yl)-2,5-diphenyltetrazolium bromide (MTT) assays were performed using the Cell Proliferation Kit I (Roche Diagnostics GmbH), according to the manufacturer's instructions. The spectrophotometric absorbance of samples was measured at 595 nm using a microtiter plate reader (FLUOstar Omega).

6.1.7 Quantitative Nuclear Magnetic Resonance (qNMR)

6.1.7.1 qNMR Analysis

The T1 relaxation times for both the standard, 1,3-dichloro-2-iodobenzene, and cannabinoid peaks of interest were determined using an inversion recovery experiment. The standard, 1,3-dichloro-2-iodobenzene, was chosen because its signals do not overlap with any signals associated with the solvent, $CDCl_3$, or key resonances of cannabinoids (9THC-A, CBD-A, 9THC, 8THC, CBD, CBN). The doublet at δ 7.35, which integrates for 2H, was chosen for the qNMR procedure. The relaxation time of the resonance for the standard was determined to be 6,796 ms, a relatively long relaxation time for organic molecules. The recycle delay (D1) was set to 5 times the longest T1 value (6,796 ms × 5 = 33,980 ms) rounded to the nearest multiple of 5. In this case the longest T1 value belonged to the standard. D1 was set to 35,000 ms, which ensured that all peaks in the experiment would fully relax prior to each subsequent magnetic pulse (required for quantitative integration of NMR signals).

6.1.7.2 Procedure for running and interpreting the qNMR

The experiment used was a ^1H NMR acquisition with a 90° excitation to ensure all peaks were fully excited. The NMR sample was prepared by dissolving a known quantity (10-20 mg) of both the standard and the material containing the cannabinoid

in approximately 0.5 mL of $CDCl_3$ in a 5 mm NMR tube. A known volume of solvent is not required, as the masses of the standard and the sample containing an unknown quantity of cannabinoid allows for determination of the relative molar ratio of the cannabinoid. Once the sample has been prepared and the NMR experiment completed, the resonances in the resulting spectrum were referenced relative to residual $CHCl_3$, which appears at δ 7.27. The signals of interest were integrated using the TopSpin® software. The signal arising from the standard, 1,3-dichloro-2-iodobenzene, at δ 7.35 (2H) is the preferred signal to use, and accordingly, was set to 2H. The number of H in the relative diagnostic signals for each cannabinoid (δ 9THC-A = 12.19 (s, 1H), CBD-A = 11.93 (s, 1H), 9THC = 3.20 (dm, 1H), 8THC = 2.70 (td, 1H), CBD = 5.57 (s, 1H), and CBN = 8.16 (s, 1H)) was determined relative to this value. The values determined by integrating the relevant signals, combined with the known masses, can be entered into the following equation (Figure 6.1) to provide cannabinoid purity, as a %, of the sample in question.

$$P\%(sample) = \frac{I(sample)}{I(standard)} \times \frac{N(standard)}{N(sample)} \times \frac{m(standard)}{m(sample)} \times \frac{M(sample)}{M(standard)} \times P\%(standard)$$

Figure 6.1: Equation for determining purity of a compound using qNMR. I = integration of signal, N = number of H in signal, m = mass (g), M = Molar mass (g/mol), and P = purity.

6.1.7.3 Examples

Table 6.1: Examples of characteristic shifts of cannabinoids that can be used for qNMR. Careful consideration into selecting the chemical shift for qNMR, especially if more than one cannabinoid exists in the sample as they may overlap.

Cannabinoid	Characteristic shifts in ^{1}H NMR spectrum ($CDCl_3$)
CBD-A	11.93 (s, 1H)
CBD	4.55 (m, 1H) 4.40 (m, 1H), 4.09 (m, 1H)
9THC-A	12.19 (s, 1H)
9THC	6.14 (d, 1H), 4.87 (s, 1H), 3.20 (dm, 1H)
8THC	2.70 (td, 1H), 4.82 (s, 1H)
CBN	8.16 (s, 1H)

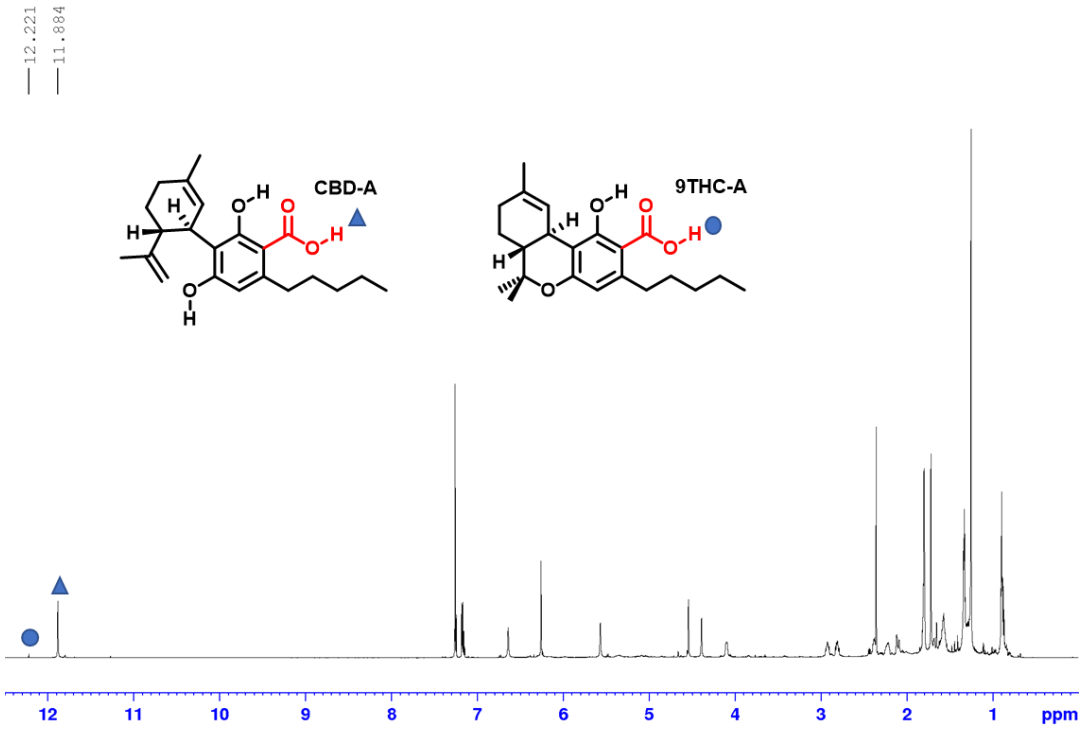

Figure 6.2: Example of quantitative ^{1}H NMR spectrum of hemp extract in $CDCl_3$ (298 K). Notable 9THC-A and CBD-A signals are indicated (δ 12.22 and 11.88)

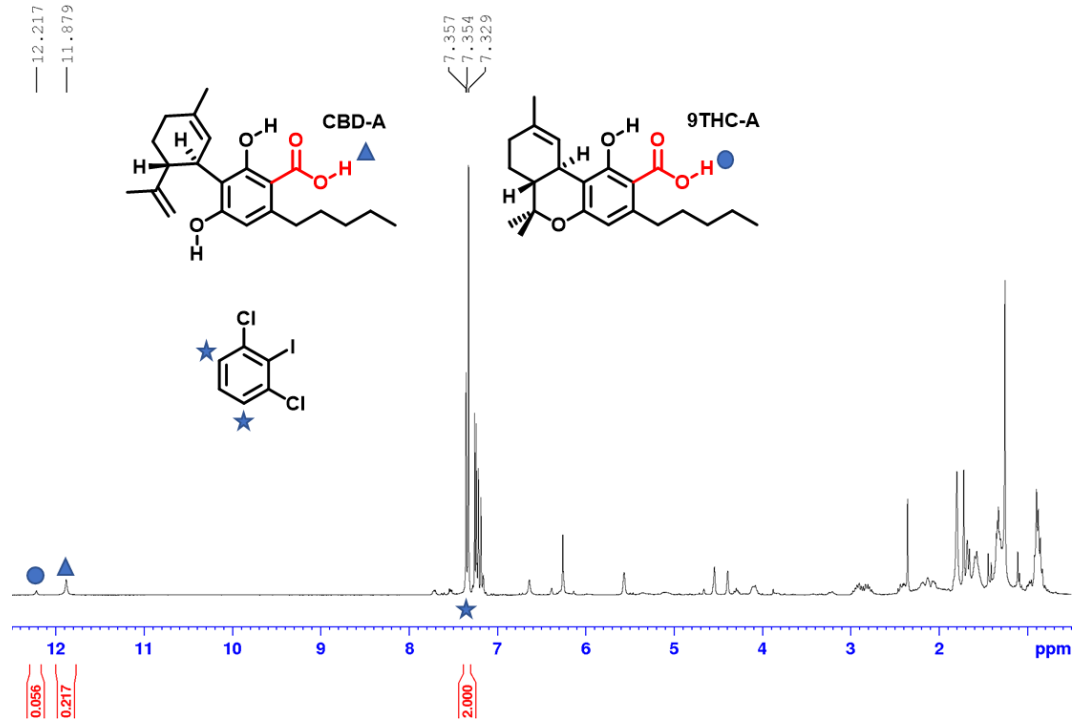

Figure 6.3: Example of quantitative ^{1}H NMR spectrum of hemp extract in $CDCl_3$ (298 K). Notable 9THC-A and CBD-A signals are indicated (δ 12.22 and 11.88). The doublet of 1,3-dichloro-2-iodobenzene selected for quantitative analysis is indicated (δ 7.35). Standard = 7.4 mg, extract = 6.0 mg, 9.08% 9THC-A and 35.2% CBD-A.

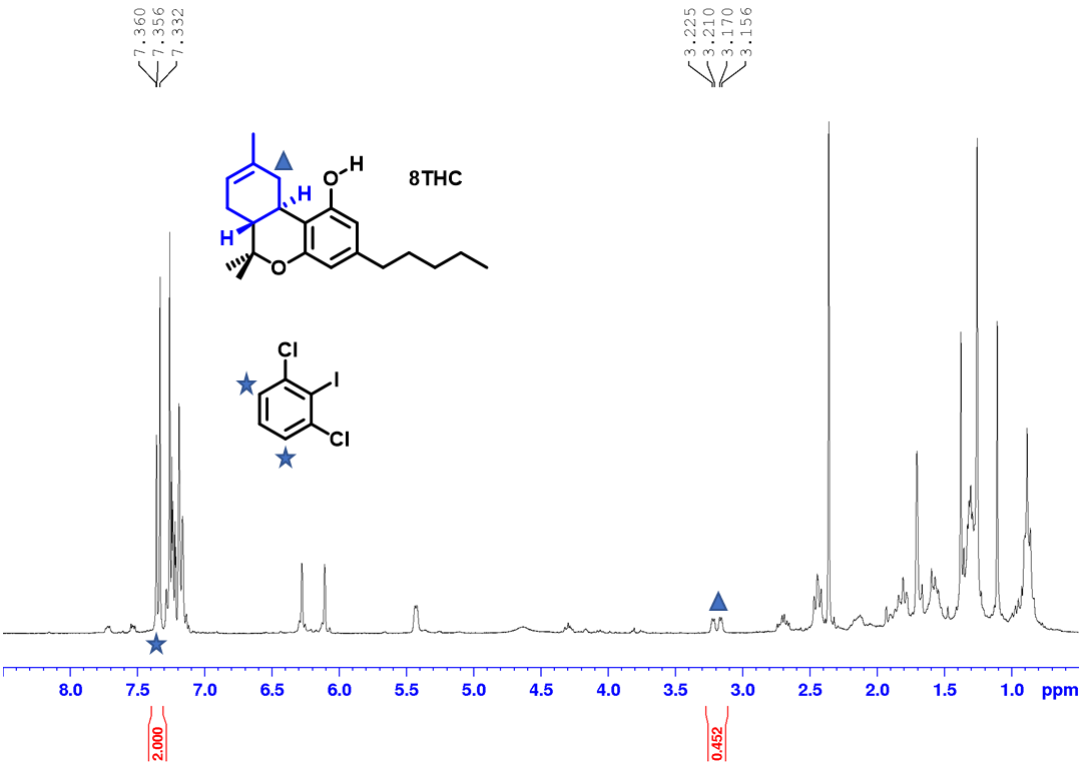

Figure 6.4: Example of quantitative ^{1}H NMR spectrum in $CDCl_3$ (298 K) of hemp extract after reaction with *p*-TsOH. Notable 8THC signa identified (δ 3.19). The doublet of 1,3-dichloro-2-iodobenzene selected for quantitative analysis is indicated (δ 7.35). Standard = 9.3 mg, extract = 6.5 mg, 74.5% 8THC.

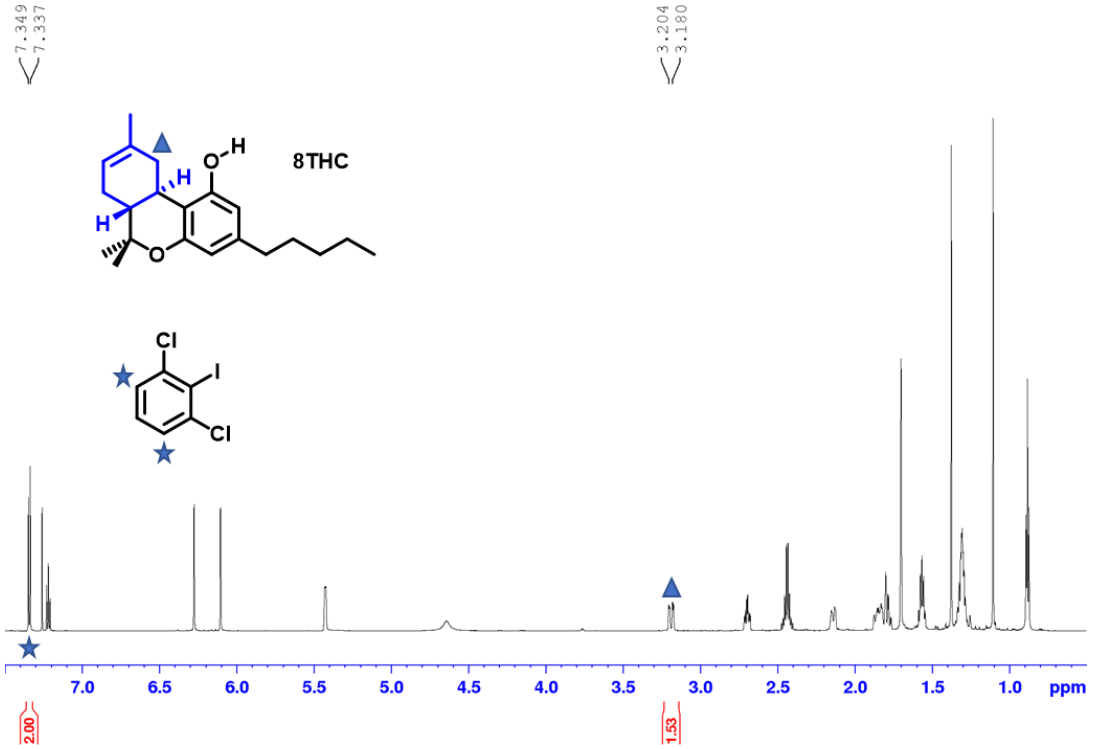

Figure 6.5: Example of quantitative ^{1}H NMR spectrum in $CDCl_3$ (298 K) of 8THC. Notable 8THC signal identified (δ 3.19). The doublet of 1,3-dichloro-2-iodobenzene selected for quantitative analysis is indicated (δ 7.35). Standard = 4.2 mg, 8THC sample = 2.2 mg, 92.4% 8THC.

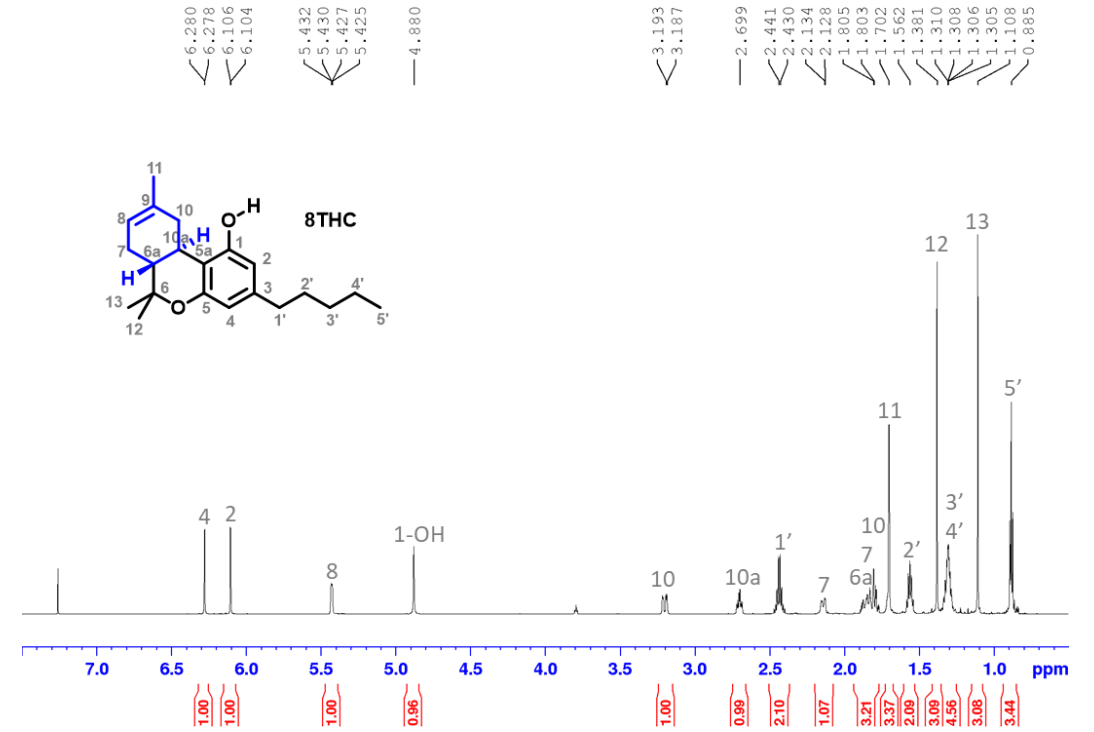

Figure 6.6: Example of ^{1}H NMR spectrum in $CDCl_3$ (298 K) of 8THC showing signals and integrations of all resonances which matched literature values.[367]

Table 6.2: Examples of toluene extractions and results of quantitative ^{1}H NMR spectroscopy in $CDCl_3$ (298 K).

Sample #	Biomass (mg)	Extract (mg)	% extract of biomass	Extract in NMR (mg)	Standard (mg)
1	543.0	81.4	15.0	7.4	6.0
2	543.0	77.8	14.3	8.0	5.5
3	501.0	69.6	13.9	4.9	4.0
4	1193.0	218.4	18.3	5.1	3.7
5	4783.4	814.9	17.0	6.1	5.1

Sample #	% CBD-A	% THC-A	Total cannabinoid % in extract	Total cannabinoid % in biomass
1	35.2	9.1	44.3	6.6
2	38.4	8.6	47.0	6.7
3	40.9	8.1	49.0	6.8
4	35.8	8.9	44.7	8.1
5	37.6	8.8	46.4	7.9

6.1.8 Computational Methods

6.1.8.1 Modelling Associated with 8THC (Section 5.4.1.1)

Models for 9THC, 8THC and 7THC were built with the native pentyl substituent replaced with a methyl group, thereby reducing the flexibility of the substituent and the number of modelled atoms. This decreased the computational complexity associated with searching the broader conformational space. Further reduction of the model to a hydrogen atom had little impact on the values of kinetic and thermodynamic parameters under consideration. All geometries were optimized in the gas phase using the B3LYP functional, while including Grimme's empirical dispersion correction with Becke-Johnson damping (D3(BJ)), in conjunction with the 6-31+G(d,p) basis set. The nature of each stationary point was confirmed with frequency calculations at the same level of theory. The transition state for conversion between 9THC and 8THC was isolated by

adding a single *para*-toluenesulfonioc acid (*p*-TsOH) molecule to the model. Intrinsic reaction coordinate (IRC) calculations were performed from the transition structure to confirm the nature of the associated reactant and product, which were subsequently fully optimized at the same level of theory. All reported relative energies were obtained using B3LYP-D3(BJ)/6-311+G(2df,2p) single-point calculations, which include zero-point corrections and thermal energy corrections to the Gibbs free energy. All energies are reported in kJ mol^{-1}, bond lengths in Angstroms (Å) and angles in degrees (º). All calculations were performed with the Gaussian 16 suite of programs.

6.1.8.2 Modelling Associated with the *ortho*-Quinone Cannainoids (Section 5.5.2)

A computational study on *o*-qCBN and *o*-q8THC was undertaken with full geometry optimization using hybrid DFT methods supplemented by empirical dispersion at the B3LYP-D3BJ/6-311+G(d,p) level of theory, including a solvation model. A more detailed investigation, also with geometry optimization, but without solvation, was undertaken on the series of charge states Q, $Q^{\bullet-}$ and Q^{2-} using a slightly simplified model. All energies are reported in kJ mol^{-1}, bond lengths in Angstroms (Å) and angles in degrees (º). All calculations were performed with the Gaussian 16 suite of programs.

6.1.9 Voltammetry

Cyclic voltammetry (CV) and square wave voltammetry (SWV) were performed in a nitrogen-atmosphere glove box using a Princeton Applied Research Potentiostat (PARSTAT) 2273 and the associated PowerSuite software. Satisfactory background scans were obtained before the addition of analyte, and plots of peak currents vs. square root of scan rates verified that the observed voltammetric peaks were due to diffusion-controlled processes. All redox processes were assessed at scan rates from 50 mV/s to

5000 mV/s. DMF was dried over 3 Å molecular sieves for 72 h, degassed with 6 freeze–pump–thaw cycles, and stored over 3 Å molecular sieves in a thick-walled (5 mm) glass vessel sealed with a Kontes® valve in an argon-filled glove box.[368] 8.62 mg of *o*-q8THC was dissolved in 5.0 mL of DMF (5.5 mM *o*-q8THC) with 0.78 g of $[Bu_4N][PF_6]$ (400 mM) as supporting electrolyte. 8.58 mg of *o*-qCBN was dissolved in 5.0 mL of DMF (5.5 mM) with 0.81 g of $[Bu_4N][PF_6]$ (420 mM) as supporting electrolyte. For both compounds, the working electrode was a 3 mm diameter Pt macrodisc, the reference electrode was Ag wire in a Luggin capillary, and the auxiliary electrode was a coil of bare Pt wire. Voltammograms were also obtained using a 3 mm diameter glassy carbon (GC) macrodisc electrode, but peaks were more discernible and line shapes better resolved using the Pt macrodisc electrode. Sublimed ferrocene (Fc) was added to the solutions towards the end of the analysis and used as an internal reference ($Fc^{+/0}$ = 0.0 V).

6.1.9.1 Voltammetry Experiments with *o*-q8THC

The scan-rate dependencies of the peak currents for oxidation and reduction for step I were shown to have a linear dependence of current on the square-root of the scan rate, indicative of diffusion-controlled processes in DMF solution at the heterogeneous electrode interface. Thus, an understanding of the processes revealed by the voltammetry experiments were sought in solution-phase chemical and electrochemical processes.

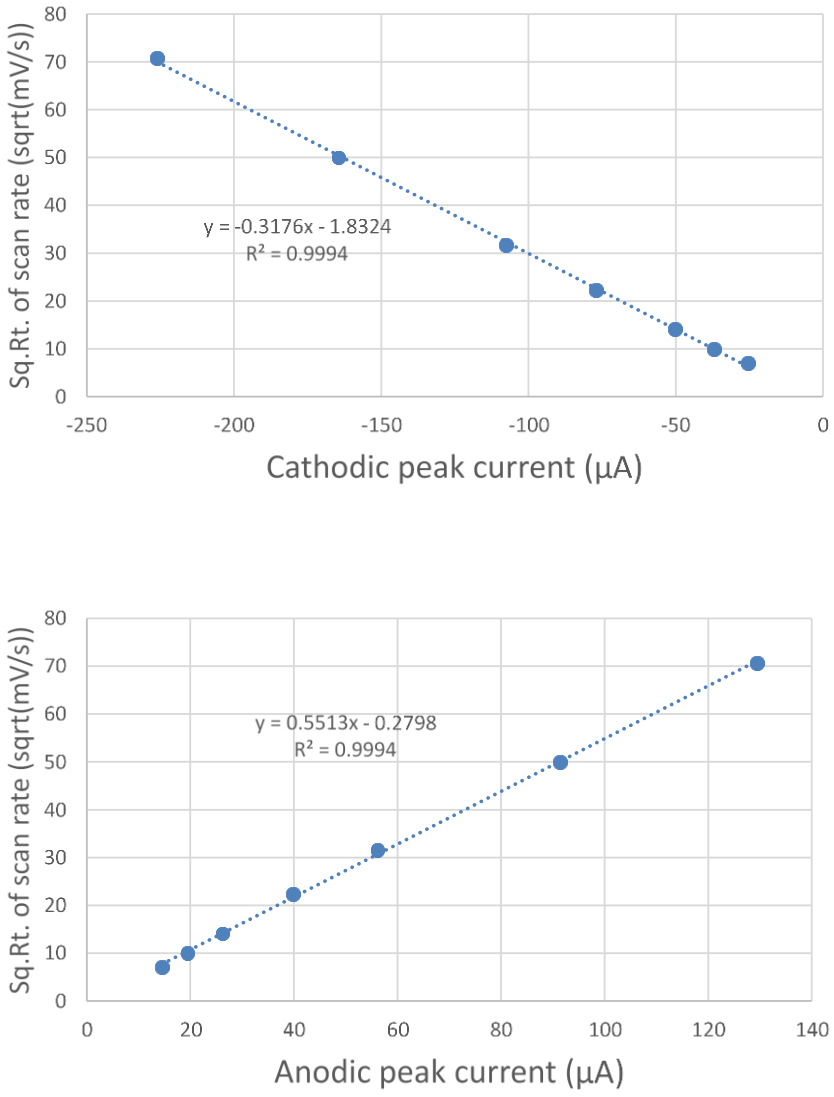

Figure 6.7: Plot of cathodic (top) and anodic (bottom) peak current vs. square root of the scan rate for *o*-q8THC from 50 mV/s to 5000 mV/s for the first reduction step $\boldsymbol{I_p^{cl}}$, and the re-oxidation $\boldsymbol{I_p^{al}}$, respectively.

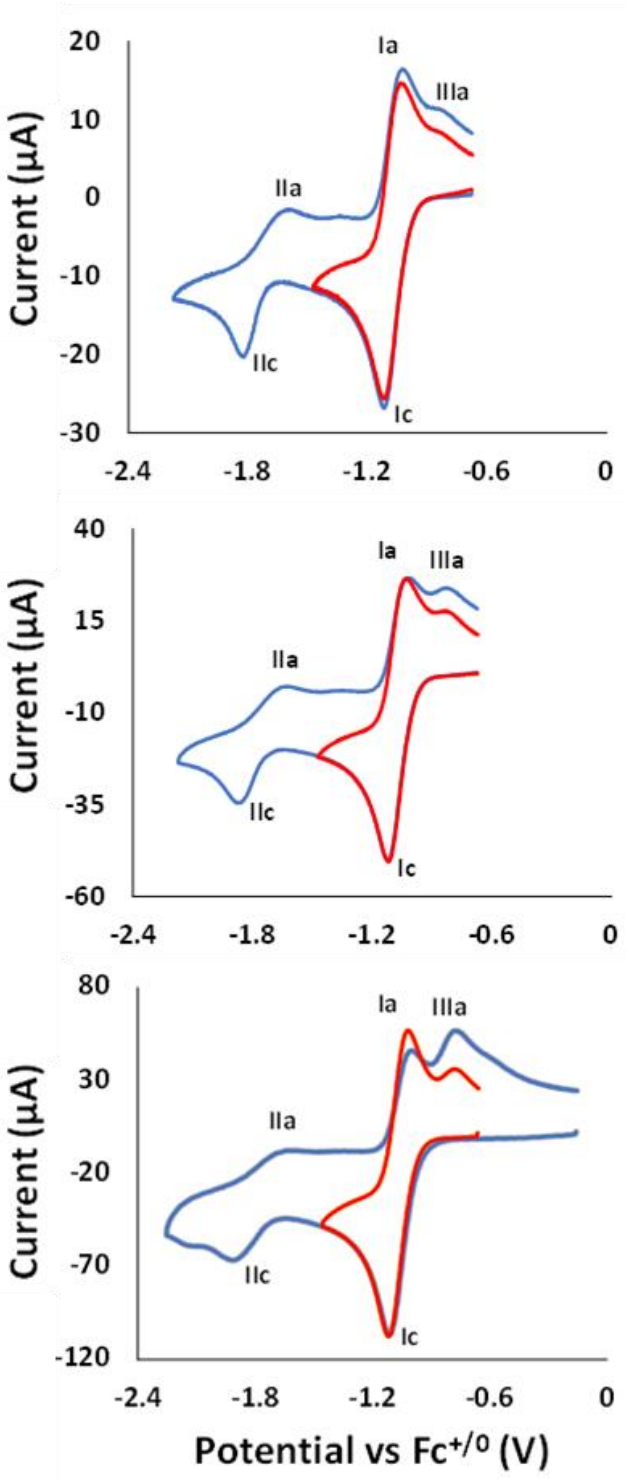

Figure 6.8: Overlay of *o*-q8THC cyclic voltammograms (CV) covering both first and second reduction processes in DMF containing $[Bu_4N][PF_6]$ at a Pt macrodisc electrode. Scan rates (top to bottom): 50mV/s; 200mV/s; 1000mV/s.

6.1.9.2 Voltammetry Experiments with *o*-qCBN

Despite the significantly different overall appearance of the CV traces, linear dependence of current on the square-root of the scan rate of peak currents for reduction process I and the merged re-oxidations I/III indicate diffusion-controlled voltammetry. Here too, the anomalous appearance of the voltammograms should be interpreted through solution-phase chemical processes involving the analyte and dissolved reactants. For *o*-qCBN, the CV peak shapes are inferior at a GC WE macrodisc compared to those at platinum. This is consistent with recent reports of the effects of surface-defects on GC WE on the voltammetry of quinones.[369]

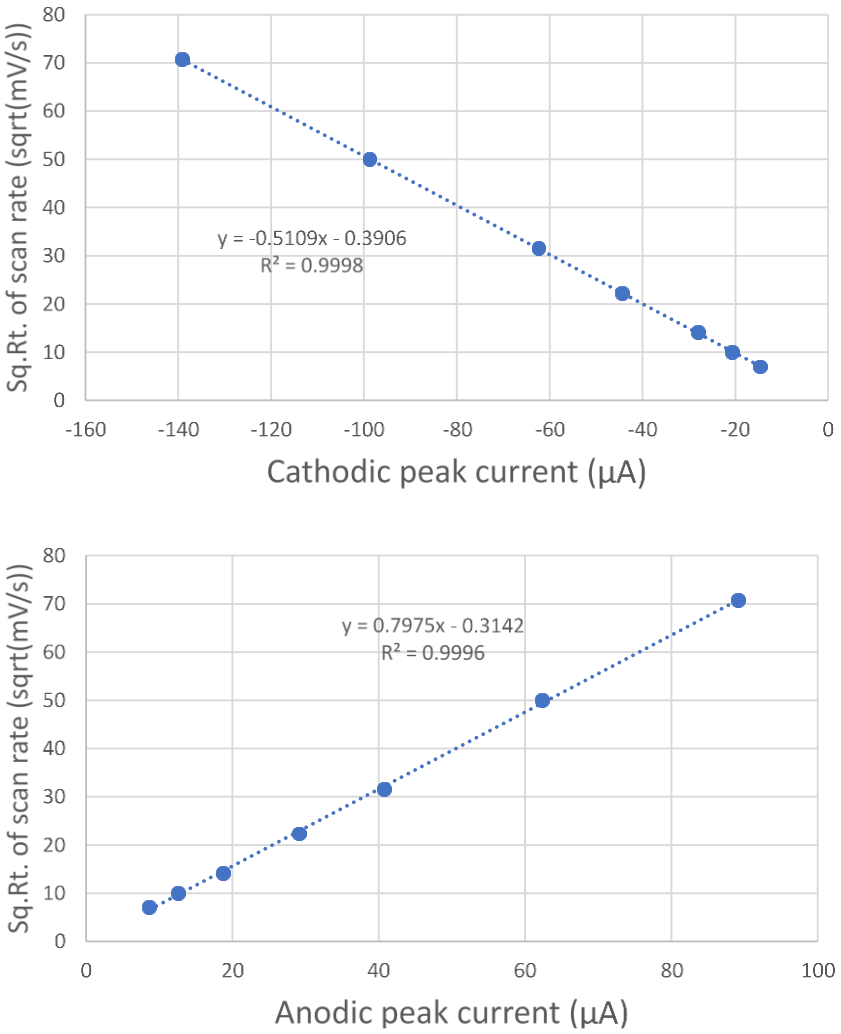

Figure 6.9: Plot of cathodic (top) and anodic peak (bottom) current vs. square root of the scan rate for *o*-qCBN from 50 mV/s to 5000 mV/s for the first reduction step $\boldsymbol{I_p^{cI}}$, and the merged re-oxidation processes $\boldsymbol{I_p^{aI/III}}$, respectively.

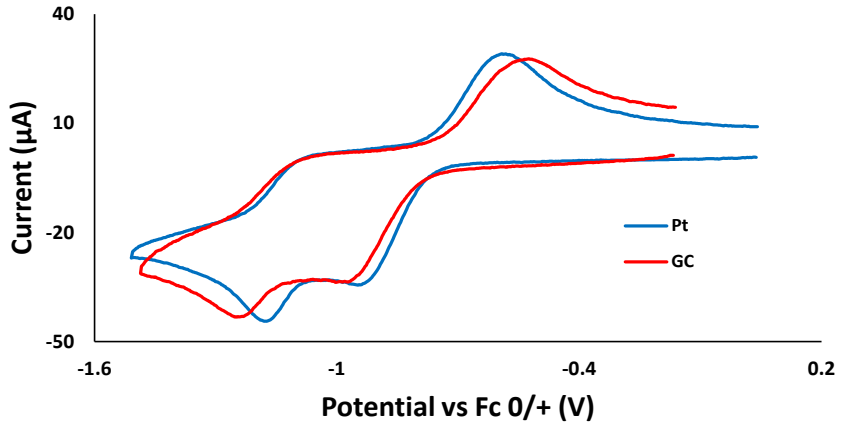

Figure 6.10: Overlay of *o*-qCBN CVs to compare performance of Pt and GC working electrodes.

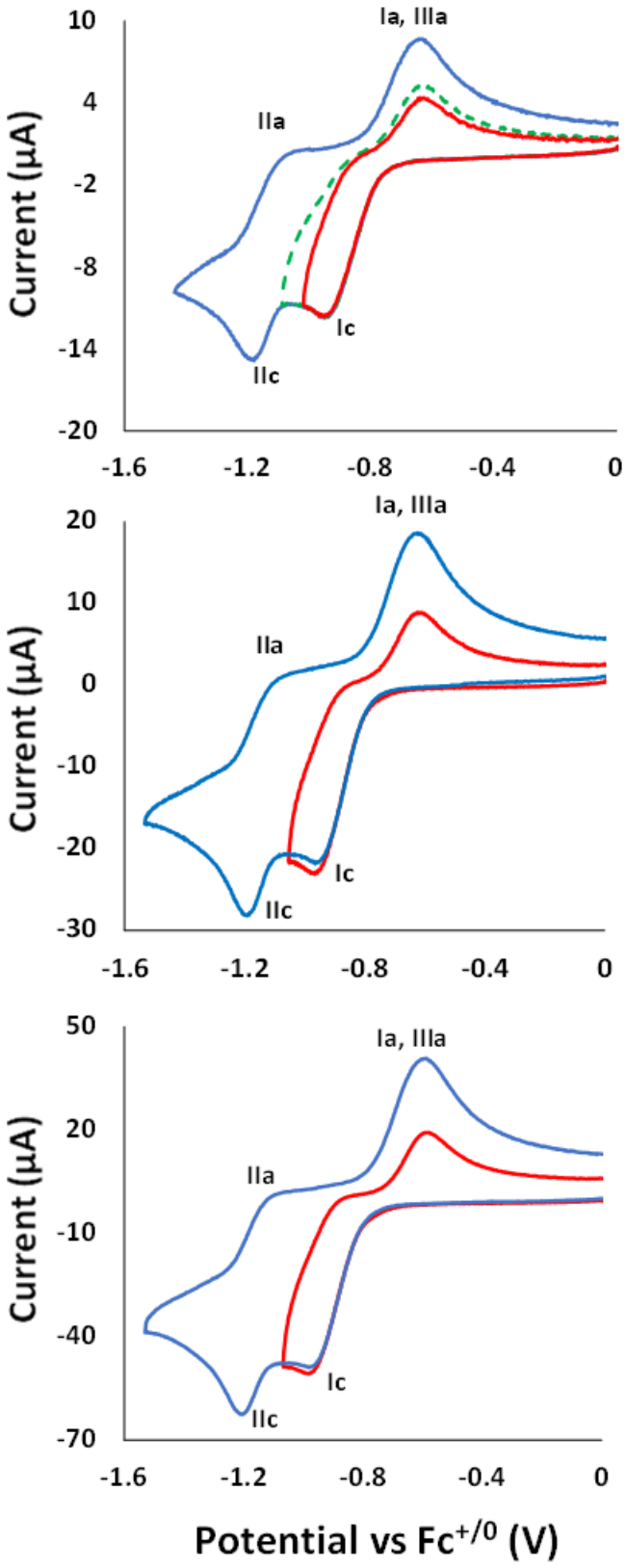

Figure 6.11: Overlay of *o*-qCBN voltammograms covering both first and second reduction processes. Scan rates (Top to bottom): 50mV/s; 200mV/s; 1000mV/s.

6.2 Synthetic Methods and Characterizations

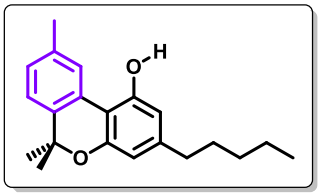

Synthesis of cannabinol production (CBN) From extract: Extract (420 mg) was dissolved in toluene (approximately 10 mL per 100 mg) and added to a thick-walled 500 mL glass vessel sealed with a Kontes® valve and charged with a Teflon® coated stir bar. Elemental iodine (268 mg or approximately 1 mg per 2 mg of extract) was added to the mixture which was heated to 130 ˚C for 3.5 h with stirring. The solution retained a dark-purple colour for the duration of heating. The reaction mixture was allowed to cool to ambient temperature and was washed with a saturated aqueous solution of $Na_2S_2O_3$ (3 × 10 mL). The organic fractions were combined, dried with $MgSO_4$ and gravity filtered. The volatiles were removed *in vacuo* yielding a dark-yellow oil. Purification was conducted using flash silica chromatography with 9:1 petroleum ether:diethyl ether used for the mobile phase (R_f = 0.32) or hexanes:diethyl ether at R_f = 0.51. A yield of 81.3 mg of 92% pure CBN (confirmed *via* qNMR) was obtained for this sample (N.B. Yield varies slightly between samples). Spectra were consistent with that reported in the literature.[370]

From CBD: A 50 mL round-bottomed flask equipped with a Teflon® coated stir bar was charged with CBD (189 mg, 0.601 mmol) and dissolved in toluene (20 mL). I_2 (268 mg, 1.06 mmol) was added to the light-yellow solution. A reflux condenser was attached, and the reaction mixture was heated to reflux for 1 h. The reaction mixture was allowed to cool to ambient temperature and then washed with a saturated solution of sodium thiosulfate (3 × 10 mL). The organic fractions were collected, dried with $MgSO_4$ and gravity filtered. The volatiles were then removed under reduced pressure yielding a dark-yellow oil. This oil was typically of sufficient purity for use in

subsequent reactions; if purification was necessary, flash silica chromatography using 9:1 petroleum ether:diethyl ether as the mobile phase was performed (Yield: 161 mg, 86.2 %, R_f = 0.32). Spectra were consistent with those reported in the literature.[367]

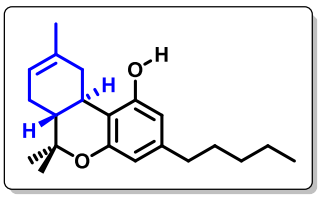

Synthesis of Δ^8-tetrahydrocannabinol (8THC) From biomass of *Cannabis sativa*: The biomass (3.8 g) was crushed using a motor and pestle to generate a fine green powder. Toluene (100 mL) was added to the biomass and the mixture was stirred for 20 min. The mixture was then filtered to give a golden solution. This step was repeated twice more, thereafter the golden colour diminished greatly. The toluene washings were combined, and volatiles removed *in vacuo* to yield a thick brown oil (0.670 g, 13-18% of the biomass). qNMR experiments indicated the extract was 24.5% CBD-A and 5.6% 9THC-A. The brown oil, herein described as "extract", was dissolved in toluene (10 mL) in a thick-walled glass vessel equipped with a Kontes® valve. *p*-TsOH (0.054 g, 0.282 mmol) was added (0.5 molar equivalents of the total cannabinoid content of the extract) to the mixture. The container was sealed and heated to 130 ˚C for 3.5 hours. The solution was cooled to ambient temperature, and then a saturated solution of $NaHCO_3$ was added (10 mL). The organic fraction was separated and washed with saturated $NaHCO_3$ solution (15 mL) two further times. The organic fractions were collected, and volatiles removed under reduced pressure to produce a thick brown oil. The crude product was determined by qNMR to contain 46.1% 8THC. Using silica as the stationary phase and petroleum ether:diethyl ether (97.5:2.5) or hexanes:diethyl ether (97.5:2.5) as the mobile phase, 8THC was isolated (*Rf* = 0.28 or R_f = 0.45, respectively). qNMR revealed the product to be 91.8% 8THC (0.144 g).

From CBD: A 50 mL round-bottomed flask equipped with a Teflon® coated stir bar was charged with CBD (202 mg, 0.642 mmol) dissolved in toluene (20 mL). *para*-Toluene sulfonic acid (123 mg, 0.644 mmol) was added to the light-yellow solution. A reflux condenser was attached, and the mixture was heated to reflux for 1 h. The reaction mixture was allowed to cool to ambient temperature and was quenched with a saturated solution of $NaHCO_3$ (50 mL). The organic fraction was further washed with saturated solutions of $NaHCO_3$ (2 × 10 mL), following which, the aqueous fractions were collected, and all organic compounds were extracted with toluene (10 mL). The organic fractions were combined, dried with $MgSO_4$ and gravity filtered. The volatiles were then removed under reduced pressure, yielding a dark-yellow oil. This oil was typically of sufficient purity to use in subsequent reactions; if purification was necessary, flash silica chromatography was conducted using 85:15 petroleum ether:diethyl ether as the mobile phase (Yield: 124 mg, 61.1%, R_f = 0.55). Spectra were consistent with those reported in the literature.[367]

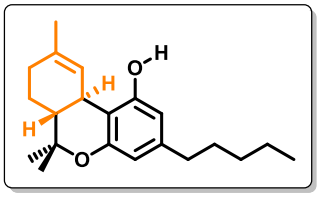

Synthesis of Δ^9-tetrahydrocannabinol (9THC) From extract: Extract (815 mg) was dissolved in toluene (approximately 10 mL per 100 mg of extract) and added to a thick-walled 500 mL glass vessel sealed with a Kontes® valve and charged with a Teflon® coated stir bar. The mixture was heated to 130 ˚C for 3.5 h with stirring. The solution was allowed to cool to ambient temperature, at which point the mixture contained only the decarboxylated cannabinoids (CBD and 9THC). The mixture was transferred to a 50 mL two-necked round-bottomed flask and volatiles were removed under vacuum. DCM (20 mL) was distilled onto the mixture. The resulting solution was placed under an inert atmosphere of argon and cooled to 0 °C whereupon $BF_3{\cdot}Et_2O$ (130 µL or 1 µL per 4.5 mg of extract) was added *via* syringe over 5 min. The solution changed from dark-

amber to green over the course of 2 h after which the reaction was quenched with a saturated aqueous solution of $NaHCO_3$ (20 mL) The organic fraction was further washed with additional saturated solution of $NaHCO_3$ (2 × 10 mL). The aqueous fractions were combined and extracted with DCM (2 × 10 mL). All organic fractions were combined, dried with $MgSO_4$ and gravity filtered. The volatiles were removed *in vacuo* yielding a dark-yellow oil. Purification was conducted using flash silica chromatography with 85:15 petroleum ether:diethyl ether as the mobile phase (R_f = 0.95) giving a yield of 69.1 mg of 85% pure 9THC (confirmed *via* qNMR) for this sample (N.B. Yield varies slightly between samples). Spectra were consistent with literature.[370]

From CBD: A 50 mL two-necked round-bottomed flask equipped with a Teflon® coated stir bar was charged with CBD (244 mg, 0.776 mmol). DCM (~25 mL) was transferred into the flask under reduced pressure. The resulting light-yellow solution was placed under an atmosphere of argon and kept at 0 °C whereupon boron trifluoride etherate (0.040 mL, 0.326 mmol) was added via syringe over 30 seconds. The solution changed from light-yellow to dark-amber over 2 h after which the reaction was quenched with a saturated solution of $NaHCO_3$ (50 mL). The organic fraction was further washed with saturated solutions of $NaHCO_3$ (2 × 10 mL). The aqueous fractions were collected, and organic compounds were extracted with DCM (10 mL). The organic fractions were combined, dried with $MgSO_4$ and gravity filtered. The volatiles were then removed *in vacuo* yielding a dark-yellow oil. This oil was typically of sufficient purity to use in subsequent reactions; if purification was necessary, flash silica chromatography using 55:45 petroleum ether:diethyl ether as the mobile phase was performed (Yield: 168 mg, 69.0%, R_f = 0.95). Spectra were consistent with those reported in the literature.[367]

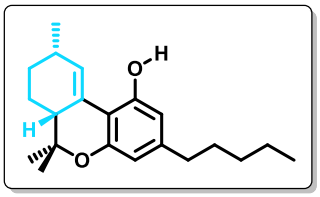

Synthesis of (*R*,*S*)-Δ^{10}-Tetrahydrocannabinol (10THC) A two-necked round-bottomed flask equipped with a Teflon® coated stir bar was charged with CBD (200 mg, 0.636 mmol) and attached to a double manifold vacuum line. Under an argon atmosphere dichloromethane (20 mL) was distilled into the flask and the solution cooled to –10 °C using an ice/acetone bath. $BF_3{\cdot}Et_2O$ (33.0 µL, 0.267 mmol) was added to the stirring colourless solution causing it to become light-yellow. The reaction mixture was stirred for an additional 1.5 h whereupon the reaction changed to an amber colour. Under air the mixture was washed with a saturated aqueous solution of $NaHCO_3$ (3 × 10 mL), dried with $MgSO_4$ and filtered. Volatiles were removed *in vacuo*. In a 50 mL round bottomed flask, under an atmosphere of argon, HMPA (10 mL) was added to the 9THC-containing residue, producing a light-yellow solution which was cooled to 0 °C. A solution of ^{n}BuLi (1.5 mL, 3.75 mol, 2.5 M in hexanes) was added dropwise over 15 min to the stirring solution which slowly became dark-green, and subsequently, deep cherry red in colour. The solution was left to react at 0 °C for 1.5 h. The excess ^{n}BuLi was quenched with ^{i}PrOH (10 mL), followed by a 1.0 M solution of HCl (10 mL). Diethyl ether (20 mL) was used to extract the organic soluble components, which were washed once with a saturated aqueous solution of $NaHCO_3$ (5 mL), followed by a saturated aqueous solution of sodium chloride (5 mL) before being dried over $MgSO_4$. The volatiles were removed under reduced pressure to afford a thick colourless oil. For purification *via* silica chromatography, either a mobile phase of 85:15 petroleum ether:diethyl or 3:2 hexanes:diethyl ether was employed to give 10THC as a thick light-yellow oil (R_f = 0.48 or R_f = 0.88 respectively) (94 mg, 46.8% yield). X-ray quality crystals of 10THC were obtained by dissolving the oil in hexanes and cooling the solution to –20 °C. In 2 days, white crystals of 10THC were obtained. Recrystallized

yield: 43 mg (21.5%). ^{1}H NMR (700 MHz, C_6D_6): δ 6.93 (d, $^{3}J_{HH}$ = 7.0 Hz, 1H, H10), 6.61 (d, $^{4}J_{HH}$ = 3.9 Hz, 1H, H4), 5.86 (d, $^{4}J_{HH}$ = 3.9 Hz, 1H, H2), 4.73 (s, 1H, OH), 2.39 (t, $^{3}J_{HH}$ = 7.4 Hz, 2H, H1'), 2.35 (m, 1H, H9), 2.32 (m, 1H, H6a), 1.49-1.58 (br ov m, 3H, H8B and H2'), 1.35 (m, 1H, H7A), 1.30 (s, 3H, H12), 1.18-1.27 (br ov m, 5H, H8A, H3' and H4'), 1.13 (m, 1H, H7B), 1.08 (s, 3H, H13), 0.97 (d, $^{3}J_{HH}$ = 6.6 Hz, 3H, H11), 0.84 (t, $^{3}J_{HH}$ = 7.0 Hz, 3H, H5'). ^{13}C{^{1}H} NMR (176 MHz, C_6D_6): δ 155.25 (C1), 155.04 (C5), 143.70 (C5a), 131.07 (C10), 128.69 (C10a), 110.66 (C4), 108.74 (C2), 108.36 (C3), 78.11 (C6), 43.87 (C6a), 36.22 (C1'), 32.10 (C3'), 31.32 (C2'), 30.00 (C9), 28.48 (C8), 28.07 (C12), 23.29 (C4'), 21.41 (C11), 20.63 (C7), 20.45 (C13) 14.58 (C5'). Anal. Calcd for $C_{21}H_{30}O$: C 80.21; H 9.62. Found: C 80.20; H 9.66. Mp: 147.1-148.5 °C.

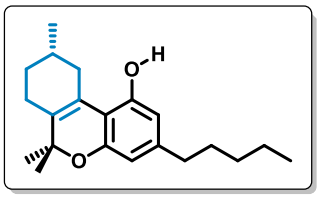

Synthesis of *R*-Δ^{10a}-Tetrahydrocannabinol (10aTHC) A sample of 10THC was exposed to wet $CDCl_3$, causing complete isomerization to 10aTHC in 1 h. Removal of the volatiles *in vacuo* gave 10aTHC as a yellow oil. ^{1}H NMR (700 MHz, $CDCl_3$): δ 6.31 (d, $^{4}J_{HH}$ = 1.8 Hz, 1H, H4), 6.14 (d, $^{4}J_{HH}$ = 1.8 Hz, 1H, H2), 4.67 (s, 1H, 1-OH), 2.64 (m, 1H, H8A), 2.46 (m, 2H, H1'), 2.30 (m, 1H, H8B), 2.20 (m, 1H, H7B), 2.08 (m, 1H, H7A), 1.78 (m, 1H, H10A), 1.65 (m, 1H, H9), 1.56 (m, 2H, H2'), 1.42 (s, 3H, H13), 1.31 (ov m, 4H, H3' and H4'), 1.30 (m, 1H, H10B), 1.22 (s, 3H, H12), 1.03 (d, $^{3}J_{HH}$ = 6.6 Hz, 3H, H11), 0.88 (t, $^{3}J_{HH}$ = 7.0 Hz, 3H, H5'). ^{13}C{^{1}H} NMR (176 MHz, $CDCl_3$): δ 153.93 (C1), 152.01 (C5), 143.49 (C5a), 133.18 (C6a), 123.17 (C10a), 110.63 (C3), 109.81 (C4), 109.70 (C2), 77.58 (C6), 36.86 (C8), 35.61 (C1'), 31.58 (C3'), 30.68 (C10), 30.66 (C2'), 29.05 (C9), 25.77 (C13), 25.64 (C7), 23.82 (C12), 22.69 (C4'), 22.01 (C11), 14.18 (C5'). Anal. Calcd for $C_{21}H_{30}O$: C 80.21; H 9.62. Found: C 80.81; H 9.71.

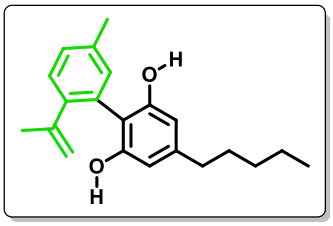

Synthesis of cannabinodiol (CBND) An oil containing >90% CBN (110 mg) was dissolved in CyH (3 mL) and added to a quartz cuvette charged with a Teflon® coated stir bar which was subsequently sealed with a ground glass joint. While stirring, the solution was exposed to UV (253 nm, 0.00128 W m^{-2}) radiation for 24 h. After the allocated time, the solution was dark-orange in colour. The volatiles were removed *in vacuo* yielding a dark-orange oil. Purification was conducted using flash silica chromatography with 7:3 hexane:diethyl ether used for the mobile phase (R_f = 0.33). Yield: 79 mg (71.8%). NMR spectra were consistent with literature (Figures S21 and S22).[337] ^{1}H NMR (300 MHz, C_6D_6): δ 7.13 (d, $^3J_{HH}$ = 9.0 Hz, 1H, H7), 6.88 (d, $^3J_{HH}$ = 9.0 Hz, 1H, H8), 6.82 (s, 1H, H10), 6.53 (s, 2H, H2 and H4), 4.92 (s, 2H, H12), 4.47 (s, 2H, 1-OH and 5-OH), 2.43 (t, $^3J_{HH}$ = 7.0 Hz, 2H, H1'), 1.97 (s, 3H, H11), 1.80 (s, 3H, H13), 1.53 (m, 2H, H2'), 1.21 (ov m, 4H, H3' and H4'), 0.84 (t, $^3J_{HH}$ = 6.9 Hz, 3H, H5'). ^{13}C{^{1}H} NMR (75 MHz, C_6D_6): δ 154.43 (C5a), 145.67 (C6), 145.55 (C6a), 143.58 (C10a), 138.68 (C9), 133.52 (C10), 130.48 (C8), 130.25 (C3), 129.26 (C7), 116.26 (C12), 113.87 (C1 and C5), 108.38 (C2 and C4), 36.56 (C1'), 32.12 (C3'), 31.48 (C2'), 23.52 (C13), 23.25 (C4'), 21.12 (C11), 14.59 (C5').

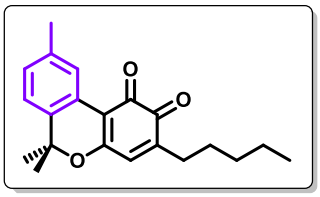

Synthesis of *ortho*-quinone-cannabinol (*o*-qCBN) A 50 mL round-bottomed flask containing a Teflon® coated stir bar was charged with CBN (80.0 mg, 0.258 mmol). Dimethylformamide (5 mL) was added creating a pale-yellow solution. 2-Iodoxybenzoic acid (144 mg, 0.515 mmol) was added in small portions to the stirring solution over a period of 10 min. After 30 min the reaction mixture became dark-red; a rusty brown colour was obtained within 1 h. The reaction mixture was stirred for 16 h. All volatiles were removed under reduced pressure at 40 °C. The waxy residue was

purified *via* silica chromatography: 3:2 petroleum ether: diethyl ether was used as the mobile phase giving analytically pure *o*-qCBN at R_f = 0.62 as a dark-purple oil (Yield: 44.0 mg, of 52.6%). ^{1}H NMR (700 MHz $CDCl_3$): δ 8.31 (d, $^4J_{HH}$ = 1.0 Hz, 1H, H10), 7.10 (dd, $^3J_{HH}$ = 7.8 Hz, $^4J_{HH}$ = 1.0 Hz, 1H, H8), 7.03 (d, $^3J_{HH}$ = 7.8 Hz, 1H, H7), 6.64 (t, $^4J_{HH}$ = 1.7 Hz, 1H, H4), 2.41 (td, $^3J_{HH}$ = 9.0 Hz, $^4J_{HH}$ = 1.7 Hz, 2H, H1'), 2.37 (s, 3H, H11), 1.71 (s, 6H, H12 and H13), 1.53 (m, 2H, H2'), 1.38-1.31 (br ov m, 4H, H3' and H4'), 0.91 (t, $^3J_{HH}$ = 6.9 Hz, 3H, H5'). ^{13}C{^{1}H} NMR (176 MHz $CDCl_3$): δ 180.36 (C1), 176.14 (C2), 163.32 (C5), 144.58 (C3), 137.96 (C9), 133.81 (C4), 131.75 (C6a), 128.91 (C8), 125.70 (C10), 124.71 (C10a), 122.30 (C7), 110.84 (C5a), 82.66 (C6), 31.43 (C3'), 29.01 (C1'), 28.33 (C12 and C13), 27.38 (C2'), 22.40 (C4'), 21.42 (C11), 13.96 (C5'). IR (FTIR): ν_{max} (cm^{-1}) 2924 (C-H), 1684 (C=O), 1638 (C=O), 1582 (C=C), 1383 (C=C), 1187 (C–O), 1111 (C–O). Anal. Calcd for $C_{21}H_{24}O_3$: C 77.75; H 7.46. Found: C 77.83; H 7.14.

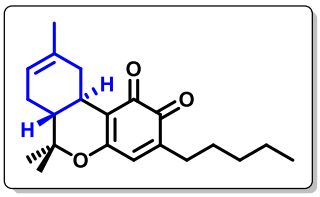

Synthesis of *ortho*-quinone-Δ^8-tetrahydrocannabinol (*o*-q8THC) A 50 mL round-bottomed flask containing a Teflon® coated stir bar was charged with 8THC (135 mg, 0.429 mmol). Dimethylformamide (5 mL) was added creating a pale-yellow solution. 2-Iodoxybenzoic acid (192 mg, 0.686 mmol) was added in small portions to the stirring solution over a period of 10 min. After 30 min the reaction mixture became intensely red, obtaining a cherry red colour in 1 h. The reaction mixture was stirred for 16 h during which it became dark-red. All volatile components were removed under reduced pressure at 40 °C. The waxy residue was purified *via* silica chromatography; 1:1 petroleum ether:diethyl ether was used as the mobile phase giving analytically pure *o*-q8THC (R_f = 0.79) as an intense red oil (Yield: 71.9 mg, 51%). ^{1}H NMR (700 MHz,

$CDCl_3$): δ 6.48 (s, 1H, H4), 5.38 (s, 1H, H8), 3.07 (dd, $^2J_{HH}$ = 17.9 Hz, $^3J_{HH}$ = 5.1 Hz, 1H, H10A), 2.48 (td, $^3J_{HH}$ = 11.2 Hz, $^3J_{HH}$ = 4.8 Hz, 1H, H10a), 2.34 (t, $^3J_{HH}$ = 7.6 Hz, 2H, H1'), 2.10 (dm, $^3J_{HH}$ = 16.2 Hz, 1H, H7A), 1.81 (dsext, $^3J_{HH}$ = 14.2 Hz, $^3J_{HH}$ = 2.2 Hz, 1H, H7B), 1.68 (s, 3H, H11), 1.67-1.59 (br ov m, 2H, H6a and H10B) 1.49 (quint, $^3J_{HH}$ = 7.1 Hz, 2H, H2'), 1.43 (s, 3H, H12), 1.36-1.28 (br ov m, 4H, H3' and H4'), 1.19 (s, 3H, H13), 0.90 (t, $^3J_{HH}$ = 7.0 Hz, 3H, H5'). $^{13}C\{^1H\}$ NMR (176 MHz $CDCl_3$): δ 181.12 (C1), 177.57 (C2), 162.93 (C5), 143.25 (C3), 134.53 (C9), 134.37 (C4), 118.57 (C8), 114.95 (C5a), 82.12 (C6), 43.60 (C6a), 35.17 (C10), 31.45 (C3'), 29.75 (C10a), 28.70 (C1'), 27.43 (C2'), 27.06 (C7), 27.00 (C12), 23.34 (C11), 22.47 (C4'), 19.53 (C13), 14.01 (C5'). IR (FTIR): ν_{max} (cm^{-1}) 2926 (C–H), 1685 (C=O), 1638 (C=O), 1584 (C=C), 1388 (C=C), 1183 (C–O), 1113 (C–O). Anal. Calcd for $C_{21}H_{28}O_3$: C 76.79; H 8.59. Found: C 76.98; H 8.68.

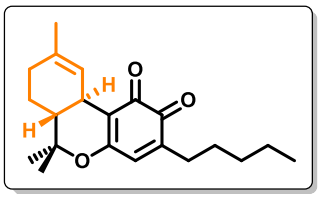

Synthesis of *ortho*-quinone-Δ^9-tetrahydrocannabinol (*o*-q9THC) A 50 mL round-bottomed flask containing a Teflon® coated stir bar was charged with 9THC (240 mg, 0.763 mmol). Dimethylformamide (5 mL) was added creating a pale-yellow solution. 2-Iodoxybenzoic acid (348 mg, 1.241 mmol) was added in small portions to the stirring solution over a period of 10 min. After 30 min the reaction mixture became intensely red, obtaining a rust red colour in 1 h. The reaction mixture was stirred for 16 h. All volatiles were removed under reduced pressure at 40 °C. The waxy residue was purified *via* silica chromatography; 1:1 petroleum ether:diethyl ether was used as the mobile phase giving analytically pure *o*-q9THC (R_f = 0.50) as a dark-red oil (Yield: 60.1 mg, 24%). Note that this compound decomposed at ambient temperature within 12 h, becoming a dark-green mixture. That was stored at –35 °C whenever possible. ^1H NMR (700 MHz $CDCl_3$): δ 6.47 (t, $^4J_{HH}$ = 1.4 Hz, 1H, H4), 6.11 (s, 1H, H10), 3.01

(d, $^{3}J_{HH}$ = 10.7 Hz, 1H, H10a), 2.33 (q, $^{3}J_{HH}$ = 7.5 Hz, 2H, H1'), 2.14 (m, 2H, H8A and H8B), 1.85 (m, 1H, H7B), 1.68 (d, $^{4}J_{HH}$ = 0.8 Hz, 3H, H11), 1.57 (m, 1H, H6a), 1.47 (s, 3H, H12), 1.46 (ov m, 2H, H2'), 1.39 (m, 1H, H7A), 1.35-1.26 (4H, br ov m, H3' and H4'), 1.18 (s, 3H, H13), 0.89 (t, $^{3}J_{HH}$ = 7.0 Hz, 3H, H5'). $^{13}C\{^{1}H\}$ NMR (176 MHz $CDCl_3$): δ 181.58 (C1), 177.83 (C2), 163.39 (C5), 143.47 (C3), 134.71 (C4), 134.47 (C9), 122.01 (C10), 113.66 (C5a), 83.16 (C6), 45.08 (C6a), 32.35 (C10a), 31.67 (C3'), 31.48 (C8), 28.95 (C1'), 27.73 (C2'), 27.23 (C12), 24.59 (C7), 23.41 (C11), 22.65 (C4'), 20.89 (C13), 14.22 (C5'). IR (FTIR): ν_{max} (cm^{-1}) 2924 (C–H), 1685 (C=O), 1638 (C=O), 1582 (C=C), 1388 (C=C), 1183 (C–O), 1113 (C–O). Anal. Calcd for $C_{21}H_{28}O_3$: C 76.79; H 8.59. Found: C 76.87; H 8.58.

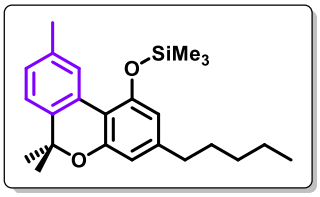

Synthesis of 1-OSiMe$_3$-cannabinol (Si-CBN) Under an inert atmosphere, a scintillation vial containing a Teflon® coated stir bar was charged with CBN (69.0 mg, 0.222 mmol) dissolved in heptane (5 mL). In a separate vial, [K][HMDS] (44.0 mg, 0.222 mmol) was dissolved in toluene (5 mL). The [K][HMDS] solution was added to the stirring CBN solution dropwise over a period of 5 min. The reaction mixture was allowed to stir for 1 h during which little colour change was observed. Neat trimethylsilyl chloride (0.028 mL, ρ = 0.856 g mL^{-1}, 0.222 mmol) was then added dropwise to the stirring solution over a period of 5 min. An off-white solid formed immediately, and the solution became lighter yellow in colour. The mixture was stirred for 1 h. The solution was filtered through Celite, and the volatiles removed *in vacuo* to yield a pale-yellow oil. For further purification, silica chromatography in 3:7 diethyl ether:hexanes as the mobile at R_f = 0.91 was appropriate (Yield: 78.3 mg, 92.2 %). ^{1}H NMR (700 MHz C_6D_6): δ 8.56 (s, 1H, H10), 6.97-6.95 (ov m, 2H, H7 and H8), 6.80 (d, $^{4}J_{HH}$ = 1.6 Hz, 1H, H4), 6.56 (d, $^{4}J_{HH}$ = 1.6 Hz, 1H, H2), 2.48 (t, $^{3}J_{HH}$ = 7.6 Hz, 2H, H1'), 2.28 (s, 3H,

H11), 1.59 (s, 6H, H12 and H13), 1.55 (t, $^{3}J_{HH}$ = 7.6 Hz, 2H, H2'), 1.26-1.18 (br ov m, 4H, H3' and H4'), 0.84 (t, $^{3}J_{HH}$ = 6.8 Hz, 3H, H5'), 0.20 (s, 9H, $OSiMe_3$). $^{13}C\{^{1}H\}$ NMR (176 MHz C_6D_6): δ 155.92 (C5), 153.61 (C1), 144.74 (C3), 137.89 (C6a), 136.66 (C9), 129.08 (C10a), 128.10 (C7 or C8), 127.95 (C10), 123.12 (C7 or C8), 114.77 (C2), 113.69 (C5a), 112.79 (C4), 77.65 (C6), 36.44 (C1'), 32.08 (C3' or C4'), 31.32 (C2'), 27.65 (C12 and C13), 23.23 (C3' or C4'), 21.81 (C11), 14.58 (C5'), 0.63 ($OSiMe_3$). Anal. Calcd for $C_{24}H_{34}O_2Si$: C 75.34; H 8.96. Found: C 75.43; H 8.96.

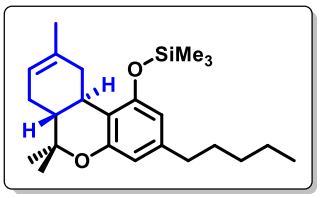

Synthesis of 1-$OSiMe_3$-Δ^8-tetrahydrocannabinol (Si-8THC)

Under an inert atmosphere, a scintillation vial containing a Teflon® coated stir bar was charged with 8THC (139.0 mg, 0.442 mmol) dissolved in heptane (5 mL). In a separate vial, [K][HMDS] (88.0 mg, 0.442 mmol) was dissolved in toluene (5 mL). The [K][HMDS] solution was added to the stirring 8THC solution dropwise over a period of 5 min. The reaction mixture was allowed to stir for 1 h during which little colour change was observed. Neat trimethylsilyl chloride (0.056 mL, ρ = 0.856 g mL^{-1}, 0.442 mmol) was then added dropwise to the stirring solution over a period of 5 min. An off-white solid formed immediately, and the solution became lighter yellow in colour. The mixture was stirred for 1 h. The solution was filtered through celite, and the volatiles removed *in vacuo* to yield a pale-yellow oil. For further purification, silica chromatography in 3:7 diethyl ether:hexanes as the mobile at R_f = 0.94 was appropriate (Yield: 143.2 mg, 87.7 %). ^{1}H NMR (700 MHz C_6D_6): δ 6.72 (d, $^{4}J_{HH}$ = 1.1 Hz, 1H, H4), 6.49 (d, $^{4}J_{HH}$ = 1.1 Hz, 1H, H2), 5.37 (s, 1H, H8), 3.44 (dd, $^{2}J_{HH}$ = 17.1 Hz, $^{3}J_{HH}$ = 3.3 Hz, 1H, H10A), 2.78 (td, $^{3}J_{HH}$ = 11.2 Hz, $^{3}J_{HH}$ = 4.6 Hz, 1H, H10b), 2.46 (t, $^{3}J_{HH}$ = 7.7 Hz, 2H, H1'), 1.91 (ov m, 1H, H7A), 1.88 (ov m, 1H, H10B), 1.84 (ov m, 1H, H6a), 1.72 (s, 3H, H11), 1.62 (ov m, 1H, H7B), 1.57 (ov m, 2H, H2'), 1.31 (s, 3H, H12), 1.25-1.18 (ov m, 4H,

H3' and H4'), 1.06 (s, 3H, H13), 0.82 (t, $^{3}J_{HH}$ = 6.9 Hz, 3H, H5'), 0.24 (s, 9H, $OSiMe_3$). $^{13}C\{^{1}H\}$ NMR (176 MHz C_6D_6): δ 156.11 (C5), 155.56 (C1), 144.74 (C3), 135.05 (C9), 120.12 (C8), 115.19 (C5a), 112.20 (C4), 112.14 (C2), 76.64 (C6), 45.81 (C6a), 36.71 (C10), 36.39 (C1'), 33.17 (C10a), 32.10 (C3' or C4'), 31.60 (C2'), 28.61 (C7), 28.08 (C12), 24.15 (C11), 18.89 (C13), 23.24 (C3' or C4'), 14.56 (C5'), 0.87 ($OSiMe_3$). Anal. Calcd for $C_{24}H_{38}O_2Si$: C 74.55; H 9.91. Found: C 74.74; H 9.99.

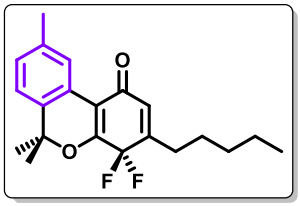

Synthesis of $4F_2$-cannabinone ($4F_2$-CBN) Either under a positive flow of argon in a 50 mL round-bottom flask equipped with a Teflon® coated stir bar or in a glass vessel sealed by a Kontes tap, CBN (211.0 mg, 0.679 mmol), *N*-fluorobenzenesulfonimide (643.0 mg, 2.038 mmol), azobisisobutyronitrile (17.0 mg, 0.102 mmol), and lithium carbonate (451.0 mg, 6.114 mmol) were added and dissolved in dry acetonitrile (10 mL). The solution was heated to 75 °C for 20 h resulting in a vibrant red solution. Volatile components were removed *in vacuo* and the resulting residue redissolved in a minimal quantity of a 1:1 hexanes:diethyl ether mixture (<5 mL). The dissolved residue was purified *via* silica chromatography; 3:2 hexanes:diethyl ether was used as the mobile phase to afford an impure product at R_f = 0.88 (bright yellow fraction). Further purification was achieved with a subsequent silica column using 4:1 hexanes:diethyl ether as the mobile phase, affording the product as a bright yellow fraction at R_f = 0.56. It is important to note that the purification step required a physically tall column (~0.75 m) in order to obtain appropriate separation (Yield: 28.9 mg, 13.4 %). ^{1}H NMR (700 MHz C_6D_6): δ 8.79 (s, 1H, H10), 6.88 (d, $^{3}J_{HH}$ = 7.8 Hz, 1H, H8), 6.66 (d, $^{3}J_{HH}$ = 7.8 Hz, 1H, H7), 6.01 (s, 1H, H2), 2.18 (t, $^{3}J_{HH}$ = 7.4 Hz, 2H, H1'), 2.14 (s, 3H, H11), 1.43 (s, 6H, H12 and H13), 1.24 (m, 2H, H2'), 1.12 (m, 2H, H4'), 1.04 (m, 2H, H3'), 0.80 (t, $^{3}J_{HH}$ = 7.3 Hz, 3H, H5'). $^{13}C\{^{1}H\}$ NMR (176 MHz C_6D_6): δ 183.31 (C1), 157.02 (t,

$^2J_{CF}$ = 23.5 Hz, C5), 147.37 (t, $^2J_{CF}$ = 24.5 Hz C3), 138.20 (C9), 134.35 (C6a), 130.14 (C8), 129.46 (t, $^2J_{CF}$ = 6.3 Hz, C2), 127.84 (C10), 125.08 (C10a), 123.04 (C7), 112.4 (t, $^2J_{CF}$ = 4.2 Hz C5a), 110.19 (t, $^1J_{CF}$ = 235.0 Hz, C4), 31.85 (C3'), 27.75 (C1'), 27.72 (C12 and C13), 26.80 (C2'), 22.97 (C4'), 21.63 (C11), 14.45 (C5'). ^{19}F NMR (659 MHz C_6D_6): δ –110.19. Anal. Calcd for $C_{24}H_{38}O_2Si$: C 72.81; H 6.98. Found: C 72.95; H 7.00.

6.3 X-ray Crystal Data

Table 6.3: X-ray crystallography data of (*R*,*S*)-Δ^{10}-Tetrahydrocannabinol(10THC)

Identification code	PH20013
Empirical formula	$C_{21}H_{30}O_2$
Formula weight	314.45
Temperature/K	100.00(10)
Crystal system	monoclinic
Space group	$P2_1$
a/Å	12.08361(17)
b/Å	6.05562(6)
c/Å	12.71633(13)
α/°	90
β/°	101.8217(13)
γ/°	90
Volume/Å^3	910.765(19)
Z	2
ρ_{calc}g/cm^3	1.147
μ/mm^{-1}	0.552
F(000)	344.0
Crystal size/mm^3	0.25 × 0.23 × 0.23
Radiation	Cu Kα (λ = 1.54184)
2Θ range for data collection/°	7.102 to 149.824
Index ranges	-12 ≤ h ≤ 14, -7 ≤ k ≤ 7, -15 ≤ l ≤ 15
Reflections collected	27208
Independent reflections	3663 [R_{int} = 0.0274, R_{sigma} = 0.0120]
Data/restraints/parameters	3663/1/213
Goodness-of-fit on F^2	1.047
Final R indexes [I>=2σ (I)]	R_1 = 0.0345, wR_2 = 0.0968
Final R indexes [all data]	R_1 = 0.0348, wR_2 = 0.0971
Largest diff. peak/hole / e Å^{-3}	0.17/-0.17
Flack parameter	-0.06(5)

6.4 Publications Arising from Part II

Webb, D. J; Hayes, P. G; Kovalchuk, I. Methods for Synthesis of Cannabis Products. **2021** US-2020262806-A1

- Content has been reformatted for 5.1, 5.3, and 5.4.2

Webb, D. J; Kovalchuk I; Li D; Hayes, P. G. A Semisynthetic Approach to Cannabinoid Production from *Cannabis sativa* and Their Corresponding Antiproliferative Effects on Cancer. To be submitted to Journal of Natural Products

- Consists of content from 5.4 and sporadic portions of Chapter 5

Webb, D. J; Kaur, R; Wetmore, S. D; Kovalchuk, I; Hayes, P. G. from Plant to Oil: A Semisynthetic Strategy and Computational Study of Δ^8-Tetrahydrocannabinol. *J.* To be submitted to ACS Medicinal Chemistry Letters.

- Consists of content from 5.4.1

Webb, D. J; Hill D. D. N; Boeré R. T; Kovalchuk, I; Li, D; Hayes, P. G. *Ortho*-quinone Derivatives of Cannabinol (CBN) and Tetrahydrocannabinol (THC) Isomers: Synthesis, Effect on Breast Cancer Cell Growth, and Electrochemistry. To be submitted to Journal of Natural Products.

- Consists of content from 5.5, 6.1.9, and 6.1.7

7 Bibliography

1. Constable, E. C., What's in a Name?—A Short History of Coordination Chemistry from Then to Now. *Chemistry* **2019**, *1*, 126-163.
2. Kauffman, G. B. *Coordination Chemistry: History. In Encyclopedia of Inorganic and Bioinorganic Chemistry*, R.A. Scott (Ed.), 2011.
3. Burdge, J.; Overby, J. *Chemistry: Atoms First*; McGraw-Hill Education, 2020.
4. Dalal, M. *A Textbook of Inorganic Chemistry – Volume 1*. Dalal Institute, 2017.
5. Fryzuk, M. D.; Haddad, T.; Berg, D. J.; Rettig, S. J. Phosphine complexes of the early metals and the lanthanoids. *Appl. Chem.* **1991**, *63*, 845-850.
6. Bhatt, V. *Essentials of Coordination Chemistry: A Simplified Approach with 3D Visuals*. Academic Press, 2015.
7. Barry, N. P. E.; Sadler, P. J. 100 years of metal coordination chemistry: from Alfred Werner to anticancer metallodrugs. *Appl. Chem.* **2014**, *86*, 1897-1910.
8. Kauffman, G. B. Christian Wilhelm Blomstrand (1826–1897) Swedish chemist and mineralogist. *Annals of Science* **1975**, *32*, 13-37.
9. Kauffman, G. B. *Alfred Werner: Founder of Coordination Chemistry*. Springer Science & Buisness Media, 2013.
10. Werner, A., Über mehrkernige Metallammoniake. *Berichte der deutschen chemischen Gesellschaft* **1907**, *40*, 2103-2125.
11. Ernst, K.-H.; Berke, H. Optical activity and Alfred Werner's coordination chemistry. *Chirality* **2011**, *23*, 187-189.
12. Stahl, G. E. *Georgii Ernesti Stahlii, Experimenta, Observationes, Animadversiones, CCC Numero, Chymicae Et Physicae*. Haude, 1731.
13. Bartoll, J. In *The early use of Prussian blue in paintings, Proceedings of the 9th International conference on NDT of Art*, Jerusalem, Israel, May 25-30, 2008
14. Finlay, V. *The Brilliant History of Color in Art*. Getty Publications, 2014.
15. Seyferth, D. Cadet's Fuming Arsenical Liquid and the Cacodyl Compounds of Bunsen. *Organometallics* **2001**, *20*, 1488-1498.
16. Zeise, W. C. Von der Wirkung zwischen Platinchlorid und Alkohol, und von den dabei entstehenden neuen Substanzen. *AnP* **1831**, *97*, 497-541.
17. Black, M.; Mais, R. H. B.; Owston, P. G. The crystal and molecular structure of Zeise's salt, $KPtCl_3.C_2H_4.H_2O$. *AcCrB* **1969**, *25*, 1753-1759.
18. Jarvis, J. A. J.; Kilbourn, B. T.; Owston, P. G. A re-determination of the crystal and molecular structure of Zeise's salt, $KPtCl_3.C_2H_4.H_2O$. *AcCrB* **1971**, *27*, 366-372.
19. Chisholm, H. *The Encyclopædia Britannica*. 11th edition.; Encyclopædia Britannica Company, Limited, 1911.
20. Mond, L.; Langer, C.; Quincke, F. L.—Action of carbon monoxide on nickel. *J. Chem. Soc., Trans.* **1890**, *57*, 749-753.

21. Fisher, E. O. In memoriam Walter Hieber 1895–1976. *Chem. Ber.* **1979**, *112*, XXI-XXXIX.

22. Zanda, M. SYNFORM ISSUE 2018/10. *Synfacts* **2018**, *14*, A153-A169.

23. Miller, S. A.; Tebboth, J. A.; Tremaine, J. F. 114. Dicyclopentadienyliron. *J. Chem. Soc.* **1952**, 632-635.

24. Pauson, P. L. Ferrocene—how it all began. *J. Organomet. Chem.* **2001**, *637-639*, 3-6.

25. Werner, H. At Least 60 Years of Ferrocene: The Discovery and Rediscovery of the Sandwich Complexes. *Angew. Chem. Int. Ed.* **2012**, *51*, 6052-6058.

26. Cossee, P. Ziegler-Natta catalysis I. Mechanism of polymerization of α-olefins with Ziegler-Natta catalysts. *J. Catal.* **1964**, *3*, 80-88.

27. Cecchin, G.; Morini, G.; Piemontesi, F. *Ziegler-Natta Catalysts*, Kirk-Othmer Encyclopedia of Chemical Technology, 2003.

28. Claverie, J. P.; Schaper, F. Ziegler-Natta catalysis: 50 years after the Nobel Prize. *MRS Bulletin* **2013**, *38*, 213-218.

29. Fink, G.; Mülhaupt, R.; Brintzinger, H. H. *Ziegler Catalysts: Recent Scientific Innovations and Technological Improvements*. Springer Science & Buisness Media, 2012.

30. Möhring, P. C.; Coville, N. J. Homogeneous group 4 metallocene ziegler-natta catalysts: The influence of cyclopentadienyl-ring substituents. *J. Organomet. Chem.* **1994**, *479*, 1-29.

31. Klosin, J.; Fontaine, P. P.; Figueroa, R. Development of Group IV Molecular Catalysts for High Temperature Ethylene-α-Olefin Copolymerization Reactions. *Acc. Chem. Res.* **2015**, *48*, 2004-2016.

32. Fortman, G. C.; Nolan, S. P. N-Heterocyclic carbene (NHC) ligands and palladium in homogeneous cross-coupling catalysis: a perfect union. *Chem. Soc. Rev.* **2011**, *40*, 5151-5169.

33. Morales-Morales, D.; Lee, D. W.; Wang, Z.; Jensen, C. M. Oxidative Addition of Water by an Iridium PCP Pincer Complex: Catalytic Dehydrogenation of Alkanes by $IrH(OH)\{C_6H_3\text{-}2,6\text{-}(CH_2PBut_2)_2\}$. *Organometallics* **2001**, *20*, 1144-1147.

34. Odian, G.; Odian, U. G. *Principles of Polymerization*, John Wiley & Sons, 2004.

35. Robert J. Young; Lovell, P. A. *Introduction to Polymers*, 3rd edition, CRC Press, 2011.

36. Cowie, J. M. G. *Polymers: Chemistry and Physics of Modern Materials, 2nd Edition*, CRC Press, 1991.

37. Rubinstein, M.; Colby, R. H. *Polymer Physics*, Oxford University Press, 2003.

38. Shah, V. *Handbook of Plastics Testing Technology*, John Wiley & Sons, 1998.

39. Shah, V. *Handbook of Plastics Testing and Failure Analysis*, John Wiley & Sons, 2007.

40. Brown, R. *Handbook of Polymer Testing: Physical Methods*, CRC Press, 1999.

41. Dechy-Cabaret, O.; Martin-Vaca, B.; Bourissou, D. Controlled Ring-Opening Polymerization of Lactide and Glycolide. *Chem. Rev.* **2004**, *104*, 6147-6176.

42. Amgoune, A.; Thomas Christophe, M.; Carpentier, J.-F. Controlled ring-opening polymerization of lactide by group 3 metal complexes. *Appl. Chem.* **2007**, *79*, 2013.

43. McNaught, A. D.; Wilkinson, A.; Jenkins, A. D. *IUPAC Compendium of Chemical Terminology: The Gold Book*, International Union of Pure and Applied Chemistry, 2006.

44. Nuyken, O.; Pask, S. D. Ring-Opening Polymerization—An Introductory Review. *Polymers* **2013**, *5*, 361-403.

45. Castro-Aguirre, E.; Iñiguez-Franco, F.; Samsudin, H.; Fang, X.; Auras, R. Poly(lactic acid)—Mass production, processing, industrial applications, and end of life. *Adv. Drug Del. Rev.* **2016**, *107*, 333-366.

46. Lim, L.-T.; Cink, K.; Vanyo, T. Processing of Poly(Lactic Acid). In *Poly(Lactic Acid)*, John Wiley & Sons, 2010; pp 189-215.

47. Agatemor, C.; Shaver, M. P. Tacticity-Induced Changes in the Micellization and Degradation Properties of Poly(lactic acid)-block-poly(ethylene glycol) Copolymers. *Biomacromolecules* **2013**, *14*, 699-708.

48. Worch, J. C.; Prydderch, H.; Jimaja, S.; Bexis, P.; Becker, M. L.; Dove, A. P. Stereochemical enhancement of polymer properties. *Nat. Rev. Chem.* **2019**, *3*, 514-535.

49. Dubois, P.; Coulembier, O.; Raquez, J. M. *Handbook of Ring-Opening Polymerization*, John Wiley & Sons, 2009.

50. Hanninen, M. M.; Zamora, M. T.; Hayes, P. G. Rare Earth Pincer Complexes: Synthesis, Reaction Chemistry, and Catalysis. In *The Privileged Pincer-Metal Platform: Coordination Chemistry & Applications*, Springer, 2015; pp 93-177.

51. Jakubowski, W.; Tsarevsky, N. V.; Higashihara, T.; Faust, R.; Matyjaszewski, K. Allyl Halide (Macro)initiators in ATRP: Synthesis of Block Copolymers with Polyisobutylene Segments. *Macromolecules* **2008**, *41*, 2318-2323.

52. Inoue, S. Immortal polymerization: The outset, development, and application. *J. Polym. Sci., Part A: Polym. Chem.* **2000**, *38*, 2861-2871.

53. Shang, X.; Liu, X.; Cui, D. Yttrium bis(alkyl) and bis(amido) complexes bearing N,O multidentate ligands. Synthesis and catalytic activity towards ring-opening polymerization of L-lactide. *J. Polym. Sci., Part A: Polym. Chem.* **2007**, *45*, 5662-5672.

54. Hiroshi, N.; Naoko, T.; Masaji, Y.; Takaaki, S.; Hiroshi, K. Tetrakis[3,5-bis(trifluoromethyl)phenyl]borate. Highly Lipophilic Stable Anionic Agent for Solvent-extraction of Cations. *Bull. Chem. Soc. Jpn.* **1984**, *57*, 2600-2604.

55. Brookhart, M.; Grant, B.; Volpe, A. F. $[(3,5\text{-}(CF_3)_2C_6H_3)_4B]\text{-}[H(OEt_2)_2]+$: a convenient reagent for generation and stabilization of cationic, highly electrophilic organometallic complexes. *Organometallics* **1992**, *11*, 3920-3922.

56. Yakelis, N. A.; Bergman, R. G. Safe Preparation and Purification of Sodium Tetrakis[(3,5-trifluoromethyl)phenyl]borate ($NaBArF_{24}$): Reliable and

Sensitive Analysis of Water in Solutions of Fluorinated Tetraarylborates. *Organometallics* **2005**, *24*, 3579-3581.

57. Krossing, I.; Raabe, I. Noncoordinating Anions—Fact or Fiction? A Survey of Likely Candidates. *Angew. Chem. Int. Ed.* **2004**, *43*, 2066-2090.

58. Heurtefeu, B.; Vaultier, F.; Leino, R.; Boisson, C.; Cramail, H. Single-Site Catalysts. In *Encyclopedia of Polymer Science and Technology*, John Wiley & Sons, 2012; pp 551-602.

59. Chen, E. Y.-X.; Marks, T. J. Cocatalysts for Metal-Catalyzed Olefin Polymerization: Activators, Activation Processes, and Structure−Activity Relationships. *Chem. Rev.* **2000**, *100*, 1391-1434.

60. Bochmann, M. The Chemistry of Catalyst Activation: The Case of Group 4 Polymerization Catalysts. *Organometallics* **2010**, *29*, 4711-4740.

61. Sarazin, Y.; Carpentier, J.-F. Discrete Cationic Complexes for Ring-Opening Polymerization Catalysis of Cyclic Esters and Epoxides. *Chem. Rev.* **2015**, *115*, 3564-3614.

62. Alt, H. G.; Köppl, A. Effect of the Nature of Metallocene Complexes of Group IV Metals on Their Performance in Catalytic Ethylene and Propylene Polymerization. *Chem. Rev.* **2000**, *100*, 1205-1222.

63. Kissin, Y. Chapter 1 The Beginner's Course: General Description of Transition Metal Catalysts and Catalytic Polymerization Reactions. In *Stud. Surf. Sci. Catal. Volume 173*, Elsevier, 2007; pp 1-34.

64. Kissin, Y. V. Active centers in Ziegler–Natta catalysts: Formation kinetics and structure. *J. Catal.* **2012**, *292*, 188-200.

65. Mitchell, N. E.; Long, B. K. Recent advances in thermally robust, late transition metal-catalyzed olefin polymerization. *Polym. Int.* **2019**, *68*, 14-26.

66. Patel, K.; Chikkali, S. H.; Sivaram, S. Ultrahigh molecular weight polyethylene: Catalysis, structure, properties, processing and applications. *Prog. Polym. Sci.* **2020**, *109*, 101290.

67. Engesser, T. A.; Lichtenthaler, M. R.; Schleep, M.; Krossing, I. Reactive p-block cations stabilized by weakly coordinating anions. *Chem. Soc. Rev.* **2016**, *45*, 789-899.

68. Gao, J.; Zhu, D.; Zhang, W.; Solan, G. A.; Ma, Y.; Sun, W.-H. Recent progress in the application of group 1, 2 & 13 metal complexes as catalysts for the ring opening polymerization of cyclic esters. *Inorg. Chem. Front.* **2019**, *6*, 2619-2652.

69. Franz, D.; Inoue, S., Cationic Complexes of Boron and Aluminum: An Early 21st Century Viewpoint. *Chem. Eur. J.* **2019**, *25*, 2898-2926.

70. Champouret, Y.; Hashmi, O. H.; Visseaux, M. Discrete iron-based complexes: Applications in homogeneous coordination-insertion polymerization catalysis. *Coord. Chem. Rev.* **2019**, *390*, 127-170.

71. Wheaton, C. A.; Hayes, P. G.; Ireland, B. J. Complexes of Mg, Ca and Zn as homogeneous catalysts for lactide polymerization. *Dalton Trans.* **2009**, 4832-4846.

72. Wheaton, C. A.; Ireland, B. J.; Hayes, P. G. Activated Zinc Complexes Supported by a Neutral, Phosphinimine-Containing Ligand: Synthesis and Efficacy for the Polymerization of Lactide. *Organometallics* **2009**, *28*, 1282-1285.

73. Hanson, S. S.; Doni, E.; Traboulsee, K. T.; Coulthard, G.; Murphy, J. A.; Dyker, C. A. Pushing the Limits of Neutral Organic Electron Donors: A Tetra(iminophosphorano)-Substituted Bispyridinylidene. *Angew. Chem. Int. Ed.* **2015**, *54*, 11236-11239.

74. Abel, E. W.; Mucklejohn, S. A. The Chemistry of Phosphinimines. *Phosphorus Sulfur Relat. Elem.* **1981**, *9*, 235-266.

75. Staudinger, H.; Meyer, J. Über neue organische Phosphorverbindungen III. Phosphinmethylenderivate und Phosphinimine. *Helv. Chim. Acta* **1919**, *2*, 635-646.

76. Gololobov, Y. G.; Zhmurova, I. N.; Kasukhin, L. F. Sixty years of staudinger reaction. *Tetrahedron* **1981**, *37*, 437-472.

77. Gololobov, Y. G.; Kasukhin, L. F. Recent advances in the staudinger reaction. *Tetrahedron* **1992**, *48*, 1353-1406.

78. Bebbington, M. W. P.; Bourissou, D. Stabilised phosphazides. *Coord. Chem. Rev.* **2009**, *253*, 1248-1261.

79. Eguchi, S.; Matsushita, Y.; Yamashita, K. The aza-wittic reaction in heterocyclic synthesis. a review. *Org. Prep. Proced. Int.* **1992**, *24*, 209-243.

80. Meng, G.; Guo, T.; Ma, T.; Zhang, J.; Shen, Y.; Sharpless, K. B.; Dong, J. Modular click chemistry libraries for functional screens using a diazotizing reagent. *Nature* **2019**, *574*, 86-89.

81. Johnson, K. R. D.; Hayes, P. G. Synthesis and Reactivity of Dialkyl Lutetium Complexes Supported by a Novel Bis(phosphinimine)carbazole Pincer Ligand. *Organometallics* **2009**, *28*, 6352-6361.

82. Johnson, K. R. D.; Hayes, P. G. Organolutetium-Mediated Dearomatization and Functionalization of Pyrimidine Rings. *Organometallics* **2013**, *32*, 4046-4049.

83. Johnson, K. R. D.; Hayes, P. G. A cascade reaction: ring-opening insertion of dioxaphospholane into lutetium alkyl bonds. *Dalton Trans.* **2014**, *43*, 2448-2457.

84. Johnson, K. R. D.; Hayes, P. G. Yttrium and scandium complexes of a bulky bis(phosphinimine)carbazole ligand. *Inorg. Chim. Acta* **2014**, *422*, 209-217.

85. Johnson, K. R. D.; Kamenz, B. L.; Hayes, P. G. Ligand influence on intramolecular cyclometalation in bis(phosphinimine) rare earth alkyl complexes. *Can. J. Chem.* **2015**, *94*, 330-341.

86. Johnson, K. R. D.; Hayes, P. G. Kinetic and Mechanistic Investigation of Metallacycle Ring Opening in an Ortho-Metalated Lutetium Aryl Complex. *Organometallics* **2011**, *30*, 58-67.

87. Johnson, K. R. D.; Hannon, M. A.; Ritch, J. S.; Hayes, P. G. Thermally stable rare earth dialkyl complexes supported by a novel bis(phosphinimine)pyrrole ligand. *Dalton Trans.* **2012**, *41*, 7873-7875.

88. Zamora, M. T.; Johnson, K. R. D.; Hänninen, M. M.; Hayes, P. G. Differences in the cyclometalation reactivity of bisphosphinimine-supported organo-rare earth complexes. *Dalton Trans.* **2014**, *43*, 10739-10750.

89. Knott, J. P.; Hänninen, M. M.; Rautiainen, J. M.; Tuononen, H. M.; Hayes, P. G. Insights into the decomposition pathway of a lutetium alkylamido complex via intramolecular C–H bond activation. *J. Organomet. Chem.* **2017**, *845*, 135-143.

90. Hänninen, M. M.; Zamora, M. T.; MacNeil, C. S.; Knott, J. P.; Hayes, P. G. Elucidation of the resting state of a rhodium NNN-pincer hydrogenation catalyst that features a remarkably upfield hydride 1H NMR chemical shift. *Chem. Commun.* **2016**, *52*, 586-589.

91. MacNeil, C. S.; Glynn, K. E.; Hayes, P. G. Facile Activation and Deoxygenative Metathesis of CO. *Organometallics* **2018**, *37*, 3248-3252.

92. MacNeil, C. S.; Hayes, P. G. An H-Substituted Rhodium Silylene. *Chem. Eur. J.* **2019**, *25*, 8203-8207.

93. Wheaton, C. A.; Hayes, P. G. Cationic organozinc complexes of a bis(phosphinimine) pincer ligand: synthesis, structural and polymerization studies. *Dalton Trans.* **2010**, *39*, 3861-3869.

94. Wheaton, C. A.; Hayes, P. G. Cationic zinc complexes: a new class of catalyst for living lactide polymerization at ambient temperature. *Chem. Commun.* **2010**, *46*, 8404-8406.

95. Wheaton, C. A.; Hayes, P. G. Exploring the versatility of a bis(phosphinimine) pincer ligand: effect of sterics on structure and lactide polymerization activity of cationic zinc complexes. *Catal. Sci. Technol.* **2012**, *2*, 125-138.

96. Wheaton, C. A.; Hayes, P. G. Electron deficient zinc complexes: Enhanced lactide polymerization activity achieved through rational ligand design. *J. Organomet. Chem.* **2012**, *704*, 65-69.

97. Zamora, M. T.; Zahir, S. M.; Johnson, K. R. D.; Barnson, C. J.; Wheaton, C. A.; Hänninen, M. M.; Hayes, P. G. Synthesis of Sterically Demanding Bis(phosphinimine) Dibenzofuran Ligands and Subsequent Zinc Metalation. *Aust. J. Chem.* **2015**, *68*, 373-384.

98. Ireland, B. J.; Wheaton, C. A.; Hayes, P. G. Cationic Organomagnesium Complexes as Highly Active Initiators for the Ring-Opening Polymerization of ε-Caprolactone. *Organometallics* **2010**, *29*, 1079-1084.

99. Wheaton, C. A.; Hayes, P. G. Designing cationic zinc and magnesium catalysts for coordination-insertion polymerization of lactide. *Comments Inorg. Chem.* **2011**, *32*, 127-162.

100. Sun, H.; Ritch, J. S.; Hayes, P. G. Toward Stereoselective Lactide Polymerization Catalysts: Cationic Zinc Complexes Supported by a Chiral Phosphinimine Scaffold. *Inorg. Chem.* **2011**, *50*, 8063-8072.

101. Wheaton, C. A.; Ireland, B. J.; Hayes, P. G. Synthesis and Structural Diversity of ZnCl2 and Zn(C6F5)2 Complexes of a Phosphinimine Ligand. *Z. Anorg. Allg. Chem.* **2011**, *637*, 2111-2119.

102. Sun, H.; Ritch, J. S.; Hayes, P. G. Ring-opening polymerisation of rac-lactide mediated by cationic zinc complexes featuring P-stereogenic bisphosphinimine ligands. *Dalton Trans.* **2012**, *41*, 3701-3713.

103. Bochmann, M.; Lancaster, S. J.; Hannant, M. D.; Rodriguez, A.; Schormann, M.; Walker, D. A.; Woodman, T. J. Role of $B(C_6F_5)_3$ in catalyst activation, anion formation, and as C_6F_5 transfer agent. *Pure Appl. Chem.* **2003**, *75*, 1183-1195.

104. Merle, N.; Törnroos, K. W.; Jensen, V. R.; Le Roux, E. Influence of multidentate N-donor ligands on highly electrophilic zinc initiator for the ring-opening polymerization of epoxides. *J. Organomet. Chem.* **2011**, *696*, 1691-1697.

105. Jensen, T. R.; Schaller, C. P.; Hillmyer, M. A.; Tolman, W. B. Zinc N-heterocyclic carbene complexes and their polymerization of d,l-lactide. *J. Organomet. Chem.* **2005**, *690*, 5881-5891.

106. Romain, C.; Rosa, V.; Fliedel, C.; Bier, F.; Hild, F.; Welter, R.; Dagorne, S.; Avilés, T. Highly active zinc alkyl cations for the controlled and immortal ring-opening polymerization of ε-caprolactone. *Dalton Trans.* **2012**, *41*, 3377-3379.

107. Scheiper, C.; Schulz, S.; Wölper, C.; Bläser, D.; Roll, J. Synthesis and Single Crystal X-ray Structures of Cationic Zinc β-Diketiminate Complexes. *Z. Anotg. Allg. Chem.* **2013**, *639*, 1153-1159.

108. Scheiper, C.; Dittrich, D.; Wölper, C.; Bläser, D.; Roll, J.; Schulz, S. Synthesis, Structure, and Catalytic Activity of Tridentate, Base-Functionalized β-Ketiminate Zinc Complexes in Ring-Opening Polymerization of Lactide. *Eur. J. Inorg. Chem.* **2014**, *2014*, 2230-2240.

109. Martinez de Leon, C.; Tlahuext, H.; Grevy, J.-M. Crystal structure of 2,5-bis(diphenylphosphanyl)furan. *Acta Cryst. E* **2015**, *71*, o922-o923.

110. Bräse, S.; Banert, K. *Organic Azides: Syntheses and Applications*, John Wiley & Sons, 2011.

111. Bräse, S.; Gil, C.; Knepper, K.; Zimmermann, V. Organic Azides: An Exploding Diversity of a Unique Class of Compounds. *Angew. Chem. Int. Ed.* **2005**, *44*, 5188-5240.

112. Barral, K.; Moorhouse, A. D.; Moses, J. E. Efficient Conversion of Aromatic Amines into Azides: A One-Pot Synthesis of Triazole Linkages. *Org. Lett.* **2007**, *9*, 1809-1811.

113. Knott, J. P. Towards Terminal Rare Earth Imido Complexes. M.Sc. Dissertation, University of Lethbridge (Canada), 2019.

114. Stott, T. L.; Wolf, M. O. Spectroscopic Study of Phosphine-Substituted Oligothiophenes. *J. Phys. Chem.* **2004**, *108*, 18815-18819.

115. Hijazi, A. K.; Taha, Z. A.; Ajlouni, A.; Radhakrishnan, N.; Voit, B.; Kühn, F. E. Improved synthesis, characterization and catalytic application of $[H(OEt_2)_2][B\{C_6H_3(m\text{-}CF_3)_2\}_4]$. *J. Organomet. Chem.* **2014**, *763-764*, 65-68.

116. Riddlestone, I. M.; Kraft, A.; Schaefer, J.; Krossing, I. Taming the Cationic Beast: Novel Developments in the Synthesis and Application of Weakly Coordinating Anions. *Angew. Chem. Int. Ed.* **2018**, *57*, 13982-14024.

117. Cussler, E. L.; Cussler, E. L., Diffusion Coefficients and Diffusion of Interacting Species, In *Diffusion: Mass Transfer in Fluid Systems*. Cambridge University Press, 1997: pp 117-211

118. Li, W.; Yao, Y.; Zhang, Y.; Shen, Q. Aluminum Complexes Stabilized by Piperazidine-Bridged Bis(phenolate) Ligands: Syntheses, Structures, and Application in the Ring-Opening Polymerization of ε-Caprolactone. *Chin. J. Chem* . **2012**, *30*, 609-615.

119. Platel, R. H.; White, A. J. P.; Williams, C. K. Bis(phosphinic)diamido Yttrium Amide, Alkoxide, and Aryloxide Complexes: An Evaluation of Lactide Ring-Opening Polymerization Initiator Efficiency. *Inorg. Chem.* **2011**, *50*, 7718-7728.

120. Kremer, A. B.; Mehrkhodavandi, P. Dinuclear catalysts for the ring opening polymerization of lactide. *Coord. Chem. Rev.* **2019**, *380*, 35-57.

121. Sarazin, Y.; Schormann, M.; Bochmann, M. Novel Zinc and Magnesium Alkyl and Amido Cations for Ring-Opening Polymerization Reactions. *Organometallics* **2004**, *23*, 3296-3302.

122. Arbaoui, A.; Redshaw, C. Metal catalysts for ε-caprolactone polymerisation. *Polym. Chem.* **2010**, *1*, 801-826.

123. Wang, X.; Brosmer, J. L.; Thevenon, A.; Diaconescu, P. L. Highly Active Yttrium Catalysts for the Ring-Opening Polymerization of ε-Caprolactone and δ-Valerolactone. *Organometallics* **2015**, *34*, 4700-4706.

124. Hu, Q.; Jie, S.; Braunstein, P.; Li, B.-G. Highly active tridentate amino-phenol zinc complexes for the catalytic ring-opening polymerization of ε-caprolactone. *J. Organomet. Chem.* **2019**, *882*, 1-9.

125. Jensen, W. B. The Place of Zinc, Cadmium, and Mercury in the Periodic Table. *J. Chem. Ed.* **2003**, *80*, 952.

126. Walborsky, H. M.; Hamdouchi, C. Mechanism of organocalcium reagent formation. *J. Org. Chem.* **1993**, *58*, 1187-1193.

127. Wolf, B. M.; Stuhl, C.; Maichle-Mössmer, C.; Anwander, R. Dimethylcalcium. *J. Am. Chem. Soc.* **2018**, *140*, 2373-2383.

128. Liu, N.; Liu, B.; Cui, D. Alkaline earth metal complexes stabilized by amidine and guanidine ligands: synthesis, structure and their catalytic activity towards polymerization of rac-lactide. *Dalton Trans.* **2018**, *47*, 12623-12632.

129. Westerhausen, M. Synthesis and spectroscopic properties of bis(trimethylsilyl)amides of the alkaline-earth metals magnesium, calcium, strontium, and barium. *Inorg. Chem.* **1991**, *30*, 96-101.

130. Cushion, M. G.; Mountford, P. Cationic and charge-neutral calcium tetrahydroborate complexes and their use in the controlled ring-opening polymerisation of rac-lactide. *Chem. Commun.* **2011**, *47*, 2276-2278.

131. Nixon, T. D.; Ward, B. D. Calcium amido-bisoxazoline complexes in asymmetric hydroamination/cyclisation catalysis. *Chem. Commun.* **2012**, *48*, 11790-11792.

132. Burger, B. J.; Bercaw, J. E. Vacuum Line Techniques for Handling Air-Sensitive Organometallic Compounds. In *Experimental Organometallic Chemistry*, American Chemical Society: 1987; pp 79-115.

133. Pangborn, A. B.; Giardello, M. A.; Grubbs, R. H.; Rosen, R. K.; Timmers, F. J. Safe and convenient procedure for solvent purification. *Organometallics* **1996**, *15*, 1518-1520.

134. Nakanishi, T.; Hirai, Y.; Hasegawa, Y.; Kitagawa, Y.; Fushimi, K. Preparation and luminescence of rare-earth complex coordination polymer with phosphine oxide bidentate ligand. WO2017191795A1, 2017.

135. Hijazi, A. K.; Taha, Z. A.; Ajlouni, A.; Radhakrishnan, N.; Voit, B.; Kühn, F. E. Improved synthesis, characterization and catalytic application of $[H(OEt_2)_2][B\{C_6H_3(m\text{-}CF_3)_2\}_4]$. *J. Organomet. Chem.* **2014**, *763*, 65-68.

136. Cosier, J. t.; Glazer, A. A nitrogen-gas-stream cryostat for general X-ray diffraction studies. *J. Appl. Crystallogr.* **1986**, *19*, 105-107.

137. *CrysAlisPRO*, CrysAlisPRO, Oxford Diffraction / Agilent Technologies UK Ltd, Yarnton, England, 2010.

138. Sheldrick, G. M. SHELXT - integrated space-group and crystal-structure determination. *Acta Cryst. A.* **2015**, *71*, 3-8.

139. Sheldrick, G. M. Crystal structure refinement with SHELXL. *Acta Cryst. C.* **2015**, *71*, 3-8.

140. Dolomanov, O. V.; Bourhis, L. J.; Gildea, R. J.; Howard, J. A.; Puschmann, H. OLEX2: a complete structure solution, refinement and analysis program. *J. Appl. Crystallogr.* **2009**, *42*, 339-341.

141. Flack, H. D. On enantiomorph-polarity estimation. *Acta Cryst. A.* **1983**, *39*, 876-881.

142. Hooft, R. W.; Straver, L. H.; Spek, A. L. Determination of absolute structure using Bayesian statistics on Bijvoet differences. *J. Appl. Crystallogr.* **2008**, *41*, 96-103.

143. Farrugia, L. J. WinGX and ORTEP for Windows: an update. *J. Appl. Crystallogr.* **2012**, *45*, 849-854.

144. All natural. *Nat. Chem. Biol.* **2007**, *3*, 351-351.

145. Samuelsson, G. *Drugs of Natural Origin: A Textbook of Pharmacognosy*, Apotekarsocieteten, 1999.

146. Hanson, J. R. *Natural products: the secondary metabolites*. Royal Society of Chemistry (Great Britain), 2003.

147. Lemke, T. L.; Williams, D. A. *Foye's Principles of Medicinal Chemistry*, 7th Edition. Wolters Kluwer Health Adis (ESP), 2012.

148. Maplestone, R. A.; Stone, M. J.; Williams, D. H. The evolutionary role of secondary metabolites — a review. *Gene* **1992**, *115*, 151-157.

149. Williams, D. H.; Stone, M. J.; Hauck, P. R.; Rahman, S. K. Why Are Secondary Metabolites (Natural Products) Biosynthesized? *J. Nat. Prod.* **1989**, *52*, 1189-1208.

150. Firn, R. D.; Jones, C. G. The evolution of secondary metabolism – a unifying model. *Mol. Microbiol.* **2000**, *37*, 989-994.

151. Demain, A. L.; Fang, A. The Natural Functions of Secondary Metabolites. In *History of Modern Biotechnology I*, Fiechter, A., Ed. Springer, 2000; pp 1-39.

152. Wink, M. Evolution of secondary metabolites from an ecological and molecular phylogenetic perspective. *Phytochemistry* **2003**, *64*, 3-19.

153. Delgoda, R.; Murray, J. E. Chapter 7 - Evolutionary Perspectives on the Role of Plant Secondary Metabolites. In *Pharmacognosy*, Academic Press, 2017; pp 93-100.

154. Li, J. W. H.; Vederas, J. C. Drug Discovery and Natural Products: End of an Era or an Endless Frontier? *Science* **2009**, *325*, 161-165.

155. Spencer, C. M.; Faulds, D. Paclitaxel. *Drugs* **1994**, *48*, 794-847.

156. Alqahtani, F. Y.; Aleanizy, F. S.; El Tahir, E.; Alkahtani, H. M.; AlQuadeib, B. T. Chapter Three - Paclitaxel. In *Profiles of Drug Substances, Excipients and Related Methodology*, Academic Press: 2019; pp 205-238.

157. Markman, M.; Mekhail, T. M. Paclitaxel in cancer therapy. *Expert Opin. Pharmacother.* **2002**, *3*, 755-766.

158. Hollinger, J. Pacific Yew, *Taxus brevifolia*. Used within creative commons. No alterations made. All rights reserved.: Panjab Creek, Blue Mts, WA, 2005.

159. Kathiravan, G.; Sureban, S. M.; Sree, H. N.; Bhuvaneshwari, V.; Kramony, E. Isolation of anticancer drug TAXOL from Pestalotiopsis breviseta with apoptosis and B-Cell lymphoma protein docking studies. *J. basic clin. pharm.* **2012**, *4*, 14-19.

160. Carroll, A. R.; Copp, B. R.; Davis, R. A.; Keyzers, R. A.; Prinsep, M. R. Marine natural products. *Nat. Prod. Rep.* **2021**, *38*, 362-413.

161. Elhady, S. S.; Al-Abd, A. M.; El-Halawany, A. M.; Alahdal, A. M.; Hassanean, H. A.; Ahmed, S. A. Antiproliferative Scalarane-Based Metabolites from the Red Sea Sponge Hyrtios erectus. *Mar. Drugs* **2016**, *14*, 130.

162. Goodman, J.; Walsh, V. *The Story of Taxol: Nature and Politics in the Pursuit of an Anti-Cancer Drug*. Cambridge University Press: 2001.

163. Sheldon, R. A. Atom efficiency and catalysis in organic synthesis. *Pure Appl. Chem.* **2000**, *72*, 1233-1246.

164. Newhouse, T.; Baran, P. S.; Hoffmann, R. W. The economies of synthesis. *Chem. Soc. rev.* **2009**, *38*, 3010-3021.

165. Greenwood, D. The quinine connection. *J. Antimicrob. Chemother.* **1992**, *30*, 417-427.

166. Woodward, R. B.; Eastman, R. H. Thiophane derivatives. *J. Am. Chem. Soc.* **1944**, *66*, 849-850.

167. Kaufman, T. S.; Rúveda, E. A. The Quest for Quinine: Those Who Won the Battles and Those Who Won the War. *Angew. Chem. Int. Ed.* **2005**, *44*, 854-885.

168. Wani, M. C.; Taylor, H. L. Plant antitumor agents. VI. The isolation and structure of taxol, a novel antileukemia and antitumor agent from [the stem bark of] Taxus brevifolia. *J. Am. Chem. Soc.* **1971**, *93*, 2325-7.

169. Wall, M. E.; Wani, M. C. Camptothecin and taxol: discovery to clinic--thirteenth Bruce F. Cain Memorial Award Lecture. *Cancer Res.* **1995**, *55*, 753-760.

170. Holton, R. A.; Somoza, C.; Kim, H. B.; Liang, F.; Biediger, R. J.; Boatman, P. D.; Shindo, M.; Smith, C. C.; Kim, S. First total synthesis of taxol. 1. Functionalization of the B ring. *J. Am. Chem. Soc.* **1994**, *116*, 1597-1598.

171. Holton, R. A.; Kim, H. B.; Somoza, C.; Liang, F.; Biediger, R. J.; Boatman, P. D.; Shindo, M.; Smith, C. C.; Kim, S. First total synthesis of taxol. 2. Completion of the C and D rings. *J. Am. Chem. Soc.* **1994**, *116*, 1599-1600.

172. Nicolaou, K. C.; Yang, Z.; Liu, J. J.; Ueno, H.; Nantermet, P. G.; Guy, R. K.; Claiborne, C. F.; Renaud, J.; Couladouros, E. A.; Paulvannan, K.; Sorensen, E. J. Total synthesis of taxol. *Nature* **1994**, *367*, 630-634.

173. Nicolaou, K. C.; Chen, J. S. *Classics in Total Synthesis III: Further Targets, Strategies, Methods*, John Wiley & Sons, 2011.

174. Armaly, A. M.; DePorre, Y. C.; Groso, E. J.; Riehl, P. S.; Schindler, C. S. Discovery of Novel Synthetic Methodologies and Reagents during Natural Product Synthesis in the Post-Palytoxin Era. *Chem. Rev.* **2015**, *115*, 9232-9276.

175. Kalkreuter, E.; Carpenter, S. M.; Williams, G. J. Chapter 11 Precursor-directed Biosynthesis and Semi-synthesis of Natural Products. In *Chemical and Biological Synthesis: Enabling Approaches for Understanding Biology*, The Royal Society of Chemistry, 2018; pp 275-312.

176. Wuts, P. G. Semisynthesis of Taxol. *Curr. opin. drug discov. dev.* **1998**, *1*, 329-337.

177. Jennewein, S.; Croteau, R. Taxol: biosynthesis, molecular genetics, and biotechnological applications. *Appl. Microbiol. Biotechnol.* **2001**, *57*, 13-19.

178. Pacher, P.; Bátkai, S.; Kunos, G. The Endocannabinoid System as an Emerging Target of Pharmacotherapy. *Pharmacol. Rev.* **2006**, *58*, 389.

179. Galiègue, S.; Mary, S.; Marchand, J.; Dussossoy, D.; Carrière, D.; Carayon, P.; Bouaboula, M.; Shire, D.; LE Fur, G.; Casellas, P. Expression of Central and Peripheral Cannabinoid Receptors in Human Immune Tissues and Leukocyte Subpopulations. *Eur. J. Biochem.* **1995**, *232*, 54-61.

180. Núñez, E.; Benito, C.; Pazos, M. R.; Barbachano, A.; Fajardo, O.; González, S.; Tolón, R. M.; Romero, J. Cannabinoid CB_2 receptors are expressed by perivascular microglial cells in the human brain: An immunohistochemical study. *Synapse* **2004**, *53*, 208-213.

181. Pacher, P.; Bátkai, S.; Kunos, G. The endocannabinoid system as an emerging target of pharmacotherapy. *Pharmacol. Rev.* **2006**, *58*, 389-462.

182. Elphick, M. R.; Egertová, M. The neurobiology and evolution of cannabinoid signalling. *Philos. Trans. R. soc. Lond., B, Biol. Sci.* **2001**, *356*, 381-408.

183. Munro, S.; Thomas, K. L.; Abu-Shaar, M. Molecular characterization of a peripheral receptor for cannabinoids. *Nature* **1993**, *365*, 61-65.

184. Basu, S.; Ray, A.; Dittel, B. N. Cannabinoid Receptor 2 Is Critical for the Homing and Retention of Marginal Zone B Lineage Cells and for Efficient T-Independent Immune Responses. *J. Immunol.* **2011**, *187*, 5720.

185. Sugiura, T.; Kodaka, T.; Nakane, S.; Miyashita, T.; Kondo, S.; Suhara, Y.; Takayama, H.; Waku, K.; Seki, C.; Baba, N.; Ishima, Y. Evidence That the Cannabinoid CB_1 Receptor Is a 2-Arachidonoylglycerol Receptor: Structure-activity relationship of 2-arachidonoylglycerol, ether-linked analogues and related compounds. *J. Biol. Chem.* **1999**, *274*, 2794-2801.

186. Pagotto, U.; Marsicano, G.; Cota, D.; Lutz, B.; Pasquali, R. The Emerging Role of the Endocannabinoid System in Endocrine Regulation and Energy Balance. *Endocr. Rev.* **2006**, *27*, 73-100.

187. Porcella, A.; Maxia, C.; Gessa, G. L.; Pani, L. The human eye expresses high levels of CB1 cannabinoid receptor mRNA and protein. *Euro. J. Neurosci.* **2000**, *12*, 1123-1127.

188. Kendall, D. A.; Yudowski, G. A. Cannabinoid Receptors in the Central Nervous System: Their Signaling and Roles in Disease. *Front. Cell. Neurosci.* **2017**, *10*.

189. Murphy, L. L.; Bartke, A., *Marijuana/Cannabinoids: Neurophysiology and Neurobiology*, CRC Press: 2019.

190. Zou, S.; Kumar, U. Cannabinoid Receptors and the Endocannabinoid System: Signaling and Function in the Central Nervous System. *Int. J. Mol. Sci.* **2018**, *19*, 833.

191. Barutta, F.; Mastrocola, R.; Bellini, S.; Bruno, G.; Gruden, G. Cannabinoid Receptors in Diabetic Kidney Disease. *Curr. Diab. Rep.* **2018**, *18*, 9.

192. Wang, J.; Lu, H.-x.; Wang, J. Cannabinoid receptors in osteoporosis and osteoporotic pain: a narrative update of review. *J. Pharm. Pharmacol.* **2019**, *71*, 1469-1474.

193. Kovalchuk, O.; Kovalchuk, I. Cannabinoids as Anticancer Therapeutic Agents. *Cell Cycle* **2020**, *19*, 961-989.

194. Shahbazi, F.; Grandi, V.; Banerjee, A.; Trant, J. F. Cannabinoids and Cannabinoid Receptors: The Story so Far. *iScience* **2020**, *23*, 101301.

195. Lambert, D. M.; Fowler, C. J. The Endocannabinoid System: Drug Targets, Lead Compounds, and Potential Therapeutic Applications. *J. Med. Chem.* **2005**, *48*, 5059-5087.

196. Pertwee, R. G. Pharmacological actions of cannabinoids. In *Cannabinoids*, Springer, 2005; pp 1-51.

197. Guzmán, M. Cannabinoids: potential anticancer agents. *Nat. Rev. Cancer* **2003**, *3*, 745-755.

198. Pellati, F.; Borgonetti, V.; Brighenti, V.; Biagi, M.; Benvenuti, S.; Corsi, L. Cannabis sativa L. and Nonpsychoactive Cannabinoids: Their Chemistry and

Role against Oxidative Stress, Inflammation, and Cancer. *Biomed res. Int.* **2018**, *2018*, 1691428-1691428.

199. Costa, B. On the Pharmacological Properties of Δ9-Tetrahydrocannabinol (THC). *Chem. Biodivers.* **2007**, *4*, 1664-1677.

200. Allan, G. M.; Finley, C. R.; Ton, J.; Perry, D.; Ramji, J.; Crawford, K.; Lindblad, A. J.; Korownyk, C.; Kolber, M. R. Systematic review of systematic reviews for medical cannabinoids: Pain, nausea and vomiting, spasticity, and harms. *Can. Fam. Physician Medecin de famille canadien* **2018**, *64*, e78-e94.

201. Campos, A. C.; Moreira, F. A.; Gomes, F. V.; Del Bel, E. A.; Guimarães, F. S. Multiple mechanisms involved in the large-spectrum therapeutic potential of cannabidiol in psychiatric disorders. *Philos. Trans. R. Soc. Lond., B, Biol. Sci.* **2012**, *367*, 3364-3378.

202. Cannaert, A.; Storme, J.; Franz, F.; Auwärter, V.; Stove, C. P. Detection and Activity Profiling of Synthetic Cannabinoids and Their Metabolites with a Newly Developed Bioassay. *Anal. Chem.* **2016**, *88*, 11476-11485.

203. Newton, D. E. *Marijuana: A Reference Handbook*, ABC-CLIO: 2013.

204. Srebnik, M.; Lander, N.; Breuer, A.; Mechoulam, R. Base-catalysed double-bond isomerizations of cannabinoids: structural and stereochemical aspects. *J. Chem. Soc., Perkin Trans. 1* **1984**, 2881-2886.

205. Gülck, T.; Møller, B. L. Phytocannabinoids: Origins and Biosynthesis. *Trends Plant Sci.* **2020**, *25*, 985-1004.

206. Tahir, M. N.; Shahbazi, F.; Rondeau-Gagné, S.; Trant, J. F. The biosynthesis of the cannabinoids. *J. Cannabis Res.* **2021**, *3*, 7.

207. Moreno-Sanz, G. Can You Pass the Acid Test? Critical Review and Novel Therapeutic Perspectives of Δ9-Tetrahydrocannabinolic Acid A. *Cannabis Cannabinoid Res.* **2016**, *1*, 124-130.

208. Perrotin-Brunel, H.; Buijs, W.; Spronsen, J. v.; Roosmalen, M. J. E. v.; Peters, C. J.; Verpoorte, R.; Witkamp, G.-J. Decarboxylation of Δ9-tetrahydrocannabinol: Kinetics and molecular modeling. *J. Mol. Struct.* **2011**, *987*, 67-73.

209. Mahadevan, A.; Siegel, C.; Martin, B. R.; Abood, M. E.; Beletskaya, I.; Razdan, R. K. Novel Cannabinol Probes for CB_1 and CB_2 Cannabinoid Receptors. *J. Med. Chem.* **2000**, *43*, 3778-3785.

210. Andre, C. M.; Hausman, J.-F.; Guerriero, G. Cannabis sativa: The Plant of the Thousand and One Molecules. *Front. Plant Sci.* **2016**, *7*.

211. Kögel, C. C.; López-Pelayo, H.; Balcells-Olivero, M. M.; Colom, J.; Gual, A. Psychoactive constituents of cannabis and their clinical implications: a systematic review/Constituyentes psicoactivos del cannabis y sus implicaciones clinicas: una revision sistematica. *Adicciones* **2018**, *30*, 140.

212. Abrams, D.; Guzman, M. Cannabis in cancer care. *Clin. Pharmacol. Ther.* **2015**, *97*, 575-586.

213. Sastre-Garriga, J.; Vila, C.; Clissold, S.; Montalban, X. THC and CBD oromucosal spray (Sativex®) in the management of spasticity associated with multiple sclerosis. *Expert Rev. Neurother.* **2011**, *11*, 627-637.

214. Lim, K.; See, Y. M.; Lee, J. A Systematic Review of the Effectiveness of Medical Cannabis for Psychiatric, Movement and Neurodegenerative Disorders. *Clin. Psychopharmacol. Neurosci.* **2017**, *15*, 301-312.

215. Boggs, D. L.; Nguyen, J. D.; Morgenson, D.; Taffe, M. A.; Ranganathan, M. Clinical and Preclinical Evidence for Functional Interactions of Cannabidiol and Δ9-Tetrahydrocannabinol. *Neuropsychopharmacology* **2018**, *43*, 142-154.

216. Pate, D. W., Possible role of ultraviolet radiation in evolution ofCannabis chemotypes. *Econ. Bot.* **1983**, *37*, 396.

217. Lydon, J.; Teramura, A. H.; Coffman, C. B. UV-B radiation effect on photosynthesis, growth and cannabinoid production of two Cannabis sativa chemotypes. *Photochem. Photobio.* **1987**, *46*, 201-206.

218. Pate, D. W. Chemical ecology of Cannabis. *J. Int. Hemp* **1994**, *2*, 32-37.

219. Black, N.; Stockings, E.; Campbell, G.; Tran, L. T.; Zagic, D.; Hall, W. D.; Farrell, M.; Degenhardt, L. Cannabinoids for the treatment of mental disorders and symptoms of mental disorders: a systematic review and meta-analysis. *Lancet Psychiat.* **2019**, *6*, 995-1010.

220. VanDolah, H. J.; Bauer, B. A.; Mauck, K. F. Clinicians' Guide to Cannabidiol and Hemp Oils. *Mayo Clin. Proc.* **2019**, *94*, 1840-1851.

221. Maroon, J.; Bost, J. Review of the neurological benefits of phytocannabinoids. *Surg. Neurol. Int.* **2018**, *9*, 91-91.

222. Sholler, D. J.; Schoene, L.; Spindle, T. R. Therapeutic Efficacy of Cannabidiol (CBD): a Review of the Evidence From Clinical Trials and Human Laboratory Studies. *Curr. Addict. Rep.* **2020**, *7*, 405-412.

223. Pisanti, S.; Malfitano, A. M.; Ciaglia, E.; Lamberti, A.; Ranieri, R.; Cuomo, G.; Abate, M.; Faggiana, G.; Proto, M. C.; Fiore, D.; Laezza, C.; Bifulco, M. Cannabidiol: State of the art and new challenges for therapeutic applications. *Pharmacol. Ther.* **2017**, *175*, 133-150.

224. Dialer, L.; Petrovic, D.; Weigl, U. Process for the production of cannabidiol and delta-9-tetrahydrocannabinol. US20180319763, 2018.

225. Gutman, A. L.; Etinger, M.; Fedotev, I.; Khanolkar, R.; Nisnevich, G. A.; Pertsikov, B.; Rukhman, I.; Tishin, B. Methods for purifying trans-(−)-Δ9-tetrahydrocannabinol and trans-(+)-Δ9-tetrahydrocannabinol. US20160199344A1, 2016.

226. Webster, G.; Sarna, L. P.; Mechoulam, R. Conversion of CBD to Δ 8-THC and Δ 9-THC. EP1409473A2, 2008.

227. Webb, D. J.; Hayes, P. G.; Kovalchuk, I. Method for synthesis of cannabis products. US20200262806A1, 2021.

228. Brenneisen, R. Chemistry and Analysis of Phytocannabinoids and Other Cannabis Constituents. In *Marijuana and the Cannabinoids*, Humana Press, 2007; pp 17-49.

229. Aizpurua-Olaizola, O.; Soydaner, U.; Öztürk, E.; Schibano, D.; Simsir, Y.; Navarro, P.; Etxebarria, N.; Usobiaga, A. Evolution of the Cannabinoid and Terpene Content during the Growth of Cannabis sativa Plants from Different Chemotypes. *J. Nat. Prod.* **2016**, *79*, 324-331.

230. Jin, D.; Dai, K.; Xie, Z.; Chen, J. Secondary Metabolites Profiled in Cannabis Inflorescences, Leaves, Stem Barks, and Roots for Medicinal Purposes. *Sci. Rep.* **2020**, *10*, 1-14.

231. Shapira, A.; Berman, P.; Futoran, K.; Guberman, O.; Meiri, D. Tandem Mass Spectrometric Quantification of 93 Terpenoids in Cannabis Using Static Headspace Injections. *Anal. Chem.* **2019**, *91*, 11425-11432.

232. Hanuš, L. O.; Meyer, S. M.; Muñoz, E.; Taglialatela-Scafati, O.; Appendino, G. Phytocannabinoids: a unified critical inventory. *Nat. Prod. Rep.* **2016**, *33*, 1357-1392.

233. Taura, F.; Sirikantaramas, S.; Shoyama, Y.; Shoyama, Y.; Morimoto, S. Phytocannabinoids in Cannabis sativa: Recent Studies on Biosynthetic Enzymes. *Chem. Biodivers.* **2007**, *4*, 1649-1663.

234. Basavarajappa, B. S. Critical Enzymes Involved in Endocannabinoid Metabolism. *Protein Pept. Lett.* **2007**, *14*, 237-246.

235. Razdan, R., Total Synthesis of Natural Products, Volume 4. In *Total Synthesis of Natural Products*, Volume 4, John Wiley & Sons, 2007; pp 185-262.

236. Taylor, E. C.; Lenard, K.; Shvo, Y. Active Constituents of Hashish. Synthesis of dl-Δ6-3, 4-trans-Tetrahydrocannabinol. *J. Am. Chem. Soc.* **1966**, *88*, 367-369.

237. Crippa, J. A. S.; Zuardi, A. W.; Hallak, J. E. C.; Miyazawa, B.; Bernardo, S. A.; Donaduzzi, C. M.; Guzzi, S.; Favreto, W. A. J.; Campos, A.; Queiroz, M. E. C. Oral Cannabidiol Does Not Convert to Δ8-THC or Δ9-THC in Humans: A Pharmacokinetic Study in Healthy Subjects. *Cannabis Cannabinoid Res.* **2019**, *5*, 89-98.

238. Nawata, Y.; Yamaguchi, T.; Fukumori, R.; Yamamoto, T. Inhibition of Monoacylglycerol Lipase Reduces the Reinstatement of Methamphetamine-Seeking and Anxiety-Like Behaviors in Methamphetamine Self-Administered Rats. *Int. J. Neuropsychopharmacol.* **2019**, *22*, 165-172.

239. Raber, J. C.; Douglass, B. J. Combination of Δ8-tetrahydrocannabinol and non-cannabinoid natural products for increasing psychoactive or non-psychoactive pharmaceutical effects. WO2019046850, 2019.

240. Abrahamov, A.; Abrahamov, A.; Mechoulam, R., An efficient new cannabinoid antiemetic in pediatric oncology. *Life Sci.* **1995**, *56*, 2097-2102.

241. Stern, E.; Lambert, D. M. Medicinal Chemistry Endeavors around the Phytocannabinoids. *Chem. Biodivers.* **2007**, *4*, 1707-1728.

242. Karniol, I. G.; Shirakawa, I.; Takahashi, R. N.; Knobel, E.; Musty, R. E. Effects of Δ9-Tetrahydrocannabinol and Cannabinol in Man. *Pharmacology* **1975**, *13*, 502-512.

243. Petitet, F.; Jeantaud, B.; Reibaud, M.; Imperato, A.; Dubroeucq, M.-C. Complex pharmacology of natural cannabivoids: Evidence for partial agonist

activity of Δ9-tetrahydrocannabinol and antagonist activity of cannabidiol on rat brain cannabinoid receptors. *Life Sci.* **1998**, *63*, PL1-PL6.

244. Dach, J.; Moore, E. A.; Kander, J., *Cannabis Extracts in Medicine: The Promise of Benefits in Seizure Disorders, Cancer and Other Conditions*, McFarland, 2015.

245. Ikuo, Y.; Hiroshi, G.; Shizuo, N.; Kazuhito, W.; Hidetoshi, Y. Cannabielsoin as a new metabolite of cannabidiol in mammals. *Pharmacol. Biochem. Behav.* **1991**, *40*, 541-546.

246. Limban, C.; Nuţă, D. C.; Chiriţă, C.; Negreș, S.; Arsene, A. L.; Goumenou, M.; Karakitsios, S. P.; Tsatsakis, A. M.; Sarigiannis, D. A. The use of structural alerts to avoid the toxicity of pharmaceuticals. *Toxicol. Rep.* **2018**, *5*, 943-953.

247. Claesson, A.; Minidis, A. Systematic Approach to Organizing Structural Alerts for Reactive Metabolite Formation from Potential Drugs. *Chem. Res. Toxicol.* **2018**, *31*, 389-411.

248. Rapaka, R. S.; Makriyannis, A.; Abuse, N. I. o. D., *Structure-activity Relationships of the Cannabinoids*. U.S., Department of Health and Human Services, Public Health Service, Alcohol, Drug Abuse, and Mental Health Administration, National Institute on Drug Abuse, 1987.

249. Le Boisselier, R.; Alexandre, J.; Lelong-Boulouard, V.; Debruyne, D. Focus on cannabinoids and synthetic cannabinoids. *Clin. Pharmacol. Ther.* **2017**, *101*, 220-229.

250. ElSohly, M. A.; Gul, W.; Wanas, A. S.; Radwan, M. M. Synthetic cannabinoids: Analysis and metabolites. *Life Sci.* **2014**, *97*, 78-90.

251. Mills, B.; Yepes, A.; Nugent, K. Synthetic Cannabinoids. *Am. J. Med. Sci.* **2015**, *350*, 59-62.

252. Martin, B. R.; Jefferson, R.; Winckler, R.; Wiley, J. L.; Huffman, J. W.; Crocker, P. J.; Saha, B.; Razdan, R. K. Manipulation of the tetrahydrocannabinol side chain delineates agonists, partial agonists, and antagonists. *J. Pharmacol. Exp. Ther.* **1999**, *290*, 1065-79.

253. Andersson, D. A.; Gentry, C.; Alenmyr, L.; Killander, D.; Lewis, S. E.; Andersson, A.; Bucher, B.; Galzi, J. L.; Sterner, O.; Bevan, S.; Högestätt, E. D.; Zygmunt, P. M. TRPA1 mediates spinal antinociception induced by acetaminophen and the cannabinoid Δ(9)-tetrahydrocannabiorcol. *Nat. Commun.* **2011**, *2*, 1-11.

254. Bow, E. W.; Rimoldi, J. M. The Structure-Function Relationships of Classical Cannabinoids: CB1/CB2 Modulation. *Perspect. Medicin. Chem.* **2016**, *8*, 17-39.

255. Prandi, C.; Blangetti, M.; Namdar, D.; Koltai, H. Structure-Activity Relationship of Cannabis Derived Compounds for the Treatment of Neuronal Activity-Related Diseases. *Molecules* **2018**, *23*, 1-17.

256. Devane, W. A.; Breuer, A.; Sheskin, T.; Jarbe, T. U.; Eisen, M. S.; Mechoulam, R. A Novel Probe for the Cannabinoid Receptor. *J. Med. Chem.* **1992**, *35*, 2065-2069.

257. Jiang, W.; Zhang, Y.; Xiao, L.; Van Cleemput, J.; Ji, S. P.; Bai, G.; Zhang, X. Cannabinoids Promote Embryonic and Adult Hippocampus Neurogenesis and Produce Anxiolytic- and Antidepressant-like Effects. *J. Clin. Invest.* **2005**, *115*, 3104-3116.

258. Ramirez, B. G.; Blazquez, C.; Gomez del Pulgar, T.; Guzman, M.; de Ceballos, M. L. Prevention of Alzheimer's Disease Pathology by Cannabinoids: Neuroprotection Mediated by Blockade of Microglial Activation. *J. Neurosci.* **2005**, *25*, 1904-1913.

259. Bedi, G.; Cooper, Z. D.; Haney, M. Subjective, Cognitive and Cardiovascular Dose-Effect Profile of Nabilone and Dronabinol in Marijuana Smokers. *Addict. Biol.* **2013**, *18*, 872-881.

260. Smith, L. A.; Azariah, F.; Lavender, V. T.; Stoner, N. S.; Bettiol, S. Cannabinoids for Nausea and Vomiting in Adults with Cancer Receiving Chemotherapy. *Cochrane Database Syst. Rev.* **2015**, CD009464, 1-86.

261. Kogan, N. M.; Schlesinger, M.; Priel, E.; Rabinowitz, R.; Berenshtein, E.; Chevion, M.; Mechoulam, R. HU-331, a Novel Cannabinoid-based Anticancer Topoisomerase II Inhibitor. *Mol. Cancer Ther.* **2007**, *6*, 173-83.

262. Kogan, N. M.; Schlesinger, M.; Peters, M.; Marincheva, G.; Beeri, R.; Mechoulam, R. A Cannabinoid Anticancer Quinone, HU-331, is More Potent and Less Cardiotoxic than Doxorubicin: a Comparative in vivo Study. *J. Pharmacol. Exp. Ther.* **2007**, *322*, 646-53.

263. Burstein, S. H.; Zurier, R. B. Cannabinoids, endocannabinoids, and related analogs in inflammation. *The AAPS journal* **2009**, *11*, 109-119.

264. Banister, S. D.; Stuart, J.; Kevin, R. C.; Edington, A.; Longworth, M.; Wilkinson, S. M.; Beinat, C.; Buchanan, A. S.; Hibbs, D. E.; Glass, M.; Connor, M.; McGregor, I. S.; Kassiou, M. Effects of Bioisosteric Fluorine in Synthetic Cannabinoid Designer Drugs JWH-018, AM-2201, UR-144, XLR-11, PB-22, 5F-PB-22, APICA, and STS-135. *ACS Chem. Neurosci.* **2015**, *6*, 1445-1458.

265. Skancke, A.; Skancke, P. N. General and theoretical aspects of quinones. In *The Quinonoid Compounds (1988)*, 1988; pp 1-28.

266. Chambers, J. Q. Electrochemistry of quinones. In *The Quinonoid Compounds (1988)*, 1988; pp 719-757.

267. O'Brien, P. J. Molecular Mechanisms of Quinone Cytotoxicity. *Chem. Bio. Interact.* **1991**, *80*, 1-41.

268. Inouye, H.; Leistner, E. Biochemistry of quinones. In *The Quinonoid Compounds (1988)*, 1988; pp 1293-1349.

269. Silva, T. L.; de Azevedo, M. d. L. S. G.; Ferreira, F. R.; Santos, D. C.; Amatore, C.; Goulart, M. O. F. Quinone-Based Molecular Electrochemistry and their Contributions to Medicinal Chemistry: A look at the Present and Future. *Curr. Opin. Electrochem.* **2020**, *24*, 79-87.

270. Bolton, J. L.; Dunlap, T. Formation and Biological Targets of Quinones: Cytotoxic versus Cytoprotective Effects. *Chem. Res. Toxicol.* **2017**, *30*, 13-37.

271. Kogan, N. M.; Peters, M.; Mechoulam, R. Cannabinoid Quinones—A Review and Novel Observations. *Molecules* **2021**, *26*, 1761.

272. Caprioglio, D.; Mattoteia, D.; Pollastro, F.; Negri, R.; Lopatriello, A.; Chianese, G.; Minassi, A.; Collado, J. A.; Munoz, E.; Taglialatela-Scafati, O.; Appendino, G. The Oxidation of Phytocannabinoids to Cannabinoquinoids. *J. Nat. Prod.* **2020**, *83*, 1711-1715.

273. Mechoulam, R.; Kogan, N. M.; Rabinowitz, R.; Schlesinger, M. Compositions Including Quinonoid Derivatives of Cannabinoids for Therapeutic Use. US8497299B2, 2013.

274. Magdziak, D.; Rodriguez, A. A.; Van De Water, R. W.; Pettus, T. R. R. Regioselective Oxidation of Phenols to o-Quinones with o-Iodoxybenzoic Acid (IBX). *Org. Lett.* **2002**, *4*, 285-288.

275. Wang, J.; Sánchez-Roselló, M.; Aceña, J. L.; del Pozo, C.; Sorochinsky, A. E.; Fustero, S.; Soloshonok, V. A.; Liu, H. Fluorine in Pharmaceutical Industry: Fluorine-Containing Drugs Introduced to the Market in the Last Decade (2001–2011). *Chem. Rev.* **2014**, *114*, 2432-2506.

276. Purser, S.; Moore, P. R.; Swallow, S.; Gouverneur, V. Fluorine in medicinal chemistry. *Chem. Soc. Rev.* **2008**, *37*, 320-330.

277. Baudoux, J.; Cahard, D. Electrophilic Fluorination with N–F Reagents. In *Organic Reactions*, pp 1-326.

278. Kirk, K. L., Fluorination in Medicinal Chemistry: Methods, Strategies, and Recent Developments. *Org. Process Res. Dev.* **2008**, *12*, 305-321.

279. Yerien, D. E.; Bonesi, S.; Postigo, A. Fluorination methods in drug discovery. *Org. Biomol. Chem.* **2016**, *14*, 8398-8427.

280. Ritter, T.; Furuya, T.; Tang, P. Fluorination of Organic Compounds. WO 2010/05994, 2010.

281. Breuer, A.; Haj, C. G.; Fogaça, M. V.; Gomes, F. V.; Silva, N. R.; Pedrazzi, J. F.; Del Bel, E. A.; Hallak, J. C.; Crippa, J. A.; Zuardi, A. W.; Mechoulam, R.; Guimarães, F. S. Fluorinated Cannabidiol Derivatives: Enhancement of Activity in Mice Models Predictive of Anxiolytic, Antidepressant and Antipsychotic Effects. *PLoS One* **2016**, *11*, 1-18.

282. Usami, N.; Kobana, K.; Yoshida, H.; Kimura, T.; Watanabe, K.; Yoshimura, H.; Yamamoto, I. Synthesis and Pharmacological Activities in Mice of Halogenated Δ9-Tetrahydrocannabinol Derivatives. *Chem. Pharm. Bull. (Tokyo)* **1998**, *46*, 1462-1467.

283. Yoshida, H.; Usami, N.; Ohishi, Y.; Watanabe, K.; Yamamoto, I.; Yoshimura, H. Synthesis and Pharmacological Effects in Mice of Halogenated Cannabinol Derivatives. *Chem. Pharm. Bull. (Tokyo)* **1995**, *43*, 335-337.

284. Crocker, P. J.; Mahadevan, A.; Wiley, J. L.; Martin, B. R.; Razdan, R. K. The role of fluorine substitution in the structure–activity relationships (SAR) of classical cannabinoids. *Bioorg. Med. Chem. Lett.* **2007**, *17*, 1504-1507.

285. Zanato, C.; Pelagalli, A.; Marwick, K. F. M.; Piras, M.; Dall'Angelo, S.; Spinaci, A.; Pertwee, R. G.; Wyllie, D. J. A.; Hardingham, G. E.; Zanda, M. Synthesis, radio-synthesis and in vitro evaluation of terminally fluorinated

derivatives of HU-210 and HU-211 as novel candidate PET tracers. *Org. Biomol. Chem.* **2017**, *15*, 2086-2096.

286. Perez, M.; Cartarozzi, L. P.; Chiarotto, G. B.; Oliveira, S. A. d.; Guimarães, F. S.; Oliveira, A. L. R. d. Neuronal preservation and reactive gliosis attenuation following neonatal sciatic nerve axotomy by a fluorinated cannabidiol derivative. *Neuropharmacology* **2018**, *140*, 201-208.

287. Leigh, C.; Zhang, Y.; Moshos, K.; Trepper, M.; Deng, H. Cannabinoids and uses thereof. WO2020230145A1, 2019.

288. Fujimoto, T.; Ritter, T. PhenoFluorMix: Practical Chemoselective Deoxyfluorination of Phenols. *Org. Lett.* **2015**, *17*, 544-547.

289. Neumann, C. N.; Ritter, T. Facile C–F Bond Formation through a Concerted Nucleophilic Aromatic Substitution Mediated by the PhenoFluor Reagent. *Acc. Chem. Res.* **2017**, *50*, 2822-2833.

290. Nodwell, M. B.; Bagai, A.; Halperin, S. D.; Martin, R. E.; Knust, H.; Britton, R., Direct photocatalytic fluorination of benzylic C–H bonds with N-fluorobenzenesulfonimide. *Chem. Commun.* **2015**, *51*, 11783-11786.

291. Halperin, S. D.; Kwon, D.; Holmes, M.; Regalado, E. L.; Campeau, L.-C.; DiRocco, D. A.; Britton, R. Development of a Direct Photocatalytic C–H Fluorination for the Preparative Synthesis of Odanacatib. *Org. Lett.* **2015**, *17*, 5200-5203.

292. Nodwell, M. B.; Yang, H.; Čolović, M.; Yuan, Z.; Merkens, H.; Martin, R. E.; Bénard, F.; Schaffer, P.; Britton, R. 18F-Fluorination of Unactivated C–H Bonds in Branched Aliphatic Amino Acids: Direct Synthesis of Oncological Positron Emission Tomography Imaging Agents. *J. Am. Chem. Soc.* **2017**, *139*, 3595-3598.

293. Yuan, Z.; Nodwell, M. B.; Yang, H.; Malik, N.; Merkens, H.; Bénard, F.; Martin, R. E.; Schaffer, P.; Britton, R. Site-Selective, Late-Stage C−H 18F-Fluorination on Unprotected Peptides for Positron Emission Tomography Imaging. *Angew. Chem. Int. Ed.* **2018**, *57*, 12733-12736.

294. Ravelli, D.; Fagnoni, M.; Fukuyama, T.; Nishikawa, T.; Ryu, I. Site-Selective C–H Functionalization by Decatungstate Anion Photocatalysis: Synergistic Control by Polar and Steric Effects Expands the Reaction Scope. *ACS Catalysis* **2018**, *8*, 701-713.

295. Miller, L. K.; Devi, L. A. The highs and lows of cannabinoid receptor expression in disease: mechanisms and their therapeutic implications. *Pharmacol. Rev.* **2011**, *63*, 461-470.

296. Ligresti, A.; Bisogno, T.; Matias, I.; De Petrocellis, L.; Cascio, M. G.; Cosenza, V.; D'Argenio, G.; Scaglione, G.; Bifulco, M.; Sorrentini, I.; Di Marzo, V. Possible endocannabinoid control of colorectal cancer growth. *Gastroenterology* **2003**, *125*, 677-687.

297. Sarfaraz, S.; Adhami, V. M.; Syed, D. N.; Afaq, F.; Mukhtar, H. Cannabinoids for cancer treatment: progress and promise. *Cancer Res.* **2008**, *68*, 339-342.

298. Bifulco, M.; Laezza, C.; Portella, G.; Vitale, M.; Orlando, P.; De Petrocellis, L.; Di Marzo, V. Control by the endogenous cannabinoid system of ras oncogene-dependent tumor growth. *FASEB J.* **2001**, *15*, 2745-2747.

299. Swietach, P.; Vaughan-Jones, R. D.; Harris, A. L.; Hulikova, A. The chemistry, physiology and pathology of pH in cancer. *Philos. Trans. R. Soc. Lond., B, Biol. Sci.* **2014**, *369*, 1-9.

300. Sosa, V.; Moliné, T.; Somoza, R.; Paciucci, R.; Kondoh, H.; Lleonart, M. E. Oxidative stress and cancer: An overview. *Ageing Res. Rev.* **2013**, *12*, 376-390.

301. Semenza, G. L. Hypoxia and cancer. *Cancer Metastasis Rev.* **2007**, *26*, 223-224.

302. Yang, M.; Brackenbury, W. Membrane potential and cancer progression. *Front. Physiol.* **2013**, *4*, 1-10.

303. Agnati, L. F.; Fuxe, K.; Zini, I.; Lenzi, P.; Hökfelt, T. Aspects on receptor regulation and isoreceptor identification. *Med. Biol.* **1980**, *58*, 182-187.

304. Papa, V.; Pezzino, V.; Costantino, A.; Belfiore, A.; Giuffrida, D.; Frittitta, L.; Vannelli, G. B.; Brand, R.; Goldfine, I. D.; Vigneri, R. Elevated insulin receptor content in human breast cancer. *J. Clin. Investig.* **1990**, *86*, 1503-1510.

305. Chen, Y.; Hughes-Fulford, M. Human prostate cancer cells lack feedback regulation of low-density lipoprotein receptor and its regulator, SREBP2. *Int. J. Cancer Res.* **2001**, *91*, 41-45.

306. Jones, D. H.; Nakashima, T.; Sanchez, O. H.; Kozieradzki, I.; Komarova, S. V.; Sarosi, I.; Morony, S.; Rubin, E.; Sarao, R.; Hojilla, C. V.; Komnenovic, V.; Kong, Y.-Y.; Schreiber, M.; Dixon, S. J.; Sims, S. M.; Khokha, R.; Wada, T.; Penninger, J. M. Regulation of cancer cell migration and bone metastasis by RANKL. *Nature* **2006**, *440*, 692-696.

307. Harrison, H.; Farnie, G.; Howell, S. J.; Rock, R. E.; Stylianou, S.; Brennan, K. R.; Bundred, N. J.; Clarke, R. B. Regulation of Breast Cancer Stem Cell Activity by Signaling through the Notch4 Receptor. *Cancer Res.* **2010**, *70*, 709-718.

308. Casaletto, J. B.; McClatchey, A. I. Spatial regulation of receptor tyrosine kinases in development and cancer. *Nat. Rev. Cancer* **2012**, *12*, 387-400.

309. Huestis, M. A. Human cannabinoid pharmacokinetics. *Chem. Biodivers.* **2007**, *4*, 1770-1804.

310. Grotenhermen, F. Pharmacokinetics and pharmacodynamics of cannabinoids. *Clin. Pharmacokinet.* **2003**, *42*, 327-360.

311. McGilveray, I. J. Pharmacokinetics of cannabinoids. *Pain Res. Manag.* **2005**, *10*, 15A-22A.

312. Decorte, T.; Potter, G. *World Wide Weed: Global Trends in Cannabis Cultivation and its Control*, Taylor & Francis: 2016.

313. Chouvy, P.-A. Cannabis cultivation in the world: heritages, trends and challenges. *EchoGéo* 2019, *48*.

314. Investopedia. https://www.investopedia.com/articles/insights/110916/economic-benefits-legalizing-weed.asp accessed 11/12/2019).

315. Marijuana Buisness Daily. https://mjbizdaily.com/chart-us-cannabis-industrys-economic-impact-could-hit-130-billion-by-2024/ (accessed 21/07/2020).

316. BuisnessWire, https://www.businesswire.com/news/home/20200207005038/en/Leafly-Jobs-Report-Cannabis-is-the-fastest-growing-American-industry-surpassing-240000-jobs (accessed 7/02/2020).

317. Chemat, F.; Abert-Vian, M.; Fabiano-Tixier, A. S.; Strube, J.; Uhlenbrock, L.; Gunjevic, V.; Cravotto, G. Green extraction of natural products. Origins, current status, and future challenges. *TrAC, Trends Anal. Chem.* **2019**, *118*, 248-263.

318. Zhang, Q.-W.; Lin, L.-G.; Ye, W.-C. Techniques for extraction and isolation of natural products: A comprehensive review. *Chin. Med.* **2018**, *13*, 1-26.

319. Koehn, F. E.; Carter, G. T. The evolving role of natural products in drug discovery. *Nat. Rev. Drug Discov.* **2005**, *4*, 206-220.

320. Government of Canada, https://www.canada.ca/en/health-canada/services/drugs-medication/cannabis.html (accessed 30/08/2020).

321. Milipore Sigma, https://www.sigmaaldrich.com/catalog/product/cerillian/h027?lang=en&region=CA (accessed 21/08/2020).

322. Mechoulam, R.; Gaoni, Y. A Total Synthesis of dl-Δ1-Tetrahydrocannabinol, the Active Constituent of Hashish1. *J. Am. Chem. Soc.* **1965**, *87*, 3273-3275.

323. Lander, N.; Ben-Zvi, Z.; Mechoulam, R.; Martin, B.; Nordqvist, M.; Agurell, S., Total syntheses of cannabidiol and Δ1-tetrahydrocannabinol metabolites. *J. Chem. Soc., Perkin Trans. 1* **1976**, 8-16.

324. Cheng, L.-J.; Xie, J.-H.; Chen, Y.; Wang, L.-X.; Zhou, Q.-L. Enantioselective total synthesis of (−)-Δ8-THC and (−)-Δ9-THC via catalytic asymmetric hydrogenation and SNAr cyclization. *Org. Lett.* **2013**, *15*, 764-767.

325. Huang, Q.; Ma, B.; Li, X. a.; Pan, X.; She, X. Total Synthesis of (-)-Δ8-trans-Tetrahydrocannabinol. *Synthesis* **2010**, *2010*, 1766-1770.

326. Michael, D. M. Ozonation of Cannabinoids. GB2567235A, 2017.

327. KumaráB, V. Protecting group free enantiospecific total syntheses of structurally diverse natural products of the tetrahydrocannabinoid family. *Chem. Commun.* **2015**, *51*, 2871-2873.

328. Ballerini, E.; Minuti, L.; Piermatti, O. High-Pressure Diels− Alder Cycloadditions between Benzylideneacetones and 1, 3-Butadienes: Application to the Synthesis of (*R,R*)-(−)-and (*S,S*)-(+)-Δ8-Tetrahydrocannabinol. *J. Org. Chem.* **2010**, *75*, 4251-4260.

329. Castillo, J. Producing cannabis extracts via selective decarboxylation. US10471113B1, 2019.

330. Bowd, A.; Swann, D. A.; Turnbull, J. H. Photochemical transformations of cannabinol. *J. Chem. Soc., Chem. Commun.* **1975**, 797-798.

331. Pollastro, F.; Caprioglio, D.; Marotta, P.; Moriello, A. S.; De Petrocellis, L.; Taglialatela-Scafati, O.; Appendino, G. Iodine-Promoted Aromatization of p-Menthane-Type Phytocannabinoids. *J. Nat. Prod.* **2018**, *81*, 630-633.

332. Blake, A.; Nahtigal, I. The evolving landscape of cannabis edibles. *Curr. Opin. Food Sci.* **2019**, *28*, 25-31.

333. Barton, D. H. R.; Crich, D.; Motherwell, W. B. The invention of new radical chain reactions. Part VIII. Radical chemistry of thiohydroxamic esters; A new method for the generation of carbon radicals from carboxylic acids. *Tetrahedron* **1985**, *41*, 3901-3924.

334. Vijh, A. K.; Conway, B. E. Electrode Kinetic Aspects of the Kolbe Reaction. *Chem. Rev.* **1967**, *67*, 623-664.

335. Johnson, R. G.; Ingham, R. K. The Degradation Of Carboxylic Acid Salts By Means Of Halogen - The Hunsdiecker Reaction. *Chem. Rev.* **1956**, *56*, 219-269.

336. Li, T.; Huo, L.; Pulley, C.; Liu, A. Decarboxylation mechanisms in biological system. *Bioorg. Chem.* **2012**, *43*, 2-14.

337. Teske, J. A.; Deiters, A. A Cyclotrimerization Route to Cannabinoids. *Org. Lett.* **2008**, *10*, 2195-2198.

338. Damm, M.; Rechberger, G.; Kollroser, M.; Kappe, C. O. An evaluation of microwave-assisted derivatization procedures using hyphenated mass spectrometric techniques. *J. Chromatogr. A* **2009**, *1216*, 5875-5881.

339. Harvey, D. J. The mass spectra of the trimethylsilyl derivatives of Δ1- and Δ6-tetrahydrocannabinol. *Biomed. Mass Spectrom.* **1981**, *8*, 575-578.

340. Kaur, A.; Ariafard, A. Mechanistic Investigation into Phenol Oxidation by IBX Elucidated by DFT Calculations. *Org. Biomol. Chem.* **2020**, *18*, 1117-1129.

341. Kogan, N. M.; Rabinowitz, R.; Levi, P.; Gibson, D.; Sandor, P.; Schlesinger, M.; Mechoulam, R. Synthesis and Antitumor Activity of Quinonoid Derivatives of Cannabinoids. *J. Med. Chem.* **2004**, *47*, 3800-3806.

342. Mattoteia, D.; Taglialatela-Scafati, O.; Muñoz, E.; de la Vega, L.; Caprioglio, D.; Appendino, G. Regiodivergent Synthesis of ortho- and para-Cannabinoquinones. *Eur. J. Org. Chem.* **2020**, *2020*, 7429-7434.

343. Pan, S. S.; Gonzalez, H. Mitomycin antibiotic reductive potential and related pharmacological activities. *Mol. Pharmacol.* **1990**, *37*, 966-970.

344. Crawford, P. W.; Gross, J.; Lawson, K.; Cheng, C. C.; Dong, Q.; Liu, D. F.; Luo, Y. L.; Szczepankiewicz, B. G.; Heathcock, C. H. Electrochemical Properties of Some Biologically Active Quinone Derivatives: Furanquinones, Pyridoquinones, and Diplamine, a Cytotoxic Pyridoacridine Alkaloid. *J. Electrochem. Soc.* **1997**, *144*, 3710-3715.

345. Quan, M.; Sanchez, D.; Wasylkiw, M. F.; Smith, D. K. Voltammetry of Quinones in Unbuffered Aqueous Solution: Reassessing the Roles of Proton Transfer and Hydrogen Bonding in the Aqueous Electrochemistry of Quinones. *J. Am. Chem. Soc.* **2007**, *129*, 12847-12856.

346. Lehmann, M. W.; Evans, D. H. Mechanism of the Electrochemical Reduction of 3,5-Di-tert-butyl-1,2-benzoquinone. Evidence for a Concerted Electron and Proton Transfer Reaction Involving a Hydrogen-Bonded Complex as Reactant. *J. Phys. Chem. B* **2001**, *105*, 8877-8884.

347. Lehmann, M. W.; Evans, D. H. Anomalous Behavior in the Two-Step Reduction of Quinones in Acetonitrile. *J. Electroanal. Chem.* **2001**, *500*, 12-20.

348. René, A.; Evans, D. H. Electrochemical Reduction of Some o-Quinone Anion Radicals: Why Is the Current Intensity so Small? *J. Phys. Chem. C* **2012**, *116*, 14454-14460.

349. Abreu, F. C.; Goulart, M. O. F.; Brett, A. M. O. Reduction of Lapachones in Aqueous Media at a Glassy Carbon Electrode. *Electroanalysis* **2002**, *14*, 29-34.

350. de Abreu, F. C.; Ferreira, D. C. M.; Wadhawan, J.; Amatore, C.; Ferreira, V. F.; da Silva, M. N.; de Souza, M. C. B. V.; Gomes, T. S.; Ximenes, E. A.; Goulart, M. O. F. Electrochemistry of β-lapachone and its diazoderivative: Relevance to their compared antimicrobial activities. *Electrochem. Commun.* **2005**, *7*, 767-772.

351. de Abreu, F. C.; Ferreira, D. C. M.; Goulart, M. O. F.; Buriez, O.; Amatore, C. Electrochemical activation of β-lapachone in β-cyclodextrin inclusion complexes and reactivity of its reduced form towards oxygen in aqueous solutions. *J. Electroanal. Chem.* **2007**, *608*, 125-132.

352. Berger, F.; Plutschack, M. B.; Riegger, J.; Yu, W.; Speicher, S.; Ho, M.; Frank, N.; Ritter, T. Site-selective and versatile aromatic C−H functionalization by thianthrenation. *Nature* **2019**, *567*, 223-228.

353. Xu, P.; Zhao, D.; Berger, F.; Hamad, A.; Rickmeier, J.; Petzold, R.; Kondratiuk, M.; Bohdan, K.; Ritter, T. Site-Selective Late-Stage Aromatic [18F]Fluorination via Aryl Sulfonium Salts. *Angew. Chem. Int. Ed.* **2020**, *59*, 1956-1960.

354. Li, J.; Chen, J.; Sang, R.; Ham, W.-S.; Plutschack, M. B.; Berger, F.; Chabbra, S.; Schnegg, A.; Genicot, C.; Ritter, T. Photoredox catalysis with aryl sulfonium salts enables site-selective late-stage fluorination. *Nat. Chem.* **2020**, *12*, 56-62.

355. Fujimoto, T.; Becker, F.; Ritter, T. PhenoFluor: Practical Synthesis, New Formulation, and Deoxyfluorination of Heteroaromatics. *Org. Process Res. Dev.* **2014**, *18*, 1041-1044.

356. Hill, C. L. Introduction of Functionality into Unactivated Carbon-Hydrogen Bonds. Catalytic Generation and Nonconventional Utilization of Organic Radicals. *Synlett* **1995**, *1995*, 127-132.

357. Hollister, L. E.; Gillespie, H. K.; Mechoulam, R.; Srebnik, M. Human pharmacology of 1S and 1R enantiomers of delta-3-tetrahydrocannabinol. *Psychopharmacology* **1987**, *92*, 505-507.

358. Rosati, O.; Messina, F.; Pelosi, A.; Curini, M.; Petrucci, V.; Gertsch, J.; Chicca, A. One-pot heterogeneous synthesis of Δ3-tetrahydrocannabinol analogues and xanthenes showing differential binding to CB1 and CB2 receptors. *Eur. J. Med. Chem.* **2014**, *85*, 77-86.

359. McAllister, S. D.; Christian, R. T.; Horowitz, M. P.; Garcia, A.; Desprez, P. Y. Cannabidiol as a novel inhibitor of Id-1 gene expression in aggressive breast cancer cells. *Mol. Cancer Ther.* **2007**, *6*, 2921-7.

360. Brown, J. M. Exploiting the hypoxic cancer cell: mechanisms and therapeutic strategies. *Mol. Med. Today* **2000**, *6*, 157-162.

361. Jiang, J.; Auchinvole, C.; Fisher, K.; Campbell, C. J. Quantitative Measurement of Redox Potential in Hypoxic Cells using SERS Nanosensors. *Nanoscale* **2014**, *6*, 12104-12110.

362. Duan, J.-X.; Jiao, H.; Kaizerman, J.; Stanton, T.; Evans, J. W.; Lan, L.; Lorente, G.; Banica, M.; Jung, D.; Wang, J.; Ma, H.; Li, X.; Yang, Z.; Hoffman, R. M.; Ammons, W. S.; Hart, C. P.; Matteucci, M. Potent and Highly Selective Hypoxia-Activated Achiral Phosphoramidate Mustards as Anticancer Drugs. *J. Med. Chem.* **2008**, *51*, 2412-2420.

363. Weiss, G. J.; Infante, J. R.; Chiorean, E. G.; Borad, M. J.; Bendell, J. C.; Molina, J. R.; Tibes, R.; Ramanathan, R. K.; Lewandowski, K.; Jones, S. F.; Lacouture, M. E.; Langmuir, V. K.; Lee, H.; Kroll, S.; Burris, H. A. Phase 1 Study of the Safety, Tolerability, and Pharmacokinetics of TH-302, a Hypoxia-Activated Prodrug, in Patients with Advanced Solid Malignancies. *Clin. Cancer Res.* **2011**, *17*, 2997-3004.

364. Protection for Phenols and Catechols. In *Greene's Protective Groups in Organic Synthesis*, John Wiley & Sons, 2014; pp 472-553.

365. Jiang, T.; Liu, H.; Zhang, H.; Huang, H. Catalytic Benzylation Reactions: From C—H Bond Activation to C—N Bond Activation. *Chin. J. Chem* . **2021**, *39*, 1070-1078.

366. Frigerio, M.; Santagostino, M.; Sputore, S. A User-Friendly Entry to 2-Iodoxybenzoic Acid (IBX). *J. Org. Chem.* **1999**, *64*, 4537-4538.

367. Choi, Y. H.; Hazekamp, A.; Peltenburg-Looman, A. M. G.; Frédérich, M.; Erkelens, C.; Lefeber, A. W. M.; Verpoorte, R. NMR Assignments of the Major Cannabinoids and Cannabiflavonoids Isolated from Flowers of Cannabis Sativa. *Phytochem. Anal.* **2004**, *15*, 345-354.

368. Williams, D. B. G.; Lawton, M. Drying of Organic Solvents: Quantitative Evaluation of the Efficiency of Several Desiccants. *J. Org. Chem.* **2010**, *75*, 8351-8354.

369. Staley, P. A.; Newell, C. M.; Pullman, D. P.; Smith, D. K. The Effect of Glassy Carbon Surface Oxides in Non-Aqueous Voltammetry: The Case of Quinones in Acetonitrile. *Anal. Chem.* **2014**, *86*, 10917-10924.

370. Choi, Y. H.; Hazekamp, A.; Peltenburg-Looman, A. M. G.; Frédérich, M.; Erkelens, C.; Lefeber, A. W. M.; Verpoorte, R., NMR assignments of the major cannabinoids and cannabiflavonoids isolated from flowers of Cannabis sativa. *Phytochem. Anal.* **2004**, *15*, 345-354.